

Alma Mater Studiorum — Università di Bologna

DOTTORATO DI RICERCA IN

Scienze Chimiche

Ciclo XXIV

Settore Concorsuale di afferenza: CHIM/06

Settore Scientifico disciplinare: CHIMICA ORGANICA

TITOLO TESI

Synthesis of Modified Amino Acids and Insertion in Peptides and Mimetics.

Structural Aspects and Impact on Biological Activity.

Presentata da: De Marco Rossella

Coordinatore Dottorato

Relatore

Prof. Adriana Bigi

Prof. Luca Gentilucci

Esame finale anno 2012

***Synthesis of Modified Amino Acids and Insertion  
in Peptides and Mimetics.***

***Structural Aspects and Impact on Biological Activity.***

***by***

***Rossella De Marco***

***2012***

*To My Self*

---

## *Table of Contents*

---

- ❖ **Cap 1. Chemical Modifications Designed to Improve Peptide Stability**
- ❖ 1. Introduction
- ❖ 1.2. Enzymatic Degradation of Peptides
- ❖ 1.3. Structure Modifications to Improve Peptide Stability
- ❖ 1.3.1. Pseudopeptides
- ❖ 1.3.2. Reduced Peptide Bonds
- ❖ 1.3.3. Azapeptides
- ❖ 1.3.4. Retro-Inverso Peptides
- ❖ 1.3.5. Peptoids
- ❖ 1.4. Incorporation of Non-Natural Amino Acids
- ❖ 1.4.1. D-Amino Acids
- ❖ 1.4.2. N-Alkylated Amino Acids
- ❖ 1.4.3.  $\alpha$ -Substituted  $\alpha$ -Amino-Acids
- ❖ 1.4.4.  $\beta$ -Substituted  $\alpha$ -Amino Acids
- ❖ 1.4.5. Proline analogues
- ❖ 1.4.6.  $\beta$ -Amino-Acids
- ❖ 1.5. Cyclization
- ❖ 1.6.  $\beta$ -Turn-Mimetics
- ❖ 1.7. Conclusion
- ❖ References

### **Chapter 2. Cyclopeptide Analogs for Generating New Molecular and 3D Diversity.**

- ❖ 2. Introduction
- ❖ 2. 1. Material and Methods
- ❖ 2.2. General Methods.
- ❖ 2.3. General Procedure for Peptide Coupling
- ❖ 2.3.1. Boc group deprotection
- ❖ 2.3.2. Fmoc group deprotection
- ❖ 2.3.3. Cbz and benzyl group deprotection
- ❖ 2.3.4. General Procedure for Peptide Cyclization
- ❖ 2.4. Conformation Analysis
- ❖ 2.5. Results
- ❖ 2.6. VT- $^1\text{H-NMR}$
- ❖ 2.7. 2D-ROESY

- ❖ 2.8. Discussion
- ❖ 2.9. Conclusions
- ❖ References

**Chapter 3.** Synthesis and Conformational Analysis of Cyclotetrapeptide Mimetic  $\beta$ -Turn Templates and Validation as 3D Scaffolds.

- ❖ 3. Introduction
- ❖ 3.1. Experimental section
  - ❖ 3.1.1. General methods
  - ❖ 3.1.2. Synthesis of 6
  - ❖ 3.1.3. Synthesis of 9
  - ❖ 3.1.4. Peptide cleavage
  - ❖ 3.1.5. Cyclization
- ❖ 3.2. Conformational analysis
- ❖ 3.3. Cell adhesion assay
- ❖ 3.4. Supporting Information
- ❖ References

**Chapter 4.** Antiangiogenic Effect of Dual/Selective  $\alpha_5\beta_1/\alpha_v\beta_3$  Integrin Antagonists Designed on Partially Modified Retro-Inverso Cyclotetrapeptide Mimetics.

- ❖ 4. Introduction
- ❖ 4.1. Results
  - ❖ 4.1.1. Inhibition of Cell Adhesion
  - ❖ 4.1.2. Effect of Integrin Antagonists on in Vitro Elicited by Basic Fibroblast Growth Factor (bFGF)
  - ❖ 4.1.3.  $\alpha_5\beta_1/\alpha_v\beta_3$  Integrin Antagonists Do Not Affect Endothelial Cell Viability
  - ❖ 4.1.4. Conformational Analysis of 2 and 3 in Solution
- ❖ 4.2. Molecular Docking
- ❖ 4.3. Discussion
- ❖ 4.4. Conclusions
- ❖ 4.5. Experimental Section
  - ❖ 4.5.1. General Methods
  - ❖ 4.5.2. Representative Synthetic Procedures and Analytical Characterization of PMRI RGD Mimetics 2 and 3.
  - ❖ 4.5.3. 14 {c[ $\beta$ Phe $\psi$ (NHCO)Asp(Ot-Bu) $\psi$ (NHCO)Gly-Arg(Mtr)]}
  - ❖ 4.5.4. 2 {c[ $\beta$ Phe $\psi$ (NHCO)Asp $\psi$ (NHCO)Gly-Arg]}
  - ❖ 4.5.5. 3 {c[(R)- $\beta$ Phe $\psi$ (NHCO)Asp $\psi$ (NHCO)Gly-Arg]}
- ❖ 4.6. Pharmacological Assays
  - ❖ 4.6.1. Materials for Biossays

- ❖ 4.6.2. Cell Culture
- ❖ 4.6.3. Cell Adhesion Assays
- ❖ 4.6.3. Flow Cytometry Assays
- ❖ 4.6.4. In Vitro Tubular Formation of HUVEC
- ❖ 4.7. Conformational Analysis
- ❖ 4.7.1. Molecular Docking
- ❖ 4.7.3. Protein Setup
- ❖ 4.7.4. Docking
- ❖ 4.8. Supporting Information
- ❖ References

**Chapter 5.** Molecular docking of opioid peptides and analogues, a powerful tool for the design of selective agonists and antagonists, and for the investigation of atypical ligand-receptor interactions.

- ❖ 5. Introduction
- ❖ 5.1. Structure and functions of the opioid receptors, and representative opioid ligands
- ❖ 5.2. Insights into the interactions between ligands and receptors
- ❖ 5.3. Principles of molecular docking.
- ❖ 5.4. Exploring the determinants of ligand affinity and selectivity: comparative docking studies
- ❖ 5.5. The docking of ligands lacking of the cationic amino group
- ❖ 5.5.1. Salvinorins
- ❖ 5.5.2. 6,6-Bicyclic enkephalin mimetics
- ❖ 5.5.3. Dhp-peptide
- ❖ 5.5.4. Fentanyl “carba”-analogues
- ❖ 5.6. The D-Trp-Phe  $\beta$ -turn MOR pharmacophoric motif
- ❖ References

**Chapter 6.** The Inverse Type II  $\beta$ -Turn on D-Trp-Phe, a Pharmacophoric Motif for MOR Agonist.

- ❖ 6. Introduction
- ❖ 6.1. Results
- ❖ 6.1.2. Cyclopeptide Design
- ❖ 6.1.3. Cyclopeptide Synthesis
- ❖ 6.1.3. Binding Affinity to the Cloned Human Opioid Receptors
- ❖ 6.1.4. Effects on Forskolin-Stimulated cAMP Production
- ❖ 6.2. Conformational Analysis
- ❖ 6.3. Molecular Backbone
- ❖ 6.4. Molecular Docking
- ❖ 6.5. Discussion
- ❖ 6.6. Conclusions

- ❖ 6.7. Experimental section
- ❖ 6.7.1. Chemistry
- ❖ 6.7.2. General Methods
- ❖ 6.7.3. Peptide Synthesis
- ❖ 6.7.4. Peptide Cleavage
- ❖ 6.7.5. Peptide Cyclization
- ❖ 6.8 Biology
- ❖ 6.8.1. Receptor Binding Assays to Cloned Human DOR and KOR
- ❖ 6.8.2. Determination of Inhibition of Cyclic AMP Accumulation
- ❖ 6.9. Conformational Analysis
- ❖ 6.9.1. Computational Methods
- ❖ 6.9.2. Molecular Docking
- ❖ 6.9.3. Hybrid QM/MM
- ❖ 6.9.4. Supporting Information
- ❖ References

**Chapter 7.** A simple route towards peptide analogues containing substituted (S)- or (R)-tryptophans.

- ❖ 7. Introduction
- ❖ 7.1. Results and Discussion
- ❖ 7.2. Conclusions
- ❖ 7.3. Supporting Information
- ❖ References

**Chapter 8.** Synthesis of Constrained Peptidomimetics Containing 2-Oxo-1,3-oxazolidine-4-carboxylic Acids.

- ❖ 8. Introduction
- ❖ 8.1. Results and Discussion
- ❖ 8.2. Conclusions
- ❖ 8.3. Experimental Section
- ❖ References

**Chapter 9.** Expedient Synthesis of Pseudo-Pro-Containing Peptides

- ❖ 9. Introduction
- ❖ 9.1. Results and discussion
- ❖ 9.1.1. Optimization of the Reaction Conditions
- ❖ 9.1.2. Synthesis of di-Oxd-peptides
- ❖ 9.2. Conformational Aspects of the Oxd peptides
- ❖ 9.3. Conclusions

- ❖ 9.4. Experimental part
- ❖ 9.4.1. Peptide Synthesis
- ❖ 9.4.2. Mono-Oxd-peptide Synthesis
- ❖ 9.4.3. Di-Oxd-peptide Synthesis
- ❖ 9.4.4. Di-Oxd-peptide Solid-Phase Synthesis
- ❖ 9.5. Theoretical Computations
- ❖ 9.5.1. Conformational Analysis
- ❖ 9.5.2.. Circular Dichroism
- ❖ 9.5.3. NMR Analysis
- ❖ 9.5.4. Roesy and Molecular Dynamics
- ❖ 9.6. Supporting information
- ❖ References

## **Conclusions**

## **Curriculum Vitae**

## **List of Publications**

---

## Abbreviations and acronyms

---

CNS = Central nervous system  
BBB = Blood-brain barrier  
ACE = Angiotensin-converting enzyme  
ADMET = Absorption distribution metabolism excretion toxicity  
SPPS = Solid phase peptide synthesis  
SAR = Structure-activity relationship  
RGD = Arg-Gly-Asp  
CCK = Cholecystokinin  
LHRH = Luteinizing hormone-releasing hormone  
TRH = Thyrotropin releasing hormone  
PEG = Polyethylene glycol  
PMRI = Partially modified retro inverso  
RCM = Ring-closing methathesis  
Boc = Tert-butyloxycarbonyl  
Fmoc = 9-*H*-fluoren-9-ylmethoxycarbonyl  
EDCI = 1-ethyl-3-(3-dimethylaminopropyl)carbodiimide  
HOBT = Hydroxybenzotriazole  
PG = Protecting group  
Bz = Benzyl  
DIC = N,N'-diisopropylcarbodiimide  
DEAD = Diethylazodicarboxylate  
Cbz = Benzyloxycarbonyl  
Dpp = Diphenylphosphinamide  
LDA = Lithium diisopropylamide  
Salen = Salicylic aldehyde ethylenediamine  
A\* = Chiral auxiliary  
TMS = Trimethylsilyl  
PyBOP = Benzotriazol-1-yl-oxytripyrrolidinophosphonium hexafluorophosphate  
DIEA = Diisopropylethylamine  
TFA = Trifluoroacetic acid  
Bom = Benzyloxymethyl  
Pip = Pípecolic acid or piperidine  
TEA = triethylamine  
DPPA = diphenylphosphorylazide  
DCM = dichlorometane  
DMA = dimethylamine

THF = tetrahydrofuran  
DMF = dimethylformamide  
EM = endomorphin  
MOR, DOR, KOR,  
 $\mu$ -,  $\delta$ -,  $\kappa$ - = opioid receptor, respectively  
EL = extracellular loop  
TMH = transmembrane helix  
2D, 3D = two-, three-dimensional, respectively  
HBTU = 2-(1H-Benzotriazole-1-yl)-1,1,3,3-tetramethyluronium hexafluorophosphate  
DMSO = dimethyl sulfoxide  
RP = reversed-phase  
ES-MS = electrospray ionization mass spectrometry  
SE = standard error  
DAMGO = H-T yr-D-Ala-Gly-N-MePhe-glyol  
DPDPE = [D-Pen<sup>2</sup>,D-Pen<sup>5</sup>]-enkephalin  
JOM-6 = Tyr-c(S-Et-S)[D-Cys-Phe-D-Pen]NH<sub>2</sub>  
MD = molecular dynamics  
Dock = molecular docking  
DO = docking orientation  
VT = variable temperature  
AMBER = assisted model building with energy refinement  
TIP3P = transferrable intermolecular potential three point  
DAD = diode array detector  
HMBC = heteronuclear multiple-bond coherence  
HSQC = heteronuclear single-quantum coherence  
rt = room temperature  
CPK = Corey, Pauling, and Koltun  
CCP4 = Collaborative Computational Project 4  
PBS = phosphate-buffered saline  
bFGF = basic fibroblast growth factor  
CTP = cyclotetrapeptide  
K562 = human erythroleukemic cells  
SK-MEL-24 = human malignant melanoma cells  
HUVEC = human umbilical vein endothelial cells  
BSA = bovine serum albumin  
ECM = extracellular matrix  
S.E.M. = standard error of mean  
ANOVA = analysis of variance test  
RMSE = root mean square deviation

MIDAS = metal-ion-dependent adhesion site

ODS = octadecyl silane

EDTA = ethylenediaminetetraacetic acid

MEM = minimum essential medium

RPMI = Roswell park Memorial Institute

FBS = fetal bovine serum

PBS = phosphate buffered saline

PMA = phorbol 12-myristate 13-acetate

PI = propidium iodide.

---

## Chapter 1

---

---

### Chemical Modifications Designed to Improve Peptide Stability

---

#### 1. Introduction

Peptides are amino acid derived compounds containing at least one amide (peptide) bond. Conventionally, peptides up to 20 amino acids are named oligopeptides, while the term polypeptide refers to peptides up to 100 amino acids. From the structural point of view, peptides encompass diverse types such as linear, cyclic peptides, depsipeptides, and peptides modified with diverse nonpeptide moieties including phosphoryl groups or carbohydrate, polyketides or terpenoids, etc [1].

The evolution of enzymatic synthesis, recombinant DNA technology, and automated synthetic methodologies in particular SPPS, allow for the production of large libraries of diverse peptides characterized by a range of pharmacological effects. Peptide or peptidomimetic drugs are currently utilized for the treatment of prostate and breast cancer, as HIV protease inhibitors or as ACE inhibitors, against hypertension and heart failures, as antibiotics, hormone, neurotransmitters, immunomodulators, and so on. Peptides have the potential to be potent pharmaceutical agents for the treatment of many diseases of the Central Nervous System (CNS)[2,3].

Unfortunately, the clinical use of these promising drugs is hampered by their rapid degradation and scarce permeation across biological barriers, such as the intestinal lumen, the intestinal mucosa, the blood-brain barriers (BBB), etc. these problems lead to short in vivo half-lives (generally <30 min) and low oral bioavailability (1-2%)[4,5].

The peptidomimetic strategy consists of altering the physico-chemical characteristics of a peptide without changing the biological activity [2]. Peptidomimetic compounds bear identifiable similarity to the parent peptides and imitate or inhibit their biochemical effects. Very often, they contain non peptidic structural elements [6], such as peptide bond-surrogates not cleaved by peptidases, a feature also found in natural peptidase inhibitors.

The design of a peptidomimetic based on the structure of a native peptide begins with an extensive SAR investigation of the parent peptide, aimed to identify the minimal sequence and the pharmacophoric groups responsible for the bioactivity. Next, the most active 3D display of these key residues is determined by means of conformationally rigid analogues [7,8]. Moving from the resulting 3D model, the pharmacophores can then be recombined by the use of non-peptidic scaffolds. Finally, the resulting compounds are tested to demonstrate the biological activity, stability, bioavailability and conformational stability, and ADMET profile.

Many non-peptide mimetics of bioactive peptides have been reported in the literature. The  $\alpha_v\beta_3$ -integrin inhibitor (1), SB223245, with a 1-4 benzodiazepine nucleus as central  $\gamma$ -turn mimetic scaffold [9], the TRH (pGlu-His-Pro-NH<sub>2</sub>) analogue (2), containing a cis-1,3,5-trisubstituted cyclohexane scaffold [10], the glucose-derived non-peptidomimetic of somatostatin (3) [11], and the C2-symmetric cyclic urea as HIV protease inhibitor (4) [12], represent outstanding examples of non-peptidomimetics with high biological activity and increased enzymatic stability, Fig (1). However, in several cases the non-peptidic compounds have failed to reproduce the biological activity of the natural peptide [13,14]. Therefore, peptidomimetics still preserve their attractiveness for replacing the original peptides.

The field of peptidomimetics has been very extensively reviewed. Some of the most relevant kinds of peptidomimetic therapeutic agents describe in the literature are the HIV protease inhibitors [15], anti thrombotic agents [16], ACE [17] and renin inhibitors [18], etc.

It is worth notice that many of the tricks used by chemists to enhance activity and stability, by protecting peptides against both endo and exo-peptidases, can also be found in active peptides of microbial or marine origin: D-amino acids or inusual amino acids instead of the natural L-residues, cyclization, glycosilation, deamination, complete removal of the first residue, N-acylation or N-formylation at the N-terminus, amidation of the C-terminus, etc [1,2].

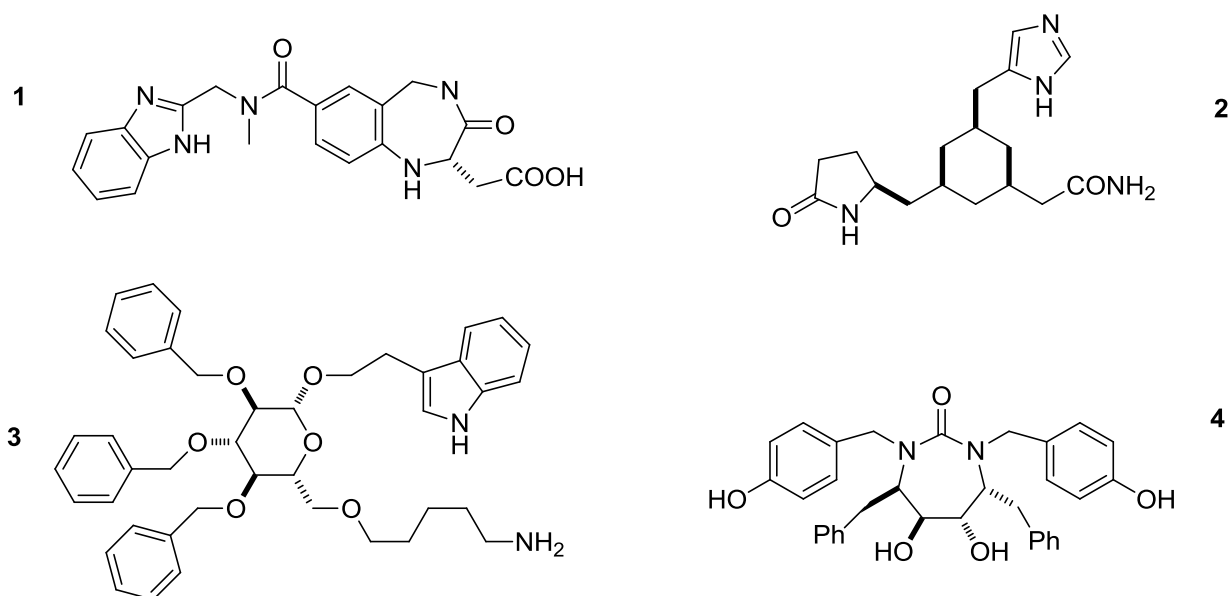


Fig.(1) Selected examples of non-peptidomimetics

It is also possible to introduce temporary modifications using a prodrug approach [19]. A peptide prodrug can be obtained by combining a biologically active peptide with additional elements which give the whole molecule increased resistance against enzymatic hydrolysis and/or bioavailability [19,20].

Proteolytic cleavage of the additional molecule, especially a short truncation at the N-terminus, in the proximity of the site of action, release the pharmacologically active drug. Prodrug or prodrug-enzyme inhibitor combinations may optimize the delivery of peptide or protein drugs to the CNS. For example, the N-terminal 4-imidazolidinone prodrugs of Leu-enkephalin, being metabolically stable and bioreversible, have been proposed as a suitable prodrug candidates for delivery of Leu-enkephalin to the brain [21].

Peptide stability can be achieved by conjugation to a polymer [22]. Polymer conjugation improves pharmacokinetics by increasing the molecular mass of protein and peptides, preventing the approach of antibodies or antigen processing cells and shielding them from proteolytic enzymes. The most promising polymer is PEG [23], which shows little toxicity and is eliminated from the body intact. Polymer conjugation allows an increase peptide stability, and reduce elimination. The conjugated PEG-DPDPE seems to act as a

pro-drug, enhancing peripheral stability, while undergoing hydrolysis in the brain and allowing nonconjugated DPDPE to act at the receptor [24].

Finally, proteolytic peptide degradation can be defeated using alternative routes of administration, including controlled-release parenteral route (subcutaneous, intramuscular or intravenous), mucosal route (nasal spray, pulmonary delivery, sublingual delivery), oral route (penetration enhancers, protease inhibitors, carriers) and transdermal route (patches) [25].

### 1.1. ENZYMATIC DEGRADATION OF PEPTIDES

The therapeutic efficacy of a peptide drug candidate is linked to its activity at the specific receptor, as well as to its pharmacokinetic properties (adsorption, transport, ability to cross biological barriers, excretion) and toxicity. Besides aqueous solubility, lipophilicity, molecular size and weight, and ability to form H-bonds (Lipinski's Rule of 5), chemical and metabolic stability plays a major role in determining peptide bioavailability. Peptide degradation by proteolytic enzyme is followed by rapid excretion of the metabolites from the circulation by the liver and kidneys [4,5].

The enzymatic stability of a peptide is dependent upon several factors, in particular kind and sequence of the amino acids, overall size, flexibility, and conformations. Side chain metabolism, such as the oxidation and reduction of disulfide bonds, can also play an important role. Amino acid composition and peptide structure also determine lipophilicity, the degree of protein binding, cellular sequestration, uptake into non-target tissue, clearance rate, and affinity for carrier mechanisms.

Peptidase that are capable of cleaving the internal peptide bonds of a substrate are designated as endopeptidases (e.g., serine proteinases, metalloproteinases). The peptidase which remove one or more residues from the termini of the peptide are classified as exopeptidases (e.g., aminopeptidases, carboxipeptidases) [26,27.] Large peptides or peptides protected at the N-terminus, or at the C-terminus, require endopeptidases to initiate hydrolysis.

After administration, peptides meet proteolytic enzymes at many compartments [28]. In case of intravenous injection, the peptide is immediately subjected to numerous proteolytic enzymes such as esterases and peptidases in the human plasma [29]. In case of oral delivery, a part from the strong acidic gastric environment, the peptide encounters two main biophysical and biochemical barriers, the lumen of the small intestine, and the brush border membrane. For peptide drugs targeting the CNS, the BBB also constitutes a formidable barrier [30].

The metabolic activity in the intestinal lumen reduces the absorption of peptide-based drugs. The gastrointestinal tract degrades proteins and peptides by using a variety of enzymes into smaller sequences, which can be easily absorbed across the intestinal mucosa [31,32]. In the duodenum, the degradation can be mediated by pancreatic proteases. The contribution of luminal hydrolysis in the overall degradation process depends on the size and composition of the peptide. Most of the degradation of peptides requires at least contact with the brush-border membrane and/or uptake into the intestinal mucosal cells.

Among the most relevant peptidases which can be found in the intestine, it is possible to mention aminopeptidase P, aminopeptidase W, aminopeptidase N and dipeptidyl peptidase IV. The lumen of the small intestine contains a number of pancreatic peptidases,  $\alpha$ -chymotrypsin, trypsin, pancreatic elastase,

carboxypeptidases A, B, D, N, U, etc., and cellular peptidases secreted by mucosal cells. The brush border membrane of the epithelial cells contains many different peptidases [33], dipeptidyl-peptidase IV, prolyl tripeptidylpeptidase, ACE, leucyl-aminopeptidase, aminopeptidase M, aminopeptidase A, neprilysin, etc.

Many enzymes are also present in the liver [34], kidney and other organs, or in different tissues. For instance, lysosomal peptidases, leukocyte elastase, cathepsins B, D, etc., can be found in epithelial or endothelial cells; other enzymes are the interstitial collagenase (MMP-1), or carboxypeptidase C or Y.

The BBB is a unique physical and enzymatic barrier that segregates the brain from the systemic circulation. BBB capillary endothelia are sealed by tight junctions, which inhibit any significant paracellular transport [30.] Specific transporters exist at the BBB that permit nutrients to enter the brain and toxicants/waste products to exit. These transporters are potential routes for mimetic designed drugs. The main peptidases which can be found in the brain microcapillaries of the BBB are gamma-glutamyl transpeptidase alkaline phosphatase, monoamine oxidase catechol-*O*-methyl transferase, butyrylcholinesterase and aromatic-L-amino-acid carboxylase (or Dopa-decarboxylase or aromatic-L-amino-acid decarboxylase), epoxidehydrolase (or epoxide hydrolase), UDP-glucuronosyl-transferase, benzyloxyresorufin-*O*-deethylase (cytochrome P-450 CYP2B1), NADPH cytochrome P-450 reductase and glutathione-S-transferase [22]. The protein-disulfide reductase, is also present in the brain and can alter peptide structures stable in plasma.

In many cases, the active peptides are enzymatically converted to products which retain some bioactivity. These bioactive metabolites may mimic but also counteract the action of the parent peptide.

The released fragment may serve as a modulator of the response of the original compound [35]. This phenomenon has been found to occur in several neuropeptide systems, including the opioid peptides, tachykinins, as well as peptides belonging to the renin-angiotensin system. Normally, the products interact with the same receptor as the native compound, but sometimes it appears that the released fragments interact with sites distinct from those of the original peptide.

## 1.2. STRUCTURE MODIFICATIONS TO IMPROVE PEPTIDE STABILITY

As mentioned in the introduction, peptidomimetics resemble native peptides or proteins but contain some synthetic element designed to reduce metabolism and to optimize the biological activity of the agent. Peptide bond hydrolysis *in vivo* can be limited by specifically protecting or replacing the targeted bond, by introducing atypical moieties, or by modifying the peptide conformation altogether, in such a way that it is no longer recognized by the protease of concern. Even modest structural changes near the scissile peptide bond can result in significant conformational differences. Example are the introduction of a N-alkyl group, that increases the incidence of the *cis* configuration of the amide bond, the use of a D-amino acid, or of a residue containing an unnatural side chain. In many cases, the introduction of non-peptidic scaffolds to imitate the secondary structure that are thought to be especially involved in binding interactions, including the  $\gamma$ - and  $\beta$ -turn,  $\beta$ -sheet and the  $\alpha$ -helix, proved to be a very effective strategy.

### 1.2.1. Pseudopeptides

The backbone of a peptide can be modified in various ways by changing at least one peptide bond with an isosteric or isoelectronic surrogate. Examples are shown in Fig. (2). The mostly utilized isosters are the reduced amides, azapeptides, retro-inverso peptides, and peptoids; these are discussed in detail in the next sections. Other isosters less frequently appeared in the literature, such as the urea peptide mimetics [36,37], sulphonamide peptides/peptoids [38], etc., are not reviewed here.

The replacement of a labile peptide bond with an isoster was of great help for designing therapeutic agents targeting proteases, like those associated with the HIV virus, as well as targets like ACE, renin, endothelin, interleukin-converting enzyme and others [15-18]. Very often, the isoster imitates the transition state of peptide bond cleavage, including the hydroxyl group resulting from enzyme nucleophilic addition, Fig. (2), hydroxyethylamino, hydroxyethylene isosters, etc.

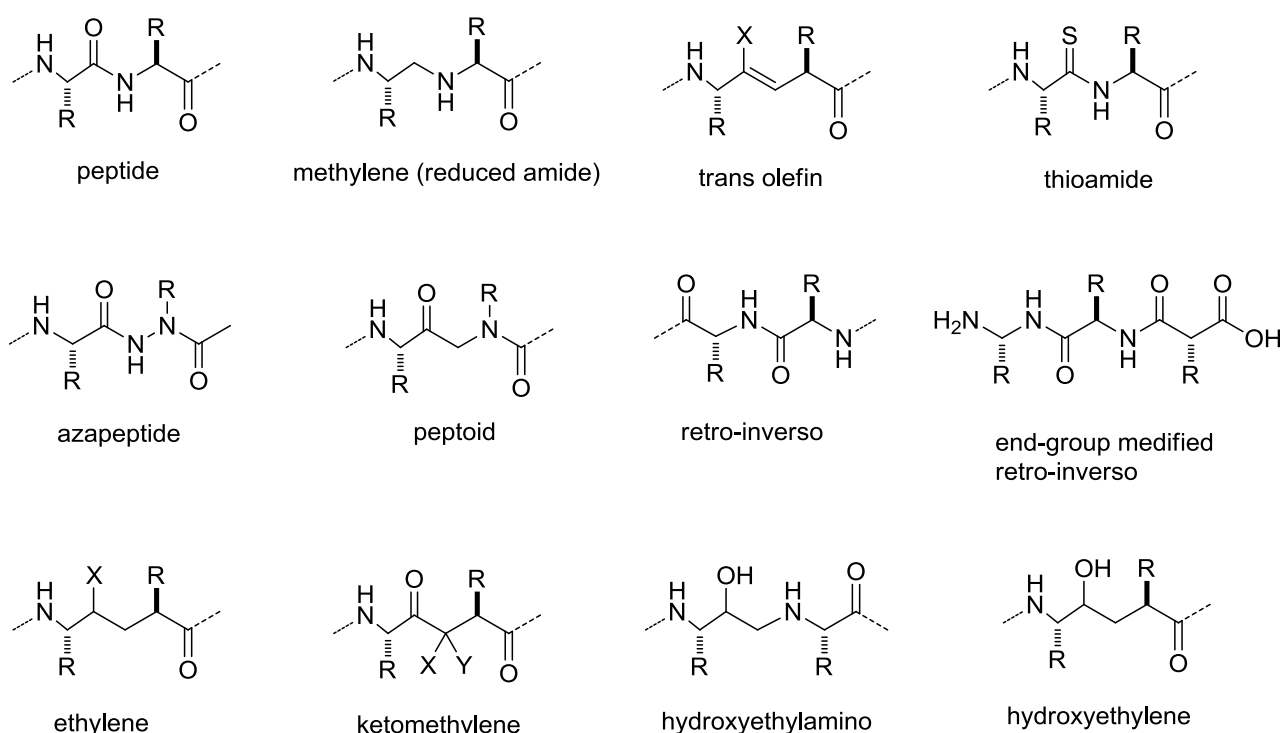


Fig.(2) Isosteric surrogates of the peptide bond

### 1.2.2. Reduced Peptide Bonds

The incorporation of reduced peptide bonds (CH<sub>2</sub>-NH), Fig. (2), renders the native sequences of opioid peptides highly resistant towards enzymatic hydrolysis in the modified positions. Synthetic peptides containing reduced bonds have found applications as vaccines for their immunogenic properties, linear pseudooligolysines, containing multiple adjacent CH<sub>2</sub>-NH bonds have been designed as DNA carriers in gene delivery. Reduced amides have also seen use in the preparation of peptide nucleic acids and antibacterial peptides [2,6]. Representative examples in the field of opioid peptides are the TIPPP-derived opioid antagonists with subnanomolar affinity and high  $\delta$ -receptor selectivity, obtained by introduction of a

reduced peptide bond between Tic2 and Phe3 residues, to give H-Tyr-Tic $\Psi$ [CH<sub>2</sub>NH]Phe-Phe-OH (TIPP[ $\Psi$ ]) and H-Tyr-Tic $\Psi$ [CH<sub>2</sub>NH] Cha-Phe-OH, Cha: cyclohexylalanine (TICP[ $\Psi$ ]). The modification conferred the molecules a high stability against chemical and enzymatic degradation [39].

Introduction of the CH<sub>2</sub>-NH peptide bond isoster can be accomplished in solid phase. The free N-terminal amino group of the resin-bound peptide is reductively alkylated by the requisite protected  $\alpha$ -aminoaldehyde in the presence of sodium cyanoborohydride (NaBH<sub>3</sub>CN) in DMF containing 1% AcOH. Microwave irradiation can be utilized to shorten the reaction times and improve the yields [40].

### 1.2.3. Azapeptides

In azapeptide isosters the  $\alpha$ -CH group of the backbone is substituted by a isoelectronic nitrogen atom, the side chains remaining unaltered, Fig. (2). Azapeptides have been developed by several groups for the design of hormone analogues, protease inhibitors, etc [41]. Examples of therapeutically useful peptides incorporating the azapeptide modification can be found in the field of serine and cysteine proteases inhibitors [42]. Atazanavir (5), Fig. (3), BMS-232632, is a highly active azapeptide inhibitor of the HIV protease, that has recently received approval as a human immunodeficiency virus (HIV) treatment [43,44]. It inhibits the protease enzyme, thereby preventing the cleavage of the viral polyproteins and resulting in an immature, non-infectious virion. It is the first, and to date the only, protease inhibitor designed to be applied once daily, with comparable anti-HIV efficacy to nelfinavir, efavirenz and the combination of ritonavir and saquinavir [45].

The synthesis of azapeptides generally starts from substituted hydrazines or hydrazides [46]. The preparation of Atazanavir (5) is shown in Fig. (3). The key building blocks are the hydrazino carbamate, obtained in turn by a Suzuki-Miyaura coupling, the amino acid-derived *N*-protected *threo*-3-amino-1,2 epoxybutane, and two equivalents of *N*-protected-*tert*-leucine [45].

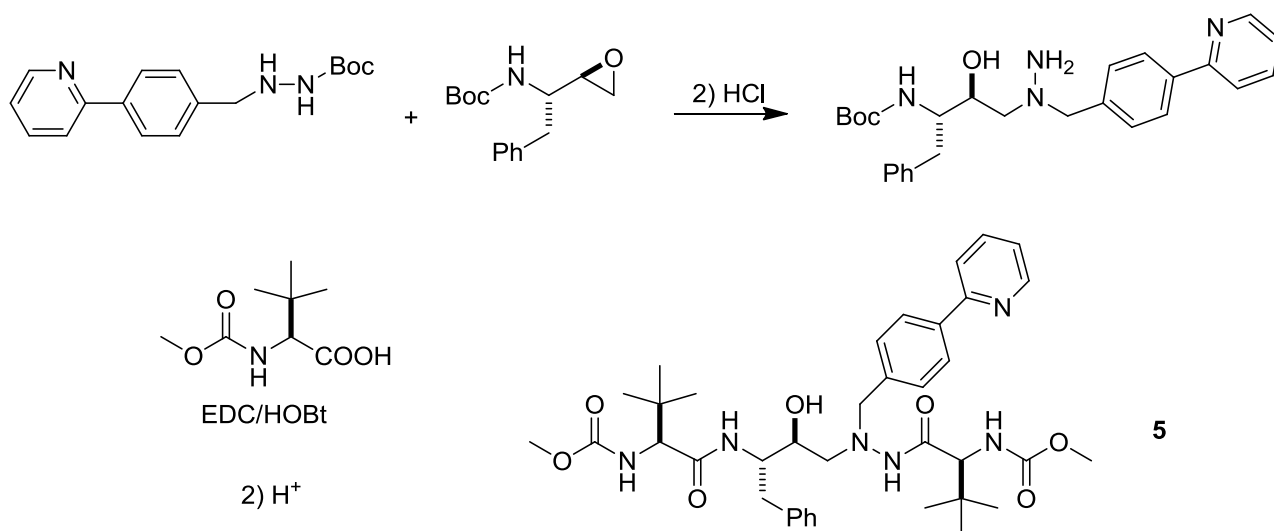


Fig.(3) Synthesis of Atazanavir

#### 1.2.4. Retro-Inverso Peptides

In these peptide-mimetics the normal sequence from *N*- to *C*-terminus is reversed, and the natural *L*-amino acids are changed by *D*-amino acids, Fig. (2) [47]. This reversal warrants that the side chain topologies of the natural peptide and the peptidomimetic are the same. Peptide-bond reversal represents an important structural alteration for peptides, and proved to be useful to reduce the degradation rate of the peptides by peptidases. In a retro-inverso sequence the *N*- and *C*-termini are reversed, therefore the positive charge located at the *N*-terminus of the natural sequence is replaced by a negative one in the peptidomimetic, and vice-versa, unless modified termini are introduced. This may be the cause of the low biological activity observed in several cases. The introduction of end-group modifications, Fig. (2), increases the complementarity with the native peptide (see also PMRI).

Retro-inverso peptides have found applications as immunogens, immunomodulators, immunostimulators; and as anti-inflammatory, antimicrobial, and diagnostic reagents, as well as modified isomers of membrane-penetrating peptides as delivery systems [48]. An evolution of the retro-inverso concept is the partially modified retro-inverso (PMRI) peptide, in which the retro-inverso structures is incorporated into a normal sequence; the retro inverso and the normal portions are connected by a diamine and/or a diacid.

The PMRI Tuftsin analogue **6** [49], Fig. (4), is degraded less than 2 % in 50 min, while maintaining the biological activity of Tuftsin, H-Thr-Lys-Pro-Arg-OH, a immune system stimulator, which is completely degraded *in vivo* in about 8 min. Other nice examples can be found as mimetics of enkephalin, CCK, RGD, gastrin antagonists, etc. [47,48]. In general, the analogues displayed higher activity than the parent peptides in an *in vitro* test. Another example is the angiotensin analogue incorporating aza- $\alpha'$ - homoamino acids of natural and inverted configuration, [Asn1, aza-  $\alpha'$ -homoTyr4, Val5]angiotensin II (**7**), Fig. (4).

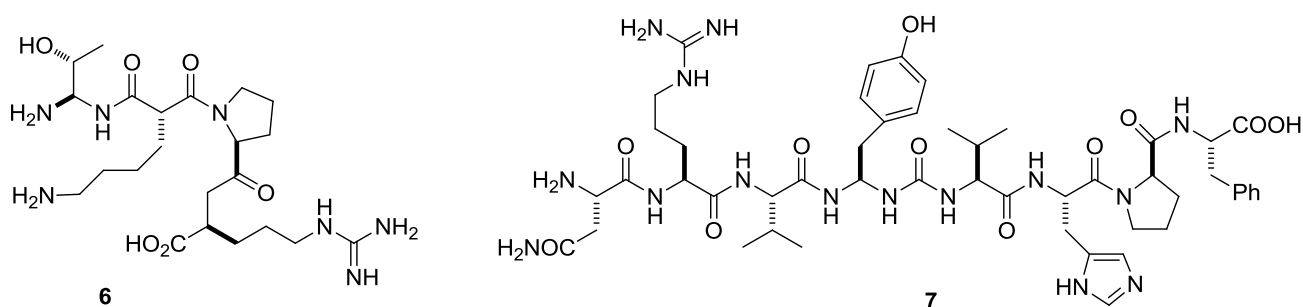


Fig.(4) PMRI analogues of Tuftsin (6) and Angiotensin II (7).

The synthesis of a PMRI peptide requires standard conditions. The principal concern of PMRI peptide synthesis is the construction of the *gem*-diaminoalkyl (**8**), Fig. (5), and C-2-substituted malonyl residues (**9**), Fig. (6).

The Curtius and Hofmann rearrangements remain the methods used most commonly for the syntheses of *gem*-diaminoalkyl derivatives (**8**); during these rearrangements the migrating groups retain the configuration, Fig. (5). Acyl azides undergo the Curtius rearrangement to yield the corresponding isocyanates, whose hydrolysis give the *gem*-diamines. Acyl azides can be prepared from the amino acids by treatment with diphenylphosphoryl azide (DPPA), or *via* the intermediate mixed anhydride [47].

The isocyanates can be reacted with a carboxylic acid derivative to yield a PMRI peptidic unit directly [50], the so-called “Goldschmidt and Wick type reaction”. The Hofmann rearrangement is extensively employed for the synthesis of PMRI peptides, using exclusively the mild oxidant iodobenzene bis(trifluoroacetate) (IBTFA). Other procedures to synthesize monoprotected *gem*diaminoalkyl (**8**), are based on the Mannich reaction [51], on the formation of intermediate oxazolones, or nitriles, etc.

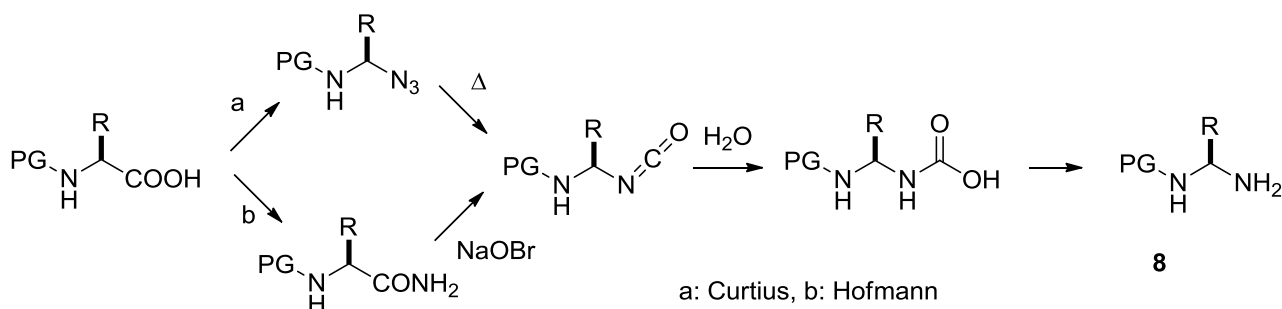


Fig.(5) Preparations of the *gem*-diaminoalkyl residues.

Concerning the preparation of C-2-substituted malonyl derivatives (**9**), the classical method is the alkylation and partial hydrolysis of malonic acid diesters, and of cyanoacetates. A very convenient method is based on the use of Meldrum’s acid, Fig. (6). The Knoevenagel reaction with aldehydes or some ketones and in situ reduction yields mono-C-5-substituted Meldrum’s acids. Subsequent alcoholysis gives C-2-substituted malonic acid monoesters. The acylation of the enolate of a *tert*-butyl carboxylate with a carbonate, a chloroformate, or a isocyanate, can be utilized to obtain C-2-substituted malonates. Special issues to take into consideration are the acidity of the C-2 hydrogen of malonates, and the configurational lability of the C-2 malonyl position during synthesis.

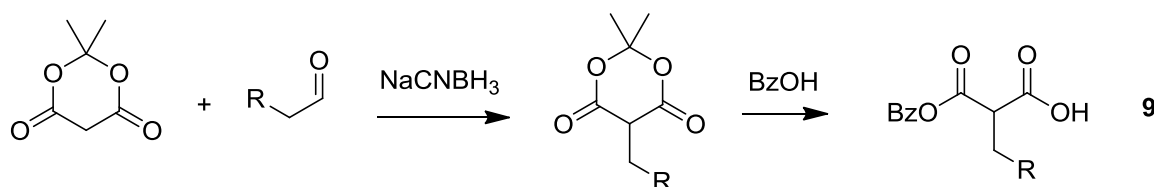


Fig.(6) Preparations of the C-2-substituted malonyls

### 1.2.5. Peptoids

In the early 1990’s Bartlett defined peptoids as pseudopeptides containing *N*-alkylated glycines linked by peptide bonds. Formally, the nitrogen atom of some residues is shifted to the α-CH position, and the NH-groups have been substituted by CH<sub>2</sub>-groups, Fig. (2).

Therefore, the side chains and the carbonyl groups remain at their positions, while the backbone CH- and NH-groups change their places. The sequence of peptoids are opposite to the ones of native peptides, and the stereogenic α-carbons of natural amino acids are lost; besides, they have higher conformational flexibility respect to natural peptides. Peptoid analogues of most natural amino acids are commercially available, or they can be easily prepared. Peptoids (**10**) can be routinely synthesized on Rink amide linker-derivatized solid supports using the submonomer synthesis method developed by Zuckermann *et al.*, Fig. (7) [52,53].

Metabolically stable, successful compounds based on the peptoid concept are the  $\alpha$ -amylase inhibitors Ac-Nhtrp-Nharg-Nhtyr-NH<sub>2</sub>, and Ac-Nhtyr-Nharg-Nhtrp-NH<sub>2</sub> [14], active as or more active than their natural parent peptides (Nh indicates the peptoid homologue of the natural amino acid); other examples are the antimicrobial peptoids derived from pexiganan, protegrins, and melittin [54].

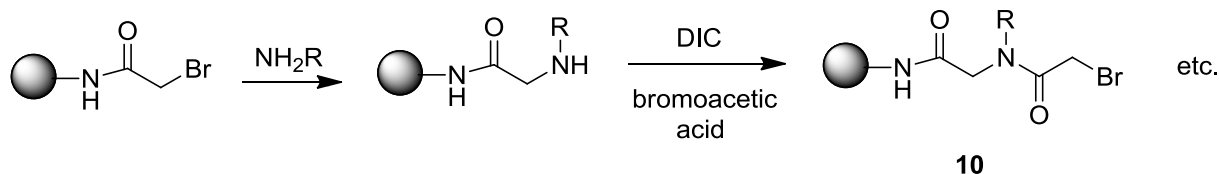


Fig.(7) Example of SPPS of peptoids.

### 1.3. Incorporation of Non-Natural Amino Acids

Peptide analogs containing non-natural residues have been obtained by diverse approaches [55], ranging from the simple replacement of the natural L-amino acids with their D-enantiomers, to the use of N-alkyl amino acids,  $\alpha$ -substituted  $\alpha$ -amino acids,  $\beta$ -substituted  $\alpha$ -amino acids, proline analogues,  $\gamma$ - and  $\beta$ -amino acids, substituted  $\alpha$ - or  $\beta$ -amino acids, and so on. For the huge number of non natural amino acids described in the literature [56,57], only these relevant families are discussed in the following paragraphs.

In some cases, it has been observed that peptide coupling with unusual amino acids can be troublesome. For instance, with N-methyl or  $\alpha,\alpha$ -disubstituted amino acids, racemisation, diketopiperazine formation, etc., are common side-reactions.

#### 1.3.1. D-amino Acids

The introduction of *D*-amino acids [58] in a sequence can give the peptide an increased stability, since only a few enzymes that effectively hydrolyse peptide bonds involving *D*-amino acids have been discovered and characterized in multicellular organisms [59].

Moreover, *D*-residues often enforce a different conformation of the peptide [60], and strongly influence receptor affinity and selectivity [61]. Some of the first successes of this approach [62] in the field of opioid peptides have been the  $\delta$ -receptor selective enkephalin analogues DADLE, H-Tyr-*D*-Ala-Gly-Phe-*D*-Leu-OH, and the  $\mu$ -receptor selective DAMGO, H-Tyr-*D*-Ala-Gly-MePhe-Glyol, widely used as a radioligand for binding experiments in its [3H]-form [3,63].

#### 1.3.2. N-Alkylated Amino Acids

N-alkylation (generally N-methylation) is present in a number of biologically active, natural peptides from different sources, in particular of marine or microbial origins, including antibiotics, monamycins, echinomycin, or insecticides, antitumor agents, such as bouvardin, or antiinflammatory peptides [64,65]. For instance, the cyclic undecapeptide cyclosporine A [66], isolated from *Trichoderma polysporum*, contains seven *N*-methylated amino acids.

This immunosuppressant with low toxicity is utilized as an effective drug after organ transplantations.

Several *N*-alkyl amino acids are commercially available, allowing their direct use in solid phase peptide synthesis, while many others can be prepared [64,67-69]. *N*-methyl amino acids (**11**) can be synthesized from *N*-protected amino acids, by direct methylation of carbamate or diphenylphosphinamide (Dpp) protected amino acids, Fig (8)A, or by the Mitsunobu reaction, with arylsulfonyl protecting group, Fig (8)B. Oxazolidinones obtained from the *N*-carbamate amino acids and formaldehyde can be reduced to *N*-methylamino acid with triethylsilane, Fig (8)C. Alternatively, oxazolidinones obtained with hexafluoroacetone can be treated with paraformaldehyde and thionyl chloride; reduction and deprotection affords the *N*-methyl amino acid.

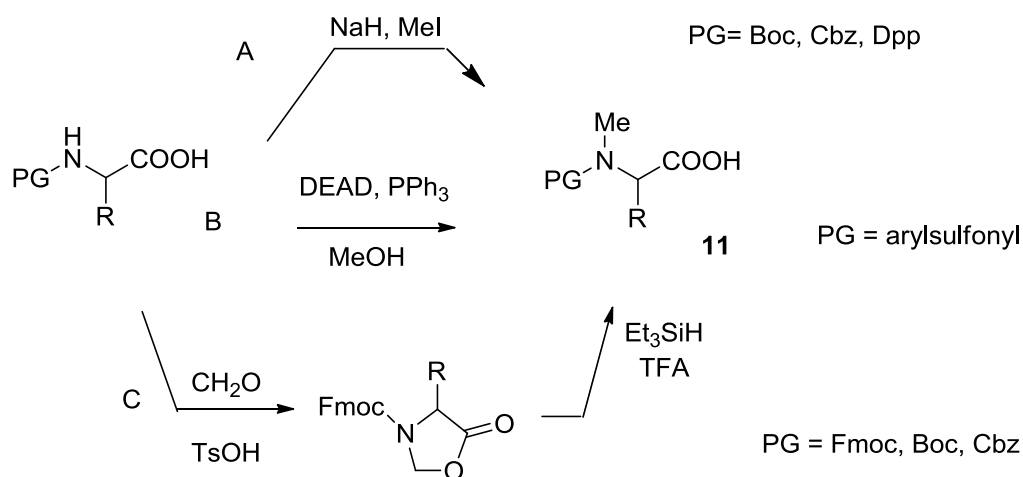


Fig. (8). Syntheses of *N*-methyl amino acids.

The alkylation of amino acids has been obtained by two successive reductive aminations of aldehydes, Fig. (9)A [64]. *N*-methylation has been performed *via* sultam-directed “enolate” hydroxyamination of non-chiral acyl chains, Fig. (9)B. The sultam chiral auxiliary served also for the alkylation of chiral enolate derived from sarcosine (*N*-methylGly).

Finally, the *N*-methylation of a peptide can be directly performed on solid support; for instance, the key step of Fig. (9)C is the selective deprotonation of the resin-bound free amine peptide protected as *o*-nitrobenzene sulfonamide with a non-ionic base, and alkylation with methyl *p*-nitrobenzenesulfonate. This strategy has been applied to the *N*-methyl scan of the thrombin receptor agonist peptide H-SFLLRNNH<sub>2</sub> [70].

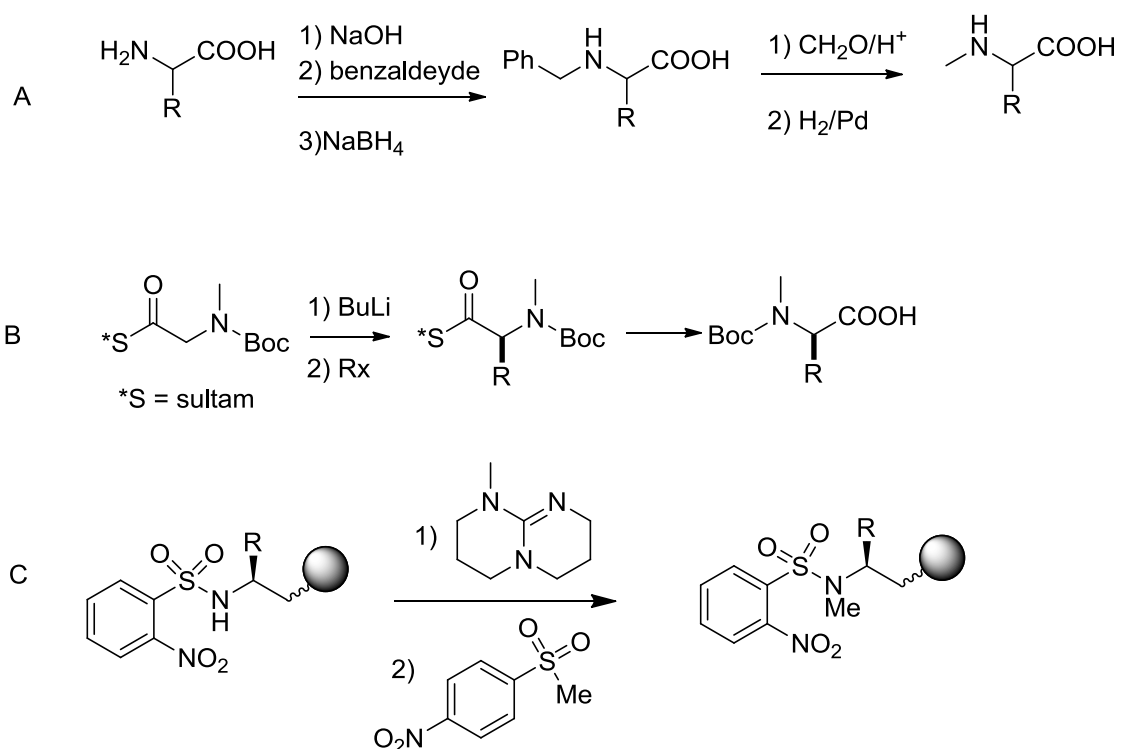


Fig. (9). Other syntheses of *N*-methyl amino acids.

Generally, peptides modified by the use of *N*-methyl amino acids resulted in analogues with improved pharmacological properties and stability. The role of the position to be *N*-methylated for peptide protection from proteolysis is essential. Substance P (Arg-Pro-Lys-Pro-Gln-Gln-Phe-Phe-Gly-Leu-Met-NH<sub>2</sub>) had been shown to be degraded in the human brain at peptide bonds 5-6, 7-8 and 8-9.

The heptapeptide analogue, Glu-Gln-Phe-NMePhe-NMeGly-Leu-Met-NH<sub>2</sub>, was almost completely resistant [71]. To mention another case, in comparison to endothelin (half-life circa 10-20 min), the *N*-methylated analogues revealed an increased stability by 500-800 fold [72]. In neurotensin(7-13) (Pro-Arg-Arg-Pro-Tyr-Ile-Leu), the scissile bonds are the positions Arg<sup>8</sup>-Arg<sup>9</sup>, Pro<sup>10</sup>-Tyr<sup>11</sup> and Tyr<sup>11</sup>-Ile<sup>12</sup>. *N*-methylation in position 8 led to increased half-life in plasma [73]. Finally, the *N*-methyl modification has been applied also to enzyme inhibitors, enkephalin, LHRH, angiotensin, and CCK [64,65].

The presence of the *N*-alkyl group affects the conformational freedom of the backbone and of the side chain of the residues close to the *N*-alkyl group. In particular it eliminates the predominance of *trans versus cis* peptide bond configuration. Besides, the substitution of *NH* by *N*-alkyl groups eliminates some inter- and intramolecular hydrogen bonds. Finally, the adjacent carbonyl group increases basicity and decreases polarity [74].

Besides to their utility to protect biologically active peptides against enzymatic degradation without concomitant loss of biological activity, *N*-alkyl residues have been also widely utilized for SAR studies. By successively alkylating each backbone NH and evaluating the biological activity (*N*-alkyl-scan), the pharmacophoric residues can be identified. A prototypic example is represented by the *N*-methyl scan performed on the cyclo RGD analogues by Kessler *et al.*, discussed in the paragraph dedicated to cyclization.

### 1.3.2. $\alpha$ -Substituted $\alpha$ -Amino Acids

$\alpha$ -Substituted  $\alpha$ -amino acids, or  $\alpha,\alpha$ -disubstituted glycines, are present in many natural sequences, for instance in several peptide antibiotics [75], such as alamethicin, an antimicrobial membraneactive peptide [76]. Among the more represented  $\alpha$ -alkyl  $\alpha$ -amino acids it is possible to cite  $\alpha$ -aminobutyric acid (Aib), diethylglycine (Deg), or isovaline (Iva), C $\alpha$ -methyl-C $\alpha$ -allylglycine (Mag), ( $\alpha$ Me)-  $\alpha,\alpha$ -diphenylalanine ( $\alpha$  MeDip), and several kinds of cyclic or heterocyclic derivatives, Fig.(10).

$\alpha$ -Substituted  $\alpha$ -amino acids have been used for the synthesis of peptidomimetics as enzyme inhibitors, and to provide peptides with a higher resistance to biodegradation. For example, in contrast to angiotensin II, the [ $\alpha$  MeTyr4] analogue is resistant to chymotrypsin [77]. Aib-containing analogues of the insect kinin neuropeptide family also demonstrate resistance to an insect ACE [78]. Incorporation of Aib has been described also for enkephalin, bradykinin, angiotensin II [64].

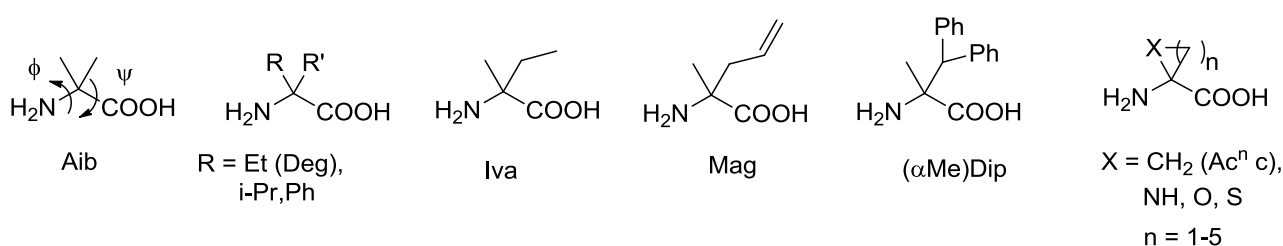


Fig. (10). Examples of  $\alpha$ -alkyl  $\alpha$ -amino acids.

One of the more relevant features of  $\alpha$ -substituted  $\alpha$ -amino acids is the conformational constraint introduced into peptide backbones [79,80]. Aib, the most widely studied of the family, restricts  $\phi$  and  $\psi$  to angles present in  $\alpha$ - or  $3_{10}$  helices. When Deg is utilized, the preferred conformation is extended with trans  $\phi$  and  $\psi$  angles. A noteworthy conformational restriction is obtained when residues having the two side chains in a ring are utilized, leading to a  $\beta$ -turn secondary structure or a helix  $3_{10}$ . Interestingly, this introduction gives the peptides increased resistance against hydrolysis [81,82]. A nice example is represented by the family of the  $\alpha$ -aminocycloalkane carboxylic acids, Ac<sup>n</sup> c. For instance, the introduction of Ac<sup>6</sup> c into various positions of Leu-Enkephalin, resulted in peptide mimetics with greater *in vivo* activity.

The synthesis of  $\alpha$ -substituted  $\alpha$ -amino acids (12) [64] can be performed by the stereoselective alkylation of imidazolidinones, Fig. (11A). Variants based on the use of other intermediate heterocycles are the alkylation of bis-lactim ether (13), obtained by treatment of the L-alanine diketopiperazine, or the alkylation of metallated imidazolidinones (14), obtained by cyclization of chiral  $\alpha$ -isocyanoamides.  $\alpha$ -Methylamino acids can be prepared by alkylation of Schiff bases derived from chiral amino acids and Oppolzer's sultam, Fig. (11B). The asymmetric alkylation of alanine enolates with chiral phase transfer catalysts, for instance with copper complexes of Salen, proceeded with ee up to 90%, Fig. (11C).

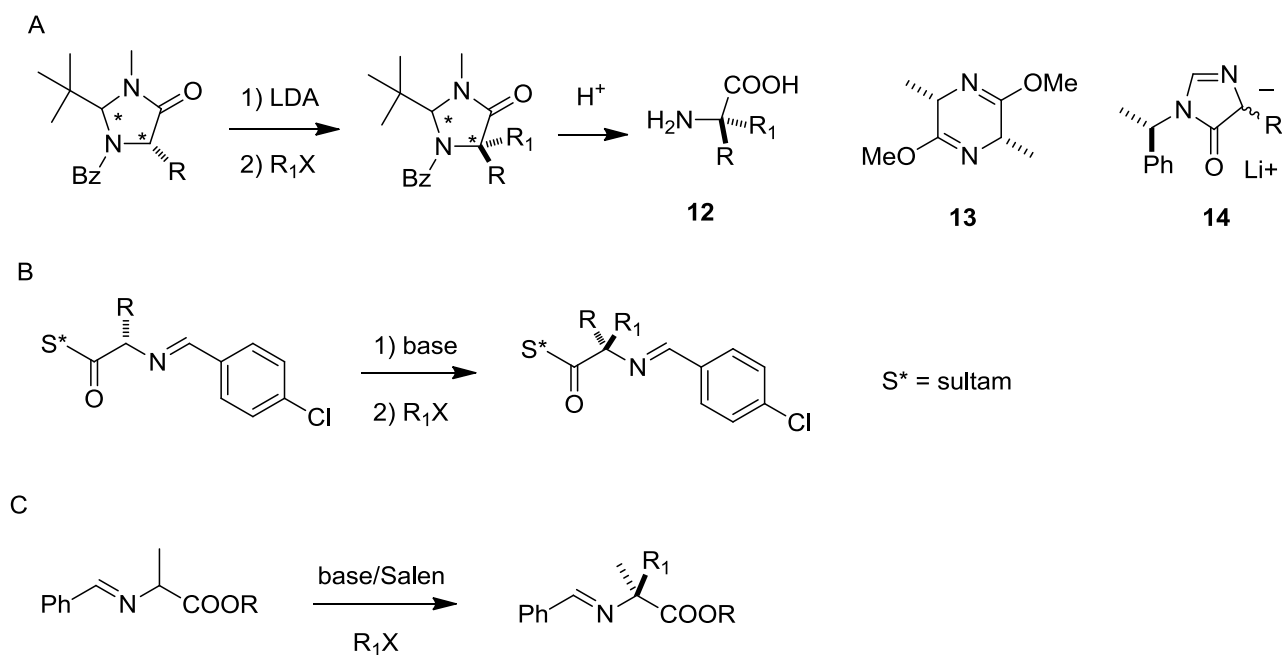


Fig. (11). Syntheses of alpha-substituted alpha-amino acids.

### 1.3.4. $\beta$ -Substituted $\alpha$ -Amino Acids

Analogues of natural amino acids alkylated at the  $\beta$ -carbon have been often utilized to induce a conformational preference in side chains. Some  $\beta$ -Me analogues of Phe, Trp, and Tyr, are shown in Fig. (12). These  $\beta$ -substituted  $\alpha$ -amino acids have also an additional  $\beta$ -stereogenic center, therefore four preferred configurations (-gauche, +gauche, and two enantiomeric trans geometries) are accessible from varying the two stereocenters, Fig. (13). 2-(Carboxycyclopropyl)- glycine (CCG) is a different kind of  $\beta$ -substituted amino acid.

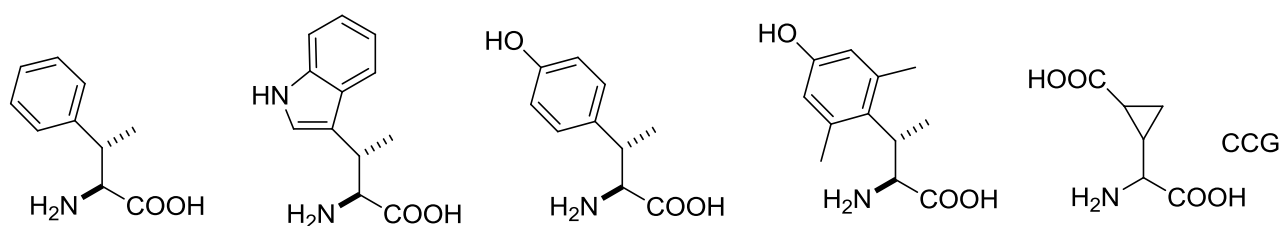


Fig. (12). Examples of beta-substituted alpha-amino acids.

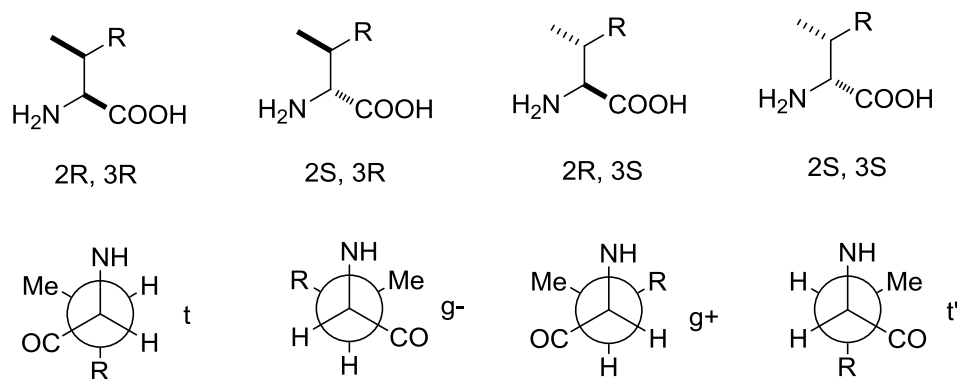


Fig. (13). Preferred conformations of beta-substituted alpha-amino acids.

Replacement of the natural amino acids often resulted in a comparably higher activity and increased biological stability with respect to the modified peptides [83]. For instance, the activity of short peptides which are active at the  $\delta$ -opioid receptor was successfully improved by exchanging phenylalanine by its  $\beta$ -Me analogue [84,85]. Also, the introduction of three methyl groups at the 2'-, 6'- and  $\beta$ -position of natural tyrosine hinders the free rotation around the  $\chi$  angle giving compounds with improved biological activity [86].

### 1.3.5. Proline Analogues

The cyclic structure of proline forces the  $\phi$  angle to  $-65^\circ \pm 15^\circ$ , thus preventing the formation of a  $\alpha$ -helix, and promoting the formation of a  $\beta$ -turn. Besides, while the barrier to secondary amide cis/trans isomerization is about 10 kcal/mol, Fig. (14), the presence of Pro reduces the barrier to just 2 kcal/mol, hence influencing the biological behaviour of peptides [87,88]. Many Pro derivatives were found in proteins of microbial or marine origins, Fig. (14), in antibiotics and cytotoxic peptides. Many other Pro derivatives were synthesized by the introduction of alkyl chains, aromatic groups, heteroatoms, or halogens in different positions of the five-membered ring [89].

Some analogues are characterized by smaller or larger rings, such as azyline-2-carboxylic acid (Azy), azetine-2-carboxylic acid (Aze), or pipercolic-2-carboxylic acid (Pip). The difference among Azy, Aze and Pro is largely the steric bulk of the side chain rather than  $\phi$  and  $\psi$  angles, while Pip prefers a chair conformation in which the COOH group is axial. Finally, the 5,5-dimethylthiazolidine-4-carboxylic acid (Dtc) allows angles in the  $\beta$ -turn region.

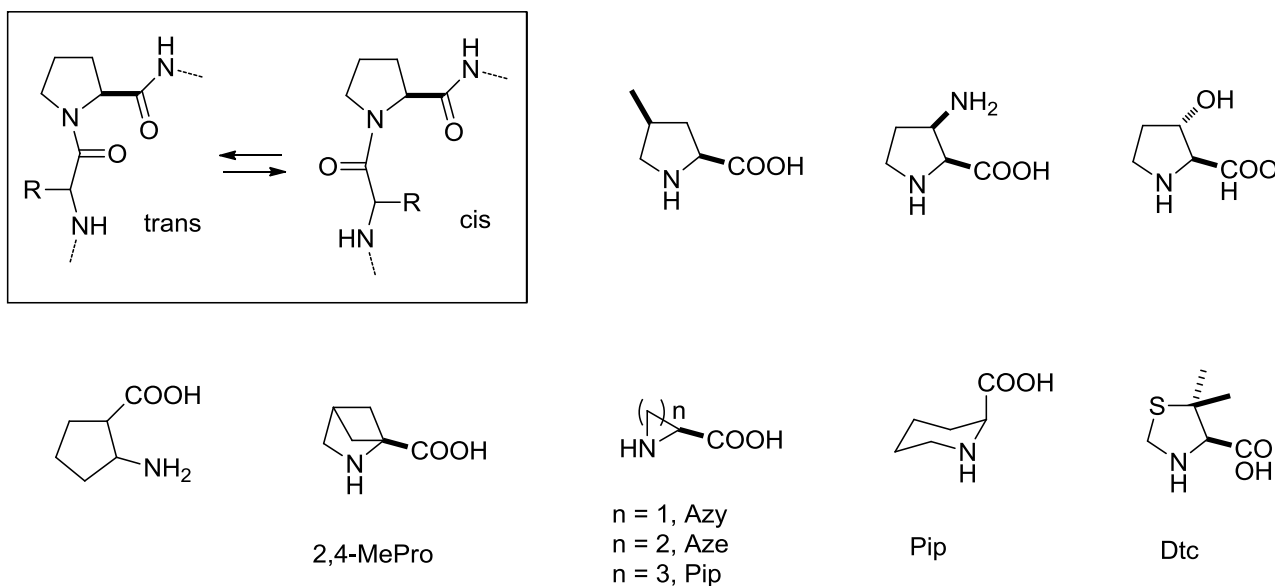


Fig.(14) Proline analogues.

It has been utilized in place of Pro in Angiotensin II, H-Asp-Arg- Val-Tyr-Ile-His-Pro-Phe-OH, a key octapeptide in blood pressure regulation, resulting in a peptidomimetic with about 40% greater activity respect to the native peptide [90].

### 1.3.6. $\beta$ -Amino Acids

$\beta$ - (and  $\gamma$ -) amino acids have been utilized to construct the mimetics of naturally occurring peptide hormones, MHC-binding beta-peptides, opioid peptides, somatostatin, or amphipathic betapeptide inhibitors of membrane-bound proteins [91]. There are different kinds of  $\beta$ -amino acids, the  $\beta^2$ - or  $\beta^3$ - versions, Fig. (15), which can be further distinguished in homologated  $\beta$ -amino acids, possessing an extra C atom, or isomeric  $\beta$ -amino acids, which maintain the same MW of the corresponding  $\alpha$ -analogue.

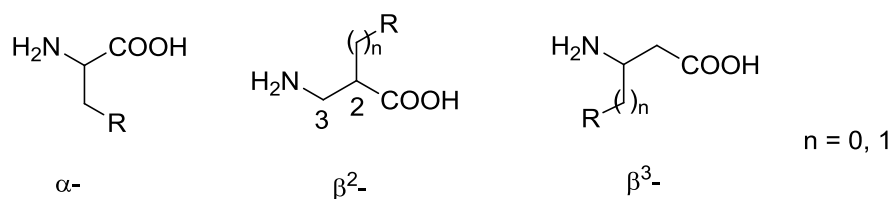


Fig.(15) Beta-amino acids

The  $\beta^3$ -amino acids are much more utilized than the  $\beta^2$  ones. All appropriately protected  $\beta^3$ -derivatives with proteinogenic side chains, with a few exceptions, are commercially available. The enzymatic resolution of racemates with isolated immobilized enzymes or with cell cultures constitutes a cheap and easy method to obtain optically active  $\beta$ -amino acids [92]. Among the many enzymes which have been utilized, chymotrypsin,  $\beta$ -lactamases, nitrilases, hydantoinases, lipases, transferases and isomerases, one of the most general and substrate-tolerant is the penicillin acylase.

The  $\beta^3$ -amino acids, with proteinogenic or non proteinogenic side chains, are readily obtained by direct Arndt–Eistert homologation of the Boc or Fmoc  $\beta$ -amino acids, Fig (16A). Other homologation procedures have been also proposed, but these are generally less efficient.

Concerning the preparation of substituted  $\beta^3$ -amino acids [93], the best options are the functionalization of intermediate di- or perhydropyrimidin- 4-ones, Fig (16B), and the conjugate addition to  $\alpha,\beta$ -unsaturated esters or imides Fig (16C). The latter procedure was developed in particular with lithium amides of chiral amines as nucleophiles, or with chiral auxiliaries.

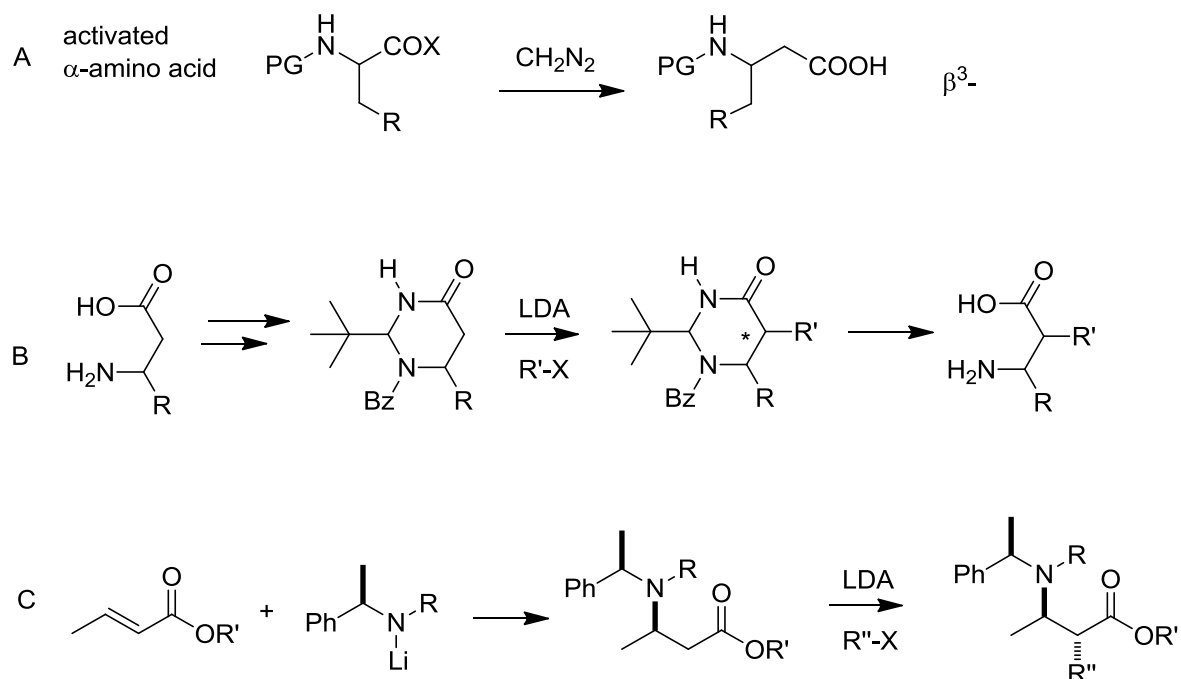


Fig.(16) Synthesis of beta-amino acids

The  $\beta^2$ -amino acids have been prepared by a number of different synthetic strategies [94]. The use of chiral auxiliaries and catalysts for C(2)–C(3) bond formation is well documented. To mention a specific approach, aminomethylating agents or synthetic equivalents (for instance CbzNHCH<sub>2</sub>O*i*-Pr [95] ) are utilized with enolates carrying chiral auxiliaries (e.g. Evans oxazolidinones), Fig. (17A).

$\beta^2$ -Amino acids can be obtained by formation of the C(2)–R bond, *via* classical  $\beta$ -alkylations of chiral enolates (with a chiral auxiliary) derived from *N*-protected  $\beta$ -aminopropanoic acid, Fig. (17B).

Alternatively, diastereoselective protonation, hydrogenation, or hydrogen- atom transfer of enols or enolates derived from 3- aminopropanoic acid afford  $\beta^2$ -amino acids by stereoselective formation of the C(2)-H bond, Fig. (17C). In some cases, the enolate was generated in situ, by addition of an *N*-nucleophile to an acrylate carrying the side chain R in the  $\alpha$ -carbonyl position.

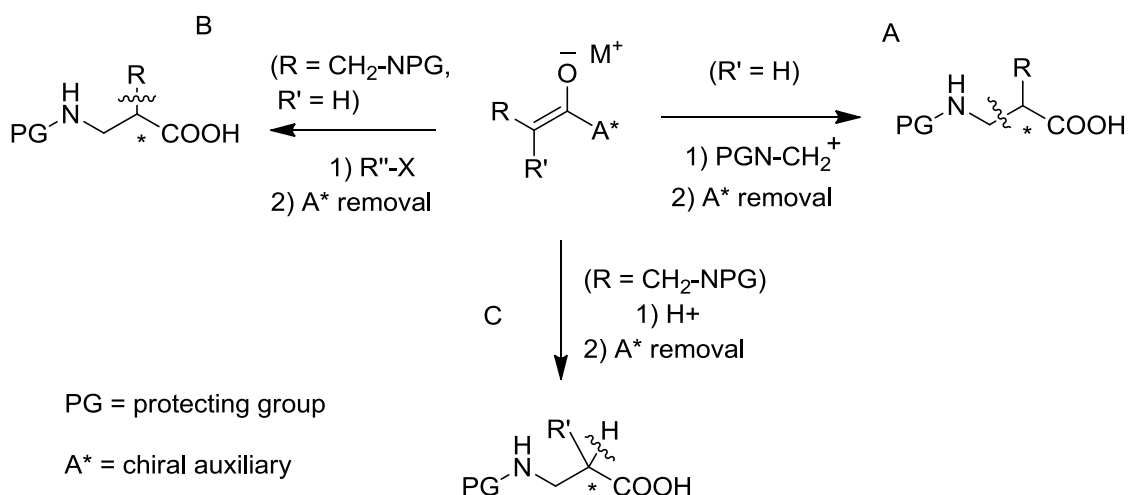


Fig.(17) Other syntheses of beta-amino acids.

Most of the reactions required the presence of a chiral auxiliary. Conversely, the use of acrylates or nitroolefins allowed the convenient synthesis of  $\beta$ -amino acids by enantioselective hydrogenation, with rhodium or ruthenium or enzymatic catalyst. Also the enantioselective formation of the C(1)–C(2) bond by conjugate additions of carbon nucleophiles to the C=C bond of  $\alpha,\beta$ -unsaturated carboxylic acid derivatives can be conducted catalytically Fig. (18).

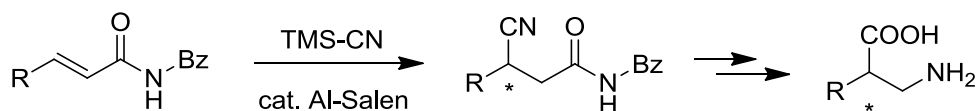


Fig.(18) Synthesis of beta amino acids.

Peptides formed by homologated  $\beta$ -amino acids have been studied for years to discover stable secondary structures [96-98]. In general, the substitution of  $\alpha$ -amino acids by their  $\beta$ -isomers in biologically active peptides gave increased activity and enzymatic stability [99]. Tests with proteolytic enzymes of all types (from mammals, microorganisms, yeasts) and *in vivo* examinations (mice, rats, insects, plants) showed  $\beta$ - and  $\gamma$ -peptides to be completely stable towards proteolysis and, as demonstrated for two  $\beta$ -peptides, extraordinarily stable towards metabolism. Even the introduction of a single  $\beta$ -amino acid in a strategic position of a native peptide can confer stability towards hydrolysis. A few examples of opioid peptidomimetics are discussed here. The introduction of  $\beta^2$ -isomeric or  $\beta^3$ -homologue amino acids in the native sequence of endomorphin-1, H-Tyr-Pro-Trp-PheNH<sub>2</sub>, gave  $\mu$ -opioid receptor agonists whose affinity largely varied depending on the  $\beta$ -amino acid. In particular, the affinity of the modified endomorphins [ $\beta^2$ -Pro<sup>3</sup>] [100], and [ $\beta^3$ -homo-Pro<sup>3</sup>]endomorphin-1 [101] were in the nanomolar range. It has been also determined that the modifications introduced allowed an enzymatic stability enhancement with respect to endomorphin-1 [101,102], and *in vivo* analgesic efficacy [103].

#### 1.4. Cyclization

The first bioactive cyclopeptide, gramicidin S, was discovered in 1947. Subsequently, a growing number of cyclopeptides of marine or microbial origins attracted attention for their potential utility in medicinal chemistry. For instance, cyclodepsipeptides widely exist in marine sponges, tunicates, cyanobacteria, fungi, etc. and exhibit varieties of biological activities, such as anti-inflammatory, anti-HIV, anti-tumor activities, etc [2]. Also worth of mention are the antimicrobial cyclopeptides defensins and their derivatives [104,105], and many other naturally occurring circular peptides, cyclotides, and proteins [106,107].

The interest in these compounds encouraged the development of cyclic mimetics of biologically active, naturally occurring linear peptides. In general, the cyclic analogues are much more stable with respect to the native peptides, conformationally more defined, and more selective towards the specific target. Some selected examples of pharmacologically relevant cyclic peptidomimetics are shown in Fig. (19).

Different kinds of connections have been utilized to restrain peptide structure into a cyclic framework, including macrolactams, ether bridges, biaryl bridges, or by disulfide bridges or mimics, etc.

Linkage of the *N*- with the *C*-terminus of the backbone is quite usual [108], but often the connection of two side chains that are not involved in the interaction with the targets (Lys, Ornithine), or eventually the connection of either the *C*- or the *N*-terminus with one of the side chains, is preferred [109]. An example is the selective and potent  $\mu$ -opioid receptor agonist (15) (Tyr-c[-*D*-Orn-2-Nal-*D*-Pro-NMe-Ala]), analogue of the natural occurring  $\beta$ -casomorphin-5, a peptide derived from the milk protein  $\beta$ -casein, Fig. (19) [110,111].

The connection between Lys and Asp has been utilized in the 31 *N*-terminal residues of the human parathyroid hormone (hPTH) to give a therapeutic osteogenic agent. This analogue contains three lactam bridges, thus resulting in a peptide with a helical structure, much more active than the natural compound [112]. Disulfide bridges are key structural features of many peptides and proteins, playing a role in folding and stabilization of bioactive conformations. Several cyclic peptidomimetics active towards the opioid receptors have been prepared by linking Cys residues or penicillamine residues *via* the oxidation to give a disulfide bridge.

This method was utilized in the cyclic enkephalin analogue DPDPE, Fig. (19), which is active at the  $\delta$ -opioid receptor [3,63].

The disulfide group is sensitive to reduction, so many efforts have been made to mimic this kind of conformational constraint, (e.g. thioether-bridges, dicarba analogues, RCM). The use of sulphur-based bridges is commonly found in the field of opioid peptidomimetics.

Selected examples are the  $\mu$ -selective JOM-6, Fig. (19), and the  $\delta$ -selective JOM-13 [3,113]. The 16-amino acid peptide  $\alpha$ -conotoxin MII, having two labile disulfide bonds between the Cys residues in positions 2-8, 3-16, was further stabilized by cyclization with a range of short peptide linkers. The cyclic MII analogue containing a seven-residue linker joining the *N* and *C* termini was as active and selective as the native peptide, and its resistance to proteolysis against a specific protease and in human plasma was significantly improved [114]. Another member of the conotoxin family is ziconotide, a cyclic synthetic analog of the  $\omega$ -conotoxin containing three disulfide bonds, presently in the final stages of clinical development as non-opioid treatment for severe chronic pain [115].

Other kinds of cyclization strategies can be appreciated in the methylamine-bridged enkephalin derivatives MABE [116,117], or in the antiangiogenic compound (**16**), a dual inhibitor of  $\alpha_5\beta_1/\alpha_v\beta_3$  integrin-mediated cell adhesion, showing a RGD sequence embedded in a PMRI structure, Fig. (**19**) [118].

Selected examples of cyclopeptidomimetics obtained by connection of phenolic side chains are shown in Fig. (**19**). The analogue of K-13 (**17**), a natural non-competitive inhibitor of ACE [119], is a competitive inhibitor for aminopeptidase B. The compounds family **18** exhibits immunopotentiating activity and were confirmed to have antitumor activity, but they lack classical toxicity [120]. Another example is the inhibitor of HIV-1 protease (**19**); the tripeptide sequence Phe-Ile-Val from the natural peptide Ac-Leu-Val-Phe-CHOHCH<sub>2</sub>-{Phe-Ile-Val}-NH<sub>2</sub> was replaced by a cyclic motif consisting of a tyrosine, a leucine and an alkyl amine [121,122].

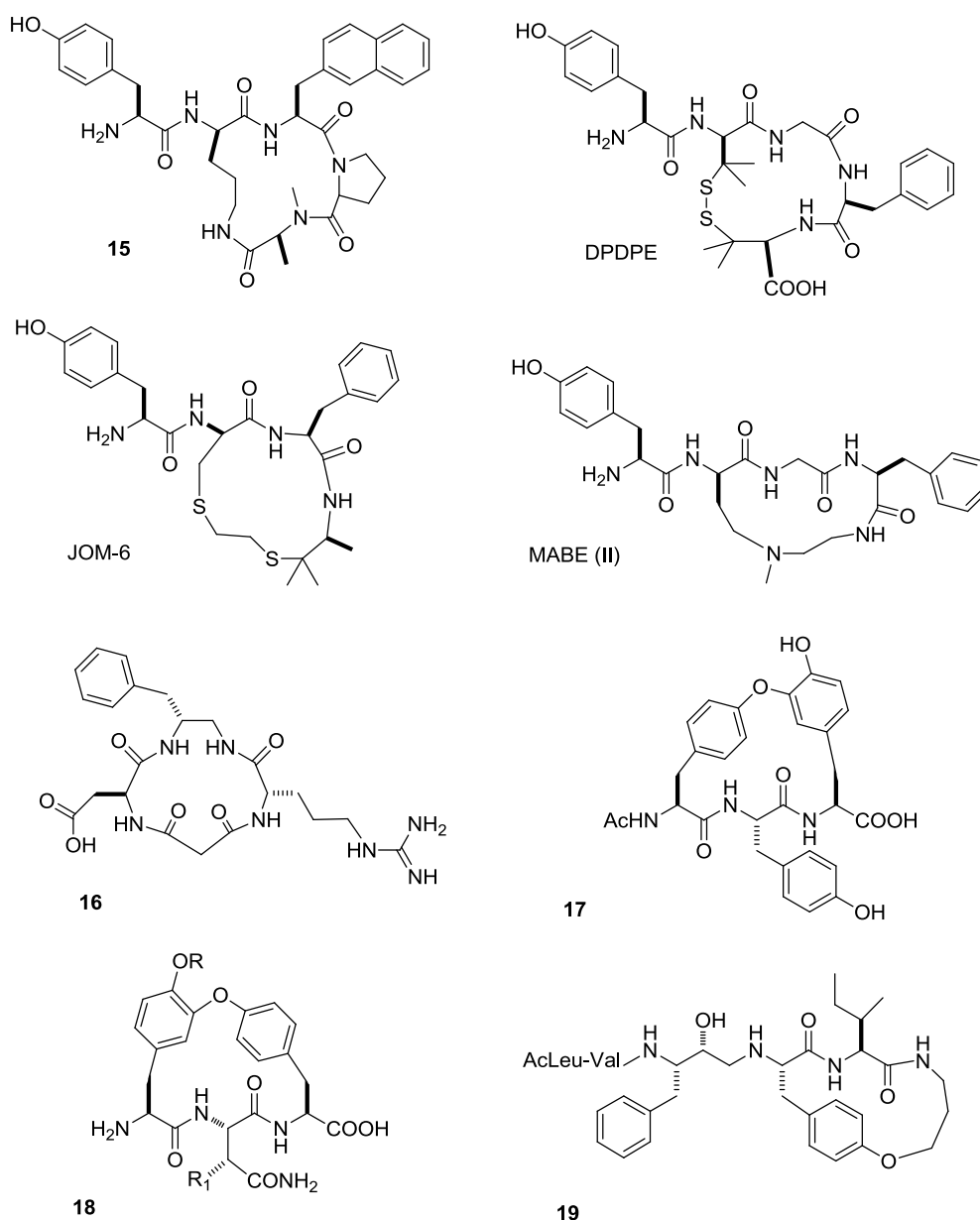


**Fig.(19)** Selected examples of pharmacologically relevant cyclic peptidomimetics.

As for the synthetic methodologies and strategies [123], cyclization can be simply performed in solution starting from the linear precursor. Macrolactamization or cycloetherification are performed in the presence of carbodiimide activating agents, or phosphonium, uronium, or uronium/aminium-type coupling reagents, the latter being more efficient. The process is affected by many parameters, concentration, temperature, base, additives, ratio of substrates, time, and requires a careful retrosynthetic analysis to identify the peptide bond designed for cyclization, in order to reduce side reactions such as oligomerization and racemization.

Examples of cyclopeptidomimetics prepared by simple cyclization with diphenylphosphoryl azide (DPPA) are the RGD integrin inhibitors developed by Kessler for treatment of human tumor metastasis and tumor induced angiogenesis, bone remodelling and osteoporosis [124,125]. *N*-methylation scan on these cyclic peptides c[Arg-Gly-Asp-D-Phe-Val] provided c[Arg-Gly-Asp-D-Phe-NMeVal], Cilengitide, with enhanced biological activity and affinity.

These conformationally defined RGD mimetics have been utilized also for investigating the relationship between the 3D display of the pharmacophores and the different selectivity towards different kinds of RGD-binding integrins [126].

Another approach is the cyclization in solid phase. This process required to take into account for parameters such as the resin, resin load, the orthogonal protecting groups, and protection/deprotection steps. However, the problem of oligomerization is completely suppressed.

The most common way is through anchoring an amino acid on resin by its side chain or its main chain at the C-terminal, Fig. (20). The amino acids whose side chain can be attached onto the resin are Asp (protected as Fmoc-Asp-Oallyl, Fmoc-Asp-ODmab, etc.), Glu, Lys, Tyr, Ser. For instance, the antibacterial peptide (20) was prepared starting from Fmoc-Asp(resin)-ODmab [127].

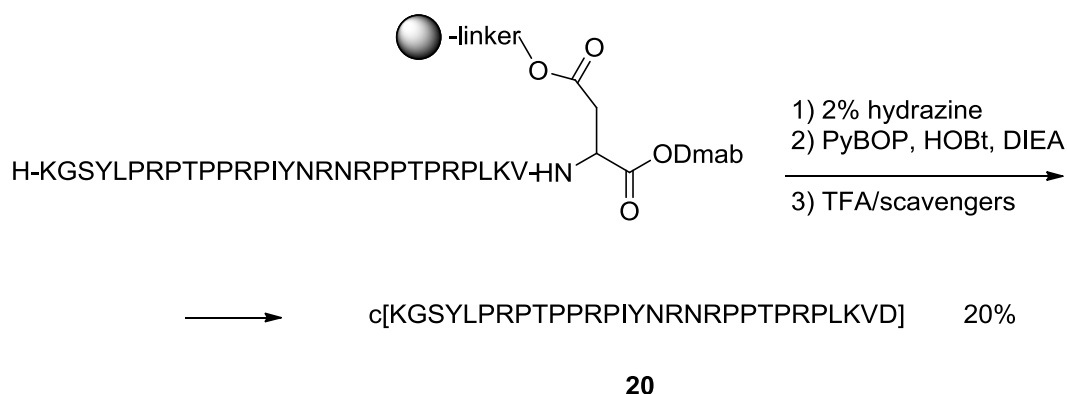


**Fig.(20)** Peptide cyclization in solid phase.

In the cleavage-by-cyclization approach, the linear precursor anchored on the resin is subjected to concurrent cleavage and cyclization, by using special linkers such as Kaiser's oxime, active esters, or safety-catch linkers. The linker should be stable during the SPPS, but should, at the same time, enable on-resin acid induced deprotection followed by nucleophilic displacement by the Nterminus.

The examples reported show the synthesis of the human calcitonin fragment analogue (**21**) by using the oxime linker <sup>[128]</sup>, and the synthesis of (**22**) by the use of a safety-catch linker <sup>[129]</sup>.

These linkers are masked variants of active esters, and can be activated by a specific chemical modification (Boc deprotection with HF, in the selected example), Fig. (**21**).

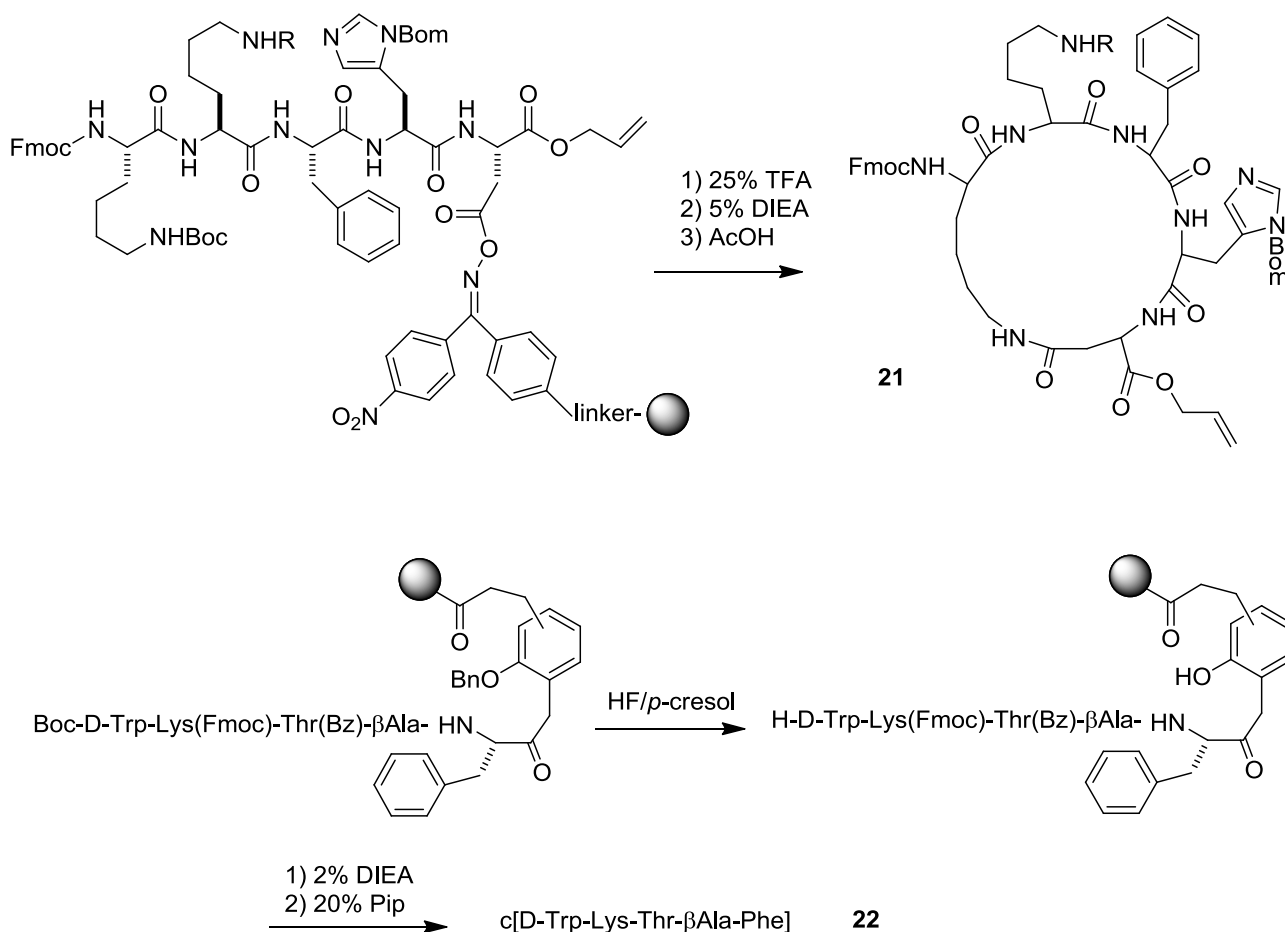
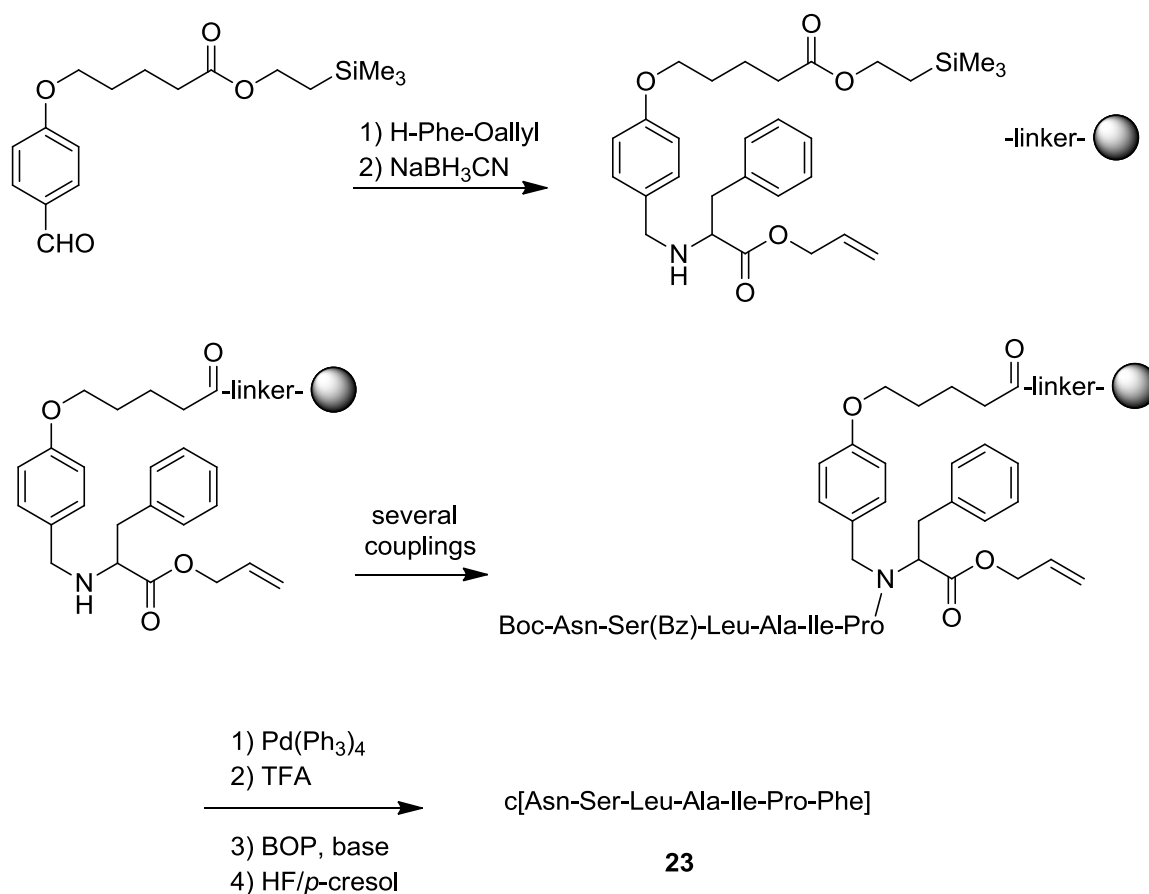


Fig.(21) Cleavage - by-cyclization

The arylsilane-based traceless linker strategy can be regarded as a variant of the side-chain anchoring method, but the preparation of the aryl silyl amino acid requires several steps, and is limited to Phe and other amino acids carrying a hydrophobic side chain. At the end of the peptide synthesis, the C-Si bond is cleaved with TFA. The backbone amide linker strategy does not require the side chain functionality, since the nitrogen of the *C*-terminal amino acid is connected to a handle by reductive amination, as shown in the synthesis of the cytotoxic stylostatin 1 (**23**) <sup>[130]</sup>, Fig. (**22**).



**Fig.(22)** Synthesis of the cytotoxic stylostatin 1.

Bisaryl ether bonds, see for instance (17) and (18), Fig. (19), exist in different naturally occurring cyclopeptides including the well known glycopeptide antibiotic vancomycin [2], a effective clinical agent useful against bacterial infections caused by drugresistant pathogens. The ruthenium-catalyzed intramolecular nucleophilic aromatic substitution allowed to prepare (17) [119].

Other synthetic methodologies for the formation of such bond are based on intramolecular aromatic substitution, or the Ullmann reaction, the oxidative thallium trinitrate-mediated macrocyclization, or arylboronic acid-mediate ring closure [123].

A extremely powerful approach to peptide cyclization is the ring-closing metathesis (RCM)<sup>[131,132]</sup> of dienes. The reaction, which can be performed also in water, is catalyzed by the Grubbs catalysts, such as benzylidene-bis(tricyclohexylphosphine) dichlororuthenium, Fig. (23) [133,134]. Cross-links consisting of hydrocarbons are much more stable *in vivo* respect to disulphide or lactam bridges, as the latter also occur in natural sequences and are susceptible to degradation. To take advantage of the reaction, protected allylglycines, or in general amino acid residues bearing an alkene side chain, can be incorporated into one chain by solid phase peptide synthesis, and they can be cyclized by the use of Grubbs catalysts [38,135]. One example is the mimic of the domain BH<sub>3</sub> of the pro-apoptotic sub-family of proteins, forced into a helical conformation through a metathesis reaction, resulting in a significantly enhanced stability and an altered *in vitro* and *in vivo* activity [136]. Other examples are shown in Fig. (23).

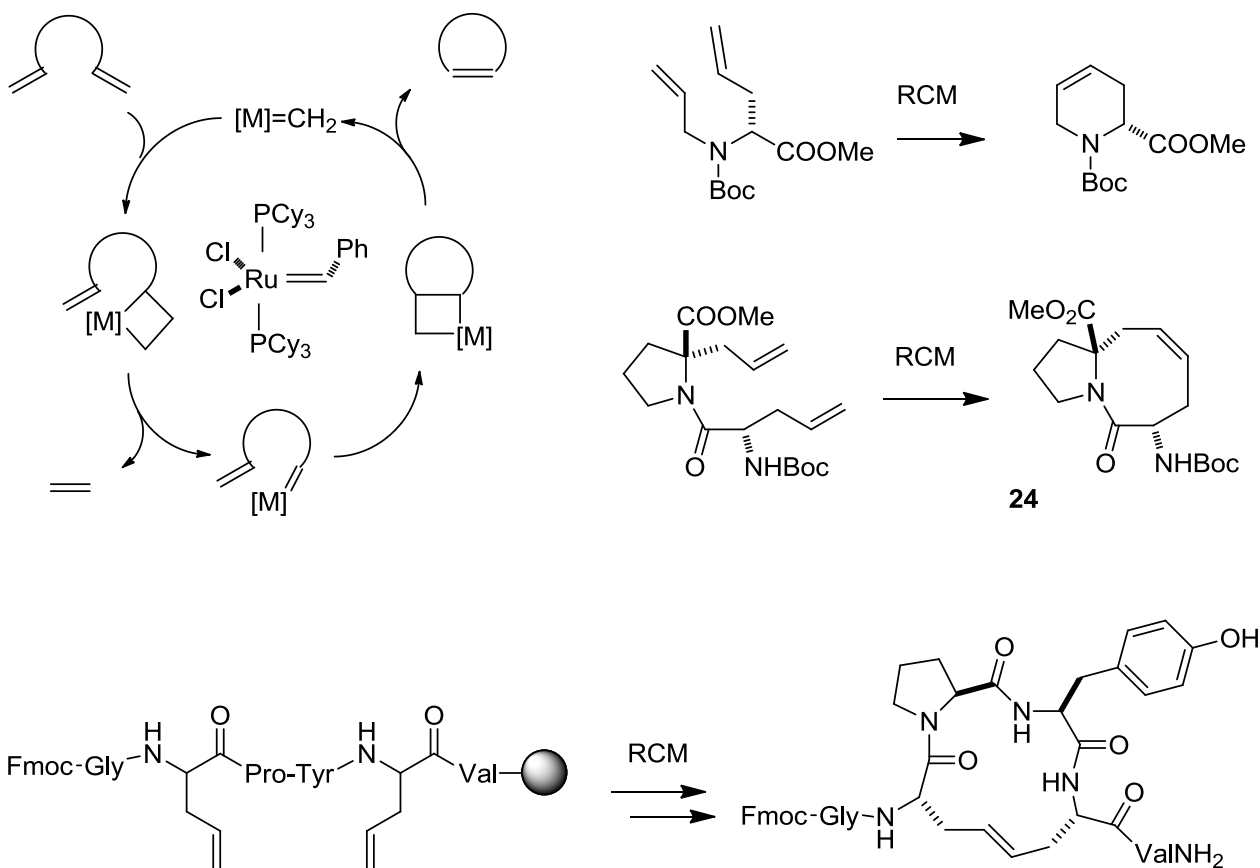


**Fig.(23)** Ring-closing metathesis.

### 1.5. $\beta$ -Turn Mimetics

$\beta$ -Turns are the most frequently mimicked protein secondary structures. They are defined as tetrapeptide sequences where the distance between the C $\alpha$  of the residues  $i$  and  $i+3$  is less or equal to 7 Å, Fig. (24). The turn can be stabilized by a ten membered ring intramolecular H-bond, or by chelation of a cation, such as Ca<sup>++</sup>. An ideal  $\beta$ -turn mimic has a rigid scaffold that orients the side chain residues in the same direction as the natural protein, while conferring good solubility and resistance to enzymatic degradation [137]. Unfortunately, many of the peptidomimetics synthesized by the use of these building blocks were inactive. Selected examples of  $\beta$ -turn mimetics are reported in Fig. (24) [138,139]. A nice example of turn mimetic is the compound (25), which has been utilized to prepare different biologically active peptidomimetics. In particular, a wide library of analogues was prepared on solid support and screened in binding assays against the fMLF receptor [137].

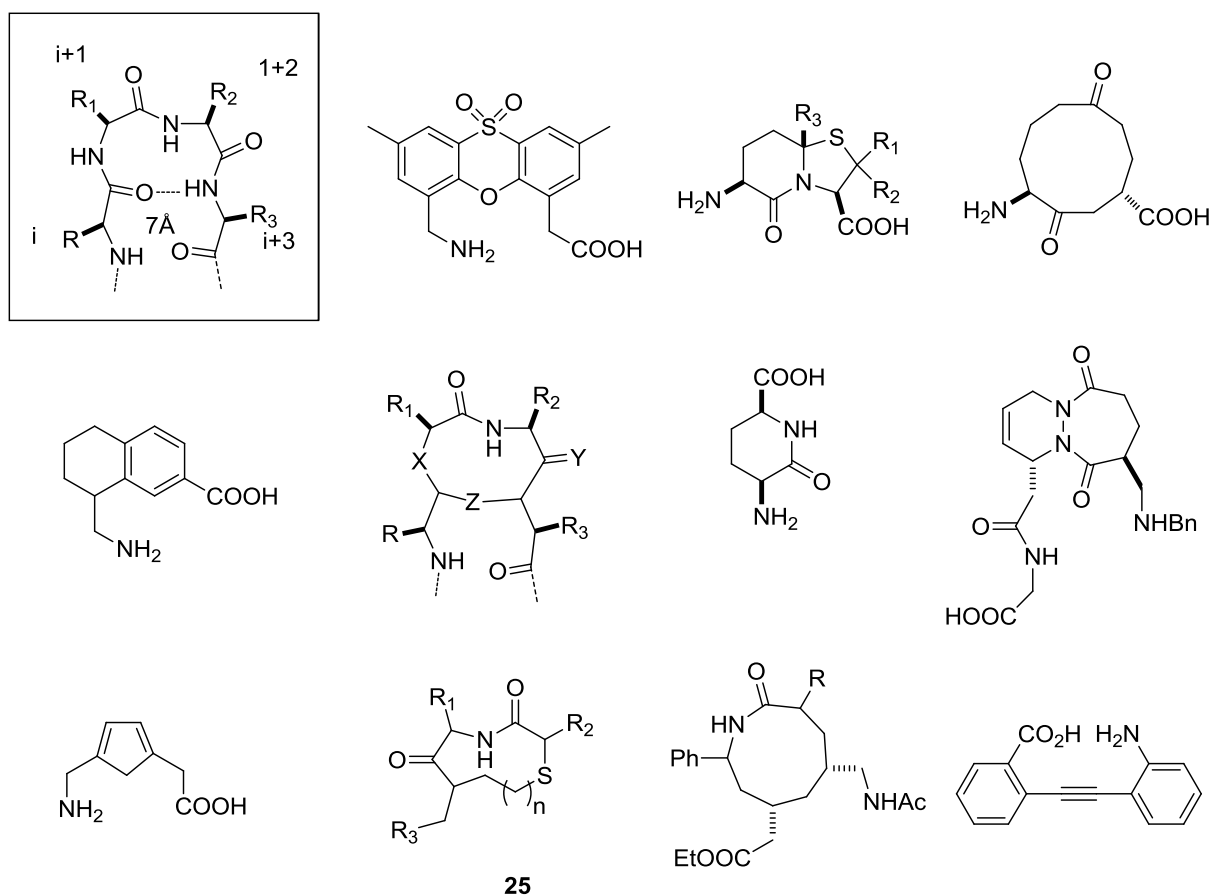


Fig.(24) Beta-turn mimetics.

The preparation of the scaffolds can be very tricky, in particular for the eventual presence of stereogenic centres. For instance, the bicyclic scaffold (**24**) was obtained by RCM, Fig (**23**)<sup>[140]</sup>. A very effective strategy to favour a geometry compatible with the  $\beta$ -turn requisites is to cyclize the peptide using a covalent linkage, by the amide nitrogen, the  $\alpha$ -carbon or a side chain<sup>[141]</sup>, Fig. (**25**). The Freidinger lactam (**26**) was designed as a mimic of Gly-Leu, and embedded in the backbone of LHRH<sup>[142,143]</sup>. The new analog showed greater potency than its parent hormone, which was attributed to a higher binding affinity for its receptor and increased metabolic stability.

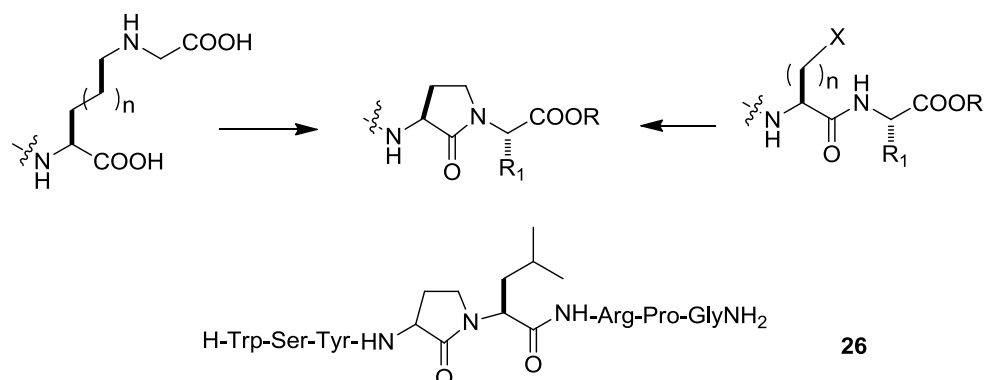
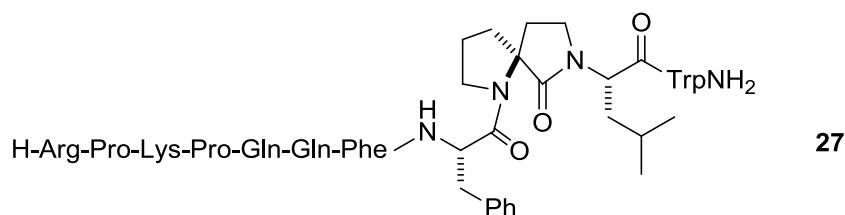


Fig.(25) Freidinger lactam.

A  $\beta$ -turn peptidomimetic based on a spiro-lactam scaffold was introduced within the structure of Substance P, H-Arg-Pro-Lys-Pro-Gln-Gln-PhePhe-Gly-Leu-MetNH<sub>2</sub>, a tachykinin neuropeptide with therapeutic potential towards gastrointestinal inflammation, arthritis, Parkinson's and Alzheimer's diseases, in place of the Phe8-Gly9 portion. Indeed, SAR studies indicated the presence of a  $\beta$ -turn centered on the sequence Phe8-Gly9-Leu10, fundamental for receptor binding. The incorporation of the spiro-lactam peptidomimetic GR71251 (**27**) resulted in a potent antagonist of the NK1 Substance P receptor, Fig. (**26**) [144].



**Fig.(26)** Example of spiro-lactam scaffold.

## 1.6. CONCLUSIONS

In spite of their potential as therapeutic agents, natural peptides have found few practical applications, mainly due to their poor stability in physiological conditions. Therefore, many efforts have been profused to design peptide-derived compounds with improved stability and ability to mimic peptide functions. The peptidomimetic approach represents a well-established strategy for developing novel, effective non-toxic therapeutic agents. Apart from the many uses in pharmacology, recent evidence have stated that the peptidomimetic strategy is the front runner in biotechnology and nanotechnology, for creating new biomaterials and biodevices, biosensors, bioelectronics, to perform specific operations within a physiological environment. In this paper we have discussed the main classes of peptide modifications intended to increase peptide stability towards proteases. The pharmacokinetic profile of a bioactive natural peptide can be strongly improved by introducing peptide bond mimetics, unnatural amino acids, conformational constraints, or non-peptide scaffolds. Many of these modifications are currently considered routine, some others are still pioneering work. These classes have been illustrated by means of selected, representative examples, supported by a brief overview of the synthetic methodologies so far developed.

## REFERENCES

- [1] Jakubke, HD; Sewald, N. Peptides from A to Z. A concise encyclopedia, Weinheim: Wiley **2008**; p. 387.
- [2] Gentilucci, L; Tolomelli, A; Squassabia, F. *Curr Med Chem.* **2006**, 13, 2449-66.
- [3] Gentilucci, L. *Curr Topics Med Chem.* **2004**, 4, 19-38.
- [4] Lee, VHL; Yamamoto, A. *Adv Drug Deliv Rev.* **1990**, 4, 171- 207.
- [5] Bocci, V. *Adv Drug Deliv Rev.* **1990**, 4, 149-69.
- [6] Hruby, VJ; Matsunaga, TO. In: Grant GA, Ed, Synthetic peptides 2nd ed. New York: Oxford University Press **2002**, pp. 292-376.
- [7] Kessler, H. *Angew Chem Int Ed.* **1982**, 2, 512-23.
- [8] Cowell, SM; Lee, YS; Cain, JP; Hruby, VJ *Curr Med Chem.* **2004**, 11, 2785-98.
- [9] Cacciari, B; Spalluto, G. *Curr Med Chem* **2005**, 51, 12-70.
- [10] Olson, GL; Cheung, HC; Chiang, E; *et al. J Med Chem* **1995**, 38, 2866-79.
- [11] Hirschmann, R; Nicolaou, KC; Pietranico, S. *J Am Chem Soc* **1993**, 115, 12550-8.
- [12] Lam, PY. *Science* **1994**, 263, 380-4.
- [13] Hruby, VJ; Balse, PM. *Curr Med Chem* **2000**, 7,945-70.
- [14] Gante, J. *Angew Chem Int Ed* **1994**, 33, 1699-720.
- [15] Randolph, JT; DeGoey, DA. *Curr Topics Med Chem* **2004**, 4, 1079-95.
- [16] Ojima, I; Chakravarty, S; Dong, Q. *Bioorg Med Chem* **1995**, 3, 337-60.
- [17] Kostis, JB; De Felice, EA; Liss, AR. In: Alan R, ed. New York: Liss Incorporated **1987**, p. 285.
- [18] Stanton, A. *Am J Cardiovasc Drugs* **2003**, 3, 389-94.
- [19] Anderson, BD. *Adv Drug Deliv Rev* **1996**, 19,171-202.
- [20] Bundgaard, H. *Adv Drug Deliv Rev* **1992**, 8,1-38.
- [21] Bak, A; Fich, M; Larsen, B.D.; Frokjaer, S; Friis, G.J. *Eur J Pharm Sci* **1999**, 7, 317-23.
- [22] Witt, K.A.; Gillespie, T.J.; Huber, J.D.; Egleton, R.D.; Davis, T.P. *Peptides* **2001**, 22, 2329-43.
- [23] Veronese, F.M. *Biomaterials* **2001**, 22, 405-17.
- [24] Witt, K.A.; Huber, J.D.; Egleton, R.D.; *et al. J Pharmacol Exp Ther* **2001**, 298, 848-56.
- [25] Pettit, D.K.; Gombotz, W.R. *Trends Biotechnol* **1998**, 8, 343-9.
- [26] Barrett, A.J.; McDonald, J.K. New York NY: Academic Press **1980**, vol. 1.
- [27] McDonald, J.K.; Barrett, A.J. New York, NY: Academic Press **1986**, Vol. 2.
- [28] Paulettia, G.M.; Gangwara, S; Siahana, T.J.; Aube´, J; Borchardt, R.T. *Adv Drug Deliv Rev* **1997**, 27, 235-56.
- [29] Powell, M.F. In: Bristol JA, Ed. Annual Reports in Medicinal Chemistry. London: Academic Press Ltd. **1993**, 28, pp. 285-94.
- [30] Witt, K.A.; Davis, T.P. *AAPS J* **2008**, 8, E76-E88.
- [31] Erickson, R.H. In: Taylor MD, Amidon GI, Eds. Peptide-based drug design: controlling transport and metabolism. DC: American Chemical Society Washington, **1995**, pp. 23-45.
- [32] Krishnamoorthy, R; Mitra, A.K. In: Taylor MD, Amidon GL Eds, Peptide-based drug design: controlling transport and metabolism. American Chemical Society. Washington, DC **1995**, 47-68.
- [33] Woodley, J.F. *Crit Rev Ther Drug Carr Syst* **1994**, 11, 61-95.

- [34] Marks, D.L.; Gores, G.J.; La Russo, N.F. Hepatic processing of peptides. In Taylor MD, Amidon GL, Eds. Washington, DC: American Chemical Society **1995**, pp. 221-48.
- [35] Nyberg, F.; Hallberg, M. *Curr Drug Targets* **2007**, 8, 147- 54.
- [36] Bakshi, P.; Wolfe, M.S. *J Med Chem* **2004**, 47, 6485-9.
- [37] Boeijen, A; Liskamp, R.M.J. *Eur J Org Chem* **1999**, 9, 2127-35.
- [38] Brouwer, A.J.; Liskamp, R.M.J. *J Org Chem* **2004**, 69, 3662-8.
- [39] Schiller, P.W.; Weltrowska, G.; Berezowska, I.; *et al. Biopolymers* **1999**, 51, 411-25.
- [40] Matej, Z.; Ziga, J.; Stanislav, G. *Curr Med Chem* **2009**, 16, 2289-304.
- [41] Gante, J.; Krug, M.; Lauterbach, G.; Weitzel, R.; Hiller, W. *J Pept Sci* **1995**, 1, 201-6.
- [42] Magrath, J.; Abeles, R.H. *J Med Chem* **1992**, 35, 4279-83.
- [43] Orrick, J.J.; Steinhart, C.R. *Ann Pharmacother* **2004**, 38,1664-74.
- [44] von Hentig, N.; Johann, W. *Drugs Today* **2008**, 44, 103-32.
- [45] dos Santos Pinheiro, E.; Ceva Antunes, O.A.; Fortunak, J.M.D. *Antiviral Res* **2008**, 79, 143-65.
- [46] Zega, A. *Curr Med Chem* **2005**, 12,589-97.
- [47] Fletcher, M.D.; Campbell, M.M. *Chem Rev* **1998**, 98, 763-96.
- [48] Chorev, M. *Biopolymers* **2005**, 80, 67-84.
- [49] Verdini, J. *Med Chem* **1991**, 34, 3372-9.
- [50] Chorev, M.; Goodman, M. *Int J Pept Protein Res* **1983**, 21,258-68.
- [51] Katritzky, A.R.; Urogdi, L.; Mayence, A. *J Org Chem* **1990**, 55, 2206-14.
- [52] Zuckermann, R.N.; Kerr, J.M.; Kent, S.B.H.; Moos, W.H.. *J Am Chem Soc* **1992**, 114, 10646-7.
- [53] Fowler, S.A.; Blackwell, H.E. *Org Biomol Chem* **2009**, 7, 1508-24.
- [54] Chongsiriwatana, N.P.; Patch, J.A.; Czyzewski, A.M.; *et al. Proc Natl Acad Sci USA* **2008**,105, 2794- 9.
- [55] Cardillo, G.; Gentilucci, L.; Tolomelli, A. *Aldrich Acta* **2003**, 36,39-50.
- [56] Cardillo, G.; Gentilucci, L.; Tolomelli, A *Mini Rev Med Chem* **2006**, 6, 293-304.
- [57] Perdih, A.; Dolenc, M.; Sollner. *Curr Org Chem* **2007**, 11, 801-32.
- [58] Luthman, K.; Hacksell, U. In Krogsgaard-Larsen P, Liljefors T, Madsen U, Eds. Textbook of drug design and discovery. *3rd Ed. London: Taylor & Francis* **2002**, pp. 459-85.
- [59] Yamada, R.; Kera, Y. *EXS* **1998**, 85, 143-55.
- [60] Durani, S. *Acc Chem Res* **2008**, 41,1301-1308.
- [61] Gentilucci, L.; Cardillo, G.; Squassabia, F.; *et al. Bioorg Med Chem Lett* **2007**,17, 2329-33.
- [62] Schiller, P.W. *Handb Exp Pharm* **1993**, 104/1(Opioids I), 681-710.
- [63] Eguchi, M. *Med Res Rev* **2004**, 24, 182-212.
- [64] Sagan, S.; Karoyan, P.; Lequin, O.; Chassaing, G.; Lavielle, S. *Curr Med Chem* **2004**, 11, 2799-822.
- [65] Wipf, P. *Chem Rev* **1995**, 95, 2115-34.
- [66] Wenger RM. Synthesis *Helv Chim Acta* **1984**, 67, 502 25.
- [67] Gilon, C.; Dechantsreiter, M.A.; Burkhart, F.; Friedler, A.; Kessler, H. *New York: Georg Thieme Verlag Stuttgart* **2003**, vol. 22, pp. 215-71.
- [68] Aurelio, L.; Brownlee, R.T.C.; Hughes, A.B. *Chem Rev* **2004**, 104, 5823-46.
- [69] Fairlie, D.P.; Abbenante, G.; March, D.R. *Curr Med Chem* **1995**, 2, 654-86.

- [70] Miller, S.C.; Scanlan, T.S. *J Am Chem Soc* **1997**, 119, 2301-2.
- [71] Sandberg, B.E.; Lee, C.M.M; Hanley, M.R.; Iversen, L.L. *Eur J Biochem* **1981**, 114, 329-37.
- [72] Cody, W.L.; He, J.X.; Reily, M.D.; *et al.* *J Med Chem* **1997**, 40, 2228-40.
- [73] Bruehlmeier, M.M; Garayoa, E.G.; Blanc, A.; *et al.* *Nucl Med Biol* **2002**, 29, 321-7.
- [74] Bach, A.C.; Eyermann, C.J.; Groos, J.D.; *et al.* *J Am Chem Soc* **1994**, 116, 3207-19.
- [75] Degenkolb, T.; Brückner, H. *Chem Biodivers* **2008**, 5, 1817-43.
- [76] Duclohier, H. *Chem Biodivers* **2007**, 4, 1023-6.
- [77] Khosla, M.C.; Stachowiak, K.; Smeby, R.R.; *et al.* *Proc Natl Acad Sci USA* **1981**, 78, 757-60.
- [78] Nachman, R.J.; Isaac, R.E.; Coast, G.M.; Holman, G.M. *Peptides* **1997**, 18, 53-7.
- [79] Toniolo, C.; Crisma, M.; Formaggio, F.; *et al.* Structures of peptides from  $\alpha$ -amino acids methylated at the  $\alpha$ -carbon. *Biopolymers* **1993**, 33,1061-72.
- [80] Karle, I.L.; Balaram, P. *Biochemistry* **1990**, 29, 6747-56.
- [81] Maity, P.; König, B. *Biopolymers* **2008**, 90, 8- 27.
- [82] Maity, P.; Zabel, M.; König, B. *J Org Chem* **2007**, 72, 8046-53.
- [83] Haskell-Luevano, C.; Toth, K.; Boteju, L.; *et al.* *J Med Chem* **1997**, 40, 2740-9.
- [84] Tourwe, D.; Mannekens, E.; Trang, N.; Thi, D.; *et al.* *J Med Chem* **1998**, 41, 5167-76.
- [85] Mosberg, H.I.; Omnaas, J.R.; Lomize, A.; Heyl, D.L. *J Med Chem* **1994**, 37, 4384-91.
- [86] Jiao, D.; Russell, K.C.; Hruby, V.J. *Tetrahedron* **1993**, 17, 3511-20.
- [87] Stewart, D.E.; Sarkar, A.; Wampler, J.E. *J Mol Biol* **1990**, 214, 253-60.
- [88] MacArthur, M.W.; Thornton, J.M. *J Mol Biol* **1991**, 218, 397-412.
- [89] Thamm, P.; Musiol, H.J.; Moroder, L. *New York: Georg Thieme Verlag Stuttgart* **2003**, vol. 22, pp. 52-86.
- [90] Samanen, J.; Cash, T.; Narindray, D.; *et al.* *J Med Chem* **1991**, 34, 3036-43.
- [91] Seebach, D.; Beck, A.K.; Bierbaum, D.J. *Chem Biodivers* **2004**,1, 1111-239.
- [92] Liljeblad, ABiocatalysis as a profound tool in the preparation of highly enantiopure  $\beta$ -amino acids. *Tetrahedron* **2006**, 62, 5831-54.
- [93] Cardillo, G.; Tomasini, C. *Chem Soc Rev* **1996**, 25, 117-28.
- [94] Seebach, D.; Beck, A.K.; Capone, S.; Deniau, G.; Groselj, U.; Zass, E. *Synthesis* **2009**, 1,1-32.
- [95] Meyer, H.; Beck, A.K.; Šebesta, R.; Seebach, D. *Org Synth* **2008**, 85, 287.
- [96] Seebach, D.; Abele, S.; Gademann, D.; *et al.* *Helv Chim Acta* **1998**, 81, 932-82
- [97] Gellman, S.H.; DeGrado, W.F. *Chem Rev* **2001**, 101, 3219-32.
- [98] Lelais, G.; Seebach, D. *Biopolymers* **2004**, 76, 206-43.
- [99] Frackenphol, J.; Arvidsson, P.I.; Schreiber, J.V.; Seebach, D. *Chem Bio Chem* **2001**, 2, 445-55.
- [100] Cardillo, G.; Gentilucci, L.; Melchiorre, P.; Spampinato, S. *Bioorg Med Chem Lett* **2000**, 10, 2755-8.
- [101] Cardillo, G.; Gentilucci, L.; Qasem, A.R.; Sgarzi, F.; Spampinato, S. *J Med Chem* **2002**, 5, 2571-8.
- [102] Cardillo, G.; Gentilucci, L.; Tolomelli, A.; Calienni, M.; Qasem, A.R.; Spampinato, S. *Org Biomol Chem* **2003**, 1, 1498-502.
- [103] Spampinato, S.; Qasem, A.R.; Calienni, M.; *et al.* *Eur J Pharmacol* **2003**, 469, 89-95.
- [104] Tang, Y.Q.; Yuan, J.; Ösapay, G.; *et al.* *Science* **1999**, 286, 498-502.
- [105] Cole, A.M.; Hong, T.; Boo, L.M.; *et al.* *PNAS* **2002**, 99,1813-8.

- [106] Colgrave, M.L.; Craik, D.J. *Biochemistry* **2004**, 43, 5965-75.
- [107] Trabi, M.; Craik, D.J. *Trends Biochem Sci* **2002**, 27, 132-8.
- [108] Cardillo, G.; Gentilucci, L.; Tolomelli, A.; *et al. J Med Chem* **2004**, 47, 5198-203.
- [109] Reichelt, A.; Martin, S.F. *Acc Chem Res* **2006**, 39, 433-42.
- [110] Teschemacher, H.; Koch, G.; Brantl, V. *Biopolymers* **1997**, 43, 99-117.
- [111] Meisel, H. *Biopolymers* **1997**, 43, 119-28.
- [112] Condon, S.M.; Morize, I.; Darnbrough, S.; *et al. J Am Chem Soc* **2000**, 122, 3007-14.
- [113] Fowler, C.B.; Pogozeva, I.D.; Lomize, A.L.; LeVine, H.; Mosberg, H.I. *Biochemistry* **2004**, 43, 15796-810.
- [114] Clark, R.J.; Fischer, H.; Dempster, L.; *et al. Proc Natl Acad Sci* **2005**, 102, 13767-72.
- [115] Miljanich, G.P. *Curr Med Chem* **2004**, 11, 3029-40.
- [116] Goodman, M.; Zapf, C.; Rew, Y. *Biopolymers* **2001**, 60, 229-45.
- [117] Shreder, K.; Zhang, L.; Dang, T.; *et al. J Med Chem* **1998**, 41, 2631-5.
- [118] Gentilucci, L.; Cardillo, G.; Spampinato, S.; *et al. J Med Chem* **2010**, 53, 106-18.
- [119] Janetka, J.W.; Raman, P.; Stayshur, K.; Flentke, G.R.; Rich, D.H. *J Am Chem Soc* **1997**, 119, 441-2.
- [120] Janetka, J.W.; Rich, D.H. *J Am Chem Soc* **1997**, 119, 6488-95.
- [121] Abbenante, G.; March, D.R.; Bergman, D.A.; *et al. J Am Chem Soc* **1995**, 117, 10220-6.
- [122] Reid, R.C.; March, D.R.; Dooley, M.J.; Bergman, D.A.; Abbenante, G.; Fairlie, D.P. *J Am Chem Soc* **1996**, 118, 8511-7.
- [123] Li, P.; Roller, P.P.; Xu, J. *Curr Org Chem* **2002**, 6, 411-40.
- [124] Schaffner, P.; Dard, M.M. *Cell Mol Life Sci* **2003**, 6, 119-32.
- [125] Aummailley, M.; Gurrath, M.; Müller, G.; Calvete, J.; Timpl, R.; Kessler, H. *FEBS Lett* **1991**, 291, 50-4.
- [126] Dechantsreiter, M.A.; Planker, E.; Mathä, B.; *et al. J Med Chem* **1999**, 42, 3033-40.
- [127] Cudic, M.; Wade, J.D.; Otvos, Jr. L. *Tetrahedron Lett* **2000**, 41, 5527-31.
- [128] Kapurniotu, A.; Taylor, J.W. *Tetrahedron Lett* **1993**, 34, 7031-4.
- [129] Bourne, G.T.; Golding, S.W.; McGeary, R.P.; *et al. J Org Chem* **2001**, 66, 7706-13.
- [130] Bourne, G.T.; Meutermans, W.D.F.; Alewood, P.F.; *et al. J Org Chem* **1999**, 64, 3095-101.
- [131] Choi, T.L.; Lee, C.W.; Chatterjee, A.K.; Grubbs, R.H. *J Am Chem Soc* **2001**, 123, 10417-8.
- [132] Martin, W.H.; Blechert, S. *Curr Top Med Chem* **2005**, 5, 1521-40.
- [133] Blackwell, H.E.; Grubbs, R.H. *Angew Chem Int Ed* **1998**, 37, 3281-4.
- [134] Blackwell, H.E.; Sadowsky, J.D.; Howard, R.J.; *et al. J Org Chem* **2001**, 66, 5291-302.
- [135] Schafmeister, C.E.; Po, J.; Verdine, G.L. *J Am Chem Soc* **2000**, 122, 5891-2.
- [136] Walensky, L.D.; Kung, A.L.; Escher, I.; *et al. Science* **2004**, 305, 1466-70.
- [137] Souers, A.J.; Ellman, J.A. *Tetrahedron* **2001**, 57, 7431-48
- [138] Hanessian, S.; McNaughton-Smith, G.; Lombart, H.G.; Lubell, W.D. *Tetrahedron* **1997**, 53, 12789-854.
- [139] MacDonald, M.; Aubé, J. *Curr Org Chem* **2001**, 5, 417-38.
- [140] Hoffmann, T.; Lanig, H.; Waibel, R.; Gmeiner, P. *Angew Chem Int Ed* **2001**, 40, 3361-4.
- [141] Toniolo, C. *Int J Pept Protein Res* **1990**, 35, 287-300.
- [142] Freidinger, R.M.; Veber, D.F.; Perlow, D.S.; Brooks, J.R.; Saperstein, R. *Science* **1980**, 210, 656-8.

- [143] Aubé, J. In: Abell A, Ed. *Advances in peptidomimetics*. Greenwich, CT: JAI Press **1996**, pp. 193-232.
- [144] Johnson, R.L *J Org Chem* **1993**, 58, 2334-7.
- [145] Burlet, S.; Pietrancosta, N.; Laras, Y.; Garino, C.; Quelever, G.; Kraus, J.L. *Curr Pharm Des* **2005**, 11, 3077-90.
- [146] Kee, K.S.; Jois, S.D. *Curr Pharm Des* **2003**, 9,1209-24.
- [147] Tozzi, C.; Giraudi, G. *Curr Pharm Des* **2006**, 12,191-203.

---

## Chapter 2

---

### Cyclopeptide Analogs for Generating New Molecular and 3D Diversity

---

#### Abstract

Cyclic peptides have been often utilized as metabolically stable, conformationally restricted mimics of different kinds of biologically active peptides, including peptide antibiotics, endogenous opioid peptides, integrin inhibitors, peptide hormones, anticancer peptides, and so on. And in particular, cyclic compounds which can mimic important secondary structure elements such as  $\beta$ -turns are of outstanding importance. Since greater chemical and structural diversity are primary features to pursue for finding novel leads for pharmacological and biotechnological applications, we explored the potential utility of the retro-inverso modification. We introduced this modification into the sequence of 13-membered cyclotetrapeptides, which can be regarded as easily available, conformationally stable analogs of cyclotetrapeptides composed of all  $\alpha$ -residues.

In this paper we describe the synthesis of a selected mini-library of partially modified retro-inverso cyclic peptides as conformationally homogeneous scaffolds for medicinal chemistry applications. The different compounds have been obtained by simple scramble of the same residues. Finally, we discuss the conformational features of such molecules as turn mimics. The comparison suggests that the retro-inverso modification allows a higher degree of three-dimensional diversity than normal peptides.

#### 2. Introduction

Protein-protein and peptide-protein/receptor interactions play a key role in most biological processes and in mediating signals, thus representing important classes of targets for human therapeutics. In addition, other peptides or short proteins are the natural inhibitors or activators of such interactions. Although these biologically active molecules have a great potential for pharmaceutical and medical applications, they generally need to be modified to overcome their poor pharmacological properties, in particular their susceptibility to enzymatic degradation<sup>[1]</sup>. Peptides are degraded by proteases in the stomach and should be administered intravenously. In the blood, peptides are degraded and cleared from the circulation very rapidly. Peptides are often too water-soluble to be able to pass the biological barriers that separate them from their targets in the cells and in the brain. Apart from their too poor bioavailability, peptides are highly flexible, a quality that counteracts a good selectivity towards a specific receptor.

All these disadvantages prevent peptides from becoming drugs and stimulate efforts to replace them with modified analogues capable of mimicking or antagonizing the biological action of the parent compounds. Many kinds of modifications have been utilized, such as *N*- or *C*- $\alpha$ -substitution, introduction of *D*-amino acids, cyclization, glycosylation. In addition, amino acids can be deleted, or added, or replaced with conformationally constrained or novel amino acids; backbone peptide bonds can be replaced with surrogates, or the backbone may be replaced altogether by a non-peptidic structure, etc [Errore. Il segnalibro non è definito.<sup>-3]</sup>. Such peptidomimetics are generally more stable than peptides and less easily cleared from the blood stream<sup>[4]</sup>. It is worth mentioning that many of the above described modifications designed to enhance peptide activity

and stability can also be found in peptides of microbial origin, such as Bestatin, Vancomycin, Lantibiotics, Epoxomicin, Lactacystin, etc. or of marine origin, including the Conotoxins, Hemiasterlin, Dolastatins, and many others peptides endowed with biological and pharmacological activity as antibiotic or anticancer agents [Errore. Il segnalibro non è definito.].

Over past decades, with the development of combinatorial techniques huge arrays of new molecules, including peptides, peptidomimetics, or non-peptidomimetics, can be produced in relatively short periods of time. Besides, various experimental high throughput screening methods as well as computational methods for rational design of peptidomimetics have been developed [5].

Despite the number of successful examples reported in the literature, the development of effective methods for finding new bioactive peptidomimetics as drug leads remains a nontrivial problem. In addition, even the biggest libraries of compounds used in screening may not reflect the rich chemical diversity of the much smaller numbers of natural products [6].

The total descriptor space that encompasses all the molecules that could in principle be created is often referred as 'chemical space', a or 'multi-dimensional descriptor space' [7]. Among the many descriptors which can be utilized to characterize a set of biomolecules (sequence, molecular mass, dimension, lipophilicity, oral absorption, side effects, toxicity, etc.). Molecular Topology deals with the complicated problems of including information on three-dimensional (3D) molecular structure and shape [8]. Topological information obtained from the analysis of naturally occurring peptides can be elaborated by means of mathematic models or virtual screening. The resulting topological model can be utilized for predicting the structural features required to give a peptidomimetic high biological activity. Many practical problems arise when the synthesis of such an "ideal" molecule leads to the generation of synthetically unfeasible or chemically unstable structures.

In many cases, it has been observed that naturally occurring peptides or proteins exert their biological activity by means of relatively small, ordered regions [9-10]. As a consequence, the ideal compound can be in principle substituted by a smaller, simple molecule which can structurally mimic the fundamental units of protein architecture. Many kinds of molecular peptidomimetic or non-peptidomimetic scaffolds capable of mimicking the structure of specific, biologically relevant regions of a peptide or a protein have been reported in the literature [11-16]. In particular, cyclic tetrapeptides or analogs [17-20] have been often used as scaffolds for the design of different kinds of turn-like structures.

We estimated that, in comparison to the parent peptides, peptidomimetics should allow a higher number of structural combinations, giving rise to higher topological diversity. In this paper we describe the preparation of a selected library of cyclotetrapeptide mimetics as scaffold models, based on a partial retro-inverso (PMRI) structure, Fig.(1), obtained by introduction of a bilateral diamine and a diacid in different positions. Further, we discuss and compare the conformational features of some of these compounds (see Results, and Discussion sections).

The convention for the construction of peptide sequence representation proceeds from the amino terminus, written on the left, to the carboxy terminus, written on the right, Fig.(1), "normal" peptide. Hence, it is possible to envisage the retro-isomer of a peptide (RI), that is an isomer in which the direction of the sequence and each amino acid stereochemistry are reversed.

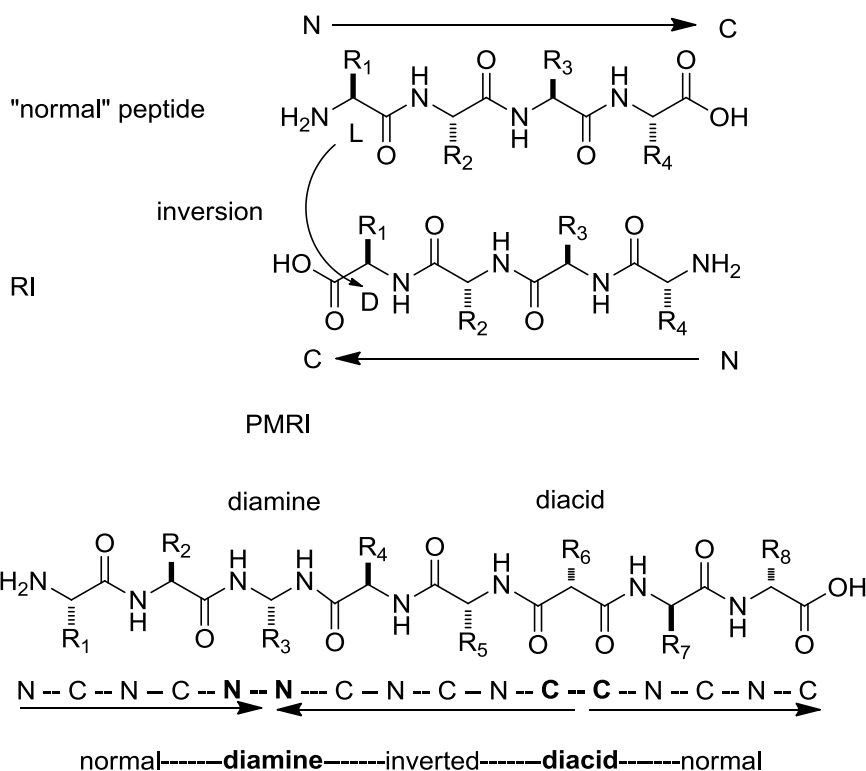


**Fig.(1).** Comparison of the structures of a "normal" peptide, a retro-inverso peptide (RI), and a partially modified retroinverso peptide (PMRI).

In a partially modified retro-inverso (PMRI) peptide, this modification involves some of the residues, while the rest of the structure is unaltered. A geminal diamine or diacid can be eventually introduced to connect the normal and the retro-inversion sections [21-26]. The retro peptide bond of a RI or a PMRI peptide can be regarded as a true peptide bond surrogate; the presence of this modified peptide bond is expected to increase the biological half-life of the compound.

## 2.1. Results

In this section we describe the preparation of the 13-membered cyclotetrapeptides **7-10**, based on a partial retro-inverso (PMRI) structure, by introduction of a 1,2-diamine as a  $\beta^2$ -amino acid mimetic, a *L*-phenylalanine, a *L*-alanine, and a *malonyl* residue in a diverse position of the peptidic sequence.

The diamine (2-amino-1-benzyl-ethyl)-carbamic acid benzyl ester (**1**) has been easily obtained by reduction of Cbz-Phe-NH<sub>2</sub> [30] with BH<sub>3</sub>, Fig. (**2**) [31]. Optically pure, differently functionalized diamines, can be prepared by a variety of methods from amino acids, amino alcohols, alkenes, unsaturated amines, dienes, aziridines, imines, diols, dihalides, nitroalkenes, amino ketones, etc [32]. The availability of all of these methods allows in principle to obtain a high chemical diversity.

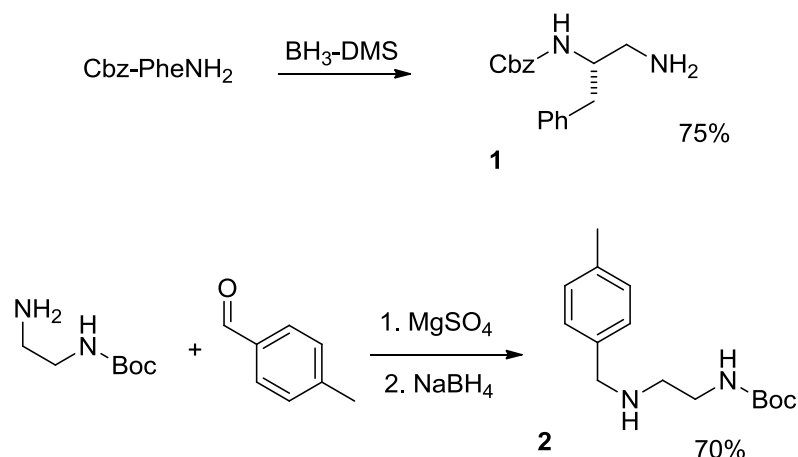


**Fig.(2).** Synthesis of substituted 1,2-diamine.

To test the feasibility of synthesizing a cyclotetrapeptide containing a *N*-substituted 1,2-diamine, we prepared also the diamine **2**. [2-(4-Methyl-benzylamino)-ethyl]-carbamic acid *tert*-butyl ester (**2**) has been prepared by reduction with NaBH<sub>4</sub> in methanol (MeOH) of the corresponding imine obtained in turn by condensation of (2-aminoethyl)carbamic acid *tert*-butyl ester [33] with *p*-methylbenzaldehyde in the presence of MgSO<sub>4</sub> in DCM. The diamines were coupled to the remaining residues under standard in-solution conditions. As an example, the synthesis of **7** is shown in Fig. (3).

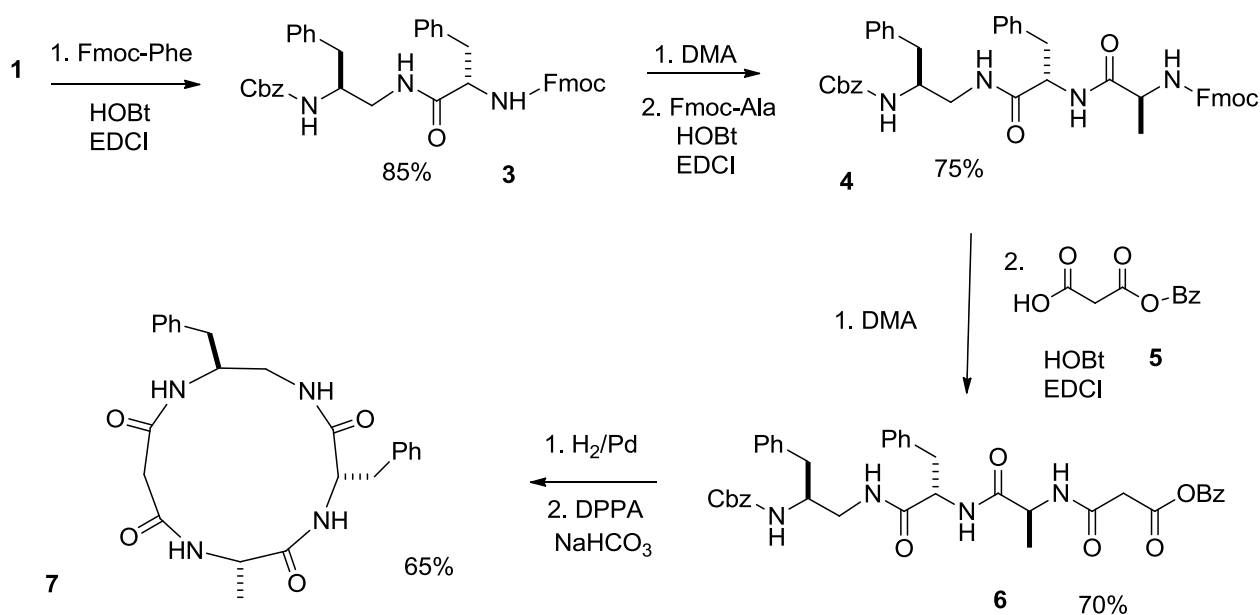


**Fig.(3).** In-solution synthesis of cyclotetrapeptide.

Coupling the Cbz-diamine (Cbz: carbobenzyloxy) with N-Fmoc protected Phe (Fmoc: fluorenylmethoxycarbonyl) gave the dipeptide **3** in good yield. Deprotection of the dipeptide by treatment with 2M dimethylamine (DMA) in tetrahydrofurane (THF) followed by coupling with Fmoc-Ala gave the tripeptide **4**. The geminal diacid has been introduced as phenylmethyl hydrogen propanedioate **5**, easily synthesized from

Meldrum's acid and benzyl alcohol [34], giving tetrapeptide **6**. The compounds were characterized by HPLC-MS analysis. Interestingly, we observed that the N-protected, linear intermediate peptides **3**, **4**, and **6** showed a noteworthy solubility in chlorinated solvents, such as chloroform and DCM, while they were practically insoluble in solvents such as ether, ethylacetate, and very poorly soluble in dimethylformamide (DMF) and MeOH, probably due to the presence of the 1,2-diamine. On the other hand, the *N*-deprotected peptides were highly soluble in ethylacetate or ether. This observation prompted us to attempt purification of the intermediate protected peptides by simple precipitation and filtration, leading to an almost solid phase-like stepwise synthesis (see Materials and Methods). As an example, the HPLC analysis of **6** after simple precipitation is shown in Fig. (4).

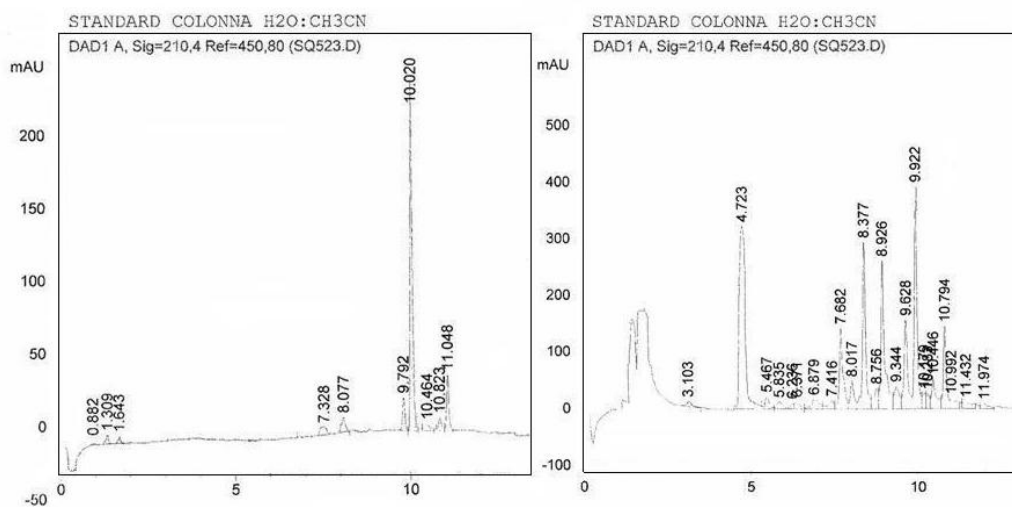


**Fig.(4).** HPLC analysis (conditions: see Experimental Section) of the crude reaction mixtures for **6** (A),  $R_t=10.02$  min, and **7** (B),  $R_t=4.72$  min.

Final deprotection of **6** by catalytic hydrogenation and cyclization of the fully deprotected tetrapeptidemimetic with diphenylphosphoryl azide (DPPA) gave the cyclic compound **7** in good yield. The HPLC analysis of the crude reaction mixture after work up is reported in Fig. (4). The compound was purified by semi-preparative RP-HPLC (see General Methods). Purity was determined to be 94% by RP-HPLC analysis.

In a similar way, we synthesized the other cyclopeptide analogs, Fig. (5). The introduction of the diamine and the diacid in diverse positions of the sequence gave rise to different compounds having one, two or three retro-peptide bonds. According to the IUPAC nomenclature, the  $\Psi$  notation for amide bond surrogates indicates that the amide bond between the two residues is reversed. Therefore, the peptide **7** can be referred to as [ $\Psi$ Phe- $\Psi$ (NHCO)-Gly-Ala-Phe], **8** as [ $\Psi$ Phe- $\Psi$ (NHCO)-Ala- $\Psi$ (NHCO)-Gly-Phe], **9** as [ $\Psi$ Phe- $\Psi$ (NHCO)-Ala- $\Psi$ (NHCO)-Phe- $\Psi$ (NHCO)-Gly-], and **10** as [*N*-Bz- $\Psi$ Ala- $\Psi$ (NHCO)-Ala- $\Psi$ (NHCO)-Gly-Phe], Fig. (6). A higher number of combinations is possible, but at the present stage we are mostly interested in addressing the atypical topological features of the cyclopeptidomimetics.

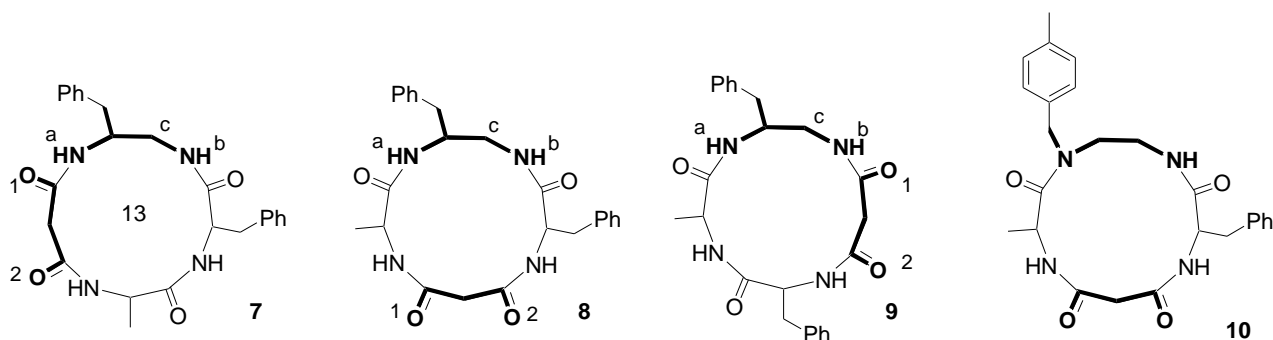


**Fig.(5).** Structures of the PMRI cyclotetrapeptides containing one (**7**), two (**8,10**), and three (**9**) retro-peptide bonds, and a N-substituted diamine (**10**).

The conformational analyses of the cyclopeptides **7**, **8** [35], and **9** were performed by spectroscopy and Molecular Dynamics (MD) simulations. The NMR analysis was conducted using standard techniques at 400 MHz in DMSO- $d_6$ . We could not perform experiments in water, for the peptides were practically insoluble. This is a familiar situation when peptidomimetics are used instead of normal peptides; in these situations DMSO is generally accepted as the solvent of choice [36]. For each peptide, the  $^1\text{H-NMR}$  revealed a single set of resonances, suggesting conformational homogeneity or a fast equilibrium, Fig. (**7**) [37-38]. The unambiguous assignment of the resonances was performed by COSY analysis.

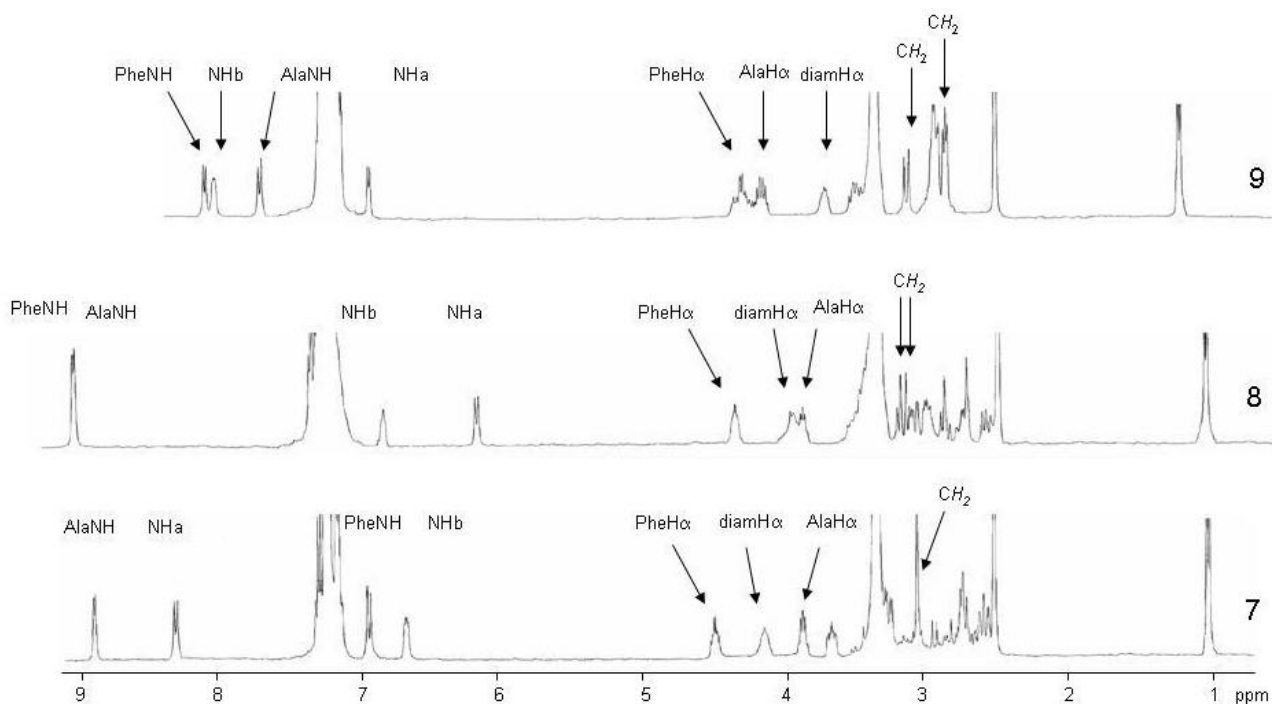


**Fig. (6).**  $^1\text{H-NMR}$  of **7,8**, and **9**, performed at 400MHz in DMSO- $d_6$ , r.t. For the attribution of diamine protons NHa, NHb, Hc (see Fig.5).

**2.1.1. VT- $^1\text{H-NMR}$**  (variable temperature) experiments were utilized to deduce the presence of H-bonds (Table 1). The analyses indicated that in cyclopeptide **7**, PheNH very likely participates to a strong H-bond,

as revealed by the  $\Delta\delta/\delta t$  value,  $-0.4$  ppb/ $^{\circ}\text{K}$  [37,39]. On the other hand, in **8** the two NHs of the diamine could be involved in H-bonds. Indeed, the  $\Delta\delta/\delta t$  values for NHa, and NHb are (ppb/ $^{\circ}\text{K}$ )  $+1.4$  and  $-1.2$ , respectively. For **9**, the VT- $^1\text{H}$ -NMR analysis suggests that the protons involved in H-bonds could be AlaNH, and NHa, being the respective  $\Delta\delta/\delta t$  values (ppb/ $^{\circ}\text{K}$ )  $-1.4$  and  $-1.3$ . These evidences are suggestive of the existence of a population of ordered structures with definite secondary structural elements, albeit for **8** and **9** different structures in equilibrium could exist.

**2.1.2. 2D-ROESY data** were utilized to investigate the spatial disposition of molecular backbones. The highly diagnostic region of amideNH – H $\alpha$  and amideNH – H $\beta$  cross peaks of **9** is reported in Fig. (7).

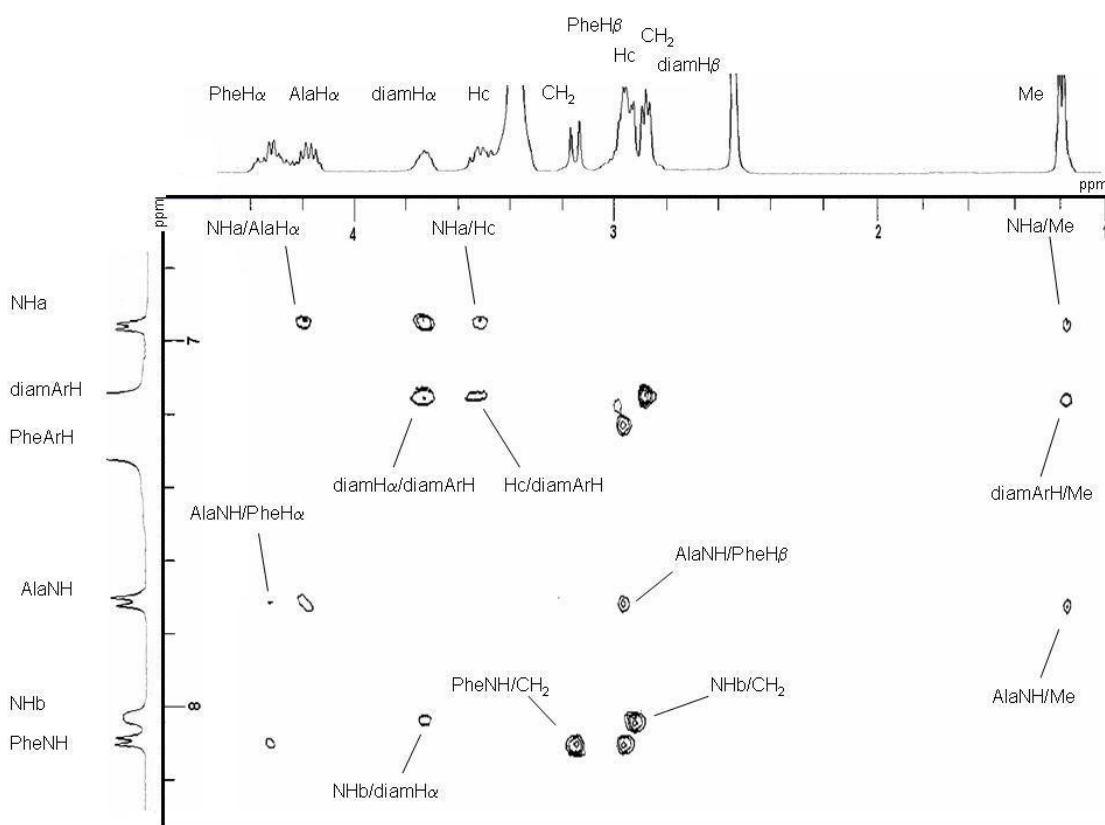


**Fig. (7).** Inset of 2D-ROESY of **9**, 400MHz, DMSO- $d_6$ , r.t. Relevant cross-peak between non-vicinal hydrogens are labelled. For the attribution of diamine protons NHa, NHb, Hc, see Fig.(5).

For the absence of H $\alpha_i$ -H $\alpha_{i+1}$  cross peaks, indicative of a cis peptide bond conformation, all of the  $\omega$  bonds were set at  $180^{\circ}$ . Conformations consistent with the spectroscopic analysis were obtained by restrained MD, using the distances deduced from ROESY as constraints, and minimized with AMBER [23] force field, with  $\epsilon = 4 \times r$ . Simulations were conducted in vacuo using a set of 100 random structures generated by means of a unrestrained high-temperature MD. The structures were subjected to restrained MD with a scaled force field, followed by a high-temperature simulation with full restraints, after which the system was gradually cooled. After minimization, the structures with the lowest internal energy and the least number of violations of the experimental data were selected and analyzed, Fig. (8).

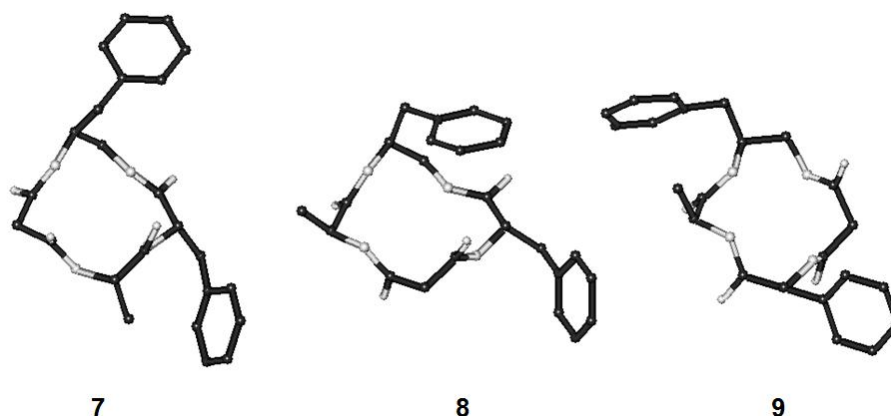


**Fig. (8).** Representative low-energy structures of **7**, **8**, and **9** consistent with ROESY analysis.

None of the structures confirms the presence of H-bonds as predicted by VT-<sup>1</sup>H-NMR analysis, probably for the occurrence of a fast equilibrium between slightly different geometries, whose average in the NMR time scale gives the NMR-derived structure. Nevertheless, ROESY-derived structures and VT-NMR analysis are consistent. The cyclopeptide **7** is roughly compatible with a structure having the diamine and Phe in the positions  $i+1$ ,  $i+2$  of a pseudo  $\beta$ -turn. However, an alternative conformation showing the residue Phe in the position  $i+1$  of an inverse  $\gamma$ -turn cannot be ruled out. The structure of **8** is compatible with the presence of two alternative type I  $\beta$ -turns, one having Phe-diamine in the positions  $i+1$ ,  $i+2$ , and the other Ala-diamine. Finally, the structure of **9** is compatible with a type II  $\beta$ -turn having in the positions  $i+1$ ,  $i+2$  the diamine and Ala, and a pseudo inverse  $\gamma$ -turn centered on the diamine. The comparatively higher number of ROESY-derived distance constraints determined for **7** (see Materials and Methods Section) suggests that this cyclopeptide likely adopts a more ordered conformation respect to **8** and **9**.

To estimate the behaviour of the cyclopeptides in water, the structures derived from NMR in DMSO were analyzed by unrestrained MD for 4.5 ns in a box of explicit, equilibrated water molecules. During the simulations, the structural features observed in the former solvent were confirmed. In addition, the examination of the trajectories revealed the occurrence of H-bonds in agreement with VT-NMR analysis. The cyclopeptide **7** shows an explicit H-bond between PheNH and malonylCO<sub>(1)</sub>, Fig. (9), **7**. Occasionally, a H-bond between NHb and malonylCO<sub>(2)</sub> can also be observed (for the attribution of the two carbonyls malonylCO<sub>(1)</sub>, malonylCO<sub>(2)</sub>, see Fig. (5)). For **8**, the simulation shows two alternating H-bonds between NHb and malonyl CO<sub>(1)</sub>, Fig. (9), **8a**, and between NHa and malonylCO<sub>(2)</sub>, Fig. (9), **8b**. For **9**, the simulation confirms the presence of a H-bond between AlaNH and malonylCO<sub>(2)</sub>, Fig. (9), **9a**. The simulation evidences also a structure compatible with an inverse  $\beta$ -turn centered on the diamine, Fig. (9), **9b**, albeit an explicit H-bond between NHa and malonylCO<sub>(2)</sub> cannot be observed.

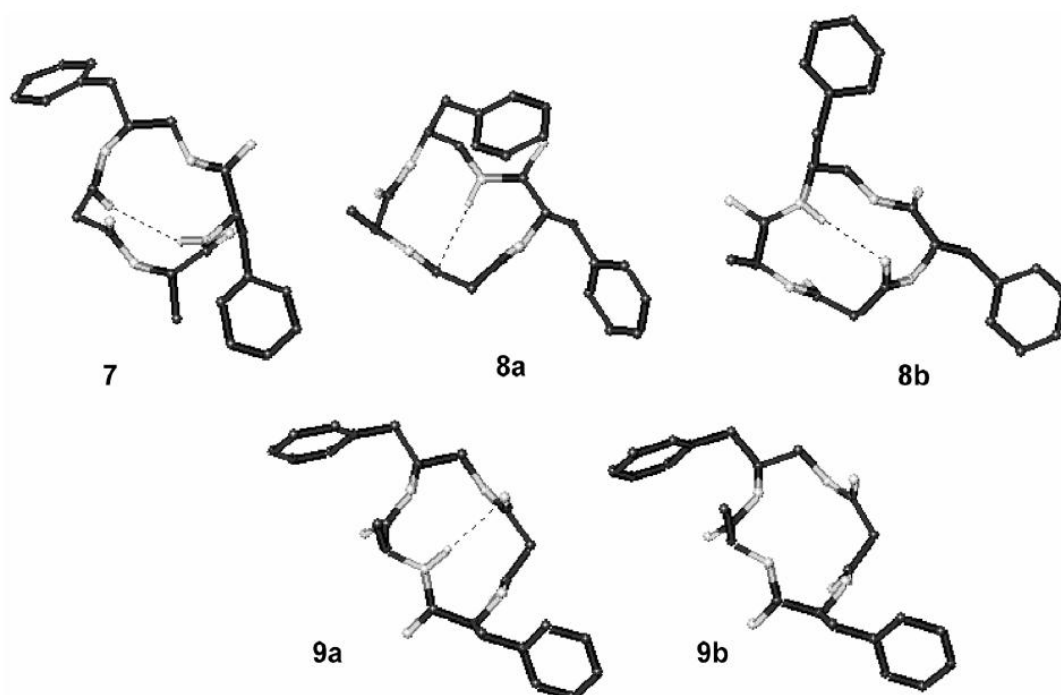
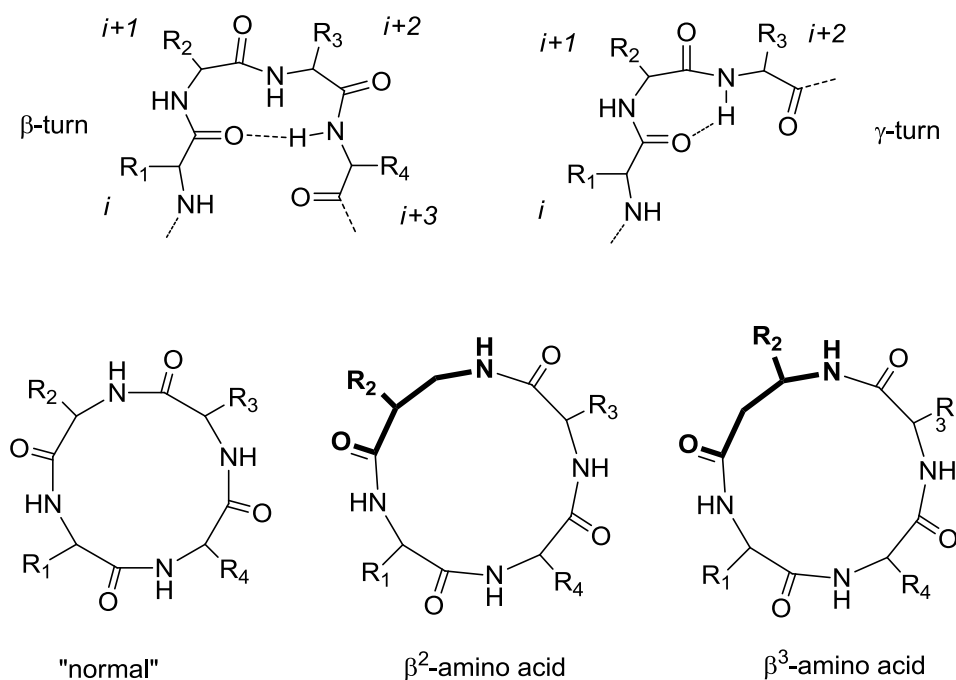


Fig. (9). Representative structures of 7, 8, and 9 showing relevant secondary elements

## 2.2. Discussion

In recent years we have been interested in cyclic peptides as restricted mimics of biologically active, naturally occurring peptides [40-41]. And in particular, we pursued the design of small, conformationally defined cyclic peptides or analogues that mimic important secondary structures such as  $\beta$ - or  $\gamma$ -turns, Fig.(10). Among the different cyclic peptides, cyclotetrapeptides are considered the smallest system capable to reproduce all kinds of turns, Fig.(10) [17], but their potential utility is often diminished by difficult synthesis. On the other hand, it has been reported that cyclotetrapeptides containing a distinct  $\beta$ -amino acid within the sequence may be easier to synthesize and conformationally more stable with respect to the "normal" cyclotetrapeptides composed of all  $\alpha$ -amino acids, and for these reasons it has been suggested that they can be effectively utilized as  $\beta$ -turn mimetics [42,43]. Two different  $\beta$ -amino acids can be utilized;  $\beta$ -amino acids having the side chain at the  $\alpha$ -carbon are named  $\beta^2$ -amino acids, while those having the side chain at the  $\beta$ -carbon are named  $\beta^3$ -amino acids, Fig.(10).



**Fig.(10).** Top:  $\beta$ - and  $\gamma$ -turnstructures; bottom: cyclotetrapeptides composed of all  $\alpha$ -amino acids, and 13-membered analogues including a  $\beta^2$ - or  $\beta^3$ -amino acids.

In order to overcome the typical limitations associated with the peptidic structure as mentioned in the Introduction, we turned our attention to the partial retro-inverso peptide bond modification, Fig.(1). We estimated that the introduction of the retro-inverso modification should lead to distinct 3D structures, depending on the specific sequence. In normal tetrapeptides, the 3D structure is largely determined by the specific combination of residue chiralities, while the nature of the residue, and hence the sequence, is less important. Therefore, in normal cyclopeptides, changing the positions of two residues (for instance from:  $Xaa^1$ - $Xaa^2$ - $Xaa^3$ - $Xaa^4$ , to  $Xaa^1$ - $Xaa^3$ - $Xaa^2$ - $Xaa^4$ ), in general has no or little consequences on the overall 3D structure of peptide backbone. On the contrary, the reversal of the sequence in a peptide containing a retro modification (such as for instance from:  $Xaa^1$ -*diamine*<sup>2</sup>- $Xaa^3$ -*diacid*<sup>4</sup>, to  $Xaa^1$ - $Xaa^3$ -*diamine*<sup>2</sup>-*diacid*<sup>4</sup>) has some consequences, since a diamine or a diacid is not comparable to an amino acid. Further, the substitution of a normal amino acid with the same residue in retro-fashion corresponds to positioning its side chain on the opposite side of the molecule. Finally, the 3D structures are less predictable, since unusual intramolecular H-bonds can occur.

Therefore, we synthesized a small library of cyclic peptidomimetics by introducing a 1,2-diamine as a  $\beta^2$ -amino acid mimetic, a L-phenylalanine, a L-alanine, and a malonyl residue in a diverse position of the peptidic sequence. To confirm the value of the cyclopeptide mimetics in generating new spatial diversity, we investigated the in-solution structures of **7**, **8** and **9**. As expected, the cyclopeptides revealed distinct geometries and characteristic secondary structural elements, Fig. (**8**) and Fig. (**9**).

In addition, the PMRI cyclotetrapeptides represent alternative 13-membered scaffolds respect to those composed of  $\alpha$ -amino acids plus a  $\beta$ -residue, reported in Fig. (**10**)<sup>[42]</sup>. For instance, the peptidomimetic **7**, [ $\beta$  Phe- $\psi$ (NHCO)-Gly-Ala-Phe], can be considered a PMRI analogue of the recently reported  $\beta^2$ -amino acid-

containing CTP,  $c[(S)\text{-}\beta^2\text{hPhe-D-Pro-Lys-Phe}]$  [42] **11**, Fig. (11). Indeed, the two peptides **7** and **11** share a common stereochemistry pattern. The first residue in **7**, the  $(S)$ -diamine, matches with the first residue  $(S)\text{-}\beta^2\text{Phe}$  in **10**. Secondly, the malonyl moiety,  $\Psi(\text{NHCO})\text{-Gly}$ , can act as a D-amino acid, mimicking D-Pro in **11**. Finally, the L-Ala in **7** matches the stereochemistry of L-Lys in **11**, and the last residue Phe is the same for **7** and **11**.

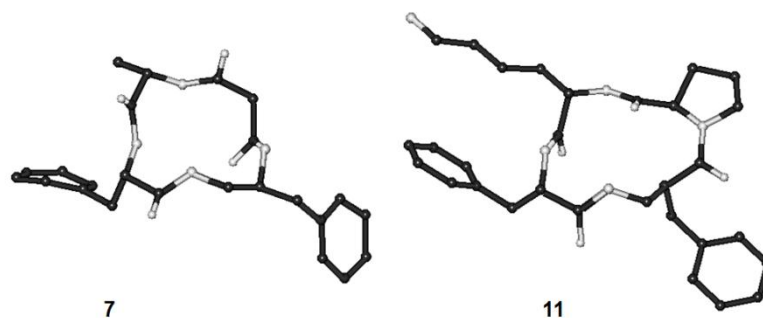


**Fig.(11).** Comparison of the PMRI cyclic RGD mimetics **12** and **13** as  $\alpha_v\beta_3$

The comparison between the two structures proves that the two scaffolds show distinct features, Fig. (11), in particular for the presence of a cis  $\beta\text{-Phe-D-Pro}$  omega bond in **11**, while **7** shows an all-trans  $\omega$  bond conformation. Besides, the two structure also differ for the position of  $\beta\text{-Phe}$  side chain, that in **11** is placed below the plane, while in **7** it points towards the opposite side.

Finally, we have recently performed a preliminary test of the potential utility of the PMRI-CTP scaffolds in medicinal chemistry, by synthesizing a couple of simple PMRI cyclotetrapeptides,  $c[\beta\text{Ala-}\Psi(\text{NHCO})\text{-Asp-}\Psi(\text{NHCO})\text{-Gly-Arg}]$  (**12**), and  $c[\beta\text{Ala-}\Psi(\text{NHCO})\text{-Asp-}\Psi(\text{NHCO})\text{-Gly-D-Arg}]$  (**13**), as RGD (Arg-Gly-Asp) mimetics, Fig. (12) [35].

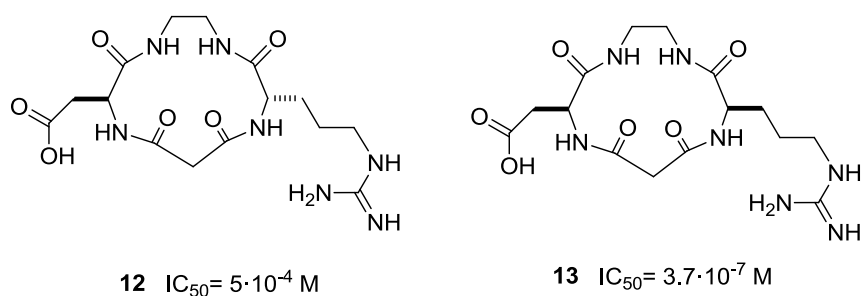


**Fig.(12).** Structures of the PMRI cyclic RGD mimetics **12** and **13** as  $\alpha_v\beta_3$  integrin inhibitors.

We tested their ability to inhibit the adhesion of an  $\alpha_v\beta_3$  integrin-expressing cell line, SK-MEL-24, to the specific ligand fibronectin. The RGD mimetics **12** and **13** showed  $\text{IC}_{50}$  values of  $5 \cdot 10^{-4}$  and  $3.7 \cdot 10^{-7}$  M, respectively [35]. The two cyclopeptides differ for the inversion of configuration at Arg. This leads to a different display of the side chains of Asp and Arg, which lie on opposite sides in **11**, while in **12** they lie on the same

side of the molecule. It is well known that a comparatively short distance between the  $\beta$  carbons (7-8 Å) of Asp and Arg favoured selective binding to  $\alpha_v\beta_3$  integrins over other RGD-binding integrins [44,45]. The inhibitory activity displayed by **13** confirmed that the pharmacophores actually adopt spatial positions compatible with an efficient ligand-receptor interaction.

### 2.3. Materials and Methods

**2.3.1. General Methods.** Unless stated otherwise, standard chemicals were obtained from commercial sources and used without further purification. Analytical RP-HPLC was performed with an ODS column, 4.6  $\mu\text{m}$  particle size, 100 Å pore diameter, 250 mm, DAD 210 nm, from 9:1 H<sub>2</sub>O/CH<sub>3</sub>CN to 2:8 H<sub>2</sub>O/CH<sub>3</sub>CN in 20 min at a 1.0 mL/min flow, followed by 10 min at the same composition. Semi-preparative RP-HPLC was performed on a C18 column, 7  $\mu\text{m}$  particle size, 21.2 x 150 mm, from 9:1 H<sub>2</sub>O/CH<sub>3</sub>CN to 3:7 H<sub>2</sub>O/CH<sub>3</sub>CN in 15 min, at a 12 mL/min flow.

<sup>1</sup>H NMR spectra were recorded using the five-millimeter tubes, using 0.01 M peptide at 400 MHz at room temperature. Chemical shifts are reported as  $\delta$  values relative to the solvent peak. VT-<sup>1</sup>H-NMR experiments were performed over the range 298-348 °K. 2D spectra were acquired in the phase sensitive mode and processed using a 90° shifted, squared sine-bell apodization. <sup>1</sup>H-NMR resonances were assigned from gCOSY and ROESY spectra. gCOSY experiments were recorded with a proton spectral width of 3103 Hz. ROESY experiments were recorded with a 300 ms mixing time with a proton spectral width of 3088 Hz.

**2.3.2. General procedure for peptide coupling.** The iterative couplings and deprotection steps have been performed in the same 100 mL two-necked round bottom reactor, with a stopcock equipped with a fritted glass filter. The reactor was loaded with a solution of the amino partner (0.5 mmol) in 9/1 DCM/DMF (5 mL). In a separate flask, a mixture of HOBt (0.6 mmol) and *N*-protected amino acid (0.5 mmol) in 9/1 DCM/DMF (5 mL) was mechanically shaken at r.t. After 5 min the homogeneous mixture was transferred into the reactor while stirring, then EDCI-HCl salt (0.6 mmol), and TEA (1.5 mmol) were added while stirring at r.t. After 4 h the mixture was diluted with Et<sub>2</sub>O (30 mL) and 0.5 HCl (10 mL) while stirring; after 5 min the liquids were removed through the stopcock under moderate suction. The crude peptide which precipitated was collected over the filter. The precipitate was washed with Et<sub>2</sub>O (30 mL) and sat. Na<sub>2</sub>CO<sub>3</sub> (10 mL). The liquids were eliminated again through the stopcock under suction, and the peptide was triturated with Et<sub>2</sub>O (30 mL). The crude peptides were dried at reduced pressure. The peptides (65-85% yield) were characterized by ES-MS analysis, see also Fig. (4), and were utilized without further purifications. Purities were determined 70-80% by RP-HPLC/ES-MS analysis (see General methods).

**2.3.3. Boc group deprotection** was performed in the same reactor by treatment with 1:2 TFA/DCM at r.t. After 20 the reactor was equipped with a condenser and solvent was removed at reduced pressure and moderate heating. The resulting oily residue was treated again for 20 min with 1:2 TFA/DCM. After final evaporated of

the mixture, the residue was triturated with Et<sub>2</sub>O, solvent was filtered under suction, and the collected deprotected amine-TFA salt which precipitated was used for the next coupling without further purification.

**2.3.4. Fmoc group deprotection** was performed in the same reactor by treatment with 2M DMA in THF at r.t. After 20 min the reactor was equipped with a condenser, and solvent was removed at reduced pressure and moderate heating. The treatment with DMA in THF was repeated. After final evaporation of the solution, the residue was triturated with 1:3 Et<sub>2</sub>O/cyclohexane, solvent was filtered under suction, and the collected deprotected amine which precipitated was used for the next coupling without further purification.

**2.3.5. Cbz and benzyl group deprotection** was performed in a 50 mL two-necked round bottom flask, by treatment of the protected tetrapeptide with H<sub>2</sub> and cat. Pd/C in EtOH at r.t. After 5 h the mixture was filtered over celite under suction, and solvent was evaporated at reduced pressure. The residue was used without further purification.

**2.3.6. General procedure for peptide cyclization.** A mixture of deprotected linear tetrapeptide (0.2 mmol), DPPA (0.5 mmol), NaHCO<sub>3</sub> (3 mmol), in DMF (60 mL) was stirred in a 250 mL two-necked round bottom flask at r.t. for 48 h. After that, solvent was distilled at reduced pressure, the residue was diluted with water, and the mixture was extracted three times with DCM. The solvent was evaporated under reduced pressure, and the residue was precipitated from DCM/Et<sub>2</sub>O. For the RP-HPLC analysis of the crude cyclopeptide, see also Fig. (4). The cyclopeptides were purified (60-70% yield) by semi-preparative RP-HPLC (see General Methods). Purities were determined 93-97% by RP-HPLC analysis (see General methods).

### 2.3.7. Conformational Analysis

The Restrained MD simulations were conducted using AMBER [27] force field with a distance dependent  $\epsilon=4.0x_r$ . A 50 ps simulation at 1200 °K was used for generating 100 random structures that were subsequently subjected to a 20 ps restrained MD with a 50% scaled force field at the same temperature, followed by 20 ps with full restraints (distance force constant: 7 kcal/mol Å<sup>2</sup>), after which the system was cooled in 5 ps to 50 °K. For the absence of H $\alpha(i, i+1)$  ROESY cross peaks, the  $\omega$  bonds were set at 180° (force constant: 16 kcal/molÅ<sup>2</sup>). Apart from the constraints on the  $\omega$  bonds, only ROESY-derived distance constraints were included in the restrained molecular dynamics. For **7**, **8** and **9**, 27, 24 and 20 ROESY-derived constraints were used, respectively. ROESY intensities were classified according to a calibration against the intensity of geminal protons (Tables 2-4) Very strong, strong, medium, and weak signals were associated to distances of 2.3 2.6, 3.0, and 4.0 Å, respectively. Geminal couplings and other obvious correlations were discarded. The resulting structures were minimized with 3000 cycles of steepest descent and 3000 cycles of conjugated gradient (convergence: 0.01kcal/Å mol). The structures that showed the lowest internal energy and the least number of violations of the experimental data were selected and analyzed.

MD simulation in explicit water was performed for 4.5 ns at 298°K using the AMBER force field in a 30x30x30 Å box of standard TIP3P models of equilibrated water [28], with a minimum solvent-solute distance of 2.3 Å, at constant temperature and pressure (Berendsen scheme [29], bath relaxation constant 0.2).

**Table 1.**  $\Delta\delta/\delta t$  values (ppb/°K) of amide protons for **7**, **8**, and **9**, determined by VT-<sup>1</sup>H-NMR analysis in DMSO-d<sub>6</sub> at 400 MHz over the range 298-348 °K

Compd	PheNH	AlaNH	NHa	NHb
<b>7</b>	-0.4	-5.2	-5.0	-1.3
<b>8</b>	-5.0 <sup>a</sup>	-5.5 <sup>a</sup>	+1.4	-1.2
<b>9</b>	-1.9	-1.4	-1.3	-2.0

<sup>a</sup> PheNH and AlaNH in **8** are superimposed.

**Table 2.** Non obvious ROESY cross-peaks observed for **7** in DMSO-d<sub>6</sub> at 400 MHz (r.t.).

Cross peak <sup>a</sup>	Intensity	Cross peak <sup>a</sup>	Intensity
AlaNH-Me	s	AlaNH-COCH <sub>2</sub> CO	vs
AlaNH-AlaH $\alpha$	m	AlaNH-PheNH	vs
AlaNH-NHa	w	NHa-diamH $\beta$	s
NHa-COCH <sub>2</sub> CO	vs	NHa-diamH $\alpha$	m
NHa-NHb	s	NHa-PheNH	w
NHa-Hc <sub>(2.6)</sub>	m	diamArH-Hc <sub>(3.7)</sub>	m
diamArH-diamH $\alpha$	s	diamArH-NHb	m
PheArH-Me	s	PheArH-PheH $\alpha$	vs
PheNH-Me	s	PheNH-AlaH $\alpha$	m
PheNH-PheH $\alpha$	s	PheNH-NHb	s
NHb-Hc <sub>(2.6)</sub>	vs	NHb-Hc <sub>(3.7)</sub>	s
NHb-diamH $\alpha$	m	NHb-AlaH $\alpha$	w
NHb-PheH $\alpha$	s	PheH $\alpha$ -Me	w
PheH $\alpha$ -AlaH $\alpha$ -	m		

<sup>a</sup>For the attribution of diamine protons NHa, NHb, Hc.(Fig.5)

**Table 3.** Non obvious ROESY cross-peaks observed for **8** in DMSO-d<sub>6</sub> at 400 MHz (r.t.).

Cross peak <sup>a</sup>	Intensity	Cross peak <sup>a</sup>	Intensity
AlaNH-NHa	s	AlaNH-COCH <sub>2</sub> CO <sub>(3.2)</sub>	vs
AlaNH-AlaH $\alpha$	m	AlaNH-COCH <sub>2</sub> CO <sub>(3.3)</sub>	w
PheNH-COCH <sub>2</sub> CO <sub>(3.2)</sub>	w	AlaNH-CH <sub>3</sub>	s
PheNH-COCH <sub>2</sub> CO <sub>(3.3)</sub>	vs	PheNH-NHb	s
NHb-PheH $\alpha$	m	PheNH-PheH $\alpha$	m
NHa-NHb	m	NHb-Hc	m
diamArH-diamH $\alpha$	m	diamArH-NHa	m
diamArH-NHb	m	diamH $\beta$ <sub>(2.75)</sub> -diamArH	s
NHa-diamH $\beta$ <sub>(2.6)</sub>	m	NHa-AlaH $\alpha$	m

diamH $\alpha$ -Hc	s	NHa-diamHa	m
diamH $\alpha$ -diamH $\beta$ <sub>(2.6)</sub>	m	diamH $\alpha$ -diamH $\beta$ <sub>(2.75)</sub>	m
PheH $\alpha$ -PheH $\beta$ <sub>(2.9)</sub>	m	PheH $\alpha$ -PheH $\beta$ <sub>(3.1)</sub>	m

<sup>a</sup>For the attribution of diamine protons NHa, NHb, Hc.(Fig.5)

**Table 4.** Non obvious ROESY cross-peaks observed for **9** in DMSO-d<sub>6</sub> at 400 MHz (r.t.).

Cross peak <sup>a</sup>	Intensity	Cross peak <sup>a</sup>	Intensity
PheNH-PheH $\alpha$	m	PheNH-COCH <sub>2</sub> CO <sub>(3.2)</sub>	vs
NHb-NHa	m	NHb-diamH $\alpha$	m
NHb-COCH <sub>2</sub> CO <sub>(2.9)</sub>	vs	AlaNH-NHa	vs
AlaNH-PheH $\alpha$	w	AlaNH-AlaH $\alpha$	m
AlaNH-PheH $\beta$	s	AlaNH-Me	m
diamArH-diamH $\alpha$	s	diamArH-Hc <sub>(3.5)</sub>	m
diamArH-Me	m	NHa-AlaH $\alpha$	m
NHa-diamH $\alpha$	s	NHa-Hc <sub>(3.5)</sub>	m
NHa-Me	m	diamH $\alpha$ -Hc <sub>(2.9)</sub>	vs
diamH $\alpha$ -Hc <sub>(3.5)</sub>	m	Hc <sub>(3.5)</sub> -diamH $\beta$	s

<sup>a</sup> For the attribution of diamine protons NHa, NHb, Hc, see Fig. (5).

## 2.4. Conclusions

In summary, we believe that the compounds described can be considered useful scaffolds for the design of stable, easy available, conformationally defined novel peptidomimetics, which allow for the exploration of a variety of chemical and spatial diversity.

The introduction of the retro modification in a 13-membered cyclotetrapeptide sequence gave us access to structurally diverse molecular scaffolds. The comparison of the structures of **7**, **8** and **9**, which share the same composition, yet differ in the scrambling of the sequence, provided evidence that the scaffolds show distinct features. The results seem to indicate that the combination of the different residues in the modified cyclopeptides gives rise to a higher degree of three-dimensionally diverse compounds with respect to normal cyclopeptides.

The availability of topologically diverse peptidomimetic scaffolds can be useful in a large range of biochemical, pharmacological, biotechnological and medical applications. Indeed, topologically definite scaffolds can be introduced in a number of peptide-derived compounds: integrin inhibitors, antibiotics, probes for non-invasive imaging, organocatalysis, self-assembling structures, nano-structures, peptide-based bio-materials, and finally bio-electronic devices such as bio-microchips, biosensors, and peptide-metal wires [Errore. Il segnalibro non è definito.]

## References

- [1] Gentilucci, L.; Tolomelli, A.; Squassabia, F. *Curr. Med. Chem.* **2006**, *13*, 2449-2466.
- [2] Hruby, V.J. *iopolymers* **1993**, *33*, 1073-1082.
- [3] Hruby, V. J.; Al-Obeidi, F.; Kazmierski, W. *Biochem. J.* **1990**, *268*, 249-262.
- [4] Baran, I.; Svobodova Varekova, R.; Parthasarathi, L.; Suchomel, S.; Casey, F.; Shields, D.C. *J. Chem. Inf. Model.* **2007**, *47*, 464-474.
- [5] Bleicher, K.H.; Boehm, H.-J.; Mueller, K.; Alanine, A.I. *Nat. Rev. Drug Discov.* **2003**, *2*, 369-378.
- [6] Feher, M.; Schmidt, J.M. *J. Chem. Inf. Comput. Sci.* **2003**, *43*, 218-227.
- [7] Dobson, C.M. *Nature* **2004**, *432*, 824-828.
- [8] Balaban, A.T. *J. Chem. Inf. Comput. Sci.* **1997**, *37*, 645-650.
- [9] Tyndall, J.D.A.; Pfeiffer, B.; Abbenante, G.; Fairlie, D.P. *Chem. Rev.* **2005**, *105*, 793-826.
- [10] Hruby, V.J.; Balse, P.M. *Curr. Med. Chem.* **2000**, *7*, 945-970.
- [11] Carotenuto, A.; D'Ursi, A. M.; Mulinacci, B.; Paolini, I.; Lolli, F.; Papini, A. M.; Novellino, E.; Rovero, P. *J. Med. Chem.* **2006**, *49*, 5072-5079.
- [12] Dings, R.P.M.; Mayo, K.H. *Acc. Chem. Res.* ACS ASAP.
- [13] Murphy, P.V.; Dunne, J.L. *Curr. Org. Synth.* **2006**, *3*, 403-437.
- [14] Le, G.T.; Abbenante, G.; Becker, B.; Grathwohl, M.; Halliday, J.; Tometzki, G.; Zuegg, J.; Meutermans, W. *Today* **2003**, *8*, 701-704.
- [15] Trabocchi, A.; Menchi, G.; Guarna, F.; Machetti, F.; Scarpi, D.; Guarna, A. *Synlett* **2006**, *3*, 331-353.
- [16] Souers, A. J.; Ellman, J. A. *Tetrahedron* **2001**, *57*, 7431-7448.
- [17] Loiseau, N.; Gomis, J.-M.; Santolini, J.; Delaforge, M.; Andre, F.. *Biopolymers* **2003**, *69*, 363-385.
- [18] Schumann, F.; Muller, A.; Kokschi, M.; Muller, G.; Sewald, N. *J. Am. Chem. Soc.* **2000**, *122*, 12009-12010.
- [19] Glenn, M. P.; Kelso, M. J.; Tyndall, J. D. A.; Fairlie, D. P. *J. Am. Chem. Soc.* **2003**, *125*, 640-641.
- [20] Mora, P.; Mas-Moruno, C.s; Tamborero, S.; Cruz, L. J.; Perez-Paya, E.; Albericio, F. *J. Pept. Sci.* **2006**, *12*, 491-496.
- [21] Chorev, M.; Goodman, M. *Acc. Chem. Res.* **1993**, *26*, 266-273.
- [22] Fletcher, M. D.; Campbell, M. M. *Chem. Rev.* **1998**, *98*, 763-796.
- [23] Chorev, M. *Biopolymers* **2005**, *80*, 67-84.
- [24] Lee, Y.; S.; Agnes, R. S.; Davis, P.; Ma, S.-w.; Badghisi, H.; Lai, J.; Porreca, F.; Hruby, V, J. *J. Med. Chem.* **2007**, *50*, 165-168.
- [25] Kim, K.-J.; Park, S.-W.; Yoon, S.S. *J. Kor. Chem. Soc.* **2000**, *44*, 286-289.
- [26] Han, Y.; Giragossian, C.; Mierke, D.F.; Chorev, M. *J. Org. Chem.* **2002**, *67*, 5085-5097.
- [27] Cornell, W. D. Cieplak, P. Bayly, C. I. Gould, I. R. Merz, K. M. Ferguson, D. M. Spellmeyer, D. C. Fox, T. Caldwell, J. W. Kollman, P. A. *J. Am. Chem. Soc.* **1995**, *117*, 5179-5197.
- [28] Jorgensen, W. L.; Chandrasekhar, J.; Madura, J.; Impey, R. W.; Klein, M. L. *J. Chem. Phys.* **1983**, *79*, 926-935.
- [29] Berendsen, H. J. C.; Postma, J. P. M.; van Gunsteren, W. F.; DiNola, A.; Haak, J. R.. *J. Chem. Phys.* **1984**, *81*, 3684-3690.

- [30] Nakabayashi, S.; Warren, C. D.; Jeanloz, R. W. *Carbohydrate Res.* **1988**, *174*, 279-289.
- [31] Morie, T.; Kato, S.; Harada, H.; Fujiwara, I.; Watanabe, K.; Matsumoto, J.-I. *J. Chem. Soc. Perkin Trans. 1* **1994**, 2565-2570.
- [32] Lucet, D.; Le Gall, T.; Mioskowski, C. *Angew. Chem. Int. Ed. Engl.* **1998**, *37*, 2580-2567.
- [33] Pittelkow, M.; Lewinsky, R.; Christensen, J. B. *Synthesis* **2002**, *15*, 2195-2202.
- [34] Felder, D.; Gutiérrez Nava, M.; del Pilar Carreón, M.; Eckert, J.-F.; Luccisano, M.; Schall, C.; Masson, P.; Gallani, J.-L.; Heinrich, B.; Guillon, D.; Nierengarten, J.-F. *Helv. Chim. Acta* **2002**, *85*, 288-319.
- [35] Gentilucci, L.; Cardillo, G.; Tolomelli, A.; Spampinato, S.; Sparta, A.; Squassabia, F. *Eur. J. Org. Chem.* **2008**, 729-735.
- [36] Gentilucci, L.; Tolomelli, A. *Curr. Topics Med. Chem.* **2004**, *4*, 105-121.
- [37] Stradley, S. J.; Rizo, J.; Bruch, M. D.; Stroup, A. N.; Gierasch, L. M. *Biopolymers* **1990**, *29*, 263-287.
- [38] Kessler, H. *Angew. Chem. Int. Ed. Engl.* **1982**, *21*, 512-523.
- [39] Toniolo, C. *CRC Crit. Rev. Biochem.* **1980**, *9*, 1-44.
- [40] Cardillo, G.; Gentilucci, L.; Tolomelli, A.; Spinosa, R.; Calienni, M.; Qasem, A. R.; Spampinato, S. *J. Med. Chem.* **2004**, *47*, 5198-5203.
- [41] Gentilucci, L.; Squassabia, F.; Artali, R. *Curr. Drug Targets* **2007**, *8*, 185-196.
- [42] Norgren, A. S.; Buttner, F.; Prabpai, S.; Kongsaree, P.; Arvidsson, P. I. *J. Org. Chem.* **2006**, *71*, 6814-6821.
- [43] Maulucci, N.; Chini, M. G.; Di Micco, S.; Izzo, I.; Cafaro, E.; Russo, A.; Gallinari, P.; Paolini, C.; Nardi, M. C.; Casapullo, A.; Riccio, R.; Bifulco, G.; De Riccardis, F. *J. Am. Chem. Soc.* **2007**, *129*, 3007-3012.
- [44] Henry, C.; Moitessier, N.; Chapleur, Y. *Mini Rev. Med. Chem.* **2002**, *2*, 531-542.
- [45] R. Haubner, R. Gratias, B. Diefenbach, S. L. Goodman, A. Jonczyk, H. Kessler. *J. Am. Chem. Soc.* **1996**, *118*, 7461-7462.

## Chapter 3

# Synthesis and Conformational Analysis of Cyclotetrapeptide Mimetic $\beta$ -Turn Templates and Validation as 3D Scaffolds

---

### 3. Introduction

The initial event that is essential for modulating a biological response is molecular recognition between a ligand and a receptor.

For peptide or protein ligands, recognition generally involves the interaction of restricted portions of the outer 3D surface with a complementary surface on the receptor. Peptide backbones generally serve as scaffolds for the key side chains that participate in the interaction. Very often, the backbones adopt secondary structure motifs, g- or b-turns, or various kinds of helices. As a consequence, the bioactive compounds can, in principle, be substituted by smaller, simpler molecules that mimic the folded architectures<sup>[1]</sup>.

In particular, cyclic peptides have been widely used as templates for the design of turn-like structures<sup>[1, 2]</sup>. However, small cyclic tetrapeptides<sup>[3]</sup> are difficult to synthesize, and they usually display mixtures of conformers due to cis/trans isomerization of peptide bonds. Conversely, larger cyclic penta- and hexapeptides are easier to prepare, but they retain significant backbone flexibility<sup>[4]</sup>.

Concerning peptidomimetic and nonpeptidic scaffolds<sup>[1,2,5]</sup>, several examples of cyclic, bicyclic, and spirocyclic compounds have been reported as turn-mimicking structures. Nevertheless, several cases have met with more limited success when the turn itself contains most of the pharmacophore elements<sup>[1a,6]</sup>.

Therefore, cyclic peptides maintain their appeal as templates for applications in medicinal chemistry. In the last few years, it has been reported that cyclic tetrapeptide structures enlarged by the introduction of a  $\beta$ -amino acid may render the structures easier to synthesize and conformationally more stable<sup>[7]</sup>. Very recently, we further customized a cyclotetrapeptide structure by implementation of a partially modified retro-inverso<sup>[8]</sup> (PMRI) sequence. A 1,2-diamine was used as  $\beta$ -amino acid analogue, and a malonic acid completed the sequence<sup>[9]</sup>. Conformational analysis revealed that the PMRI models containing an unsubstituted diamine exhibit notable flexibility. In contrast, the presence of a chiral, substituted 1,2-diamine (compound 1, Figure 1) rendered the backbone more rigid, inducing  $\beta$ -turn structures and showing alternative conformations with respect to those of previously reported cyclotetrapeptide mimetics<sup>[7]</sup>.

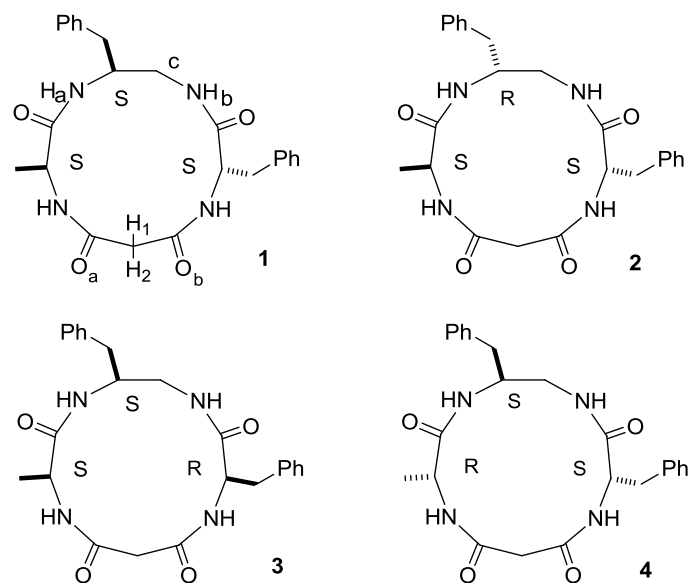
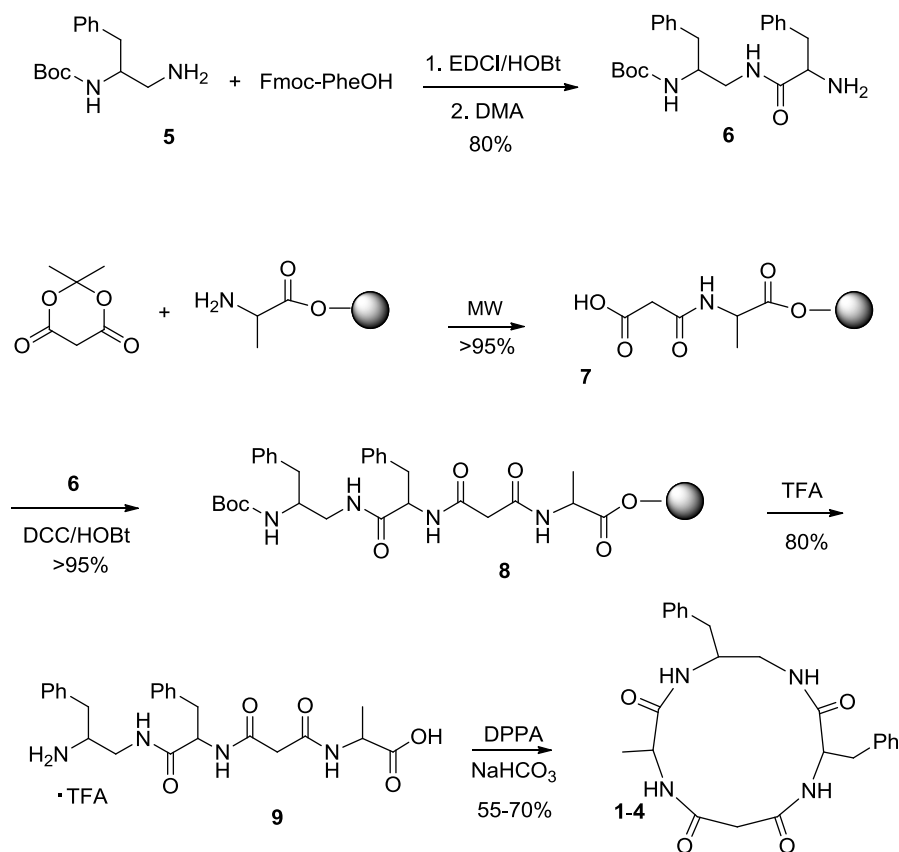


**Fig. (1).** Structure of the partially modified retro-inverso cyclic tetrapeptide models 1-4

Herein we describe the syntheses and conformational analyses of all stereoisomers of PMRI cyclotetrapeptide models of the general sequence cyclo-[bPhe-yACHTUNG TRENUNG(NHCO)Ala-yACHTUNG TRENUNG(NHCO)Gly-Phe], obtained by introducing a chiral (S)- or (R)-1,2-diamine<sup>[10]</sup> as a b2-amino acid mimetic, (S)- or (R)-phenylalanine, (S)- or (R)- alanine, and a malonyl residue (Figure 1). Furthermore, we provide preliminary validation of these compounds as effective scaffolds for the design of molecules with predictable 3D displays of the pharmacophores, useful for targeting specific bioactive conformations. As a prototypic example, we used those models for testing some selected novel RGD peptidomimetic compounds capable of interfering with integrin receptors.

We prepared models 1–4 as shown in Scheme 1, with the remaining being the enantiomers. The cyclic tetrapeptide analogues were prepared by solid-phase coupling of two dipeptide analogues **6** and **7**. Fragment **6** was prepared by a standard solution-phase procedure by coupling Fmoc-Phe-OH and Boc-protected diamine **5**<sup>[10b,11]</sup>, obtained, in turn, by reduction of Boc-PheNH<sub>2</sub> with BH<sub>3</sub><sup>[12]</sup>. The dipeptide was deprotected with dimethylamine (DMA), and the resulting crude product **6** was used without purification. Wang resin pre-loaded with alanine was treated with Meldrum's acid under microwave irradiation (MW) at 300 W. The complete conversion of resin-supported alanine to the dipeptide acid **7** was monitored by Kaiser's test. The solid-phase coupling of **7** with **6** afforded the tetrapeptide **8**. Subsequent cleavage from the resin with trifluoroacetic acid (TFA) and scavengers gave **9**, which was subjected to cyclization by treatment with diphenylphosphorylazide (DPPA). After 48 h, the cyclic tetrapeptide analogues were isolated in 55–70% yield (cyclization step) by semipreparative RPHPLC, and were 92–95% pure as determined by analytical RPHPLC.



**Scheme 1.** Synthesis of partially modified retro-inverso cyclic models **1-4**.

The presence of stereoisomers originating from epimerization was excluded on the basis of HPLC–ESMS and  $^1\text{H}$  NMR analyses.

The 3D structures of models **1-4** were investigated by NMR spectroscopy and molecular dynamics (MD) simulations. The NMR analysis was conducted using standard techniques at 400 MHz in the biomimetic medium  $[\text{D}_6]\text{DMSO}/\text{H}_2\text{O}$  8:2<sup>[13]</sup>; (the compounds were nearly insoluble in water). For **1** and **3**, the analyses generally confirmed the results previously obtained in  $[\text{D}_6]\text{DMSO}$ <sup>[9]</sup>, with few differences. In any case, their conformational features are discussed herein for comparison.

For each peptide,  $^1\text{H}$  NMR data revealed a single set of resonances, indicative of conformational homogeneity or a fast equilibrium<sup>[4]</sup>. COSY analysis allowed unambiguous assignment of the resonances. Variable temperature (VT)- $^1\text{H}$  NMR experiments were used to deduce the presence of H bonds involving amide protons (Table 1)<sup>[14]</sup>. For **1**, **3**, and **4**, the comparatively low  $\Delta\delta/\Delta T$  values of diamine NHa and NHb (Figures 1, and 2) with respect to PheNH and AlaNH suggest the presence of secondary structures in equilibrium, alternatively stabilized by H bonds involving NHa or NHb, whereas for **2**, only the NHb amide proton seems to be H bonded.

<b>Table 1.</b> $\Delta\delta/\Delta T$ values [ppbK <sup>-1</sup> ] of amide protons for <b>1–4</b> determined by VT- <sup>1</sup> H NMR. <sup>[a]</sup>				
Compd	PheNH	AlaNH	NH <sup>a[b]</sup>	NH <sup>b[b]</sup>
<b>1</b>	−5.0	−6.0	+ 1.2	−1.3
<b>2</b>	−6.0	−5.6	−4.5	−2.0
<b>3</b>	−3.5	−4.1	−1.3	−0.4
<b>4</b>	−3.9	−2.8	−0.75	−1.5

[a] Determined in [D<sub>6</sub>]DMSO/H<sub>2</sub>O (8:2) at 400 MHz over the range  $T=298\text{--}338$  K. [b] NH<sup>a</sup> and NH<sup>b</sup>, see Figures 1 and 2.

Molecular backbone conformations were investigated by 2D ROESY. The full list of ROESY crosspeaks is given in the Supporting Information (S.I.).

The analyses indicated that the cyclic tetrapeptide analogues adopt all-trans conformations of the w bonds, deduced from the absence of Hai-Hai+1 cross-peaks, indicative of cis peptide bonds. Structures consistent with the spectroscopic analyses were obtained by restrained MD, using the distances obtained from ROESY as constraints, and minimized with the AMBER<sup>[15]</sup> force field, with  $\epsilon=4x$ r. Simulations were conducted in vacuo by using a set of 50 random structures generated by an unrestrained high-temperature MD. The structures were subjected to restrained MD with a scaled force field, followed by a high-temperature simulation with full restraints.

Finally, the system was gradually cooled, and the structures were minimized. The conformations with the lowest internal energy and the fewest number of violations of the experimental data were selected and analyzed (Figure 2 and S.I.).

The vastmajority of the structures calculated for **1** and **2** by restrained MD did not show any violations of the restraints, and were well ordered. For **3** and **4**, on the other hand, the computations essentially gave two families of structures, **3a/3b** and **4a/4b** ( Figure 2), with nearly the same energy, differing exclusively, each showing some constraintviolations.

As expected, for **1** and **3**, the analyses confirmed the results previously obtained in [D<sub>6</sub>]DMSO<sup>[9]</sup>.

To estimate the dynamic behavior of the cyclopeptides in water, and in particular to determine secondary structures stabilized by H bonds, the structures derived from ROESY were analyzed by unrestrained MD for 10 ns in a box of explicit, equilibrated water molecules. During the simulations, the structural features deduced by ROESY were maintained, and the examination of the trajectories revealed the occurrence of H bonds in agreement with VT-NMR analysis, not explicitly revealed by ROESY.

The representative structure of **1** calculated by ROESY-restrained MD in Figure 2 is compatible with a type I  $\beta$ -turn centered on Phe-diamine, and a second one centered on Ala-diamine.

This structure shows no H bonds. However, analysis of the trajectories of the unrestrained MD revealed the presence of the two  $\beta$ -turn conformations in equilibrium, with NH<sub>a</sub> and NH<sub>b</sub> either alternately or simultaneously engaged in explicit H bonds with CO<sub>b</sub> and CO<sub>a</sub>, respectively (S.I.).

Concerning compound **2**, the ROESY-derived conformation shows a distinct H bond between NHb and COa, as anticipated on the basis of VT-NMR, and an overall type II  $\beta$ -turn conformation on Ala-diamine (Figure 2). This conformation was very stable during the unrestrained MD simulation.

The occurrence of two slightly different structures for **3** and **4** reflects the observation of contradictory ROESY cross-peaks between H<sup>1</sup>/H<sup>2</sup> protons and PheNH or AlaNH (Figure 2). In **3**, both AlaNH and PheNH show strong cross-peaks with H<sup>1</sup>, and this situation is compatible with the structure **3a**. On the other hand, PheNH also gives a cross-peak of medium intensity with H<sup>2</sup>. Moreover, while AlaNH gives a medium cross-peak with AlaHa, PheNH gives a strong cross-peak with PheHa. These observations are compatible with the structure **3b**, showing PheNH reversed relative to its position in **3a**. Both **3a** and **3b** are compatible with a type I  $\beta$ -turn on the Ala-diamine fragment, and **3a** manifests an explicit H bond between NHb and COa. Compound **3b** is also compatible with a type I  $\beta$ -turn on Phe-diamine. The two structures **3a/3b** reasonably represent conformers in equilibrium. However, **3b** shows fewer distance violations and a structure more compatible with VT-NMR data, which are suggestive of two H bonds on both NHa and NHb.

Unrestrained MD simulations performed on **3a** confirmed the stability of the H bonded structure. The unrestrained MD performed on **3b** show the H bonded structures involving NHa and/or NHb (S.I.). The simulations failed to reproduce the inversion of PheNH; evidently, this rotation is slow relative to the time selected for the simulation.

In a similar manner as with **3**, for compound **4** the strong cross-peaks between H<sup>2</sup> and both AlaNH and PheNH account for the structure **4a**, compatible with a type I  $\beta$ -turn centered on Phe-diamine. On the other hand, the cross-peak of medium intensity between AlaNH and H<sup>1</sup>, and the strong cross-peak between AlaNH and AlaHa account for the structure **4b**, (Figure 2) characterized by a reversed orientation of AlaNH, compatible with a type I  $\beta$ -turn centered on Phe-diamine, and a second one on Ala-diamine. As for **3a/3b**, the two structures **4a/4b** likely represent conformers in equilibrium. During the unrestrained MD performed on **4a** and **4b**, analysis of the trajectories revealed the presence H bonded structures involving NHa and NHb (S.I.), as suggested by VT-NMR data.

In summary, compounds **1** and **2** show stable preferred backbone conformations, although **1** presents modest residual flexibility. The diastereomers **3** and **4** exhibit two slightly different conformers **a** and **b** in equilibrium; nevertheless, the overall 3D displays of the side chains are almost coincident. Notably, the different stereoisomers tend to adopt a similar 3D structure, with a  $\beta$ -turn centered on Ala-diamine and a second  $\beta$ -turn on Phe-diamine (with the exception of **2**), regardless of the stereochemistry assortment. This observation is not trivial; indeed, it is generally observed that the stereochemistry inversion of a distinct residue in a cyclic peptide leads to alternative secondary structures<sup>[4, 8b, 16]</sup>. This difference can be ascribed to the peculiar structure of the mimetics. Apparently, the PMRI cyclotrapeptides show a strong tendency to stabilize type I or type II  $\beta$ -turn conformations involving the diamine amide protons.

It is accepted that the conformation of a cyclic peptide is scarcely controlled by the precise nature of the residues<sup>[4, 8b]</sup>.

Therefore, the  $\beta$ -turn templates **1–4** and the respective enantiomers **5–8** can be used as topologically defined scaffolds for the design of biologically active compounds that having their pharmacophoric side chains in precise and well-defined diverse spatial arrangements. A schematic topographic depiction of the

eight stereoisomeric PMRI cyclotetrapeptide models, simplified according to the Dunitz–Waser concept<sup>[8b, 17]</sup>, is shown in Figure 3. Relevant distances (in Å) between the C $\beta$  atoms of the residues and H bonds are also shown.

To endorse the effectiveness of the novel PMRI scaffolds in medicinal chemistry, we used a selection of the models described above for the design of some unprecedented RGD peptidomimetic compounds capable of interfering with integrin receptors<sup>[18]</sup>. Integrins are a large family of heterodimeric transmembrane receptors involved in cell–cell adhesion and in the adhesion of cells to proteins of the extracellular matrix, such as fibronectin and vitronectin, as well as in signal transduction.

Integrins are also involved in many major diseases, including cancer, asthma, thrombosis, osteoporosis, and atherosclerosis.

Among the various kinds of integrins,  $\alpha_v\beta_3$ -integrins are generally considered privileged targets for anticancer therapy.

Many types of integrins, including  $\alpha_v\beta_3$ , bind their ligands by recognition of the same tripeptide motif: the Arg-Gly-Asp (RGD) sequence. As a consequence, many RGD-like ligands have been reported as  $\alpha_v\beta_3$ -integrin inhibitors. Massive SAR investigations of ligands based on peptide, peptidomimetic, or nonpeptide scaffolds have given detailed structural information about ligand–receptor interactions<sup>[1d, 4a, 19]</sup>. More recently, the crystal structure of the extracellular section of the receptor, with a cyclic RGD peptide bound to the active site, has been disclosed<sup>[20]</sup>, providing the opportunity to design novel antagonists based on the receptor-bound conformation of the RGD tripeptide<sup>[21]</sup>.

In essence, the criteria for designing effective  $\alpha_v\beta_3$ -integrin inhibitors reside in specific reciprocal orientations and distances between the Asp and Arg side chains, and in the orientation and analyzed (Figure 2 and S.I.).

The vast majority of the structures calculated for **1** and **2** by restrained MD did not show any violations of the restraints, and were well ordered. For **3** and **4**, on the other hand, the computations essentially gave two families of structures, **3a/3b** and **4a/4b** (Figure 2), with nearly the same energy, differing exclusively by the opposite orientation of PheNH, and AlaNH, respectively, each showing some constraint violations.

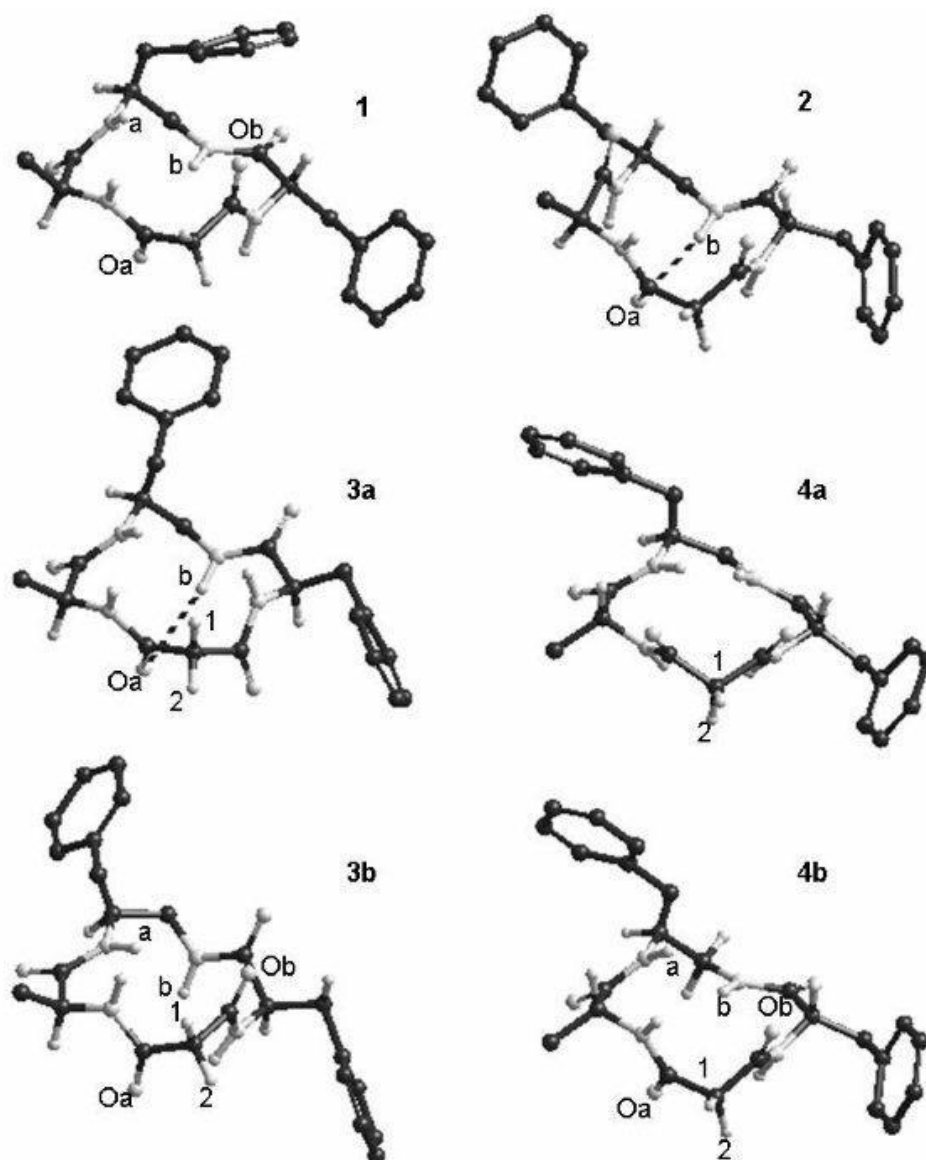


**Fig. (2).** Representative lowest-energy structure of 1-4 calculated by ROESY-restrained MD with the fewest violations of ROESY data

Formation of a third aromatic pharmacophore flanking Asp. Also, the presence of secondary structures in RGD ligands has often been correlated with specificity<sup>[19, 22]</sup>. For this purpose, based on models 1–3 and 7, we substituted Ala and Phe with Asp and Arg, respectively, to give the stereoisomeric cyclic PMRI RGD analogues 9–12 of general sequence cyclo-[bPhe-y- ACHTUNG TRENUNG(NHCO)Asp-y ACHTUNG TRENUNG(NHCO)Gly-Arg] (or cyclo-[bF-y ACHTUNG TRENUNG(NHCO)D-y ACHTUNG TRENUNG(NHCO)GR] in brief; Table 2). For this preliminary investigation, models 1 and 2 were selected on the basis of their comparatively higher conformational stability, while models 3 and 7 were tentatively chosen for comparison.

We tested the activity of 9–12 as integrin antagonists by measuring the percent inhibition of fibronectin adhesion to the  $\alpha_v\beta_3$ -integrin-expressing cell line SK-MEL-24 (human malignant melanoma)<sup>[23]</sup>. Fibronectin

was immobilized on each well of a standard assay plate. Cells were pre-incubated with the cyclopeptides and dispensed on the wells. After removal of nonadherent cells, the number of adherent cells was quantified by fluorimetry. The activity of potential antagonists was determined by the number of adherent cells relative to the control. Table 2 shows the sequences of RGD mimetics **9–12**, the corresponding parent models **1–3**, and **7**, and the inhibitory activity (%) of **9–12**, at a concentration of  $10^{-6}$ M, toward  $\alpha_v\beta_3$ -integrin-mediated cell adhesion. The activity of the well-known  $\alpha_v\beta_3$ -integrin antagonists Ac-DRGDS<sup>[23b]</sup> and GRGDNP<sup>[24]</sup>, assayed under the same conditions, was also measured as a positive control. For the inhibitory activity at various ligand concentrations, see the S.I.

<b>Table 2.</b> Inhibition of $\alpha_v\beta_3$ -integrin-mediated SK-MEL-24 cell adhesion of fibronectin in the presence of <b>9–12</b> , Ac-DRGDS, and GRGDNP.			
Ligand	Structure	Model	Inhibition [%] <sup>[a]</sup>
<b>9</b>	<i>cyclo</i> -[(S)- $\beta$ F- $\psi$ (NHCO)D- $\psi$ (NHCO)GR]	<b>1</b>	32 $\pm$ 3
<b>10</b>	<i>cyclo</i> -[(R)- $\beta$ F- $\psi$ (NHCO)D- $\psi$ (NHCO)GR]	<b>2</b>	55 $\pm$ 2
<b>11</b>	<i>cyclo</i> -[(S)- $\beta$ F- $\psi$ (NHCO)D- $\psi$ (NHCO)G-(R)-R]	<b>3</b>	43 $\pm$ 1
<b>12</b>	<i>cyclo</i> -[(S)- $\beta$ F- $\psi$ (NHCO)-(R)-D- $\psi$ (NHCO)GR]	<b>7</b>	35 $\pm$ 2
–	Ac-DRGDS	–	69 $\pm$ 1
–	GRGDNP	–	40 $\pm$ 3

[a] Determined at a compound concentration of  $10^{-6}$ M; values represent the mean  $\pm$  SEM of three experiments.

Statistical analysis reveals that all the compounds display significant and concentration-dependent potency in blocking SK-MEL-24 cell adhesion (S.I.). The biological activities of the four peptides vary radically ( $10 > 11 > 12 > 9$ ), although the constitution of the peptides is identical. This observation confirms the anticipation that compounds based on the PMRI cyclotetrapeptide models behave as topologically distinct structures.

These results can be tentatively rationalized by comparing the topographic depiction of the parent models **1–3** and **7** (Figure 3) with the structural requisites reported for  $\alpha_v\beta_3$ -integrin inhibitors (the conformations of **9–12** have not been reexamined <sup>[25]</sup>). An illustrative model of the bioactive conformation of a prototypic  $\alpha_v\beta_3$ -selective cyclopentapeptide ligand<sup>[19a, 26]</sup> is shown in Figure 4A<sup>[20, 21]</sup>. The simplified Dunitz–Waser sketch, Figure 4B and the relevant distances between the pharmacophoric groups and between the C $\beta$  atoms are also presented.

For the noteworthy conformational freedom of the side chains, the precise disposition of the pharmacophoric groups of a cyclopeptide in solution and in the bioactive conformation can be very different. For this reason, the 3D structure of a cyclopeptide is often characterized by the disposition of the C $\beta$  atoms with respect to the cyclopeptide scaffold<sup>[4a, 8b, 16, 19a]</sup>.

Therefore, the use of topographic models, such as those depicted in Figures 3 and 4B, can be very useful to compare the structures of different compounds. Compound **10** shows the best activity as an inhibitor of integrin-mediated adhesion; it is inferior, but still comparable to that of the reference compound Ac-DRGD (Table 2). It can be perceived that **10** (see model **2**, Figure 3) shows a comparatively higher topological similarity with the prototypic pharmacophore (Figure 4B) in comparison with the other compounds (see

models), both in terms of the orientations and distances between the C $\beta$  atoms. The lower activities displayed by **11** and **12** seem to be correlated with a short distance between the C $\beta$  atoms of Asp and Arg, and the diamine (models **3** and **7**, Figure 3). Interestingly, compound **9** shows the lowest inhibitory activity, despite having a similar disposition of Asp and Arg side chains with respect to **10** (based on the comparison of the parent models **1** and **2**), highlighting the role of the aromatic pharmacophoric group of the diamine. In conclusion, we have presented cyclotetrapeptide mimetic  $\beta$ -turn templates based on the retro-inverso concept, and we have described their conformational and topological features.

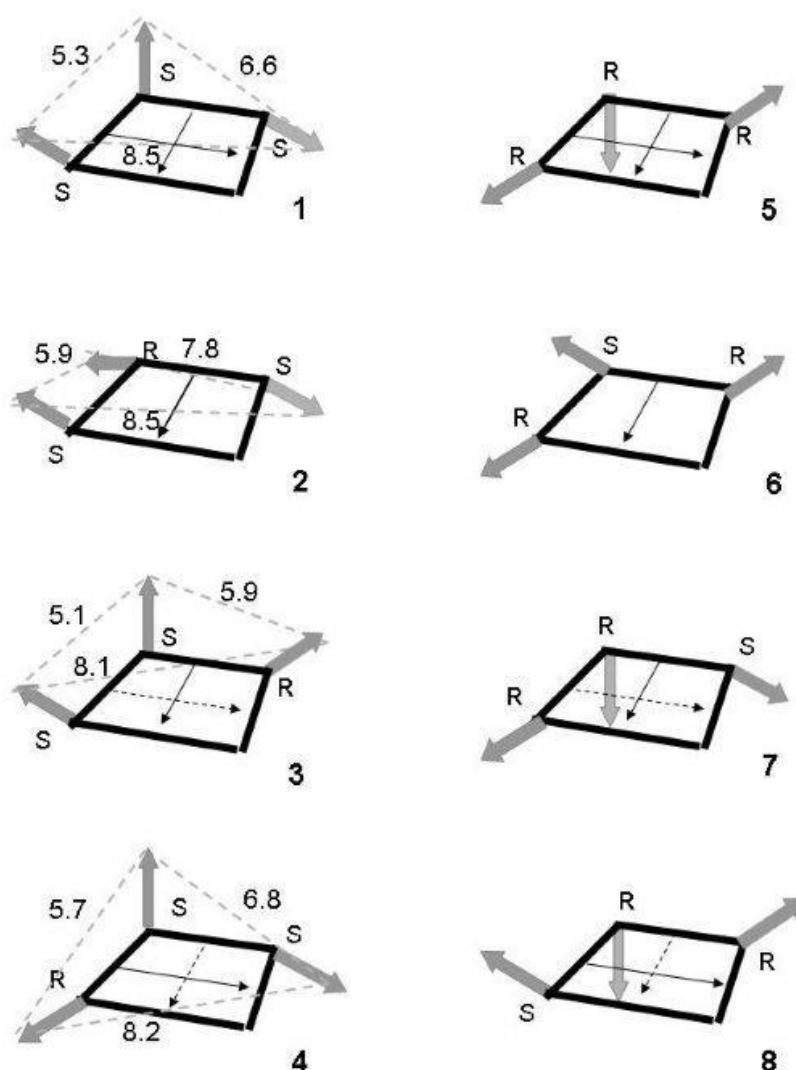


**Fig. (3).** Schematic topographic depiction of the PMRI cyclotetrapeptide models **1-4** and their respective enantiomers **5-8**, with the distance ( $\text{\AA}$ ) between the C $\beta$  atoms indicated. Large grey arrows show the pseudo-axial or pseudo-equatorial disposition of the side chains (C $\alpha$ -C $\beta$  vectors). Thin arrows indicate the H bonds.

The 3D structures are largely dominated by the tendency of the diamine residue to stabilize  $\beta$ -turn structures. As a consequence, the various stereoisomers can be viewed as diverse scaffolds assembled on a common

$\beta$ -turn template, which can find applications in medicinal chemistry. To confirm the assumptions, we prepared a selected set of RGD peptidomimetics based on the structures of the scaffold models.

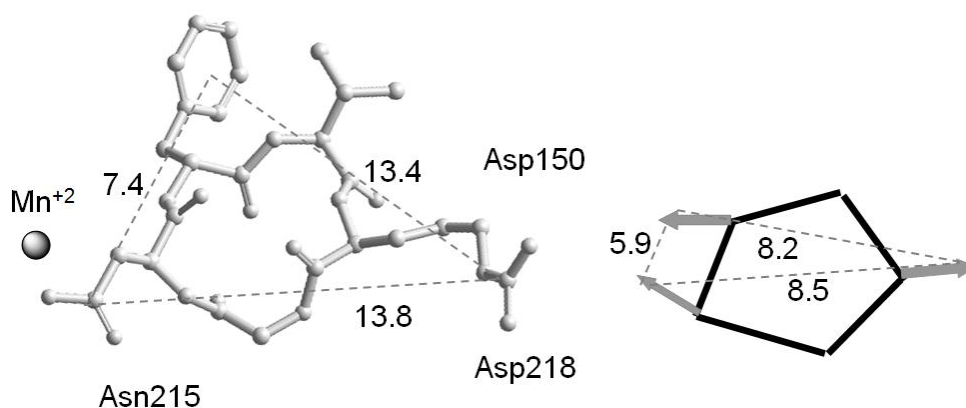


**Fig.(4).** Models of the bioactive conformation of the  $\alpha_v\beta_3$ -selective ligand cyclo-[RGDf(NMe)V], along with A) the distances (Å) between the pharmacophores, and B) between the C $\beta$  atoms of Asp, D-Phe, and Arg.

The biological assay gave evidence for a clear relationship between the supposed 3D structures of the RGD mimetics and the experimental activities as inhibitors of integrin-mediated cell adhesion.

### 3.1. Experimental Section

**3.1.1. General methods.** Unless stated otherwise, standard chemicals were obtained from commercial sources and used without further purification. Analytical RP-HPLC was performed with an ODS column (4.6  $\mu\text{m}$  particle size, 100 Å pore diameter, 250 mm, DAD 210 nm) using a linear gradient of H<sub>2</sub>O/CH<sub>3</sub>CN (9:12→2:8) over 20 min at a flow rate of 1.0 mLmin<sup>-1</sup>, followed by 10 min isocratic H<sub>2</sub>O/CH<sub>3</sub>CN 2:8. Chiral HPLC analysis was performed on a Chiralcel ODH column [0.46 cm ( $\varnothing$ ) x 25 cm (l)], n-hexane/2-propanol 85:15, at 0.8 mLmin<sup>-1</sup>. Semipreparative RP-HPLC was performed on a C18 column (7  $\mu\text{m}$  particle size, 21.2x150 mm) with a linear gradient of H<sub>2</sub>O/CH<sub>3</sub>CN (7:3→100% CH<sub>3</sub>CN) over 15 min, at a flow rate of 12 mLmin<sup>-1</sup>. Fluorimetry to evaluate the number of adherent cells was performed with a Victor2 multilabel counter. <sup>1</sup>H NMR spectra were recorded at 400 MHz at room temperature with 5- mm tubes, using 0.01<sub>M</sub> peptide. Chemical shifts ( $\delta$ ) are reported relative to the solvent peak. VT-<sup>1</sup>H NMR experiments were performed over the range T=298–348 K; 2D spectra were acquired in the phase-sensitive mode and processed using a 90° shifted, squared sine-bell apodization. <sup>1</sup>H NMR resonances were assigned from 2D gCOSY and 2D ROESY spectra; gCOSY experiments were recorded with a proton spectral width of 3103 Hz. ROESY experiments were recorded with a mixing time of 300 or 350 ms with a proton spectral width of 3088 Hz. Materials for bioassays were purchased from Invitrogen (Carlsbad, CA, USA) and Cambrex (Walkersville, MD, USA). SK-MEL-24 (human malignant melanoma) cells were obtained from American Type Culture Collection (ATCC, Rockville, MD, USA). Plates (96-well) were obtained from Corning, New York, NY, USA. The Victor2 multilabel counter was obtained from PerkinElmer (Waltham, MA, USA).

**3.1.2. Synthesis of 6.** HOBt (0.12 g, 0.9 mmol) was added to a stirred solution of Fmoc-Phe-OH (0.29 g, 0.75 mmol) in 9/1 CH<sub>2</sub>Cl<sub>2</sub>/DMF (9:1, 10 mL) at room temperature. After 10 min, 5<sup>[10b,11]</sup> (0.19 g, 0.75 mmol, 94% pure by chiral HPLC analysis, see General methods), EDCI·HCl salt (0.19 g, 0.9 mmol) and TEA (0.15 mL, 1.1 mmol) were added while stirring at room temperature. After 3 h, the mixture was diluted with CH<sub>2</sub>Cl<sub>2</sub>, and the solution was washed with 0.5M HCl, and saturated Na<sub>2</sub>CO<sub>3</sub>. The organic layer was dried over Na<sub>2</sub>SO<sub>4</sub>, and the solvent was removed at reduced pressure. The protected dipeptide was isolated by crystallization from CH<sub>2</sub>Cl<sub>2</sub>/ Et<sub>2</sub>O (0.39 g, 83 %, 85% pure by RP-HPLC). ESMS m/z: 620.3 [M+1]; calcd: 620.3. The crude protected dipeptide was treated while under magnetic stirring with 2M DMA in THF (5 mL) at room temperature. After 30 min, the solution was evaporated at reduced pressure, and the treatment was repeated. The residue was triturated in n-hexane. The dipeptide 6 (0.23 g, 96%, 82% pure by RPHPLC) was used without further purification. ESMS m/z: 398.3 [M+1], calcd: 398.2.

**3.1.3. Synthesis of 9.** Wang resin pre-loaded with alanine (0.5 g, 0.6 (mmol Ala)g<sup>-1</sup>) was suspended in DMF (4 mL) and treated with Meldrum's acid (0.36 g, 2.4 mmol). The suspension was heated by MW irradiation at 300 W. After 90 min, the resin was filtered and washed with MeOH, DMF, and CH<sub>2</sub>Cl<sub>2</sub> (5 mL each), and the procedure was repeated twice. The complete conversion of resin-supported Ala to the resin-bound dipeptide acid 7 was monitored by Kaiser's test. The resin-bound dipeptide 7 was suspended in CH<sub>2</sub>Cl<sub>2</sub> (5 mL) and treated with 6 (0.24 g, 0.6 mmol), DCC (0.13 g, 0.7 mmol), and HOBt (0.10 g, 0.8 mmol). The mixture was mechanically shaken for 6 h. The mixture was then filtered, and the resin was washed with MeOH, DMF, and CH<sub>2</sub>Cl<sub>2</sub> (5 mL each). The washing procedure was repeated twice.

**3.1.4. Peptide cleavage.** The resulting resin-bound 8 was suspended in a mixture of TFA (5 mL), H<sub>2</sub>O (0.15 mL), TIPS (0.1 mL), and PhOH (0.15 g), and mechanically shaken at room temperature. After 2 h, the mixture was filtered, the resin was washed twice with 10% TFA in Et<sub>2</sub>O (5 mL), and twice with Et<sub>2</sub>O. The collected filtrates were evaporated, and the residue was precipitated from ice-cold Et<sub>2</sub>O. The resulting precipitate was centrifuged at 4000 rpm (ALC Centrifugette 4206), and the crude solid peptide·TFA salt 9 was crystallized from MeOH/Et<sub>2</sub>O (0.14 g, 80 %, 82% pure by RP-HPLC). ESMS m/z: 455.3 [M+1]; calcd: 455.2.

**3.1.5. Cyclization to 1–4.** The peptide·TFA salt 9 (0.14 g, 0.24 mmol) was dissolved in dry DMF (60 mL) and treated, while under magnetic stirring, with NaHCO<sub>3</sub> (0.25 g, 3 mmol) and DPPA (0.17 g, 0.6 mmol) at room temperature. After 72 h, the mixture was filtered, and the solvent was distilled at reduced pressure. The residue was diluted with H<sub>2</sub>O (5 mL), and the mixture was extracted with EtOAc (4x20 mL). The collected organic layers were dried over Na<sub>2</sub>SO<sub>4</sub>, and the solvent was evaporated at reduced pressure. The oily residue was purified by semipreparative RP-HPLC to afford the cyclopeptides 1–4 (0.58–0.73 g, 55–70% yield, 92–95% pure by RP-HPLC). ES MS m/z: 437.3 [M+1]; calcd: 437.2.

**3.2. Conformational analysis.** The restrained MD simulations were conducted using the AMBER<sup>[15]</sup> force field with a distance-dependent  $\epsilon=4\epsilon_r$ . A 100-ps simulation at 1200 K was used for generating 50 random

structures that were subsequently subjected to a 20-ps restrained MD with a 50% scaled force field at the same temperature, followed by 20 ps with full restraints (distance force constant: 7 kcalmol<sup>-1</sup>·Å<sup>-2</sup>), after which the system was cooled over 10 ps to 50 K. Due to the absence of H<sub>ai</sub> and H<sub>ai+1</sub> ROESY cross-peaks, the w bonds were set at 1808 (force constant: 16 kcalmol<sup>-1</sup>·Å<sup>-2</sup>). Only ROESY-derived constraints were included in the restrained MD.

H bond interactions as well as torsion angle restraints were excluded. ROESY intensities were classified as very strong, strong, medium, and weak, and were associated with distances of 2.3, 2.6, 3.0, and 4.0 Å, respectively. Geminal couplings and other clear correlations were discarded. The resulting structures were minimized with 3000 cycles of steepest descent and 3000 cycles of conjugated gradient (convergence: 0.01 kcal<sup>-1</sup>mol<sup>-1</sup>). The structures that showed the lowest internal energy and the fewest violations of the experimental data were selected and analyzed. MD simulation in explicit water was performed for 10.0 ns at 298 K using the AMBER force field in a 30x30x30 x3 box of standard TIP3P models of equilibrated water<sup>[27]</sup>, with a minimum solvent–solute distance of 2.3Å, at constant temperature and pressure (Berendsen scheme<sup>[28]</sup>, bath relaxation constant: 0.2).

**3.3. Cell adhesion assays.** SK-MEL-24 cells were routinely grown in minimal essential medium (MEM) supplemented with 10% fetal bovine serum, nonessential amino acids, and sodium pyruvate.

Cells were kept at 37°C in a 5% CO<sub>2</sub> humidified atmosphere.

Plates (96-well) were coated by passive adsorption with fibronectin (10 mgmL<sup>-1</sup>) overnight at 4°C. Cells were counted and exposed to the drug at three different concentrations (10<sup>-8</sup>, 10<sup>-6</sup>, and 10<sup>-4</sup>M) for 30 min at room temperature to allow ligand–receptor equilibrium.

Stock solutions (10<sup>-2</sup>M) of the assayed compounds were prepared in 33% DMSO and 66% phosphate buffered saline (PBS) (v/ v), and were further diluted with PBS alone. Control cells were exposed to the same concentration of DMSO (vehicle). At the end of the incubation time, the cells were plated (50000 cells per well) and incubated at room temperature for 1 h. All the wells were then washed with PBS to remove the nonadherent cells, and the hexosaminidase substrate, 4-nitrophenyl-N-acetyl-b-d-glucosaminide (50 mL, dissolved at 7.5 mM in 0.09M citrate buffer solution, pH 5, and mixed with an equal volume of 0.5% Triton X-100 in H<sub>2</sub>O), was added. This product is a chromogenic substrate for β-Nacetylglucosaminidase that is transformed in 4-nitrophenol, the absorbance of which is measured at λ=405 nm. As previously described<sup>[29]</sup>, there is a linear correlation between absorbance and enzymatic activity. It is therefore possible to identify the number of adherent cells in treated wells, interpolating the absorbance values of the unknowns in a calibration curve. The reaction was blocked by adding 100 μL stop solution (50 μm glycine, 5 μm EDTA, pH 10.4), and the plate was read in a multilabel counter. Experiments were carried out in triplicate. All data are expressed as the mean ±SEM for the number of experiments indicated. Statistical comparisons were made by ANOVA and post hoc Dunnet's or Turkey's tests with differences of p<0.05 considered significant. Data were analyzed using Prism 5.0 software (GraphPad Software Inc., San Diego, CA, USA).

### 3.4 Supporting Information

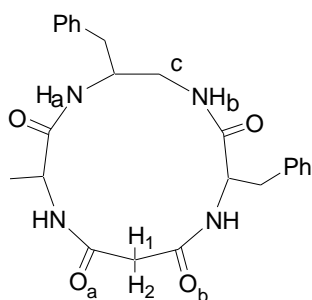


Figure S1. Structures of 1-4

**Characterization of 1-4.** Residue stereochemistry has been omitted; NHa, NHb, Hc, H<sub>1</sub>, H<sub>2</sub>, see Figure S1.

c[βPhe-ψ(NHCO)-Ala-ψ(NHCO)-Gly-Phe] (**1**). 94% pure by RP-HPLC. ES-MS m/z: 437.1 (M+1); calcd: 437.2; <sup>1</sup>H-NMR (8/2 DMSO-d<sub>6</sub>/H<sub>2</sub>O): 1.06 (d, J=7.1 Hz, 3H, CH<sub>3</sub>), 2.60 (dd, J=9.8, 13.8 Hz, 1H, diamHβ), 2.73 (dd, J=5.6, 13.8 Hz, 1H, diamHβ), 2.90 (dd, J=8.5, 14.7 Hz, 1H, PheHβ), 2.90-3.10 (m, 2H, Hc), 3.11 (dd, J=3.6, 14.7 Hz, 1H, PheHβ), 3.15 (d, J=10.2, 1H, H<sub>1</sub>), 3.20 (d, J=10.2, 1H, H<sub>2</sub>), 3.90 (dq, J=5.7, 7.5 Hz, 1H, AlaHα), 3.90-3.99 (m, 1H, diamHα), 4.30-4.40 (m, 1H, PheHα), 6.13 (d, J=8.3 Hz, 1H, NHa), 6.81 (br.t, 1H, NHb); 7.06-7.17 (m, 10H, ArH), 8.99 (br.d, 1H, AlaNH), 9.02 (br.d, 1H, PheNH); [α]<sup>20</sup><sub>D</sub> = -1.6 (c 1.2, MeOH).

c[D-βPhe-ψ(NHCO)-Ala-ψ(NHCO)-Gly-Phe] (**2**). 95% pure by RP-HPLC. ES-MS m/z: 437.2 (M+1); calcd: 437.2; <sup>1</sup>H-NMR (8/2 DMSO-d<sub>6</sub>/H<sub>2</sub>O): 1.09 (d, J=6.8 Hz, 3H, CH<sub>3</sub>), 2.68 (dd, J=6.4, 13.2 Hz, 1H, diamHβ), 2.75-2.82 (m, 1H, diamHβ), 2.82-2.90 (m, 1H, PheHβ), 2.90-3.00 (m, 1H, Hc), 3.00 (d, J=11.0, 1H, H<sub>1</sub>), 3.05 (d, J=11.0, 1H, H<sub>2</sub>), 3.00-3.10 (m, 1H, PheHβ), 3.40-3.50 (m, 1H, Hc), 3.61-3.72 (m, 1H, diamHα), 4.12 (quintet, J=7.2 Hz, 1H, AlaHα), 4.21-4.30 (m, 1H, PheHα), 7.06 (br.t, 1H, NHb), 7.22 (d, 1H, NHa), 7.12-7.24 (m, 5H, PheArH), 7.25-7.36 (m, 5H, diamArH), 8.52 (d, J=8.4 Hz, 1H, PheNH), 8.62 (d, J=7.2 Hz, 1H, AlaNH); [α]<sup>20</sup><sub>D</sub> = -12.5 (c 2.0, MeOH).

c[βPhe-ψ(NHCO)-Ala-ψ(NHCO)-Gly-D-Phe] (**3**). 92% pure by RP-HPLC. ES-MS m/z: 437.2 (M+1); calcd: 437.2; <sup>1</sup>H-NMR (8/2 DMSO-d<sub>6</sub>/H<sub>2</sub>O): 1.15 (d, J=7.1 Hz, 3H, CH<sub>3</sub>), 2.70 (dd, J=8.3, 14.1 Hz, 1H, diamHβ), 2.78 (dd, J=6.4, 14.1 Hz, 1H, diamHβ), 2.78-2.89 (m, 1H, Hc), 2.90 (d, J=10.4, 1H, H<sub>2</sub>), 3.00 (dd, J=9.6, 13.2 Hz, 1H, PheHβ), 3.19 (d, J=10.4, 1H, H<sub>1</sub>), 3.28 (dd, J=4.9, 13.2 Hz, 1H, PheHβ), 3.44-3.53 (m, 1H, Hc), 3.78-3.84 (m, 1H, diamHα), 3.89 (quintet, J=7.2 Hz, 1H, AlaHα), 4.10-4.21 (m, 1H, PheHα), 6.60 (d, J=7.9 Hz, 1H, NHa), 6.90 (br.t, 1H, NHb); 7.00-7.26 (m, 10H, ArH), 8.60 (d, J=7.4 Hz, 1H, PheNH), 8.69 (d, J=5.6 Hz, 1H, AlaNH); [α]<sup>20</sup><sub>D</sub> = +45.2 (c 0.8, MeOH).

c[βPhe-ψ(NHCO)-D-Ala-ψ(NHCO)-Gly-Phe] (**4**). 93% pure by RP-HPLC. ES-MS m/z: 437.2 (M+1); calcd: 437.2; <sup>1</sup>H-NMR (8/2 DMSO-d<sub>6</sub>/H<sub>2</sub>O): 1.08 (d, J=7.0 Hz, 3H, CH<sub>3</sub>), 2.65-2.70 (m, 2H, diamHβ), 2.70-2.79 (m, 1H, PheHβ), 2.80 (d, J=11.6, 1H, H<sub>1</sub>), 2.90 (dd, J=6.8, 14.0 Hz, 1H, Hc), 3.11 (dd, J=4.2, 14.2 Hz, 1H, PheHβ), 3.22 (d, J=11.6, 1H, H<sub>2</sub>), 3.45-3.55 (m, 1H, Hc), 3.85-3.96 (m, 1H, diamHα), 4.06 (quintet, J=7.2 Hz,

1H, AlaH $\alpha$ ), 4.38-4.46 (m, 1H, PheH $\alpha$ ), 6.99 (d, J=8.4 Hz, 1H, NHa), 7.09 (t, J=4.8 Hz, 1H, NHb); 7.15-7.22 (m, 5H, diamArH), 7.22-7.35 (m, 5H, PheArH), 8.29 (d, J=8.0 Hz, 1H, PheNH), 8.31 (d, J=7.2 Hz, 1H, AlaNH);  $[\alpha]_D^{20} = -14.1$  (c 0.6, MeOH).

**Tables S1-S4.** Non obvious ROESY cross-peaks observed for **1-4** in 8/2 DMSO-d<sub>6</sub>/H<sub>2</sub>O at 400 MHz (r.t.). Residue stereochemistry has been omitted. Very strong, strong, medium, weak cross peaks, have been associated to distances of 2.3, 2.6, 3.0, and 4.0 Å, respectively. NHa, NHb, Hc, H<sub>1</sub>, H<sub>2</sub>, see Figure S1.

Table S1, 1.

Cross peak	Intensity	Cross peak	Intensity
AlaNH-NHa	s	AlaNH-H1	vs
AlaNH-AlaH $\alpha$	m	AlaNH-H2	w
PheNH-H1	w	AlaNH-CH <sub>3</sub>	s
PheNH-H2	vs	PheNH-NHb	s
NHb-PheH $\alpha$	m	PheNH-PheH $\alpha$	m
NHa-NHb	m	NHb-NHbCH <sub>2</sub>	m
diamArH-diamH $\alpha$	m	diamArH-NHa	m
diamArH-NHb	m	diamH $\beta_{(2.7)}$ -diamArH	s
NHa-diamH $\beta_{(2.6)}$	m	NHa-AlaH $\alpha$	m
diamH $\alpha$ -Hc	s	NHa-diamH $\alpha$	m
diamH $\alpha$ -diamH $\beta$	m	PheH $\alpha$ -PheH $\beta_{(3.1)}$	m
PheH $\alpha$ -PheH $\beta_{(2.9)}$	m		

Table S2, 2.

Cross peak	Intensity	Cross peak	Intensity
AlaNH-NHa	w	PheNH-NHb	vs
PheNH-PheArH	m	AlaNH-Me	s
AlaNH-AlaH $\alpha$	m	AlaNH-H1	vs
PheNH-PheH $\alpha$	m/s	PheNH-PheH $\beta_{(2.8)}$	m
NHb-Hc <sub>(2.9)</sub>	s	PheNH-H2	vs
NHb-PheH $\alpha$	s	NHb-NHa	vs
NHa-AlaH $\alpha$	vs	NHb-diamH $\alpha$	m
diamArH-diamH $\alpha$	vs	NHa-diamH $\alpha$	s
NHa-Hc <sub>(2.9)</sub>	m	PheArH-PheH $\beta_{(3.0)}$	w
PheArH-PheH $\beta$	s	PheArH-PheH $\beta_{(2.8)}$	s
NHb-Hc <sub>(3.4)</sub>	m	diamArH-diamH $\beta_{(2.7)}$	m
diamArH-diamH $\beta_{(2.75)}$	m	diamH $\beta_{(2.7)}$ -NHa	s
PheH $\alpha$ -PheH $\beta_{(2.8)}$	m	PheH $\alpha$ -PheH $\beta_{(3.0)}$	s
diamH $\alpha$ -diamH $\beta_{(2.65)}$	s	diamH $\alpha$ -diamH $\beta_{(2.75)}$	w

Table S3, 3.

Cross peak	Intensity	Cross peak	Intensity
AlaNH-NHa	s	AlaNH-PheNH	w
AlaNH-AlaH $\alpha$	m	AlaNH-H1	vs
PheNH-H1	s	AlaNH-H2	w
PheNH-H2	m	AlaNH-CH <sub>3</sub>	w
NHb-PheH $\alpha$	s	PheNH-NHb	s
NHa-NHb	m	PheNH-PheH $\alpha$	s
diamH $\alpha$ -NHb	m	PheNH-NHa	w
NHb-HC <sub>(3.5)</sub>	m	NHb-HC <sub>(2.9)</sub>	vs
NHa-diamH $\beta$	s	NHa-AlaMe	m
NHa-HC <sub>(3.5)</sub>	w	NHa-AlaH $\alpha$	m
PheH $\alpha$ -PheH $\beta$ <sub>(3.3)</sub>	vs	NHa-diamH $\alpha$	s
PheH $\alpha$ -PheAr	s	PheH $\alpha$ -PheH $\beta$ <sub>(3.0)</sub>	m
diamH $\alpha$ -HC <sub>(3.5)</sub>	m	diamH $\alpha$ -diamH $\beta$	s
diamH $\alpha$ -diamH $\beta$	vs	diamH $\alpha$ -HC <sub>(2.9)</sub>	vs
HC <sub>(3.5)</sub> -diamH $\beta$	m	HC <sub>(3.5)</sub> -diamH $\beta$	s

Table S4, 4.

Cross peak	Intensity	Cross peak	Intensity
AlaNH-Me	m	AlaNH-H1	m
AlaNH-AlaH $\alpha$	s	AlaNH-NHa	m
AlaNH-H2	s	PheNH-H2	vs
PheNH-PheH $\alpha$	m	PheNH-NHb	s
PheNH-Phe $\beta$ <sub>(2.8)</sub>	m	NHb-HC <sub>(2.9)</sub>	s
NHb-diamH $\beta$	w	NHb-diamH $\alpha$	w
NHb-PheH $\alpha$	vs	NHb-PheNH	vs
NHb-HC <sub>(3.5)</sub>	m	NHa-diamH $\beta$	s
NHa-HC <sub>(2.9)</sub>	m	NHa-diamH $\alpha$	s
NHa-AlaH $\alpha$	vs	NHa-PheH $\alpha$	w
diamArH-HC <sub>(2.9)</sub>	m	diamArH-diamH $\beta$	vs
diamArH-diamH $\alpha$	vs	diamArH-AlaH $\alpha$	w
PheArH-PheH $\alpha$	vs	diamArH-HC <sub>(3.5)</sub>	m
PheH $\alpha$ -PheH $\beta$ <sub>(2.7)</sub>	m	PheH $\alpha$ -PheH $\beta$ <sub>(3.1)</sub>	s
diamH $\alpha$ -diamH $\beta$	vs	diamH $\alpha$ -HC <sub>(2.9)</sub>	m
diamH $\alpha$ -HC <sub>(3.5)</sub>	s		

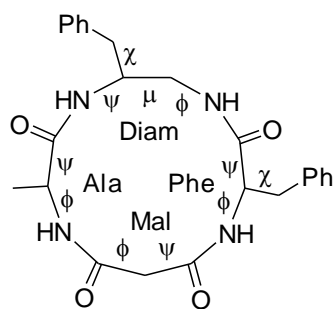


Figure S2. Torsion angles of **1-4**.

**Table S4.** Torsion angles of the NMR-derived structures of **1-4** (see Figure S2);  $\Psi$  bonds are all trans.

Compd	$\beta$ -Phe				Ala		Mal		Phe		
	$\phi$	$\mu$	$\psi$	$\chi$	$\phi$	$\psi$	$\phi$	$\psi$	$\phi$	$\psi$	$\chi$
<b>1</b>	-139	-44	-83	+75	-68	-37	-94	-75	-93	+19	-63
<b>2</b>	-108	-52	+133	+61	-84	+86	-76	-68	-127	+17	-55
<b>3a</b>	-111	-43	-94	-165	-77	-22	-132	+86	+122	-40	+58
<b>3b</b>	-124	+20	-147	-169	-109	-1	-76	-54	-64	-68	+57
<b>4a</b>	+174	-27	-127	-59	+142	-49	+83	-88	-141	+46	-65
<b>4b</b>	-151	-37	-101	-56	-52	-55	-73	-70	-131	+41	-63

Figures S3-S8. Stereoviews of **1-4** from Figure 2.

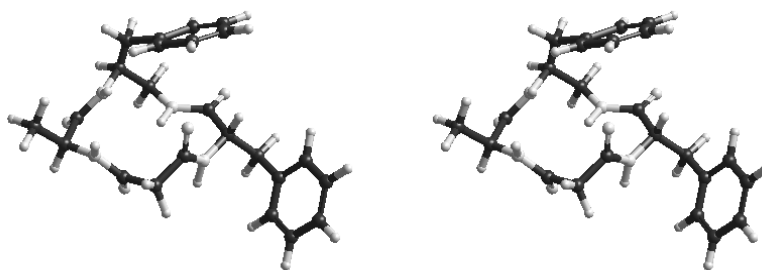
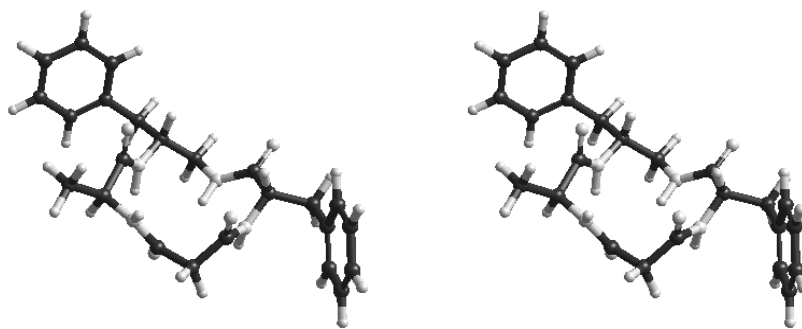


Figure S3. Stereo picture of **1**.



**Figure S4.** Stereo picture of 2.



**Figure S5.** Stereo picture of 3a.

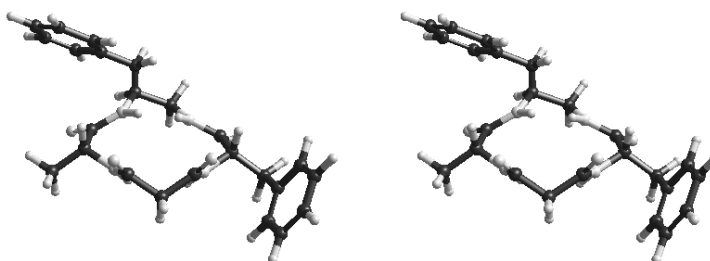


**Figure S6.** Stereo picture of 4a.

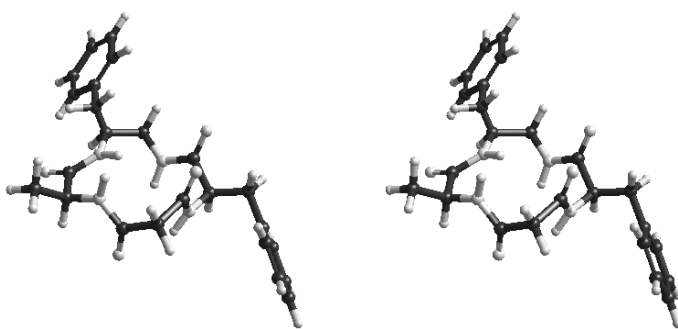


Figure S7. Stereo picture of 3b.

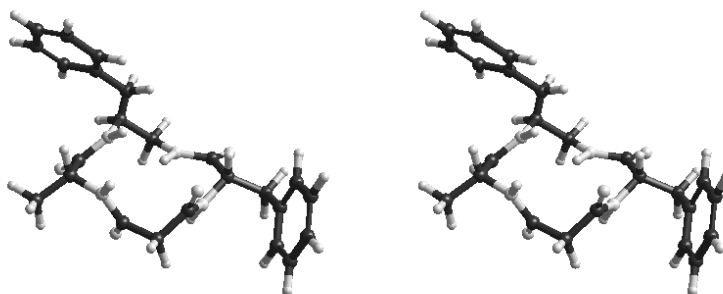


Figure S8. Stereo picture of 4b.

Figures S3-S6. Representative, minimized structures of 1, 3b, 4a, 4b, sampled during a 10 ns unrestrained MD simulation in explicit water, characterized by secondary structural elements stabilized by H-bonds.

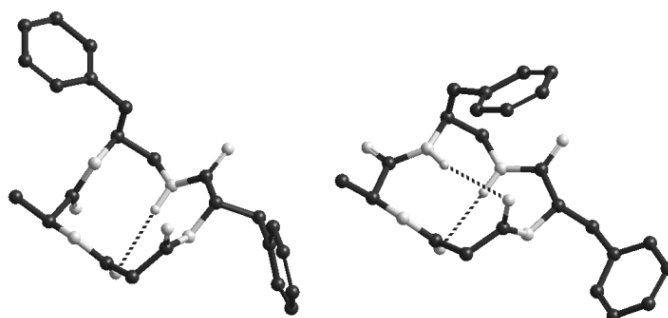


Figure S9. 1

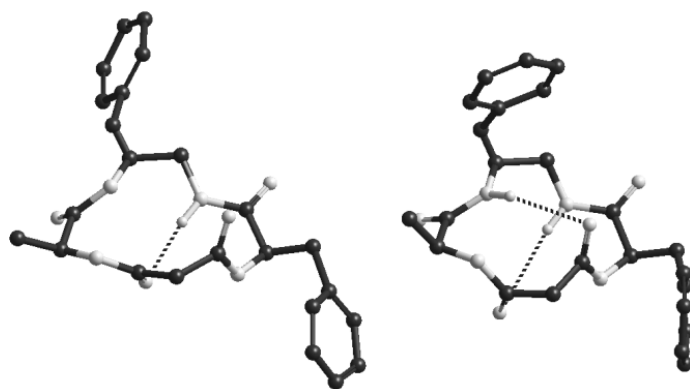


Figure S10. 3b

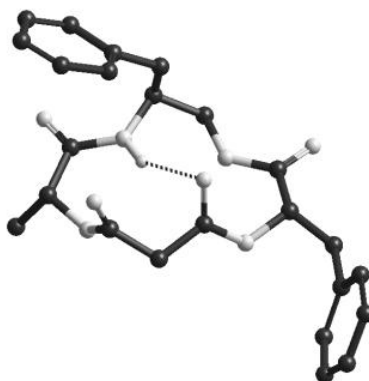


Figure S11. 4a

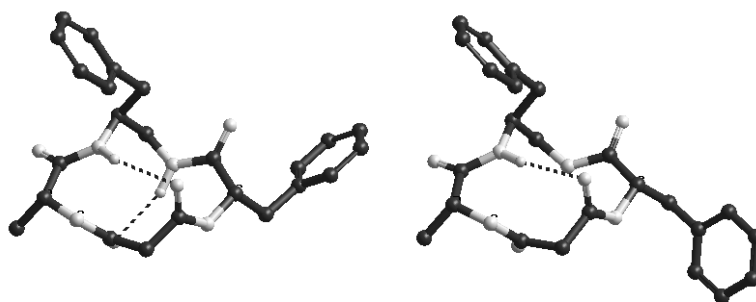
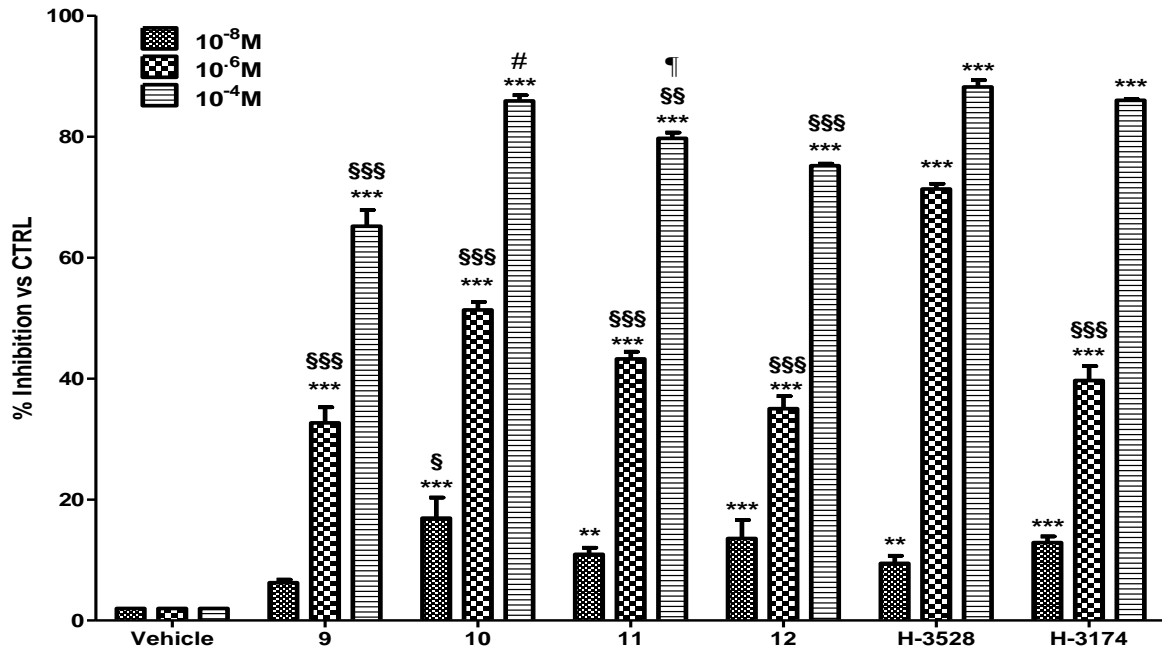


Figure S12. 4b



**Figure S13.** Inhibition (%) of  $\alpha_v\beta_3$  integrin-mediated SK-MEL-24 cell adhesion to fibronectin in the presence of **9-12** and of the reference compounds H-3528 (Ac-DRGDS) and H-3174 (GRGDNP) at three different concentrations ( $10^{-8}$ ;  $10^{-6}$ , and  $10^{-4}$  M). Control cells were treated with the vehicle alone as described under the experimental section. Data represent the means of triplicate determinations ( $n=3$ ) and the error bars indicate  $\pm$  SEM. One-way ANOVA was performed, followed by a Dunnet's multiple comparison test. \*\*\*  $p < 0.0001$  vs vehicle; \*\*  $p < 0.001$  vs vehicle; \$\$\$  $p < 0.0001$  vs H-3528 ( $10^{-4}$  M); \$\$  $p < 0.001$  vs H-3528 ( $10^{-4}$  M); \$  $p < 0.05$  vs H-3528 ( $10^{-4}$  M); #  $p < 0.05$  vs 9, 11 and 12 ( $10^{-4}$  M);  $p < 0.0001$  vs 9 ( $10^{-4}$  M).

## References and note

- [1] a) Hruby, V. J.; Balse, P. M.; *Curr. Med. Chem.* **2000**, *7*, 945–970; b) Tyndall, J. D. A.; Pfeiffer, B.; Abbenante, G.; Fairlie, D. P. *Chem. Rev.* **2005**, *105*, 793–826; c) Hruby, V. J.; Agnes, R. S. *Biopolymers* **1999**, *51*, 391–410; d) Gentilucci, L.; Tolomelli, A.; Squassabia, F. *Curr. Med. Chem.* **2006**, *13*, 2449–2466.
- [2] MacDonald, M.; Aub, J. *Curr. Org. Chem.* **2001**, *5*, 417–438.
- [3] a) Loiseau, N.; Gomis, J.-M.; Santolini, J.; Delaforge, M.; Andre, F. *Biopolymers* **2003**, *69*, 363–385; b) Mora, P.; Mas-Moruno, C.; Tamborero, S.; Cruz, L.; Perez-Paya, J. E.; Albericio, F. *J. Pept. Sci.* **2006**, *12*, 491–496.
- [4] a) Kessler, H. *Angew. Chem.* **1982**, *94*, 703–703; *Angew. Chem. Int. Ed. Engl.* **1982**, *21*, 512–523; b) Stradley, S. J.; Rizo, J.; Bruch, M. D.; Stroup, A. N.; Gierasch, L. M. *Biopolymers* **1990**, *29*, 263–287; c) Zhang, X. M.; Nikiforovich, G. V.; Marshall, G. R. *J. Med. Chem.* **2007**, *50*, 2921–2925.
- [5] Schneider, G.; Schneider, P.; Renner, S. *QSAR Comb. Sci.* **2006**, *25*, 1162–1171.
- [6] a) Giannis, A.; Kolter, T. *Angew. Chem.* **1993**, *105*, 1303–1326; *Angew. Chem. Int. Ed. Engl.* **1993**, *32*, 1244–1267; b) Gante, J. *Angew. Chem.* **1994**, *106*, 1780–1802; *Angew. Chem. Int. Ed. Engl.* **1994**, *33*, 1699–1720.
- [7] a) F. Schumann, A. Muller, M. Koksche, G. Muller, N. Sewald. *J. Am. Chem. Soc.* **2000**, *122*, 12009–12010; b) M. P. Glenn, M. J. Kelso, J. D. A. Tyndall, D. P. Fairlie. *J. Am. Chem. Soc.* **2003**, *125*, 640–641; c) A. S. Norgren, F. Buttner, S. Prabpai, P. Kongsaree, P. I. Arvidsson. *J. Org. Chem.* **2006**, *71*, 6814–6821; d) N. Maulucci, M. G. Chini, S. Di Micco, I. Izzo, E. Cafaro, A. Russo, P. Gallinari, C. Paolini, M. C. Nardi, A. Casapullo, R. Riccio, G. Bifulco, F. De Riccardis. *J. Am. Chem. Soc.* **2007**, *129*, 3007–3012.
- [8] a) M. Chorev, M. Goodman. *Acc. Chem. Res.* **1993**, *26*, 266–273; b) J. Wermuth, S. L. Goodman, A. Jonczyk, H. Kessler. *J. Am. Chem. Soc.* **1997**, *119*, 1328–1335; c) M. D. Fletcher, M. M. Campbell. *Chem. Rev.* **1998**, *98*, 763–795; d) K.-J. Kim, S.-W. Park, S. S. Yoon. *J. Kor. Chem. Soc.* **2000**, *44*, 286–289; e) Y. Han, C. Giragossian, D. F. Mierke, M. Chorev. *J. Org. Chem.* **2002**, *67*, 5085–5097; f) H. Tamamura, M. Mizumoto, K. Hiramatsu, S. Kusano, S. Terakubo, N. Yamamoto, J. O. Trent, Z. Wang, S. C. Peiper, H. Nakashima, A. Otaka, N. Fujii. *Org. Biomol. Chem.* **2004**, *2*, 1255–1257; g) M. Chorev. *Biopolymers* **2005**, *80*, 67–84; h) Y. S. Lee, R. S. Agnes, P. Davis, S.-W. Ma, H. Badghisi, J. Lai, F. Porreca, V. J. Hruby. *J. Med. Chem.* **2007**, *50*, 165–168.
- [9] L. Gentilucci, G. Cardillo, A. Tolomelli, S. Spampinato, A. Spartà, F. Squassabia. *Eur. J. Org. Chem.* **2008**, 729–735.
- [10] a) D. Lucet, T. Le Gall, C. Mioskowski. *Angew. Chem.* **1998**, *110*, 2724–2772; *Angew. Chem. Int. Ed.* **1998**, *37*, 2580–2627; b) V. Fedi, M. Altamura, G. Balacco, F. Canfarini, M. Criscuoli, D. Giannotti, A. Giolitti, S. Giuliani, A. Guidi, N. J. S. Harmat, R. Nannicini, F. Pasqui, R. Patacchini, E. Perrotta, M. Tramontana, A. Triolo, C. A. Maggi. *J. Med. Chem.* **2004**, *47*, 6935–6947.
- [11] a) H. Sajiki, K. Y. Ong. *Tetrahedron* **1996**, *52*, 14507–14514.
- [12] T. Morie, S. Kato, H. Harada, I. Fujiwara, K. Watanabe, J.-I. Matsumoto. *J. Chem. Soc. Perkin Trans.* **1994**, *1*, 2565–2569.
- [13] a) For a leading reference on the use of a cryoprotective [D<sub>6</sub>]DMSO/H<sub>2</sub>O mixture as a biomimetic medium, see: P. A. Temussi, D. Picone, G. Saviano, P. Amodeo, A. Motta, T. Tancredi, S. Salvadori, R.

- Tomatis. *Biopolymers* **1992**, 32, 367–372; b) L. Gentilucci, A. Tolomelli. *Curr. Topics Med. Chem.* **2004**, 4, 105–121, and references herein.
- [14] C. Toniolo. *CRC Crit. Rev. Biochem.* **1980**, 9, 1–44.
- [15] W. D. Cornell, P. Cieplak, C. I. Bayly, I. R. Gould, K. M. Merz, D. M. Ferguson, D. C. Spellmeyer, T. Fox, J. W. Caldwell, P. A. Kollman. *J. Am. Chem. Soc.* **1995**, 117, 5179–5197.
- [16] R. Haubner, R. Gratiyas, B. Diefenbach, S. L. Goodman, A. Joczzyk, H. Kessler. *J. Am. Chem. Soc.* **1996**, 118, 7461–7472.
- [17] a) J. D. Dunitz, J. Waser. *J. Am. Chem. Soc.* **1972**, 94, 5645–5650; b) H. Kessler, R. Gratiyas, G. Hessler, M. Gurrath, G. Muller. *Pure Appl. Chem.* **1996**, 68, 1201–1205.
- [18] G. P. Curley, H. Blum, M. J. Humphries. *Cell. Mol. Life Sci.* **1999**, 56, 427–441.
- [19] a) M. A. Dechantsreiter, E. Planker, B. Matha, E. Lohof, G. Holzemann, A. Jonczyk, S. L. Goodman, H. Kessler. *J. Med. Chem.* **1999**, 42, 3033–3040;  
b) C. Henry, N. Moitessier, Y. Chapleur. *Mini-Rev. Med. Chem.* **2002**, 2, 531–542; c) B. Cacciari, G. Spalluto. *Curr. Med. Chem.* **2005**, 12, 51–70.
- [20] J.-P. Xiong, T. Stehle, R. Zhang, A. Joachimiak, M. Frech, S. L. Goodman, M. Amin Arnaut. *Science* **2002**, 296, 151–155.
- [21] L. Marinelli, A. Lavecchia, K.-E. Gottschalk, E. Novellino, H. Kessler. *J. Med. Chem.* **2003**, 46, 4393–4404.
- [22] M. Gurrath, G. Muller, H. Kessler, M. Aumailley, R. Timpl. *Eur. J. Biochem.* **1992**, 210, 911–921.
- [23] a) S. Caltabiano, W. T. Hum, G. J. Atwell, D. N. Gralnick, L. J. Budman, A. M. Cannistraci, F. Bex. *J. Biochem. Pharm.* **1999**, 58, 1567–1578; b) H. Fujii, H. Komazawa, H. Mori, M. Kojima, I. Itoh, J. Murata, I. Azuma, I. Saiki. *Biol. Pharm. Bull.* **1995**, 18, 1681–1688.
- [24] M. S. Goligorsky, G. F. Dibona. *Proc. Natl. Acad. Sci. USA* **1993**, 90, 5700–5704.
- [25] VT-<sup>1</sup>H NMR analysis of 10 is consistent with the secondary structure expected on the basis of the parent model 2; Dd/DT (ppbK<sub>1</sub>): AspNH, -6.0; ArgNH, -5.0; NHa, -4.2; NHb, -1.0.
- [26] cyclo-[RGDfACHTUNG(TREUNUNG(NMe)V)] (Cilengitide, EMD 121974) inhibits the adhesion of fibronectin and other extracellular matrix proteins to various kinds of α<sub>v</sub>β<sub>3</sub>-integrin-expressing cell lines at micromolar concentrations; for selected examples, see: a) T. Taga, A. Suzuki, I. Gonzalez-Gomez, F. H. Gilles, M. Stins, H. Shimada, L. Barsky, K. I. Weinberg, W. E. Laug. *Int. J. Cancer* **2002**, 98, 690–697; b) L. Belvisi, T. Riccioni, M. Marcellini, L. Vesci, I. Chiarucci, D. Efrati, D. Potenza, C. Scolastico, L. Manzoni, K. Lombardo, M. A. Stasi, A. Orlandi, A. Ciucci, B. Nico, D. Ribatti, G. Giannini, M. Presta, P. Carminati, C. Pisano. *Mol. Cancer Ther.* **2005**, 4, 1670–1680; c) S. Loges, M. Butzal, J. Otten, M. Schweizer, U. Fischer, C. Bokemeyer, D. K. Hossfeld, G. Schuch, W. Fiedler. *Biochem. Biophys. Res. Commun.* **2007**, 357, 1016–1020, and references therein.
- [27] W. L. Jorgensen, J. Chandrasekhar, J. Madura, R. W. Impey, M. L. Klein. *J. Chem. Phys.* **1983**, 79, 926–935.
- [28] H. J. C. Berendsen, J. P. M. Postma, W. F. van Gunsteren, A. DiNola, J. R. Haak. *J. Chem. Phys.* **1984**, 81, 3684–3690.
- [29] H. Shibata, T. Yagi. *Clin. Chim. Acta* **1996**, 251, 53–64.

---

## Chapter 4

---

# Antiangiogenic Effect of Dual/Selective $\alpha_5\beta_1/\alpha_v\beta_3$ Integrin Antagonists Designed on Partially Modified Retro-Inverso Cyclotetrapeptide Mimetics

---

Recent evidence highlighted the role of  $\alpha_5\beta_1$  integrin in angiogenesis and in regulating  $\alpha_v\beta_3$  integrin function. As a consequence, selective  $\alpha_5\beta_1$  integrin inhibitors or dual  $\alpha_5\beta_1/\alpha_v\beta_3$  integrin inhibitors are considered promising candidates for the development of cancer therapeutic agents. In this paper, we describe the synthesis and pharmacological characterization of a minilibrary of cyclotetrapeptide mimetics containing a PMRI Arg-Gly-Asp sequence. In particular, c[(R)- $\beta$ Phe $\psi$ (NHCO)Asp $\psi$ -(NHCO)Gly-Arg] (**3**) displayed a good activity in inhibiting the  $\alpha_v\beta_3$  integrin-mediated cell adhesion of fibronectin or vitronectin, as well as the adhesion of fibronectin to the  $\alpha_5\beta_1$  integrin. Interestingly, the diastereomeric compound c[(S)- $\beta$ Phe $\psi$ (NHCO)Asp $\psi$ (NHCO)Gly-Arg] (**2**) maintained a good efficacy in inhibiting  $\alpha_5\beta_1$  integrin while gaining a certain selectivity over  $\alpha_v\beta_3$  integrin. These two integrin antagonists significantly inhibited bFGF-induced human endothelial cell tube formation at submicromolar concentrations. Conformational analysis and Molecular Docking calculations suggest that the different  $\alpha_5\beta_1$  versus  $\alpha_v\beta_3$  selectivity of **2** and **3** can be rationalized on the basis of the alternative display of the aromatic side chain adjacent to Asp.

### 4. Introduction

Among the different members of the integrin receptor family,  $\alpha_v\beta_3$  integrin is generally considered a privileged target for antiangiogenic therapy<sup>[1-6]</sup>. At the same time,  $\alpha_5\beta_1$  integrin has emerged as a new promising target for the development of cancer therapeutic agents. Besides an important function in the migration of activated lymphocytes during the immune response and the involvement in diabetes and inflammatory diseases like rheumatoid arthritis<sup>[7]</sup>, the proangiogenic function of the  $\alpha_5\beta_1$  receptor has been clearly demonstrated<sup>[8]</sup>. Interestingly, the  $\alpha_5\beta_1$  integrin has been shown to affect  $\alpha_v\beta_3$ -mediated endothelial cell migration and angiogenesis via regulation of  $\alpha_v\beta_3$  integrin function<sup>[9]</sup>. A study with  $\alpha_v\beta_3$  and  $\alpha_5\beta_1$  specific antibodies demonstrated that integrin  $\alpha_5\beta_1$  regulates the function of integrin  $\alpha_v\beta_3$  on endothelial cells during their migration in vitro or angiogenesis in vivo<sup>[10]</sup>.

Likewise, it has been reported that the combined antagonism of both  $\alpha_v\beta_3$  and  $\alpha_5\beta_1$ , as opposed to  $\alpha_v\beta_3$  alone, induces apoptosis of angiogenic endothelial cells cultured on type I collagen<sup>[11]</sup>.

Another approach to developing integrin inhibitors is to modify extracellular matrix proteins like angiostatin, tamustatin, arresten, and endostatin capable of antagonizing  $\alpha_v\beta_3$  and  $\alpha_5\beta_1$ <sup>[12]</sup>. A laminin-1-derived peptide that similarly blocks  $\alpha_v\beta_3$  and  $\alpha_5\beta_1$  has been shown to inhibit growth of melanoma cells in vivo<sup>[13]</sup>.

The endogenous extracellular matrix ligands vitronectin and fibronectin bind to the  $\alpha_v\beta_3$  integrin, and fibronectin binds also to  $\alpha_5\beta_1$  integrin by recognition of the acidic and guanidino side chain groups of the same tripeptide motif, the Arg-Gly-Asp (RGD) sequence<sup>[14]</sup>. Therefore, small RGD-mimetic molecules that are able to interfere with the  $\alpha_5\beta_1$  and/or  $\alpha_v\beta_3$  integrins are currently considered of interest for the angiostatic

therapy of cancer<sup>[15-17]</sup>. The RGD sequence is the recognition site for various integrin receptors, and the conformation of the sequence in the individual adhesion protein or peptide is critical for the specificity of this recognition<sup>[18,19]</sup>.

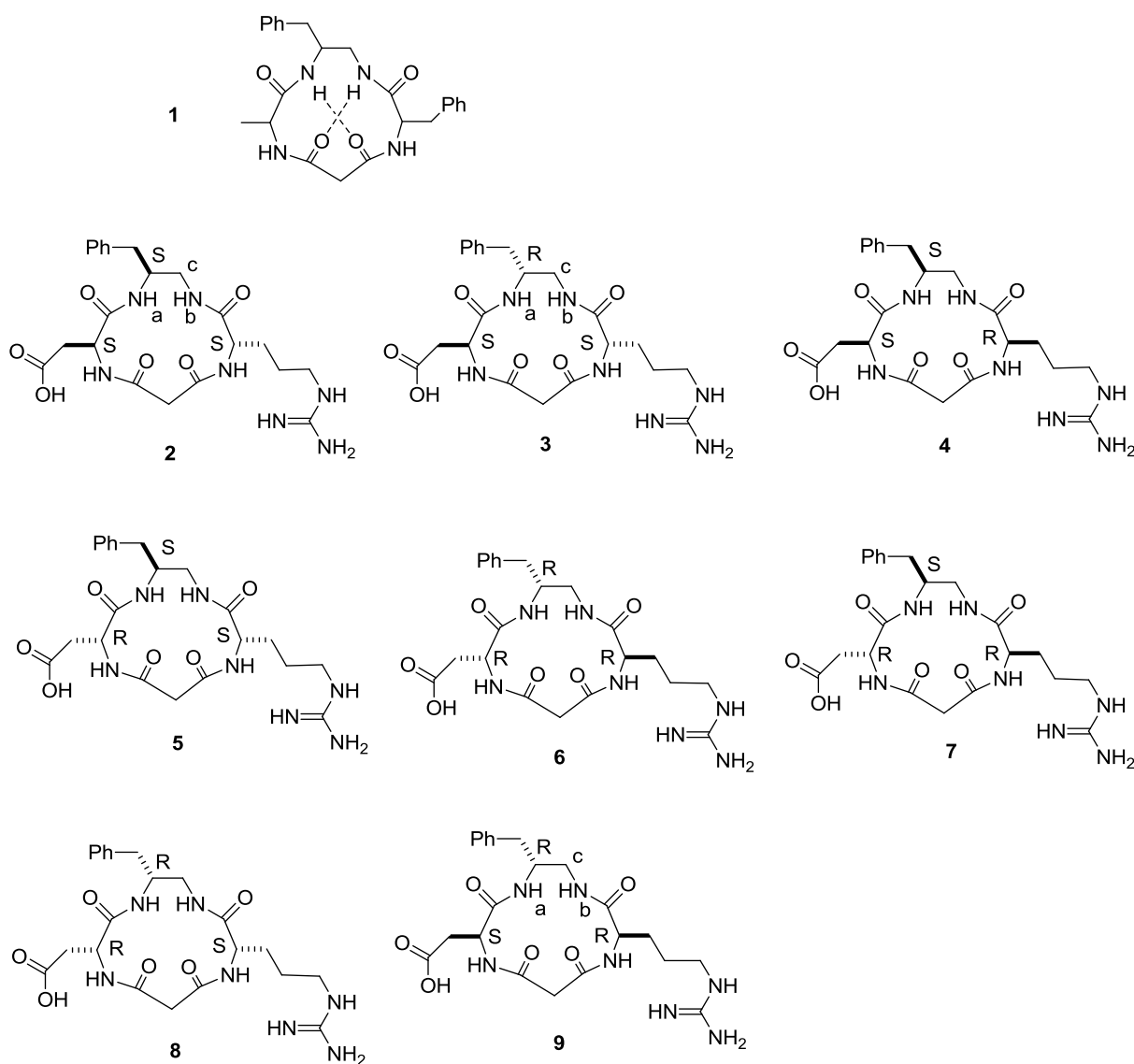


**Fig.(1).** General structure of the PMRI-cyclotetrapeptide models  $c[(S/R)\text{-}\beta\text{Phe}\Psi(\text{NHCO})(S/R)\text{-Ala}\Psi(\text{NHCO})\text{Gly}\text{-}(S/R)\text{-Phe}]$  **1**, and structures of stereoisomeric PMRI RGD-mimetics  $c[(S/R)\text{-}\beta\text{Phe}\Psi(\text{NHCO})(S/R)\text{-Asp}\Psi(\text{NHCO})\text{Gly}\text{-}(S/R)\text{-Arg}]$  **2-9**.

With regard to the  $\alpha_v\beta_3$  integrin receptor, a large number of peptidic, peptidomimetic<sup>[20,21]</sup>, and non peptidomimetic<sup>[22]</sup> scaffolds have been successfully employed to provide the desired conformational constraint to maintain the acidic and basic side chains at the appropriate distance and in a conformation suitable for binding. The cyclopentapeptide  $c[\text{Arg}\text{-Gly}\text{-Asp}\text{-}(R)\text{-Phe}\text{-Val}]$  has represented the first highly active and selective  $\alpha_v\beta_3$  integrin antagonist<sup>[23-25]</sup> and has served as a lead structure for the development by Kessler et al. of the cyclic pentapeptide cilengitide,  $c[\text{Arg}\text{-Gly}\text{-Asp}\text{-}(R)\text{-Phe}\text{-NMeVal}]$  (EMD121974)<sup>[26]</sup>, currently in clinical trials for antiangiogenic cancer therapy<sup>[27,28]</sup>. Furthermore, the crystal structure of the

extracellular segment of the  $\alpha_v\beta_3$  integrin with cilengitide bound to the active site has been disclosed previously<sup>[29]</sup>, giving the opportunity to design novel integrin antagonists based on the receptor-bound conformation of the RGD tripeptide<sup>[30]</sup>.

On the other hand, the experimental 3D structure of  $\alpha_5\beta_1$  integrin is not available, and few structural details about ligand-receptor interactions have been obtained until now<sup>[31,32]</sup>.

As a consequence, only some potent and selective antagonists of  $\alpha_5\beta_1$  or dual  $\alpha_5\beta_1/\alpha_v\beta_3$  antagonists have been described<sup>[33-36]</sup>.

Recently, a homology model of the receptor has been published<sup>[37]</sup>, which has successfully been used to optimize ligand activity and selectivity<sup>[38]</sup>.

In essence, the criteria for designing integrin antagonists showing selectivity for a certain RGD-binding integrin type over the others seem to reside for the most part in subtle differences in the reciprocal orientation and distance between the Asp and Arg side chains, and in the disposition of an aromatic side chain adjacent to Asp. In particular, the presence of definite secondary structure elements in RGD linear or cyclic peptides has often been correlated to the ligand's specificity<sup>[20,30,31,38]</sup>. Therefore, the synthesis of novel, conformationally definite RGD-containing scaffolds to mimic important secondary structure elements such as  $\gamma$ - or  $\beta$ -turns is of great interest.

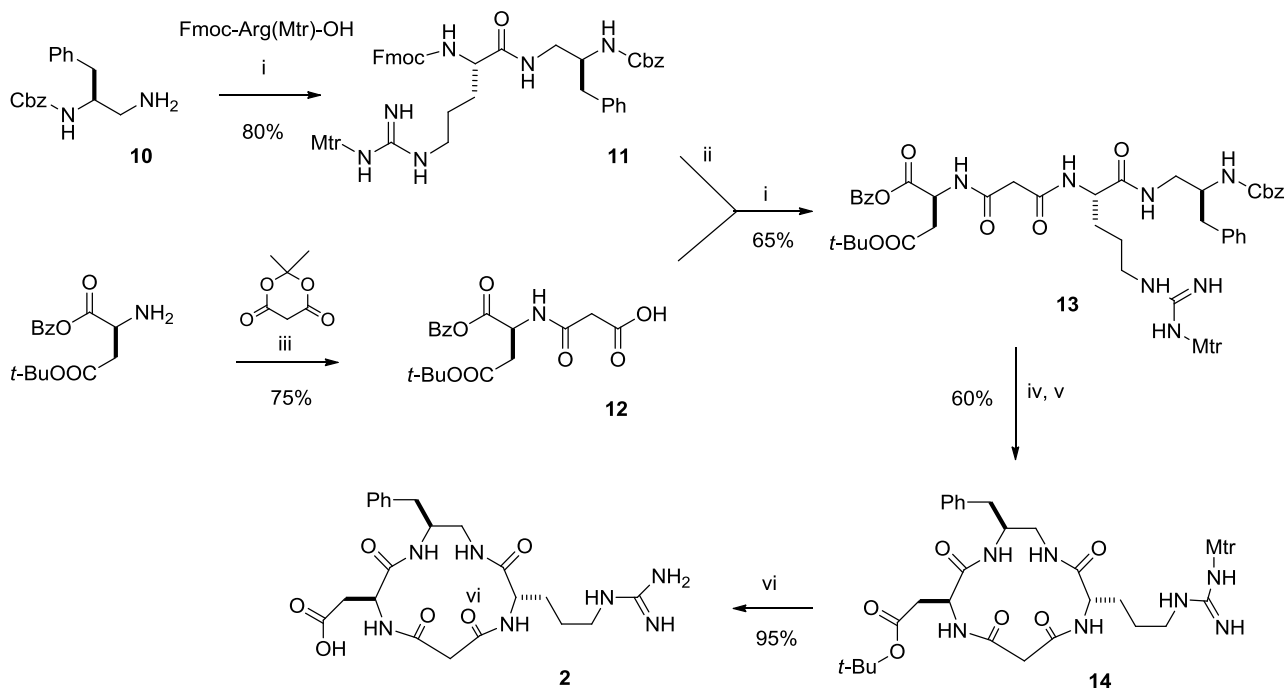
Very recently<sup>[39,40]</sup>, we designed a new kind of cyclotetrapeptide (CTP) scaffold based on a partially modified retroinverso (PMRI) variant of CTP containing a  $\beta$ -amino acid, forming 13-membered rings<sup>[41]</sup>. Retro-inverso and PMRI analogues have been widely utilized to improve the performance of a bioactive parent peptide<sup>[42-46]</sup>. We envisaged the opportunity to utilize these scaffolds for designing peptidomimetic molecules with a well-defined 3D display of the RGD sequence and aimed to discover selective  $\alpha_5\beta_1$  integrin antagonists or dual  $\alpha_v\beta_3/\alpha_5\beta_1$  integrin antagonists, whose activity could be synergistically effective in preventing angiogenesis.

#### 4.1. Results

**Design and Synthesis.** Compared to CTPs composed of all  $\alpha$ -amino acids, which can be considered the smallest turnmimetic structure, 13-membered analogues incorporating a  $\beta^3$ - or  $\beta^2$ -amino acid proved to be easier to synthesize and conformationally more defined<sup>[41,47-49]</sup>. The eight stereoisomeric PMRI-CTP models (1) of the general sequence  $c[(S/R)-\beta\text{Phe}\psi\text{-(NHCO)}(S/R)\text{-Ala}\psi\text{(NHCO)Gly-(S/R)-Phe}]$  (Figure 1) contain a 1,2-diamine to replace the  $\beta$ -amino acid, and a diacid as a Gly mimetic. Conformational analysis revealed that these 13-membered scaffolds manifest specific 3D geometries in comparison to normal 13-membered CTPs<sup>[39]</sup> and have a strong tendency to adopt turn structures. This preference can be ascribed to the propensity of the PMRI-CTP structures to stabilize H-bonded conformations involving the diamine amide protons<sup>[50]</sup>.

On the basis of the structures of the scaffolds **1**, we designed a minilibrary of PMRI RGD-mimetic compounds<sup>[21]</sup>, aiming to obtain integrin antagonists having the pharmacophoric side chains in well-defined, predictable spatial dispositions. For this purpose, we prepared the stereoisomeric compounds  $c[(S/R)-\beta\text{Phe}\psi\text{(NHCO)}(S/R)\text{-Asp}\psi\text{(NHCO)Gly-(S/R)-Arg}]$  **2-9** by introducing (S)- or (R)-Asp and (S)- or (R)-Arg in place of (S)- or (R)-Ala and (S)- or (R)-Phe, respectively (some preliminary results of the  $\alpha_v\beta_3$  integrin-

mediated cell adhesion inhibition in the presence of **2-4** and **8**, at a single concentration, have been reported in a previous paper<sup>[50]</sup>).



**Scheme 1.** Synthesis of **2**. Reagents and conditions: (i) EDCI/HOBt/TEA, DCM/DMF; (ii) DMA/THF; (iii) CH<sub>3</sub>CN, 70°C; (iv) H<sub>2</sub> Pd/C, EtOH; (v) DPPA/NaHCO<sub>3</sub>, DMF; (vi) TFA/PhOH/PhSH/H<sub>2</sub>O/Et<sub>2</sub>S 94/2/1/2/1.

The cyclic PMRI RGD mimetics were easily obtained from the corresponding linear precursors. As a prototypic example, the synthesis of **2**, the first member of the minilibrary, is shown in Scheme 1, the syntheses of the other stereoisomers (**3-9**) being the same.

The retrosynthetic analysis of the protected linear precursor **13** was thought to proceed by in-solution coupling of fragments **11** and **12**. Reduction of Cbz-Phe-NH<sub>2</sub><sup>[51]</sup> with BH<sub>3</sub><sup>[52]</sup> gave chiral Cbz-1,2-diamine **10** in excellent yield. The coupling of **10** under standard conditions with Fmoc-Arg-(Mtr)-OH afforded dipeptide **11**, whose deprotection was performed by treatment with 2 M DMA in THF.

The second fragment was straightforwardly prepared from Meldrum's acid and H-Asp(Ot-Bu)-OBz, giving dipeptide acid **12**, not needing further deprotection steps. The standard coupling of dipeptides **11** and **12** gave fully protected linear tetrapeptide **13**. The removal of the Cbz and benzyl ester protecting groups at the N- and C-termini, respectively, by hydrogenolysis, followed by cyclization with DPPA, gave cyclopeptide **14** in good yield and purity after preparative RP-HPLC. The final deprotection of Asp and Arg side chains was performed with TFA in the presence of a mixture of scavengers. PMRI-CTP **2** was isolated by preparative RP-HPLC.

Accordingly, we prepared the remaining PMRI RGD analogues **3-9**; purities and mass characterizations are reported in Table 1.

**4.1.2. Inhibition of Cell Adhesion.** The ability of compounds **2-9** to inhibit the adhesion of K562 (human erythroleukemic cells, expressing  $\alpha_5\beta_1$  integrin) or SK-MEL-24 (human malignant melanoma cells, expressing  $\alpha_v\beta_3$  integrin) to immobilized fibronectin and the adhesion of HUVEC (human umbilical vein endothelial cells, expressing  $\alpha_v\beta_3$  integrin) to immobilized vitronectin was evaluated. These cell models are widely used to investigate potential antagonists of  $\alpha_v\beta_3$  integrin (HUVEC and SK-MEL-24)<sup>[53,54]</sup> or of  $\alpha_5\beta_1$  integrin (K562)<sup>[55]</sup>. In these experiments, the cells were seeded onto plates coated with different substrata and allowed to adhere before quantitation of the number of adherent cells. Under these conditions, no significant cell adhesion was observed for BSA-coated plates (negative control) or nonspecific substrate-coated plates (i.e., collagen I for SK-MEL-24 and HUVEC expressing  $\alpha_v\beta_3$  integrin and vitronectin for K562 expressing  $\alpha_5\beta_1$  integrin) (data not shown). Results are summarized in Table 1. The compound c[Arg-Gly-Asp- (R)-Phe-Val] was included as reference cyclic peptide, being a potent inhibitor of cell adhesion<sup>[23,56,57]</sup> and the peptide c[Arg-Ala-Asp-(R)-Phe-Val] was used as a negative control<sup>[58]</sup>.

Compound **3**, c[(R)- $\beta$ Phe $\psi$ (NHCO)Asp $\psi$ (NHCO)Gly-Arg], containing (S)-Arg and (S)-Asp, exhibited the highest potency as an inhibitor of cell adhesion mediated by  $\alpha_v\beta_3$  and  $\alpha_5\beta_1$  integrins. The IC<sub>50</sub> value versus  $\alpha_5\beta_1$  integrin-mediated cell adhesion was 10 times lower than that versus  $\alpha_v\beta_3$  integrin (Table 1). The diastereoisomer **2**, c[(S)- $\beta$ Phe $\psi$ (NHCO)Asp $\psi$ (NHCO)Gly-Arg], which differs from **3** exclusively for the stereochemistry of the diamine moiety, maintained a notable efficacy as  $\alpha_5\beta_1$  integrin inhibitor and gained selectivity versus  $\alpha_v\beta_3$  integrin. Indeed, although **2** exhibited an IC<sub>50</sub> of 0.52  $\mu$ M as an  $\alpha_5\beta_1$  integrin antagonist, the activity toward  $\alpha_v\beta_3$  integrin dropped to an IC<sub>50</sub> value of 11  $\mu$ M against fibronectin and of 25.2  $\mu$ M against vitronectin. PMRI RGD mimetic **4** containing (S)-Asp and (R)-Arg, and mimetic **8** containing (R)-Asp and (S)-Arg, gave comparatively inferior results with respect to **2** and **3**. Both compounds exhibited modest IC<sub>50</sub> values, in the micromolar range (Table 1). The rest of the compounds poorly affected adhesion of cells to immobilized fibronectin or vitronectin, with an IC<sub>50</sub> of >100  $\mu$ M.

Compounds **2-4** and **8** possess IC<sub>50</sub> values comparable to those of  $\alpha_v\beta_3$  integrin inhibitors in the two cell models expressing this integrin toward the two ligands fibronectin (employed in SK-MEL-24) and vitronectin (employed in HUVEC)<sup>[59,60]</sup>.

In agreement with previous studies<sup>[23,56,57,61]</sup>, c[Arg-Gly-Asp-(R)-Phe-Val] displayed a micromolar inhibitory activity on the cell adhesive capacity driven by  $\alpha_v\beta_3$  and  $\alpha_5\beta_1$  integrin, whereas the cyclic peptide c[Arg-Ala-Asp-(R)-Phe-Val] had IC<sub>50</sub> values of >100  $\mu$ M. Interestingly, compound **3** was more potent than reference compound c[Arg-Gly-Asp-(R)-Phe-Val] as it inhibited cell adhesion mediated by  $\alpha_v\beta_3$  and  $\alpha_5\beta_1$  integrin possessing IC<sub>50</sub> values 40- and 1445-fold less, respectively.

**Table 1.** Analytical characterization of **2-9** and inhibition of  $\alpha_v\beta_3$ - and  $\alpha_5\beta_1$  integrin mediated cell adhesion to fibronectin (FN) and vitronectin (VN) in the presence of **2-9**, or the reference cyclic peptide c[Arg-Gly-Asp-(R)-Phe-Val] and the negative control peptide c[Arg-Ala-Asp-(R)-Phe-Val], c[RGDFV] and c[RADfV], respectively, in brief.

compd	Purity (%)	MS [M+1] <sup>a</sup>	$\alpha_v\beta_3$ vs FN	$\alpha_v\beta_3$ vs VN	$\alpha_5\beta_1$ vs FN
			(SK-MEL-24 cells) IC <sub>50</sub> ( $\mu$ M) <sup>b</sup>	(HUVEC cells) IC <sub>50</sub> ( $\mu$ M) <sup>b</sup>	(K562 cells) IC <sub>50</sub> ( $\mu$ M) <sup>b</sup>
<b>2</b>	97	490.2	11 $\pm$ 6	25.2 $\pm$ 5.2	0.52 $\pm$ 0.04
<b>3</b>	96	490.3	0.18 $\pm$ 0.05	0.24 $\pm$ 0.08	0.024 $\pm$ 0.003
<b>4</b>	95	490.3	2.3 $\pm$ 0.3	1.5 $\pm$ 0.4	4.7 $\pm$ 0.4
<b>5</b>	95	490.4	> 100	> 100	> 100
<b>6</b>	95	490.2	> 100	> 100	> 100
<b>7</b>	95	490.1	> 100	> 100	> 100
<b>8</b>	96	490.2	2.1 $\pm$ 0.3	0.92 $\pm$ 0.09	1.3 $\pm$ 0.1
<b>9</b>	96	490.3	> 100	> 100	> 100
c[RGDFV] <sup>c</sup>	-	-	7.1 $\pm$ 2.7	9.6 $\pm$ 2.9	34.7 $\pm$ 8.4
c[RADfV] <sup>c</sup>	-	-	> 100	> 100	> 100

<sup>a</sup> Calculated [M+1]: 490.2. <sup>b</sup> Values are means  $\pm$  standard error of three experiments carried out in quadruplicate. <sup>c</sup> Purchased from Bachem.

**4.1.3. Effect of Integrin Antagonists on in Vitro Angiogenesis Elicited by Basic Fibroblast Growth Factor (bFGF).** The formation of capillary-like tube structures by HUVEC in the extracellular matrix (ECM) is the pivotal step in angiogenesis and is also involved in cell migration and invasion<sup>[62-64]</sup>. To evaluate any potential antiangiogenic activity of these novel  $\alpha_v\beta_3/\alpha_5\beta_1$  integrin antagonists, in vitro angiogenesis assays were conducted by evaluating bFGF-induced angiogenesis of HUVEC cultured in a 3D gel consisting of Matrigel. As shown in Figure 2, when HUVEC were plated on wells coated with Matrigel without the addition of the growth factor, they showed only a few spontaneous tube formations (taken as an index of neo-angiogenesis), and most of them were still in a highly proliferating state with a cobblestone shape. On the other hand, when HUVEC were plated on Matrigel with addition of bFGF (30  $\mu$ g/mL), cells formed a capillary-like network within 16 h (Figure 2). In the presence of compounds **2** and **3** (1  $\mu$ M), the extent of tube formation induced by bFGF was significantly reduced (Figure 2) in comparison to that in cells treated with the vehicle alone (containing up to 1% DMSO dissolved in cell culture medium). Interestingly, **3** exhibited the greatest inhibitory effect in blocking bFGF-induced angiogenesis. The number of tube branches per square millimeter was reduced from 10  $\pm$  3 (bFGF-treated HUVEC) to 5.1  $\pm$  0.7 (3-treated HUVEC), and 6.8  $\pm$  0.9 (2-treated HUVEC). The minimal concentration of these compounds yielding a complete inhibition of endothelial morphogenesis on Matrigel was 1  $\mu$ M; lower concentrations (100 and 500 nM) were less effective or (10 nM) ineffective (data not shown), whereas compound **8** (10  $\mu$ M) did not cause any significant reduction in the level of angiogenesis (Figure 2). Similarly, compounds **4-7** and **9**, added to the cells to a final concentration of up to 10  $\mu$ M, were not effective as angiogenesis inhibitors (see the Supporting Information).

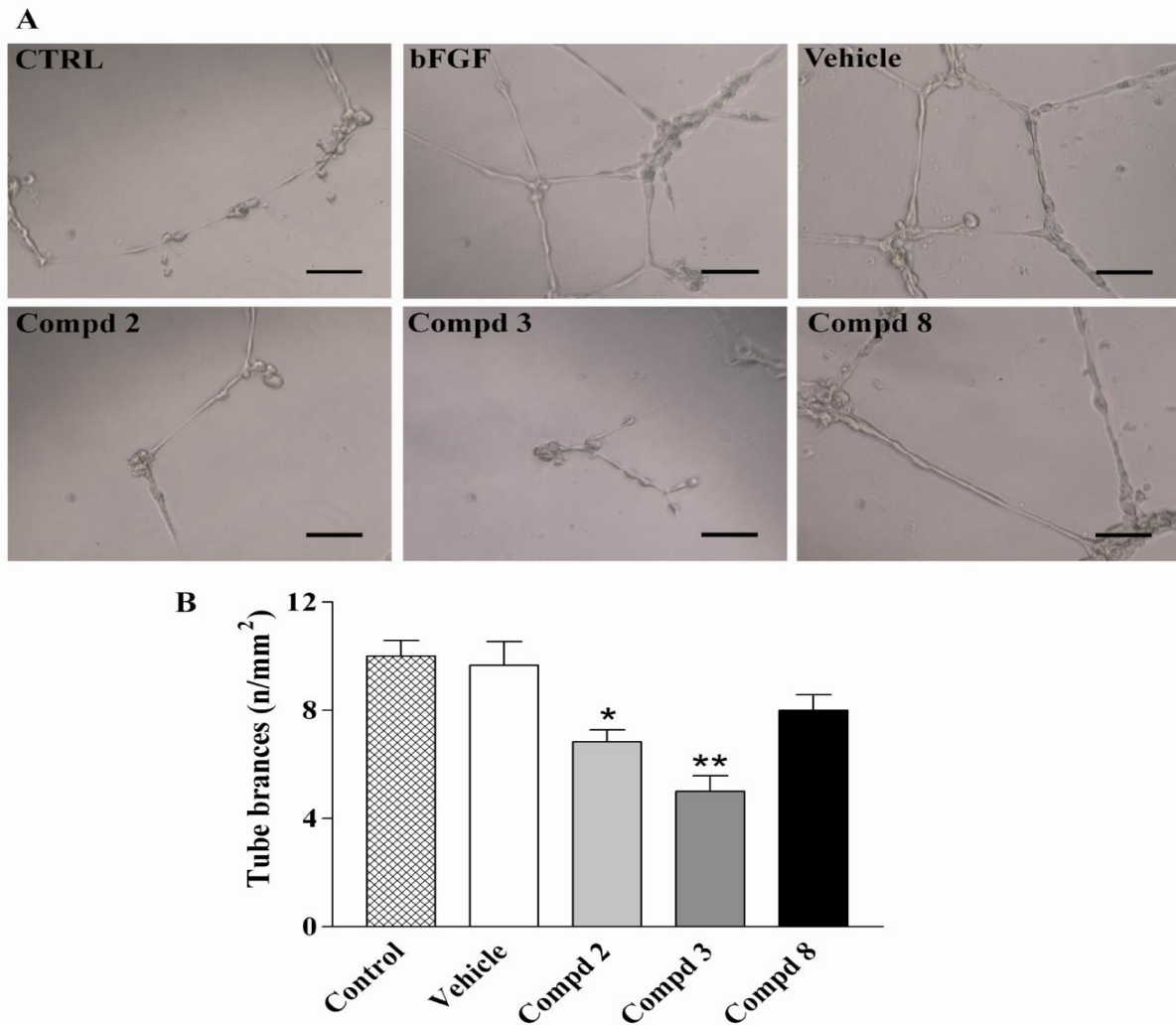


**Fig. (2).**  $\alpha_v\beta_3/\alpha_5\beta_1$  integrins antagonists inhibit bFGF-induced HUVEC tube formation on Matrigel. Representative pictures of capillary-like structures (black bar in the pictures corresponds to 100  $\mu\text{m}$ ). **CTRL)** HUVEC cells plated on Matrigel in the absence of bFGF. **bFGF)** HUVEC cells plated on Matrigel in the presence of bFGF (30 ng/mL) for 16 h. **Vehicle)** HUVEC cells treated with vehicle alone (containing up to 1% of DMSO dissolved in cell culture medium). **Compd2)** HUVEC cells treated with compound 2 (1  $\mu\text{M}$ ); **Compd3)** HUVEC cells treated with compound 3 (1  $\mu\text{M}$ ); **Compd8)** HUVEC cells treated with compound 8 (10  $\mu\text{M}$ ). The ability to form capillary-like sproutings on Matrigel was significantly diminished when HUVEC cells were treated with compounds 2 and 3. Data are presented as mean  $\pm$  S.E.M. of the number of tubes/ $\text{mm}^2$ . These experiments were carried out in quadruplicate and repeated three times. \* $P < 0.01$ ; \*\* $P < 0.05$  vs control (Newman-Keuls test after ANOVA).

#### 4.1.4. $\alpha_5\beta_1/\alpha_v\beta_3$ Integrin Antagonists Do Not Affect Endothelial Cell Viability.

To determine whether  $\alpha_5\beta_1$  and  $\alpha_v\beta_3$  integrin antagonists could alter endothelial cell viability, morphology and flow cytometric analysis were evaluated in HUVEC after treatment for 16 h with 1 and 10  $\mu\text{M}$  RGD cyclopeptides.

These data indicate that neither significant changes in the morphology (data not shown) nor significant increases in the level of apoptosis or necrosis (Supporting Information) were observed in endothelial cells, suggesting that these compounds do not display any relevant cytotoxicity in HUVEC.

#### 4.2. Conformational Analysis of 2 and 3 in Solution.

Then biological activities of some of the compounds vary radically (Table 1), although the sequence of the peptides is identical.

This observation confirms the anticipation that RGDmimetic compounds based on the PMRI CTPs behave as topologically distinct structures. It is accepted that the conformation of a cyclic peptide is controlled by the stereochemistry array of the residues, while the precise nature of the residues has a minor impact<sup>[21,65,66]</sup>. In this section, we discuss the in-solution structural features of **2** and **3**, aiming to deduce useful clues about the biologically active structures of this class of pseudopeptides, while the conformations of the less active or inactive compounds **4** and **5** are discussed in the Supporting Information. The conformations of **6-9**, the mirror images of **2-5**, respectively, were not re-examined.

The conformational analyses were performed by NMR spectroscopy and molecular dynamics (MD) simulations.

The NMR analyses of cyclopeptides **2** and **3** were conducted using standard techniques in the 8:2 DMSO  $d_6/H_2O$  biomimetic medium<sup>[67]</sup>. We could not perform experiments in water, since the peptides were very poorly soluble. The  $^1H$  NMR analyses of **2** and **3** revealed a single set of resonances, suggesting conformational homogeneity or a fast equilibrium<sup>[21,65]</sup>. VT  $^1H$  NMR experiments were utilized to deduce the presence of H-bonds (Table 2). The analyses indicated that in the two cyclopeptides, AspNH and ArgNH do not seem to be involved in intramolecular H-bonds. On the other hand, for both compounds, diamineNHb [NHa, NHb, and Hc (see Figures 1 and 3-6)] very likely participates in a strong H-bond ( $|\Delta\delta/\Delta t| \approx 1$  ppb/K)<sup>65,68</sup>. With regard to diamineNHa, while in **2** the low  $\Delta\delta/\Delta t$  value is suggestive of the involvement in H-bonds ( $\Delta\delta/\Delta t = 1.4$  ppb/K), the comparatively higher  $|\Delta\delta/\Delta t|$  value observed in **3** accounts for solvent-exposed protons ( $\Delta\delta/\Delta t = -4.0$  ppb/K).

**Table 2.**  $\Delta\delta/\Delta t$  values (ppb/°K) of amide protons for **2** and **3**, determined by VT- $^1H$ -NMR analysis in 8/2 DMSO- $d_6/H_2O$  at 400 MHz over the range 298-348 °K (NHa, NHb, see Figure 1 and Figures 5-8).

Compd	AspNH	ArgNH	NHa	NHb
<b>2</b>	-6.1	-5.8	+1.4	-0.6
<b>3</b>	-6.3	-5.0	-4.0	-1.0

2D ROESY data were utilized to investigate the spatial disposition of molecular backbones (Tables 3 and 4). For the absence of  $H_{i+1}-H_i$  cross-peaks, indicative of a cis peptide bond conformation, all of the  $\omega$  bonds were set to 180°.

Conformations consistent with the spectroscopic analysis were obtained by restrained MD in a box of explicit, equilibrated water molecules<sup>[69]</sup>, using the distances deduced from ROESY as constraints and minimized with the AMBER 70 force field. A set of 50 random structures generated by means of a unrestrained high-temperature MD simulation was subjected to restrained MD with a scaled force field, followed by a high-temperature simulation with full restraints, after which the system was gradually cooled.

These structures were clustered by the rmsd analysis of the backbone atoms. For both peptides, one major cluster comprising more than 90% of the structures was obtained; the lowest-energy structures of the major clusters are shown in Figures 3 and 5.

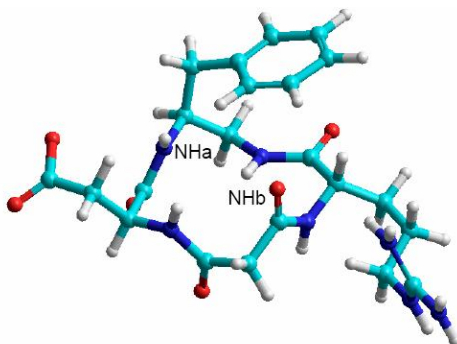


**Fig. (3).** Representative structure of **2** consistent with ROESY analysis.

The ROESY-derived structure of **2** (Figure 3) does not show explicit H-bonds, which were predicted on the basis of the VT NMR analysis. Apparently, the conformations determined by ROESY analyses represent the average on the NMR time scale of different geometries in equilibrium<sup>[21,65]</sup>.

To estimate the residual flexibility of the cyclopeptide, the dynamic behavior of the structure derived from ROESY was analyzed by unrestrained MD for 10 ns in a box of explicit water. During the simulation, the main structural features described on the basis of ROESY were maintained. In addition, the examination of the trajectories revealed the occurrence of explicit H-bonds in agreement with VT NMR analysis.

Indeed, the trajectories of **2** clearly revealed the occurrence of two slightly different backbone structures. One is characterized by a type I  $\beta$ -turn centered on Arg-diamine and stabilized by a H-bond between malonylCO and diamine-NHa (Figure 4, left). The second one is characterized by a type I  $\beta$ -turn centered on Asp-diamine, with a H-bond between the other malonylCO and diamineNHb (Figure 4, right).

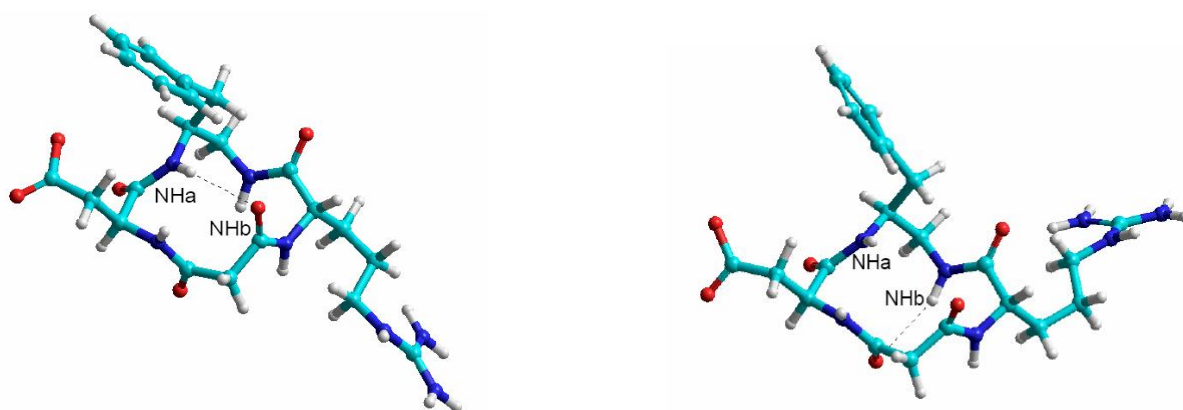


**Fig. (4).** Representative, minimized structures **2a** (left) and **2b** (right) calculated by unrestrained MD in a 30x30x30 Å box of standard TIP3P water molecules, characterized by explicit H-bonds and secondary structural elements.

As for compound **3**, the ROESY-derived conformation shows a distinct H-bond between NHb and malonylCO, as anticipated on the basis of VT NMR, and an overall type II  $\beta$ -turn conformation on Asp diamine (Figure 5). Unrestrained MD simulation was performed as reported for **2**.

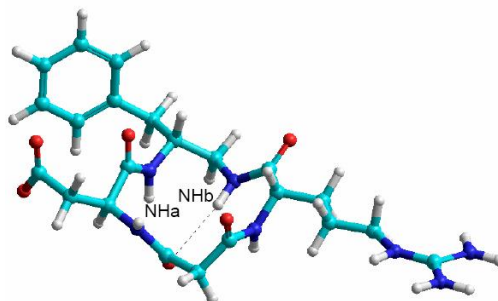


**Fig.(5).** Representative structure **3a** consistent with ROESY analysis.

In addition to the conformation of **3a** shown in Figure 5, the analysis of the trajectories of **3** gave a second conformer, **3b**, whose structure is in agreement with a pseudoinverse  $\gamma$ -turn centered on Asp, and an inverse  $\gamma$ -turn on Arg<sup>[71]</sup>. This alternative secondary structure (Figure 6) is still compatible with the involvement of the NHb proton in a H-bond as predicted by VT NMR analysis. Despite the different secondary structures, the two conformers, **3a** and **3b**, still maintain a very similar display of the pharmacophores.

However, the two situations slightly differ for the distance between the C $\beta$  atoms of Asp and Arg:  $\sim 8.3$  Å in **3a** and  $\sim 8.8$  Å in **3b**.

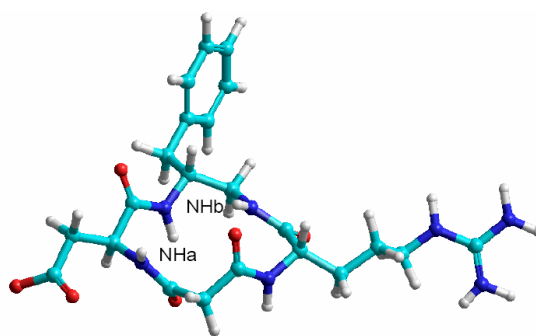


**Fig. (6).** Representative, minimized structure **3b** calculated by unrestrained MD in a 30x30x30 Å box of standard TIP3P water molecules, characterized by secondary structural elements.

The structures of **2** and **3** share a certain similarity in the RGD-mimetic region. The main difference among the two structures resides in the different orientations of the diamine aromatic side chain and of NHa. In **2**, the aromatic side chain and NHa point above the molecular plane; in **3**, the situation is reversed. In particular, in **2**, the diamine phenyl side chain adopts a pseudoaxial disposition; in **3**, it adopts a pseudoequatorial disposition.

### 4.3. Molecular Docking.

To interpret on a molecular basis the different affinities of compounds **2** and **3** for the  $\alpha_v\beta_3$  receptor, docking studies were performed using Glide (version 4.5)<sup>[72]</sup> by starting from the representative macrocycle conformations sampled during the unrestrained MD simulations. Molecular docking of compounds **4-9** is discussed in the Supporting Information. The protein binding site was derived from the X-ray crystal structure of the extracellular segment of integrin  $\alpha_v\beta_3$  in complex with the cyclic pentapeptide ligand cilengitide [Protein Data Bank (PDB) entry 1L5GJ]<sup>[29]</sup> In this X-ray structure, the potent  $\alpha_v\beta_3$  antagonist cilengitide, bound to the headgroup of the integrin, features an extended conformation of the RGD sequence with a distance of  $\sim 9$  Å between the C $\beta$  atoms of Asp and Arg. The crystal complex interaction pattern involves the formation of an electrostatic clamp between the guanidinium group of the ligand and the negatively charged side chains of Asp<sup>218</sup> and Asp<sup>150</sup> in the  $\alpha$  unit and between the carboxylic group of cilengitide and the metal cation in the metal ion-dependent adhesion site (MIDAS) region of the  $\beta$  unit. Moreover, further stabilization occurs through hydrogen bonds between the NH group of the ligand Asp residue and the carbonyl oxygen atom of Arg<sup>216</sup> in the  $\beta$  subunit as well as between the ligand carboxylate oxygen not coordinated to MIDAS and the backbone amides of Asn<sup>215</sup> and Tyr<sup>122</sup> in the  $\beta$  unit (Figure 7).

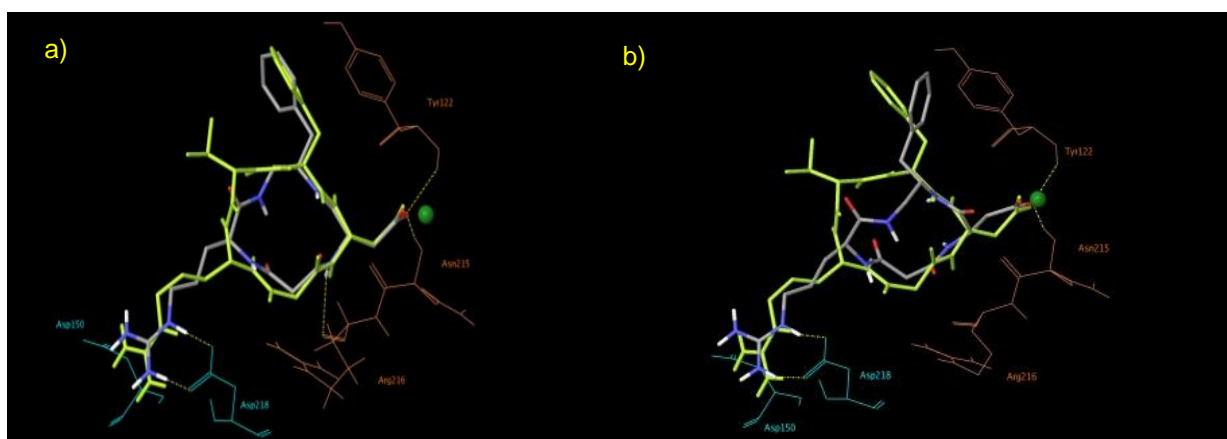


**Fig.(7).** Top-ranked docking poses of (a) ligand **3** (atom colour tube representation, macrocycle geometry “inverse  $\gamma$ /inverse  $\gamma$ ” **3b**) and (b) ligand **2** (atom colour tube representation, macrocycle geometry “ $\beta$ -turn” **2b**) into the crystal structure of the extracellular domain of  $\alpha_v\beta_3$  integrin ( $\alpha$  unit cyan and  $\beta$  unit orange wire representation) overlaid on the bound conformation of cilengitide (green tube representation). Only selected integrin residues involved in the interactions with cilengitide are shown. The Mn<sup>2+</sup> ion at MIDAS is shown as a green CPK sphere. Nonpolar hydrogen atoms were removed for clarity.

The experimentally observed binding mode of cilengitide with  $\alpha_v\beta_3$  integrin was taken as a reference model for the interpretation of the docking results in terms of the ligandbound conformation and ligand-protein interactions.

The models built for the interaction of compounds **2** and **3** with  $\alpha_v\beta_3$  integrin through docking studies showed that suitable macrocycle conformations of these ligands enable them to fit properly in the shallow cleft of the receptor, sharing the binding features of the crystal structure of the cilengitide- $\alpha_v\beta_3$  complex, especially those governing the recognition process. Among the conformations selected from the MD simulations of **2** and **3**, only the macrocycle geometries “inverse  $\gamma$ /inverse  $\gamma$ ” **3b** and “ $\beta$ -turn” **2b** generate top-ranked docking poses

conserving the relevant ligand-protein interactions observed in the crystal structure of the cilengitide- $\alpha_v\beta_3$  complex. However, the inverse  $\gamma$ /inverse  $\gamma$  geometry of **3b** reproduces the RGD backbone of the X-ray ligand better than the  $\beta$ -turn geometry of **2b** (Figure 7).

Moreover, the pseudoequatorial benzyl group in **3b** points to the same direction of the Phe side chain of the reference ligand, that is, toward the outside of the integrin binding site, allowing the aromatic ring to fit unhindered and to form a T-shaped interaction with the Tyr<sup>122</sup> side chain of the  $\beta$  subunit (Figures 7 and 8).

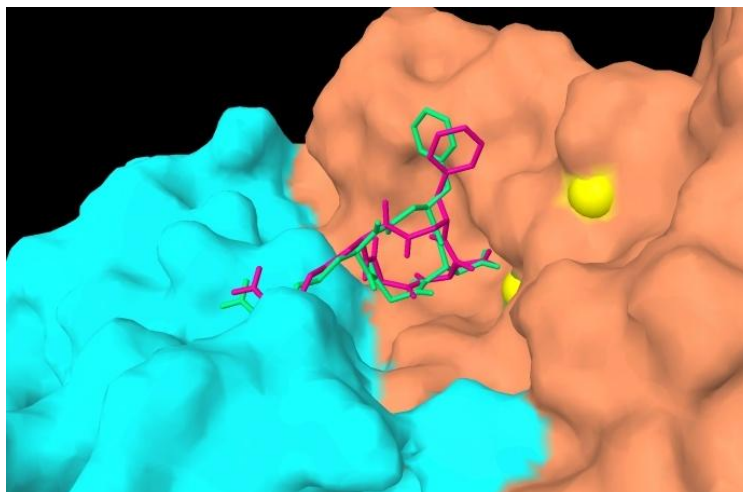


**Fig.(8).** Top-ranked docking poses of mimics **3b** (green tube representation) and **2b** (purple tube representation) into the crystal structure of the extracellular domain of  $\alpha_v\beta_3$  integrin represented as a molecular surface ( $\alpha$  unit cyan,  $\beta$  unit orange).  $Mn^{2+}$  ions are represented as yellow CPK spheres.

The  $\beta$ -turn structure of **2b** properly drives the pharmacophoric groups within the binding site to form the key electrostatic interactions with the receptor. Nevertheless, the pseudoaxial benzyl group forces the entire molecule to enter the receptor lopsided. The benzyl group fails in forming the T-shaped interaction with the aromatic ring of the Tyr<sup>122</sup> side chain. Accordingly, the Glide score values suggest a slightly better binding for epimer 3.

#### 4.4. Discussion

In this study, a selected minilibrary of stereoisomeric, modified retro-inverso cyclotetrapeptides **2-9** having the general structure  $c[(S/R)\text{-}\beta\text{Phe}\psi(\text{NHCO})(S/R)\text{-}\text{Asp}\psi(\text{NHCO})\text{Gly}\text{-}(S/R)\text{-}\text{Arg}]$  inhibited adhesion of cells to vitronectin- or fibronectin- coated surfaces and inhibited angiogenesis. The different compounds displayed variable activities as  $\alpha_v\beta_3$  or  $\alpha_5\beta_1$  integrin receptor antagonists, as determined by testing the inhibition of adhesion of fibronectin and vitronectin to  $\alpha_v\beta_3$  or  $\alpha_5\beta_1$  integrin receptor-expressing cell lines. Interestingly,  $c[(S)\text{-}\beta\text{Phe}\psi(\text{NHCO})\text{Asp}\psi(\text{NHCO})\text{Gly}\text{-}\text{Arg}]$  (**2**) displayed a submicromolar activity for  $\alpha_5\beta_1$  integrin, and a certain selectivity over  $\alpha_v\beta_3$  integrin, while  $c[(R)\text{-}\beta\text{Phe}\psi\text{-}(\text{NHCO})\text{Asp}\psi(\text{NHCO})\text{Gly}\text{-}\text{Arg}]$  (**3**) was demonstrated to be a potent dual antagonist, with **10-8** and **10-7** activities for  $\alpha_5\beta_1$  and  $\alpha_v\beta_3$  integrins, respectively. On the other hand,  $c[(S)\text{-}\beta\text{Phe}\psi(\text{NHCO})(S)\text{-}\text{Asp}\psi(\text{NHCO})\text{Gly}\text{-}(R)\text{-}\text{Arg}]$  (**4**) and  $c[(R)\text{-}\beta\text{Phe}\psi(\text{NHCO})(R)\text{-}\text{Asp}\psi(\text{NHCO})\text{Gly}\text{-}(S)\text{-}\text{Arg}]$  (**8**) revealed moderate micromolar inhibitory activities, while the remaining

compounds, **5-7** and **9**, were ineffective. These results demonstrate that compound **2** is more specific as an  $\alpha_5\beta_1$  integrin antagonist whereas compounds **3**, **4**, and **8** nonselectively antagonized  $\alpha_v\beta_3$  and  $\alpha_5\beta_1$  integrins, albeit with different efficacies, **3** being the most potent.

Moreover, we showed that  $\alpha_5\beta_1$  and  $\alpha_v\beta_3$  integrin antagonists inhibited bFGF-induced human endothelial cell tube formation at submicromolar concentrations as examined using the Matrigel assay. Among them, compound **3** showed the most potent antiadhesion and antiangiogenic effects; it can directly interact with  $\alpha_v\beta_3$  integrin expressed on melanoma and endothelial cells and can prevent adhesion of endothelial cells to vitronectin displaying higher binding selectivity for  $\alpha_v\beta_3$  integrin in cell culture.

Blockade of  $\alpha_v\beta_3$  integrin-mediated functions by antibodies or RGD peptides disrupts blood vessel formation in various animal models;  $\alpha_v\beta_3$  antagonists may perturb the growth and/ or maturation of blood vessels without detectable alteration on the preexisting blood vessels<sup>[73]</sup>.

Angiogenesis is also directly regulated by binding of fibronectin to its receptor, the  $\alpha_5\beta_1$  integrin. Specific antibodies, peptides, and novel nonpeptide antagonists of  $\alpha_5\beta_1$  integrin can block angiogenesis induced by several growth factors in both chick embryo and murine models. In fact, these  $\alpha_5\beta_1$  antagonists inhibited tumor angiogenesis, thereby causing regression of human tumors in animal models<sup>[74]</sup>. Antagonists of  $\alpha_v\beta_3$  and  $\alpha_5\beta_1$  integrins substantially prevent angiogenesis induced by bFGF, suggesting that these integrins regulate similar pathways of angiogenesis.

The results of this study suggest that the partially retroinverso RGD motif in the cyclotetrapeptide retains the  $\alpha_v\beta_3$  and  $\alpha_5\beta_1$  integrin antagonist activity. Therefore, we propose that the potent antiangiogenic effect of **3** in cell adhesion and tube formation assays is probably due to the interference of the  $\alpha_v\beta_3$  and  $\alpha_5\beta_1$  integrin-mediated interactions between endothelial cells and ECM protein. Indeed, **3** significantly decreased the level of bFGF-induced angiogenesis in an in vitro model. Therefore, the mechanism of action of these compounds in suppressing bFGF-elicited angiogenesis could be mediated by the specific blockade of  $\alpha_v\beta_3$  ligation. Finally, these integrin antagonists did not cause any cytotoxic effect as evidenced by flow cytometric analysis. The sequence of peptides **2-9** is identical, the only difference being the stereochemistry array. The comparatively higher inhibitory efficacy toward  $\alpha_5\beta_1$  integrin observed for compounds **2** and **3**, the most potent of the minilibrary, can be correlated to the specific (S,S) stereochemistry of the retro-inverso RGD sequence,  $\psi(\text{NHCO})(\text{S})\text{-Asp-}\psi(\text{NHCO})\text{-Gly-(S)-Arg}$ . Indeed, the remaining compounds possess (S,R), (R,R), or (R,S) (Arg,Asp) configurations.

It is worth mentioning that, due to the partial retro-inverso nature of the RGD sequence, the (S,S) stereochemistry of Arg and Asp in **2** and **3** leads to overall conformations showing the Arg and Asp pharmacophoric side chains on the opposite sides of the molecular scaffold, an unusual biologically active conformation in comparison to other well-known RGD cyclopentapeptide integrin antagonists, such as c[Arg-Gly-Asp-(R)-Phe-Val] or c[Arg-Gly-Asp-(R)-Phe-NMeVal] (cilengitide), having the pharmacophoric side chains placed on the same side. Apparently, in the smaller cyclotetrapeptide structures, an opposite orientation allows for a correct distance between the pharmacophores. For both **2** and **3**, during the unrestrained MD simulations, the average distance between Asp and Arg C $\beta$  was  $\sim 8.5$  Å, and that between the carboxylate and guanidino functions was  $\sim 13$  Å, very similar to that of the  $\alpha_5\beta_1$  or  $\alpha_v\beta_3$  selective cyclopentapeptides<sup>[29,30,38]</sup>.

As revealed by conformational analysis (Results), the two compounds show a very similar display of the retro-inverso RGD sequence. On the other hand, the different  $\alpha_5\beta_1$  versus  $\alpha_v\beta_3$  selectivity displayed by **2** and **3**, sharing the same (S,S) stereochemistry of the RGD-mimetic sequence, can be attributed to the presence of an (S)-diamine in **2** and an (R)-diamine in **3**. The most relevant 3D difference can be identified in the disposition of the diamine portion. Apart from the different location of diamineNH<sub>a</sub> andNH<sub>b</sub>, in **2** the diamine phenyl side chain adopts an axial position while in **3** it is equatorial (Figure 9).

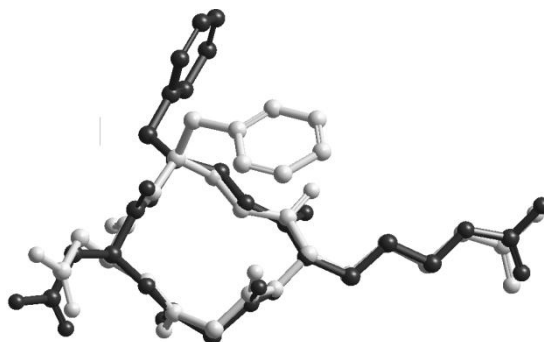


**Fig. (9).** Overlap of the backbone structures of **2** (**2b**, white) and **3** (**3b**, black) determined by ROESY and MD analysis. Side chains have been positioned in trans extended conformation.

The experimental 3D structure of  $\alpha_5\beta_1$  integrin is not yet available. As a consequence, the comparison of the structures of **2** and **3** with the structures of a few ligands, and with a *in silico* model, previously reported in the literature, could furnish some useful information about the biologically active conformation at this receptor. Goodman et al. described the receptor-bound conformation of the RGD sequence in the partially <sup>15</sup>N-labeled  $\alpha_5\beta_1$  integrin weak antagonist c[Mpa<sup>15</sup>N-Arg-<sup>15</sup>N-Gly-<sup>15</sup>N-Asp-<sup>15</sup>N-Asp-<sup>15</sup>N-Val-Cys]-NH<sub>2</sub> (IC<sub>50</sub>=1.2  $\mu$ M), determined by <sup>15</sup>N-edited 2D transferred nuclear Overhauser effects<sup>[31]</sup>. Data were indicative of a tilted conformation, leading to a very short average distance between Arg and Asp C $\beta$  of ~5.6 Å. More recently, Sewald et al. reported for the  $\alpha_5\beta_1$  integrin cyclohexapeptide ligand c[Arg-Gly-Asp-D-Phe-Val- $\beta$ Ala] (IC<sub>50</sub>=2 ( 1  $\mu$ M in K562 adhesion assays) a preferred extended RGD conformation showing a quite longer average distance between Arg C $\beta$  and Asp C $\beta$  of ~9.3 Å <sup>[32]</sup>. Apparently, the average C $\beta$ -C $\beta$  distance of 8.5Å observed for **2** and **3** is somewhat between the two values reported above.

More recently, a homology model of the  $\alpha_5\beta_1$  integrin has been reported by Kessler, Novellino, and co workers<sup>[37]</sup>. The model, obtained by comparative protein modeling and validated with experimental data of nonpeptide ligands, allowed identification of a distance between the carboxylate function and the basic moiety of ~13Å. This value is very close to the distance of ~13.8Å between the carboxylate and basic groups determined for  $\alpha_v\beta_3$  integrin-bound ligands<sup>[20,29,30]</sup>. As a consequence, the distance between the basic and acid moieties does not constitute a discriminant for  $\alpha_v\beta_3$  versus  $\alpha_5\beta_1$  selectivity. Therefore, the different pharmacological profile of **2** and **3** toward  $\alpha_v\beta_3$  and  $\alpha_5\beta_1$  integrins cannot be explained on the basis of the C $\beta$ -C $\beta$  distance alone.

However, the comparison of  $\alpha_5\beta_1$  and  $\alpha_v\beta_3$  binding pockets revealed the occurrence of mutated residues in the  $\beta$  subunit.

Indeed, ( $\beta^3$ )-Arg<sup>214</sup> is replaced with ( $\beta^1$ )-Gly<sup>217</sup>, and ( $\beta_3$ )-Arg<sup>216</sup> is mutated to ( $\beta^1$ )-Leu<sup>219</sup>. The substitution of both the bulky Arg residues expands the site of the  $\alpha_5\beta_1$  binding pocket in comparison to the  $\alpha_v\beta_3$  integrin. The authors concluded that ligands carrying bulky aromatic substituents in the proximity of the Asp (or Asp mimetic) residue can still fit the larger  $\alpha_5\beta_1$  binding pocket, but not the cramped  $\alpha_v\beta_3$  binding pocket, therefore showing a certain selectivity for  $\alpha_5\beta_1$  over  $\alpha_v\beta_3$  integrins.

The model highlights the fundamental role of the aromatic residue flanking Asp in determining selectivity. This rationalization is corroborated by the molecular docking computations performed by us on compounds **2** and **3** positioned within the  $\alpha_v\beta_3$  integrin receptor binding site (see Results).

The results lead to conjecture that the different disposition of diamine side chain is responsible of the different activity of **2** and **3** toward  $\alpha_v\beta_3$  integrin.

Molecular modeling studies showed that the pseudoequatorial benzyl group of **3** points toward the outside of the integrin binding site, allowing the aromatic ring to fit unhindered and reproducing the orientation of cilengitide (Results), matching side by side the Tyr<sup>122</sup> side chain. Conversely, the axial disposition of the benzyl group of **2** gives rise to less favorable interactions, forcing the entire molecule to go into the receptor lopsided.

With regard to the  $\alpha_5\beta_1$  integrin, on the basis of the homology model discussed above, the  $\alpha_5\beta_1$  integrin seems to be more tolerant in hosting the aromatic side chain of both **2** and **3**. In particular, its larger binding site would more easily accommodate the phenyl ring of **2** with respect to the  $\alpha_v\beta_3$  integrin, leading to a pronounced  $\alpha_5\beta_1$  selectivity, while the disposition of **3** would be adequate for both integrins, leading to a generally good affinity (Figure 10).

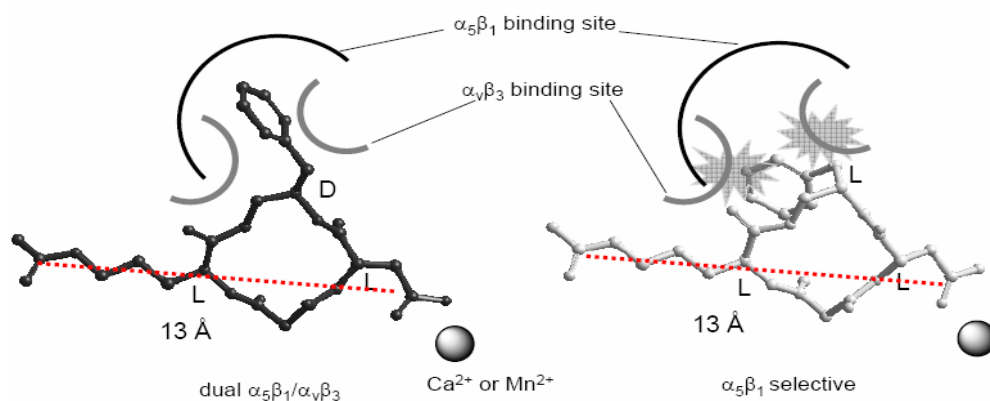


**Fig.(10).** Schematic representation of the proposed disposition of **3** (left, black) and **2** (right, white) within  $\alpha_5\beta_1$  (black line) and  $\alpha_v\beta_3$  (grey lines) integrin binding site sketches. Unfavourable interactions are also shown (transparent grey flashes).

Despite the moderate or absent activity as adhesion inhibitors, compounds **4-9** can be utilized to confirm the validity of the model proposed above for the more active compounds, **2** and **3**. Indeed, the structures of **4-9** obtained by conformational analysis (see the Supporting Information) in general correlate well with the activity profile of the compounds toward  $\alpha_5\beta_1$  and  $\alpha_v\beta_3$  integrins. Finally, the different affinities of **4-9** for the  $\alpha_v\beta_3$  receptor can be explained on the basis of docking analyses performed by Glide (see the Supporting Information).

## 4.5. Conclusions

In summary, we have reported the synthesis of a selected small library of RGD mimetics as  $\alpha_v\beta_3$  and/or  $\alpha_5\beta_1$  integrin antagonists. The compounds have been designed starting from 13-membered CTP scaffolds based on a partially retroinverso structure, containing (S)- or (R)-Asp, (S)- or (R)-Arg, and an (S)- or (R)-diamine as a  $\beta$ -Phe surrogate.

The different compounds exhibited variable activities as  $\alpha_v\beta_3$  or  $\alpha_5\beta_1$  integrin receptor antagonists, as determined by testing the inhibition of adhesion of fibronectin or vitronectin to  $\alpha_v\beta_3$  or  $\alpha_5\beta_1$  integrin receptor-expressing cell lines. c[(S)- $\beta$ Phe $\psi$ (NHCO)Asp $\psi$ (NHCO)Gly-(R)-Arg] (4) and c[(R)- $\beta$ Phe $\psi$ (NHCO)(R)-Asp $\psi$ (NHCO)Gly-Arg] (8) revealed moderate micromolar inhibitory activities; c[(S)- $\beta$ Phe $\psi$ (NHCO)Asp $\psi$ (NHCO)Gly-Arg] (2) displayed a submicromolar activity for  $\alpha_5\beta_1$  integrins, and a certain selectivity over  $\alpha_v\beta_3$  integrins, while c[(R)- $\beta$ Phe $\psi$ (NHCO)Asp $\psi$ (NHCO)-Gly-Arg] (3) was demonstrated to be a potent dual antagonist, with activities of  $10^{-8}$  and  $10^{-7}$  M for  $\alpha_5\beta_1$  and  $\alpha_v\beta_3$  integrins, respectively, and significantly inhibited bFGF-induced angiogenesis of HUVEC cultured in vitro. The different  $\alpha_5\beta_1$  versus  $\alpha_v\beta_3$  selectivity of **2** and **3** has been explained on the basis of their alternative secondary structures, discussed on the basis of NMR, ROESY, MD, and molecular docking analyses. In particular, the 3D display of the phenyl substituent of the diamine, pseudoaxial in **2** and pseudoequatorial in **3**, seems to be a major contributor to receptor selectivity.

These  $\alpha_v\beta_3$  and  $\alpha_5\beta_1$  antagonists may be potentially effective and safe for therapeutic purposes. Small RGD-containing peptidomimetics may be used as lead compounds for developing the potential therapeutic agents for angiogenesis-related diseases, including cancer.

## 4.6. Experimental Section

**4.6.1. General Methods.** Unless stated otherwise, standard chemicals were obtained from commercial sources and used without further purification. Flash chromatography was performed on silica gel (230-400 mesh), using mixtures of distilled EtOAc and MeOH. Semipreparative RP-HPLC was performed on a C18 column (7  $\mu$ m particle size, 21.2mm x150 mm, from a 7:3H<sub>2</sub>O/ CH<sub>3</sub>CN mixture to 100% CH<sub>3</sub>CN in 15 min) at a flow rate of 12 mL/min. The purity (>95%) of tested compounds was assessed by analytical RP-HPLC, on an ODS column (4.6  $\mu$ m particle size, 100Å pore diameter, 250 mm, DAD 210 nm, from a 9:1 H<sub>2</sub>O/CH<sub>3</sub>CN mixture to a 2:8 H<sub>2</sub>O/CH<sub>3</sub>CN mixture in 20 min) at a flow rate of 1.0 mL/min, followed by 10 min at the same composition. <sup>1</sup>H NMR spectra were recorded using 5 mm tubes, using 0.01 M peptide at 400 MHz at room temperature.

Solvent suppression was performed by the solvent presaturation procedure implemented in varian (presat). Chemical shifts are reported as  $\delta$  values relative to the solvent peak. The unambiguous assignment of <sup>1</sup>H NMR resonances was performed by gCOSY, HMBC, and HSQC. gCOSY experiments were conducted with a proton spectral width of 3103 Hz. VT <sup>1</sup>H NMR experiments were performed over the range of 298-348 K. Peaks were calibrated on DMSO. Conformational rearrangement was excluded since signal broadening was absent. 2D spectra were recorded in the phase sensitive mode and processed using a 90°-shifted, squared sine-bell apodization. ROESY experiments were recorded with a 300 or 350 ms mixing time with a proton spectral width of 3088 Hz.

#### 4.6.2. Representative Synthetic Procedures and Analytical Characterization of PMRI RGD Mimetics 2 and 3.

**11.** HOBT (0.16 g, 1.2 mmol) was added to a stirred solution of Fmoc-Asp(Mtr)-OH (0.61 g, 1.0 mmol) in a 9:1 DCM/DMF mixture (15 mL) at rt. After 10 min, 10 (0.28 g, 1.0 mmol), EDCI-HCl salt (0.24 g, 1.2 mmol), and TEA (0.40 mL, 3.0 mmol) were added while the mixture was stirred at rt. After 4 h, the mixture was diluted with DCM, and the solution was washed with 0.5 M HCl and saturated Na<sub>2</sub>CO<sub>3</sub>. The organic layer was dried over Na<sub>2</sub>SO<sub>4</sub>, and the solvent was removed under reduced pressure. The Fmoc dipeptide **11** was isolated by crystallization from a DCM/Et<sub>2</sub>O mixture [0.74 g, 85%, 88% pure by RP-HPLC (see General Methods); R<sub>f</sub>=11.7 min]: ES-MS m/z 875.3(M+1), calcd 875.4; <sup>1</sup>H NMR (200 MHz, CDCl<sub>3</sub>) δ 1.40-1.60 (m, 2H), 1.60-1.80 (m, 2H), 2.10 (s, 3H), 2.60 (s, 3H), 2.68 (s, 3H), 2.70-2.78 (m, 3H), 3.00-3.15 (m, 2H), 3.15-3.22 (m, 2H), 3.78 (s, 3H), 4.05 (m, 1H), 4.20 (m, 1H), 4.30-4.50 (m, 2H), 4.99 (s, 2H), 5.45 (br d, 1H), 5.50 (br d, 1H), 5.70 (br s, 1H), 6.10 (br s, 2H), 6.50 (s, 1H), 7.05-7.42 (m, 15H), 7.55 (br d, 2H), 7.75 (br d, 2H).

Fmoc group deprotection was performed by treatment with 2 M DMA in THF (6 mL) at rt. After 30 min, the solution was evaporated at reduced pressure, and the treatment was repeated.

After final evaporation of the solution, the residue was triturated twice in n-pentane. The deprotected dipeptide [0.50 g, 90%, 86% pure by RP-HPLC (see General Methods); R<sub>f</sub>=8.8 min] was used without further purification: ES-MS m/z 653.3 (M + 1), calcd 653.3. **12.**

A solution of Meldrum's acid (0.85 g, 6 mmol) and H-Asp(Ot-Bu)-OBz (1.4 g, 5 mmol) in CH<sub>3</sub>CN (15 mL) was warmed to 70 °C under an inert atmosphere. After 3 h, a 4:1 cyclohexane/Et<sub>2</sub>O mixture (40 mL) was added, and the oily residue that precipitated was separated. This residue was washed twice with a 4:1 hexane/Et<sub>2</sub>O mixture (20 mL), and the resulting dense oil was dissolved in EtOAc (40 mL) and washed with 0.1 M HCl (5 mL). The organic layer was dried over Na<sub>2</sub>SO<sub>4</sub>, and solvent was evaporated at reduced pressure (<40°C), giving **12** as a waxy solid, which was used for the following step without further purification (1.2 g, 68%, 84% pure by NMR analysis): <sup>1</sup>H NMR (300 MHz, CDCl<sub>3</sub>) δ 1.31 (s, 9H), 2.72 (dd, J=5.1, 17.2 Hz, 1H), 2.86 (dd, J=4.8, 17.2 Hz, 1H), 3.28 (br s, 2H), 4.82 (m, 1H), 5.05 (d, J=12.1 Hz, 1H), 5.14 (d, J = 12.1 Hz, 1H), 7.25-7.40 (m, 5H), 7.86 (br d, 1H), 9.70-10.4 (br s, 1H).

**13.** Dipeptides **11** (0.33 g, 0.5 mmol) and **12** (0.18 g, 0.5 mmol) were coupled under the same conditions used for the synthesis of **11** with HOBT (0.082 g, 0.6 mmol), EDCI-HCl salt (0.12 g, 0.6 mmol), and TEA (0.20 mL, 1.5 mmol) in a 9:1 DCM/DMF mixture (10 mL) at rt. After 5 h, the usual workup afforded the fully protected tetrapeptide **13**, isolated by crystallization from a DCM/Et<sub>2</sub>O mixture [0.32 g, 65%, 86% pure by RP-HPLC (see General Methods); R<sub>f</sub>=11.2 min]: ES-MS m/z 1001.3 (M + 1), calcd 1001.4; <sup>1</sup>H NMR (200 MHz, CDCl<sub>3</sub>) δ 1.48 (s, 9H) 1.54-1.70 (m, 2H), 1.77 (m, 1H), 1.92 (m, 1H), 2.10 (s, 3H), 2.50 (br s, 1H), 2.70 (s, 3H), 2.76 (s, 3H), 2.74-2.85 (m, 3H), 3.18-3.38 (m, 3H), 3.39-3.50 (m, 3H), 3.90 (s, 3H), 4.10 (m, 1H), 4.60 (m, 1H), 4.93 (m, 1H), 5.03-5.25 (m, 4H), 6.01 (d, J= 8.0 Hz, 1H), 6.20-6.40 (br s, 1H), 6.42 (br s, 2H), 6.60 (s, 1H), 7.18-7.42 (m, 15H), 7.78 (br t, 1H), 7.97 (br d, 1H), 8.10 (br d, 1H); <sup>13</sup>C NMR (300 MHz, 9:1 CDCl<sub>3</sub>/DMSO-d<sub>6</sub>) δ 14.5, 17.1, 23.6, 27.3, 29.0, 29.2, 35.5, 37.9, 38.5, 39.8, 48.7, 49.2, 53.3, 55.0, 56.1, 69.6, 73.7, 111.0, 121.3, 125.8, 127.3, 127.3, 127.5, 128.3, 128.3, 128.4, 128.4, 128.6, 128.6, 128.7, 128.7, 130.1, 130.1, 130.6, 132.3, 132.9, 133.8, 136.5, 138.8, 150.2, 157.2, 162.6, 163, 165.7, 167.6, 170.9, 170.9, 172.0, 174.7.

**4.6.3.14 {c[βPheψ(NHCO)Asp(Ot-Bu)ψ(NHCO)Gly-Arg(Mtr)]}**. Removal of the protecting group from **13** (0.32 g, 0.32 mmol) was performed by treatment with H<sub>2</sub> and catalytic Pd/C in EtOH (15 mL) at rt. After 6 h, the mixture was filtered over Celite, and the solvent was evaporated at reduced pressure, giving the linear tetrapeptide H-βPheψ(NHCO)Asp(Ot-Bu)ψ-(NHCO)Gly-Arg(Mtr)-OH [0.24 g, 96%, 84% pure by RP-HPLC (see General Methods); R<sub>f</sub>= 5.9 min], used without further purification: ES-MS m/z 776.3 (M + 1), calcd 776.4. A mixture of the deprotected tetrapeptide (0.24 g, 0.31 mmol), DPPA (0.15 mL, 0.62 mmol), and NaHCO<sub>3</sub> (0.42 g, 5.0 mmol) in DMF (70 mL) was stirred at rt. After 72 h, the solvent was distilled under reduced pressure, the residue was diluted with water, and the mixture was extracted three times with DCM.

The solution was evaporated under reduced pressure, and the residue was precipitated from a DCM/Et<sub>2</sub>O mixture. Semipreparative RP-HPLC (General Methods) gave **14** [0.16 g, 69%, 96% pure by RP-HPLC (see General Methods); R<sub>f</sub>=8.3 min]: ES-MS m/z 758.5 (M + 1), calcd 758.4; <sup>1</sup>H NMR (400 MHz, DMSO-d<sub>6</sub>) δ 1.39 (s, 9H, t-Bu), 1.40-1.60 (m, 3H, ArgH<sub>γ</sub> + ArgH<sub>β</sub>), 1.70 (m, 1H, ArgH<sub>β</sub>), 2.07 (s, 3H, CH<sub>3</sub>), 2.29 (dd, J=10.0, 16.5 Hz, 1H, AspH<sub>β</sub>), 2.49 (dd, J=4.1, 16.5 Hz, 1H, AspH<sub>β</sub>), 2.52 (s, 3H, CH<sub>3</sub>), 2.62 (s, 3H, CH<sub>3</sub>), 2.62-2.85 (m, 2H, diamH<sub>β</sub>), 2.95-3.18 (m, 4H, Hc+ArgH<sub>δ</sub>), 3.18 (d, J=11.0 Hz, 1H, COCH<sub>2</sub>CO), 3.26 (d, J=11.0 Hz, 1H, COCH<sub>2</sub>CO), 3.81 (s, 3H, OCH<sub>3</sub>), 3.85 (m, 1H, diamH<sub>α</sub>), 4.05 (m, 1H, ArgH<sub>α</sub>), 4.25 (m, 1H, AspH<sub>α</sub>), 6.30-6.50 (m, 2H, ArgNH<sub>η</sub>), 6.46 (d, J=8.4 Hz, 1H, NH<sub>a</sub>), 6.70 (s, 1H, 50-ArH), 6.82 (t, J=5.4 Hz, 1H, NH<sub>b</sub>), 6.92 (m, 1H, ArgNH<sub>ε</sub>), 7.15-7.35 (m, 5H, ArH), 8.88 (d, J=6.6 Hz, 1H, ArgNH), 9.04 (d, J=6.6 Hz, 1H, AspNH); <sup>13</sup>C NMR (400 MHz, DMSO-d<sub>6</sub>) δ 18.5, 19.1, 24.0, 25.9, 29.1, 29.3, 36.0, 37.5, 39.1, 39.8, 48.8, 50.4, 51.8, 55.0, 56.3, 73.2, 112.2, 121.3, 125.8, 128.3, 128.3, 128.6, 128.6, 132.6, 132.9, 136.3, 139.2, 162.9, 165.8, 170.9, 170.9, 172.2, 174.7, 175.0.

**4.6.4. 2 {c[βPheψ(NHCO)Aspψ(NHCO)Gly-Arg]}**. The protected cyclotetrapeptide **14** (0.16 g, 0.21 mmol) was treated with a 94:2:1:2:1 mixture of TFA and scavengers [TFA/PhOH/PhSH/ H<sub>2</sub>O/Et<sub>2</sub>S (5 mL)] at rt for 30 min. The mixture was distilled under reduced pressure, and the treatment was repeated. The residue was suspended in Et<sub>2</sub>O, and the precipitate was centrifuged.

The resulting crude residue was purified by semipreparative RP-HPLC (General Methods), giving **2** [0.077 g, 76%, 97% pure by analytical RP-HPLC (see General Methods); R<sub>f</sub>=1.8 min]: ES-MS m/z 490.2 (M + 1), calcd 490.2; <sup>1</sup>H NMR (400 MHz, 8:2 DMSO-d<sub>6</sub>/H<sub>2</sub>O) δ 1.45-1.60 (m, 3H, ArgH<sub>γ</sub> + ArgH<sub>β</sub>), 1.74 (m, 1H, ArgH<sub>β</sub>), 2.30 (dd, J=9.5, 16.0 Hz, 1H, AspH<sub>β</sub>), 2.47 (dd, J=4.0, 16.0 Hz, 1H, AspH<sub>β</sub>), 2.60-2.86 (m, 2H, diamH<sub>β</sub>), 2.92-3.20 (m, 4H, Hc+ArgH<sub>δ</sub>), 3.19 (d, J=10.8 Hz, 1H, COCH<sub>2</sub>CO), 3.24 (d, J=10.8 Hz, 1H, COCH<sub>2</sub>CO), 3.68 (m, 1H, diamH<sub>α</sub>), 3.96 (m, 1H, ArgH<sub>α</sub>), 4.20 (m, 1H, AspH<sub>α</sub>), 6.70 (d, J=8.4 Hz, 1H, NH<sub>a</sub>), 6.90 (br t, 1H, NH<sub>b</sub>), 7.10-7.35 (m, 5H, ArH), 7.90 (br s, 1H, ArgNH<sub>ε</sub>), 9.10 (br d, 1H, ArgNH), 9.28 (br d, 1H, AspNH); <sup>13</sup>C NMR (400 MHz, 8:2 DMSO-d<sub>6</sub>/ H<sub>2</sub>O) δ 26.0, 29.2, 36.5, 37.5, 39.0, 39.8, 40.0, 48.8, 50.2, 51.8, 55.0, 126.0, 128.1, 128.3, 128.8, 128.7, 138.8, 163.9, 171.0, 171.2, 174.7, 175.1, 177.7.

**4.6.5. 3 {c[(R)-βPheψ(NHCO)Aspψ(NHCO)Gly-Arg]}**: <sup>1</sup>H NMR (400 MHz, 8:2 DMSO-d<sub>6</sub>/H<sub>2</sub>O) δ 1.42-1.50 (m, 2H, ArgH<sub>γ</sub>), 1.56 (m, 1H, ArgH<sub>β</sub>), 1.74 (m, 1H, ArgH<sub>β</sub>), 2.40 (dd, J=6.0, 16.8 Hz, 1H, AspH<sub>β</sub>), 2.58 (dd, J=7.2, 16.8 Hz, 1H, AspH<sub>β</sub>), 2.75 (dd, J=6.6, 16.0 Hz, 1H, diamH<sub>β</sub>), 2.83 (dd, J=8.0, 16.0 Hz, 1H, diamH<sub>β</sub>), 2.95-3.15 (m, 3H, Hc + ArgH<sub>δ</sub>), 3.20 (d, J=10.2 Hz, 1H, COCH<sub>2</sub>CO), 3.21 (d, J=10.2 Hz, 1H, COCH<sub>2</sub>CO), 3.28

(m, 1H, Hc), 3.67 (m, 1H, diamHa), 3.95 (m, 1H, ArgHa), 4.26 (m, 1H, AspHa), 7.02 (br t, 1H, NHb), 7.10-7.35 (m, 5H, ArH), 7.62 (d, J=6.9 Hz, 1H, NHa), 7.90 (br s, 1H, ArgNHε), 8.85 (br d, 1H, ArgNH), 9.22 (br d, 1H, AspNH); <sup>13</sup>CNMR (400 MHz, 8:2 DMSO-d<sub>6</sub>/H<sub>2</sub>O) δ 26.0, 29.0, 34.5, 36.6, 39.3, 39.8, 39.9, 48.8, 50.4, 52.8, 56.6, 124.5, 127.9, 127.9, 129.0, 129.1, 138.8, 163.8, 171.3, 175.0, 175.1, 176.1.

#### 4.7. Pharmacological Assays

**4.7.1. Materials for Bioassays.** Trypsin/ EDTA, nonessential amino acids, minimum essential medium (MEM), RPMI-1640 with L-glutamine, antibiotic and antimycotic solution, and glycine were purchased from Invitrogen (Carlsbad, CA). Fetal bovine serum (FBS) and phosphatebuffered saline (PBS) were from Cambrex (Walkersville, MD).

Citrate buffer solution, EDTA, DMSO, Triton X-100, 4-nitrophenylN- acetyl-β-D-glucosaminide, phorbol 12 myristate 13-acetate (PMA), pyruvic acid, fibronectin, and vitronectin, both from human plasma, were obtained from Sigma-Aldrich SRL (Milan, Italy). SK-MEL-24 (human malignant melanoma) and K-562 (human erythroleukemia) were obtained from American Tissue Culture Collection (ATCC, Rockville, MD). HUVEC (human umbilical vein endothelial cells) were obtained from Clonetics (Cambrex). Matrigel-precoated 96-well plates and human recombinant bFGF were from BD Biosciences (Bedford, MA).

**4.7.2. Cell Culture.** SK-MEL-24 were routinely grown in MEM supplemented with 10% FBS, nonessential amino acids, and sodium pyruvate. K-562 were maintained as a stationary suspension culture in RPMI-1640 and L-glutamine with 10% FBS. HUVEC were cultured in endothelial growth medium (EGM, Clonetics), containing fetal bovine serum, bovine brain extract, human epidermal growth factor, hydrocortisone, gentamicin, and amphotericin B; cells from passages 2-7 were used in this study. Cells were kept at 37 °C in a 5% CO<sub>2</sub> humidified atmosphere.

Forty hours before the experiment, K-562 were treated with 25 ng/mL PMA to induce differentiation with an increased level of expression of cell surface antigens<sup>[75]</sup>.

**4.7.3. Cell Adhesion Assays<sup>[76]</sup>** Plates (96 wells) (Corning, New York, NY) were coated by passive adsorption with fibronectin (10 µg/mL) or vitronectin (10 µg/mL) overnight at 4°C. Cells were counted and exposed to different concentrations of each compound for 30 min at room temperature to allow the ligand-receptor equilibrium to be reached. Stock solutions (10<sup>-2</sup> M) of the assayed compounds were prepared in 33% DMSO in phosphate-buffered saline (v/v); further dilutions were done in PBS alone. The highest concentration of DMSO in the assays was 1% of the stock solution. Control cells were exposed to the same concentration of DMSO. At the end of the incubation time, the cells were plated (50000 cells/well) and incubated at room temperature for 1 h. Then, all the wells were washed with PBS to remove nonadherent cells, and 50 µL of hexosaminidase [4-nitrophenylN-acetyl-β-D-glucosaminide dissolved at a concentration of 7.5 mM in 0.09 M citrate buffer solution (pH 5) and mixed with an equal volume of 0.5% Triton X-100 in water] was added. This product is a chromogenic substrate for β-N-acetylglucosaminidase that is transformed in 4-nitrophenol whose absorbance is measured at 405 nm. As previously described<sup>[77]</sup>, there is a linear correlation between absorbance and enzymatic activity. Therefore, it is possible to identify the number of adherent cells in treated

wells, interpolating the absorbance values of the unknowns in a calibration curve. The reaction was blocked by addition of 100  $\mu\text{L}$  of a stopping solution [50  $\mu\text{M}$  glycine and 5  $\mu\text{M}$  EDTA (pH 10.4)], and the plates were read in a Victor2 Multilabel Counter (Perkin-Elmer, Waltham, MA). Experiments were conducted in quadruplicate and were repeated at least three times. Data analysis and  $\text{IC}_{50}$  values were calculated using Graph-Pad Prism 3.0 (GraphPad Software, San Diego, CA).

**4.7.4. Flow Cytometry Assay.** To assess the amount of intact, apoptotic or necrotic cells, an Annexin V-Fluos (Roche)/propidium iodide (PI) (Sigma-Aldrich) assay was performed. Double staining against annexin V together with PI separates cells, not necrotic, currently undergoing apoptosis from cells that have died of necrosis. HUVEC were treated with different concentrations of the assayed compounds for 30 min at 37°C; the cells were detached and fixed with 1% paraformaldehyde for 15 min and then washed with PBS. Thereafter, HUVEC were resuspended in Annexin-V-Fluos incubation buffer [10 mM Hepes/ NaOH (pH 7.4), 140 mM NaCl, and 5 mM  $\text{CaCl}_2$ ] with prediluted Annexin-V-Fluos and PI, according to the manufacturers' instructions. After incubation for 15 min at room temperature in the dark, the cells were analyzed with EPICS XLMCL (Beckman Coulter).

**4.7.6. In Vitro Tubular Formation of HUVEC.** The endothelial tube formation assay was performed as described<sup>[78]</sup>. Matrigel precoated 96-well plates were used, and HUVEC (5000 cells/ well) were seeded in the presence of different concentrations of test compounds, in the absence (negative control) or presence of bFGF (30 ng/mL). Cells were incubated for 16 h at 37°C. After incubation, these cells underwent differentiation into capillarylike tube structures; tube formation was examined by a NIKON microscope equipped with a camera. The experiments were repeated three times.

#### 4.8. Conformational Analysis.

ROESY intensities were classified very strong, strong, medium, and weak and were associated with distances of 2.3, 2.6, 3.0, and 4.0 Å, respectively. Geminal couplings and other obvious correlations were discarded. For the absence of HR-COCH<sub>2</sub>CO or HR-NHCH (i, i + 1) ROESY cross-peaks, the  $\omega$  bonds were set at 180° (force constant of 16 kcal mol<sup>-1</sup> Å<sup>-2</sup>). Only ROESY-derived constraints were included in the restrained MD. The restrained MD simulations were conducted using the AMBER70 force field in a 30 Å x 30 Å x 30 Å box of standard TIP3P models of equilibrated water. All water molecules with atoms that come closer to a solute atom than 2.3 Å were eliminated. A 50 ps simulation at 1200 K was used for generating 50 random structures that were subsequently subjected to a 20 ps restrained MD with a 50% scaled force field at the same temperature, followed by 20 ps with full restraints (distance force constant of 7 kcal mol<sup>-1</sup> Å<sup>-2</sup>), after which the system was cooled in 5 ps to 50 K. H-Bond interactions were not included, nor were torsion angle restraints. The resulting structures were minimized with 3000 cycles of steepest descent and 3000 cycles of conjugated gradient (convergence of 0.01 kcal Å<sup>-1</sup> mol<sup>-1</sup>). The backbones of the structures were clustered by the rmsd analysis module of HyperChem. Unrestrained MD simulation in explicit water was performed for 10 ns at 298 K, at constant temperature and pressure (Berendsen scheme,<sup>79</sup> bath relaxation

constant of 0.2)<sup>[80]</sup>. For 1-4 scale factors, van der Waals and electrostatic interactions are scaled in AMBER to half their nominal value. The integration time step was set to 0.1 fs. Box equilibration was set to 10 ps.

**4.8.1. Molecular Docking.** All calculations were run using the Schrödinger suite of programs (<http://www.schrodinger.com>) through the Maestro graphical interface.

**4.8.2. Protein Setup.** The recently determined crystal structure of the extracellular domain of the integrin  $\alpha_v\beta_3$  receptor in complex with cilengitide and in the presence of the proadhesive ion  $Mn^{2+}$  (PDB entry 1L5G) was used for docking studies. Docking was performed only on the globular head of the integrin because the headgroup of integrin has been identified in the X-ray structure as the ligand-binding region. The protein structure was set up for docking as follows; the protein was truncated to residues 41-342 for chain  $\alpha$  and residues 114-347 for chain  $\beta$ .

Due to a lack of parameters, the  $Mn^{2+}$  ions in the experimental protein structure were modeled via replacement with  $Ca^{2+}$  ions.

The resulting structure was prepared using the Protein Preparation Wizard of the graphical user interface Maestro and the OPLSAA force field.

**4.8.3. Docking.** The automated docking calculations were performed using Glide<sup>[72]</sup> (Grid-based Ligand Docking with Energetics) within the framework of Impact version 4.5 in a standard precision mode (SP). The grid generation step started from the extracellular fragment of the X-ray structure of the  $\alpha_v\beta_3$  complex with cilengitide, prepared as described in Protein Setup. The center of the grid-enclosing box was defined by the center of the bound ligand. The enclosing box dimensions, which are automatically deduced from the ligand size, fit the entire active site. For the docking step, the size of the bounding box for placing the ligand center was set to 12Å. No further modifications were applied to the default settings. The Glide-Score function was used to select 20 poses for each ligand. Glide was initially tested for its ability to reproduce the crystallized binding geometry of cilengitide. The program was successful in reproducing the experimentally found binding mode of this compound, as it corresponds to the best-scored pose.

## 4.9. Supporting Information

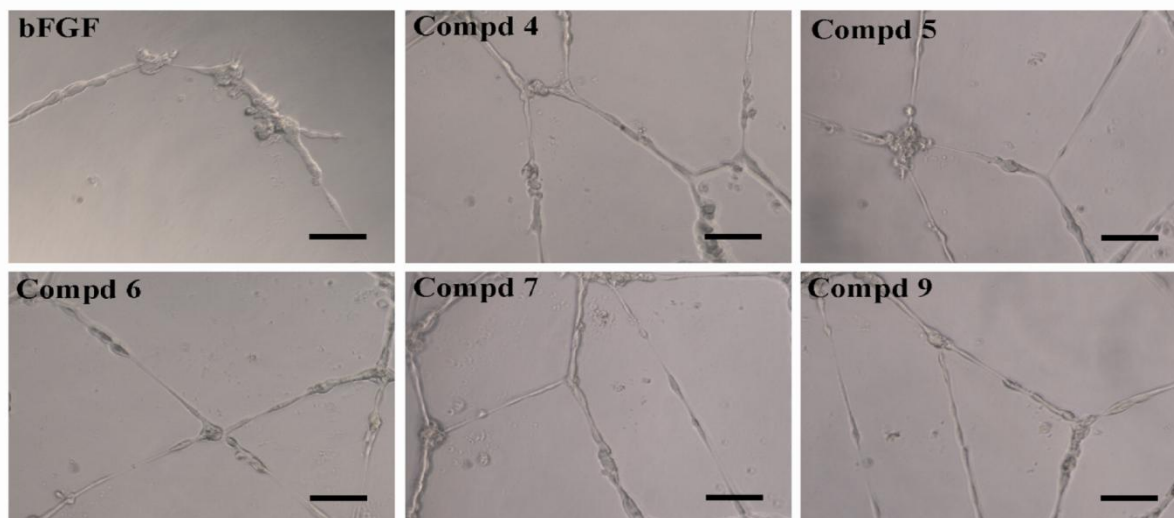


**Figure S1.** Tube formation of HUVEC cells on Matrigel. Representative pictures of capillary-like structures (black bar in the pictures corresponds to 100  $\mu\text{m}$ ). HUVEC cells were treated with or without integrin antagonists (10  $\mu\text{M}$ ) and then plated on Matrigel in the absence or presence of bFGF (30 ng/mL) for 16h. Compounds **4**, **5**, **6**, **7** and **9** were not effective as angiogenesis inhibitors.

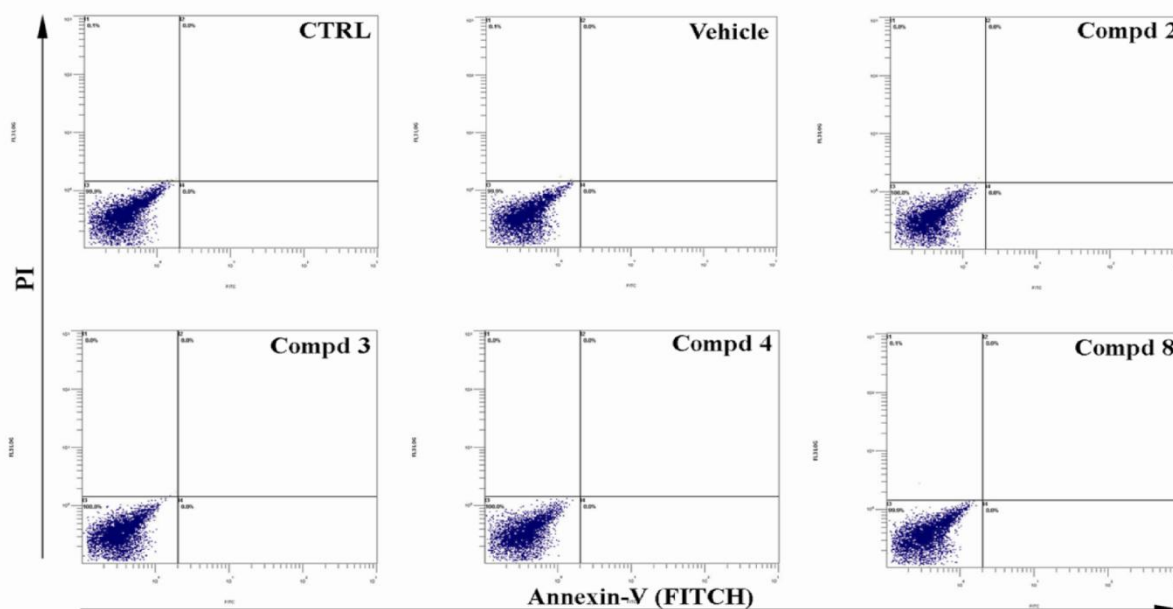


**Figure S2.**  $\alpha_v\beta_3/\alpha_5\beta_1$  integrin antagonists did not induce apoptosis or necrosis in endothelial cells. No significant increase in apoptotic or necrotic cells was observed among endothelial cells treated with 10  $\mu\text{M}$  integrin antagonists. HUVEC cells were treated with integrin antagonists for 16 h; then the cells were detached and stained with Annexin-V and PI to distinguish healthy cells (Annexin-V<sup>-</sup> and PI<sup>-</sup>), early apoptotic cells (Annexin-V<sup>+</sup> and PI<sup>-</sup>), and late apoptotic/necrotic cells (Annexin-V<sup>+</sup> and PI<sup>+</sup>). A representative experiment of three done with superimposable results is shown.

### Analytical characterization of PMRI RGD-mimetics 4, 5.

Compounds 6-9 are the enantiomers of 2-5, respectively. The syntheses of 3-9 were performed as reported for 2.

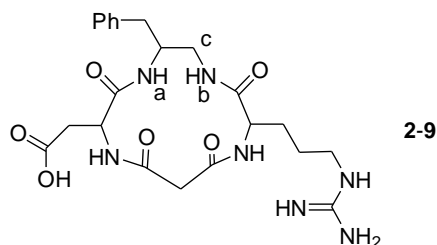


Figure S3

(4), c[βPheψ(NHCO)Aspψ(NHCO)Gly-(*R*)-Arg]. <sup>1</sup>H-NMR (400 MHz, 8/2 DMSO-d<sub>6</sub>/H<sub>2</sub>O): δ = 1.40-1.55 (m, 3H, ArgH<sub>γ</sub>+ArgH<sub>β</sub>), 1.67 (m, 1H, ArgH<sub>β</sub>), 2.36 (dd, J = 9.0, 15.0 Hz, 1H, AspH<sub>β</sub>), 2.50 (dd, J = 4.0, 15.0 Hz, 1H, AspH<sub>β</sub>), 2.58-2.87 (m, 3H, Hc+diamH<sub>β</sub>), 2.91 (d, J = 10.4 Hz, 1H, COCH<sub>2</sub>CO), 2.92-3.20 (m, 2H, ArgH<sub>δ</sub>), 3.20 (d, J = 10.4 Hz, 1H, COCH<sub>2</sub>CO), 3.55 (m, 1H, Hc), 3.80 (m, 1H, diamH<sub>α</sub>), 3.90 (m, 1H, ArgH<sub>α</sub>), 4.18 (m, 1H, AspH<sub>α</sub>), 6.65 (d, J = 8.4 Hz, 1H, NH<sub>a</sub>), 6.95 (br.t, 1H, NH<sub>b</sub>), 7.10-7.35 (m, 5H, ArH), 8.00 (br.s, 1H, ArgNH<sub>ε</sub>), 8.61 (br.d, 1H, ArgNH), 8.75 (br.d, 1H, AspNH). <sup>13</sup>C-NMR (400 MHz, 8/2 DMSO-d<sub>6</sub>/H<sub>2</sub>O): δ = 27.0, 30.2, 36.0, 37.4, 38.5, 40.0, 40.6, 48.2, 49.9, 51.4, 55.3, 125.1, 128.0, 128.3, 129.0, 129.2, 138.2, 163.6, 171.8, 173.2, 173.5, 175.0, 176.5.

(5), c[βPheψ(NHCO)-(*R*)-Aspψ(NHCO)Gly-Arg]. <sup>1</sup>H-NMR (400 MHz, 8/2 DMSO-d<sub>6</sub>/H<sub>2</sub>O): δ = 1.38-1.57 (m, 3H, ArgH<sub>γ</sub>+ArgH<sub>β</sub>), 1.61 (m, 1H, ArgH<sub>β</sub>), 2.41 (dd, J = 9.0, 15.0 Hz, 1H, AspH<sub>β</sub>), 2.54 (dd, J = 4.0, 15.0 Hz, 1H, AspH<sub>β</sub>), 2.70-2.80 (m, 2H, diamH<sub>β</sub>), 2.81 (d, J = 10.6 Hz, 1H, COCH<sub>2</sub>CO), 2.90 (m, 1H, Hc), 2.91-3.19 (m, 2H, ArgH<sub>δ</sub>), 3.22 (d, J = 10.4 Hz, 1H, COCH<sub>2</sub>CO), 3.50 (m, 1H, Hc), 3.90 (m, 1H, diamH<sub>α</sub>), 4.05 (m, 1H, ArgH<sub>α</sub>), 4.25 (m, 1H, AspH<sub>α</sub>), 6.99 (d, J = 8.4 Hz, 1H, NH<sub>a</sub>), 7.08 (br.t, 1H, NH<sub>b</sub>), 7.10-7.38 (m, 5H, ArH), 8.30 (br.s, 1H, ArgNH<sub>ε</sub>), 8.40 (br.d, 1H, ArgNH), 8.75 (br.d, 1H, AspNH). <sup>13</sup>C-NMR (400 MHz, 8/2 DMSO-d<sub>6</sub>/H<sub>2</sub>O): δ = 26.7, 30.6, 36.9, 37.3, 38.4, 39.8, 40.4, 48.8, 49.7, 52.3, 55.3, 125.7, 128.2, 128.8, 129.4, 129.6, 135.2, 164.6, 169.8, 173.7, 174.0, 175.6, 176.4.

**Table S1.** Non-obvious ROESY cross-peaks observed for 4. Stereochemistry has been omitted. For Ha, Hb, Hc, see Figure S3; u = upfield, d = downfield; vs = very strong, s = strong, m = medium, w = weak

Cross peak	Intensity	Cross peak	Intensity
AspNH-NHa	s	AspNH-ArgNH	w
AspNH-AspH <sub>α</sub>	m	AspNH-COCH <sub>2</sub> CO <sub>u</sub>	vs
ArgNH-COCH <sub>2</sub> CO <sub>u</sub>	s	AspNH-COCH <sub>2</sub> CO <sub>d</sub>	w
ArgNH-COCH <sub>2</sub> CO <sub>d</sub>	m	AspNH-AspH <sub>βd</sub>	w
NH <sub>b</sub> -ArgH <sub>α</sub>	s	ArgNH-NH <sub>b</sub>	s
NH <sub>a</sub> -NH <sub>b</sub>	m	ArgNH-ArgH <sub>α</sub>	s
diamH <sub>α</sub> -NH <sub>b</sub>	m	ArgNH-NHa	w

NHb-Hc <sub>u</sub>	m	NHb-Hc <sub>d</sub>	vs
NHa-diamH $\beta$	s	NHa-AspH $\beta$ <sub>d</sub>	m
NHa-Hc <sub>u</sub>	w	NHa-AspH $\alpha$	m
AspH $\alpha$ -AspH $\beta$ <sub>d</sub>	m	AspH $\alpha$ -AspH $\beta$ <sub>u</sub>	w
ArgH $\alpha$ -ArgH $\beta$ <sub>u</sub>	vs	NHa-diamH $\alpha$	s
ArgH $\alpha$ -ArgH $\beta$ <sub>d</sub>	m	diamH $\alpha$ -diamH $\beta$	s
ArgH $\alpha$ -ArgH $\gamma$	w	ArgH $\alpha$ -ArgH $\delta$	m
diamH $\alpha$ -Hc <sub>u</sub>	m	diamH $\alpha$ -Hc <sub>d</sub>	vs
diamH $\alpha$ -diamH $\beta$	vs	Hc <sub>u</sub> -diamH $\beta$	s
Hc <sub>u</sub> -diamH $\beta$	m	ArgH $\delta$ -ArgH $\gamma$	s
ArgH $\beta$ -ArgH $\gamma$	vs		

**Table S2.** Non-obvious ROESY cross-peaks observed for **5**. Stereochemistry has been omitted. For Ha, Hb, Hc, see Figure S3; u = upfield, d = downfield; vs = very strong, s = strong, m = medium, w = weak

Cross peak	Intensity	Cross peak	Intensity
AspNH-AspH $\beta$ <sub>d</sub>	m	AspNH-COCH <sub>2</sub> CO <sub>d</sub>	m
AspNH-AspH $\alpha$	s	AspNH-NHa	s
AspNH-COCH <sub>2</sub> CO <sub>u</sub>	s	ArgNH-COCH <sub>2</sub> CO <sub>u</sub>	vs
ArgNH-ArgH $\alpha$	m	ArgNH-NHb	s
ArgNH-ArgH $\beta$ <sub>d</sub>	m	NHb-Hc <sub>d</sub>	s
NHb-diamH $\beta$	w	NHb-diamH $\alpha$	w
NHb-ArgH $\alpha$	vs	NHb-ArgNH	vs
NHb-Hc <sub>u</sub>	m	NHa-diamH $\beta$	s
NHa-Hc <sub>d</sub>	m	NHa-diamH $\alpha$	s
AspH $\alpha$ -AspH $\beta$ <sub>d</sub>	m	AspH $\alpha$ -AspH $\beta$ <sub>u</sub>	w
NHa-AspH $\alpha$	vs	NHa-ArgH $\alpha$	w
diamArH-Hc <sub>d</sub>	m	diamArH-diamH $\beta$	vs
diamArH-diamH $\alpha$	vs	diamArH-AspH $\alpha$	w
ArgH $\alpha$ -ArgH $\beta$ <sub>d</sub>	m	diamArH-Hc <sub>u</sub>	m
ArgH $\alpha$ -ArgH $\gamma$	w	ArgH $\alpha$ -ArgH $\delta$	m
diamH $\alpha$ -diamH $\beta$	vs	ArgH $\alpha$ -ArgH $\beta$ <sub>u</sub>	s
diamH $\alpha$ -Hc <sub>u</sub>	s	diamH $\alpha$ -Hc <sub>d</sub>	m
ArgH $\beta$ -ArgH $\gamma$	s	ArgH $\delta$ -ArgH $\gamma$	s

#### Conformational analysis of **4** and **5** in solution.

The conformational analyses of **4** and **5** were performed by NMR spectroscopy and Molecular Dynamics (MD) simulations as reported for **2**, **3**. The <sup>1</sup>H-NMR of **4** and **5** revealed a single set of resonances. Variable

temperature  $^1\text{H-NMR}$  experiments were utilized to deduce the presence of H-bonds involving amide protons (Table S3).

**Table S3.**  $\Delta\delta/\Delta t$  values (ppb/ $^\circ\text{K}$ ) of amide protons for **4** and **5**, determined by VT- $^1\text{H-NMR}$  analysis in 8/2 DMSO- $d_6$ /H $_2$ O at 400 MHz over the range 298-348  $^\circ\text{K}$ . (NHa, NHb, see Figure S3)

Compd	AspNH	ArgNH	NHa	NHb
4	-4.0	-3.0	-1.3	-0.2
5	-2.8	-3.0	-0.7	-1.5

As for **2**, in **4** and **5** the comparatively low  $\Delta\delta/\Delta t$  values of diamine NHa and NHb with respect to AspNH and ArgNH suggest the existence of secondary structures in equilibrium, alternatively stabilized by H-bonds involving NHa or NHb.

Molecular backbone conformations were investigated by 2D ROESY and restrained molecular dynamics performed in a box of explicit water. For the absence of  $\text{H}\alpha_i\text{-H}\alpha_{i+1}$  cross peaks, all of the  $\omega$  bonds were set at  $180^\circ$ . After cluster analysis, for both **4** and **5** the computations essentially gave two kinds of structures, **4a/4b** (Figure S4) and **5a/5b** (Figure S5), differing exclusively by the opposite orientation of ArgNH, and AspNH, respectively, each showing some constraint violations (Table S4).

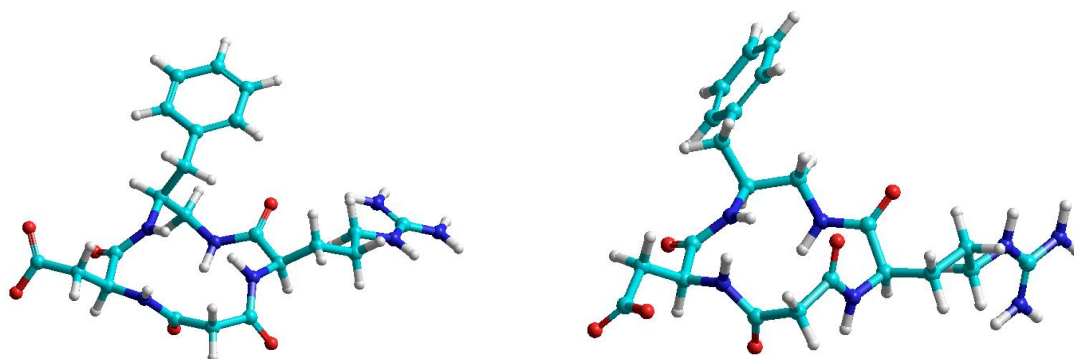


**Figure S4.** Representative, low-energy structure **4a** (left) and **4b** (right) consistent with ROESY analysis.

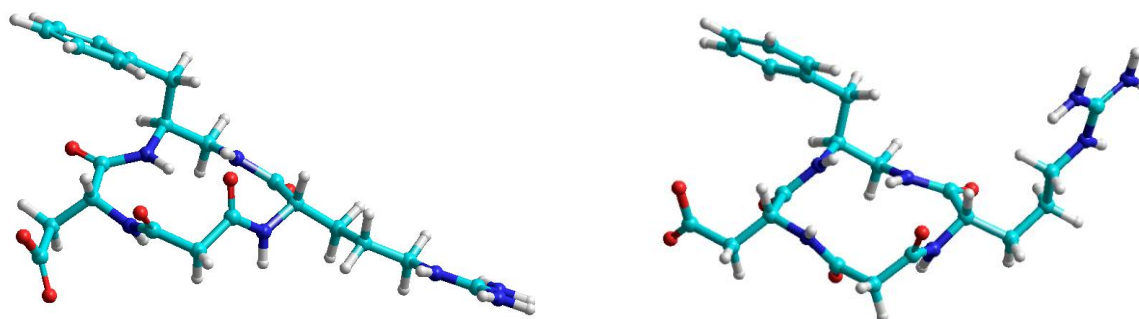


**Figure S5.** Representative, low-energy structure **5a** (left) and **5b** (right) consistent with ROESY analysis.

The couples **4a/4b** and **5a/5b** reasonably represent conformers in equilibrium. The structure **4a** is compatible with the strong cross-peaks observed between COCH<sub>2</sub>CO<sub>u</sub> and both AspNH and ArgNH; the structure **4b** is compatible with the medium cross peak between COCH<sub>2</sub>CO<sub>d</sub> and ArgNH, and with the strong cross-peak between ArgNH and ArgH<sub>α</sub>. For compound **5**, the strong cross peaks between COCH<sub>2</sub>CO<sub>u</sub> and both AspNH and ArgNH account for the structure **5a**; the cross peak of medium intensity between AspNH and COCH<sub>2</sub>CO<sub>d</sub>, and the strong cross-peak between AspNH and AspH<sub>α</sub> account for the structure **5b**.

The structures **4b** and **5b** show a smaller number of distance violations (Table S4) with respect to **4a** and **5a**, respectively, and conformations more compatible with VT-NMR data, which are suggestive of H-bonds on both NH<sub>a</sub> and NH<sub>b</sub>.

**Table S4.** Distance violations, calculated vs constraint (Å)<sup>a</sup> for ROESY-derived structures. Residue stereochemistry has been omitted.

4a	4b	5a	5b
ArgNH-ArgH <sub>α</sub> 2.9 vs 2.6	ArgNH-ArgH <sub>α</sub> 2.3 vs 2.6	AspNH-AspH <sub>α</sub> 2.9 vs 2.6	AspNH-AspH <sub>α</sub> 2.3 vs 2.6
ArgNH-NH <sub>b</sub> 2.9 vs 2.6		AspNH-NH <sub>a</sub> 2.9 vs 2.6	
ArgNH-COCH <sub>2</sub> CO <sub>u</sub> 2.3 vs 2.6	ArgNH-COCH <sub>2</sub> CO <sub>u</sub> 3.5 vs 2.6	AspNH-COCH <sub>2</sub> CO <sub>u</sub> 2.3 vs 2.6	AspNH-COCH <sub>2</sub> CO <sub>u</sub> 3.5 vs 2.6
ArgNH-COCH <sub>2</sub> CO <sub>d</sub> 3.5 vs 2.9		AspNH-COCH <sub>2</sub> CO <sub>d</sub> 3.5 vs 2.9	

<sup>a</sup> The authors are aware that being concerned about distance differences that are a few tenths of an Angstrom different could be misleading in this context.

During the unrestrained MD in explicit solvent performed on **4a**, **4b**, **5a**, and **5b**, the analysis of the trajectories revealed the presence of H-bonded structures involving NH<sub>a</sub> and/or NH<sub>b</sub> (not shown), as suggested by VT-NMR data. The simulations failed to reproduce the inversion of ArgNH for **4**, and the inversion of AspNH for **5**; evidently, these rotations are slow compared to the time selected for the simulation. The compounds **6-9** were not investigated; their structures were generated as the mirror mages of the respective enantiomers **2-5**.

The comparison of the in-solution structures of **2** and **3** with the structures of **4-9**, and the correlation with their experimental affinity for α<sub>5</sub>β<sub>1</sub> and α<sub>v</sub>β<sub>3</sub> integrins give several clues to discuss the interaction with the receptors.

Compounds **4**, **5**, **8**, and **9**, show a cis disposition of Asp and Arg (Figure S4 and S5 and respective mirror images). The analysis of the trajectories of unrestrained molecular dynamics confirms that the average distance between the pharmacophores is shorter with respect to the distance considered optimal for binding α<sub>5</sub>β<sub>1</sub> and α<sub>v</sub>β<sub>3</sub> integrins.

In **4**, the guanidino group of (R)-Arg is placed on the opposite side of the cyclic scaffold with respect to **2**, **3** (see the main text). Apparently, the long and flexible side chain of Arg still allows a certain interaction with the receptors. In the preferred conformation **4b**, the benzyl side chain of the diamine points below the molecular plane, as for **2**, but the pseudo-equatorial position seems scarcely effective in discriminating the different sizes/shapes of the lipophilic pockets of the  $\alpha_v\beta_3$  (small pocket) or  $\alpha_5\beta_1$  (large pocket) receptors. This situation is consistent with a moderate affinity towards both the receptors, in the micromole range, with no selectivity.

While in **4** the carboxylic group of Asp points towards the receptor's cation in a straight line, as in **2** and **3**, in **5** the carboxylic group of (R)-Asp is placed on the opposite side of the cyclic scaffold. This difference accounts for the lack of activity of **5**.

Compound **6** and **7** are the enantiomers of **2** and **3**, respectively, and the same distance between the pharmacophores can be observed (the conformational analysis was not repeated). This distance matches the one required for a good interaction with the receptors. However, as for **5**, the D-Asp residue places the carboxylic group on the opposite side of the scaffold respect to the compounds **2-4**. As a consequence, **6** and **7** seem to be scarcely adapt to interact the receptors.

In contrast, compound **8** shows a moderate experimental affinity for both  $\alpha_5\beta_1$  and  $\alpha_v\beta_3$  integrins despite of the presence of (R)-Asp. Besides, the complete lack of activity of **9** towards both the  $\alpha_v\beta_3$  and  $\alpha_5\beta_1$  receptors remains for the moment elusive. Further insight can be obtained for the  $\alpha_v\beta_3$  integrin by molecular docking.

#### **Molecular docking of 4-9.**

In order to rationalize, on a molecular basis, the affinity of the compounds for the  $\alpha_v\beta_3$  receptor, docking studies were performed following the same virtual screening protocol used for compounds **2** and **3**. Ligands **4** and **8** produced top-ranked poses conserving all the important interactions of the X-ray complex (Figure S6) with the benzyl side chain of the diamine pointing toward the outside of the integrin binding site, allowing the aromatic ring to fit unhindered. In the calculated docking poses, compound **4** fits the receptor by reproducing the RGD backbone of the X-ray ligand better than the conformations of ligand **8** (Figure S6). Altogether these computational findings agree with the comparable micromolar activity observed for **2**, **3**, **4** and **8** for the integrin  $\alpha_v\beta_3$ .

On the contrary, most poses generated by the automated docking calculations for the inactive compounds **5**, **6**, **7** and **9** failed in forming all the key ligand-protein interactions, as revealed by the less favourable Glide score values. The stereochemistry array of the residues in compounds **5**, **6**, **7** and **9** produce three-dimensional pharmacophoric arrangements forcing the entire molecule to enter the receptor lopsided. In particular, the electrostatic interactions drive the fit of these ligands into the receptor binding site, but cause the loss of the complex network of hydrogen bonds. Especially, the presence of a (R)-Asp residue seems to hamper the proper fit of the ligands in the receptor cleft (see **5**, **6**, **7**).

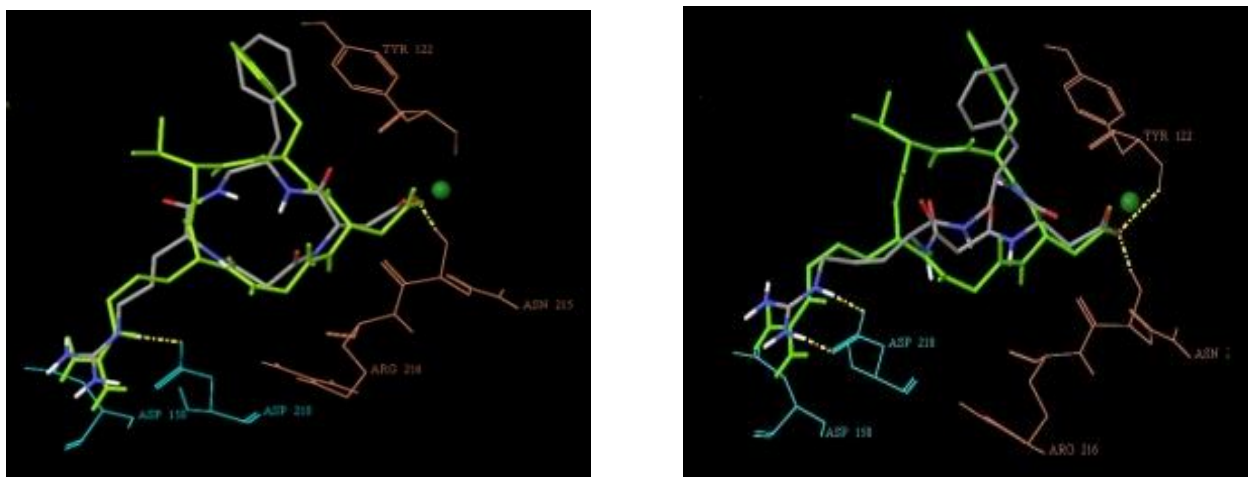


**Figure S6.** Top-ranked docking poses of ligands 4 (left side) and 8 (right side) (atom colour tube representation) into the crystal structure of the extracellular domain of  $\alpha_5\beta_3$  integrin ( $\alpha$  unit cyan and  $\beta$  unit orange wire representation) overlaid on the bound conformation of cilengitide (green tube representation). Only selected integrin residues involved in the interactions with cilengitide are shown. The  $Mn^{2+}$  ion at MIDAS is shown as a green CPK sphere. Nonpolar hydrogen atoms were removed for clarity.

In conclusion, the conformational analyses and molecular docking computations of **2-9** confirm that the distance between the pharmacophores is the primary requisite for a correct interaction with the receptors, as expected, but this feature has no effect on selectivity. Data explain the experimental observation that the presence of (S)-Asp and (S)-Arg is a pre-requisite to obtain the highest affinity. The presence of (R)-Arg can be tolerated, due to the flexibility of its side chain, while the presence of (R)-Asp is generally deleterious for activity. The only exception is **8**, which likely adopts an alternative receptor-bound conformation (calculated only for  $\alpha_5\beta_3$  integrin).

In the proposed model, the disposition of the benzyl group of the diamine plays a fundamental role in selectivity. It is possible to perceive that a pseudo-equatorial orientation of the benzyl group is well tolerated by both  $\alpha_5\beta_1$  and  $\alpha_5\beta_3$  integrins. Interestingly, compound **2**, the only compound with a well precise axial disposition of the benzyl, is also the only compound selective for  $\alpha_5\beta_1$  over  $\alpha_5\beta_3$  integrin.

## References

- [1] Brower, V. *Nat. Biotechnol.* **1999**, 17, 963–968.
- [2] Arndt, T.; Arndt, U.; Reuning, U.; Kessler, H. Integrins in angiogenesis: Implications for tumor therapy. In *Cancer Therapy: Molecular Targets in Tumor-Host Interactions*; Weber, G. F., Ed.; *Horizon Bioscience: Norfolk, U.K.*, **2005**.
- [3] Curley, G. P.; Blum, H.; Humphries, M. J.. *Cell. Mol. Life Sci.* **1999**, 56, 427–441.
- [4] Brooks, P. C.; Clark, R. A.; Cheresch, D. A. *Science* **1994**, 264, 569–571.
- [5] Hynes, R. O. *Nat. Med.* **2002**, 8, 918–921.
- [6] Reynolds, L. E.; Wyder, L.; Lively, J. C.; Taverna, D.; Robinson, S. D.; Huang, X.; Sheppard, D.; Hynes, R. O.; Hodivala-Dikle, K. M. *Nat. Med.* **2002**, 8, 27–34.
- [7] Cardarelli, P. M.; Lobl, T. J. Peltz, G., Ed.; *Springer: Heidelberg, Germany*, **1996**; pp 275-294.
- [8] Ruoslahti, E. *Tumor Biol.* **1996**, 17, 117–124.
- [9] Okada, N.; Watarai, M.; Ozeri, V.; Hanski, E.; Caparon, M.; Sasakawa, C. *J. Biol. Chem.* **1997**, 272, 26978–26984.
- [10] Kim, S.; Harris, M.; Varner, J. A. *J. Biol. Chem.* **2000**, 275, 33920–33928.
- [11] Ikari, Y.; Yee, K. O.; Schwartz, S. M. *Thromb. Haemostasis* **2000**, 84, 701–705.
- [12] Bewick, M. A.; Lafrenie, R. M. *Curr. Pharm. Des.* **2006**, 12, 2833–2848.
- [13] Mitjans, F.; Meyer, T.; Fittschen, C.; Goodman, S.; Jonczyk, A.; Marshall, J. F.; Reyes, G.; Piulats, J.. *Int. J. Cancer* **2000**, 87, 716–723.
- [14] Plow, E. F.; Haas, T. A.; Zhang, L.; Loftus, J.; Smith, J. W. *J. Biol. Chem.* **2000**, 275, 21785–21788.
- [15] Ruoslahti, E. *Annu. Rev. Cell Dev. Biol.* **1996**, 12, 697–715.
- [16] Thijssen, V. L. J. L.; van Beijnum, J. R.; Mayo, K. H.; Griffioen, A. W. *Curr. Pharm. Des.* **2007**, 13, 3576–3583.
- [17] Schmidmaier, R.; Baumann, P. *Curr. Med. Chem.* **2008**, 15, 978–990.
- [18] Ruoslahti, E.; Pierschbacher, M. D. *Cell* **1986**, 44, 517–518.
- [19] DeSouza, S. E.; Ginsberg, M. H.; Plow, E. F. *Trends Biochem. Sci.* **1991**, 16, 246–250.
- [20] Henry, C.; Moitessier, N.; Chapleur, Y. *Mini-Rev. Med. Chem.* **2002**, 2, 531–42.
- [21] Wermuth, J.; Goodman, S. L.; Jonczyk, A.; Kessler, H. *J. Am. Chem. Soc.* **1997**, 119, 1328–1335.
- [22] Cacciari, B.; Spallato, G. *Curr. Med. Chem.* **2005**, 12, 51–70.
- [23] Pfaff, M.; Tangemann, K.; Muller, B.; Gurrath, M.; Müller, G.; Kessler, H.; Timpl, R.; Engel, J. *J. Biol. Chem.* **1994**, 269, 20233–20238.
- [24] Gurrath, M.; Muller, G.; Kessler, H.; Aumailley, M.; Timpl, R. *Eur. J. Biochem.* **1992**, 210, 911–921.
- [25] Nisato, R. E.; Tille, J.-C.; Jonczyk, A.; Goodman, S. L.; Pepper, M. S. *Angiogenesis* **2003**, 6, 105–119.
- [26] Dechantsreiter, M. A.; Planker, E.; Matha, B.; Lohof, E.; Holzemann, G.; Jonczyk, A.; Goodman, S. L.; Kessler, H. *J. Med. Chem.* **1999**, 42, 3033–3040.
- [27] Cai, W.; Chen, X. *Anticancer Agents Med. Chem.* **2006**, 6, 407–428.
- [28] Heckmann, D.; Kessler, H. *Methods Enzymol.* **2007**, 426, 463–503.
- [29] Xiong, J.-P.; Stehle, T.; Zhang, R.; Joachimiak, A.; Frech, M.; Goodman, S. L.; Amin Arnaut, M. *Science* **2002**, 296, 151–155.

- [30] Marinelli, L.; Lavecchia, A.; Gottschalk, K.-E.; Novellino, E.; Kessler, H. *J. Med. Chem.* **2003**, *46*, 4393–4404.
- [31] Zhang, L.; Mattern, R.-H.; Malaney, T. I.; Pierschbacher, M. D.; Goodman, M. *J. Am. Chem. Soc.* **2002**, *124*, 2862–2863.
- [32] Zimmermann, D.; Guthc-hrlein, E. W.; Malesevic<sup>0</sup>, M.; Sewald, K.; Wobbe, L.; Heggemann, C.; Sewald, N. *ChemBioChem* **2005**, *6*, 272–276.
- [33] Benfatti, F.; Cardillo, G.; Fabbroni, S.; Galzerano, P.; Gentilucci, L.; Juris, R.; Tolomelli, A.; Baiula, M.; Sparta', A.; Spampinato, S. *Bioorg. Med. Chem.* **2007**, *15*, 7380–7390.
- [34] Takagi, J.; Strokovich, K.; Springer, T. A.; Walz, T *EMBO J.* **2003**, *22*, 4607–4615.
- [35] Smallheer, J. M.; Weigelt, C. A.; Woerner, F. J.; Wells, J. S.; Daneker, W. F.; Mousa, S. A.; Wexler, R. R.; Jadhav, P. K. *Bioorg. Med. Chem. Lett.* **2004**, *14*, 383–387.
- [36] Kumar, C. C.; Malkowski, M.; Yin, Z.; Tanghetti, E.; Yaremko, B.; Nechuta, T.; Varner, J.; Liu, M.; Smith, E. M.; Neustadt, B.; Presta, M.; Armstrong, L. *Cancer Res.* **2001**, *61*, 2232–2238.
- [37] Marinelli, L.; Meyer, A.; Heckmann, D.; Lavecchia, A.; Novellino, E.; Kessler, H. *J. Med. Chem.* **2005**, *48*, 4204–4207.
- [38] Heckmann, D.; Meyer, A.; Marinelli, L.; Zahn, G.; Stragies, R.; Kessler, H. *Angew. Chem., Int. Ed.* **2007**, *46*, 3571–3574.
- [39] Gentilucci, L.; Cardillo, G.; Tolomelli, A.; Spampinato, S.; Sparta, A.; Squassabia, F. *Eur. J. Org. Chem.* **2008**, 729–735.
- [40] Gentilucci, L.; Cardillo, G.; Tolomelli, A.; Squassabia, F.; De Marco, R.; Chiriano, G. *Comb. Chem. High Throughput Screening* **2009**, *12*, 929–939.
- [41] Schumann, F.; Muller, A.; Kokschi, M.; Muller, G.; Sewald, N. *J. Am. Chem. Soc.* **2000**, *122*, 12009–12010.
- [42] Chorev, M.; Goodman, M. *Acc. Chem. Res.* **1993**, *26*, 266–273.
- [43] Chorev, M. *Biopolymers* **2005**, *80*, 67–84.
- [44] Han, Y.; Giragossian, C.; Mierke, D. F.; Chorev, M. *J. Org. Chem.* **2002**, *67*, 5085–5097.
- [45] Lee, Y. S.; Agnes, R. S.; Davis, P.; Ma, S.-w.; Badghisi, H.; Lai, J.; Porreca, F.; Hruby, V. J. *J. Med. Chem.* **2007**, *50*, 165–168.
- [46] Fletcher, M. D.; Campbell, M. M. *Chem. Rev.* **1998**, *98*, 763–795.
- [47] Glenn, M. P.; Kelso, M. J.; Tyndall, J. D. A.; Fairlie, D. P. *J. Am. Chem. Soc.* **2003**, *125*, 640–641.
- [48] Norgren, A. S.; Buttner, F.; Prabpai, S.; Kongsaree, P.; Arvidsson, P. I. *J. Org. Chem.* **2006**, *71*, 6814–6821.
- [49] Maulucci, N.; Chini, M. G.; Di Micco, S.; Izzo, I.; Cafaro, E.; Russo, A.; Gallinari, P.; Paolini, C.; Nardi, M. C.; Casapullo, A.; Riccio, R.; Bifulco, G.; De Riccardis, F. *J. Am. Chem. Soc.* **2007**, *129*, 3007–3012.
- [50] Gentilucci, L.; Cardillo, G.; Tolomelli, A.; De Marco, R.; Garelli, A.; Spampinato, S.; Sparta', A.; Juaristi, E. *ChemMedChem* **2009**, *4*, 517–523.
- [51] Nakabayashi, S.; Warren, C. D.; Jeanloz, R. W. *Carbohydr. Res.* **1988**, *174*, 279–289.
- [52] Morie, T.; Kato, S.; Harada, H.; Fujiwara, I.; Watanabe, K.; Matsumoto, J.-I. *J. Chem. Soc., Perkin Trans. 1* **1994**, 2565–2569.

- [53] Conner, S. R.; Scott, G.; Aplin, A. E. *J. Biol. Chem.* **2003**, *278*, 34548–34554.
- [54] Park, K.; Kim, Y.-S.; Lee, G. Y.; Parl, R.-W.; Kim, I.-S.; Kim, S. Y.; Byun, Y. *Pharm. Res.* **2008**, *25*, 2786–2798.
- [55] Lundell, B. I.; McCarthy, J. B.; Kovach, N. L.; Verfaillie, C. M. *Blood* **1996**, *87*, 2450–2458.
- [56] Belvisi, L.; Riccioni, T.; Marcellini, M.; Vesce, L.; Chiarucci, I.; Efrati, D.; Potenza, D.; Scolastico, C.; Manzoni, L.; Lombardo, K.; Stasi, M. M.; Orlandi, A.; Ciucci, A.; Nico, B.; Ribatti, D.; Giannini, G.; Presta, M.; Carminati, P.; Pisano, C. *Mol. Cancer Ther.* **2005**, *4*, 1670–1680.
- [57] Del Gatto, A.; Zaccaro, L.; Grieco, P.; Novellino, E.; Zannetti, A.; Del Vecchio, S.; Iommelli, F.; Salvatore, M.; Pedone, C.; Saviano, M. *J. Med. Chem.* **2006**, *49*, 3416–3420.
- [58] Giannis, A.; Rubsam, F. *Angew. Chem., Int. Ed.* **1997**, *36*, 588–590.
- [59] Gentilucci, L.; Cardillo, G.; Squassabia, F.; Tolomelli, A.; Spampinato, S.; Sparta, A.; Baiula, M. *Bioorg. Med. Chem. Lett.* **2007**, *17*, 2329–2333.
- [60] Cheresch, D. A. *Proc. Natl. Acad. Sci. U.S. A.* **1987**, *84*, 6471–6475.
- [61] Kawaguchi, M.; Hosotani, R.; Ohishi, S.; Fujii, N.; Singh Tulachan, S.; Koizumi, M.; Toyoda, E.; Masui, T.; Nakajima, S.; Tsuji, S.; Ida, J.; Fujimoto, K.; Wada, M.; Doi, R.; Imamura, M. *Biochem. Biophys. Res. Commun.* **2001**, *288*, 711–717.
- [62] Carmelit, P.; Jain, R. K. *Circ. Res.* **2000**, *87*, 176–178.
- [63] Liotta, L.; Steeg, P.; Stetler-Stevenson, W. *Cell* **1991**, *64*, 327–336.
- [64] Hanahan, D.; Folkman, J. *Cell* **1996**, *86*, 353–364.
- [65] Kessler, H. *Angew. Chem., Int. Ed.* **1982**, *21*, 512–523.
- [66] Stradley, S. J.; Rizo, J.; Bruch, M. D.; Stroup, A. N.; Gierasch, L. M. *Biopolymers* **1990**, *29*, 263–287.
- [67] For a leading reference on the use of a cryoprotective DMSO-d<sub>6</sub>/H<sub>2</sub>O mixture as a biomimetic medium, see: Temussi, P. A.; Picone, D.; Saviano, G.; Amodeo, P.; Motta, A.; Tancredi, T.; Salvadori, S.; Tomatis, R. *Biopolymers* **1992**, *32*, 367–372 and references cited herein .
- [68] Toniolo, C. *CRC Crit. Rev. Biochem.* **1980**, *9*, 1–44.
- [69] HyperChem, release 8.0.3; Hypercube Inc.: Gainesville, FL, **2007**.
- [70] Cornell, W. D.; Cieplak, P.; Bayly, C. I.; Gould, I. R.; Merz, K. M.; Ferguson, D. M.; Spellmeyer, D. C.; Fox, T.; Caldwell, J. W.; Kollman, P. A. *J. Am. Chem. Soc.* **1995**, *117*, 5179–5197.
- [71] In a preliminary investigation of the conformational features of the PMRI RGD mimetics by ROESY and MD, we analyzed the insolution structural features of c[βPheψ(NHCO)Asp(Ot-Bu)ψ(NHCO)Gly-Arg(Mtr)] (14) and c[(R)-βPheψ(NHCO)Asp(Ot-Bu)ψ(NHCO)Gly-Arg(Mtr)], the protected synthetic precursors of **2** and **3**, respectively. While the conformation of fully protected **2** (14) was practically coincident to the type I β-turn/ type I β-turn structure of **2** (Figures 5 and 6), the predominant conformation of fully protected **3** was compatible with the inverse γ/inverse γ structure reported in Figure 8. Apparently, increasing the size of the side chains of the PMRI CTPs tends to stabilize the inverse γ/ inverse γ structure over the type II β-turn structure (Figure 8).
- [72] Glide, version 4.5; Schrodinger, LLC: New York, **2007**.
- [73] Brooks, P. C.; Montgomery, A. M. P.; Rosenfeld, M. *Cell* **1994**, *79*, 1157–1164.
- [74] Kim, S.; Bell, K.; Mousa, S.; Varner, J. A. *Am. J. Pathol.* **2000**, *156*, 1345–1362.

- [75] Hunakova, L.; Sedlak, J.; Klobusicka, M.; Sulikova, M.; Chorvath, B. *Neoplasma* **1995**, 42, 249–253.
- [76] Caltabiano, S.; Hum, W. T.; Attwell, G. J.; Gralnick, D. N.; Budman, L. J.; Cannistraci, A. M.; Bex, F. J. *Biochem. Pharmacol.* **1999**, 58, 1567–1578.
- [77] Shibata, H.; Yagi, T. *Clin. Chim. Acta* **1996**, 251, 53–64.
- [78] Maeshima, Y.; Manfredi, M.; Reimer, C.; Holthaus, K. A.; Hopfer, H.; Chandamuri, B. R.; Kharbanda, S.; Kalluri, R.. *J. Biol. Chem.* **2001**, 276, 15240–15248.
- [79] Berendsen, H. J. C.; Postma, J. P. M.; van Gunsteren, W. F.; Di Nola, A.; Haak, J. R. *J. Chem. Phys.* **1984**, 81, 3684–3690.
- [80] Jorgensen, W. L.; Chandrasekhar, J.; Madura, J.; Impey, R. W.; Klein, M. L.. *J. Chem. Phys.* **1983**, 79, 926–935.

---

## Chapter 5

---

# Molecular Docking of Opioid Peptides and Analogues, a Powerful Tool for the Design of Selective Agonists and antagonists, and for the Investigation of Atypical Ligand-Receptor Interactions.

---

**Abstract.** In the last years, molecular docking emerged as a powerful tool to investigate the interactions between opioid ligands and their receptors, thus driving the design and development of new selective agonists or antagonists of therapeutic interest. This review especially covers the most representative and recent comparative molecular docking analysis of structurally related compounds, as well as of agonists and antagonists within the active and inactive states of the receptors. The comparative analyses gave important information on the structural determinants responsible for the affinity and selectivity of the ligands, and defined the features responsible for the activation of the receptors. A special section is dedicated to the analyses of recently discovered, unusual agonists lacking of the tyramine pharmacophore, such as Salvinorin A, and the cyclopeptides including the D-Trp-Phe pharmacophoric motif. For the atypical structure of these compounds, the docking proved to be essential to disclose how they interact with and activate the receptors.

### 5. Introduction

In medicinal chemistry, the rational drug design (structure based drug design or de novo drug design), is the process of finding new bioactive molecules based on the knowledge of the biological target. The final goal is to design molecules that are complementary in shape and charge to their receptor to which they interact and bind to. When the drug design is centered on computer modeling, it is often referred to as Computer-Aided Drug Design (CADD). In particular, the molecular docking is a method which estimates the preferred, energetically favorable orientations of a candidate drug inside its receptor. Molecular docking emerged as a powerful tool in drug discovery to find and optimize lead compounds. Structural information derived from the theoretically modeled complex may clarify the mechanism of molecular recognition, and can be also used to discover novel ligands by predicting binding affinities with the receptor before they are synthesized. Indeed, docking can be utilized to prescreen *in silico* “real” or “virtual” compounds, avoiding expensive *in vitro* or *in vivo* assays. This opportunity is of particular interest in regard to the screening of large compound libraries generated by Combinatorial Chemistry (*in silico* highthroughput screening). The distinction between docking and *de novo* design methods can be subtle and, in many cases, significant overlap in methodology occurs between the strategies.

In the last years, continuous efforts have been dedicated to the quest for new potent analgesics devoid of the typical undesired side effects of the opiates. In this respect, docking may represent a useful technique; an accurate insight of the ligand-receptor complex and the comprehension of the mode of interaction might help in clarifying the origins of the adverse effects exerted by the opiates, in particular addiction and

tolerance, and might drive to the development of new opioid drugs and therapies with more desirable properties.

A number of somewhat differing models have been proposed to explain the binding and selectivity of opioid agonists and antagonists. Albeit the structural differences might be minimal, the biochemical effects of agonists and antagonists are well distinct: agonists stabilize the receptor conformation in the active form whereas antagonists stabilize the receptor conformation in the inactive form and interfere with the binding of agonists. The classic pharmacophoric models of opiates have been exhaustively reviewed by Eguchi [1], Mosberg et al. [2], and by Ferguson et al. [3]. For this reason, this review intends to discuss in details two issues: the most relevant and recent comparative docking analyses of opioid peptides and peptidomimetics bound to the active and inactive states of the  $\mu$ -,  $\delta$ -,  $\kappa$ -opioid receptors (MOR, DOR, and KOR), and the docking analyses of some atypical agonists deprived of the tyramine pharmacophore. The latter is of particular interest; the docking procedure proved to be fundamental for the determination of the mechanism by which these unusual ligands interact with and activate the receptors.

### 5.1 Structure and Functions of the Opioid Receptors, and Representative Opioid Ligands

The opioid receptors belong to the class a G protein coupled receptor (GPCR) [4], and are expressed in different areas of the CNS: pons, medulla, spinal cord, telencephalon, diencephalon, mesencephalon, and myelencephalon. Three opioid receptors DOR, MOR, and KOR were cloned in the early 1990s [5]. The MOR and KOR subtypes are widely distributed in the gastrointestinal tract, in particular in the stomach and proximal colon, while the DOR is expressed on neurons within myenteric and submucous ganglia [6].

The receptors are composed of seven transmembrane helices (TMH) that are packed together in an anti clockwise disposition, and have long extracellular *N*-terminus and intracellular *C*-terminus sequences. The helices are connected by three intra- and three extracellular loops (EL) that vary in size and composition.

The opioid receptors share extensive sequence homology; in particular, the intracellular loops and the TMHs show high identity, while EL2, EL3, and the *C*-terminus share little to no homology.

Based on the selectivity profiles of some agonists or antagonists, there are at least two variants for each receptor type, namely MOR1/2, DOR1/2, and KOR1/2. However, the cloning studies did not confirm the existence of distinct genes, therefore these subdivisions may result from splice variants, or different post translational modifications, distinct cellular localizations, dimerization, or interaction with some proteins.

In the intracellular domain, the receptors are linked to a heterotrimeric G protein, composed of the  $G\alpha$ ,  $G\beta$ , and  $G\gamma$  subunits. Upon binding with an agonist, the receptors undergo a conformational change, which promotes the exchange of GDP for GTP at the  $G\alpha$  subunit. This induces the dissociation from the  $G\beta,\gamma$  dimer; the subunits activate several effectors, until the GTP is hydrolyzed to GDP (intrinsic GTPase activity), leading to the reassembly of the subunits [7]. The inhibition of adenylyl cyclase activity is induced by the GTP bound  $G\alpha_i$  subunit, so reducing the activity of cAMP-dependent PKA, while the  $G\beta,\gamma$  subunits mediate the activation of potassium conductance and inhibition of voltagegated calcium channels, decreasing excitability.

There is evidence of homo- and heteromerization of the opioid receptors; these heteromers possess unique biochemical properties including allosteric modulation between units, changes in ligand recognition, G protein-coupling and trafficking [8, 9].

The alkaloids found in the opium poppy plant have been used as remedies for pain relief for centuries [1]. The most abundant is morphine (1), which was isolated in 1803, and is still the drug of choice for treating severe pain caused by cancer or surgical operation; codeine (2), isolated in 1832, is the second-most predominant alkaloid in opium. Many semisynthetic derivatives of morphine revealed an agonist or antagonist behaviour. The progressive reduction of morphine structure resulted in several new classes of therapeutically useful opioid ligands such as morphinans, e.g. levorphanol (3), benzomorphan, e.g. pentazocine (4), 4-phenylpiperidines, e.g. meperidine (5), N-phenylpiperazines, e.g. fentanyl (6), and methadone-type compounds (7), Fig. (1). For instance, oripavine derivatives, e.g. buprenorphine (8), display a circa one thousand fold potency with respect to morphine. Other selected examples of opioid ligands described throughout the text are also given in Fig. (1), naltrindole (9), naltrexone (10), loperamide (11).

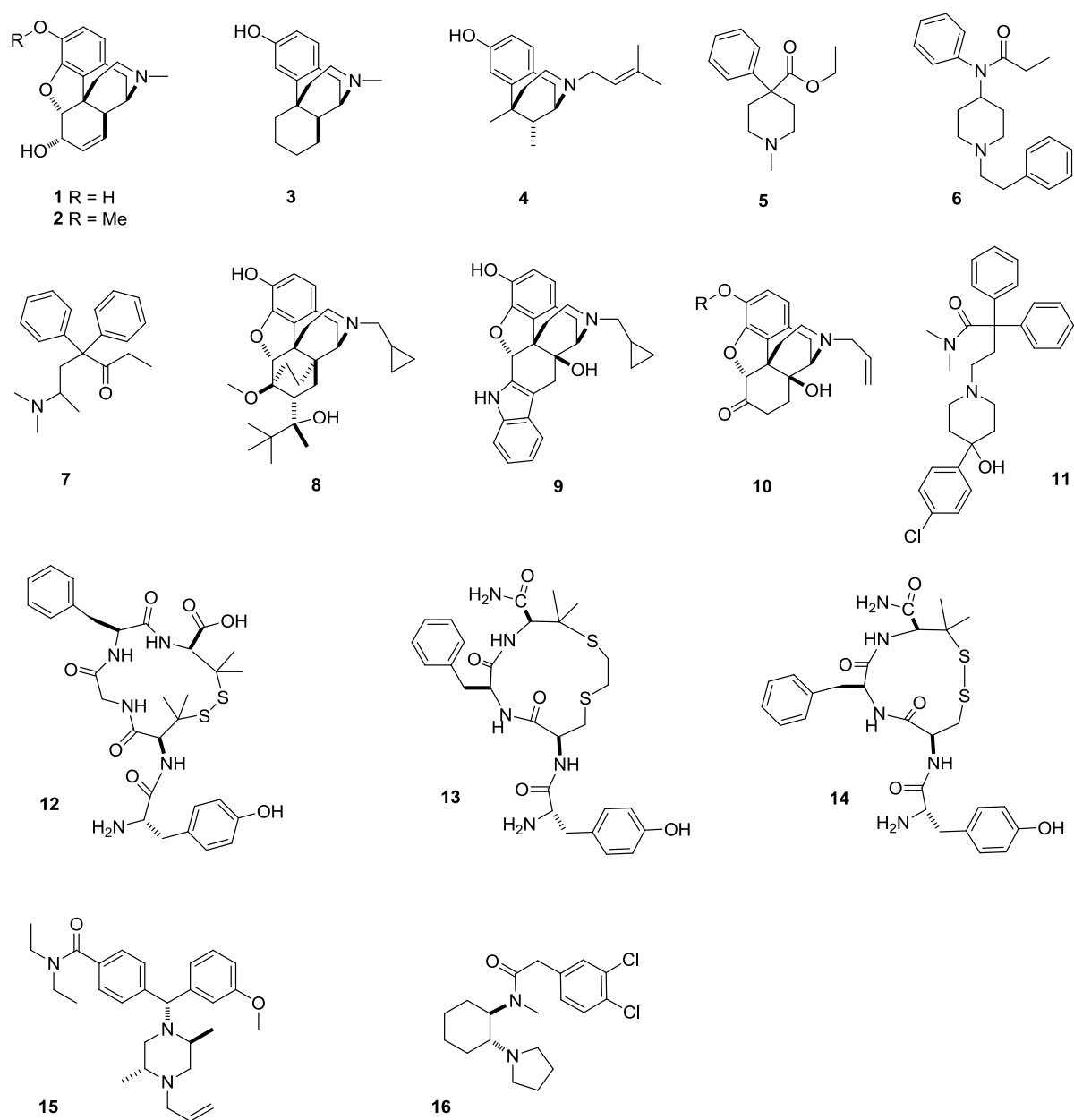


Fig. (1). Structures of representative opioid ligands.

The endogenous opioid agonists Met-enkephalin, H-Tyr-Gly-Gly-Phe-Met-OH, and Leu-enkephalin, H-Tyr-Gly-Gly-Phe-Leu-OH, were discovered in the mammalian brain in 1975; these peptides showed high affinity for DOR and MOR. A few years later, other endogenous peptides were described, namely  $\beta$ -endorphin, a 31 amino acid peptide that revealed affinity to both MOR and DOR, and dynorphins (e.g. Dyn A: H-Tyr-Gly-Gly-Phe-Leu-Arg-Arg-Ile-Arg-Pro-Lys-Leu-Lys-Trp-Asp-Asn-Gln-OH), selective ligands of the KOR [10]. The tetrapeptides endomorphin-1 (EM1) and endomorphin-2 (EM2), H-Tyr-Pro-Trp-PheNH<sub>2</sub> and HTyr-Pro-Phe-PheNH<sub>2</sub>, showing high affinity and selectivity for MOR, were discovered in mammalian brain only in 1997 [11, 12].

Most endogenous peptides originate from their propeptide precursors through hydrolysis by specific proteases.

Proopiomelanocortin (POMC) is the precursor of  $\beta$ -endorphin, proenkephalin is the precursor of Met- and Leu-enkephalin, prodynorphin produces several dynorphin peptides, including Dyn A and B, while for the EMs, no propeptide precursors have been discovered yet, and very likely they are synthesized de-novo.

The clinical use of these endogenous peptides is hampered by their rapid degradation and scarce permeation across biological barriers, especially the blood-brain barrier. One way to overcome these inherent limitations is the introduction of structural modification, including the insertion of non-peptidic structural elements, giving rise to the family of the peptidomimetics [13]. The peptidomimetics bear identifiable similarity to the parent peptides and imitate or inhibit their biochemical effects. The pseudopeptides have sequences in which at least one peptide bond is replaced with a isosteric or isoelectronic surrogate, such as a reduced peptide bond, or the azapeptides, the retro-inverso peptides, or the peptoids.

Other strategies are the incorporation of non-natural amino acids, D-configured residues, N-alkylated amino acid,  $\alpha$ - or  $\beta$ -substituted  $\alpha$ -amino acids,  $\beta$ - or  $\gamma$ -amino acids, or the cyclization of the peptide sequence, etc [14, 15]. Examples of opioid peptidomimetics are DAMGO, H-Tyr-D-Ala-Gly-MePhe-Glyol, DADLE, H-Tyr-D-Ala-Gly-Phe-D-Leu-OH, and the cyclopeptides DPDPE, Tyr-c[-D-Pen-Gly-Phe-D-Pen-]-OH (**12**), JOM-6, Tyr-c(S-Et-S)[D-Cys-Phe-D-Pen]NH<sub>2</sub> (**13**) and JOM-13, Tyr-c[D-Cys-Phe-D-Pen]OH (**14**), the palindromic biphalin, (H-Tyr-D-Ala-Gly-Phe-NH-)<sub>2</sub>, etc. In several cases these modifications resulted in high stability and bioavailability and consequently in a increased analgesic efficacy *in vivo* [16]. Besides, the constrained peptidomimetics, such as the cyclopeptides or the turn mimetics, have been utilized for the investigation of the bioactive conformation of the parent peptides.

These extensive investigations led to the general definition of the proper spatial orientation of a cationic amine, a phenol group, and an additional hydrophobic group, that are necessary to manifest the biological activity through interaction with opioid receptors [17].

The mimetics of the opioid peptides in which the peptide character is no longer preponderant are referred to as non-peptidomimetics.

Examples are the N-benzylpiperazine derivative SNC 80 (**15**), selective DOR agonists, and the KOR agonist U50,488 (**16**) [1], Fig. (1).

## 5.2. Insights Into the Interaction between Ligands and Receptors

Ideally, the best approach for determining the 3D structure of a receptor and the interactions with its agonists and antagonists would be the X-ray analysis of the ligand-receptor complex [18]. Many of the required information can be found easily by consulting a variety of on-line services and databases. The *Protein Data Bank* (PDB) [19], Brookhaven National Library, is a database of experimentally determined 3D structures of almost 78500 proteins, nucleic acids, macromolecular complexes, etc. The *Cambridge Structural Database* (CSD) stores the crystallographic structures of small organic or metallo-organic molecules [20]. The Zinc Database [21] is a free database of more than  $1.3 \times 10^7$  commercially-available and ready-to-dock compounds for virtual screening. Pubchem [22] is a database of chemical molecules and their activities against biological assays that contains descriptions of small molecules with less than 1000 atoms. The system is maintained by the National Center for Biotechnology Information (NCBI) and can be accessed for free through a web user interface. ChEMBL (or ChEMBLdb) [23] is a chemical database of bioactive molecules with drug-like properties, maintained by the European Bioinformatics Institute (EBI). ChEMBLdb can be accessed *via* a web interface or downloaded by File Transfer Protocol and is also integrated into other large-scale chemistry resources, including PubChem and the ChemSpider system of the Royal Society of Chemistry. The DrugBank [24] is a bioinformatics and cheminformatics resource that combines detailed drug data together with comprehensive drug target information. The database is available at the University of

Alberta and contains nearly 6707 drug entries including 1436 FDA-approved small molecule drugs, 134 FDA-approved biotech (protein/peptide) drugs, 83 nutraceuticals, and 5086 experimental drugs.

As a matter of fact, the opioid receptors belong to the wide class of the GPCRs, and the X-ray diffraction of membrane-bound GPCRs met with considerable experimental obstacles. Structural and biophysical information of ligand-receptor binding can be obtained by several modern techniques, such as the in-solution and solid-state NMR, fluorescence spectroscopy and single molecule fluorescence methods, flow cytometry, surface plasmon resonance, isothermal titration calorimetry, and atomic force microscopy [25, 26].

Alternatively, the putative ligand binding site of the receptor and the pharmacophores of the ligands involved in the interaction can be simulated by manual or automated docking computations [1- 3, 27]. This method predicts the preferred orientation of one molecule into a receptor to form a stable complex. Virtual models of the opioid receptors have been generated by homology modeling using templates constructed on the basis of the electron crystallographic study or the X-ray crystal structure of rhodopsin.

For many years, rhodopsin has been the only GPCR with available crystallographic structural information. Solved 10 years ago [28], the crystal structure of inactive state rhodopsin covalently linked to *cis*-retinal provided the first near-atomic view of the GPCR architecture. In 2007, a new high-resolution crystal structure of GPCR, the  $\beta 2$  adrenergic receptor ( $\beta 2$ -AR), was reported [29, 30].

Subsequently, the structures of other members of the GPCR class have been elucidated: avian  $\beta 1$ -adrenoceptor [31], squid rhodopsin [32], the human adenosine A2A receptor [33], and the human D3 receptor in complex with a D2/D3 selective antagonist [34]. As for the opioid receptors, there is a high degree of sequence similarity at the TMH and intracellular domains, which leads to the assumption that the homologous TMH regions of all opioid receptors have the same secondary structures. In some cases, multi-template models produced better structures than single-template models.

The combination of experimental studies and modeling allowed the development of more realistic models, accounting for problematic issues such as helix distortions or divergent extracellular loops included in the binding pocket. Therefore, in some cases the rhodopsin X-ray template was supplemented by experimental structural constraints appropriate for the active or inactive receptor conformations, together with receptor-specific and ligand-specific interactions.

Experimental information has been derived from the investigation of the receptors features, site-directed mutagenesis and/or chimeric studies, or conversely from the investigation of the ligands structures by structure-activity relationship (SAR) studies.

Other approaches are cross-linking studies, the substituted cysteine accessibility method, affinity labeling, correlative replacements of ligand and receptor groups, incorporation of metal binding sites between residues of receptors or receptors and ligands, etc [2, 35].

The conformational switch between the active form and inactive form of the receptor is currently the matter of much interest. For instance, plasmon resonance spectroscopy revealed the structural difference between agonist binding and antagonist binding conformations of the human DOR [36].

The site-directed mutagenesis grounds on the exchange of individual amino acids in the receptor protein with a Ala residue, to verify their role in ligand-receptor interaction [37]. The chimeric receptors approach consists in interchanging sequences of the MOR, DOR, and KOR. These chimeras allowed to identify receptor regions necessary for ligand recognition, as well as regions responsible for selectivity [38].

These methods revealed that several residues in the binding pocket are conserved across all of the opioid receptors, in particular Asp(3.32), Tyr(3.33), Lys(5.39), Phe(5.47), Trp(6.48), Ile(6.51), His(6.52), Ile(6.53), Ile(7.39), Tyr(7.43). On the other hand, these studies highlighted the fundamental role of non-conserved residues in the composition of specificity pockets, responsible for the binding with the selective ligands.

The SAR approach consists in the comparison of the biological activities of large sets of structurally correlated opioid compounds (opiate, peptide, peptidomimetic, non-peptidomimetic agonists or antagonists), to evaluate the role of the different pharmacophores in ligand-receptor binding [39]. The SAR studies analyze the pharmacophores of the ligands, so that some information on the receptor can be obtained as a negative contour. Very often, the introduction of conformational and topographical constraints in endogenous opioid peptides proved to be beneficial in developing peptide ligands with high activity and selectivity, giving more definitive information. In essence, SAR studies revealed that opioid ligands contain different recognition elements that are responsible for their activities. The portion in common, generally a tyrosine or a tyramine, represents the "message," responsible for receptor interaction, while the variable portion represents the "address," responsible for the selectivity towards one subtype respect to the others.

### **5.3. Principles of Molecular Docking**

Initially, docking simulations were done quite manually, with both the receptor and the ligand represented by explicit atoms and the resulting complexes approximated as rigid bodies, fixing all internal degrees of freedom except for the translational and rotational ones; eventually, it was possible to make use of pregenerated conformational libraries of ligands. The development of molecular surface calculations and

their successive use in docking applications (DOCK [40]) significantly reduced the number of possible complexes and the time required for the simulation.

Today there are many docking programs available, differing mainly in the sampling or search algorithms, scoring functions [41] and treatment of conformational freedom (flexibility) of ligand and receptor. Examples of recent programs developed to automatically dock ligands into receptor models are DOCK, AutoDock [42], AutoDock Vina [43], GOLD [44], FlexX [45], FDS, [46] Glide [47], LigandFit [48], ICM [49], and others. Many of these programs perform semiflexible docking, with a the flexible ligand and a rigid protein. Since a conformational search to identify the most favorable geometry is generally necessary, docking algorithms can be classified as systematic, stochastic, and deterministic [50].

Systematic search algorithms are based on the “anchor-and-grow” approach that consists of splitting a ligand into separate fragments, docking the fragments to the receptor, followed by linking again the fragments to obtain the whole ligand. An example of systematic search is represented by the fragment-based methods, as implemented in software like eHiTS [51].

Monte Carlo is an example of stochastic method, implemented in QXP [52] and LigandFit and useful for large systems. Since only some solutions are evaluated, the method might afford different and unrepeatable results. The ligand is considered as a whole and random changes are made to modify the torsion angles, as well as to translate and rotate the ligand. This is followed by energy minimization.

To increase the chance of stochastic methods to achieve the global energy minimum, the simulation may consist of several cycles. The first cycle is performed at high temperature and later cycles are done at decreasing temperatures (simulated annealing).

AutoDock was the first docking program to implement simulated annealing by using evolutionary (or genetic) algorithms. The best structures are carried on to the next generation and random or biased mutations can be made to increase genetic diversity and prevent premature convergence. GOLD, AutoDock, AutoDock Vina and FlexyDock, use a genetic search strategy.

A different mathematical optimization method belonging to the class of trajectory-based techniques is Tabu search [53]. Tabu search enhances the performance of a local search method by using memory structures that describe the visited solutions: once a potential solution has been determined, it is marked as “taboo” so that the algorithm does not visit that possibility repeatedly.

Finally, the ESCHER procedure (Evaluation of Surface Complementarity, Hydrogen bonding, and Electrostatic interaction in molecular Recognition) transforms a 3D structure in a set of polygons, with three modules that work in series: the first evaluates the geometric complementarity and produces a set of rough solutions, the second identifies molecular collisions within those solutions, and the third one evaluates their electrostatic complementarity [54].

Regardless of the strategy used, at the end of each docking run the reliability of the pose is numerically rendered with a *score* that permits, *a priori*, to appreciate interesting orientations [55]. Scoring functions estimate the binding free energy of a molecule or a molecular fragment in the active site of receptor and consists of both enthalpic and entropic contributions. The ranking of ligand docking poses according to certain scoring systems that identify the best fit, is the central step in virtual database screening for drug discovery.

The need for a fast, yet accurate, scoring function for docking studies has led to a number of different functions like the scaling approach, consensus scoring approaches and the addition of selected accuracy [56]. For example the scoring function of the docking program DOCK includes force field, contact score and chemical complementary score, while Gold, Glide, AutoDock, use empirical scoring functions.

Anyway, ligand-receptor complexes are formed between partners that are complementary in structure as well as in physicalchemical properties. They are stabilized by intermolecular Van der Waals, electrostatic, dipole-dipole, and  $\pi$ - $\pi$  interactions, and by H-bonds and hydrophobic effects [57]. Before binding, both molecules interact with the solvent. Desolvating polar and charged parts of the molecule upon complex formation come at a penalty, while desolvating nonpolar parts of the surface releases water molecules, thus increasing entropy. This entropy gain is favorable to complex formation so that the hydrophobic effect is a major stabilizing term for biomolecular complexes, while the Coulomb interactions and H-bonds provide specificity to protein-ligand interactions.

To reach the binding site, ligands have to move from the transport fluid to the receptor through different phases characterized by increasingly ordered water, decreasing dielectric constant and reduced H-bonding activity. The trajectory of the ligands from the aqueous environment to the receptors is generally ignored. Very recently, the possible pathway for entry of the nonselective antagonist naloxone from the water environment into the binding pocket of DOR was explored using metadynamics simulations [58].

If the location of the binding site is unknown, it is possible to proceed using a method known as "blind docking". In this case the docking is conducted to search the entire surface of the macromolecule of interest [59, 60]. The first docking program to implement the use of automated grids was AutoDock.

It has been also pointed out that the membrane promotes ligandreceptor docking. Since the docking event of a receptor and a ligand must take place near the membrane, ligand-membrane interactions should be important. Hence, understanding membrane-bound structures of ligands is indispensable for further insight into their diverse biological behaviors [61].

The rigid body and the flexible ligand approximations have clear limitations, in particular they do not account for the "inducedfit".

In the "induced fit" model hypothesis, the receptor and the ligand adapt their structures to bind to each other [62]; to reduce complexity, only selected receptor side chains are allowed to move.

In MOBILE [63], an ensemble of homology models was generated and the ligands were docked into an averaged binding site representation using Autodock. The same result can be obtained using Molecular Dynamics (MD) experiments. Molecular dynamics is a deterministic simulation of physical movements of atoms and molecules. The trajectories of molecules and atoms are determined by numerically solving the Newton's equations of motion for a system of interacting particles, where forces between the particles and potential energy are defined by molecular mechanics force fields such as AMBER [64], CHARMM [65] and OPLS [66]. To account for the screening effect of the solvent on electrostatic interactions, a distance-dependent dielectric constant is used. More accurate simulations require the introduction of the complex within a box of explicit, equilibrated solvent molecules with periodic boundary conditions. In this way MD simulations may account for dynamic phenomena not observed in X-ray structures.

Recently, with the development of very fast computing systems, hybrid quantum mechanics/molecular mechanics (QMMM) methods have become a standard tool for the characterization of complex molecular systems [67]. Initially used to study enzyme complexes, these methods treat the part of the system that undergoes the most important electronic changes upon binding a substrate quantum mechanically, and the rest of the system by traditional molecular mechanics. In this way, a QM/MM optimization of the ligand-receptor complexes give a more accurate description of the electronic and steric properties effects of the “induced fit”, and a complete description of reaction mechanisms and electronic properties.

#### 5.4. Exploring the Determinants of Ligand Affinity and Selectivity: Comparative Docking Studies

By crossing the results of SAR analyses, mutagenesis, studies with chimeric receptors, homology modeling, etc., it appears that there are differences in binding cavity geometry among MOR, DOR, and KOR, related to the divergence in size, polarity, and charge of residues, especially from the top of TMHs 5 to 6, EL2, and EL3. The greatest difference is observed for KOR, whose 3-residue longer EL2 occupies more space between TMH3 and TMH7 and between TMH3 and TMH5, so that the binding pocket in KOR is consequently smaller. To allow a better comparison of the three opioid receptors, the residue numbers have been given also using the Ballesteros-Weinstein nomenclature.

In general, great care should be taken in interpreting docking analyses for different classes of compounds, and even small differences in related structures might lead to alternative binding modes. The summation of all experimental data suggests that the different classes of ligands, morphine and the opiates, the fentanyl, peptides, cyclopeptides, and the atypical ligands, such as the benzodiazepine derivatives [68], the salvinorins (see next paragraph), etc., have distinct modes of receptor interaction and, for the agonists, different activation mechanisms. In these respects, comparative docking analyses proved to be very effective in the visualization of the structural features responsible for the selectivity of a given ligand towards the three receptor types, and in the identification of the specificities responsible for the different binding modes of the different ligands with a given receptor.

Morphine, the prototypical MOR agonist, has been studied extensively with all of the techniques mentioned in the previous paragraphs. Nevertheless, these studies did not furnish a definitive and convincing ligand-receptor 3D model. In general, the main interaction was that of the protonable tertiary amine with Asp<sup>147</sup>(3.32), but the rest of the structure was oriented in different ways [1, 69, 70], mainly due to its compact structure, which can be easily accommodated within the receptor binding site. One study [69] proposed a hydrophobic interaction between the phenol group of morphine and the phenol group of Tyr<sup>299</sup>(6.54) in TM VI and the hydrogen bonding interaction between the phenolic-OH of morphine and both the amino group of Lys<sup>303</sup>(6.58) and the phenolic-OH of Tyr<sup>148</sup>(3.33). In an more recent model [70], the aromatic ring of morphine interacts with side chain of Ile<sup>234</sup>(5.40), Trp<sup>293</sup>(6.48), Ile<sup>296</sup>(6.51), and Val<sup>300</sup>(6.55), Fig. (2a). The phenolic hydroxy group forms a hydrogen bond with the imidazole group of His<sup>297</sup>(6.52). The piperidine ring has a hydrophobic interaction with the side chains of Tyr<sup>148</sup>(3.33) and Ile<sup>322</sup>(7.39).

The cyclohexene ring is placed in the hydrophobic pocket formed by the side chains of the Ile<sup>234</sup>(5.40) and Tyr<sup>148</sup>(3.33), and Asn<sup>230</sup>(5.36) and Trp<sup>318</sup>(7.35).

Also the molecular recognition of the MOR-selective agonist fentanyl (**6**) is poorly defined; besides, it has been pointed out that morphine and the fentanyls interact with the MOR in different ways [71]. The pharmacophores of fentanyl are the protonable tertiary amine, which interacts with Asp<sup>147</sup>(3.32), the *N*-phenyl-*N*-piperidinyl propionamide, and the phenethyl group (but the phenyl can be substituted with a thiophene or methyl ester, in sufentanyl and remifentanyl, respectively). For the fentanyls, flexibility is the most relevant practical complication to docking analysis.

Automated docking resulted in several docking orientations and conformations for each ligand, differing in particular for the position of the phenethyl group [1, 72-74].

For instance, in a recent study of fentanyl [73] the most probable model shows the piperidine ring positioned vertically in the region between the helices TM3 and TM7, with the protonated nitrogen at a distance of 3.38 Å from the oxygen of Asp<sup>147</sup>(3.32), Fig. (2). The aromatic ring of *N*-phenethyl group is oriented towards His<sup>297</sup>(6.52), and the *N*-phenylpropanamide group is near to Trp<sup>318</sup>(7.35) and His<sup>319</sup>(7.36). The Tyr<sup>148</sup>(3.33) approaches the hydrocarbon part of the piperidine ring, and the Tyr<sup>326</sup>(7.43) is close to the linear bridge of the *N*-phenethyl group. Finally, Asn<sup>230</sup>(5.36) is close to the alkyl group of the *N*-phenylpropanamide group of the ligand. The computations gave other plausible binding poses with comparable scores, but these alternatives were excluded on the basis of experimental results reported in the literature, indicating the important amino acids constituting the ligand binding site within the receptor.

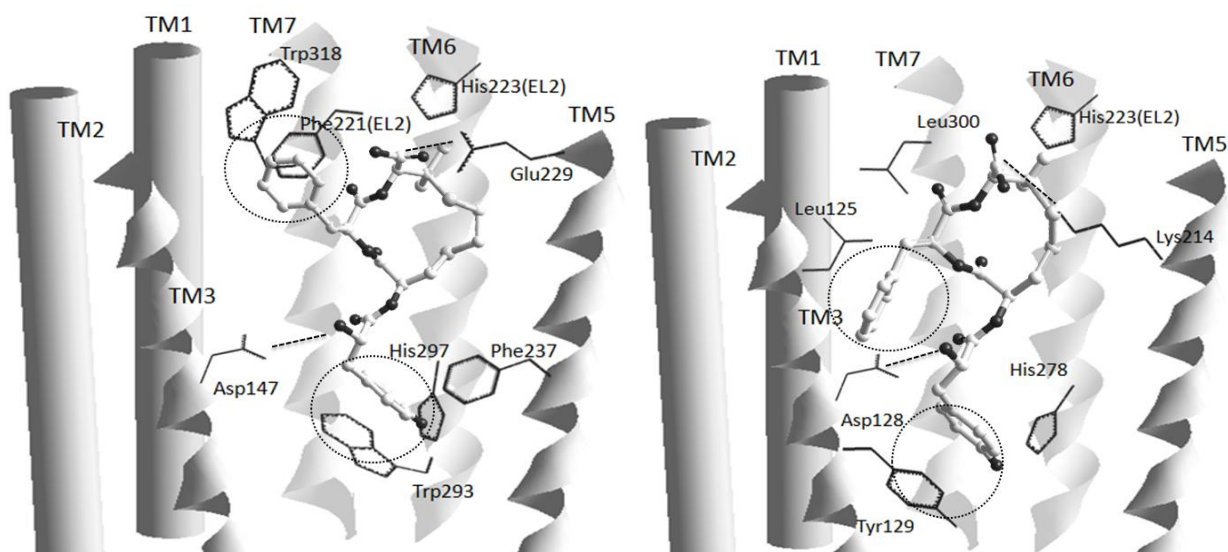


**Fig. (2).** Schematic sketches of the interactions between the JOMs and the opioid receptors. Left, JOM-6 and MOR; right, JOM-13 and DOR. The TMHs 3, 5, 6, and 7, delimitating the binding-site, are rendered as ribbons, while the TMHs 1 and 2 are rendered as cylinders. TMH4, in front of the observer, has been removed for clarity; pale gray TMHs (6 and 7) are positioned far from the observer. Dotted lines indicate relevant interactions (ionic, H-bonds), dotted circles indicate other contacts (hydrophobic, stacking interactions).

For the opiates, the tyramine moiety is generally regarded to as the classic message, while large substituents on the C ring represent the address. For example, naltrindole (**9**) contains a indole moiety, and is a DOR-selective ligand, while 5-guandinylnaltrindole, containing a guanidiny moiety, displays selectivity

for the KOR, and naltrexone (**10**) does not contain an address and thus is not selective [75-78]. In some cases, even minor differences showed a strong impact on activity and selectivity: 5'-guanidinonaltrindole (GNTI) is an antagonist, and 6'-GNTI is an agonist, as discussed in a recent docking analysis which compared these two very similar structures [79].

The universal opioid antagonist naltrexone (**10**) has been utilized as a probe molecule to identify the antagonist binding site in all three opioid receptors. Naltrexone was docked and the critical amino acid residues for binding were identified [80], revealing an alternative aromatic "address" binding domain in the extracellular loops of the MOR. On the basis of this model, a pyridinyl side chain was introduced in C-6 of the structure to target the aromatic binding locus at the extracellular loops of the MOR, resulting in a compound with high MOR selectivity [81].

Loperamide (**11**) is a piperidine analogue, acting as agonist on peripheral opioid receptors, and exhibiting affinity and selectivity for the cloned human MOR compared with the human DOR. The automatic docking studies of loperamide on human MOR and DOR was described; whilst no meaningful difference was detected concerning the docking of the arylpiperidine moiety, MOR/DOR selectivity was explained as a different accommodation of the two phenyl groups in the lipophilic pockets of receptors [82].

Very recently, an attempt to encompass the different kinds of ligands was discussed. A ligand-based pharmacophore modeling study on a medium-size training set of ligands including specific MOR, DOR and KOR agonists, was used to extract common and specific chemical features for three receptor subtypes. Other ligands were used as test set. Then, homology models of human MOR, DOR, and KOR were built based on the crystal structure of  $\beta$ 2-AR, and interactions between each receptor and their specific agonists were explored by subsequent molecular docking [83]. The docking complexes were compared to understand the detailed interactive mode of every subtype-agonist interaction, suggesting that MOR agonists could form two strong H bonds, whereas DOR and KOR ones form many hydrophobic interactions; KOR agonists could specifically form a strong H-bond with Tyr<sup>312</sup>, whereas that interaction was not found in DOR and MOR; MOR and DOR could form one H-bond with the Tyr<sup>150</sup> or Tyr<sup>129</sup>, respectively (TMH3).

Because of their extreme flexibility, linear peptides are difficult subjects for the docking protocols. On the other hand, the endomorphins EM1, H-Tyr-Pro-Trp-Phe-NH<sub>2</sub>, EM1, and EM2, HTyr-Pro-Phe-Phe-NH<sub>2</sub>, discovered by Zadina et al. in 1997 [11], are very short molecules, so that their investigation should be comparatively easier. Nevertheless, the docking analyses appeared so far in the literature could not shed light into the bioactive structure, even in regard to the relevance of the cis or trans conformation of the Tyr-Pro peptide bond. These tetrapeptides exhibited the highest affinity and selectivity for MOR receptor, and a strong antinociceptive effect on acute and neuropathic pain.

According to the 'message-address' concept, it is possible to consider that H-Tyr-Pro-Trp/Phe and Phe-NH<sub>2</sub> correspond to the message and address domains, respectively. Representative conformers of EM2 were utilized for a docking study of a MOR receptor model [84]. Some key residues defining the binding pocket were already known by site-directed mutagenesis studies, such as Asp<sup>147</sup>(3.32), Tyr<sup>148</sup>(3.33), Glu<sup>229</sup>(5.35), His<sup>297</sup>(6.52), Trp<sup>318</sup>(7.35), Tyr<sup>326</sup>(7.43), therefore the possible docking site was devised in such a way that EM2 interacts with these residues of the receptor model as much as possible; the Tyr<sup>1</sup> residue was placed at the bottom of the cavity, and Glu<sup>229</sup>(5.35) was considered as a possible residue for interacting with the C-

terminal amide. The procedure gave a S-type open docked structure with a trans Tyr-Pro peptide bond, showing some interactions, among which the most relevant were those between Tyr<sup>1</sup>NH and Asp<sup>147</sup>(3.32), Tyr<sup>1</sup>OH and His<sup>297</sup>(6.52), Tyr<sup>1</sup>Ar and Trp<sup>293</sup>(6.48), CONH<sub>2</sub> and Glu<sup>229</sup>(5.35), while the aromatic rings of Phe<sup>3</sup> and Phe<sup>4</sup> were parallel and formed a pliers-like structure gripping the indole of Trp<sup>318</sup>(7.35).

Some years later, an automated docking approach that allows ligand flexibility was performed starting from the NMR conformations of the EMs and some analogues, and the complexes were refined by molecular dynamics simulations in a membrane environment [85]. For all analogs the protocol gave similar structures, with refined contact interactions and scoring. Peculiarly, the authors omitted to discuss the resulting cis conformation of the Tyr-Pro peptide bond.

One opportunity to investigate the bioactive conformation of the linear peptides is the integration of the results furnished by 3D-QSAR and docking analyses. Aiming at developing a quantitative model on the basis of molecular flexibility, Martinek et al. established a statistical thermodynamically supported 3D flexibility descriptor type which accounts for the conformational free energy changes upon receptor binding [86]. The resulting 3+3D-QSAR models were validated with a training set of a series of flexible tetrapeptide EM analogues (and a second set of prostaglandins, which are not discussed here). The methodology gave the predicted conformations for the different derivatives. The authors superimposed their rigid structure for EM2 (without minimization) to the 3D structure of JOM-6 (**13**) (see next paragraph) inside the receptor cavity, and observed a good agreement between the two conformations. However, the resulting structure strongly differed from the previously described ones [84, 85] in the disposition of the aromatic ring Phe<sup>3</sup>, that in this case is perpendicular with respect to that of Phe<sup>4</sup>.

Conformational and topographical constraint of the linear natural opioid peptides has played a major role in developing peptide ligands with high selectivity, since it allowed to understand the conformational, topographical, and stereoelectronic requirements for the interactions of the opioid peptides with opioid receptors [87]. The constraints can be introduced by means of nonnatural amino acids, non-peptide portions, turn-mimetics, or by cyclization (N to C terminus, side-chain to side-chain, side-chain to C terminus) [13].

Conformationally constrained cyclopeptide analogues of linear opioid peptides gave the opportunity to investigate ligand affinity and selectivity in much detail. Prototypic examples are the two structurally related cyclotetrapeptides JOM-6 (**13**), Tyr-c(S-Et-S)[D-Cys-Phe-D-Pen]NH<sub>2</sub>, and JOM-13 (**14**) [88], Tyr-c[D-Cys-Phe-D-Pen]OH. Molecular docking [89] gave interesting clues about the specific interactions responsible for the MOR selectivity of JOM-6 and the DOR selectivity of JOM-13, confirming that the preference shown by a peptide for a specific receptor subtype over the other depends on the presence of structurally distinct pockets [2], Fig. (3). The bioactive conformation of both the peptides showed the expected interaction of the protonated amine of Tyr<sup>1</sup> with the carboxylate side chain of the conserved Asp(3.32) from TMH3 (Asp<sup>147</sup> and Asp<sup>128</sup> in MOR and DOR, respectively); moreover, the phenolic-OH group is H-bonded with His(6.52) from TMH6 (His<sup>297</sup> and His<sup>278</sup>), Fig. (3). This second pharmacophore is much less relevant than the former; the transposition of the Tyr<sup>1</sup> with Phe<sup>3</sup> in JOM-6, gave a MOR agonist JH-54 with only fourfold reduced affinity [90]. The remaining portion of the ligands occupy the address-binding region of the receptors and are responsible for the specificity.

In particular, in the position (7.35) MOR has Trp<sup>318</sup>, while DOR has Leu<sup>300</sup>. As a consequence, the interaction of the transoriented Phe<sup>3</sup> side chain of JOM-6 with Trp<sup>318</sup>(7.35) consents high-affinity binding to MOR, whereas the same side chain would have a bad contact with the Leu<sup>300</sup>(7.35), resulting in a very poor DOR affinity. On the other hand, the gauche orientation of Phe<sup>3</sup> side chain of JOM-13 nicely fits the address-binding region of the DOR, but not that of MOR, Fig. (3).

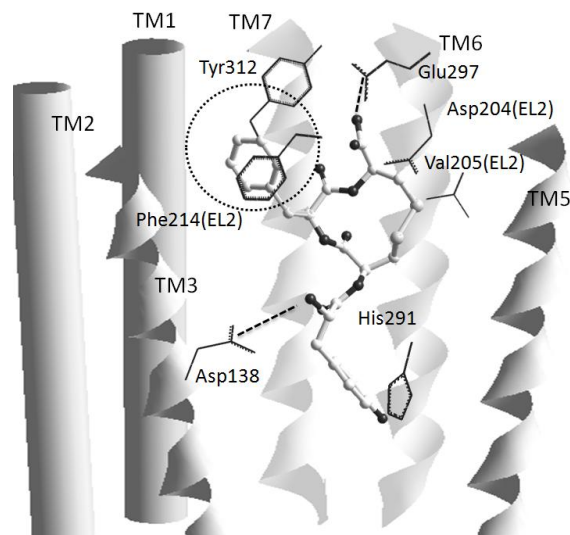


**Fig. (3).** Schematic sketch of the interactions between JOM derivative Tyr-c[D-Cys-Phe-D-Cys]NH<sub>2</sub>, S-S bridge, and KOR, to be compared to Fig. (3). The TMHs 3, 5, 6, and 7, delimitating the binding-site, are rendered as ribbons, while the TMHs 1 and 2 are rendered as cylinders. TMH4, in front of the observer, has been removed for clarity; pale gray TMHs (6 and 7) are positioned far from the observer. Dotted lines indicate relevant interactions (ionic, H-bonds), dotted circles indicate other contacts (hydrophobic, stacking interactions).

A more detailed structural analysis allowed studying the different inner shapes of the binding pockets of the active and inactive states. These are slightly different, which implies distinct interaction modes of agonists and antagonists [91]. The improved models were obtained by site-directed mutagenesis studies and design of Zn<sup>2+</sup>-binding centers. The interaction of Tyr with the Trp<sup>293</sup>(6.48) of the receptor in the active state is of particular interest, since it appears to induce a circa 20° rotation of the TMH6, an event that triggers the dissociation of the G protein.

On the basis of the above discussed modeling of the active and inactive conformations of the receptors, the same authors designed new cyclopeptide ligands, aiming at tuning MOR/DOR/KOR selectivity, as well as the agonist and antagonist behavior. Modeling of the KOR in the active state indicated that the address-binding pocket is smaller than that in the other receptors. This assumption led to the design of a series of new compounds, among which Tyr-c[D-Cys-Phe-D-Cys]-NH<sub>2</sub> demonstrated high binding affinity toward all opioid receptors [92]. This tetrapeptide was docked in the homology model of KOR. In the area of the Tyr<sup>1</sup>-binding site, the compound showed the same interactions created by JOM-6 in the MOR. However, in the KOR the cleft between TMH7 and EL2 is narrowed because of two residues of EL2, Asp<sup>204</sup>, and Val<sup>205</sup>, Fig. (4). As a consequence, the space available for interaction with the ligand's fourth residue and disulfide/dithioether

bridge is reduced. For this reason, Tyr-c[D-Cys-Phe-D-Cys]-NH<sub>2</sub>, having a smaller-size cycle, can fit not only MOR and DOR, but also KOR.

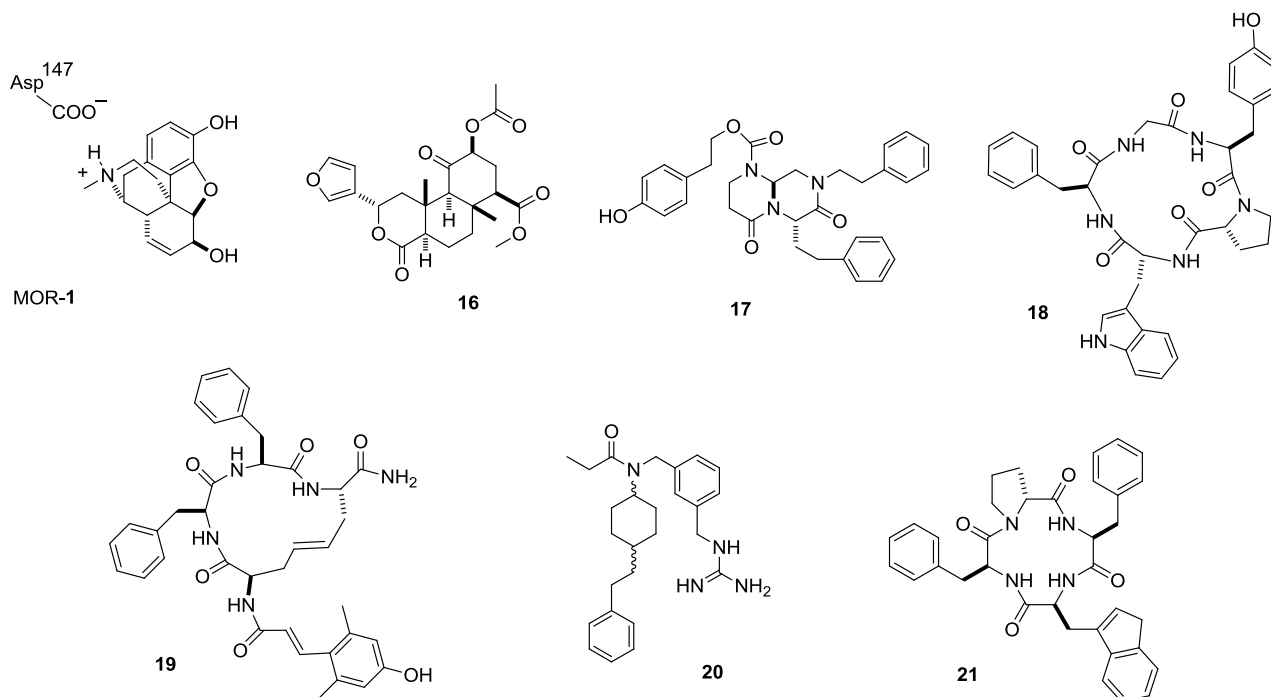


**Fig. (4).** Structures of opioid agonists lacking in the “classic” amino group.

Another set of experiments was attempted aiming at obtaining dual ligands with similar MOR/DOR affinities, but displaying agonism at MOR and antagonism at DOR. Evidence implicating a role of DOR in modulating MOR-induced tolerance suggested that such compounds might find clinical applications for the treatment of chronic pain. Initially, the peptide Tyr-c(S-CH<sub>2</sub>-S)[D-Cys-Phe-Phe-Cys]NH<sub>2</sub> [93] displayed a promising mixed-efficacy profile, exhibiting full agonism at MOR and KOR but only partial agonism at DOR. The peptide was virtually docked in models of active and inactive conformations of MOR and DOR in a similar manner as JOM-6 and JOM-13. The results showed favorable aromatic interactions between its Phe<sup>3</sup> side chain and the Trp<sup>318</sup>(7.35), accounting for the binding to MOR, as compared to DOR, which has Leu<sup>300</sup>(7.35) at the corresponding position. The same peptide, when fitted into the active conformation of DOR, demonstrated a clash between Phe<sup>4</sup> and Trp<sup>284</sup>(6.58), which was not observed in the inactive DOR.

Starting from this model, it was supposed that the incorporation of a bulkier naphthylalanine side chain in either the third or fourth position of the pentapeptide would differentially affect binding and efficacy properties at MOR and DOR, resulting in potent MOR agonist/DOR antagonist ligands. This hypothesis was partially achieved with the cyclopeptide Tyr-c(S-CH<sub>2</sub>-S)[D-Cys-Phe-2-Nal-Cys]NH<sub>2</sub> [94], that showed similar affinity for MOR and DOR but decreased DOR efficacy without compromising MOR agonism.

This behavior was rationalized by docking the peptide in the modeled active and inactive conformations of MOR and DOR. As premised, the 2-naphthylAla<sup>4</sup> side chain showed minimal hindrance with receptor residue Lys<sup>303</sup>(6.58) in the MOR active conformation but an increased steric overlap with Trp<sup>284</sup>(6.58) side chain in

the DOR active conformation. These hindrances were absent in the inactive conformations of both MOR and DOR. This reduced compatibility for the active state of DOR supported the decreased agonism at DOR.

Examples of constrained non natural amino acids are the phenylalanine analogue 1,2,3,4-tetrahydroisoquinoline-3-carboxylic acid (Tic), 4-amino-1,2,4,5-tetrahydro-indolo[2,3-c]azepin-3-one (Aia), and 4-amino-1,2,4,5-tetrahydro-2-benzazepin-3-one (Aba) scaffolds. It was determined that Dmt-Tic-Gly-NH-Bn (Dmt =dimethylTyr) and similar dipeptides, display a DOR over MOR selectivity, whereas MOR binding is preferred for the Aba containing analogues [95]. To rationalize the observed SAR data, the automated docking simulations of the Tic and Aba compounds in MOR and DOR were compared to that of the prototypic JOM-6 and JOM-13 (see previous paragraph), respectively. The Tic and Aba compounds maintained the same interactions between the receptors and Dmt as shown for Tyr<sup>1</sup> of the JOMs. The Tic group of DOR specific compounds occupies the same binding pocket as the Phe<sup>3</sup> group of JOM-13, and also the benzyl group plays a role in DOR-specific binding. The Aba group of the MOR-specific compounds, on the other hand, stacks with Trp<sup>318</sup>(7.35), and occupies the same binding pocket as the Phe<sup>3</sup> ring of JOM6. The benzyl group forms a cation- $\pi$  interaction with the positively charged nitrogen atom of Lys<sup>233</sup>(5.39) of MOR. In essence, the different profiles seemed to be mostly due to the different geometries adopted by the six and seven membered rings within the receptors.

Stereoisomeric 4- or 5-methyl-substituted Aba scaffolds have been introduced within the sequence of the tetrapeptide H-Dmt-DAla-Phe-Gly-NH<sub>2</sub> in place of Phe<sup>3</sup>. Interesting effects of the Aba configuration on ligand binding affinity were observed: the erythro-(4S,5S) and threo-(4R,5S) 5-methyl variants exhibited subnanomolar affinity for OPRM, while in the 4-methyl substituted analogues, the (4R)-Me isomer was significantly more potent than the (4S) one. These results were rationalized by automated molecular docking; the simulations revealed that the (4R)-Me isomer binds in a different mode compared with the other analogues [96].

Replacement of the Tyr<sup>1</sup> residue in the peptide TIPP, H-Tyr-Tic-Phe-Phe-OH, with the phenylalanine analogues 4'-[N-((4'-phenyl)phenethyl) carboxamido]phenylalanine (Bcp) and 2',6'-dimethyl-4'-[N-((4'-phenyl)phenethyl)carboxamido]phenylalanine (Dbcp) resulted in tetra-, tri-, and dipeptides with subnanomolar DOR binding affinity and high selectivity [97]. Interestingly, [Bcp1]TIPP was an agonist, whereas [Dbcp1]TIPP an antagonist.

The flexible docking studies indicated that in both cases, the Nterminal amino group of the ligand formed a salt bridge with Asp<sup>128</sup>(3.32) of the receptor. The large biphenylethyl group contained in the Bcp residue of the agonist interacts with an accessory binding site of the activated receptor distinct from the binding site of the biphenylethyl group of the Dbcp residue of the antagonist bound to the receptor in the inactive state. In particular, the biphenyl moiety differentially interacts with Glu<sup>201</sup>(EL2), Ser<sup>204</sup>(EL2), Asp<sup>210</sup>(5.35), and Thr<sup>211</sup>(5.36) in the case of the agonist and with Ile<sup>183</sup>(4.60), Thr<sup>213</sup>(5.38), and Val<sup>217</sup>(5.42) in the case of the antagonist.

### 5.5. The Docking of Ligands of the Cationic Amino

The ionic bond between a protonated amino group of the agonist and the conserved Asp(3.32) of the receptor is generally regarded to as the driving force of ligand-receptor interaction for all kinds of ligands,

including morphine, fentanyls, and the endogenous peptides [17, 73, 87, 98, 99]. In most cases, the removal or derivatization of this group resulted in inactive derivatives or antagonists; some outstanding examples of antagonists are given: the cyclic  $\beta$ -casomorphin-derived opioid peptide CHO-Dmt-c[D-Orn-2-Nal-Pro-Gly] showed MOR and DOR antagonist activity [100]; the cyclic opioid peptides containing 3-(2,6-dimethyl-4-hydroxyphenyl)propanoic acid (Dhp), (2S)-2-methyl-3-(2,6-dimethyl-4-hydroxyphenyl)-propanoic acid [(2S)-Mdp], or (3S)-3-methyl-3-(2,6-dimethyl-4-hydroxyphenyl) propanoic acid [(3S)-Mdp] instead of the classic Tyr1 residue, resulted in opioid antagonists [101-103]; the MOR and KOR antagonist *N*-formylnormorphine [104]; the dynorphin A analogue cyclo (N,5)[Trp<sup>3</sup>,Trp<sup>4</sup>,Glu<sup>5</sup>] dynorphin A-(1-11)NH<sub>2</sub>, an *N*-terminal to-side chain cyclic peptide showed good KOR antagonism [105].

However, in the last few years some compounds having no classic, protonable amino group proved to be full or partial nagonists. These very few examples are shown in Fig. (5) (for the references, see the next sections): the diterpene Salvinorin A (16) and its many analogues and derivatives; the bicyclic enkephalin mimetic by Eguchi (17); the cyclopentapeptide analogue of EM1, c[Tyr-D-Pro-D-Trp-Phe-Gly] (18); a cyclic enkephalin analogue containing Dhp in the place of Tyr (19); a “carba”- analogue of fentanyl, in which the classic piperidine nitrogen of the fentanyls was replaced by a carbon, but equipped with a ionisable guanidino group (20); the cyclotetrapeptide CJ-15,208 (21), discovered earlier, whose agonist character *in vivo* was proved only very recently, and some analogues.

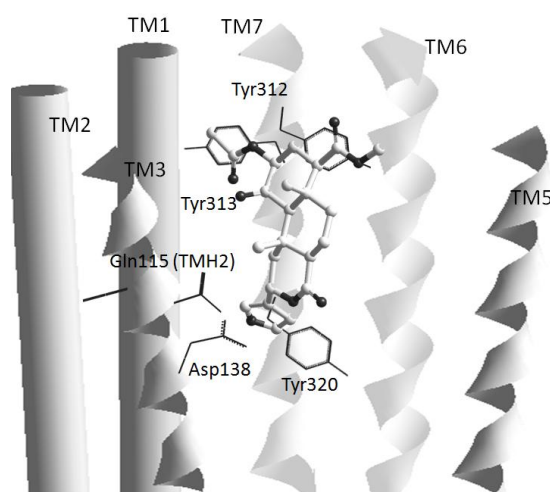


**Fig. (5).** Schematic sketch of the interactions between salvinorin A and KOR. The TMHs 3, 5, 6, and 7, delimitating the binding-site, are rendered as ribbons, while the TMHs 1 and 2 are rendered as cylinders. TMH4, in front of the observer, has been removed for clarity; pale gray TMHs (6 and 7) are positioned far from the observer.

For their atypical structure, it is likely that these compounds elicit their opioid activity through alternative or more complex mechanisms than typical opioid receptor ligands. For this reason, some of them have been the object of extensive SAR analysis and/or molecular docking studies, aiming at obtaining information on the interactions with the receptors responsible for the activation.

### 5.5.1. *Salvinorins*

Salvinorin A (**16**), isolated from the plant *Salvia divinorum* [106], is a highly potent and selective KOR receptor agonist and the most potent naturally occurring hallucinogen known, used for centuries by the Mazatec Indians of Mexico for divination. Salvinorin A is unique among opioids in that its chemical structure lacks a basic amine group, quite it has no N at all. For this reason, it can be anticipated that salvinorin A and its derivatives interact with the KOR *via* residues that are not utilized by conventional agonists.

Salvinorin A consists of a rigid hydrophobic core that contains eight H-bond accepting oxygen atoms. During the years, Salvinorin A was the subject of many docking analyses, which often gave incoherent results even by the same authors. Extensive modifications were brought especially at the C-2 position, but also at C-4 and at the furan ring, and these analogues were utilized for SAR studies and for refining the results of the docking computations. In the first model [107] four H-bonding interactions were identified: between amide-NH of Gln<sup>115</sup>(2.60) and furanoic oxygen, phenolic-OH of Tyr<sup>139</sup>(3.33) and lacton-CO, phenolic-OH of Tyr<sup>312</sup>(7.35) and methoxycarbonyl group, and phenolic-OH of Tyr<sup>313</sup>(7.36) and acetyl group. The screening of several derivatives confirmed the importance of the methyl ester and furan ring but reduced the role of the lactone and ketone functionalities [108]. More recent data using an improved model of the KOR revolutionized this initial hypothesis [109], revealing interactions with Tyr<sup>313</sup>(7.36) and Tyr<sup>320</sup>(7.43) and Tyr<sup>119</sup>(2.64), plus a hydrophobic interaction of Tyr<sup>313</sup>(7.36) with 2-acetoxy group of Salvinorin A. A few years later also this second model was revisited. A combination of studies performed on wild-type, chimeric, and single-point mutant opioid receptors [110-112], lead to the proposal of a model showing the interaction of the furane with Tyr<sup>320</sup>(7.43), while the acetyl group interacts with Tyr<sup>312</sup>(7.35) and Tyr<sup>313</sup>(7.36), the methyl ester with Tyr<sup>119</sup>(2.64), and Gln<sup>115</sup>(2.60) serves as a H-bond donor for lacton carbonyl. Other recognition elements of the receptor initially regarded to as relevant for the interaction were not confirmed.

Further experiments and docking analyses consistent with sitedirected mutagenesis studies, chimeric receptor studies [113], and affinity labeling experiments [114] again revolutionized the binding model [115-117], Fig. (6). The oxygen of the furan ring may form a H-bond with both Gln<sup>115</sup>(2.60) and Tyr<sup>320</sup>(7.43). An additional H-bond may possibly exist between Tyr<sup>312</sup>(7.35) and the methoxy oxygen of the C-4 position methyl ester. In addition, there is a likely hydrophobic interaction between Tyr<sup>313</sup>(7.36) and the acetoxy moiety of Salvinorin. Besides to the already mentioned Gln<sup>115</sup>(2.60), Tyr<sup>119</sup>(2.64), Tyr<sup>313</sup>(7.36), and Tyr<sup>320</sup>(7.43), it appears that Salvinorin A interacts also with Ile<sup>316</sup>(7.39), as revealed by the complete lack of binding to the Ile<sup>316</sup>Ala mutant [118].

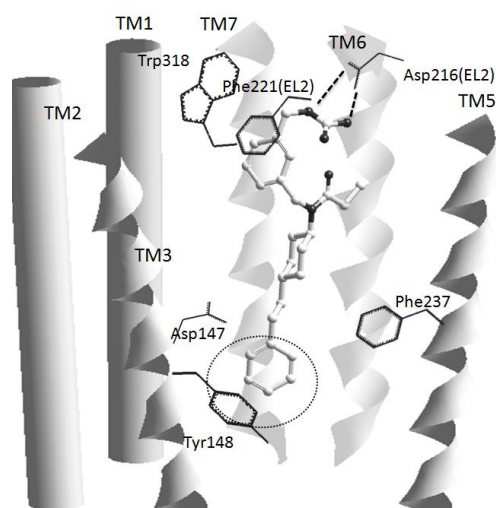


**Fig. (6).** Interactions between the MOR and the carba-guanidinic fentanyl (**20**). The TMHs 3, 5, 6, and 7, delimitating the binding-site, are rendered as ribbons, while the TMHs 1 and 2 are rendered as cylinders. TMH4, in front of the observer, has been removed for clarity; pale gray TMHs (6 and 7) are positioned far from the observer. Dotted lines indicate relevant interactions (ionic, H-bonds), dotted circles indicate other contacts (hydrophobic, stacking interactions).

### 5.5.2. 6,6-Bicyclic Enkephalin Mimetics

The highly constrained 6,6-bicyclic system **17** belongs to a series of constrained peptidomimetics designed to mimic enkephalin or EM  $\beta$ -turn models. It showed an initial level of analgesic activity similar to that of morphine, but *in vivo* half-life was shorter [119]. On the basis of 2D NMR analysis and molecular mechanics computations, the authors noticed a good super-imposition of the structure of **17** with a trans EM1 type III  $\beta$ -turn backbone structure. Based on this similarity and on the MOR-selectivity profile, the authors implicitly suggested that the interaction with the receptor could mimic that of EM or enkephalins, but docking simulation to visualize a plausible 3D structure were not performed.

### 5.5.3. Dhp-Peptide

Cyclic enkephalin analogues were obtained by ring closing metathesis using a second generation Grubbs catalyst from precursors containing D-allylGly and (2S)-2-amino-5-hexenoic acid (Aha) in position 2 and 5, respectively. Compounds of this series containing 3-(2,6-dimethyl-4-hydroxyphenyl)propanoic acid (Dhp) in place of Tyr such as trans Dhp-c[D-AllylGly-Phe-Phe-Aha]NH<sub>2</sub> (**19**) or the cis isomer, or the saturated analogue, all lacking a positively charged nitrogen, were mixed DOR agonist MOR antagonists by the GPI and MVD bioassays. This peptide **19** was presented as the first example of a neutral compound with DOR agonist activity [120], but no docking analysis was reported to explain the unexpected agonism.

### 5.5.4. Fentanyl "Carba"-Analogues

In the MOR agonist fentanyl, the positively charged nitrogen is contained in the piperidine ring. The substitution of the piperidine nitrogen with a carbon atom and introduction of a 3-(guanidinomethyl)-benzyl group in place of the phenyl moiety attached to the ethylamido group gave "carba"-analogues of fentanyl (**20**) (cis and trans isomers).

These compounds showed reduced binding affinities, but retained full agonist activity [121]. Flexible docking studies indicated that the phenylethyl group is accommodated in a binding pocket formed by TMHs 3, 5, and 6; in the trans isomer this group is in an extended conformation, while it assumes a bent conformation in the cis isomer. For both, the guanidino group forms a salt bridge with the side chain of Asp<sup>216</sup>(EL2), and its aromatic ring interacts with Phe<sup>313</sup>(7.30), Trp<sup>318</sup>(7.35), Thr<sup>218</sup>(EL2), Fig. (7).

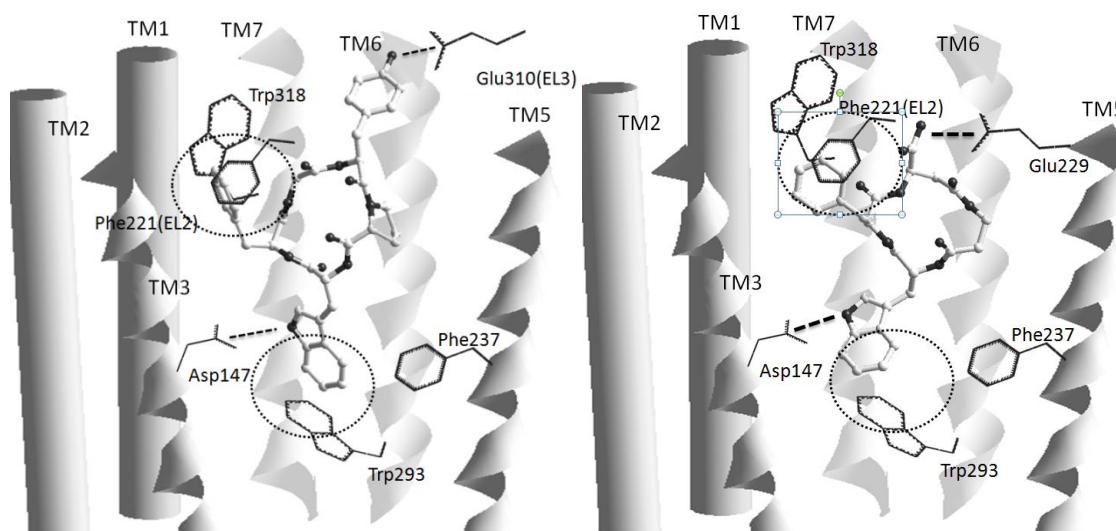


**Fig. (7).** Left, interactions between the MOR and CycloEM/1 (**18**); right, interactions between MOR and CycleEM/3. The TMHs 3, 5, 6, and 7, delimitating the binding-site, are rendered as ribbons, while the TMHs 1 and 2 are rendered as cylinders. TMH4, in front of the observer, has been removed for clarity; pale gray TMHs (6 and 7) are positioned far from the observer. Dotted lines indicate relevant interactions (ionic, H-bonds), dotted circles indicate other contacts (hydrophobic, stacking interactions).

The calculated reduction in receptor binding energy is due to the inability of these “carba”-analogues to engage in an electrostatic interaction with Asp<sup>147</sup>(3.32), but this deficiency is partially compensated by the interaction between the guanidine group with Asp<sup>216</sup>(EL2), which contributes to binding the active conformation of the receptor and, thereby, maintaining the agonist activity.

### 5.6. The D-Trp-Phe Pharmacophoric Motif

The cyclopentapeptide c[Tyr-D-Pro-D-Trp-Phe-Gly], CycloEM-1 (**18**), is an analogue of EM1 lacking in the free amino group of Tyr<sup>1</sup> but which can still bind and activate MOR. It is the most active member of a mini-library of cyclic EM1 analogues having the same amino acids in L or D configuration [122], connected by a Gly. The diverse stereochemistry arrays of the diastereoisomers conferred them alternative 3D displays and different pharmacological features, since only the LDDL configured CycloEM-1 revealed a 10<sup>-8</sup> M receptor affinity.

CycloEM-1 produced a concentration dependent inhibition of forskolin-stimulated production of cAMP, thus acting as an agonist.

In the visceral pain test, used for detecting both central and peripheral analgesia, CycloEM-1 significantly reduced the number of writhes; MOR antagonist, but not KOR and DOR antagonists, blocked antinociception

[123]. CycloEM-1 was even more effective in preemptive antinociception, with a similar profile, and maintained the effect when delivered by subcutaneous injection, which correlates to its lipophilicity and stability. In the tail flick test, the cyclopeptide i.p. administered gave a moderate response, suggestive of a partial penetration of the BBB.

The significant receptor affinity and the agonist profile suggested that this atypical compound activates the MOR, but it must necessarily interact in a different way with respect to the large majority of the cases. The in-solution conformations were docked into a model of the MOR [124], and computations were refined by hybrid QM/MM, giving an unprecedented orientation, showing the peptide deeply inserted between the TMH3, 5, and 7, and featuring the indole NH of D-Trp<sup>3</sup> H-bonded to Asp<sup>147</sup>(3.32), Fig. (8a). The absence of the ionic interaction is partially compensated by this Hbond; ligand polarization also represents a strong contribution to the overall binding energy, as determined by QM/MM. Tyr<sup>1</sup>-OH is Hbonded to Glu<sup>310</sup>, Phe<sup>4</sup> interacts with the residues Phe<sup>221</sup>(EL2) and Trp<sup>318</sup>(7.35). Tyr also contributes to the overall binding with some stabilizing hydrophobic contacts. The interaction between D-Trp of the ligand and Trp<sup>293</sup>(6.48) is relevant, since the induced fit on this region of the receptor would be responsible for MOR activation, as proposed by Mosberg [91]. The overall bioactive conformation is compatible with an inverse type II  $\beta$ -turn centered on D-Trp-Phe. To corroborate this unprecedented model, a second generation of more rigid or, conversely, more flexible cyclopeptides modified in the position 5 was prepared and tested (CycloEMs-2).

All the derivatives adopted the same binding poses of CycloEM-1, with different calculated docking scores and energies. The correlation between the calculated docking energies and the experimental free energies derived from the affinity parameters showed a nice linear regression with excellent statistics, supporting the liability of the model.

The cyclopeptides adopt in the receptor a quite different conformation with respect to the preferred ones shown in solution, so that for optimal fit the backbone of the ligands is forced to assume a higher energy conformation. In principle, it should be possible to improve the efficacy of such compounds, taking into consideration that "the more the structures of the free ligands in solution resemble the structures at the receptor, the stronger the binding and affinity" [125]. Despite of some limitations, this assumption can be utilized as an indicative guide for structure optimization. Starting from the proposed model, new cyclopeptides were designed, fostering the beta-turn motif on D-Trp-Phe. The docking model indicated that neither D-Pro<sup>2</sup> nor Gly<sup>5</sup> in CycloEMs really interacted with the receptor, being their role fundamental in stabilizing backbone geometries. In particular, D-Pro plays a major role in preventing CycloEM from assuming the bioactive conformation.

A third generation of cyclopentapeptides was designed on the basis of these assumptions; backbone conformations were predetermined on the basis of the well-known structures of cyclo-Ala<sup>5</sup> models or other cyclopentapeptides containing one or two D-residues already reported in the literature, widely used as  $\beta/\gamma$ -turn mimetics. Among the new cyclopeptides, c[Tyr-Gly-D-Trp-Phe-Gly], CycloEM-3, proved to be a selective ligand of MOR with nanomolar affinity, almost as good as the reference DAMGO, and about 10-fold better compared to the parent CycloEM/1 (18), a very good result for a compound lacking of the cationic amino group [126]. Another compound c[Tyr-Ala-D-Trp-Ala-Gly] was a selective, modest ligand of the DOR, and c[Tyr-Gly-D-Trp-Ala-Gly] had a significant affinity and selectivity for the KOR.

As expected, CycloEM-3 had a greater conformational freedom. The docking analysis revealed at least a couple of plausible poses; the binding pose with the best score is compatible with the required inverse  $\beta$ -turn on D-Trp-Phe. However, the intrinsic flexibility both in solution and in the receptor-bound state, diminished the reliability of the proposed model of bioactive conformation. For this reason, cyclopeptide candidates were modelled, characterized by lower conformational freedom and a predisposition to reproduce the inverse type II  $\beta$ -turn, whose conformational homogeneity allowed more definitive conclusions. The cyclotrapeptide c[DAsp- 1-amide- $\beta$ -Ala-D-Trp-Phe] (**22**), CycloEM-4, deprived of the Tyr, and including two  $\beta$ -amino acids, clearly adopted the expected backbone conformation, and showed a nanomolar MOR affinity, high selectivity, and an agonist behaviour. Docking analysis confirmed that CycloEM-4 retained the same geometry also into the receptor, Fig. (8b). The indole of D-Trp occupies the same hydrophobic cavity occupied by the corresponding residue of CycloEM-1. The most relevant contacts were the H-bond of indoleNH with Asp<sup>147</sup>(3.32), the two H-bonds of D-AspCONH<sub>2</sub>, one with Leu<sup>219</sup>(EL2), the other with Glu<sup>229</sup>(5.35), and the two H-bonds of  $\beta$ -Ala, one with Glu<sup>229</sup>(5.35), the other with Thr<sup>218</sup>(EL2). The phenyl of Phe has strong hydrophobic interaction with Phe<sup>221</sup>(EL2) and Trp<sup>318</sup>(7.35).

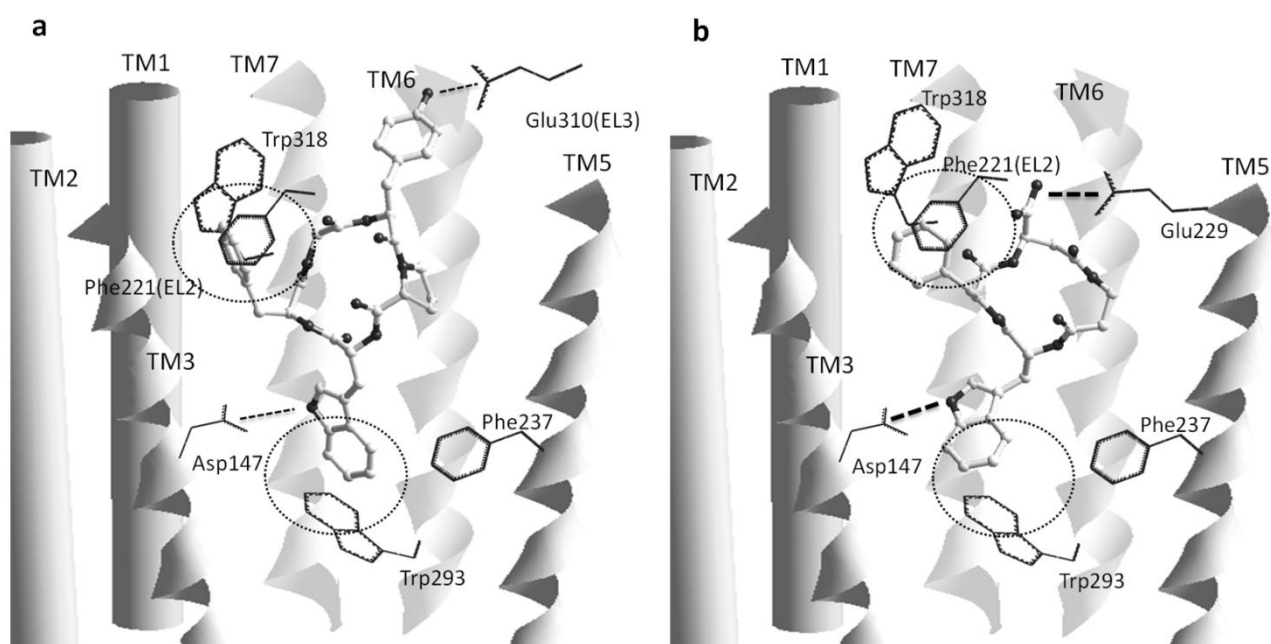


**Fig. (8).** Schematic sketches of the interactions of CycloEM/1 (**18**) (left, **a**), and of CycloEM/3 (**22**) (right, **b**) with the MOR. The TMHs 3, 5, 6, and 7, delimitating the binding-site, are rendered as ribbons, while the TMHs 1 and 2 are rendered as cylinders. TMH4, in front of the observer, has been removed for clarity; pale gray TMHs (6 and 7) are positioned far from the observer. Dotted lines indicate relevant interactions (ionic, H-bonds), dotted circles indicate other contacts (hydrophobic, stacking interactions).

To improve the ability to cross the BBB, the structure of CycloEM-4 was reduced to the minimal bioactive sequence.

According to the docking model, the most relevant pharmacophores were the indole and the phenyl aromatic rings, and the CONH<sub>2</sub> group, while the remaining portion of D-Asp- $\beta$ -Ala had scarce or no interactions at all

with the receptor. Accordingly, the linear peptide Ac-D-Trp-Phe-GlyNH<sub>2</sub> (CycloEM-5) maintained the MOR agonism, and a nanomolar affinity [127]. Conformational analysis revealed that, despite of intrinsic flexibility, in solution this linear peptide had a significant tendency to fold in an inverse  $\beta$ -turn stabilized by a H-bond between Ac(CO) and GlyNH, due to the presence of a D-configured amino acid in the position *i+1*.

The cyclopeptides CycloEM-1 represents the first examples of MOR-agonists described in the literature (2004) whose bioactivity resides in the D-Trp-Phe sequence. Very recently, this pharmacophoric motif was proposed again in regard to c[D-Pro-Phe-D-Trp-Phe] and correlated compounds [128], derived from the naturally occurring cyclotetrapeptide c[D-Pro-Phe-Trp-Phe], CJ-15,208 (**21**) [129], isolated as a metabolite of a fungus. CJ-15,208 was reported to preferentially bind to KOR (IC<sub>50</sub> 47 nM, using a guinea pig brain membrane), and antagonize the activity of a KOR agonist in the rabbit vas deferens smooth muscle preparation. The D-configured Trp residue rendered the derivatives more potent than the natural product. c[D-Pro-Phe-D-Trp-Phe] was a KOR antagonist devoid of agonist activity, with a modest MOR affinity.

The analogue c[D-Pro-Phe-D-Trp-Ala] practically maintained the same activity and selectivity as KOR antagonist. This suggests that the pharmacophoric sequence likely is Phe-D-Trp, rather than D-Trp-Phe. Therefore, the different pharmacologic profile of the MOR agonists CycloEM/1-5 with respect to the KOR-antagonists derived from CJ-15,208 very likely originates in the inverted positions of D-Trp and Phe within the sequence, and in the 3D display of their side chains, correlated to the different sizes of the cyclopeptide structures. These differences strongly impact not only the affinity for a specific opioid receptor type, but also the ability to trigger the activation of G-proteins and activate signal transduction.

Although CJ-15,208 (**21**) did not exhibit any agonist activity at either KOR or MOR *in vitro*, very recently Aldrich et al. observed an unexpected agonist activity *in vivo* in the 55°C warm-water tail withdrawal antinociceptive assay in addition to KOR-selective antagonist activity [130].

The same authors prepared and tested analogues of CJ-15,208 having one Ala instead of each of the natural residues [131]. The substitution of one Phe to give c[D-Pro-Phe-Trp-Ala] increased both KOR and MOR affinities by 4.4- and 19-fold, respectively. In contrast, substitution of the other three residues with Ala decreased KOR affinity from 3- to 44-fold, with the largest decrease occurring if the Trp residue is replaced. None of the peptides exhibited appreciable agonism *in vitro* (stimulation of [35S]GTP $\gamma$ S binding) *via* either KOR or MOR, consistent with the lack of agonist activity of the parent peptide in this assay. Like the parent peptide, each of the analogues exhibited agonist activity in an antinociceptive assay *in vivo*. As observed for the CycloEMs, the agonist activity of the analogues was mediated predominantly by MOR; indeed, their antinociceptive activity was almost completely blocked by pretreatment with the MOR-selective irreversible antagonist  $\beta$ -funaltrexamine. These results strongly support the hypothesis above discussed for the CycloEMs, that Trp and Phe represent an unusual kind of agonist pharmacophoric motif in cyclopeptides. The stereochemistry of Trp, the disposition of Trp and Phe, and the secondary conformation of the dipeptide strongly influence affinity and selectivity and, likely, agonism vs antagonism.

## 5.7. CONCLUSIONS

In the last decades, continuous efforts have been dedicated to the design and synthesis of new opioid agonists or antagonists; in particular, the former raise much interest as potential analgesics devoid of the

unwanted side effects of the opiates. In this contest, the molecular docking approach emerged as a powerful tool in drug discovery to find and optimize lead compounds. Molecular docking is a method which estimates the preferred orientations of a candidate drug inside its receptor. The results of this computational analysis are much more realistic when the simulations take into account for the data furnished by experimental methods, especially SAR, mutagenesis, chimeric receptors, etc. The survey of the examples discussed in this review clearly shows that the different classes of ligands, such as morphine and the opiates, the fentanyl, the peptides, the peptidomimetics, etc., have distinct modes of receptor interaction and, for the agonists, activation. As a consequence, a number of specific models have been proposed to explain the binding and selectivity of each class. In addition, the analyses of ligands lacking of a well defined message or address, or of highly flexible ligands, often gave alternative models. For instance, morphine, the prototypic agonist of the MOR, is deprived of a relevant address portion, and therefore docking analyses gave different orientations within the receptor cavity. Nevertheless, some ligand classes, such as the conformationally constrained cyclic peptidomimetic JOMs, proved to be very effective in disclosing the structural requirements for receptor affinity and selectivity, as well as of agonism versus antagonism. Besides, docking has represented a useful technique for the analysis of the opioid agonists lacking in the cationizable amino group, generally regarded to as the fundamental pharmacophore interacting with the conserved Asp of TMH3, such as the salvinorins, and the cyclopeptides including the inverse  $\beta$ -turn on D-Trp-Phe. In particular, the results deduced for the latter might be of help to disclose the unexpected agonist activity of the structurally related cyclopeptide CJ-15,208 and its derivatives.

## REFERENCES

- [1] Eguchi, M.; Recent advances in selective opioid receptor agonists and antagonists. *Med. Res. Rev.*, **2004**, *24*, 182-212.
- [2] Pogozheva, I.D.; Przydzial, M.J.; Mosberg, H.I. Homology modeling of opioid receptor-ligand complexes using experimental constraints. *AAPS J.*, **2005**, *7*, Article 43.
- [3] Kane, B.E.; Svensson, B.; Ferguson, D.M. Molecular recognition of opioid receptor ligands. *The AAPS J.*, **2006**, *8*, E126-E137.
- [4] Knapp, R.J.; Malatynska, E.; Collins, N.; Fang, L.; Wang, J.Y.; Hruby, V.J.; Roeske, W.R.; Yamamura, H.I. Molecular biology and pharmacology of cloned opioid receptors. *FASEB J.*, **1995**, *9*, 516-525.
- [5] Kieffer, B.L. Recent advances in molecular recognition and signal transduction of active peptides: receptors for opioid peptides. *Cell. Mol. Neurobiol.*, **1995**, *15*, 615-635.
- [6] Elde, R.; Arvidsson, U.; Riedl, M.; Vulchanova, L.; Lee, J.H.; Dado, R.; Nakano, A.; Chakrabarti, S.; Zhang, X.; Loh, H.H.; Law, P.Y.; Hokefelt, T.; Wessendorf, M. Distribution of neuropeptide receptors. New views of peptidergic neurotransmission made possible by antibodies to opioid receptors. *Ann. N. Y. Acad. Sci.*, **1995**, *757*, 390-404.
- [7] Trescot, A.M.; Datta, S.; Lee, M.; Hansen, H. Opioid Pharmacology. *Pain Physician*, **2008**, Opioid Special Issue: *11*, S133-S153
- [8] Ferré, S.; Navarro, G.; Casadó, V.; Cortés, A.; Mallol, J.; Canela, E.I.; Lluís, C.; Franco, R.G. protein-coupled receptor heteromers as new targets for drug development. *Prog. Mol. Biol. Transl. Sci.*, **2010**; *91*, 41-52.
- [9] Guidolin D.; Ciruela F.; Genedani S.; Guescini M.; Tortorella C.; Albertin G.; Fuxe K.; Agnati L.F. Bioinformatics and mathematical modelling in the study of receptor-receptor interactions and receptor oligomerization: focus on adenosine receptors. *Biochim. Biophys. Acta*, **2011**, *1808*, 1267-1283.
- [10] Janecka, A.; Fichna, J.; Janecki, T. Opioid receptors and their ligands. *Curr. Top. Med. Chem.*, **2004**, *4*, 1-17.
- [11] Zadina, J.E.; Hackler, L.; Ge, L.J.; Kastin, A.J. A potent and selective endogenous agonist for the mu-opiate receptor. *Nature*, **1997**, *386*, 499-502.
- [12] Jakub, F.; Janecka, A.; Constantin, J.; Do Rego, J.C. The endomorphin system and its evolving neurophysiological role. *Pharmacol. Rev.*, **2007**, *59*, 88-123.
- [13] Gentilucci, L.; De Marco, R.; Cerisoli, L. Chemical modifications designed to improve peptide stability: incorporation of non-natural amino acids, pseudo-peptide bonds, and cyclization. *Curr. Pharm. Design*, **2010**, *16*, 3185-3203.
- [14] Janecka A.; Perlikowska R.; Gach K.; Wyrebska, A.; Fichna, J. Development of Opioid Peptide Analogs for Pain Relief. *Curr. Pharm. Des.*, **2010**, *16*, 1126-1135
- [15] Cardillo, G.; Gentilucci, L., Qasem, A.R., Sgarzi, F.; Spampinato, S. Endomorphin-1 analogues containing  $\beta$ -proline are  $\mu$ -opioid receptor agonists and display enhanced enzymatic hydrolysis resistance. *J. Med. Chem.* **2002**, *45*, 2571-2578
- [16] Gentilucci, L. New trends in the development of opioid peptide analogues as advanced remedies for pain relief. *Curr. Top. Med. Chem.*, **2004**, *4*, 19-38.

- [17] Gentilucci, L.; Tolomelli, A. Recent advances in the investigation of the bioactive conformation of peptides active at the  $\mu$ -opioid receptor. Conformational analysis of endomorphins. *Curr. Top. Med. Chem.*, **2004**, *4*, 105-121.
- [18] Chrysina, E.D.; Chajistamatiou, A.; Chegkazi, M. From structure-based to knowledge-based drug design through x-ray protein crystallography: sketching glycogen phosphorylase binding sites. *Curr. Med. Chem.*, **2011**, *18*, 2620-2629.
- [19] <http://www.wwpdb.org/>
- [20] <http://www.ccdc.cam.ac.uk/products/csd/>
- [21] <http://zinc.docking.org/>
- [22] Wang, Y.; Bolton, E.; Dracheva, S.; Karapetyan, K.; Shoemaker, B.A.; Suzek, T.O.; Wang, J.; Xiao, J.; Zhang, J.; Bryant, S.H., An overview of the PubChem BioAssay resource. *Nucleic Acids Res.*, **2010**, *38*, D255-266.
- [23] Bellis, L.J.; Akhtar, R.; Al-Lazikani, B.; Atkinson, F.; Bento, A.P.; Chambers, J.; Davies, M.; Gaulton, A.; Hersey, A.; Ikeda, K.; Krüger, F.A.; Light, Y.; McGlinchey, S.; Santos, R.; Stauch, B.; Overington, J.P. Collation and data-mining of literature bioactivity data for drug discovery. *Biochem. Soc. Trans.*, **2011**, *39*, 1365-1370.
- [24] Wishart, D.S.; Knox, C.; Guo, A.C.; Cheng, D.; Shrivastava, S.; Tzur, D.; Gautam, B.; Hassanali, M. DrugBank: a knowledgebase for drugs, drug actions and drug targets. *Nucleic Acids Res.*, **2008**, *36*, D901-906.
- [25] Tapaneeyakorn, S.; Goddard, A.D.; Oates, J.; Willis, C.L.; Watts, A. Solution- and solid-state NMR studies of GPCRs and their ligands. *Biochim. Biophys. Acta.*, **2011**, *1808*, 1462-1475.
- [26] Langelaan, D.N.; Ngweniform, P.; Rainey, J.K. Biophysical characterization of G-protein coupled receptorpeptide ligand binding. *Biochem. Cell. Biol.*, **2011**, *89*, 98-105.
- [27] Hou, T.; Xu, X. Recent development and application of virtual screening in drug discovery: an overview. *Curr. Pharm. Design*, **2004**, *10*, 1011-1033.
- [28] Palczewski, K.; Kumasaka, T.; Hori, T.; Behnke, C.A.; Motoshima, H.; Fox, B.A.; Le Trong, I.; Teller, D.C.; Okada, T.; Stenkamp, R.E.; Yamamoto, M.; Miyano, M. Crystal structure of rhodopsin: A G protein-coupled receptor. *Science*, **2000**, *289*, 739-745.
- [29] Cherezov, V.; Rosenbaum, D.M.; Hanson, M.A.; Rasmussen S.G.; Thian, F.S.; Kobilka, T.S.; Choi, H.J.; Kuhn, P.; Weis, W.I.; Kobilka, B.K.; Stevens, R.C. High resolution crystal structure of an engineered human beta2-adrenergic G protein-coupled receptor. *Science*, **2007**, *318*, 1258-1265.
- [30] Rosenbaum, D.M.; Cherezov, V.; Hanson, M.A.; Rasmussen, S.G.; Thian, F.S.; Kobilka, T.S.; Choi, H.J.; Kuhn, P.; Weis, W.I.; Kobilka, B.K.; Stevens, R.C. GPCR engineering yields high-resolution structural insights into beta2-adrenergic receptor function. *Science*, **2007**, *318*, 1266-1273.
- [31] Warne, T.; Serrano-Vega, M.J.; Baker, J.G.; Moukhametzianov, R.; Edwards, P.C.; Henderson, R.; Leslie, A.G.; Tate, C.G.; Schertler, G.F. Structure of a beta1-adrenergic G-protein-coupled receptor. *Nature*, **2008**, *454*, 486-491.
- [32] Murakami, M.; Kouyama, T. Crystal structure of squid rhodopsin. *Nature*, **2008**, *453*, 363-367.

- [33] Jaakola, V.P.; Ijzerman, A.P. The crystallographic structure of the human adenosine A2A receptor in a high-affinity antagonist-bound state: implications for GPCR drug screening and design. *Curr. Opin. Struct. Biol.*, **2010**, *20*, 401-414.
- [34] Chien, E.Y.T.; Liu, W.; Zhao, Q.; Katritch, V.; Gye G.W.; Hanson, M.A.; Shi, L.; Newman, A.H.; Javitch, J.A.; Cherezov, V.; Stevens, R.C. Structure of the Human Dopamine D3 Receptor in Complex with a D2/D3 Selective Antagonist. *Science*, **2010**, *330*, 1091-1095.
- [35] Yarnitzky, T.; Levit, A.; Niv, M.Y. Homology modeling of G-proteincoupled receptors with X-ray structures on the rise. *Curr. Opin. Drug Discov. Devel.*, **2010**, *13*, 317-325.
- [36] Salamon, Z.; Cowell, S.; Varga, E.; Yamamura, H.I.; Hruby, V.J.; Tollin, G. Plasmon resonance studies of agonist/antagonist binding to the human deltaopioid receptor: New structural insights into receptor-ligand interactions. *Biophys J.*, **2000**, *79*, 2463-2474.
- [37] Blake, A.D.; Bot, G.; Reisine, T. Structure-function analysis of the cloned opiate receptors: peptide and small molecule interactions. *Chem. Biol.*, **1996**, *3*, 967-972.
- [38] Law, P.Y.; Wong, Y.H.; Loh, H.H. Mutational analysis of the structure and function of opioid receptors. *Biopolymer*, **1999**, *51*, 440-455.
- [39] Filizola, M.; Villar, H.O.; Loew, G.H. Differentiation of delta, mu, and kappa opioid receptor agonists based on pharmacophore development and computed physicochemical properties. *J. Comput. Aided Mol. Des.*, **2001**, *15*, 297-307.
- [40] Ewing, T.J.; Makino, S.; Skillman, A.G.; Kuntz, I.D. DOCK 4.0: search strategies for automated molecular docking of flexible molecule databases. *J. Comput. Aided Mol. Des.*, **2001**, *15*, 411-428.
- [41] Walters, P.E.; Charifson, P.S. A detailed comparison of current docking and scoring methods on systems of pharmaceutical relevance. *Proteins*, **2004**, *56*, 235-249.
- [42] Morris, G.M.; Goodsell, D.S.; Halliday, R.S.; Huey, R.; Hart, W.E.; Belew, R.K. Olson, A.J. Automated docking using a Lamarckian genetic algorithm and an empirical binding free energy function. *J. Comput. Chem.*, **1998**, *19*, 1639-1662.
- [43] Trott, O.; Olson, A.J. AutoDock Vina: improving the speed and accuracy of docking with a new scoring function, efficient optimization and multithreading. *J. Comput. Chem.*, **2010**, *31*, 455-461
- [44] Jones, G.; Willett, P.; Glen, R.C.; Leach, A.R.; Taylor, R. Development and validation of a genetic algorithm for flexible docking. *J. Mol. Biol.*, **1997**, *267*, 727-748.
- [45] Rarey, M.; Wefing, S.; Lengauer, T. Placement of medium-sized molecular fragments into active sites of proteins. *J. Comput. Aided Mol. Des.*, **1996**, *10*, 41-54.
- [46] Taylor, R.D.; Jewsbury, P.J.; Essex, J.W. FDS: flexible ligand and receptor docking with a continuum solvent model and soft-core energy function. *J. Comput. Chem.*, **2003**, *24*, 1637-1656 .
- [47] Friesner, R.A.; Banks, J.L.; Murphy, R.B.; Halgren, T.A.; Klicic, J.J.; Mainz, D.T.; Repasky, M.P.; Knoll, E.H.; Shelley, M.; Perry, J.K.; Shaw, D.E.; Francis, P.; Shenkin, P.S. Glide: a new approach for rapid, accurate docking and scoring. 2. Enrichment factors in database screening. *J. Med. Chem.*, **2004**, *47*, 1750-1759.
- [48] Venkatachalam, C.M.; Jiang, X.; Oldfield, T.; Waldman, M. Ligand Fit: a novel method for the shape-directed rapid docking of ligands to protein active sites. *J. Mol. Graph. Model.*, **2003**, *21*, 289-307.

- [49] Cavasotto, C N.; Abagyan, R.A. Protein flexibility in ligand docking and virtual screening to protein kinases. *J. Mol. Biol.*, **2004**, *337*, 209-225.
- [50] Brooijmans, N.; Kuntz, I.D. Molecular recognition and docking algorithms. *Annu. Rev. Biophys. Biomol. Struct.*, **2003**, *32*, 335-373.
- [51] <http://www.simbiosys.ca/ehits/index.html>
- [52] Alisaraie, L.; Haller, L.A.; Fels, G. A QXP-Based Multistep Docking Procedure for Accurate Prediction of Protein  $\alpha$  Ligand Complexes. *J. Chem. Inf. Mod.*, **2006**, *46*, 1174-1187.
- [53] Glover, F.; Laguna, M. In Reeves, C. R., Modern Heuristic Techniques for Combinatorial Problem. **1993**, Blackells, Oxford, UK, pp. 70-150.
- [54] Ausiello, G.; Cesareni, G.; Helmer-Citterich, M. ESCHER: a new docking procedure applied to the reconstruction of protein tertiary structure. *Proteins*, **1997**, *28*, 556-567.
- [55] Taylor, R.D.; Jewsbury, P.J.; Essex, J.W. A review of protein-small molecule docking methods. *J. Comput. Aided Mol. Des.*, **2002**, *16*, 151-166.
- [56] Zhong, S.J.; Zhang, Y.P.; Xiu, Z.L. Rescoring ligand docking poses. *Curr. Opin. Drug Disc. Dev.*, **2010**, *13*, 326-334.
- [57] Kauzmann W. Some factors in the interpretation of protein denaturation. *Adv. Prot. Chem.*, **1959**, *14*, 1-63.
- [58] Provasi, D.; Bortolato, A.; Filizola, M. Exploring molecular mechanisms of ligand recognition by opioid receptors with etadynamics. *Biochemistry*, **2009**, *48*, 10020-10029.
- [59] Hetenyi, C.; van der Spoel, D. Efficient docking of peptides to proteins without prior knowledge of the binding site. *Prot. Science*, **2002**, *11*, 1729-1737.
- [60] Hetenyi, C.; van der Spoel, D. Blind docking of drug-sized compounds to proteins with up to a thousand residues. *FEBS Lett.*, **2006**, *580*, 1447-1450.
- [61] Yamamoto, T.; Nair, P.; Jacobsen, N.E.; Davis, P.; Ma, S.; Navratilova, E.; Moye, S.; Lai, J.; Yamamura, H. I.; Vanderah, T.W.; Porreca, F.; Hruby, V.J. The importance of micelle-bound states for the bioactivities of bifunctional peptide derivatives for  $\delta/\mu$  opioid receptor agonists and neurokinin 1 receptor antagonists. *J. Med. Chem.*, **2008**, *51*, 6334-6347.
- [62] Koshland, D.E. Jr. Application of a theory of enzyme specificity to protein synthesis. *Proc. Natl. Acad. Sci. USA*, **1958**, *44*, 98-104.
- [63] Evers, A.; Gohlke, H.; Klebe, G. Ligand-supported homology modelling of protein binding-sites using knowledge-based potentials. *J. Mol. Biol.*, **2003**, *334*, 327-345.
- [64] Cornell, W. D.; Cieplak, P.; Bayly, C. I.; Gould, I. R.; Merz, K. M.; Ferguson, D. M.; Spellmeyer, D. C.; Fox, T.; Caldwell, J. W.; Kollman, P. A. *J. Am. Chem. Soc.*, **1995**, *117*, 5179 - 5197.
- [65] Brooks, B.R.; Brucoleri, R.E.; Olafson, B.D.; States, D.J.; Swaminathan, S.; Karplus, M. CHARMM: A program for macromolecular energy, minimization, and dynamics calculations. *J. Comp. Chem.*, **1983**, *4*, 187-217.
- [66] Jorgensen, W.L.; Tirado-Rives, J. The OPLS force field for proteins. Energy minimizations for crystals of cyclic peptides and crambin. *J. Am. Chem. Soc.*, **1988**, *110*, 1657-1666.

- [67] Menikarachchi, L.C.; Gascón, J.A. QM/MM approaches in medicinal chemistry research. *Curr. Top. Med. Chem.*, **2010**, *10*, 46-54.
- [68] Anzini, M.; Canullo, L.; Braile, C.; Cappelli, A.; Gallelli, A.; Vomero, S.; Menziani, M.C.; De Benedetti, P.G.; Rizzo, M.; Collina, S.; Azzolina, O.; Sbacchi, M.; Ghelardini, C.; Galeotti, N. Synthesis, biological evaluation, and receptor docking simulations of 2-[(acylamino)ethyl]-1,4- benzodiazepines as kappa-opioid receptor agonists endowed with antinociceptive and anti-amnesic activity. *J. Med. Chem.*, **2003**, *46*, 3853-3864.
- [69] Sagara, T.; Egashira, H.; Okamura, M.; Fujii, I.; Shimohigashi, Y.; Kanematsu, K. Ligand recognition in mu opioid receptor: Experimentally based modeling of mu opioid receptor binding sites and their testing by ligand docking. *Bioorg. Med. Chem.*, **1996**, *4*, 2151-2166.
- [70] Pogozhev, I.D.; Lomize, A.L.; Mosberg, H.I. Plasmon resonance studies of agonist/antagonist binding to the human delta-opioid receptor: new structural insights into receptor-ligand interactions. *Biophys. J.*, **1998**, *75*, 612-634.
- [71] Subramanian, G.; Paterlini, M.G.; Portoghese, P.S.; Ferguson, D.M. Molecular docking reveals a novel binding site model for fentanyl at the  $\mu$ -opioid receptor. *J. Med. Chem.*, **2000**, *43*, 381-391.
- [72] Xu, H.; Lu Y.F.; Partilla, J.S.; Zheng, Q.X.; Wang, J.B.; Brine, G.A.; Carroll, F.I.; Rice, K.C.; Chen, K.X.; Chi, Z.Q.; Rothman, R.B. Opioid peptide receptor studies, 11: involvement of Tyr<sup>148</sup>, Trp<sup>318</sup> and His<sup>319</sup> of the rat mu-opioid receptor in binding of mu-selective ligands. *Synapse*, **1999**, *32*, 23-28.
- [73] Dosen-Micovic, L.; Ivanovic, M.; Micovic, V. Steric interactions and the activity of fentanyl analogs at the  $\mu$ -opioid receptor. *Bioorg. Med. Chem.*, **2006**, *14*, 2887-2895.
- [74] Subramanian, G.; Paterlini, M.G.; Larson, D.L.; Portoghese, P.S.; Ferguson, D.M. Structure modeling of the chemokine receptor CCR5: implications for ligand binding and selectivity. *J. Med. Chem.*, **1998**, *41*, 4777-4789.
- [75] Portoghese, P.S.; Sultana, M.; Takemori, A.E. Naltrindole: a highly selective and potent non-peptide delta opioid receptor antagonist. *Eur. J. Pharm.*, **1988**, *146*, 185-186.
- [76] Jones, R.M.; Hjorth, S.A.; Schwartz, T.W.; Portoghese, P.S. Mutational evidence for a common  $\beta$  antagonist binding pocket in the wild-type  $\delta$  and mutant  $\mu$  [K303E] opioid receptors. *J. Med. Chem.*, **1998**, *41*, 4911-4914.
- [77] Resnick, R.B.; Volavka, J.; Freedman, A.M.; Thomas, M. Studies of EN- 1639A (naltrexone): a new narcotic antagonist. *Am. J. Psychiatry*, **1974**, *131*, 646-650.
- [78] Bera, I.; Laskar, A.; Ghoshal, N. Exploring the structure of opioid receptors with homology modeling based on single and multiple templates and subsequent docking: A comparative study. *J. Mol. Model.*, **2011**, *17*, 1207-1221.
- [79] Kolinski, M.; Filipek, S. Study of a structurally similar kappa opioid receptor agonist and antagonist pair by molecular dynamics simulations. *J. Mol. Model.*, **2010**, *16*, 1567-1576.
- [80] Zhang, Y.; Sham, Y.S.; Rajamani, R.; Gao, J.; Portoghese, P.S. Homology modeling and molecular dynamics simulations of the mu opioid receptor in a membrane-aqueous system. *Chem. Bio. Chem.*, **2005**, *6*, 853-859.

- [81] Li, G.; Aschenbach, L.C.; Chen, J.; Cassidy, M.P.; Stevens, D.L.; Gabra, B.H.; Selley, D.E.; Dewey, W.L.; Westkaemper, R.B.; Zhang, Y. Design, synthesis, and biological evaluation of 6- and 6-*N*-heterocyclic substituted naltrexamine derivatives as  $\mu$  opioid receptor selective antagonists. *J. Med. Chem.*, **2009**, *5*, 1416-1427.
- [82] Di Bosco, A.M.; Grieco, P.; Diurno, M.V.; Campiglia, P.; Novellino, E.; Mazzoni, O. Binding site of loperamide: automated docking of loperamide in human mu- and delta-opioid receptors. *Chem. Biol. Drug. Des.*, **2008**, *71*, 328-335.
- [83] Cheng, J.; Liu, G.; Zhang, J.; Xu, Z.; Tang, Y. Insights into subtype selectivity of opioid agonists by ligand-based and structure-based methods. *J. Mol. Mod.*, **2011**, *17*, 477-493.
- [84] In, Y.; Minoura, K.; Tomoo, K.; Sasaki, Y.; Lazarus, H.L.; Okada, Y.; Ishida, T. Structural function of C-terminal amidation of endomorphin. Conformational comparison of  $\mu$ -selective endomorphin-2 with its C-terminal free acid, studied by 1H-NMR spectroscopy, molecular calculation, and X-ray crystallography. *FEBS J.*, **2005**, *272*, 5079-5097.
- [85] Liu, X.; Kai, M.; Jin, L.; Wang, R. Molecular modeling studies to predict the possible binding modes of endomorphin analogs in  $\mu$  opioid receptor. *Bioorg. Med. Chem. Lett.*, **2009**, *19*, 5387-5391.
- [86] Martinek, T.A.; Otvös, F.; Dervarics, M.; Tóth, G.; Fülöp, F. Ligand-based prediction of active conformation by 3D-QSAR flexibility descriptors and their application in 3+3D-QSAR models. *J. Med. Chem.* **2005**, *48*, 3239-3250.
- [87] Hruby, V.J.; Agnes, R.S. Conformation-Activity Relationships of Opioid Peptides with Selective Activities at Opioid Receptors. *Biopolymers*, **1999**, *51*, 391-410.
- [88] Mosberg, H.I.; Omnaas, J.R.; Medzihradsky, F.; Smith, C.B. Cyclic, disulfide- and dithioether-containing opioid tetrapeptides: development of a ligand with high delta opioid receptor selectivity and affinity. *Life Sci.*, **1988**, *43*, 1013-1020.
- [89] Mosberg, H.I.; Fowler, C.B. Development and validation of opioid ligand-receptor interaction models: The structural basis of mu vs. delta selectivity. *J. Pept. Res.*, **2002**, *60*, 329-335.
- [90] Mosberg, H.I.; Ho, J.C.; Sobczyk-Kojiro, K. A high affinity, mu-opioid receptor-selective enkephalin analogue lacking an N-terminal tyrosine. *Bioorg. Med. Chem. Lett.*, **1998**, *8*, 2681-2684.
- [91] Fowler, C.B.; Pogozeva, I.D.; Lomize, A.L.; LeVine, H.-III; Mosberg, H.I. Complex of an active mu-opioid receptor with a cyclic peptide agonist modeled from experimental constraints. *Biochemistry*, **2004**, *43*, 15796-15810.
- [92] Przydzial, M.J.; Pogozeva, I.D.; Bosse, K.E.; Andrews, S.M.; Tharp, T.A.; Traynor, J.R.; Mosberg, H.I. Roles of residues 3 and 4 in cyclic tetrapeptide ligand recognition by the  $\kappa$  opioid receptor. *Peptide Res.*, **2005**, *65*, 333-342.
- [93] Przydzial, M.J.; Pogozeva, I.D.; Ho, J.C.; Bosse, K.E.; Sawyer, E.; Traynor, J.R.; Mosberg, H.I. Design of high affinity cyclic pentapeptide ligands for kappa-opioid receptors. *J. Pept. Res.*, **2005**, *66*, 255-262.
- [94] Purington, L.C.; Pogozeva, I.D.; Traynor, J.R.; Mosberg, H.I. Pentapeptides displaying  $\mu$  opioid receptor agonist and  $\mu$  opioid receptor partial agonist/antagonist properties. *J. Med. Chem.*, **2009**, *52*, 7724-7731.

- [95] Ballet, S.; Feytens, D.; De Wachter, R.; De Vlaeminck, M.; Marczak, E.D.; Salvadori, S.; de Graaf, C.; Rognan, D.; Negri, L.; Lattanzi, R.; Lazarus, L.H.; Tourwé, D.; Balboni, G. Conformationally constrained opioid ligands: the Dmt-Aba and Dmt-Aia versus Dmt-Tic scaffold. *Bioorg. Med. Chem. Lett.*, **2009**, *19*, 433-437.
- [96] De Wachter, R., de Graaf, C., Keresztes, A.; Vandormael, B.; Ballet, S.; Tóth, G.; Rognan, D., Tourwé, D. Synthesis, biological evaluation, and automated docking of constrained analogues of the opioid peptide H-Dmt-DAla-Phe-Gly-NH<sub>2</sub> Using the 4- or 5-methyl substituted 4-amino-1,2,4, tetrahydro-2-benzazepin-3-one scaffold. *J. Med. Chem.*, **2011**, *54*, 6538–6547
- [97] Berezowska, I.; Chung, N.N.; Lemieux, C.; Wilkes, B.C.; Schiller, P.W. Agonist vs antagonist behavior of  $\mu$  opioid peptides containing novel phenylalanine analogues in place of Tyr<sup>1</sup>. *J. Med. Chem.*, **2009**, *52*, 6941-6945.
- [98] Keresztes, A.; Borics, A.; Tóth, G. Recent advances in endomorphin engineering. *Chem. Med. Chem.*, **2010**, *5*, 1176-1196.
- [99] Janecka, A.; Staniszewska, R.; Fichna, J.; Tóth, G., Poels, J.; Gach, K.; Vanden -Broeck, J. Synthesis and Biological Activity of Endomorphin-2 Analogs Incorporating Piperidine-2-, 3- or 4-carboxylic acids instead of proline in position 2. *Chem. Biol. Drug Des.*, **2008**, *72*, 91-94.
- [100] Schiller, P.W.; Berezowska, I.; Nguyen, T.M.D.; Schmidt, R.; Lemieux, C.; Chung, N.N.; Falcone-Hindley, M.L.; Yao, W.; Liu, J.; Iwama, S.; Smith, A.B.; Hirschmann, R.F. Novel ligands lacking a positive charge for the  $\delta$ - and  $\mu$ -opioid receptors. *J. Med. Chem.*, **2000**, *43*, 551-559.
- [101] Lu, Y.; Nguyen, T.M.D.; Weltrowska, G.; Berezowska, I.; Lemieux, C.; Chung, N.N.; Schiller, P. W. [20,60-Dimethyltyrosine<sup>1</sup>]-dynorphin A(1-11)-NH<sub>2</sub> analogues lacking an N-terminal amino group: potent and selective  $\mu$ -opioid antagonists. *J. Med. Chem.*, **2001**, *44*, 3048-3053.
- [102] Schiller, P.W.; Weltrowska, G.; Nguyen, T.M.D.; Lemieux, C.; Chung, N.N.; Lu, Y. Conversion of  $\delta$ -, K-, and  $\mu$ -receptor selective opioid peptide agonists into  $\delta$ -, K- and  $\mu$ -selective antagonists. *Life Sci.*, **2003**, *73*, 691-698.
- [103] Weltrowska, G.; Lu, Y.; Lemieux, C.; Chung, N.N.; Schiller, P.W. A Novel cyclic enkephalin analogue with potent opioid antagonist activity. *Bioorg. Med. Chem. Lett.*, **2004**, *14*, 4731-4733.
- [104] Li, J. G.; Chen, C.; Yin, J.; Rice, K.; Zhang, Y.; Matecka, D.; de Riel, J.K.; Des Jarlais, R.L.; Liu-Chen, L.Y. Asp147 in the third transmembrane helix of the rat  $\mu$  opioid receptor forms ion-pairing with morphine and naltrexone. *Life Sci.* **1999**, *65*, 175–185.
- [105] Vig, B.S.; Murray, T.F.; Aldrich, J.V. A novel N-terminal cyclic dynorphin A analogue cyclo(N,5)[Trp(3),Trp(4),Glu(5)] dynorphin A-(1-11)NH(2) that lacks the basic N-terminus. *J. Med. Chem.*, **2003**, *46*, 1279-1282.
- [106] Ortega, A.; Blount, J.F.; Manchand, P.S. Salvinorin, a new transneoclerodanemdiolide from *Salvia divinorum* (Labiatae). *J. Chem. Soc. Perkins Trans.*, **1982**, *1*, 2505–2508.
- [107] Roth, B.L.; Baner, K.; Westkaemper, R.B.; Siebert, D.; Rice, K.C.; Steinberg, S.; Ernsberger, P.; Rothman, R.B. Salvinorin A: a potent naturally occurring non-nitrogenous  $\kappa$  opioid selective agonist. *Proc. Natl. Acad. Sci. U.S.A.*, **2002**, *99*, 11934-11939.

- [108] Munro, T.A.; Rizzacasa, M.A.; Roth, B.L.; Tóth, B.A.; Yan, F. Studies toward the pharmacophore of salvinorin A, a potent  $\mu$ -opioid receptor agonist. *J. Med. Chem.*, **2005**, *48*, 345-348.
- [109] Yan, F.; Mosier, P.D.; Westkaemper, R.B.; Stewart, J.; Zjawiony, J.K.; Vortherms, T.A.; Sheffler, D J. Roth, B.L. Identification of the molecular mechanisms by which the diterpenoid salvinorin A binds to  $K$ -opioid receptors. *Biochemistry*, **2005**, *44*, 8643-8651.
- [110] Beguin, C.; Richards, M.R.; Wang, Y.; Chen, T.; Liu-Chen, L.Y.; Ma, Z.; Lee, D.Y.W.; Carlezon, W.A. Jr.; Cohen, B.M. Synthesis of salvinorin A analogues as opioid receptor probes. *Bioorg. Med. Chem. Lett.*, **2005**, *15*, 2761-2765.
- [111] Harding, W.W.; Tidgewell, K.; Byrd, N.; Cobb, H.; Dersch, C.M.; Butelman, E.R.; Rothman, R.B.; Prisinzano, T.E. Neoclerodane diterpenes as a novel scaffold for mu opioid receptor ligands. *J. Med. Chem.*, **2005**, *48*, 4765-4771.
- [112] Kane, B.E.; Nieto, M.J.; McCurdy, C.R.; Ferguson, D.M. A unique binding epitope for Salvinorin A, a non-nitrogenous kappa opioid receptor agonist. *FEBS J.*, **2006**, *273*, 1966-1974.
- [113] Vortherms, T.; Mosier, P.D.; Westkaemper, R.B.; Roth, B.L. Differential helical orientations among related G protein-coupled receptors provide a novel mechanism for selectivity: studies with Salvinorin A and the k-opioid receptor. *J. Biol. Chem.*, **2007**, *282*, 3146-3156.
- [114] Yan, F.; Bikbulatov, R.V.; Mocanu, V.; Dicheva, N.; Parker, C.E.; Wetsel, W.C.; Mosier, P.D.; Westkaemper, R.B.; Allen, J.A.; Zjawiony, J.K.; Roth, B.L. Structure-based design, synthesis, and biochemical and pharmacological characterization of novel Salvinorin A analogues as active state probes of the k-opioid receptor. *Biochemistry*, **2009**, *48*, 6898-6908.
- [115] Singh, N.; Cheve, G.; Ferguson, D.M.; McCurdy, C.R. A combined ligandbased and target-based drug design approach for G-protein coupled receptors: application to Salvinorin A, a selective kappa opioid receptor agonist. *J. Comput. Aided Mol. Des.*, **2006**, *20*, 471-493.
- [116] Yan, F.; Mosier, P.D.; Westkaemper, R.B.; Roth, B.L. G-subunits differentially alter the conformation and agonist affinity of k-opioid receptors. *Biochemistry*, **2008**, *47*, 1567-1578.
- [117] McGovern, D.L.; Mosier, P.D.; Roth, B.L.; Westkaemper, R.B. CoMFA analyses of C-2 position Salvinorin A analogs at the kappa-opioid receptor provides insights into epimer selectivity. *J. Mol. Graph. Model.*, **2010**, *28*, 612-625.
- [118] Kane, B.E.; McCurdy, C.R.; Ferguson, D.M. Toward a structure-based model of salvinorin A recognition of the  $\mu$ -opioid receptor. *J. Med. Chem.*, **2008**, *51*, 1824-1830.
- [119] Eguchi, M.; Shen, R.Y.; Shea, J.P.; Lee, M.S.; Kahn, M. Design, synthesis, and evaluation of opioid analogues with non-peptidic  $\beta$ -turn scaffold: enkephalin and endomorphin mimetics. *J. Med. Chem.*, **2002**, *45*, 1395-1398.
- [120] Berezowska, I.; Lemieux, C.; Chung, N.N.; Wilkes, B.C.; Schiller, P.W. Cyclic opioid peptide agonists and antagonists obtained *via* ring-closing metathesis. *Chem. Biol. Drug Des.*, **2009**, *74*, 329-334.
- [121] Weltrowska, G.; Chung, N.N.; Lemieux, C.; Guo, J.; Lu, Y.; Wilkes, B. C.; Schiller, P.W. "Carba"-Analogues of Fentanyl are Opioid Receptor Agonists. *J. Med. Chem.*, **2010**, *53*, 2875-2881.

- [122] Cardillo, G.; Gentilucci, L.; Tolomelli, A.; Spinosa, R.; Calienni, M.; Qasem, A. R.; Spampinato, S. Synthesis and evaluation of the affinity toward  $\mu$ - opioid receptors of atypical, lipophilic ligands based on the sequence  $\alpha$ -[Tyr-Pro-Trp-Phe-Gly-]. *J. Med. Chem.*, **2004**, *47*, 5198-5203.
- [123] Bedini, A.; Baiula, M.; Gentilucci, L.; Tolomelli, A.; De Marco, R.; Spampinato, S. *Peptides*, **2010**, *31*, 2135-2140.
- [124] Gentilucci, L.; Squassabia, F.; De Marco, R.; Artali, R.; Cardillo, G.; Tolomelli, A.; Spampinato, S.; Bedini, A. Investigation of the interaction between the atypical agonist c[YpwFG] and MOR. *FEBS J.*, **2008**, *275*, 2315–2337.
- [125] Kessler, H. Conformation and biological activity of cyclic peptides. *Angew. Chem. Int. Ed. Engl.*, **1982**, *21*, 512– 523.
- [126] Gentilucci, L.; Tolomelli, A.; De Marco, R.; Spampinato, S.; Bedini, A.; Artali, R. The inverse type II  $\beta$ -turn on D-Trp-Phe, a pharmacophoric motif for MOR agonists. *Chem. Med. Chem.*, **2011**, *6*, 1640-1653.
- [127] De Marco, R.; Gentilucci, L.; Tolomelli, A.; Feddersen, S.; Spampinato, S.; Bedini, A.; Artali, R. Design and synthesis of opioid peptide analogues and mimetics. *Pharmacol. Rep.*, **2011**, *63*, 226.
- [128] Dolle, R.E.; Michaut, M.; Martinez-Teipel, B.; Seida, P.R.; Ajello, C.W.; Muller, A.L.; De Haven, R.N.; Carroll, P.J. Nascent structure–activity relationship study of a diastereomeric series of kappa opioid receptor antagonists derived from CJ-15,208. *Bioorg. Med. Chem. Lett.*, **2009**, *19*, 3647-3650.
- [129] Saito, T.; Hirai, H.; Kim, Y. J.; Kojima, Y.; Matsunaga, Y.; Nishida, H.; Sakakibara, T.; Suga, O.; Sujaku, T.; Kojima, N. The tryptophan isomers of the cyclic tetrapeptide CJ-15,208, reported to be a kappa opioid receptor (KOR) antagonist. *J. Antibiot.*, **2002**, *55*, 847-854.
- [130] Ross, N.C.; Reilley, K.J.; Murray, T.F.; Aldrich, J.V.; McLaughlin, J. P. *Br. J. Pharmacol.*, DOI: 10.1111/j.1476-5381.2011.01544.x
- [131] Aldrich, J.V.; Kulkarni, S.S.; Senadheera, S.N.; Ross, N.C.; Reilley, K.J.; Eans, S.O.; Ganno, M.L.; Murray, T.F.; McLaughlin, J.P. Unexpected opioid activity profiles of analogues of the novel peptide kappa opioid receptor ligand CJ-15,208. *Chem. Med. Chem.*, **2011**, *6*, 1739-1745.

## Chapter 6

# The Inverse Type II $\beta$ -Turn on D-Trp-Phe, a Pharmacophoric Motif for MOR Agonist.

---

### 6. Introduction

Herein we propose the D-Trp-Phe sequence within an inverse type II  $\beta$ -turn as a new kind of pharmacophoric motif for  $\mu$ -opioid receptor (MOR) cyclopeptide agonists. Initially, we observed that c[Tyr-D-Pro-D-Trp-Phe-Gly] (**4**), an analogue of endomorphin-1 (H-Tyr-Pro-Trp-Phe-NH<sub>2</sub>) lacking the crucial protonatable amino group of Tyr<sup>1</sup>, is a MOR agonist with 10<sup>-8</sup>M affinity.

Molecular docking analysis suggested that the relevant interactions with the receptor involve D-Trp-Phe. The bioactive conformation of this region was investigated by selected derivatives of **4** designed to adopt an inverse type II  $\beta$ -turn. These efforts led to c[Tyr-Gly-D-Trp-Phe-Gly] (**14**) and to the cyclotetrapeptide c[D-Asp-1-amide- $\beta$ -Ala-D-Trp-Phe] (**15**), showing improved nanomolar affinity. Both **14** and **15** selectively bind MOR, as they have negligible affinity for the  $\kappa$ - and  $\delta$ -opioid receptors. The compounds **14** and **15** behave as partial MOR agonists in functional assays. Conformational and docking analyses confirm the role of the inverse  $\beta$ -turn in binding. These results indicate that the D-Trp-Phe inverse  $\beta$ -turn structure can be used for designing non-endomorphin-like peptidomimetic opioid agonists in general, characterized by an atypical mechanism of interaction between ligand and receptor introduction

The tetrapeptides Endomorphin-1 (EM1, H-Tyr-Pro-Trp-Phe-NH<sub>2</sub>) and Endomorphin-2 (H-Tyr-Pro-Phe-Phe-NH<sub>2</sub>)<sup>[1]</sup>, have been isolated from mammalian brain and were found to activate  $\mu$ -opioid receptors (MOR) with high affinity and selectivity. Morphine and EMs act as agonists at the same receptor, but the latter are thought to inhibit pain without some of the undesired side effects of plant opiates<sup>[2]</sup>. This observation prompted extensive studies of EM mimetics<sup>[3]</sup>, with the aim of obtaining analgesic compounds<sup>[4]</sup> with higher resistance against enzymatic degradation and better penetration of the blood–brain barrier (BBB).

A survey of the many reported peptidomimetics reveals that the amino group of Tyr<sup>1</sup> is generally maintained unaltered.

Indeed, the ionic bond between the protonated amine and a conserved Asp of the receptor is considered the driving force of the ligand–receptor interaction for all kinds of endogenous opioid peptides<sup>[3, 5]</sup> as well as for exogenous agonists<sup>[6]</sup>, such as morphine (**1**) and fentanyl<sup>[7]</sup>. In most cases, the removal or derivatization of this group resulted in inactive derivatives or antagonists<sup>[8]</sup>.

The very few compounds made without this pharmacophore<sup>[9]</sup> which retain agonist behavior are shown, consecutively numbered by the year of publication: the MOR-selective bicyclic enkephalin mimetic **2**<sup>[10]</sup>, the  $\kappa$ -opioid receptor (KOR)-selective neoclerodane diterpene salvinorin A (**3**)<sup>[11]</sup>, the MOR-active cyclic analogue of EM1 c[Tyr-D-Pro-D-Trp-Phe-Gly] (**4**)<sup>[12]</sup>, and the “carba” analogues (both *cis* and the *trans* isomers) of a fentanyl equipped with a guanidino group (compound **5**), in which the piperidine ring nitrogen atom is replaced by carbon<sup>[13]</sup>. Compound **5** likely retains the same binding mode as the “normal” fentanyl; however, it was observed that the ionic bridge between the guanidine moiety of the ligands and an Asp in the

second extracellular loop (EL) is significant for receptor binding. In contrast, compounds **3** and **4**, which are deprived of any ionic interactions, have receptor binding modes different from that of the classical agonists<sup>[14]</sup>. The cyclopentapeptide **4** was the most active member of a mini-library of stereomeric, 3D distinct analogues of EM1 of general sequence c[L/D-Tyr-L/D-Pro-L/D-Trp-L/D-Phe-Gly], designed as lipophilic compounds with improved ability to cross the BBB and higher in vivo stability. Among them, **4** proved to be an agonist with an affinity of  $10^{-8}$ M for MOR. Further studies revealed in vivo analgesic efficacy upon peripheral administration which correlated to its lipophilicity and metabolic stability<sup>[15]</sup>, whereas the parent opioid peptide EM1 was completely inactive<sup>[2, 16]</sup>.

As **4** represents a lipophilic, atypical opioid agonist deprived of the primary pharmacophore, we performed investigations to understand how the compound might interact and activate the MOR<sup>[14c]</sup>. As revealed by NMR spectroscopy and molecular dynamics (MD), **4** in solution adopts two different conformations in equilibrium, one characterized by a type II  $\beta$ -turn on Tyr-D-Pro and an inverse  $\gamma$ -turn on Phe (Figure 1 a), the second by an inverse type I  $\beta$ -turn on D-Pro<sup>2</sup>-D-Trp<sup>3</sup> and a  $\gamma$ -turn on Gly (Figure 1 b).

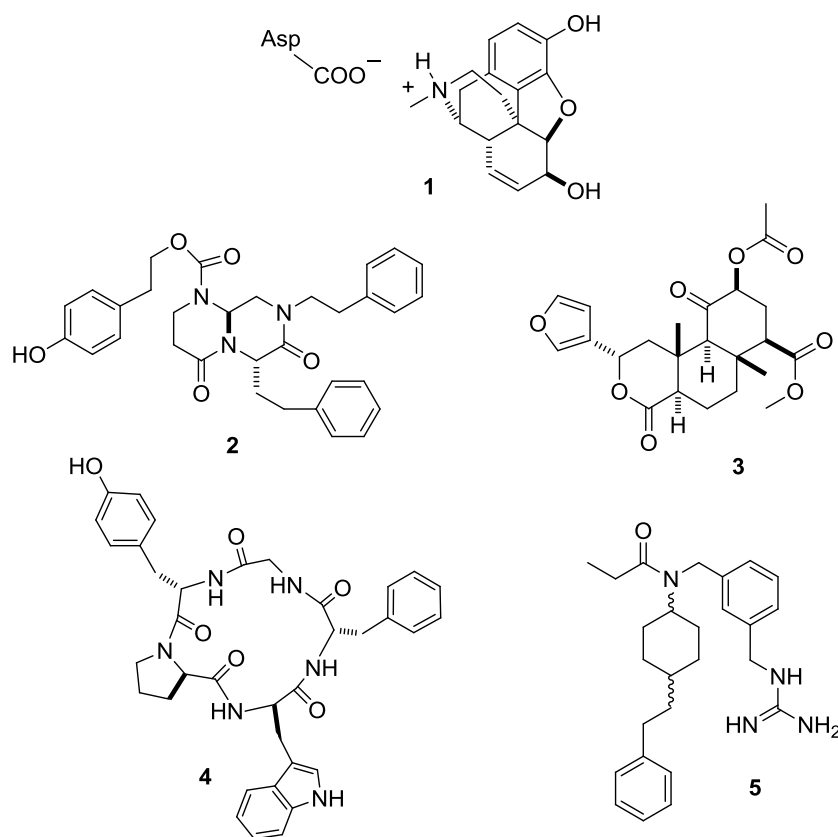


**Fig. (1).** Structures of the MOR agonists **1**, **3-5**, and of the KOR agonist **2**.

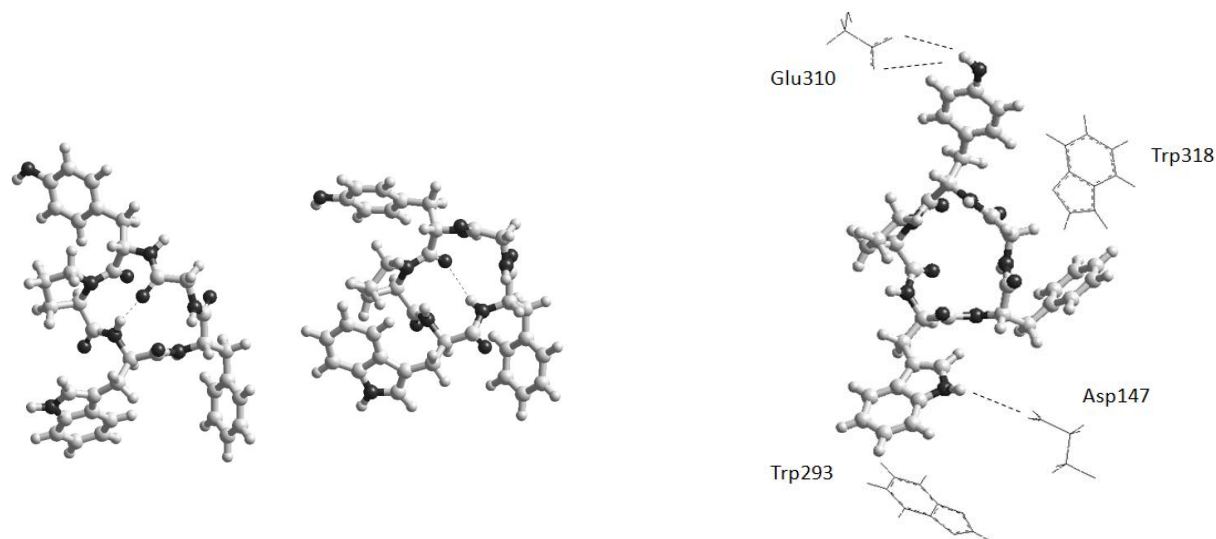


**Fig. (2).** Preferred conformations of **4** in solution (left), and schematic sketch of the receptor-bound conformation (right) with some relevant contacts (stick rendering). *Errore. Il segnalibro non è definito.*

However, a molecular docking investigation suggested that the ligand might have quite a different geometry within the receptor pocket. This analysis revealed a fundamental hydrogen bond between the indolic NH of D-Trp and the carboxylate of Asp<sup>147</sup> (TMH-III), which partially compensates for the absence of the ionic interaction, and an overall conformation roughly compatible with an inverse  $\beta$ -turn centered on D-Trp- Phe (Figure 1c).

Herein we show that an inverse type II  $\beta$ -turn centered on D-Trp-Phe is fundamental for activity, and represents a novel pharmacophoric motif for this atypical class of cyclopeptide MOR agonists. To this purpose, we used the putative bioactive conformation of **4** shown in Figure 1 as a model for designing new cyclopeptides with higher propensity to adopt the inverse  $\beta$ -turn on D-Trp-Phe, and with increased MOR affinity, therefore demonstrating the utility of the model. To further corroborate the model, we designed a cyclopeptide not based on the sequence of EM1, whose activity as a selective MOR agonist is clearly correlated to the D-Trp-Phe inverse  $\beta$ -turn bioactive conformation.

## 6.1. Results

### 6.1.1. Cyclopeptide design

Despite the inadequate 3D structure in solution, ligand **4** can still attain a significant interaction with the receptor by taking advantage of its flexibility. In addition, the receptor itself can adapt its shape to host the ligand (induced fit)<sup>[17]</sup>. In principle, it is possible to improve the efficacy of such a flexible molecule by modifying its geometry<sup>[5a]</sup>, taking into consideration that “the more the structure of a free ligand in solution resembles the structure in the complex, the stronger the binding”<sup>[18]</sup>. Despite the many limitations, this assumption sometimes works very well as an indicative guide for structure optimization.

Consequently, we supposed that analogues of **4** having the inverse type II  $\beta$ -turn on D-Trp-Phe might show improved receptor affinity, therefore confirming that this secondary structure represents the bioactive conformation.

The docking procedure indicated that neither D-Pro nor Gly in **4** really interact with the receptor, but their role is fundamental in stabilizing the geometries observed in solution. In particular, it is well documented that D-Pro induces alternative backbone conformations with respect to the other amino acids<sup>[5a, 18, 19]</sup>.

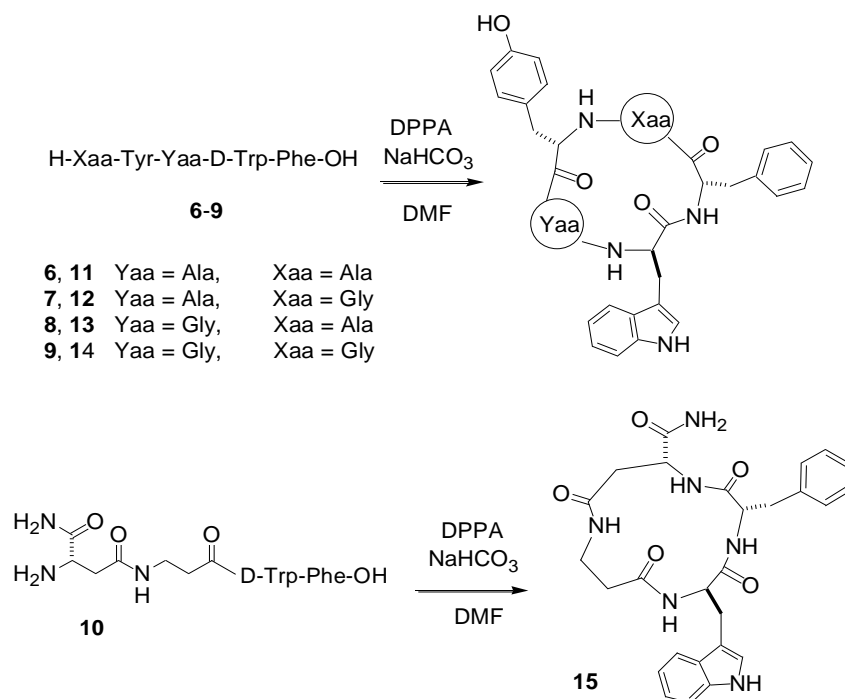
The desired conformation can be predetermined on the basis of the well-known structures of cyclo-Ala<sup>5</sup> models, or other cyclopentapeptides already reported in the literature containing one D-residue, widely used as  $\beta/\gamma$ -turn mimetics. In particular, it is well known that an L,L,D,L,L chirality induces an inverse type II  $\beta$ -turn with the D-amino acid in the position  $i+1$ , with a few exceptions (see Conformational analysis and Discussion below)<sup>[18–20]</sup>.

Based on these premises, we retained the amino acids of the pharmacophores, D-Trp, Phe, and Tyr, and we completed the sequences with L-Ala and/or Gly, giving cyclopeptides **11–14** of general sequence c[Tyr-Yaa-D-Trp-Phe-Xaa], where Yaa, Xaa=Ala or Gly (Gly can act either as an L- or D-configured residue). We also designed and synthesized the non-EM1-like 14-membered cyclotetrapeptide c[D-Asp-1-amide- $\beta$ -Ala-D-Trp-Phe] (**15**), deprived of the Tyr, and characterized by a rigid backbone.

It should be mentioned that replacement of D-Pro with its enantiomer to give c[Tyr-Pro-D-Trp-Phe-Gly] (**16**)<sup>[12]</sup> does not induce the desired conformation. In fact, **16** had ~1000-fold lower affinity than **4**. L-Pro likely precludes the inverse  $\beta$ -turn on D-Trp-Phe, in particular, cyclopeptides containing an L-Xaa-L-Pro sequence strongly increase the probability of the peptide bond preceding Pro having a cis conformation<sup>[19,21]</sup>.

### **6.1.2. Cyclopeptide synthesis**

The new cyclic pentapeptides **11–14** were obtained by cyclization of the linear precursors H-Xaa-Tyr-Yaad-Trp-Phe-OH, Yaa, Xaa=Ala or Gly (**6–9**), whereas **15** was prepared from the linear precursor H-D-Asp-1-amide- $\beta$ -Ala-D-Trp-Phe-OH (**10**) (Scheme 1). The peptides **6–10** were obtained in turn by SPPS by coupling Fmoc-protected amino acids on a Wang resin under standard conditions<sup>[22]</sup> using an automated peptide synthesizer. Fmoc deprotection was performed with piperidine in DMF, and coupling of the amino acids was done with HBTU/DIPEA as coupling agents. The cleavage from the resin was performed with trifluoroacetic acid (TFA) in the presence of scavengers. The sequence of **10** contains two  $\beta$ -amino acids,  $\beta$ -Ala, and D-aspartic acid-1-amide (Scheme 1), the latter introduced in its Boc-protected form; Boc was removed during the cleavage of the peptide from resin.



Scheme 1. Synthesis of cyclopeptides **11-15** from the linear precursors **6-10**.

The crude peptides **6-10** were subjected to in-solution cyclization (high dilution) with diphenylphosphoryl azide (DPPA) and NaHCO<sub>3</sub> without prior purification (Scheme 1). The cyclic peptides **11-15** were obtained pure (95-97%) after semipreparative RP-HPLC. Cyclization yields, purities, and ESI-MS characterizations are reported in Table 1.

Table 1. Synthesis, MS characterization, and affinities for MOR binding sites of DAMGO, <b>4</b> , and <b>11-15</b> .						
Compd	Yield [%] <sup>[a]</sup>	Purity [%] <sup>[b]</sup>	$M_r$ [ $M + 1$ ] <sup>[c]</sup>	$K_i$ [nM] <sup>[d]</sup>	IC <sub>50</sub> [nM] <sup>[d]</sup>	$n_H$
DAMGO	–	–	–	1.5 ± 0.1	9.9 ± 0.6	0.98 ± 0.10
<b>4</b> <sup>[12]</sup>	62	96	651.2/651.2	34 ± 7	44 ± 6	0.44 ± 0.08 *
<b>11</b>	70	96	639.2/639.3	> 10 <sup>5</sup>	> 10 <sup>5</sup>	–
<b>12</b>	55	95	625.3/625.3	> 10 <sup>5</sup>	> 10 <sup>5</sup>	–
<b>13</b>	60	95	625.3/625.3	> 10 <sup>5</sup>	> 10 <sup>5</sup>	–
<b>14</b>	65	97	611.3/611.3	3.6 ± 0.3	4.9 ± 0.1	0.85 ± 0.15
<b>15</b>	65	97	519.2/519.3	5.9 ± 0.1	7.9 ± 0.2	0.25 ± 0.13 *

[a] Yield of the cyclization step after purification. [b] Determined by analytical RP-HPLC (see Experimental Section). [c] Experimental/calculated. [d] Values represent the mean ± SE of three experiments; data were analyzed by one-way ANOVA followed by Tukey's test; \* $p < 0.1$  versus DAMGO and **14**.

### 6.1.3. Binding affinity to the cloned human opioid receptors

The affinities of compounds **11-15** toward the human MOR were determined by displacement binding assays; the  $K_i$  and IC<sub>50</sub> values are reported in Table 1. The potent MOR-selective agonist DAMGO (H-Tyr-D-Ala-Gly-N-MePhe-Glyol) and compound **4** were chosen as reference compounds. Compounds were added to HEK-293 cells stably expressing human MOR, using [<sup>3</sup>H]DAMGO as a  $\mu$ -specific radioligand and were assayed in a wide range of concentrations, from 10<sup>-12</sup> to 10<sup>-4</sup>M. The potency of DAMGO was in the

nanomolar range as previously reported<sup>[12, 23]</sup>. Compounds **11**, **12**, and **13** displaced [<sup>3</sup>H]DAMGO very poorly within the range of concentrations used, so preventing the calculation of  $K_i$  and  $IC_{50}$ , whereas **14** and **15** displayed an easily measurable concentration-dependent displacement of [<sup>3</sup>H]DAMGO, with affinity values in the region of  $10^{-9}$ M. DAMGO and **14** had Hill coefficients ( $n_H$ ) not significantly different from unity (Table 1). In contrast, **4** and **15** showed  $n_H$  values significantly lower than unity. This phenomenon suggests that they displaced [<sup>3</sup>H]DAMGO binding with multiple affinities and can be interpreted by a negative cooperativity, that is, their binding at one side may lower the affinity at another site.

Table 2 reports the affinities ( $K_i$  and  $IC_{50}$ ) of compounds **4**, **11–15**, and of the reference compounds DPDPE and U50,488, toward the cloned human  $\delta$ -opioid receptor (DOR) or KOR expressed on HEK-293 cells. These values were determined by displacement binding assays using [<sup>3</sup>H]diprenorphine and [<sup>3</sup>H]U69,593 as DOR and KOR specific radioligands, respectively.

As expected, the affinity of DPDPE<sup>[24]</sup> and U50,488<sup>[25]</sup> were in the nanomolar range.

Compound **11** displayed a concentration-dependent displacement of [<sup>3</sup>H]diprenorphine from cloned human DOR, with a moderate  $10^{-7}$ M affinity, whereas the other compounds were ineffective; their  $K_i$  and  $IC_{50}$  values were higher than  $10^{-4}$ M (Table 2). On the other hand, all the compounds were ineffective in displacing [<sup>3</sup>H]U69,593 from cloned human KOR, apart from compound **13** that had an affinity of  $10^{-8}$ M.

In summary, the cyclopeptide **14**, c[Tyr-Gly-D-Trp-Phe-Gly], showed the highest MOR affinity, having  $K_i$  and  $EC_{50}$  values in the nanomolar range, approximately tenfold improved over the parent compound **4**<sup>[12]</sup>, c[Tyr-D-Pro-D-Trp-Phe-Gly], and almost as good as the reference compound DAMGO. Cyclopeptide **15**, c[D-Asp-1-amide- $\beta$ -Ala-D-Trp-Phe], was slightly less effective, whereas **11–13** were practically inactive.

The ligands **4**, c[Tyr-D-Pro-D-Trp-Phe-Gly], **14**, c[Tyr-Gly-D-Trp-Phe-Gly], and **15**, c[D-Asp-1-amide- $\beta$ -Ala-D-Trp-Phe], selectively bind to the MOR, as they have negligible affinity for the KOR and DOR. Interestingly, **11**, c[Tyr-Ala-D-Trp-Phe-Ala], showed a modest affinity for DOR, but not for MOR and KOR, whereas compound **13**, c[Tyr-Gly-D-Trp-Phe-Ala], which was ineffective as a MOR and DOR ligand, displayed a significant affinity for KOR (Table 2).

Table 2. Affinities for DOR binding sites of DPDPE, <b>4</b> and <b>11–15</b> and for KOR binding sites of U50,488, <b>4</b> , and <b>11–15</b> . <sup>[a]</sup>					
Compd	DOR		KOR		$n_H$
	$K_i$ [nM]	$IC_{50}$ [nM]	$K_i$ [nM]	$IC_{50}$ [nM]	
DPDPE	3.30 ± 0.05	3.10 ± 0.02	–	–	–
U50,488	–	–	2.90 ± 0.04	2.70 ± 0.03	–
<b>4</b>	> 10 <sup>5</sup>	> 10 <sup>5</sup>	> 10 <sup>5</sup>	> 10 <sup>5</sup>	–
<b>11</b>	170 ± 30	180 ± 20	> 10 <sup>5</sup>	> 10 <sup>5</sup>	1.1 ± 0.12
<b>12</b>	> 10 <sup>5</sup>	> 10 <sup>5</sup>	> 10 <sup>5</sup>	> 10 <sup>5</sup>	–
<b>13</b>	> 10 <sup>5</sup>	> 10 <sup>5</sup>	29 ± 4	33 ± 3	0.71 ± 0.20
<b>14</b>	> 10 <sup>5</sup>	> 10 <sup>5</sup>	> 10 <sup>5</sup>	> 10 <sup>5</sup>	–
<b>15</b>	> 10 <sup>5</sup>	> 10 <sup>5</sup>	> 10 <sup>5</sup>	> 10 <sup>5</sup>	–

[a] Values represent the mean ± SE of three experiments.

#### 6.1.4. Effects on forskolin-stimulated cAMP production

To assess if **14** and **15** behave as MOR agonists or antagonists, we evaluated their effects on forskolin-stimulated cAMP formation in whole HEK-293 cells stably expressing MOR. The IC<sub>50</sub> and maximal effect (Emax) values are reported in Table 3. The MOR agonist DAMGO<sup>[26]</sup> produced a concentration-dependent reduction of cAMP. Compounds **14** and **15** display a similar potency to DAMGO as they have similar IC<sub>50</sub> values, although they show a reduced Emax in comparison with DAMGO, consistent with an activity as partial agonists (Table 3). The IC<sub>50</sub> values of **14** and **15** as inhibitors of forskolin-stimulated cAMP production were similar to those elicited by **4**<sup>[12]</sup>. In control HEK-293 cells DAMGO, EM1, **14**, and **15** did not inhibit cAMP production induced by forskolin (data not shown).

The partial agonist activity of the cyclopeptides **14**, an analogue of EM1, and **15**, relative to the full agonism of DAMGO is not surprising. Also the efficacy of EMs in many bioassays is lower than that of DAMGO (but higher than that of morphine), albeit that their antinociceptive efficacy is higher<sup>[1-3]</sup>. In general, EM1 and EM2 behave as partial agonists of the MORs<sup>[27]</sup>, but in a few cases full agonist activities have been reported<sup>[1, 28]</sup>.

#### 6.1.5. Conformational analysis

The in-solution conformations of **11**, **13**, **14**, and **15** were investigated by NMR spectroscopy and MD simulations. The analysis of **12** was omitted because of its inactivity as an opioid ligand. As the compounds were poorly soluble in water, the NMR analyses were conducted using standard techniques at 400 MHz in the biomimetic medium 8:2 [D<sub>6</sub>]DMSO/H<sub>2</sub>O<sup>[29]</sup>.

Apart from the solubility issue, a very recent comparative structural analysis of MOR ligands with similar affinity and selectivity confirmed that DMSO may be a better approximation for the mechanical and electrostatic environment of binding to the MOR than H<sub>2</sub>O is<sup>[30]</sup>.

The <sup>1</sup>H NMR analysis of the compounds **13**, **14**, and **15** revealed a single set of sharp resonances, indicating conformational homogeneity or a fast equilibrium between conformers.

The <sup>1</sup>H NMR of **11** appeared as a single set of resonances, but with a noteworthy broadening of the signals of TyrOH, TyrNH, XAlaNH (XAla: Xaa=Ala), and a less pronounced broadening of YAlaNH (YAla: Yaa=Ala), indicative of a slow switch between different NH orientations in the XAla-Tyr region. COSY and HMBC experiments allowed unambiguous assignment of all the resonances.

Variable temperature (VT)-<sup>1</sup>H NMR experiments were used to deduce the presence of hydrogen bonds (Table 4). For **11** and **13**, the comparatively lower  $\Delta\delta/\Delta T$  values of the amide protons of Yaa and Xaa with respect to D-Trp, Phe, and Tyr, are suggestive of structures in which one or both of the AlaNH in **11**, c[Tyr-Ala-D-Trp-Phe-Ala], and GlyNH and/or AlaNH in **13**, c[Tyr-Gly-D-Trp-Phe-Ala], are involved in hydrogen bonds ( $\Delta\delta/\Delta T < \text{or close to } 2 \text{ ppbK}^{-1}$ )<sup>[31]</sup>. For **14**, c[Tyr-Gly-D-Trp-Phe-Gly], the low  $\Delta\delta/\Delta T$  values suggest that D-TrpNH and GlyNH very likely contribute to hydrogen bonds. Finally, for compound **15**, c[D-Asp-1-amide- $\beta$ -Ala-D-Trp-Phe], the d-AspNH (=Xaa in Table 4) is certainly involved in a very strong hydrogen bond ( $\Delta\delta/\Delta T = -0.5 \text{ ppbK}^{-1}$ ).

**Table 3.** Inhibitory effects of DAMGO, **4**, **14**, and **15** on forskolin-induced cAMP formation in HEK-293 cells stably expressing MOR.<sup>[a]</sup>

Compd	IC <sub>50</sub> [nM] <sup>[b]</sup>	E <sub>max</sub> [% vehicle] <sup>[c]</sup>
DAMGO	19 ± 1	95 ± 4
<b>4</b>	29 ± 9	73 ± 4 <sup>**[d]</sup>
<b>14</b>	31 ± 3	65 ± 8 <sup>**</sup>
<b>15</b>	37 ± 5	58 ± 5 <sup>**</sup>

[a] Values represent the mean ± SE of 5–6 independent experiments performed in triplicate. [b] Half-maximal inhibitory concentration. [c] Maximal obtainable effect. [d] Data were analyzed by one-way ANOVA followed by Tukey's test; <sup>\*\*</sup>*p* < 0.01 versus DAMGO.

**Table 4.**  $\Delta\delta/\Delta T$  values [ppb/K] of amide protons for **11**, **13**, **14**, and **15**.<sup>[a]</sup>

Compd	Yaa	D-TrpNH	PheNH	Xaa	Tyr
<b>11</b>	−1.5	−4.0	−6.5	−2.2	−5.0
<b>13</b>	−1.3	−5.0	−9.0	−1.6	−5.7
<b>14</b>	−6.4	−2.5	−7.7	−1.5	−7.5
<b>15</b>	−4.8	−5.2	−6.6	−0.5	−

[a] Determined by VT-<sup>1</sup>H NMR analysis in [D<sub>6</sub>]DMSO/H<sub>2</sub>O (8:2) at 400 MHz over the range 298–348 K.

### 6.1.6. Molecular backbone conformations were investigated by 2D

ROESY analysis, and the intensities of the resulting cross-peak were ranked to infer plausible inter-proton distances (see Supporting Information tables S1–S4). Structures consistent with the spectroscopic analyses were obtained by restrained MD simulations<sup>[32]</sup>, using the distances derived from ROESY as constraints, and minimized with AMBER<sup>[33]</sup> force field. The w bonds were set at 1808, as the absence of Hai-Hai+1 cross-peaks excluded cis peptide bonds. Simulations were conducted in a box of explicit, equilibrated TIP3P water molecules<sup>[34]</sup> using a set of 50 random structures generated by means of unrestrained high-temperature MD. The structures were subjected to high-temperature restrained MD with a scaled force field, followed by a simulation with full restraints. Finally, the system was gradually cooled, and the structures were minimized. The results were clustered by the RMSD analysis of the backbone atoms.

For **11**, c[Tyr-Ala-D-Trp-Phe-Ala], computations essentially gave two clusters altogether comprising more than 95% of the structures. For each cluster, the representative geometries **11a** and **11b** with the lowest internal energy were selected and analyzed, Figure 2 (see figures S2 and S3, Supporting Information).

The two conformers are characterized by nearly the same energy, and differ almost exclusively in the opposite orientation of the peptide bond of XAla-Tyr. The occurrence of these two different structures for **11** reflects the lack of clear ROESY cross-peaks for TyrNH, XAlaNH, and YAlaNH, whose resonances appear as broad signals. These two conformations closely match that of other cyclopentapeptides sharing the same

L,L,D,L,L stereochemistry array<sup>[18–20]</sup>, such as c[Asp-Trp-D-Met-Asp-Phe] and related peptides<sup>[20b]</sup>. Both **11a** and **11b** show an inverse type II  $\beta$ -turn centered on D-Trp-Phe, with an explicit hydrogen bond between YAlaCO and XAlaNH. In addition, **11a** also shows a  $\gamma$ -turn on Tyr, with a hydrogen bond between XAlaCO and YAlaNH.

The structures **11a** and **11b** were analyzed by unrestrained MD for 10 ns in a box of explicit, equilibrated water molecules.

The analysis of the trajectories did not show the conversion of one conformation into the other. Probably, the flip of the peptide bond of XGly-Tyr is slow with respect to the time scale of the simulation.

The analysis of **13**, c[Tyr-Gly-D-Trp-Phe-Ala], was conducted as for **11**. ROESY-restrained MD and cluster analysis gave the two structures **13a** and **13b** (>95% of the structures), the latter being slightly more stable, whose representative low energy conformations are shown in Figure 3a and 3b, respectively.

The two structures differ in the opposite orientations of the Ala-Tyr peptide bond, and show some violations of the distance constraints in this region. In particular, the strong crosspeaks of TyrNH-AlaHa, and TyrNH-TyrHa, and the medium cross-peak of TyrNH-AlaNH, account for the conformation of **13b** (Figure 3 b). Both these structures do not show any of the hydrogen bonds predicted by VT-NMR analysis, probably because of a fast equilibrium between different geometries whose average in the NMR time scale gave the ROESY-derived structures. Nevertheless, the VT-NMR analysis of **13** is indicative of some preference for conformations stabilized by hydrogen bonds involving GlyNH and/or AlaNH.

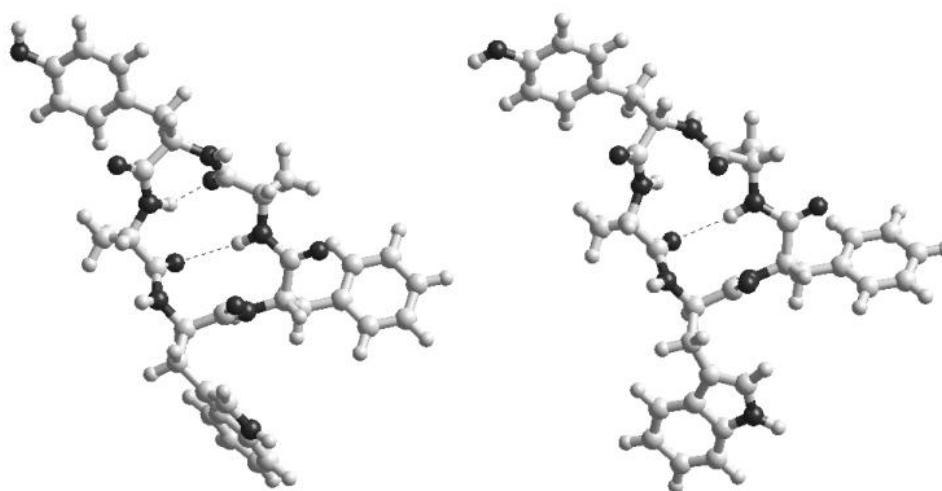


**Fig. (3).** Representative low-energy structures of **11a** (left) and **11b** (right) consistent with ROESY analysis, calculated by restrained MD in a 30x30x30 Å box of standard TIP3P water molecules

To investigate the dynamic behavior, the structures **13a** and **13b** were analyzed by unrestrained MD for 10 ns in a box of explicit, equilibrated water molecules. During the simulation, the conversion of **13a** into **13b** was not observed. Besides the different random conformations, the analysis of the trajectories of **13a** revealed the occurrence of well-defined secondary structures (see figures S4 and S5, Supporting Information). The representative conformation **13c** (Figure 4) is characterized by an inverse type II  $\beta$ -turn

having D-Trp-Phe in the positions  $i+1$ ,  $i+2$ , stabilized by a hydrogen bond between GlyCO and AlaNH, as predicted by the VT-NMR temperature coefficient (Table 4). In a similar way, structures congruent to the same kind of  $\beta$ -turn were also observed during the unrestrained MD simulation of **13b**. Cyclopentapeptides usually show fast rotations of the peptide bonds preceding Gly<sup>[18, 19]</sup>. As expected, the rotation of the peptide bond between Tyr-Gly in **13b** led to the formation of a  $\gamma$ -turn centered on Tyr, with a hydrogen bond between AlaCO and GlyNH in agreement with VT-NMR, as represented by the structure **13d** (Figure 4), the backbone of which is practically coincident with that of **11 a**.

For **14**, c[Tyr-Gly-D-Trp-Phe-Gly], containing two glycines, a greater conformational freedom was expected. ROESY-restrained MD and cluster analysis performed as described above gave a preferred geometry (>90% of the structures), whose representative low-energy conformation is shown in Figure 4a. The VT-NMR analysis of **14** accounts for conformations stabilized by hydrogen bonds involving XGlyNH and/or D-TrpNH. However, the structure determined by ROESY-restrained analysis does not show any hydrogen bond, confirming that the compound can adopt different geometries in equilibrium.

The structure **14** was analyzed by unrestrained MD for 10 ns in a box of H<sub>2</sub>O molecules. Among the different random conformations, the analysis of the trajectories revealed the occurrence of alternative secondary structures with hydrogen bonds predicted by the VT-NMR (see figures S6 and S7, Supporting Information).

The conformation of **14a** (Figure 4b) is characterized by a type II  $\beta$ -turn centered on Tyr-YGly (YGly: Yaa=Gly), stabilized by a hydrogen bond involving XGlyCO and D-TrpNH, and by an inverted  $\gamma$ -turn centered on Phe. During the simulation, the rotation of the peptide bonds between Phe-XGly and Tyr-YGly was observed, the latter leading to an alternative type I  $\beta$ -turn on Tyr-YGly. The conformation of **14b** (Figure 4 c) is compatible with an inverse type II  $\beta$ -turn having D-Trp-Phe in the positions  $i+1$ ,  $i+2$ , stabilized by a hydrogen bond between YGlyCO and XGlyNH.

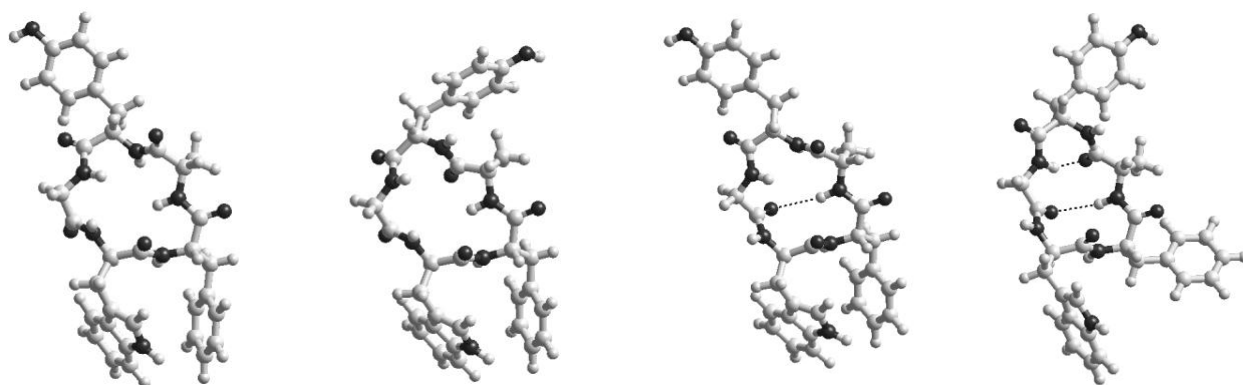


**Fig. (4).** Representative low-energy structures of **13a** (top, left), **13b** (top, right) consistent with ROESY analysis, calculated by restrained MD, and of **13c** (bottom, left), **13d** (bottom, right), obtained by unrestrained MD, all in a 30x30x30 Å box of standard TIP3P water molecules.

For the most part, the overall conformation of a cyclopentapeptide depends on the stereochemistry array. Therefore, the secondary structures of **13** and **14** can be rationalized by comparison with the structures of

cyclo-Ala<sup>5</sup> models, or other cyclopentapeptides sharing the same chirality described in the literature<sup>[18–20]</sup>. Gly can act as either an L- or a D-residue, therefore different chirality arrays can be attributed to the compounds **13**, c[Tyr-Gly-D-Trp-Phe-Ala], and **14**, c[Tyr-YGly-D-Trp-Phe-XGly].

Apparently, the structures **13c**, **13d**, and **14b** adopt the same secondary structure as L,L,D,L,L cyclopentapeptides, namely an inverse type II  $\beta$ -turn centered on D-aa 3 L-aa 4 (see the discussion concerning **11** in the previous paragraph). In contrast, the structure **14a** behaves as an L,D,D,L,D-cyclopentapeptide, as its backbone reproduces the mirror image of that of D,L,L,D,L-cyclo-Ala<sup>5</sup>, as well as the mirror image of the backbone of the  $\alpha_v\beta_3$ -integrin inhibitor c[D-Phe-Val-Arg-Gly-Asp] (generally reported as c[RGDFV]<sup>[20a]</sup>), having D,L,L,D,L chirality, the opposite of L,D,D,L,D both featuring an inverse type II  $\beta$ -turn on D-aa1L-aa2, and a  $\gamma$ -turn on L-aa 4. On the other hand, L,D,D,L,L-cyclo-Ala<sup>5</sup> still maintains the type II  $\beta$ -turn on L-aa 1-D-aa<sup>[19, 20]</sup>. Finally, the conformational analysis of **15**, c[D-Asp-1-amide- $\beta$ -Ala-D-Trp-Phe], performed as before, gave one major cluster comprising more than 95% of the structures, whose representative lowest-energy structure is shown in Figure 5 (see figure S8, Supporting Information).

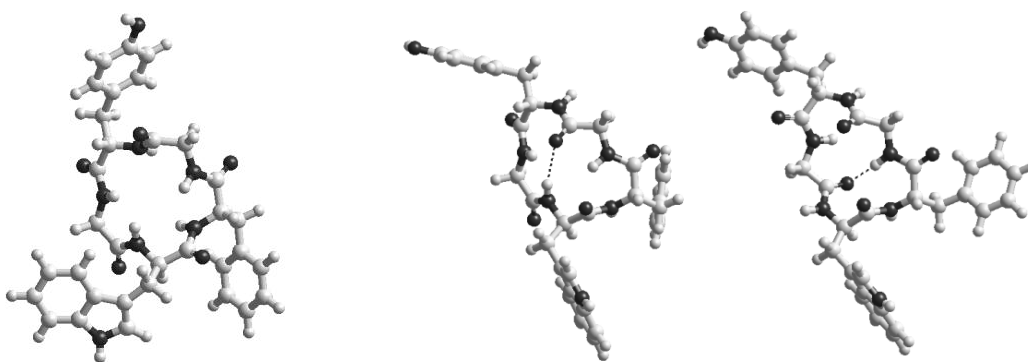


**Fig. (5).** Representative low-energy structures of **14** consistent with ROESY analysis calculated by restrained MD (top), and representative low-energy structures of **14a**, (left) and **14b** (right) obtained by unrestrained MD; all these structures were calculated in a 30x30x30 Å box of standard TIP3P water molecules.

The structure shows the inverse type II  $\beta$ -turn centered on D-Trp-Phe, stabilized by an explicit hydrogen bond between  $\beta$ -AlaCO and D-AspNH, fully compatible with the VT-NMR analysis (Table 4, Xaa=D-AspNH, Yaa= $\beta$ -Ala). This conformation has no violations of the distance constraints, nevertheless, a 10 ns unrestrained MD simulation in explicit water revealed that the amide bond of D-Asp- $\beta$ -Ala can rotate, pointing toward the opposite sides of the molecular plane. Apart from this residual flexibility, **15** shows higher conformational homogeneity with respect to the cyclopentapeptides, probably due to the smaller size of the cyclopeptide ring and strong hydrogen bond. For stereo views of the structures described in this section, see the Supporting Information, figures S2–S8.

### 6.1.7. Molecular docking

To explore the structural determinants responsible for the different MOR affinities of compounds **11** and **13–15**, molecular modeling studies were carried out in our previously obtained MOR model<sup>[14c]</sup> (see Supporting

Information, figure S1 and table S5) using AutoDock (ver. 4)<sup>[35]</sup>, a docking suite that uses an automated approach that allows ligand flexibility, and it is able to locate poses in a consistent way with respect to the X-ray crystal structures<sup>[36]</sup>.

The docking computations were performed by starting from the representative conformations **11a**, **11b**, **13c**, **13d**, **14a**, **14b**, and **15** observed in solution.

For most docking analyses reported in the literature, the construction of ligand–MOR complex models postulated an electrostatic interaction of the protonated amine with Asp<sup>147</sup> in TMH III<sup>[3, 6, 7, 9, 37]</sup>. Conversely, the compounds **11** and **13–15** do not include any ionic functionalities, so the main binding force toward the receptor should comprise hydrophobic and hydrogen bonding interactions.

After docking, MD, energy minimization, clustering, and QM/MM induced fit calculations, the models obtained for compounds **14** and **15** showed suitable macrocycle conformations that enable them to fit the shallow cleft of the MOR. On the contrary, no satisfying poses were obtained for **11** and **13**, presumably due to bad contacts of the Ala methyl side chain(s).

The docking of **14** led to a few alternative docking orientation (DO), characterized by different binding energies, whereas only one orientation was obtained for **15**. This can be correlated to the higher conformational flexibility of **14** with respect to **15** (see the previous section). The top-ranking 14-DO1 and 14-DO2 are shown in Figure 6 a and 6b, respectively, whereas 15-DO is shown in Figure 7; for supplementary views of these DOs, see figures S9 and S10 in the Supporting Information.

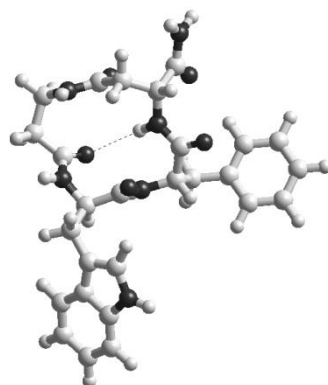


**Fig. ( 6).** Representative low-energy structure of **15** consistent with ROESY analysis, calculated by restrained MD in a 30x30x30 Å box of standard TIP3P water molecules.

The binding site of 14-DO1, 14-DO2, and 15-DO is located in the central core of MOR, delimited by TMH III, VI, and VII, and EL III, IV. The list of the MOR residues in contact with the ligands is reported in table S6 (Supporting Information). The D-Trp of **14** and **15** points toward the bottom of the binding site, with the indole NH in contact with the carboxyl group of Asp<sup>147</sup> (TMH III); the rest of the ligand resides in a cavity delimited on top by EL III.

Four hydrogen bonds are formed between 14-DO1 and the receptor. Two strong hydrogen bonds are located between the heterocyclic NH of D-Trp and Od1 Asp<sup>147</sup> (2.48 Å), and between the phenolic OH of the

Tyr and Oe2 Glu<sup>310</sup> (2.57 Å), whereas the other two are formed between the oxygen of YGly and the Og1H group of Thr<sup>218</sup> (2.57 Å), and between the amide group of XGly and NzH of Lys<sup>233</sup> (2.81 Å).

The aromatic moieties of 14-DO1 are stabilized by many stacking interactions (see table S2, Supporting Information).

The indole of D-Trp points toward a hydrophobic pocket composed mainly of the aromatic residues Phe<sup>152</sup> (TMH III), Phe<sup>237</sup> (TMH V), and Trp<sup>293</sup> (TMH VI). The aromatic group of Tyr is involved in one cation- $\pi$  interaction with the side chain of Lys<sup>303</sup> (TMH VI) and two  $\pi$ - $\pi$  stacking interactions with the aromatic centers of Phe<sup>221</sup> and His<sup>233</sup> (EL III). The phenyl group of Phe interacts the residues Phe<sup>221</sup> (EL III) and Trp<sup>318</sup> (TMH VI). This interaction pattern leads to a calculated binding free energy (DG<sub>b</sub>) value of -9.88 kcalmol<sup>-1</sup>. The structure 14-DO2, Figure 6 (see figure S9, Supporting Information), is rotated by ~180° with respect to 14-DO1, and is involved in interactions with nearly the same residues of TMH III, V-VII, and EL III, IV, but also with Ile<sup>198</sup> and Val<sup>202</sup> from TMH IV (see table S2, Supporting Information).

Four hydrogen bonds are formed between 14-DO2 and the receptor. The hydrogen bond between D-TrpNH and Od1 Asp<sup>147</sup> is retained, but with an appreciable elongation of the distance (2.59 Å versus 2.48 Å). The other hydrogen bonds involve the phenolic OH of Tyr and Oe2 Glu<sup>229</sup> (2.54 Å), the backbone oxygen of XGly and the Ne2H of His<sup>223</sup> (2.60 Å), and one between the backbone oxygen of D-Trp and the Og1H of Thr<sup>218</sup> (2.76 Å).

The phenyl of Phe is now involved in stacking interactions with the side chain of Tyr<sup>148</sup> (TMH III) whereas the indole of D-Trp occupies nearly the same hydrophobic cavity of 14-DO1 (Phe<sup>152</sup> of TMH III and Trp<sup>293</sup> of TMH VI). In this orientation the aromatic side chain of Tyr is rotated toward Glu<sup>229</sup> and does not establish significant stacking interactions with residues of the hydrophobic cavity delimited mainly by Val<sup>300</sup> and Ala<sup>304</sup> (TMH IV) and Thr<sup>307</sup> (EL IV), giving a lower contribution to the complex stability that, in concert with the inferior interaction of D-Trp with Asp<sup>147</sup>, results in an overall calculated binding free energy value of -6.03 kcalmol<sup>-1</sup>.

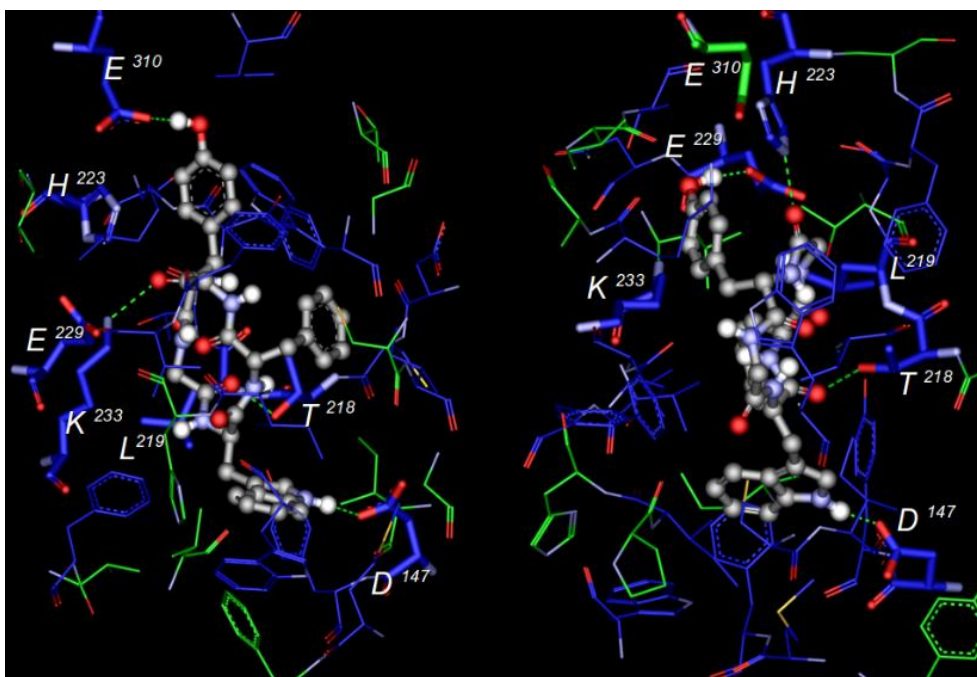


**Figure 7.** Side views of the top ranking docking orientations of **14-DO1** (left) and **14-DO2** (right) and the MOR binding site. The protein residues are represented in wireframe and sticks for the key-residues, with the C-atoms colored in blue for the residues in the first interaction shell,  $<3.5\text{\AA}$  from the ligand, green for those at a distance  $<5\text{\AA}$ ; the ligand is depicted by balls and cylinders (CPK). The figure highlights essential H-bond interactions (green dotted lines).

Interestingly, the structure **14-DO1** maintains a reasonable similarity to the structure **14b** observed in solution (Figure 4).

This, along with the more favorable binding energy, implies that **14-DO1** might be the bioactive conformation of the ligand.

Concerning **15**, the docking protocol revealed only one topranked pose, **15-DO** (Figure 7, see figure S10, Supporting Information), likely due to its greater conformational rigidity. This structure maintains the inverse type II  $\beta$ -turn and the other features observed in solution (Figure 5), the only difference being the orientation of the peptide bond between D-Asp and  $\beta$ -Ala.

The rotation of this peptide bond was also observed in solution during the unrestrained MD simulation. **15-DO** has five hydrogen bonds. The most relevant is between the indole NH and Od1 Asp <sup>147</sup> (2.57  $\text{\AA}$ ). The CONH<sub>2</sub> of D-Asp, situated within the upper part of the MOR, near EL III and surrounded by Thr <sup>220</sup>, Phe<sup>221</sup>, His <sup>223</sup>, and Glu <sup>229</sup>, is involved in two hydrogen bonds, one with the backbone amide of Leu<sup>219</sup> (3.06  $\text{\AA}$ ) and the other with Oe2 Glu <sup>229</sup> (2.59  $\text{\AA}$ ).

Two hydrogen bonds involve the  $\beta$ -Ala residue, one between the NH and Oe2Glu <sup>229</sup> (2.82  $\text{\AA}$ ), and the other between the backbone oxygen and the Og1H of Thr<sup>218</sup> (2.73  $\text{\AA}$ ).

The phenyl of Phe has strong hydrophobic interaction with residues of EL III, in particular the  $\pi$ - $\pi$  and cation- $\pi$  interactions with His <sup>216</sup>. The indole of D-Trp occupies the same hydrophobic cavity of **14** (Tyr<sup>148</sup> and Phe<sup>152</sup> of TMH III, and Trp<sup>293</sup> of TMH VI). The macrocyclic portion of the ligand interacts with the

hydrophobic rim of the tubular pocket (Figure 7), establishing hydrophobic interactions with Thr<sup>218</sup>, Leu<sup>219</sup>, and Thr<sup>220</sup> (EL III), Ile<sup>296</sup>, Val<sup>300</sup>, and Ala<sup>304</sup> (TMH VI), Thr<sup>307</sup> (EL IV), and Ile<sup>322</sup> (TMH VII).

The calculated binding energy value of 15-DO is 9.53 kcalmol<sup>-1</sup>, very close to that of 14-DO1. This is consistent with the similar poses, hydrogen bond interactions, and hydrophobic contacts shown by the D-Trp-Phe portion of the two ligands with the same regions of the receptor, confirming that this can be regarded to as the dominant pharmacophoric motif of this class of cyclopeptides.

## 6.2. Discussion

Data presented in the previous sections support evidence that a D-Trp-Phe sequence situated in positions *i*+1, *i*+2 of an inverse type II  $\beta$ -turn, might confer MOR agonist behavior to cyclopeptides.

Initially, conformational and docking analyses led us to suppose that the atypical MOR agonist **4**, c[Tyr-D-Pro-D-Trp-Phe-Gly], adopted a bioactive conformation compatible with an inverse  $\beta$ -turn centered on D-Trp-Phe. To confirm this hypothesis, we designed cyclopeptide derivatives c[Tyr-Yaa-D-Trp-Phe-Xaa] clearly adopting such a conformation. We supposed that these analogues should display higher receptor affinity with respect to the parent compound **4**, therefore substantiating the proposed bioactive structure. Backbone conformations of the new generation of ligands were predetermined on the basis of the well-known structures of cyclo-Ala<sup>5</sup> models or other cyclopentapeptides containing one or two D-residues already reported in the literature widely used as  $\beta/\gamma$ -turn mimetics (see previous sections).

Gratifyingly, we observed that compound **14**, c[Tyr-Gly-D-Trp-Phe-Gly], proved to be a selective MOR ligand with an approximate tenfold improved nanomolar affinity, while still maintaining the agonism. In solution, this compound adopts a couple of alternative secondary structures in equilibrium, amongst which is **14b**, characterized by the desired inverse type II  $\beta$ -turn on D-Trp-Phe. The docking analysis furnished two alternative orientations of **14** within the receptor, the best of which (14-DO1) was compatible with the in-solution structure **14b**. On the other hand, the cyclopeptides **11–13**, including one or two Ala as Yaa Xaa residues in c[Tyr-Yaa-D-Trp-Phe-Xaa], gave very poor MOR affinities, although **11** revealed a modest affinity for DOR and **13** a moderate KOR affinity.

The complete lack of efficacy of **11** and **13** as MOR ligands was discussed on the basis of conformational and docking analysis. Conformational analysis confirmed that in solution, **11** stably adopts the inverse  $\beta$ -turn conformation on D-Trp-Phe, whereas **13** is more flexible, but is still cable to adopt the same geometry. However, docking analyses gave no suitable orientations of **11–13** inside the receptor cavity.

These data highlight the functional role of the D-Trp-Phe for this class of cyclopeptides. This atypical opioid pharmacophoric motif can be used for designing non-endomorphin-like opioid cyclopeptide agonists. The intrinsic flexibility of **14**, both in solution and in the receptor-bound state, might diminish the reliability of the proposed model of bioactive conformation.

For this reason, we designed and tested the derivative **15**, whose great conformational homogeneity allowed more definitive conclusions.

The compound **15**, c[D-Asp-1-amide- $\beta$ -Ala-D-Trp-Phe], is deprived of the Tyr residue, and includes two  $\beta$ -amino acids, D-Asp-1-amide and  $\beta$ -Ala. Compound **15** was designed on the basis of a preliminary conformational analysis conducted by MD in a box of explicit water molecules (not shown), which led us to

conjecture decreased conformational freedom and a predisposition to reproduce the inverse type II  $\beta$ -turn for this 14-membered cyclotetrapeptide. The CONH<sub>2</sub> side chain of D-Asp-1-amide was engineered on the basis of the analogue group present in the potent MOR-selective agonist JOM-6<sup>[38]</sup>.

Interestingly, **15** had a nanomolar affinity, high selectivity for the MOR, and an agonist behavior.

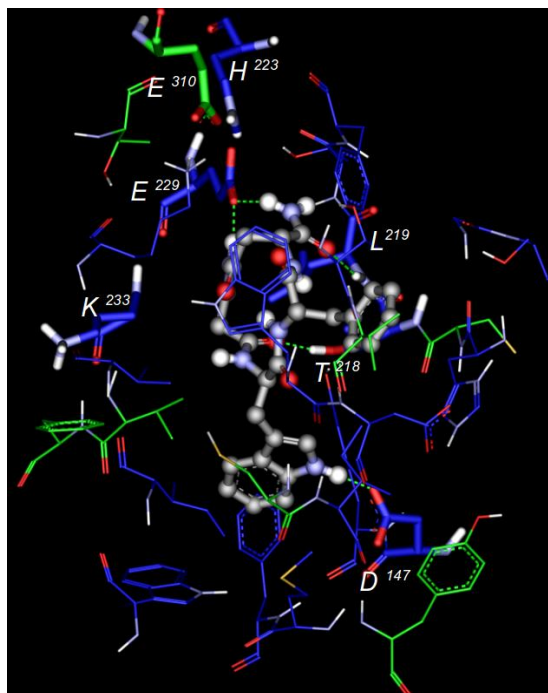
Conformational analysis confirmed the stability of the inverse  $\beta$ -turn on D-Trp-Phe. Docking analysis indicated that **15** retains practically the same structure also in the receptor (see figure S10, Supporting Information, showing the comparison between the rear views of the receptor-bound 15-DO and of the in-solution structure).

Figure 8 shows the nice overlap of the D-Trp-Phe  $\beta$ -turn regions of **11a**, **13d**, **14b**, and **15** observed in solution. It can be observed that an Ala methyl substituent of **11** and **13** occupy the same region of CONH<sub>2</sub> of **15**, but the former precludes a proper receptor fitting, as revealed by the very poor binding affinities of **11** and **13**, and consistent with the docking analyses.

Apparently, the amino acids flanking D-Trp-Phe in the positions *i* and *i*+3 of the  $\beta$ -turn seem to be limited in respect of the dimensions and kinds of side chains tolerated by the receptor.

The comparison between the docking structures 14-DO1 and 15-DO revealed a few differences. 15-DO shows a strong hydrogen bond between CONH<sub>2</sub> and Glu<sup>229</sup>. On the other hand, the phenolic OH of Tyr in 14-DO1 makes a strong hydrogen bond with Glu<sup>310</sup>. Tyr also contributes to the overall binding with some stabilizing hydrophobic contacts. This subtle distinction could justify the slightly better experimental affinity of **14** with respect to **15**.

15-DO and 14-DO1 share many features and show similar binding energy values, in agreement to the nanomolar experimental affinities. For both compounds, Phe strongly interacts the residues Phe<sup>221</sup> (EL III) and Trp<sup>318</sup> (TMH VI). The main interaction of D-Trp is the ionic bond between indolyl NH and Asp<sup>147</sup> of TMH III, accompanied hydrophobic interactions with the aromatic residues Tyr<sup>148</sup>, Phe<sup>152</sup> (TMH III), and Trp<sup>293</sup> (TMH VI).



**Figure 8.** Side view of the top-ranked docking pose of **15** and the MOR binding site. Only selected MOR residues involved in the interactions are shown. The protein is represented in wireframe and sticks (for the key-residues), with the C-atoms colored in blue for the residues in the first interaction shell,  $<3.5\text{\AA}$  from the ligand, green for those at a distance  $<5\text{\AA}$ ; the ligand is depicted by balls and cylinders (CPK). The figure highlights the essential H-bond interactions (green dotted lines).

The stabilizing contact between D-Trp and Trp<sup>293</sup> of TMH VI is of particular interest. Exhaustive investigations performed on the potent agonist JOM-6 indicated that the interaction with Trp<sup>293</sup> might be responsible for receptor activation<sup>[38]</sup>. The rearrangement of Trp<sup>293</sup> induced by the ligand would be accompanied by a rotation of the entire TMH VI, so determining the activation of the G protein.

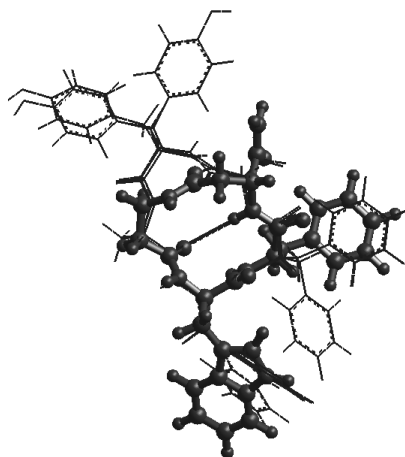


**Fig.(9).** Overlap of the D-Trp-Phe  $\beta$ -turn structures of **11a**, **13d**, **14b** (rendered in sticks) and **15** (balls and cylinders rendering) observed in solution

Cyclopeptide **4** represents the first example of a MOR-selective agonist reported (in 2004)<sup>[12]</sup> the bioactivity of which resides in the D-Trp-Phe sequence. Very recently, the same pharmacophoric motif has been proposed

again with regard to c[D-Pro-Phe-D-Trp-Phe] and correlated compounds<sup>[39]</sup> derived from the naturally occurring cyclotetrapeptide c[D-Pro-Phe-Trp-Phe], CJ-15,208<sup>[40]</sup>, isolated as a metabolite of a fungus. CJ-15,208 was a modestly selective KOR antagonist ligand (IC<sub>50</sub>=47 nm, using guinea pig brain membrane). The D-configured Trp residue rendered the derivatives more potent than the natural product. c[D-Pro-Phe-D-Trp-Phe] was a KOR antagonist devoid of agonist activity, with a modest MOR affinity.

The analogue c[D-Pro-Phe-D-Trp-Ala] maintained practically the same activity and selectivity as a KOR antagonist. This means that the pharmacophoric sequence very likely is Phe-D-Trp, rather than D-Trp-Phe. Therefore, the different pharmacologic profile of the agonists **4**, **14**, and **15** with respect to the antagonist derivatives of CJ-15,208 very likely resides in the inverted positions of D-Trp and Phe within the sequence, and in the 3D display of their side chains, which correlated to the different sizes of the cyclopeptide structures. These differences strongly impact not only the affinity for a specific opioid receptor type, but also the ability to trigger the activation of G-proteins and signal transduction.

### 6.3. Conclusions

Herein we discuss our investigations in support of an unprecedented pharmacophore for the MOR, the inverse type II  $\beta$ -turn on D-Trp-Phe. This bioactive structure was formerly supposed on the basis of conformational and docking analyses performed on the agonist c[Tyr-D-Pro-D-Trp-Phe-Gly] (**4**), a cyclic analogue of EM1 showing a 10<sup>-8</sup>M affinity for the MOR. To validate this initial hypothesis, we designed a new generation of analogues with improved receptor affinity, by fostering the inverse  $\beta$ -turn on D-Trp-Phe.

Among the new compounds **11–14** of general sequence c[Tyr-Yaa-D-Trp-Phe-Xaa] (Yaa, Xaa=Ala, Gly), the cyclopeptide c[Tyr-Gly-D-Trp-Phe-Gly] (**14**) was a selective MOR agonist with 10<sup>-9</sup>M affinity. This result is of particular interest, taking into consideration that **14** is deprived of any ionic interactions which are generally considered fundamental in binding and activating the opioid receptor. Despite of the backbone flexibility generated by the two Gly residues, the conformational analysis revealed that in solution **14** can adopt an inverse type II  $\beta$ -turn (the conformation 14b).

To further validate and to expand the scope of the D-Trp-Phe pharmacophore, we designed the cyclotetrapeptide c[D-Asp-1-amide- $\beta$ -Ala-D-Trp-Phe] (**15**), not based on the sequence of EM1, and characterized in solution by a stable D-Trp<sub>i+1</sub>-Phe<sub>i+2</sub> inverse type II  $\beta$ -turn. This compound showed a selective, nanomolar MOR affinity, and a partial agonist behavior.

Docking analyses further confirmed that the inverse type II  $\beta$ -turn on D-Trp-Phe allow the cyclopeptides **14** and **15** to assume the correct poses within the binding site, while the structures of the other analogues **11–13** were unsuitable for receptor fitting, possibly because of the presence of methyl substituents on the residues *i*, *i*+3 of the  $\beta$ -turn. These results indicate that cyclopeptides comprising a D-Trp-Phe motif in the proper secondary conformation may represent leads for the discovery of novel lipophilic opioid agonists, characterized by an atypical mechanism of receptor activation.

The functional selectivity observed for the novel MOR ligands described in this study can be explored in further investigations to ascertain if they can direct the receptor toward a conformational selectivity, evoking a specific response. Recent pharmacological data and modeling studies strongly support the hypothesis that GPCRs, including opioid receptors, exist as dynamic entities that can occupy multiple conformations and

signaling states, depending on the ligand and accessory proteins within the signaling complex<sup>[41]</sup>.

## 6.4. Experimental Section

### 6.4.1. Chemistry

**General methods:** Unless stated otherwise, standard chemicals were obtained from commercial sources and used without further purification. Flash chromatography was performed on silica gel (230–400 mesh), using mixtures of EtOAc and MeOH; solvents were simply distilled. Semipreparative RP-HPLC was performed on a C18 column (7 mm particle size, 21.2 mm x150 mm, from 7:3 H<sub>2</sub>O/CH<sub>3</sub>CN to 100% CH<sub>3</sub>CN in 15 min), flow rate of 12 mLmin<sup>-1</sup>.

The purity (>95%) of tested compounds was assessed by analytical RP-HPLC on an ODS column (4.6 mm particle size, 100 μpore diameter, 250 mm, DAD 210 nm, from 9:1 H<sub>2</sub>O/CH<sub>3</sub>CN to 2:8 H<sub>2</sub>O/ CH<sub>3</sub>CN in 20 min), flow rate of 1.0 mLmin<sup>-1</sup>, followed by 10 min at the same composition. <sup>1</sup>H NMR spectra were recorded at 400 MHz in 5 mm tubes, using 0.01M peptide in 8:2 [D<sub>6</sub>]DMSO/H<sub>2</sub>O, at RT.

Solvent suppression was performed by the solvent presaturation procedure implemented in Varian (presat). Chemical shifts are reported as δ values. The unambiguous assignment of <sup>1</sup>H NMR resonances was performed by 2D gCOSY, HMBC, and HSQC. gCOSY experiments were conducted with a proton spectral width of 3103 Hz. VT-<sup>1</sup>H NMR experiments were performed over the range of 298–348 K. Peaks were calibrated on DMSO. 2D spectra were recorded in the phase sensitive mode and processed using a 908-shifted, squared sine-bell apodization. 2D ROESY experiments were recorded with a 250 ms mixing time with a proton spectral width of 3088 Hz.

**6.4.2. Peptide synthesis:** The linear precursors **6–10** were obtained by standard SPPS using an automated synthesizer apparatus on a Wang resin preloaded with Fmoc-Phe (0.5 g, 0.4–0.8 mmolg<sup>-1</sup>).

Fmoc removal was performed with 4:1 DMF/piperidine (5 mL) under mechanical shaking. After 15 min, the mixture was filtered, the resin was washed with DMF (5 mL), and treated under mechanical shaking with a second portion of 4:1 DMF/piperidine. After 40 min, the mixture was filtered, and the resin was washed three times in sequence with DMF (5 mL) and CH<sub>3</sub>OH (5 mL). The resin was suspended in CH<sub>2</sub>Cl<sub>2</sub> (5 mL), and a solution of the next Fmoc protected amino acid (0.6 mmol) and HOBt (0.6 mmol) in DMF (3 mL) was added, followed by HBTU (0.6 mmol) and DIPEA (1.2 mmol). The mixture was mechanically shaken, and after 3 h the resin was filtered and washed three times with DMF (5 mL) and CH<sub>3</sub>OH (5 mL) in sequence. Coupling efficacy was determined by means of the Kaiser tests.

**6.4.3. Peptide cleavage:** The N-deprotected resin-bound peptide was suspended in a mixture of TFA (4.7 mL), H<sub>2</sub>O (0.15 mL), and PhOH (0.15 mL), and mechanically shaken at RT. After 2 h, the mixture was filtered, the resin was washed twice with 10% TFA in Et<sub>2</sub>O (5 mL), and twice with Et<sub>2</sub>O. Filtrate and washes were collected and the solvent and volatiles were removed under N<sub>2</sub> flow at RT.

The resulting residue was suspended in Et<sub>2</sub>O, and the crude solid which precipitated was triturated and collected by centrifuge. Peptides were characterized by analytical RP-HPLC and ESI-MS (see General methods).

**6.4.4. Peptide cyclization:** The peptides (0.15 mmol) were dissolved in dry DMF (40 mL) and treated while being magnetically stirred with NaHCO<sub>3</sub> (2.0 mmol) and DPPA (0.5 mmol) at RT. After two days, the mixture was filtered, the solvent was distilled at reduced pressure, and the residue was transferred in a separating funnel. The residue was diluted with water (5 mL), and the mixture was extracted with EtOAc (4x20 mL). The collected organic layers were dried over Na<sub>2</sub>SO<sub>4</sub>, and the solvent was evaporated at reduced pressure. The oily residue was rapidly purified by flash chromatography over silica gel (eluent: 97:3 EtOAc/MeOH), followed by semipreparative RP-HPLC (see General methods), affording the cyclopeptides in 55–70% yield, 95–97% pure (Table 1) by analytical RP-HPLC analysis (see General methods). Cyclopeptides were characterized by analytical ESI-MS (Table 1 and General methods) and <sup>1</sup>H NMR.

**Peptide 11:** <sup>1</sup>H NMR (400 MHz, 8:2 [D<sub>6</sub>]DMSO:H<sub>2</sub>O): δ=1.09 (d, J=6.4 Hz, 3H, YAlaMe), 1.90 (d, J=6.8 Hz, 3H, XAlaMe), 2.65–2.85 (m, 2H, TyrHβ+D-TrpHβ), 2.85–2.94 (m, 3H, TyrHβ+D-TrpHβ+PheHβ), 2.98 (dd, J=4.0, 13.6 Hz, 1H, PheHβ), 4.04 (q, J=7.2 Hz, 1H, TyrHα), 4.15 (quint, J=7.4 Hz, 1H, XAlaHα), 4.27 (quint, J=7.0 Hz, 1H, YAlaHα), 4.33 (m, 1H, PheHα), 4.42 (q, J=7.2 Hz, 1H, D-TrpHα), 6.64 (d, J=7.6 Hz, 2H, TyrArH), 6.96 (s, 1H, IndH2), 6.97 (br t, 1H, IndH5), 6.98 (d, J=7.6 Hz, 2H, TyrArH), 7.06 (t, J=7.2 Hz, 1H, IndH6), 7.11–7.25 (m, 5H, PheArH), 7.32 (d, J=8.0 Hz, 1H, IndH7), 7.49 (d, J=7.6 Hz, 1H, IndH4), 8.06 (br d, 1H, YAlaNH), 8.18 (br d, 1H, XAlaNH), 8.38 (br d, 1H, TyrNH), 8.47 (d, J=8.0 Hz, 1H, PheNH), 8.58 (d, J=7.2 Hz, 1H, d-TrpNH), 9.25 (br s, 1H, TyrOH), 10.70 ppm (s, 1H, IndH1).

**Peptide 13:** <sup>1</sup>H NMR (400 MHz, 8:2 [D<sub>6</sub>]DMSO:H<sub>2</sub>O): δ=1.20 (d, J=8.8 Hz, 3H, AlaMe), 2.76 (dd, J=10.8, 13.2 Hz, 1H, PheHb), 2.80–2.90 (m, 3H, TyrHb+D-TrpHb), 2.90–3.00 (m, 2H, D-TrpHb+PheHb), 3.58 (dd, J=4.8, 15.6 Hz, 1H, GlyHα), 3.72 (dd, J=8.0, 15.6 Hz, 1H, GlyHα), 4.03 (q, J=7.6 Hz, 1H, TyrHα), 4.12 (quint, J=7.4 Hz, 1H, AlaHα), 4.19–4.33 (dt, J=5.6, 8.0 Hz, 1H, PheHα), 4.33 (q, J=6.8 Hz, 1H, D-TrpHα), 6.61 (d, J=8.0 Hz, 2H, TyrArH), 6.93 (d, J=8.0 Hz, 2H, TyrArH), 6.96 (m, 2H, IndH2+IndH5), 7.05–7.15 (m, 3H, PheArH+IndH6), 7.15–7.25 (m, 3H, PheArH), 7.27 (d, J=7.6 Hz, 1H, IndH7), 7.50 (d, J=7.2 Hz, 1H, IndH4), 7.81 (d, J=7.8 Hz, 1H, AlaNH), 7.84 (t, J=6.6 Hz, 1H, GlyNH), 8.11 (d, J=6.8 Hz, 1H, d-TrpNH), 8.20 (d, J=7.2 Hz, 1H, TyrNH), 8.41 (d, J=7.2 Hz, 1H, PheNH), 9.21 (s, 1H, TyrOH), 10.70 ppm (s, 1H, IndH1).

**Peptide 14:** <sup>1</sup>H NMR (400 MHz, 8:2 [D<sub>6</sub>]DMSO:H<sub>2</sub>O): δ=2.60–2.70 (m, 2H, TyrHβ+D-TrpHβ), 2.80–2.90 (m, 2H, TyrHβ+D-TrpHβ), 2.95–3.05 (m, 2H, PheHβ), 3.25–3.35 (m, 1H, XGlyHα), 3.35–3.45 (m, 1H, YGlyHα), 3.55–3.65 (m, 1H, YGlyHα), 3.95–4.15 (m, 1H, XGlyHα), 4.10–4.25 (m, 1H, TyrHα), 4.40–4.51 (m, 2H, PheHα+d-TrpHα), 6.64 (d, J=8.4 Hz, 2H, TyrArH), 6.85 (s, 1H, IndH2), 6.96 (br t, 1H, IndH5), 7.01 (d, J=8.4 Hz, 2H, TyrArH), 7.11 (t, J=7.2 Hz, 1H, IndH6), 7.11–7.25 (m, 5H, PheArH), 7.31 (br t, 1H, IndH7), 7.54 (d, J=8 Hz, 1H, IndH4), 7.78 (br t, 1H, XGlyNH), 7.86 (d, J=6.4 Hz, 1H, d-TrpNH), 8.25 (br t, 1H, YGlyNH), 8.71 (d, J=6.4 Hz, 1H, TyrNH), 8.76 (d, J=8.0 Hz, 1H, PheNH), 9.25 (br s, 1H, TyrOH), 10.66 ppm (s, 1H, IndH1).

**Peptide 15:** <sup>1</sup>H NMR (400 MHz, 8:2 [D<sub>6</sub>]DMSO:H<sub>2</sub>O): δ=2.08 (m, 1H, β-AlaH<sub>α</sub>), 2.30 (dd, J=4.6, 15.4 Hz, 1H, D-AspH<sub>β</sub>), 2.40 (m, 1H, β-AlaH<sub>α</sub>), 2.67 (dd, J=6.8, 15.4 Hz, 1H, D-AspH<sub>β</sub>), 2.75 (dd, J=6.8, 14.0 Hz, 1H, D-TrpH<sub>β</sub>), 2.80–2.90 (m, 2H, PheH<sub>β</sub>+D-TrpH<sub>β</sub>), 2.98 (dd, J=4.2, 14.2 Hz, 1H, PheH<sub>β</sub>), 3.18 (m, 1H, β-AlaH<sub>β</sub>), 3.42 (m, 1H, β-AlaH<sub>β</sub>), 4.27 (m, 2H, PheH<sub>α</sub>+D-AspH<sub>α</sub>), 4.57 (q, J=8.0 Hz, 1H, D-TrpH<sub>α</sub>), 6.90 (s, 1H, IndH<sub>2</sub>), 6.96 (t, J=7.2 Hz, 1H, IndH<sub>5</sub>), 7.05–7.15 (m, 4H, PheArH<sub>2,6</sub>+IndH<sub>6</sub>+CONH<sub>2</sub>), 7.15–7.25 (m, 4H, PheArH<sub>3–5</sub>+CONH<sub>2</sub>), 7.33 (d, J=7.6 Hz, 2H, IndH<sub>7</sub>+d-AspNH), 7.45 (d, J=7.6 Hz, 1H, IndH<sub>4</sub>), 7.64 (t, J=5.6 Hz, 1H, β-AlaNH), 8.19 (d, J=8.4 Hz, 1H, D-TrpNH), 8.43 (d, J=8.4 Hz, 1H, PheNH), 10.7 ppm (s, 1H, IndH<sub>1</sub>).

## 6.5. Biology

Receptor binding to cloned human MOR on intact cells: HEK-293 cells stably expressing human MOR were employed to perform displacement binding assays on intact cells to evaluate the binding affinity of compounds **11–15** toward MOR. HEK-293 cells were transfected with the human MOR encoding plasmid pcDNA3.1+ OPRM1 (UMR cDNA Resource Center, Rolla, MO, USA) by using EXGEN 500 (Fermentas, Hanover, MD, USA) according to the manufacturer's recommendations. Stable transfectants were selected by exposure to G418 (500 mgmL<sup>-1</sup>) for four weeks and then seeded in normal minimum essential medium (MEM; Sigma, Steinheim, Germany) to perform binding assays. Cell surface human MOR receptors were measured on intact cells using [<sup>3</sup>H]DAMGO (0.1–5 nM) as radioligand and naloxone (30 nM) to determine nonspecific binding.

[<sup>3</sup>H]DAMGO binding to HEK-293 cells expressing human MOR was saturable, with a K<sub>d</sub> (apparent dissociation constant of the radioligand) of 1.45x0.14 nM and a B<sub>max</sub> (maximal number of binding sites) of 3189x18 dpm (5x10<sup>5</sup> cells)x1 (n=4). For displacement binding assays, HEK-293 cells expressing human MOR were incubated at RT for 2 h with [<sup>3</sup>H]DAMGO (5 nM), in the presence or absence of compounds at various concentrations (10<sup>-12</sup>–10<sup>-4</sup>M); nonspecific binding was determined in the presence of naloxone (30 nM). Compounds were prepared as stock solutions (10<sup>-2</sup> M) in ethanol and protected from light; compound dilutions were made in assay buffer. After incubation with the listed ligands, cells were washed in PBS (pH 7.4) and lysed with 0.1N NaOH. Lysed samples were buffered with an equal amount of 0.1N HCl and left in scintillation fluid for 8 h before counting. Data from at least three independent experiments were fitted by nonlinear regression analysis using GraphPad Prism. K<sub>i</sub> values were calculated from the IC<sub>50</sub> values using the Cheng–Prusoff equation<sup>[42]</sup>. IC<sub>50</sub> values represent mean values from no less than four experiments. IC<sub>50</sub> values, relative potency estimates, and their associated standard errors were determined by fitting the data to the Hill equation by a computerized nonlinear least-squares method.

**6.5.1. Receptor binding assays to cloned human DOR and KOR:** HEK-293 cells stably expressing human DOR (2700x100 fmolmg<sup>-1</sup> protein; n=6) or KOR (2600x400 fmolmg<sup>-1</sup> protein; n=6) were generated by EXGEN500 (Fermentas) by transfection with cDNAs cloned into the pcDNA3.1(+) vector (Invitrogen). The cDNAs were obtained from UMR cDNA Resource Center (Rolla, MO, USA). HEK-293 cells expressing DOR or KOR were grown as a monolayer culture in tissue culture flasks that were incubated at 37°C in a humidified atmosphere (5% CO<sub>2</sub>) in MEM (Lonza) containing 2 mM l-glutamine, 1\_ nonessential amino acids (Invitrogen) and supplemented with 10% fetal calf serum (Lonza), and maintained in the presence of 400

mgmL<sup>-1</sup> geneticin (Invitrogen). Cells were washed with icecold PBS, pH 7.4; scraped into an ice-cold buffer containing 10 mm HEPES/NaOH, pH 7.4 and 1 mm EDTA; and lysed with a Dounce tissue grinder. The cell lysate was centrifuged at 1000 g for 2 min at 4 °C. The supernatant was collected and centrifuged at 32 000 g for 20 min at 4 °C. The pellet was resuspended in homogenization buffer at a protein concentration (determined by BCA assay) of 1.0 to 1.5 mgmL<sup>-1</sup> and stored in aliquots at -80°C. Receptor binding assays were carried out by using [<sup>3</sup>H]diprenorphine to label DOR and [<sup>3</sup>H]U69,593 to label KOR and by incubating the membrane preparations at 25 °C for 90 min in buffer containing 100 mm Tris- HCl and 0.3% BSA. For saturation binding assays, the concentrations of [<sup>3</sup>H]diprenorphine and [<sup>3</sup>H]U69,593 ranged from 40 pm to 3 nm and from 20 pm to 5 nm, respectively ([<sup>3</sup>H]diprenorphine K<sub>d</sub>=0.22-0.03 nm; n=3) ([<sup>3</sup>H]U69,593 K<sub>d</sub>=1.1-0.1 nm; n=3). For competition binding assays, the concentration of [<sup>3</sup>H]diprenorphine or [<sup>3</sup>H]U69,593 was 1 nm and 2 nm, respectively.

Nonspecific binding was determined in the presence of either 10 mm DPDPE (DOR) or 10 mm U50,488 (KOR) and corresponded to 8 –12% and 12–15% of total [<sup>3</sup>H]diprenorphine and [<sup>3</sup>H]U 69,593 binding, respectively. Triplicate determinations were made for each experiment. Reactions were terminated by filtration through Whatman GF/C filters presoaked with 0.3% polyethylenimine, which were washed three times with 5 mL of ice-cold buffer containing 50 mm Tris-HCl, pH 7.4. The radioactivity trapped was determined by liquid scintillation spectrometry. Data from at least three independent experiments were fitted by nonlinear regression analysis using GraphPad Prism. K<sub>i</sub> values were calculated from IC<sub>50</sub> values by the Cheng–Prusoff equation. IC<sub>50</sub> values represent mean values from no fewer than four experiments. IC<sub>50</sub> values, relative potency estimates, and their associated standard errors were determined by fitting the data to the Hill equation by a computerized nonlinear least-squares method.

**6.5.2. Determination of inhibition of cyclic AMP accumulation:** The agonist activity was determined by measuring the inhibition of forskolin-stimulated cyclic AMP accumulation in whole HEK-293 cells stably expressing MOR. Cells were grown at 37°C and 5% CO<sub>2</sub> in MEM, 2 mm l-glutamine, 1\_ nonessential amino acids supplemented with 10% FBS. A 75 cm flask at 95–100% confluence was split into 24 wells and incubated overnight. When the confluence arrived at 85–95%, the medium was removed and the cells were washed three times with PBS; thereafter, cells were incubated in serumfree medium containing 0.5 mm 3-isobutyl-1-methylxanthine (Sigma–Aldrich) and exposed for 15 min to 10 mm forskolin without and with each compound (0.01 nm–100 nm) at 37°C. Cells were then lysed in 0.1N HCl, scraped off and centrifuged (2000 g, 5 min).

Supernatants were assayed for cAMP concentration by using a Cyclic AMP EIA kit (Cayman Chemical Company, Ann Arbor, MI, USA) according to the manufacturer's instructions. Each well was determined individually, the triplicates were averaged, and IC<sub>50</sub> values were determined. In these experimental conditions, forskolin-stimulated cAMP production in control cells was 35-1 pmolmg<sup>-1</sup> protein (n=4) and basal production of cAMP in untreated cells was 1.7-0.3 pmolmg<sup>-1</sup> protein (n=4). Activity of DAMGO, EM1, and compounds **4**, **14**, and **15** has been expressed as percent inhibition of forskolin-induced cAMP production.

## 6.6. Conformational analysis

ROESY intensities were classified as very strong, strong, medium, and weak, and were associated with distances of 2.2, 2.6, 3.0, and 4.2 Å, respectively. Geminal couplings and other obvious correlations were discarded. For the absence of  $H\alpha(i, i+1)$  ROESY crosspeaks, the w bonds were set at 1808 (force constant: 16 kcalmol<sup>-1-2</sup>). Only ROESY-derived constraints were included in the restrained MD. The restrained MD simulations were conducted using the AMBER force field in a 30x30x30Å box of standard TIP3P models of equilibrated water. All water molecules with atoms that come closer than 2.3 Å to a solute atom were eliminated. A 50 ps simulation at 1200 K was used for generating 50 random structures that were subsequently subjected to a 20 ps restrained MD with a 50% scaled force field at the same temperature, followed by 20 ps with full restraints (distance force constant of 7 kcalmol<sup>-1-2</sup>), after which the system was cooled in 5 ps to 50 K. Hydrogen bond interactions were not included, nor were torsion angle restraints.

The resulting structures were minimized with 3000 cycles of the steepest descent and 3000 cycles of the conjugated gradient (convergence of 0.01 kcal<sup>-1</sup>mol<sup>-1</sup>). The backbones of the structures were clustered by the RMSD analysis module of HyperChem. Unrestrained MD simulation in explicit water was performed for 10 ns at 298 K, at constant temperature and pressure (Berendsen scheme<sup>[43]</sup>, bath relaxation constant of 0.2). For 1–4 scale factors, van der Waals and electrostatic interactions are scaled in AMBER to half their nominal value. The integration time step was set to 0.1 fs. Box equilibration was set to 10 ps.

### 6.6.1. Computational methods

Molecular modeling studies and graphic manipulations were performed using the optimized Mac OSX versions of NAMD<sup>[44]</sup>, Auto-Dock (ver. 4), MGL tools, and UCSF chimera software packages<sup>[45]</sup> on an Apple MacPro quad-Xeon workstation running Mac OSX Tiger (ver. 10.4.9). The analysis of the outputs from the docking runs as well as images were performed with PyMOL<sup>[46]</sup> and Accelrys DS Visualizer (<http://www.accelrys.com>) and rendered with POVRay<sup>[47]</sup>. The UCSF chimera was used to calculate the hydrogen bond distances measured between the hydrogen and its assumed binding partner.

Preparation of the MOR-substrate systems: As the experimentally determined 3D structure of a MOR is not yet available, the MOR 3D model used in this study was that obtained in our previous work concerning comparative modeling. The MOR model was checked through MGL tools and the UCSF chimera to guarantee system conformity with the molecular modeling programs (in particular, the names of the side chains that must be congruent with the AMBER force field used). The amino acid chain of the MOR model was terminated with COO<sup>-</sup> and NH<sup>3+</sup> groups in their zwitterionic forms, and the polar hydrogen atoms were added in their calculated positions. The protonation state was set to the normal ionization state at pH 7.0 for all the ionizable residues (in particular, Asp<sup>147</sup>, Asp<sup>216</sup>, Glu<sup>229</sup>, and Glu<sup>310</sup>) and His residues (His<sup>223</sup>, His<sup>297</sup>, and His<sup>319</sup>), and both the topology and connectivity of the molecule had been created. Model building was followed by energy minimization up to an energy gradient lower than 10<sup>-4</sup> kcalmol<sup>-1-1</sup>, choosing AMBER as the force field as implemented in the NAMD package.

The ligands experimental conformation were used as starting structures and the first model building and geometry optimization of the studied compounds were accomplished with the Gchemical package,<sup>[48]</sup>

whereas the refinement was obtained using a systematic conformer search followed by geometry optimization of the lowest energy structure with MOPAC2009 (PM3 Method, RMS gradient 0.0100)<sup>[49]</sup>. The atomic charges were assigned using the Gasteiger–Marsili formation, which uses the type of atomic charges used in calibrating the AutoDock empirical free energy function.

**6.6.2. Molecular docking:** The docking of the cyclopeptides into the MOR model was performed with AutoDock. Default parameters (including a distance-dependent dielectric 'constant') were used as described in the AutoDock manual, and both the receptor model and the ligands were prepared for docking by following the default protocols (except for those changes mentioned below). Auto-Dock uses an empirical scoring function that is able to approximate the binding free energies, because it includes a solvation free energy term. As a result of the absence of information on the binding region of compounds **11**, **13**, **14**, and **15**, the docking process was performed in two steps. The docking procedure was applied to the binding region of the protein target, represented by a box of 20x20x20 Å, centered on the best scored conformation obtained in our previous work (corresponding to x, y, and z values of -13.71, 9.56 and 0.47 Å, respectively), with a grid spacing of 0.300 Å. Movement of the ligands was limited to inside this search space during docking. Atomic solvation parameters were assigned to the protein, and the default parameters for the Lamarckian genetic algorithm were used as the search protocol, except for the maximum number of energy evaluations, which was changed to 10 million (the population size was raised to 500). For the GA algorithm, the default parameters were kept for mutation, crossover, and elitism.

Ligand-induced fit phenomenon occurring at the ligand binding domain of the MOR was investigated by MD calculations. The ligand orientations resulting from the docking run were clustered into families, considering a RMSD clustering tolerance of 2.0 Å, and the lowest docking energy conformations were equilibrated for 4.0 ns by MD, using the AMBER force field as implemented in the NAMD package. To study the induced fit phenomenon, the docked MOR–ligand complexes were prepared to use a smaller reacting subsystem consisting of the cyclopeptides and side chains of the amino acids within 10 Å from the ligands, whereas the rest of the protein was restrained by using the harmonic restraints feature of NAMD. The protocol for each instance involved an energy minimization of the initial structure (2000 steps), heating to 298 K (10 ps), equilibration at 298 K and 1 atm (50 ps), and the production run (to 5 ns). A round of optimization included 100 steps of steepest descent and 400 steps of the conjugated gradient method. Both minimization and equilibration were conducted gradually by releasing initial harmonic constraints on the reacting subsystem (25 kcalmol<sup>-1</sup>). The schedules for removing the restraints involved decrements of 10 kcalmol<sup>-1</sup> (5 kcalmol<sup>-1</sup> in the end) every 500 steps or every 10 ps. The first 10 ps of equilibration were conducted at constant (E,V), after which the system was coupled to a (T,p) reservoir at a temperature of 298 K with a coupling time of 0.1 ps, and the pressure was held at 1 bar, with a coupling time of 0.2 ps, using a Berendsen thermostat to maintain the constant temperature and pressure. Global rotations and translations were removed every 100 steps, and the corresponding energy was accounted for by scaling the atomic velocities. The list of nonbonded atom pairs was updated at ten step intervals during MD, and every step during minimization. The time step used in the simulation was 1.0 fs and Particle-Mesh Ewald summation with a 10 Å short-range cutoff was used to treat long-range electrostatics. SHAKE<sup>[50]</sup> was used to constrain bond lengths between

heavy and hydrogen atoms. Hydrogen bonds and contacts were automatically identified using the 'contact' module of CCP4<sup>[51]</sup> and the UCSF chimera, and the other interactions were identified visually.

**6.6.3. Hybrid QM/MM calculations:** In the current study, we used the pseudo-bond ab initio QM/MM approach as implemented in Gaussian 03.<sup>[52]</sup> For the QM/MM calculations, the MOR–ligand system resulting from the docking study was first partitioned into a QM subsystem and an MM subsystem. The reaction system used a smaller QM subsystem consisting of the cyclopeptide and side chains of the amino acids within 3.5 Å, whereas the rest of the protein (the MM subsystem) was treated using the AMBER force field, together with a low memory convergence algorithm. The boundary problem between the QM and MM subsystems was treated using the pseudobond approach. With this MOR–substrate QM/MM system, an iterative optimization procedure was applied to the QM/MM system, using B3LYP/3-21G\* QM/MM calculations, leading to an optimized structure for the reactants. The convergence criterion used was set to obtain an energy gradient of  $<10^{-4}$ , using the twinrange cutoff method for nonbonded interactions, with a longrange cutoff of 14 Å and a short-range cutoff of 8 Å.

## 6.7. Supporting Information

**Table S1.** Non-obvious ROESY cross-peaks observed for **11**.

Cross peak <sup>a</sup>	Intensity <sup>b</sup>	Cross peak <sup>a</sup>	Intensity <sup>b</sup>
TrpNH-PheNH	w	TrpH4-TrpH $\alpha$	s
TrpNH-TrpH4	w	PheArH-PheH $\beta$ 2.9	vs
TrpNH-TrpH2	m	PheArH-PheH $\beta$ 3.1	vs
TrpNH-TrpH $\alpha$	m	PheArH-PheH $\alpha$	s
TrpNH-YAlaH $\alpha$	vs	TyrArH-TyrH $\beta$	vs
TrpNH-TrpH $\beta$ 2.9	m	TyrArH-TyrH $\alpha$	s
TrpNH-TrpH $\beta$ 3.0	m	TrpH2-TrpH $\beta$ 2.9	m
TrpNH-YAlaMe	m	TrpH2-TrpH $\beta$ 3.0	vs
PheNH-PheArH	m	TrpH2-TrpH $\alpha$	s
PheNH-TrpH $\alpha$	vs	TrpH $\alpha$ -YAlaMe	w
PheNH-PheH $\alpha$	m	TrpH $\alpha$ -TrpH $\beta$ 2.9	m
PheNH-PheH $\beta$ 2.9	s	TrpH $\alpha$ -TrpH $\beta$ 3.0	s
PheNH-PheH $\beta$ 3.1	w	PheH $\alpha$ -PheH $\beta$ 2.9	s
TrpH4-TrpH $\beta$ 2.9	s	PheH $\alpha$ -PheH $\beta$ 3.1	vs
TrpH4-TrpH $\beta$ 3.0	s	TyrH $\alpha$ -TyrH $\beta$	vs

<sup>a</sup> Stereochemistry has been omitted. <sup>b</sup> vs = very strong, s = strong, m = medium, w = weak

**Table S2.** Non-obvious ROESY cross-peaks observed for **13**.

Cross peak <sup>a</sup>	Intensity <sup>b</sup>	Cross peak <sup>a</sup>	Intensity <sup>b</sup>
PheNH-PheH $\beta$ 2.8	vs	PheNH-PheH $\beta$ 3.0	m
PheNH-PheH $\alpha$	m	PheNH-TrpH $\alpha$	vs
PheNH-AlaNH	s	PheNH-PheArH	s
TyrNH-AlaMe	vs	TyrNH-TyrH $\alpha$	s
TyrNH-GlyNH	s	TyrNH-AlaH $\alpha$	s
TyrNH-AlaNH	m	TyrNH-TyrArH	m
TrpNH-TrpH $\beta$ 3.0	w	TrpNH-TrpH $\beta$ 2.9	s
TrpNH-GlyH $\alpha$ 3.7	m	TrpNH-GlyH $\alpha$ 3.6	vs
TrpNH-GlyNH	m	TrpNH-TrpH $\alpha$	m
TrpNH-TrpH4	w	GlyNH-GlyH $\alpha$ 3.6	s
GlyNH-TyrH $\alpha$	s	GlyNH-GlyH $\alpha$ 3.7	s
AlaNH-AlaH $\alpha$	s	GlyNH-TyrH $\beta$	m
AlaNH-PheH $\beta$ 2.8	m	AlaNH-AlaMe	s
AlaNH-PheH $\alpha$	m	AlaNH-PheH $\beta$ 3.0	s
AlaNH-TyrH $\alpha$	w	AlaNH-TrpH $\alpha$	m
TrpH4-Trp $\beta$ 3.0	m	TrpH4-Trp $\beta$ 2.9	s
PheArH-PheH $\alpha$	s	TrpH4-Trp $\alpha$	s
PheArH-PheH $\beta$ 3.0	vs	PheArH-PheH $\beta$ 2.8	vs
TrpH2-TrpH $\beta$ 3.0	s	TrpH2-TrpH $\beta$ 2.9	s
TyrArH-AlaMe	m	TrpH2-TrpH $\alpha$	m
TyrArH-TyrH $\beta$	vs	TyrArH-TyrH $\alpha$	s

PheH $\alpha$ -PheH $\beta$ 2.8	s	PheH $\alpha$ -PheH $\beta$ 3.0	s
TrpH $\alpha$ -TrpH $\beta$ 2.9	s	PheH $\alpha$ -TrpH $\beta$ 3.0	m
TyrH $\alpha$ -TyrH $\beta$	m		

<sup>a</sup> Stereochemistry has been omitted. <sup>b</sup> vs = very strong, s = strong, m = medium, w = weak

**Table S3.** Non-obvious ROESY cross-peaks observed for **14**.

Cross peak <sup>a</sup>	Intensity <sup>b</sup>	Cross peak <sup>a</sup>	Intensity <sup>b</sup>
PheNH-TyrNH	w	TrpNH-TrpH $\beta$ 2.6	m
PheNH-YGlyNH	w	TrpNH-TrpH $\beta$ 2.8	m
PheNH-TrpNH	m	XGlyNH-PheH $\alpha$	s
PheNH-XGlyNH	m	XGlyNH-XGlyH $\alpha$ 3.3	m
PheNH-PheArH	m	XGlyNH-XGlyH $\alpha$ 4.0	m
PheNH-PheH $\alpha$	m	TrpH4-TrpH $\alpha$	w
PheNH-TrpH $\alpha$	vs	TrpH4-TrpH $\beta$ 2.6	m
PheNH-PheH $\beta$	m	TrpH4-TrpH $\beta$ 2.8	m
TyrNH-YGlyNH	m	PheArH-PheH $\beta$	m
TyrNH-XGlyNH	m	PheArH-PheH $\alpha$	m
TyrNH-TyrArH	m	TyrArH2,6-TyrH $\alpha$	vs
TyrNH-TyrH $\alpha$	m	TyrArH2,6-TyrH $\beta$ 2.6	s
TyrNH-XGlyH $\alpha$ 4.2	s	TyrArH2,6-TyrH $\beta$ 2.8	s
TyrNH-TyrH $\beta$ 2.7	m	TrpH2-TrpH $\alpha$	s
TyrNH-TyrH $\beta$ 2.9	m	TrpH2-TrpH $\beta$ 2.6	m
YGlyNH-TrpNH	vs	TrpH2-TrpH $\beta$ 2.8	m
YGlyNH-XGlyNH	w	PheH $\alpha$ -PheH $\beta$	s
YGlyNH-TyrH $\alpha$	vs	TrpH $\alpha$ -TrpH $\beta$ 2.6	m
YGlyNH-YGlyH $\alpha$ 3.6	m	TrpH $\alpha$ -TrpH $\beta$ 2.8	m
YGlyNH-YGlyH $\alpha$ 3.4	m	TyrH $\alpha$ -TyrH $\beta$ 2.6	m
TrpNH-XGlyNH	m	TyrH $\alpha$ -TyrH $\beta$ 2.8	m
TrpNH-TrpH $\alpha$	m		

<sup>a</sup> Stereochemistry has been omitted. <sup>b</sup> vs = very strong, s = strong, m = medium, w = weak

**Table S4.** Non-obvious ROESY cross-peaks observed for **15**.

Cross peak <sup>a</sup>	Intensity <sup>b</sup>	Cross peak <sup>a</sup>	Intensity <sup>b</sup>
PheNH-AspNH	s	AspNH-AspH $\alpha$	m
PheNH-PheArH	w	AspNH-PheH $\alpha$	m
PheNH-TrpH $\alpha$	vs	AspNH-PheH $\beta$ 3.0	w
PheNH-PheH $\alpha$	m	AspNH-PheH $\beta$ 2.9	w
PheNH-PheH $\beta$ 3.0	w	AspNH-AspH $\beta$ 2.7	m
PheNH-PheH $\beta$ 2.9	s	PheArH-PheH $\beta$ 3.0	s
TrpNH-TrpH2	w	PheArH-PheH $\beta$ 2.9	s
TrpNH-TrpH $\alpha$	m	PheArH-PheH $\alpha$	vs
TrpNH- $\beta$ -AlaH $\beta$ 3.2	w	TrpH2-TrpH $\alpha$	m
TrpNH-TrpH $\beta$ 2.9	m	TrpH2-PheH $\alpha$	w
TrpNH-TrpH $\beta$ 2.8	s	TrpH2-TrpH $\beta$ 2.9	m

TrpNH- $\beta$ -AlaH $\alpha$ 3.2	vs	TrpH2-TrpH $\beta$ 2.8	w
$\beta$ -AlaNH- $\beta$ -AlaH $\beta$ 3.4	m	TrpH $\alpha$ -TrpH $\beta$ 2.9	s
$\beta$ -AlaNH- $\beta$ -AlaH $\beta$ 3.2	s	TrpH $\alpha$ -TrpH $\beta$ 2.8	s
$\beta$ -AlaNH-AspH $\beta$ 2.7	vs	PheH $\alpha$ -PheH $\beta$ 3.0	vs
$\beta$ -AlaNH- $\beta$ -AlaH $\alpha$ 2.4	m	PheH $\alpha$ -PheH $\beta$ 2.9	s
$\beta$ -AlaNH-AspH $\beta$ 2.3	s	AspH $\alpha$ -AspH $\beta$ 2.7	s
$\beta$ -AlaNH- $\beta$ -AlaH $\alpha$ 2.1	m	AspH $\alpha$ -AspH $\beta$ 2.3	s
TrpH4-TrpH $\alpha$	m	$\beta$ -AlaH $\beta$ 3.4- $\beta$ -AlaH $\alpha$ 2.4	m
TrpH4-TrpH $\beta$ 2.9	m	$\beta$ -AlaH $\beta$ 3.4- $\beta$ -AlaH $\alpha$ 2.1	s
TrpH4-TrpH $\beta$ 2.8	s	$\beta$ -AlaH $\beta$ 3.2- $\beta$ -AlaH $\alpha$ 2.4	s
AspNH-TrpH $\alpha$	w	$\beta$ -AlaH $\beta$ 3.2- $\beta$ -AlaH $\alpha$ 2.1	m

<sup>a</sup> Stereochemistry has been omitted. <sup>b</sup> vs = very strong, s = strong, m = medium, w = weak

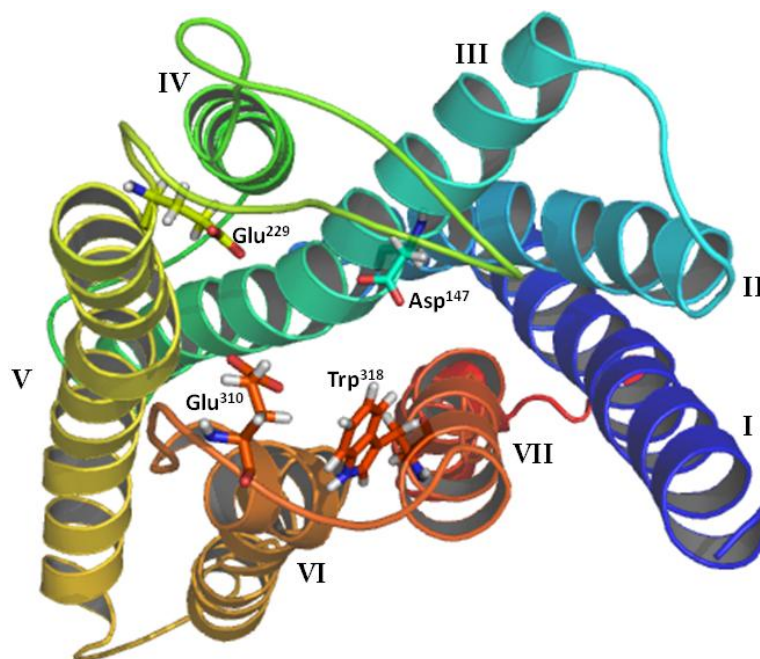


**Figure S1.** Top view of the MOR model, with the trans-membrane domains (ribbon) evidenced in different colors, numbered from I to VII, and the key-residues involved in the interaction with the ligands (stick).

**Table S5.** Residue contents and position of the MOR structural elements.

Domain Type	Position	Range	Length	Domain Type	Position	Range	Length
Loop	EL I	1 – 66	66	Loop	EL III	212 – 236	25
Transmembrane	TMH I	67 – 96	30	Transmembrane	TMH V	237 – 259	23
Loop	CL I	97 – 105	9	Loop	CL III	260 – 282	23
Transmembrane	TMH II	106 – 123	18	Transmembrane	TMH VI	283 – 305	23
Loop	EL II	124 – 145	22	Loop	EL IV	306 – 313	8
Transmembrane	TMH III	146 – 165	20	Transmembrane	TMH VII	314 – 330	17
Loop	CL II	166 – 195	30	Loop	CL IV	331 – 400	70
Transmembrane	TMH IV	196 – 211	16				

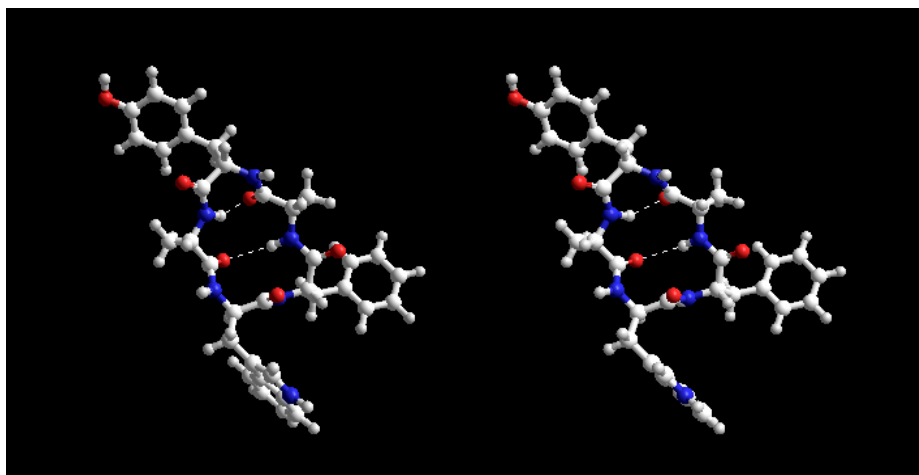


Figure S2. Stereoview of the in-solution structure 11a.

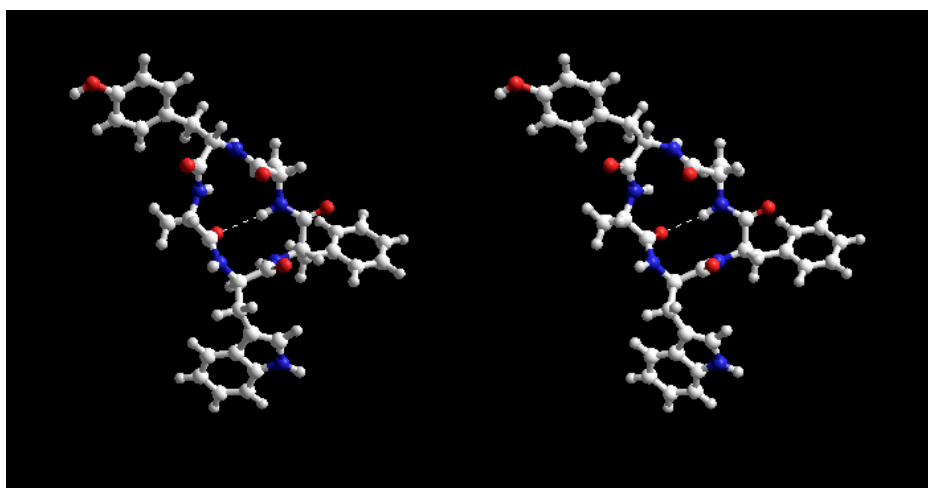


Figure S3. Stereoview of the in-solution structure 11b.

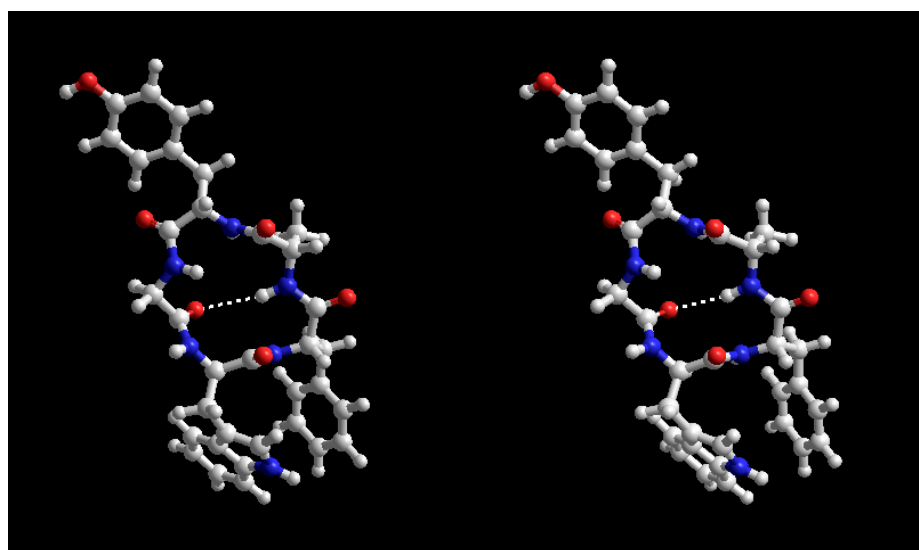


Figure S4. Stereoview of the in-solution structure 13c.

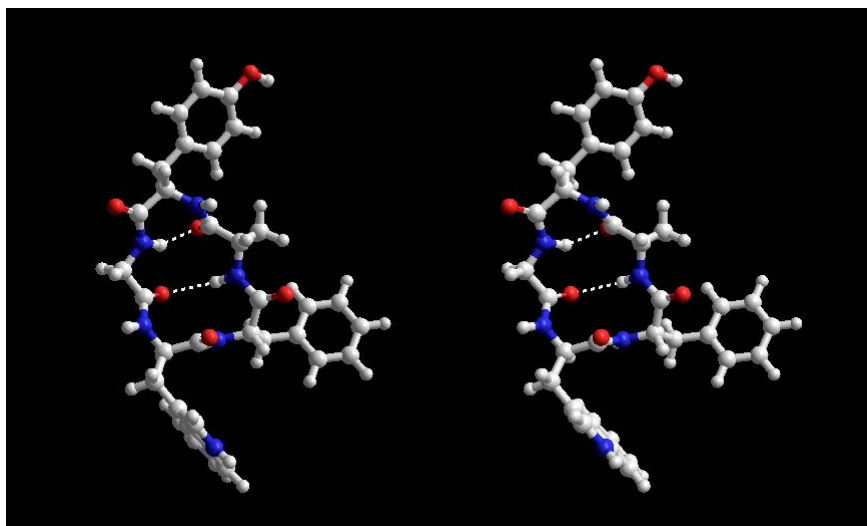


Figure S5. Stereoview of the in-solution structure 13d.

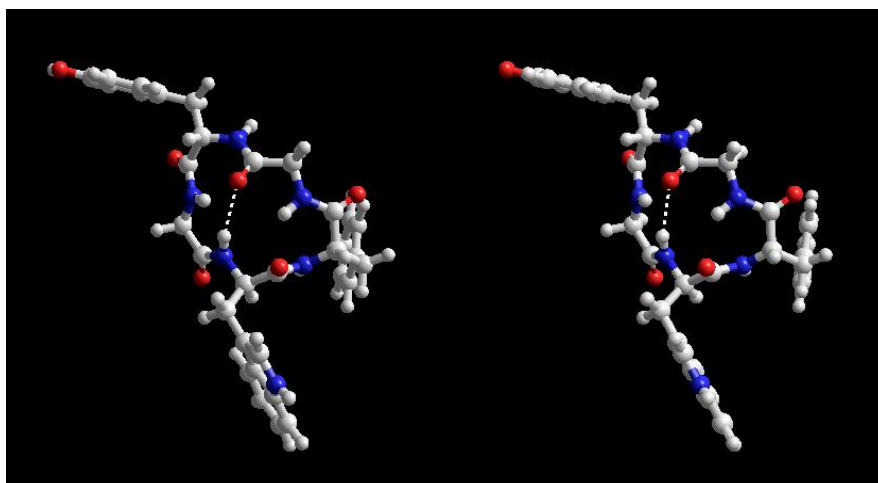


Figure S6. Stereoview of the in-solution structure 14a.

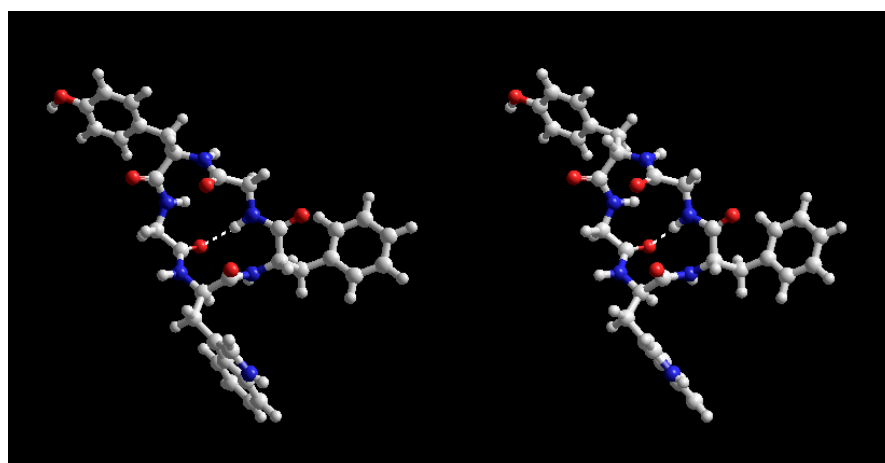
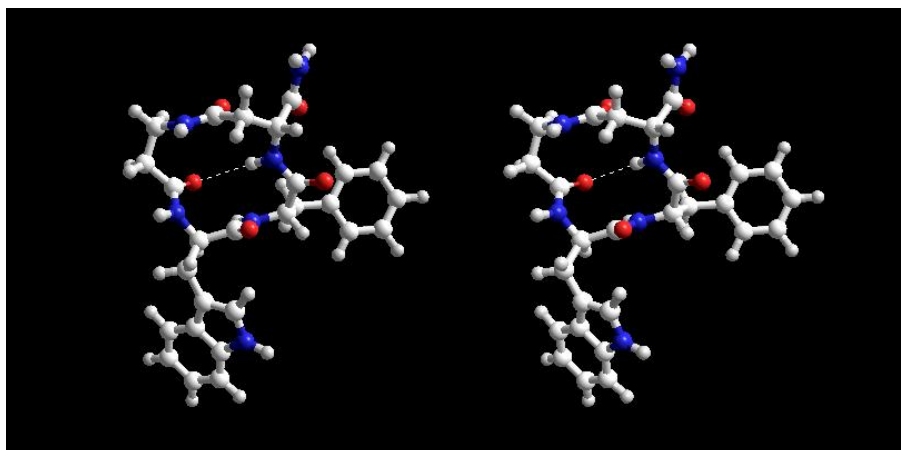
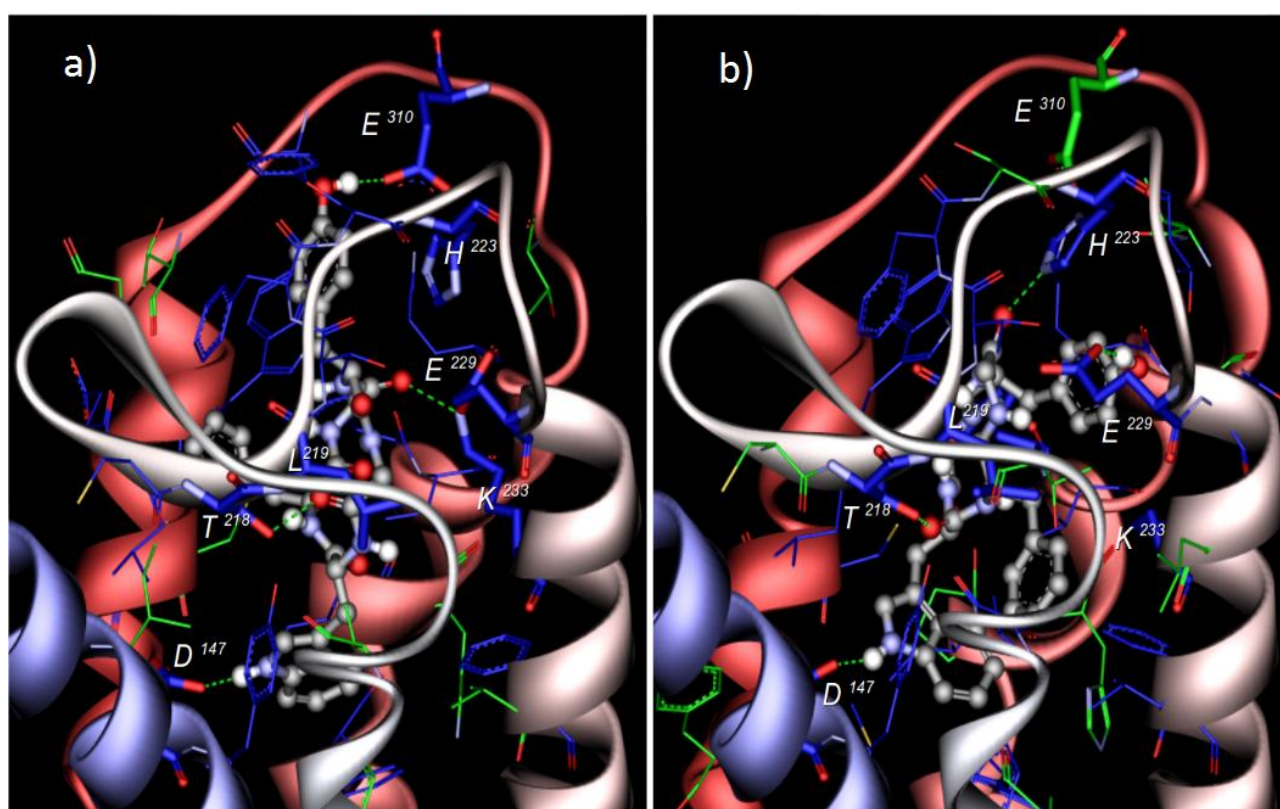


Figure S7. Stereoview of the in-solution structure 14b.



**Figure S8.** Stereoview of the in-solution structure **15**.



**Figure S9.** Rear view of the two top ranking docking orientations of **14** orientation 1 (a) and 2 (b) and the MOR binding site. The protein residues are represented in wireframe and sticks for the key-residues, with the C-atoms colored in blue for the residues in the first interaction shell,  $<3.5\text{\AA}$  from the ligand, green for those at a distance  $<5\text{\AA}$ ; the ligand is depicted by balls and cylinders (CPK). The figure highlights essential H-bond interactions (green dotted lines).

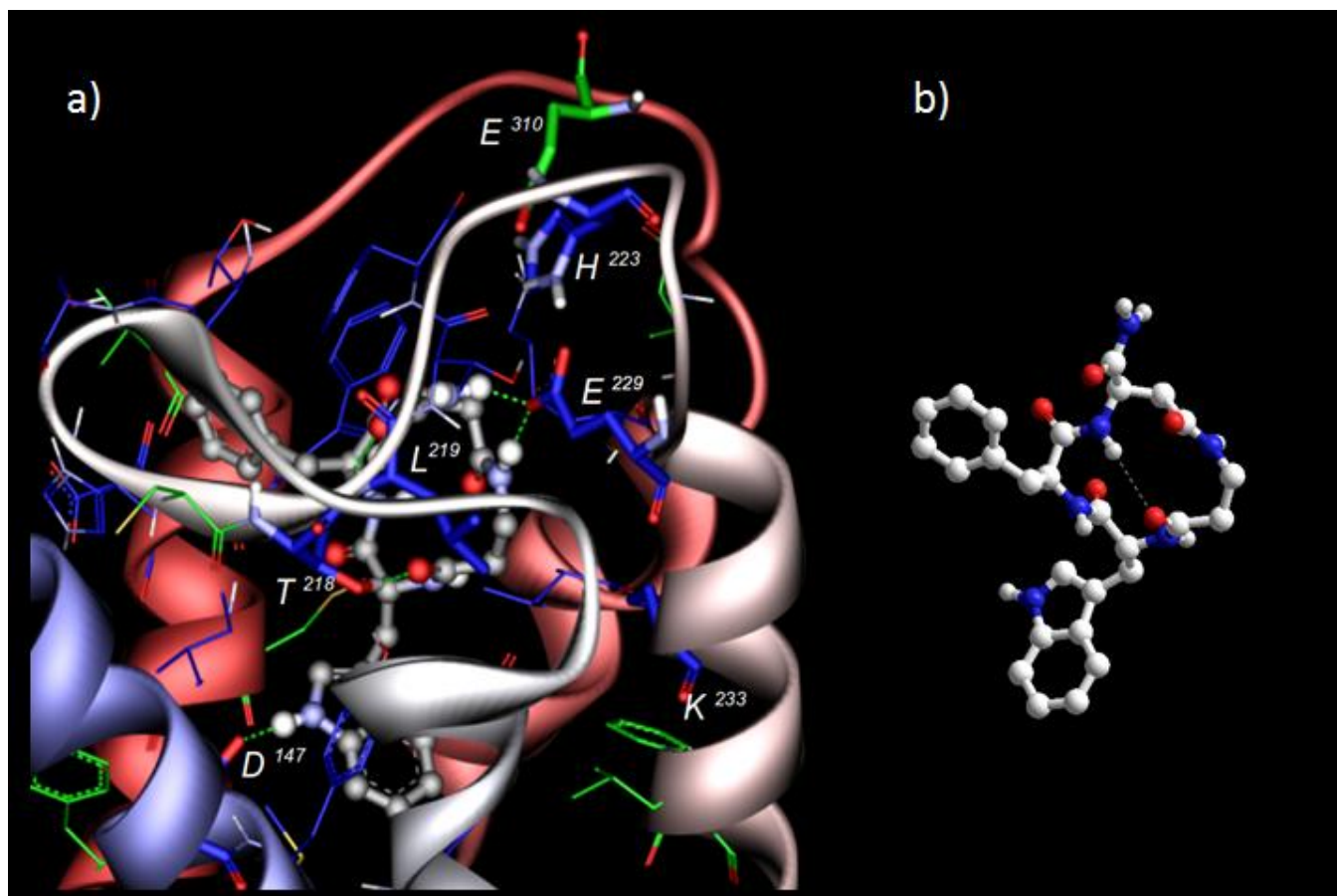


**Figure S10.** Rear view of the top-ranked docking pose of **15** (a) and the MOR binding site. Only selected MOR residues involved in the interactions are shown. The protein is represented in wireframe and sticks (for the key-residues), with the C-atoms colored in blue for the residues in the first interaction shell,  $<3.5\text{\AA}$  from the ligand, green for those at a distance  $<5\text{\AA}$ ; the ligand is depicted by balls and cylinders (CPK). The figure highlights the essential interactions between the MOR and the CONH<sub>2</sub> (upper part) and indole (lower part) fragments of **15**. Rear view of the in-solution conformation of **15** (b) in balls and cylinders.

**Table S6.** List of MOR residues involved in the interaction with compound **14** orientation (or) 1 & 2 and **15**, classified according to their structural elements. In the table, the Xs represents the contacts in the ligand-MOR complex at a distance  $<5\text{\AA}$ .

region	residue	15	14-or 1	14-or 2	region	residue	15	14-or 1	14-or 2
TMH III	Asp147	x	x	x	TMH V	Phe237	x	x	x
	Tyr148	x	x	x	TMH VI	Trp293	x	x	x
	Met151	x	x	Pro295					x
	Phe152	x	x	Ile296		x	x	x	
	Ile155			His297		x	x		
TMH IV	Ile198			x	Tyr299	x	x	x	
	Val202			x	Val300	x	x	x	
EL III	Gln212	x			Ile301			x	
	Gly213	x			Lys303	x	x	x	x
	Ser214	x			Ala304	x	x	x	x

Ash216	x	x		EL IV	Ile306		x	
Cys217	x				Thr307	x	x	x
Thr218	x	x	x		Glu310	x	x	x
Leu219	x	x	x		Thr311		x	
Thr220	x	x	x		Phe313		x	
Phe221	x	x	x	TMH VII	Thr315	x		
His223	x	x	x		Trp318	x	x	x
Glu229	x	x	x		His319	x	x	
Asn230			x		Cys321			x
Leu232			x		Ile322	x	x	x
Lys233	x	x	x		Tyr326			x

## References

- [1] J. E. Zadina, L. Hackler, L.-J. Ge, A. J. Kastin, *Nature* **1997**, 386, 499–502.
- [2] J. Fichna, A. Janecka, J. Costentin, J.-C. Do Rego, *Pharmacol. Rev.* **2007**, 59, 88–123.
- [3] a) A. Keresztes, A. Borics, G. Tóth, *ChemMedChem*. **2010**, 5, 1176–1196; b) A. Janecka, R. Staniszevska, J. Fichna, *Curr. Med. Chem.* **2007**, 14, 3201–3208.
- [4] L. Gentilucci, *Curr. Top. Med. Chem.* **2004**, 4, 19–38.
- [5] a) V. J. Hruby, R. S. Agnes, *Biopolymers* **1999**, 51, 391–410; b) L. Gentilucci, A. Tolomelli, *Curr. Top. Med. Chem.* **2004**, 4, 105–121.
- [6] M. Eguchi, *Med. Res. Rev.* **2004**, 24, 182–212.
- [7] a) L. Dosen-Micovic, M. Ivanovic, V. Micovic, *Bioorg. Med. Chem.* **2006**, 14, 2887–2895; b) G. Subramanian, M. G. Paterlini, P. S. Portoghese, D. M. Ferguson, *J. Med. Chem.* **2000**, 43, 381–391.
- [8] Some outstanding examples: a) B. S. Vig, T. F. Murray, J. V. Aldrich, *J. Med. Chem.* **2003**, 46, 1279–1282; b) Y. Lu, T. M.-D. Nguyen, G. Weltrowska, I. Berezowska, C. Lemieux, N. N. Chung, P. W. Schiller, *J. Med. Chem.* **2001**, 44, 3048–3053; c) P. W. Schiller, G. Weltrowska, T. M.-D. Nguyen, C. Lemieux, N. N. Chung, Y. Lu, *Life Sci.* **2003**, 73, 691–698; d) G. Weltrowska, Y. Lu, C. Lemieux, N. N. Chung, P. W. Schiller, *Bioorg. Med. Chem. Lett.* **2004**, 14, 4731–4733.
- [9] L. Gentilucci, F. Squassabia, R. Artali, *Curr. Drug Targets* **2007**, 8, 185–196.
- [10] M. Eguchi, R. Y. Shen, J. P. Shea, M. S. Lee, M. Kahn, *J. Med. Chem.* **2002**, 45, 1395–1398.
- [11] B. L. Roth, K. Baner, R. Westkaemper, D. Siebert, K. C. Rice, S. Steinberg, P. Ernsberger, R. B. Rothman, *Proc. Natl. Acad. Sci. USA* **2002**, 99, 11934–11939.
- [12] G. Cardillo, L. Gentilucci, A. Tolomelli, R. Spinosa, M. Calienni, A. R. Qasem, S. Spampinato, *J. Med. Chem.* **2004**, 47, 5198–5203.
- [13] G. Weltrowska, N. N. Chung, C. Lemieux, J. Guo, I. Lu, B. C. Wilkes, P. W. Schiller, *J. Med. Chem.* **2010**, 53, 2875–2881.
- [14] a) F. Yan, P. D. Mosier, R. B. Westkaemper, J. Stewart, J. K. Zjawiony, T. A. Vortherms, D. J. Sheffler, B. L. Roth, *Biochemistry* **2005**, 44, 8643–8651; b) B. E. Kane, C. R. McCurdy, D. M. Ferguson, *J. Med. Chem.* **2008**, 51, 1824–1830; c) L. Gentilucci, F. Squassabia, R. De Marco, R. Artali, G. Cardillo, A. Tolomelli, S. Spampinato, A. Bedini, *FEBS J.* **2008**, 275, 2315–2337.
- [15] A. Bedini, M. Baiula, L. Gentilucci, A. Tolomelli, R. De Marco, S. Spampinato, *Peptides* **2010**, 31, 2135–2140.
- [16] S. Spampinato, A. Qasem, M. Calienni, G. Murari, L. Gentilucci, A. Tolomelli, G. Cardillo, *Eur. J. Pharmacol.* **2003**, 469, 89–95.
- [17] A. M. Davis, S. J. Teague, *Angew. Chem.* **1999**, 111, 778–792; *Angew. Chem. Int. Ed.* **1999**, 38, 736–749.
- [18] H. Kessler, *Angew. Chem.* **1982**, 94, 509–520; *Angew. Chem. Int. Ed. Engl.* **1982**, 21, 512–523.
- [19] a) S. J. Stradley, J. Rizo, M. D. Bruch, A. N. Stroup, L. M. Gierasch, *Biopolymers* **1990**, 29, 263–287; b) H. Weisshoff, T. Wieprecht, P. Henklein, C. Frömmel, C. Antz, C. Mge, *FEBS Lett.* **1996**, 387, 201–207.

- [20] a) J. Wermuth, L. Goodman, A. Jonczyk, H. Kessler, *J. Am. Chem. Soc.* **1997**, 119, 1328–1335; b) H. Weisshoff, C. Prsang, P. Henklein, C. Frçmmel, A. Zschunke, C. Mgge, *Eur. J. Biochem.* **1999**, 259, 776–788; c) C. Paulitz, W. Steglich, *J. Org. Chem.* **1997**, 62, 8474–8478.
- [21] a) H. Heller, M. Sukopp, N. Tsomaia, M. John, D. F. Mierke, B. Reif, H. Kessler, *J. Am. Chem. Soc.* **2006**, 128, 13806–13814; b) L. Gentilucci, A. Tolomelli, F. Squassabia, *Protein Pept. Lett.* **2007**, 14, 51–56.
- [22] Solid-Phase Synthesis: A Practical Guide, (Eds.: S. A. Kates, F. Albericio), Marcel Dekker Inc., New York, **2001**.
- [23] a) C. Harrison, S. McNulty, D. Smart, D. J. Rowbotham, D. K. Grandy, L. A. Devi, D. G. Lambert, *Br. J. Pharmacol.* **1999**, 128, 472–478; b) L. Toll, *J. Pharmacol. Exp. Ther.* **1995**, 273, 721–727.
- [24] H. Schmidt, S. Vormfelde, K. Klinder, U. Gundert-Remy, C. H. Gleiter, G. Skopp, R. Aderjan, U. Fuhr, *Pharmacol. Toxicol.* **2002**, 91, 57–63.
- [25] J. A. Clark, G. W. Pasternak, *Neuropharmacology* **1988**, 27, 331–332.
- [26] J. Gong, J. A. Strong, S. Zhang, X. Yue, R. N. DeHaven, J. D. Daubert, J. A. Cassel, G. Yu, E. Mansson, L. Yu, *FEBS Lett.* **1998**, 439, 152–126.
- [27] a) L. J. Sim, Q. Liu, S. R. Childers, D. E. Selley, *J. Neurochem.* **1998**, 70, 1567–1576; b) A. Z. R\_nai, M. Al-Khrasani, S. Benyhe, I. Lengyel, L. Kocsis, G. Orosz, E. Kat\_, L. T\_thfalusi, *Peptides* **2006**, 27, 1507–1513.
- [28] M. Spetea, K. Monory, C. Tçmbçly, G. T\_th, E. Tzavara, S. Benyhe, J. Hanoune, A. Borsodi, *Biochem. Biophys. Res. Commun.* **1998**, 250, 720–725.
- [29] P. A. Temussi, D. Picone, G. Saviano, P. Amodeo, A. Motta, T. Tancredi, S. Salvadori, R. Tomatis, *Biopolymers* **1992**, 32, 367–372, and references herein.
- [30] A. Borics, G. Toth, *J. Mol. Graph. Modell.* **2010**, 28, 495–505.
- [31] C. Toniolo, *CRC Crit. Rev. Biochem.* **1980**, 9, 1–44.
- [32] HyperChem (release 8.0.3), Hypercube Inc., Gainesville, FL (USA), **2007**: <http://www.hyper.com/> (accessed June 1, 2011).
- [33] W. D. Cornell, P. Cieplak, C. I. Bayly, I. R. Gould, K. M. Merz, D. M. Ferguson, D. C. Spellmeyer, T. Fox, J. W. Caldwell, P. A. Kollman, *J. Am. Chem. Soc.* **1995**, 117, 5179–5197.
- [34] W. L. Jorgensen, J. Chandrasekhar, J. Madura, R. W. Impey, M. L. Klein, *J. Chem. Phys.* **1983**, 79, 926–935.
- [35] G. M. Morris, R. Huey, W. Lindstrom, M. F. Sanner, R. K. Belew, D. S. Goodsell, A. J. Olson, *J. Comput. Chem.* **2009**, 30, 2785–2791.
- [36] a) C. Het\_nyi, D. van der Spoel, *FEBS Lett.* **2006**, 580, 1447–1450; b) O. Dym, I. Xenarios, H. Ke, J. Colicelli, *Mol. Pharmacol.* **2002**, 61, 20–25.
- [37] X. Liu, M. Kai, L. Jin, R. Wang, *Bioorg. Med. Chem. Lett.* **2009**, 19, 5387–5391.
- [38] a) H. I. Mosberg, C. B. Fowler, *J. Pept. Res.* **2002**, 60, 329–335; b) C. B. Fowler, I. D. Pogozheva, A. L. Lomize, H. LeVine, H. I. Mosberg, *Biochemistry* **2004**, 43, 15796–15810.
- [39] R. E. Dolle, M. Michaut, B. Martinez-Teipel, P. R. Seida, C. W. Ajello, A. L. Muller, R. N. DeHaven, P. J. Carroll, *Bioorg. Med. Chem. Lett.* **2009**, 19, 3647–3650.

- [40] T. Saito, H. Hirai, Y. J. Kim, Y. Kojima, Y. Matsunaga, H. Nishida, T. Sakakibara, O. Suga, T. Sujaku, N. Kojima, *J. Antibiot.* **2002**, 55, 847–854.
- [41] J. D. Urban, W. P. Clarke, M. von Zastrow, D. E. Nichols, B. Kobilka, H. Weinstein, J. A. Javitch, B. L. Roth, A. Christopoulos, P. M. Sexton, K. J. Miller, M. Spedding, R. B. Mailman, *J. Pharmacol. Exp. Ther.* **2007**, 320, 1–13.
- [42] Y. Cheng, W. H. Prusoff, *Biochem. Pharmacol.* **1973**, 22, 3099–3108.
- [43] H. J. C. Berendsen, J. P. M. Postma, W. F. van Gunsteren, A. Di Nola, J. R. Haak, *J. Chem. Phys.* **1984**, 81, 3684–3690.
- [44] L. Kalchauer, R. Skeel, M. Bhandarkar, R. Brunner, A. Gursoy, N. Krawetz, J. Phillips, A. Shinozaki, K. Varadarajan, K. Schulten, *J. Comput. Phys.* **1999**, 151, 283–312.
- [45] E. F. Pettersen, T. D. Goddard, C. C. Huang, G. S. Couch, D. M. Greenblatt, E. C. Meng, T. E. Ferrin, *J. Comput. Chem.* **2004**, 25, 1605–1612.
- [46] PyMOL Molecular Graphics System (version 1.2r1), W. L. DeLano, DeLano Scientific, San Carlos, CA (USA), 2002: <http://www.pymol.org> (accessed June 1, 2011).
- [47] Persistence of Vision Raytracer (POV-Ray) ver. 3.6, Persistence of Vision Pty. Ltd., Williamstown, VIC (Australia), 2004: <http://www.povray.org/>(accessed June 1, 2011).
- [48] Ghemical (version 2.00), A. Acton, M. Banck, J. Brufford, M. Cruz, D. Curtis, T. Hassinen, V. Heikkilä, G. Hutchison, J. Huuskonen, J. Jensen, R. Liboska, C. Rowley: <http://www.uku.fi/~thassine/projects/ghemical/> (accessed June 1, 2011); [T. Hassinen, M. Perkkylä, *J. Comput. Chem.* **2001**, 22, 1229–1242].
- [49] MOPAC2009, J. J. P. Stewart, Stewart Computational Chemistry, Colorado Springs, CO (USA), **2008**: <http://OpenMOPAC.net> (accessed June 1, 2011).
- [50] M. Yoneya, H. J. C. Berendsen, K. A. Hirasawa, *Mol. Simul.* **1994**, 13, 395–405.
- [51] Collaborative Computational Project Number 4, “The CCP4 Suite: Programs for Protein Crystallography”, *Acta Crystallogr. Sect. D Biol. Crystallogr.* **1994**, 50, 760–763.
- [52] Gaussian 03, Revision A.1: M. J. Frisch, G. W. Trucks, H. B. Schlegel, G. E. Scuseria, M. A. Robb, J. R. Cheeseman, J. A. Montgomery, Jr., T. Vreven, K. N. Kudin, J. C. Burant, J. M. Millam, S. S. Iyengar, J. Tomasi, V. Barone, B. Mennucci, M. Cossi, G. Scalmani, N. Rega, G. A. Petersson, H. Nakatsuji, M. Hada, M. Ehara, K. Toyota, R. Fukuda, J. Hasegawa, M. Ishida, T. Nakajima, Y. Honda, O. Kitao, H. Nakai, M. Klene, X. Li, J. E. Knox, H. P. Hratchian, J. B. Cross, C. Adamo, J. Jaramillo, R. Gomperts, R. E. Stratmann, O. Yazyev, A. J. Austin, R. Cammi, C. Pomelli, J. W. Ochterski, P. Y. Ayala, K. Morokuma, G. A. Voth, P. Salvador, J. J. Dannenberg, V. G. Zakrzewski, S. Dapprich, A. D. Daniels, M. C. Strain, O. Farkas, D. K. Malick, A. D. Rabuck, K. Raghavachari, J. B. Foresman, J. V. Ortiz, Q. Cui, A. G. Baboul, S. Clifford, J. Cioslowski, B. B. Stefanov, G. Liu, A. Liashenko, P. Piskorz, I. Komaromi, R. L. Martin, D. J. Fox, T. Keith, M. A. Al-Laham, C. Y. Peng, A. Nanayakkara, M. Challacombe, P. M. W. Gill, B. Johnson, W. Chen, M. W. Wong, C. Gonzalez, J. A. Pople, Gaussian Inc., Pittsburgh, PA (USA), **2003**.

## Chapter 7

# A Simple Route Towards Peptide Analogues Containing Substituted (S)- or (R)-Tryptophans

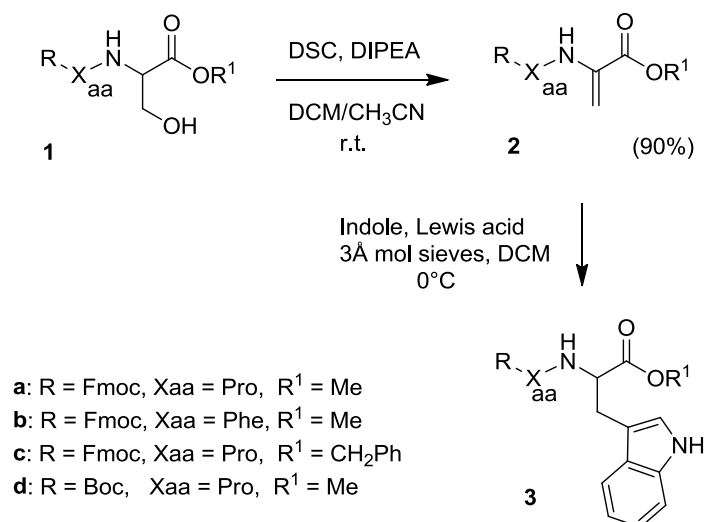
---

### 7. Introductyion

Peptides based on natural amino acids are widely used as therapeutic agents<sup>[1]</sup>. However, their efficacy is hampered by several problems, in particular high conformational flexibility, low in vivo stability against proteolysis and scarce ability to cross biological barriers, resulting in poor receptor selectivity, short duration of action and poor bioavailability. The preparation of unusual amino acids and their introduction in peptide sequences have attracted considerable interest to overcome the pharmacological limitations of bioactive peptides<sup>[1,2]</sup>. Modification of individual amino acids has been shown to be responsible for changes in peptide conformation and for increased enzymatic stability<sup>[3]</sup>. Besides, the introduction of modified amino acids has been utilized for the elucidation of an individual residue's biological function<sup>[3,4]</sup>. In connection with on going projects<sup>[5]</sup> on the synthesis, conformational analysis and pharmacological behaviour of endomorphin-1<sup>[6]</sup> (H Tyr-Pro-Trp-Phe-NH<sub>2</sub>) analogues as potential drugs for pain management<sup>[7]</sup>, we have been interested in the preparation of new peptide derivatives containing modified tryptophans. Several examples of tryptophans bearing substituent on the indole ring can be found in complex structures. For instance, halotryptophans are present in peptides of microbial<sup>[8]</sup> or marine origins<sup>[9]</sup>. A few preparations of (S)- or (R)-Trp analogues have been reported in the literature<sup>[10]</sup>. Halotryptophans can be obtained by palladium-mediated heteroannulation of a chiral auxiliary<sup>[11]</sup>; by electrochemical oxidation of proline followed by Fischer indole synthesis<sup>[12]</sup>; from serine, by means of the lysate of a commercially available microorganism containing tryptophan synthase<sup>[13]</sup>. (S)- and (R)-Br-tryptophans have been obtained with L-aminoacylase or D-aminoacylase<sup>[14]</sup>. More often, reactions lead to the preparation of racemates. Very recently, the regioselective electrophilic substitution of indoles with *N*-acetyl dehydroalanine (Dha), promoted by different transition metal salts, provided an efficient protocol towards racemic-functionalized tryptophans<sup>[15]</sup>. In this context, we envisaged the opportunity to develop a simple procedure to synthesize modified (S)- or (R)-tryptophans within a peptide sequence. Herein, we report our results on the Friedel-Crafts alkylation of indoles<sup>[15,16]</sup> with dipeptides containing dehydroalanine (Xaa-Dha) in the presence of different Lewis acids. Further, to endorse the methodology, we describe the preliminary synthesis in a few steps of two novel endomorphin-1<sup>[6]</sup> analogues, [(S)-2-MeTrp]-endomorphin-1 and [(R)-2-MeTrp]-endomorphin-1. Among the different endogenous opioid peptides<sup>[1]</sup>, endomorphin-1 is unique for high receptor affinity and selectivity, being considered the endogenous agonist of the  $\mu$ -opioid receptor (MOR). Since none of the other naturally occurring opioid peptides contain a Trp in the sequence, the preparation and pharmacological assay of endomorphin-1 analogues containing modified Trp in position 3 could be of help to investigate the role of this pharmacophore in ligand-receptor recognition<sup>[17]</sup>. Besides, the presence of substituted Trp can also enhance lipophilicity and blood-brain barrier (BBB) permeability of peptide active towards the CNS<sup>[18]</sup>.

## 7.1. Results and discussion

As anticipated in the introduction, indoles undergo Friedel-Crafts (F-C) alkylation with N-Ac-Dha methyl ester in the presence of Lewis acids, giving racemic 3-indolyl- $\alpha$ -amino acids<sup>[15]</sup>. Since we were interested in optically pure amino acids, we thought to carry out a diastereoselective version of this reaction with dipeptides of type Xaa-Dha, taking advantage of the asymmetric induction exerted by Xaa. The protected dipeptides Xaa-Dha **2** were easily obtained from dipeptides Xaa-serine **1**, prepared in turn by standard in-solution peptide synthesis, using 1-ethyl-3-[3-dimethylaminopropyl] carbodiimide hydrochloride (EDC-HCl) and 1-hydroxybenzotriazole hydrate (HOBt) as activating agents (Supplementary data). The dehydration of **1** with N,N-disuccinimidyl carbonate (DSC) and N,N-diisopropylethylamine (DIPEA) gave **2** in very good yield<sup>[19]</sup>, isolated by flash chromatography over silica gel (Scheme 1). Initially, the reaction was tested with indole. The treatment of Pro-Dha **2a** with a Lewis acid and indole, in the presence of 3 Å molecular sieves, afforded the protected dipeptide Pro-Trp **3a** as a mixture of diastereoisomers (Scheme 1). Yields and diastereomeric ratios strongly varied depending on the Lewis acid selected (Table 1). In the absence of molecular sieves, the reaction gave variable quantities of by-products arising from peptide bond and/or ester hydrolysis, as revealed by reversed phase (RP)-HPLC and electron-spray (ES)-MS analyses. On the other hand, molecular sieves lead to better yields, while the unreacted starting material was recovered unaltered. The diastereomeric ratios of the reaction mixtures (Table 1) were measured by normal phase-HPLC, with an analytical Kromasil Diol column. The separation of the diastereoisomers by analytical RP-HPLC under different conditions was unfeasible. Racemization was excluded on the basis of chiral HPLC by using a CHIRALPAK IC column. The configuration of the newly created stereocentre on Trp was determined by comparison with that of the authentic samples of (S,S)-**3a** and (S,R)-**3a**, prepared by standard peptide synthesis in solution from the commercially available amino acids. Yields (Table 1) were determined after isolation by flash chromatography over silica gel. The use of 1 equiv of ZnOTf<sub>2</sub>, FeCl<sub>3</sub>, InF<sub>3</sub>, CeCl<sub>3</sub>, RuCl<sub>3</sub> and Yb(OTf)<sub>3</sub> gave no reaction or traces of the dipeptide **3a**. Other Lewis acids, MgBr<sub>2</sub>, BBU<sub>2</sub>OTf, TiCl<sub>4</sub>, Cu(OTf)<sub>2</sub>, Sc(OTf)<sub>3</sub>, ZrCl<sub>4</sub>, AlEtCl<sub>2</sub> and AlEt<sub>2</sub>Cl (1 equiv), gave the product **3a** in low yields (<5%, data not shown). All reactions were carried out at 0 °C for 24 h in dichloromethane (DCM). Increasing time and temperature gave negligible improvements. The only exception was Yb(OTf)<sub>3</sub>; indeed, performing the reaction with 1 equiv of Yb(OTf)<sub>3</sub> at 80 °C in dichloroethane (DCE) for 24 h, **3a** was obtained in 20% yield (entry 1) and when the reaction was conducted under microwave (MW) irradiation (400 W) for 3.5 h, yield increased up to 55%, with a satisfactory 22/78 diastereomeric ratio in favour of (S,R)-**3a** (entry 2).



**Scheme 1.** Synthesis of the protected dipeptides Xaa-Dha **2a-d** and Lewis acid-induced F.-C. alkylation of indole.

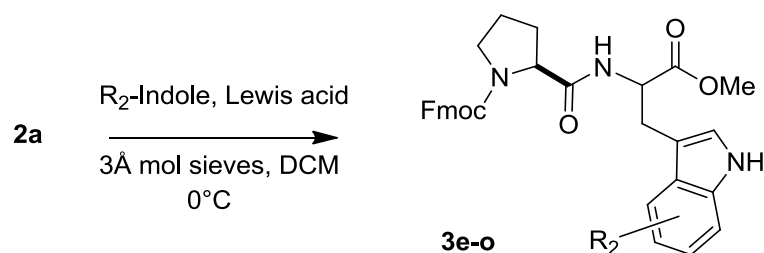
Making use of a catalytic amount of Yb(OTf)<sub>3</sub> led to a drop of the yield, while the use of an excess seemed inexpedient, for the high molecular weight of such Lewis acid. Reactions with MgBr<sub>2</sub>, BBu<sub>2</sub>OTf, TiCl<sub>4</sub>, Cu(OTf)<sub>2</sub>, Sc(OTf)<sub>3</sub> and ZrCl<sub>4</sub> were slightly improved by increasing the amount of Lewis acid (yields 5–25%, Table 1, entries 3–8).

**Table 1.** Synthesis of dipeptides Xaa-Trp **3a-d** by F.-C. reaction of indole with dipeptides Xaa-Dha **2a-d** promoted by different Lewis acids, at 0°C for 24h in DCM (with the exception of Entries 1, 2).

Entry	Lewis acid	Equiv.	<b>3</b>	Yield (%) <sup>[c]</sup>	S,S/S,R
1	Yb(OTf) <sub>3</sub> <sup>[a]</sup>	1	<b>a</b>	20	-
2	Yb(OTf) <sub>3</sub> <sup>[b]</sup>	1	<b>a</b>	55	22/78
3	MgBr <sub>2</sub>	4	<b>a</b>	5	-
4	BBu <sub>2</sub> OTf	2	<b>a</b>	5	-
5	TiCl <sub>4</sub>	4	<b>a</b>	15	-
6	CuOTf <sub>2</sub>	2	<b>a</b>	10	-
7	ScOTf <sub>3</sub>	2	<b>a</b>	10	-
8	ZrCl <sub>4</sub>	2	<b>a</b>	25	-
9	AlEtCl <sub>2</sub>	3.5	<b>a</b>	70	50/50
10	AlEt <sub>2</sub> Cl	3.5	<b>a</b>	60	24/76
11	AlEtCl <sub>2</sub>	3.5	<b>b</b>	65	45/55
12	AlEt <sub>2</sub> Cl	3.5	<b>b</b>	55	35/65
13	AlEtCl <sub>2</sub>	3.5	<b>c</b>	65	55/45
14	AlEt <sub>2</sub> Cl	3.5	<b>c</b>	55	62/38
15	AlEtCl <sub>2</sub>	3.5	<b>d</b>	55	50/50
16	AlEt <sub>2</sub> Cl	3.5	<b>d</b>	35	30/70

<sup>[a]</sup> DCE, reflux. <sup>[b]</sup> DCE, MW, 400 W. <sup>[c]</sup> After isolation by flash chromatography over silica-gel.

Finally, in the presence of an excess of AlEtCl<sub>2</sub> (3.5 equiv)<sup>15</sup> the reaction gave the desired dipeptide **3a** in reasonable yield, after isolation by flash chromatography over silica gel, albeit with a disappointing 50/50 diastereomeric ratio (entry 9). On the other hand, in the presence of AlEt<sub>2</sub>Cl (3.5 equiv) the reaction gave lesser amount of **3a**, but with a reasonable 24/76 diastereomeric ratio, in favour of the (S,R)-**3a** stereoisomer (entry 10). The eventual effect of the residue Xaa preceding Dha and the protecting groups R, R1 on yield and stereoselectivity was examined. The reaction of indole with the dipeptide Phe-Dha **2b** occurred with comparable yield, but with lower stereoselectivity (entries 11 and 12). Changing the methyl ester with a benzyl ester (**2c**) lead to a moderate stereoselectivity, in favour of the isomer (S,S)-**3c** (entries 13 and 14). The presence of a Boc-protecting group (**2d**) instead of Fmoc gave lower yield and selectivity (entries 15 and 16). The configuration of Trp in the dipeptides **3b–d** was determined by comparison with authentic samples, prepared by standard peptide synthesis in solution. Interestingly, apart from the slightly different yields, changing the ester allowed preparing preferentially the dipeptides containing either (S)-Trp or (R)-Trp. Besides, the analysis of the crude reaction mixtures revealed no trace of concurrent  $\alpha$ -amidoalkylation reaction<sup>[15,20]</sup>. The reaction of **2a** with substituted indoles in the presence of 3.5 equiv of AlEt<sub>2</sub>Cl or AlEtCl<sub>2</sub> (Scheme 2) was performed at 0°C for 24 h in DCM and in the presence of 3 Å molecular sieves (Supplementary data). The reaction afforded the dipeptides **3e–o** (Table 2). For the moment, we were mainly interested in verifying the applicability of the procedure to diverse kinds of indoles, therefore the diastereoselectivity issue was not faced in detail. The absolute configurations of the diastereoisomers were determined by comparison of the chiral-HPLC analyses with that of **3a**.



**Scheme 2.** Synthesis of the dipeptides **3e–o** by Lewis acid-induced F.-C. alkylation of substituted indoles.

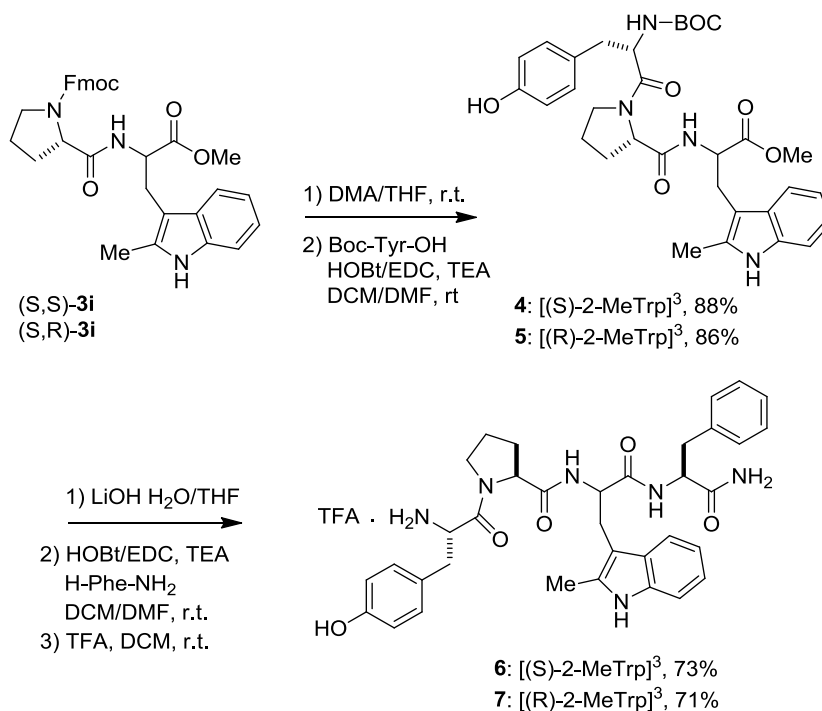
The reaction of **2a** with 5-fluoroindole promoted by AlEtCl<sub>2</sub> (entry 1) or AlEt<sub>2</sub>Cl (entry 2) gave **3e** in sufficient yield, albeit only AlEt<sub>2</sub>Cl ensured acceptable stereoselectivity. The reaction of **2a** and 5'-chloro indole or 5'-bromoindole with AlEtCl<sub>2</sub> proceeded in lower yields of **3f** and **3g**, respectively (entries 3 and 4), while AlEt<sub>2</sub>Cl was almost ineffective. In a similar way, **2a** reacted with 1-methylindole in the presence of AlEtCl<sub>2</sub> affording **3h** (entry 5) with scarce selectivity. The reaction with 2-methylindole in the presence of AlEtCl<sub>2</sub> (entry 6) or AlEt<sub>2</sub>Cl (entry 7) gave **3i** in excellent yields. 7-Methylindole, 2'-methyl-7'-bromoindole, 2'-methyl-5'-bromoindole and 2-aminophenylindole gave **3l**, **3m**, **3n** and **3o**, respectively (entries 8–11), in sufficient to good yields. Finally, 5-nitroindole scarcely reacted with **2a** giving **3p** (entry 12), while 2-benzylsulfonylindole gave only traces of the corresponding product (not shown). In addition, we confirmed that changing the methyl ester with a benzyl ester gave a moderate switch of stereoselectivity, from (S,R) to (S,S), also with some substituted indoles. Indeed, the reaction of 5'-F-indole with **2c** in the presence of AlEt<sub>2</sub>Cl, under the

same conditions reported for **2a**, gave the 5'-F-Trp containing dipeptide in 55% yield and 65/35 d.r., while 2'-Me-indole gave the corresponding product in 70% yield with the same d.r. In order to validate the procedure as a facile access to analogues containing modified Trp in either (S) or (R) configuration, we synthesized in a few steps the unprecedented analogues of endomorphin-1 **6** and **7**, containing (S)-2'-MeTrp and (R)-2'-MeTrp, respectively (Scheme 3). The endomorphin analogues **6** and **7** were obtained from the dipeptides (S,S)-**3i** and (S,R)-**3i**, obtained in turn by alkylation of 2-methylindole with **2a** (Table 2, entry 6). The identities of all the intermediates were confirmed by ES-MS analyses. Purities were determined by RP-HPLC and by normal phase HPLC. After separation by flash chromatography over silica gel, (S,S)-**3i** (41%) and (S,R)-**3i** (49%) were quantitatively deprotected by treatment with 2 M DMA in THF and reacted without prior purification with Boc-Tyr-OH in the presence of HOBt/EDC. The tripeptides Boc-Tyr- Pro-[(S)-2-MeTrp]-OMe, or Boc-Tyr-Pro-[(R)-2-MeTrp]-OMe, were isolated in high yield by flash chromatography over silica gel. The tripeptides were treated with LiOH in H<sub>2</sub>O/THF and the resulting tripeptide acids were utilized without further purification.

**Table 2.** Synthesis of dipeptides **3e-p** by F.C. reaction of substituted indoles with **2a**, promoted by 3.5 equiv. of Lewis acids, at 0°C for 24h in DCM.

Entry	R <sub>2</sub>	Lewis acid	<b>3</b>	Yield (%) <sup>[a]</sup>	S,S/S,R
1	5'-F	AlEtCl <sub>2</sub>	<b>e</b>	65	45/55
2	5'-F	AlEt <sub>2</sub> Cl	<b>e</b>	55	25/75
3	5'-Cl	AlEtCl <sub>2</sub>	<b>f</b>	30	45/55
4	5'-Br	AlEtCl <sub>2</sub>	<b>g</b>	20	-
5	1'-Me	AlEtCl <sub>2</sub>	<b>h</b>	45	45/55
6	2'-Me	AlEtCl <sub>2</sub>	<b>i</b>	90	45/55
7	2'-Me	AlEt <sub>2</sub> Cl	<b>i</b>	75	28/72
8	7'-Me	AlEtCl <sub>2</sub>	<b>l</b>	60	40/60
9	2'-Me-7'-Br	AlEtCl <sub>2</sub>	<b>m</b>	50	40/60
10	2'-Me-5'-Br	AlEtCl <sub>2</sub>	<b>n</b>	40	40/60
11	2-amino Ph	AlEtCl <sub>2</sub>	<b>o</b>	50	-
12	5'-NO <sub>2</sub>	AlEtCl <sub>2</sub>	<b>p</b>	15	-

<sup>[a]</sup> After isolation by flash chromatography over silica-gel.



**Scheme 3.** Synthesis of the endomorphin-1 analogues **6** and **7** starting from the dipeptides (S,S)-3i and (S,R)-3i.

Activation of the tripeptide acids with HOBt/EDC and coupling with H-Phe-NH<sub>2</sub> gave Boc-6 and Boc-7, isolated by flash chromatography. Final deprotection with TFA gave the endomorphin-1 analogues **6** and **7** in good yields, 95% pure after semi-preparative RP-HPLC.

## 7.2. Conclusions

In summary, we have proposed a practical route for the preparation of protected dipeptides containing substituted tryptophans in either (S) or (R) configuration. The F-C alkylation of dipeptides containing Dha allowed the direct asymmetric synthesis of the tryptophanes within the peptidic structure. The reaction gave (S,S)- or (S,R)-dipeptides, albeit with moderate stereoselectivity. After isolation by normal-phase chromatography, the diastereomeric dipeptides can be readily utilized for preparing peptides of pharmacological interest. As a preliminary demonstration, we synthesized analogues of endomorphin-1 with a 2-methyltryptophan in position 3. Work is in progress to expand the scope of the reaction, in particular to improve the stereoselectivity. Further, the procedure will be utilized to synthesize a mini-library of endomorphin analogues, aiming to obtain new opioid peptides with improved performances as in vivo analgesic<sup>[21]</sup>, as well as new clues about the role of Trp in receptor recognition and activation.

### 7.3. Supporting Information

#### Experimental Section

**General methods.** Standard chemicals were obtained from commercial sources and used without further purification. Analytical RP-HPLC was performed with an ODS column (4.6 mm particle size, 100 Å pore diameter, 250 mm, DAD 210 nm) using a linear gradient of H<sub>2</sub>O/CH<sub>3</sub>CN, 9:1 to 2:8 over 20 min at a flow rate of 1.0 mL min<sup>-1</sup>, followed by 10 min isocratic H<sub>2</sub>O/CH<sub>3</sub>CN 2:8. Chiral HPLC analysis was performed on a CHIRALPAK IC column (0.46 cm x 25 cm), n-hexane/2-propanol 1:1, at 0.8 mL min<sup>-1</sup>. Semipreparative RP-HPLC was performed on a C18 column (7 mm particle size, 21.2 x 150 mm) with H<sub>2</sub>O:CH<sub>3</sub>CN 7:3, at a flow rate of 10 mL min<sup>-1</sup>. <sup>1</sup>H NMR spectra were recorded at 400 MHz at r.t. with 5 mm tubes, using 0.05 M compound. Chemical shifts (δ) are reported relative to the solvent peak.

Fmoc-Pro-Dha-OMe (**2a**). DSC (0.39 g, 1.51 mmol) was added to a stirred solution di **1** (0.44 g, 1.0 mmol) in acetonitrile (10 mL) followed by a 5% solution of DIEA (1.5 mmol) in anhydrous DCM solution (5.22 mL) at r.t., under inert atmosphere. After 4 h, the solvent was removed at reduced pressure, the residue is diluted with 1M HCl (5 mL), and the mixture was extracted three times with EtOAc (3 x 10 mL). The combined organic layers were dried over sodium sulfate, filtered, and concentrated at reduced pressure. The residue was purified by flash chromatography over silica-gel (9:1 hexane:EtOAc, column size: 15×1.5 cm<sup>2</sup>) to give the product **2a** as waxy solid (0.38 g, 90%). <sup>1</sup>H-NMR (CDCl<sub>3</sub>) δ: 1.95-2.20 (m, 4H, ProH<sub>γ</sub>+ ProH<sub>β</sub>), 3.30-3.50 (m, 2H, ProH<sub>δ</sub>), 3.80 (s, 3H, OMe), 4.30 (m, 1H, ProH<sub>α</sub>), 4.48 (m, 3H, Fmoc), 5.93 (s, 1H, =CH), 6.62 (s, 1H, =CH), 7.25-7.45 (m, 5H, ArH + NH), 7.50-7.70 (m, 2H, ArH), 7.70-7.82 (m, 2H, ArH). <sup>13</sup>C-NMR (CDCl<sub>3</sub>) δ: 27.1, 47.4, 53.1, 61.6, 68.1, 109.6, 120.2, 125.3, 125.5, 127.3, 127.9, 129.2, 141.5, 144.0. ES-MS m/z: 421.2 [M+1]; calcd: 421.2.

Fmoc-Pro-(S/R)-Trp-OMe (**3a**). A 1 M solution of AlEt<sub>2</sub>Cl in hexane (0.7 mmol, 0.7 mL) was added dropwise to a stirred mixture of **2a** (0.084 g, 0.2 mmol), indole (0.094 g, 0.8 mmol), and molecular sieves (3Å, 0.2 g) in dry CH<sub>2</sub>Cl<sub>2</sub> (4 mL) at 0°C, under a nitrogen atmosphere. The mixture was stirred for 24 h, then it was poured into saturated aqueous sodium hydrogen carbonate (5 mL). The resulting suspension of was filtered through Celite and the aqueous layer was extracted with dichloromethane (3 x 15 mL). The combined organic layers were dried over sodium sulphate, filtered, and concentrated at reduced pressure. The crude residue was purified by flash chromatography over silica-gel (DCM:EtOAc 85:15, column size: 15 × 1.5 cm<sup>2</sup>) to give (S,S)-**3a** (0.015 g, 14%) and (S,R)-**3a** (0.049 g, 46%).

(S,S)-**3a**. <sup>1</sup>H-NMR (CDCl<sub>3</sub>) δ: 1.78-1.95 (m, 2H, ProH<sub>γ</sub>), 2.00-2.20 (m, 2H, ProH<sub>β</sub>), 3.30 (d, J = 14.0 Hz, 2H, TrpH<sub>β</sub>), 3.38-3.48 (m, 2H, ProH<sub>δ</sub>), 3.55 (minor conformer) + 3.65 (major conformer) (s, 3H, OMe), 4.20-4.35 (m, 3H, Fmoc), 4.30-4.40 (m, 1H, ProH<sub>α</sub>), 4.87-5.00 (m, 1H, TrpH<sub>α</sub>), 6.50 (br.d, 1H, TrpNH minor conformer), 6.87-7.70 (m, 12H, ArH + TrpNH major conformer), 7.75-7.85 (m, 2H, ArH), 8.30 (major conformer) + 8.40 (minor conformer) (s, 1H, TrpH<sub>1</sub>). <sup>13</sup>C-NMR (CDCl<sub>3</sub>) major conformer δ: 4.7, 27.8, 28.6, 47.2, 47.3, 52.6, 52.9, 53.2, 60.6, 67.9, 77.5, 109.9, 111.4, 118.6, 119.6, 120.2, 122.2, 123.4, 125.4, 125.5, 127.4, 128.1, 136.3, 141.5, 144.3, 156.0, 171.5, 172.5. [α]<sub>D</sub> = +26.0 (c 1, CHCl<sub>3</sub>). ES-MS m/z: 537.1 [M+1]; calcd: 537.2.

(S,R)-**3a**. <sup>1</sup>H-NMR (CDCl<sub>3</sub>) δ: 1.60-2.00 (m, 4H, ProH<sub>γ</sub> + Pro H<sub>β</sub>), 3.15-3.35 (m, 2H, TrpH<sub>β</sub>), 3.35-3.58 (m, 2H, ProH<sub>δ</sub>), 3.68 (s, 3H, OMe), 3.88-4.08 (m, 1H, ProH<sub>α</sub>), 4.20-4.55 (m, 3H, Fmoc), 4.80-4.95 (m, 1H, TrpH<sub>α</sub>), 6.45 (br.d, 1H, TrpNH minor conformer), 6.80-7.70 (m, 13H, ArH + TrpNH major conformer + TrpH<sub>1</sub> major conformer), 7.81 (d, J = 14.0 Hz, 2H, ArH), 7.95 (s, 1H, TrpH<sub>1</sub> minor conformer). <sup>13</sup>C-NMR (CDCl<sub>3</sub>) major conformer δ: 23.6, 24.6, 27.6, 29.3, 31.4, 47.3, 47.6, 52.5, 52.8, 61.1, 67.9, 77.5, 111.5, 118.3, 118.6, 119.7, 120.3, 122.3, 122.9, 123.3, 125.3, 127.3, 128.1, 136.3, 141.5, 144.6, 156.1, 172.2, 172.3. [α]<sub>D</sub> = -61.2. (c 1, CHCl<sub>3</sub>). ES-MS m/z: 537.2 [M+1]; calcd: 537.2.

**Fmoc-Pro-[(S/R)-2-MeTrp]-OMe (3i)**. 1 M AlEtCl<sub>2</sub> in hexane (0.7 mmol, 0.7 mL) was added to a mixture of **2a** (0.084 g, 0.2 mmol), 2-methylindole (0.105 g, 0.8 mmol), and molecular sieves (3Å, 0.2 g) in dry CH<sub>2</sub>Cl<sub>2</sub> (4 mL) at 0 °C, under a nitrogen atmosphere. The same work-up and isolation procedures reported for **3a** afforded (S,S)-**3i** (0.045 g, 41%) and (S,R)-**3i** (0.054 g, 49%).

(S,S)-**3i**. <sup>1</sup>H-NMR (CDCl<sub>3</sub>) δ: 1.60-2.00 (m, 4H, ProH<sub>β</sub> + ProH<sub>γ</sub>), 2.32 (s, 3H, Me), 3.10-3.27 (m, 2H, TrpH<sub>β</sub>), 3.30-3.52 (m, 2H, ProH<sub>δ</sub>), 3.62 (s, 3H, OMe), 3.88-4.08 (m, 1H, ProH<sub>α</sub>), 4.20-4.37 (m, 3H, Fmoc), 4.65-4.90 (m, 1H, TrpH<sub>α</sub>), 6.40 (br.d, 1H, TrpNH minor conformer), 6.80-7.70 (m, 13H, ArH + TrpNH major conformer + TrpH<sub>1</sub>), 7.80 (d, J = 14.5 Hz, 2H, ArH). ES-MS m/z: 551.2 [M+1]; calcd: 551.2.

(S,R)-**3i**. <sup>1</sup>H-NMR (CDCl<sub>3</sub>) δ: 1.60-1.90 (m, 4H, ProH<sub>β</sub> + ProH<sub>γ</sub>), 2.32 (s, 3H, Me), 3.18-3.28 (m, 2H, TrpH<sub>β</sub>), 3.30-3.52 (m, 2H, ProH<sub>δ</sub>), 3.65 (s, 3H, OMe), , 3.90-4.09 (m, 1H, ProH<sub>α</sub>), 4.20-4.55 (m, 3H, Fmoc), 4.65-4.85 (m, 1H, TrpH<sub>α</sub>), 6.45 (br.d, 1H, TrpNH minor conformer), 6.90-7.60 (m, 13H, ArH + TrpNH major conformer + TrpH<sub>1</sub>), 7.82 (d, J = 14.5 Hz, 2H, ArH). ES-MS m/z: 551.1 [M+1]; calcd: 551.2.

**Boc-Tyr-Pro-[(S)-2-MeTrp]-OMe (4)**. The dipeptide (S,S)-**3i** (0.045 g, 0.082 mmol) was dissolved in 2M DMA in THF (3 mL) at r.t. The mixture was stirred for 20 min, then the solution was concentrated at reduced pressure. The procedure was repeated, affording H-Pro-[(S)-2-MeTrp]-OMe, used for the next step without further purification. ES-MS m/z: 329.1 [M+1]; calcd: 329.2. The crude H-Pro-[(S)-2-MeTrp]-OMe was dissolved in DCM (3 mL), and the solution was added at r.t. to a stirred mixture of HOBt (0.014 mg, 0.10 mmol), Boc-Tyr-OH (0.027 g, 0.10 mmol), in DCM (2 mL) and DMF (1 mL). After 10 min, EDCI-HCl (0.018 mg, 1.0 mmol), and TEA (0.028 mL, 0.20 mmol), were added to the mixture at r.t. After 3 h the reaction mixture was diluted with AcOEt (20 mL), and the suspension was washed with HCl 1M (4 mL) and with saturated aqueous sodium carbonate (4 mL). The organic layers were dried over sodium sulfate, and solvent was removed at reduced pressure. The crude product was purified by flash chromatography over silica gel (cyclohexane:EtOAc 1:1, column size: 10 × 1.0 cm<sup>2</sup>) to give the product **4** (0.042 g, 88%) as a waxy solid. ES-MS m/z: 592.3 [M+1]; calcd: 592.3.

**Boc-Tyr-Pro-[(R)-2-MeTrp]-OMe (5)**. The dipeptide (S,R)-**3i** (0.054 g, 0.098 mmol) was dissolved with 2M DMA in THF (4 mL) as reported for (S,S)-**3i**, giving H-Pro-[(R)-2-MeTrp]-OMe. ES-MS m/z: 329.1 [M+1]; calcd: 329.2. Treatment of H-Pro-[(R)-2-MeTrp]-OMe with HOBt (0.016 mg, 0.12 mmol), Boc-Tyr-OH (0.034 g, 0.12 mmol), EDCI-HCl (0.023 mg, 0.12 mmol), and TEA (0.033 mL, 0.24 mmol), in DCM (5 mL) and DMF

(1 mL), under the same conditions and work-up procedures reported for **4**, gave **5** (0.050 g, 86%). ES-MS  $m/z$ : 592.2 [M+1]; calcd: 592.3.

**TFA.[(S)-2-Me-Trp]-endomorphin-1 (6)**. To a stirred solution of the protected tripeptide **4** (0.042 g, 0.071 mmol) in THF (2 mL), 0.6N LiOH in H<sub>2</sub>O (1 mL) was added at r.t. After 36 h the reaction was concentrated at reduced pressure to give Boc-Tyr-Pro-[(S)-2-MeTrp]-OH, which was used without further purification. ES-MS  $m/z$ : 578.2 [M+1]; calcd: 578.3. The crude Boc-Tyr-Pro-[(S)-2-MeTrp]-OH was dissolved in DCM (4 mL) and DMF (1 mL), and treated while stirring with HOBt (0.012 g, 0.085 mmol) at r.t. After 10 min the mixture was treated at r.t. with EDC-HCl (0.016 g, 0.085 mmol), TEA (0.024 mL, 0.17 mmol), and H-Phe-NH<sub>2</sub>-HCl (0.017 mg, 0.085 mmol). After 3 h, the reaction was quenched as reported for the synthesis of **4**. Purification by flash chromatography over silica-gel (AcOEt, column size: 10 × 1.0 cm<sup>2</sup>) gave Boc-Tyr-Pro-[(S)-2-MeTrp]-PheNH<sub>2</sub> (0.039 g, 76%). ES-MS  $m/z$ : 725.4 [M+1]; calcd: 725.4. Boc-Tyr-Pro-[(S)-2-MeTrp]-PheNH<sub>2</sub> (0.039 g, 0.054 mmol) was dissolved in DCM (3 mL) and TFA (1 mL) at r.t. After 1h, the solvent was removed at reduce pressure, and the crude peptide was precipitated with cold ether (30 mL). The solid was collected by centrifugation, and purified by semi-preparative RP-HPLC on a C18 column, as reported in General Methods, affording **6** as TFA salt (0.038 g, 96%, 95% pure by analytical RP-HPLC). <sup>1</sup>H-NMR (8:2 DMSO-d<sub>6</sub>:H<sub>2</sub>O) major conformer  $\delta$ : 1.49 (m, 1H), 1.72-1.84 (m, 2H), 1.95 (m, 1H), 2.10 (s, 3H), 2.62 (dd, J = 6.5, 14.5 Hz, 1H), 2.78 (dd, J = 7.5, 15.0 Hz, 1H), 2.82 (dd, J = 8.0, 14.0 Hz, 1H), 2.90 (m, 1H), 2.95-3.10 (m, 2H), 3.08 (dd, J = 7.0, 15.5 Hz, 1H), 3.55 (m, 1H), 4.35-4.47 (m, 3H), 4.55 (m, 1H), 6.68 (d, J = 7.8 Hz, 2H), 6.90 (dd, J = 4.8, 7.2 Hz, 1H), 6.98-7.05 (m, 2H), 7.10 (d, J = 7.8 Hz, 2H), 7.10-7.25 (m, 7 H), 7.50 (d, J = 7.2 Hz, 1H), 7.81 (d, J = 7.8 Hz, 1H), 7.87 (br.s, 2H), 8.21 (d, J = 9.0 Hz, 1H), 9.33 (s, 1H), 10.66 (s, 1H). ES-MS  $m/z$ : 625.3 [M+1]; calcd: 625.3.

**TFA.[(R)-2-MeTrp]-endomorphin-1 (7)**. The protected tripeptide **5** (0.050 g, 0.085 mmol) dissolved in THF (2 mL) was treated with 0.6N LiOH in H<sub>2</sub>O (1 mL), under the same conditions and work-up procedures described for **4**, giving Boc-Tyr-Pro-[(R)-2-MeTrp]-OH. ES-MS  $m/z$ : 578.3 [M+1]; calcd: 578.3. The crude Boc-Tyr-Pro-[(R)-2-MeTrp]-OH was reacted with HOBt (0.014 g, 0.10 mmol), EDC-HCl (0.019 g, 0.10 mmol), TEA (0.028 mL, 0.2 mmol), and H-Phe-NH<sub>2</sub>-HCl (0.020 mg, 0.10 mmol), in DCM (5 mL) and DMF (1 mL), as above reported for the synthesis of **6**. Purification by flash chromatography over silica-gel (AcOEt, column size: 12 × 1.0 cm<sup>2</sup>) gave Boc-Tyr-Pro-[(R)-2-MeTrp]-PheNH<sub>2</sub> (0.049 g, 79%). ES-MS  $m/z$ : 725.4 [M+1]; calcd: 725.4. Boc-Tyr-Pro-[(S)-2-MeTrp]-PheNH<sub>2</sub> (0.049 g, 0.068 mmol) in DCM (2 mL) was reacted with TFA (1 mL) as described for the synthesis of **6**, giving TFA.**7** (0.045 g, 90%, 94% pure by analytical RP-HPLC). <sup>1</sup>H-NMR (8:2 DMSO-d<sub>6</sub>:H<sub>2</sub>O) major conformer  $\delta$ : 1.42-1.52 (m, 2H), 1.63 (m, 1H), 1.75 (m, 1H), 2.25 (s, 3H), 2.55 (m, 1H), 2.70-2.80 (m, 2H), 2.88 (m, 1H), 2.97-3.05 (m, 2H), 3.07 (m, 1H), 3.60 (m, 1H), 4.32 (m, 1H), 4.39 (m, 1H), 4.45 (m, 1H), 4.56 (m, 1H), 6.67 (d, J = 7.8 Hz, 2H), 6.85 (m, 1H), 6.90-7.00 (m, 2H), 7.10 (d, J = 13.8 Hz, 2H), 7.10-7.25 (m, 7 H), 7.51 (d, J = 7.8 Hz, 1H), 8.01 (d, J = 8.4 Hz, 1H), 8.06 (br.s, 2H), 8.09 (d, J = 9.0 Hz, 1H), 9.28 (s, 1H), 10.63 (s, 1H). ES-MS  $m/z$ : 625.4 [M+1]; calcd: 625.3.

## References and notes

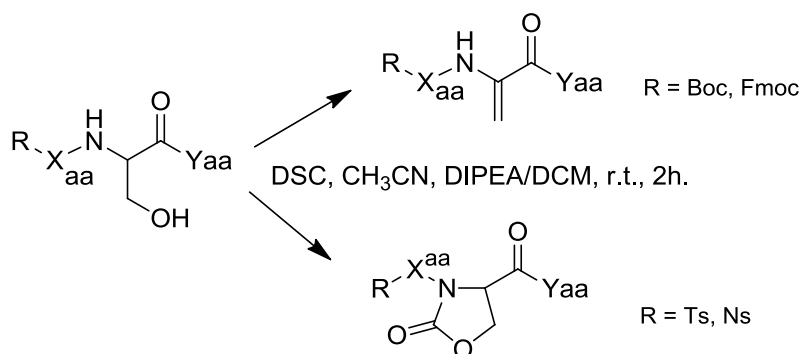
- [1] Gentilucci, L.; Tolomelli, A.; Squassabia, F. *Curr. Med. Chem.* **2006**, *13*, 2449–2466.
- [2] (a) Hruby, V. J.; Qian, X. *Methods Mol. Biol.* **1994**, *35*, 249–286; (b) Cardillo, G.; Gentilucci, L.; Tolomelli, A. *Mini Rev. Med. Chem.* **2006**, *6*, 293–304.
- [3] (a) Hruby, V. J. *Biopolymers* **1993**, *33*, 1073–1082; (b) Grauer, A.; König, B. *Eur. J. Org. Chem.* **2009**, 5099–5111.
- [4] Gentilucci, L.; Tolomelli, A. *Curr. Topics Med. Chem.* **2004**, *4*, 105–121.
- [5] Selected examples: (a) Cardillo, G.; Gentilucci, L.; Melchiorre, P.; Spampinato, S. *Bioorg. Med. Chem. Lett.* **2000**, *10*, 2755–2758; (b) Cardillo, G.; Gentilucci, L.; Qasem, A. R.; Sgarzi, F.; Spampinato, S. *J. Med. Chem.* **2002**, *45*, 2571–2578; (c) Cardillo, G.; Gentilucci, L.; Tolomelli, A.; Calienni, M.; Qasem, A. R.; Spampinato, S. *Org. Biomol. Chem.* **2003**, *1*, 1498–1502; (d) Cardillo, G.; Gentilucci, L.; Tolomelli, A.; Spinosa, R.; Calienni, M.; Qasem, A. R.; Spampinato, S. *J. Med. Chem.* **2004**, *47*, 5198–5203; (e) Gentilucci, L.; Squassabia, F.; De Marco, R.; Artali, R.; Cardillo, G.; Tolomelli, A.; Spampinato, S.; Bedini, A. *FEBS J.* **2008**, *275*, 2315–2337.
- [6] Zadina, J. E.; Hackler, L.; Ge, L.-J.; Kastin, A. *J. Nature* **1997**, *383*, 499–502.
- [7] (a) Gentilucci, L. *Curr. Topics Med. Chem.* **2004**, *4*, 19–38; (b) Lipkowski, A. W.; Misicka, A.; Carr, D. B.; Ronsisvalle, G.; Kosson, D.; Maszczyńska Bonney, I. *Pure Appl. Chem.* **2004**, *76*, 941–950.
- [8] Yeh, E.; Garneau, S.; Walsh, C. T. *Proc. Natl. Acad. Sci. U.S.A.* **2005**, *102*, 3960–3965.
- [9] (a) Bittner, S.; Scherzer, R.; Harlev, E. *Amino Acids* **2007**, *33*, 19–42; (b) Lindquist, N.; Fenical, W.; Van Dyne, C. D.; Clardy, J. *J. Am. Chem. Soc.* **1991**, *113*, 2303–2304.
- [10] (a) Perry, C. W.; Brossi, A.; Deitcher, K. H.; Tautz, W.; Teitel, S. *Synthesis* **1977**, 492–493; (b) Li, X.; Yin, W.; Srirama Sarma, P. V. V.; Zhou, H.; Ma, J.; Cook, J. M. *Tetrahedron Lett.* **2004**, *45*, 8569–8573.
- [11] Ma, C.; Liu, X.; Li, X.; Flippen-Anderson, J.; Yu, S.; Cook, J. *J. Org. Chem.* **2001**, *66*, 4525–4542.
- [12] Irie, K.; Ishida, A.; Nakamura, T.; Oh-Ishi, T. *Chem. Pharm. Bull.* **1984**, *32*, 2126–2139.
- [13] Goss, R. J. M.; Newil, P. L. A. *Chem. Commun.* **2006**, 4924–4925.
- [14] Konda-Yamada, Y.; Okada, C.; Yoshida, K.; Umeda, Y.; Arima, S.; Sato, N.; Kai, T.; Takayanagi, H.; Harigaya, Y. *Tetrahedron* **2002**, *58*, 7851–7861.
- [15] Angelini, E.; Balsamini, C.; Bartocchini, F.; Lucarini, S.; Piersanti, G. *J. Org. Chem.* **2008**, *73*, 5654–5657.
- [16] (a) Bandini, M.; Melloni, A.; Tommasi, S.; Umani-Ronchi, A. *Synlett* **2005**, 1199–1222; (b) Tabatabaeian, K.; Mamaghani, M.; Mahmoodi, N. O.; Khorshidi, A. *J. Mol. Cat. A* **2007**, *270*, 112–116.
- [17] Paterlini, M. G.; Avitabile, F.; Ostrowski, B. G.; Ferguson, D. M.; Portoghese, P. S. *Biophys. J.* **2000**, *78*, 590–599.
- [18] Witt, K. A.; Gillespie, T. J.; Huber, J. D.; Egleton, R. D.; Davis, T. P. *Peptides* **2001**, *22*, 2329–2343.
- [19] Polinsky, A.; Cooney, M. G.; Toy-Palmer, A.; Osapay, G.; Goodman, M. *J. Med. Chem.* **1992**, *35*, 4185–4194.
- [20] Jia, Y.-X.; Zhong, J.; Zhu, S.-F.; Zhang, C.-M.; Zhou, Q.-L. *Angew. Chem., Int. Ed.* **2007**, *46*, 5565–5567.
- [21] Janecka, A.; Staniszevska, R.; Gach, K.; Fichna, J. *Peptides* **2008**, *29*, 2066–2073.

## Chapter 8

# Synthesis of Constrained Peptidomimetics Containing 2-Oxo-1,3-oxazolidine-4-carboxylic Acids

### 8. Introduction

In principle, many naturally occurring, biologically active peptides can be regarded as potential pharmaceutical agents. However, there are intrinsic weaknesses that hinder their clinical use, in particular, their rapid metabolism in vivo, which can lead to short half-life stability, and their poor permeation across membrane barriers. These inherent limitations can be bypassed by adopting the peptidomimetic strategy, which involves altering the structure of a peptide. Peptidomimetics very often contain non-amino acidic elements, but still bear identifiable similarity to the parent peptides, and either imitate or inhibit their biochemical effects<sup>[1]</sup>. During the course of our studies on biologically active mimetics of naturally occurring opioid peptides<sup>[2]</sup>, we became interested in the preparation of dehydroalanine (DHA) containing peptides<sup>[3]</sup> as intermediates for the synthesis of sequences including substituted (*S*)- or (*R*)-tryptophans<sup>[4]</sup>. We obtained the DHA residue (80–90%) by dehydration of Boc- or Fmoc-protected serine-containing peptides with bis(succinimidyl) carbonate (DSC), according to a procedure reported in the literature (Scheme 1)<sup>[5]</sup>. Interestingly, we observed that, on submitting the corresponding sulfonyl peptides to the same reaction conditions, the serine residue underwent cyclization to form the 2-oxo-1,3-oxazolidine-4-carboxylate (Oxd; Scheme 1).



**Scheme 1.** Different reactivities of Fmoc-, Boc-, or sulfonylpeptides containing serine.

Peptides containing an oxazolidinone constitute a relatively uncommon class of peptidomimetics<sup>[6]</sup>. In some cases, they have been utilized as prodrugs<sup>[7]</sup> or as intermediates for the preparation of other peptidomimetics<sup>[8]</sup>. In medicinal chemistry, the oxazolidinone ring is present in some bioactive peptides or mimetics, such as the GPIIb/IIIa integrin antagonists, which are based on the (oxo-oxazolidinyl)-methyl scaffold<sup>[9]</sup>, or the HIV-1 protease inhibitors, which incorporate an oxo-*N*-phenyloxazolidine-5-carboxylic acid moiety, that are designed to improve the cellular antiviral potency<sup>[10]</sup>. Very recently, oxazolidin-2-one-containing peptides have found applications in the field of foldamers, which are short synthetic oligomers that

tend to assume ordered conformations<sup>[11]</sup>. Short Oxd-peptides were shown to form well-defined 3D structures, such as the dimeric Boc-(Phe-D-Oxd)<sub>2</sub>-OBn, which forms nanofibers with an antiparallel  $\beta$ -sheet structure<sup>[12]</sup>. The synthesis of the oxazolidin-2-one ring from an amino alcohol and a carbonate or a dicarbonate (CDI, diethyl or diphenyl carbonate, Boc<sub>2</sub>O, etc.) is well documented<sup>[13]</sup>. However, this work describes a new, highly efficient synthesis of some representative examples of Oxd-peptides directly from a peptide sequence, either in solution or in the solid phase.

Furthermore, to demonstrate the utility of the procedure in medicinal chemistry, a constrained analogue of the endogenous opioid peptide endomorphin-1 (EM1)<sup>[14]</sup>, H-Tyr-Pro-Trp-PheNH<sub>2</sub>, with the 2-oxo-oxazolidine-4-carboxylate in position 2 was prepared as a proline mimetic; the compound was characterized by a *trans* conformation of the preceding peptide bond.

### 8.1. Results and Discussion

Peptides with DHA were obtained by treating a mixture of the corresponding serine-containing *N*-Boc- or Fmoc protected peptides and DSC in acetonitrile with a solution of DIPEA in dichloromethane at room temperature (Scheme 1). However, when the same conditions were applied to *N*-sulfonyl di-, tri-, or tetrapeptides **1** having the serine (or threonine) residue in different positions, the reaction gave the *N*-sulfonyl peptides **2**, containing a 2-oxo-oxazolidine-4-carboxylate ring, without significant formation of either DHA or aziridine<sup>[15]</sup> (Scheme 2). Optimization of the reaction conditions led to the adoption of some minor changes with respect to the conditions described in the literature, such as the replacement of acetonitrile with *N,N*-dimethylformamide (DMF); the modifications resulted in excellent yields (Table 1) and reduced reaction times.

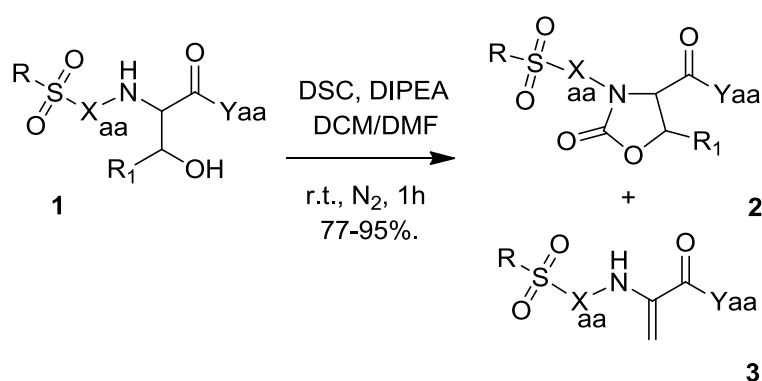
Table 1. Yields (%) of the Oxd-peptides **2** prepared as described in Scheme 2.

<b>1</b>	R	Xaa	Yaa	R1	<b>2</b> (%) <sup>[a]</sup>	<b>3</b> (%) <sup>[a]</sup>
<b>a</b>	4-MePh	Pro	OMe	H	[b]	82
<b>b</b>	4-MePh	-	PheNH <sub>2</sub>	H	80	[b]
<b>c</b>	4-MePh	Pro	PheNH <sub>2</sub>	H	85	[b]
<b>d</b>	4-MePh	Ala	PheNH <sub>2</sub>	H	88	-
<b>e</b>	4-MePh	Ala	PheNH <sub>2</sub>	Me	85	-
<b>f</b>	4-NO <sub>2</sub> Ph	Ala	PheNH <sub>2</sub>	H	90	-
<b>g</b>	4-MePh	Ala-Ala	PheNH <sub>2</sub>	H	95	-
<b>h</b> <sup>[c]</sup>	4-MePh	Ala	Phe-OH <sup>[d]</sup>	H	77 <sup>[e]</sup>	-
<b>i</b>	4-MePh	Tyr	Trp- PheNH <sub>2</sub>	H	85	-

<sup>[a]</sup> Determined after isolation by flash chromatography over silica-gel. <sup>[b]</sup> Traces. <sup>[c]</sup> Ts-Ala-Ser-Phe-Wang. <sup>[d]</sup> Reaction performed in solid-phase (Wang resin), followed by peptide cleavage. <sup>[e]</sup> Determined after isolation by semi-preparative RP-HPLC.

Tosyl (Ts) protected amino acids were prepared by allowing the amino acids, TsCl, and NaHCO<sub>3</sub> in H<sub>2</sub>O/dioxane to react according to the literature<sup>[16]</sup>; the synthesis of 4-O<sub>2</sub>NC<sub>6</sub>H<sub>4</sub>SO<sub>2</sub>-(Nosyl or Ns)-Ala-OH was performed with Ns-Cl in H<sub>2</sub>O at pH = 8<sup>[17]</sup>. The dipeptide ester Ts-Pro-Ser-OMe (**1a**) was obtained in

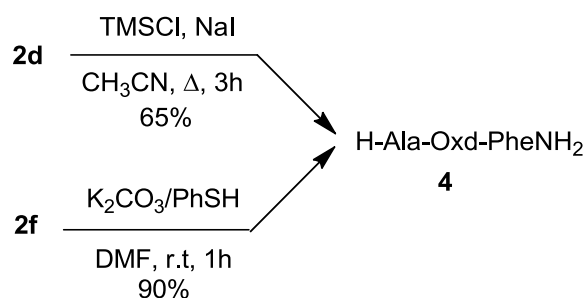
solution from Ts-Pro-OH and H-Ser-OMe·HCl under standard conditions by using 1-[3-(dimethylamino)propyl]-3-ethylcarbodiimide hydrochloride (EDC·HCl) and 1-hydroxybenzotriazole hydrate (HOBt) as activating agents. The sulfonyl di-, tri-, and tetrapeptide-amides of general sequence RSO<sub>2</sub>-Xaa-Ser/Thr-Yaa-NH<sub>2</sub> (**1b–g** and **1i**) were readily obtained by standard solid-phase peptide synthesis (SPPS) on a Rink amide resin with Fmoc-protected amino acids, with *N,N'*-dicyclohexyl carbodiimide (DCC) and HOBt as coupling agents. After cleavage with trifluoroacetic acid (TFA) in the presence of scavengers, the peptides were isolated by flash chromatography on silica gel and analyzed by RP-HPLC and ES-MS (see Experimental Section, Table 2). Alternatively, the Ts-peptide **1h** was prepared on Wang resin by using Fmoc-protected amino acids, DCC, and HOBt; Ts-Ala-Ser-Phe-Wang was then utilized for the following cyclization reaction on a solid phase prior to cleavage. The cyclization reaction of sulfonyl-peptides **1a–g** and **1i** was performed in solution (Scheme 2). The corresponding Oxd-peptide amides **2** were isolated by flash chromatography on silica gel (purity higher than 95% by RP-HPLC analysis), whereas the Oxd-peptide acid **2h** was obtained after cleavage from the resin (see below). The Oxd-peptides were characterized by IR, NMR, RP-HPLC, ES-MS, and HRMS (FAB) analyses. <sup>1</sup>H NMR resonances were assigned by using 2D gCOSY techniques.



**Scheme 2.** Synthesis of Oxd-containing peptides **2**.

Only the reaction of dipeptide Ts-Pro-Ser-OMe (**1a**), containing a serine methyl ester, gave the dehydration product Ts-Pro-DHA-OMe (**3a**) as the major product (82%, Table 1). Apparently, in this case, the comparatively high acidity of the α-H atom of the serine methyl ester with respect to that of the serine amides (**1b–j**)<sup>[18]</sup> promoted the elimination of the intermediate Ser-*O*-succinimidyl carbonate. In contrast, all of the other Ts or Ns oligopeptides containing Ser or Thr amides gave the corresponding Oxd-peptides, as reported in Table 1. This is a significant result, because, provided the sulfonyl group is present, these conditions allow the introduction of the Oxd group directly into oligopeptides. Indeed, when the protecting group is a carbamate, such as Boc, Fmoc, or Cbz, the reaction of peptides containing a Ser amide gives rise to the formation of DHA, as previously reported<sup>[5a,5e]</sup>. For confirmation, we submitted the corresponding Fmoc- or Boc-protected versions of **1d** (and **1f**), **1g**, and **1h** to the same conditions described above; as expected, in all cases, the reactions gave dehydration products in variable yields, without any trace of Oxd (data not shown). The reaction of the dipeptide Ts-Ser-Phe-NH<sub>2</sub> (**1b**) gave Ts-Oxd-Phe-NH<sub>2</sub> (**2b**) in good yield and only traces of the dehydration product (**3b**). The tripeptides Ts-Pro-Ser-Phe-NH<sub>2</sub> (**1c**) and Ts-Ala-

Ser-Phe-NH<sub>2</sub> (**1d**), containing a tosyl group that was not directly appended to the Ser residue, gave the corresponding Oxd-peptides **2c** and **2d**, respectively, in high yields. In a similar way, Ts-Ala-Thr-Phe-NH<sub>2</sub> (**1e**), which contains a Thr residue, gave the corresponding tripeptide with a *trans*-5-methyl-2-oxo-oxazolidine-4-carboxylate (**2e**). In this case, the (2*S*,3*R*) stereochemistry of the threonine residue was retained, as determined from the <sup>1</sup>H NMR coupling constant of the 4-H-5-H doublet (*J* = 4.8 Hz). The reaction could also be performed with a different sulfonyl group; thus, the Nosyl-peptide Ns-Ala-Ser-Phe-NH<sub>2</sub> (**1f**), gave the expected product Ns-Ala-Oxd-Phe-NH<sub>2</sub> (**2f**) with comparable yield. Furthermore, the tetrapeptide Ts-Ala-Ala-Ser-Phe-NH<sub>2</sub> (**1g**), having the Ser residue in position 3 of the sequence, underwent cyclization to the corresponding Oxd-tetrapeptides Ts-Ala-Ala-Oxd-Phe-NH<sub>2</sub> (**2g**) in almost quantitative yield. To expand the synthetic scope of the reaction, the Oxd tripeptide acid Ts-Ala-Oxd-Phe-OH (**2h**) was synthesized entirely on a solid phase (Table 1). The resin-bound precursor Ts-Ala-Ser-Phe-Wang (**1h**) was prepared under standard conditions, and then subjected to cyclization by treatment with a moderate excess of DSC and DIPEA in dichloromethane/DMF (4:1) for 2 h. The cleavage of the Oxd-peptide was performed by treatment with two consecutive portions of 10% TFA in dichloromethane and scavengers. Analysis of the crude reaction mixture by RP-HPLC and ES-MS analysis revealed the presence of the peptide Ts-Ala-Ser-Phe-OH (ca. 5%). The peptide **2h** was isolated by semipreparative RP-HPLC with satisfactory yield (77%, based on an average resin loading of 0.6 mmol/g). The feasibility of sulfonyl group removal under reasonably mild conditions was then investigated (Scheme 3). The tripeptide Ts-Ala-Oxd-PheNH<sub>2</sub> (**2d**) was treated with iodotrimethylsilane <sup>[19]</sup> to give the deprotected product H-Ala-Oxd-PheNH<sub>2</sub> (**4**) in moderate yield, together with a mixture of by-products. As an alternative, treatment of **2d** with Sml<sub>2</sub>/pyrrolidine/water<sup>[20]</sup>, was attempted, but this method gave **4** in only low yield.



**Scheme 3.** Removal of Ts from **2d** and Ns from **2f** affording the deprotected Oxd-containing peptide **4**.

In contrast, cleavage of the Ns group was much easier (Scheme 3), and treatment of Ns-Ala-Oxd-PheNH<sub>2</sub> (**2f**) with K<sub>2</sub>CO<sub>3</sub>/PhSH <sup>[21]</sup> gave **4** in good yield. The superior performance of Ns compared with Ts is not unexpected<sup>[22]</sup>. Based on this result, the Ns group can be regarded as the best choice for the preparation of deprotected Oxd-peptides.

Finally, to demonstrate the usefulness of Oxd-peptides as conformationally defined peptidomimetics containing a pseudo-proline<sup>[6]</sup>, an analogue of the endogenous opioid peptide endomorphin-1 (EM1), H-Tyr-Pro-Trp-PheNH<sub>2</sub> was prepared. Among the different natural or synthetic opioid peptides<sup>[23]</sup>, EM1 is unique for high receptor affinity and selectivity towards the  $\mu$ -opioid receptor (MOR). However, despite many structural

investigations performed on EM1 and its analogues, the identification of the bioactive conformation remains elusive<sup>[24]</sup>. Extensive NMR studies revealed that, in solution, EM1 exists as an approximate 1:3 *cis/trans* mixture of conformers with respect to the Tyr<sup>1</sup>–Pro<sup>2</sup> peptide bond. The tetrapeptide Ts-Tyr-Ser-Trp-Phe-NH<sub>2</sub> (**1i**) gave Ts-Tyr-Oxd-Trp-Phe-NH<sub>2</sub> (**2i**) in satisfactory yield. In solution, the Oxd-tetrapeptide **2i** adopts an all-*trans* conformation of the peptide bonds, as revealed by the NMR spectrum of the compound, which shows a single set of sharp resonances (Figure 1).

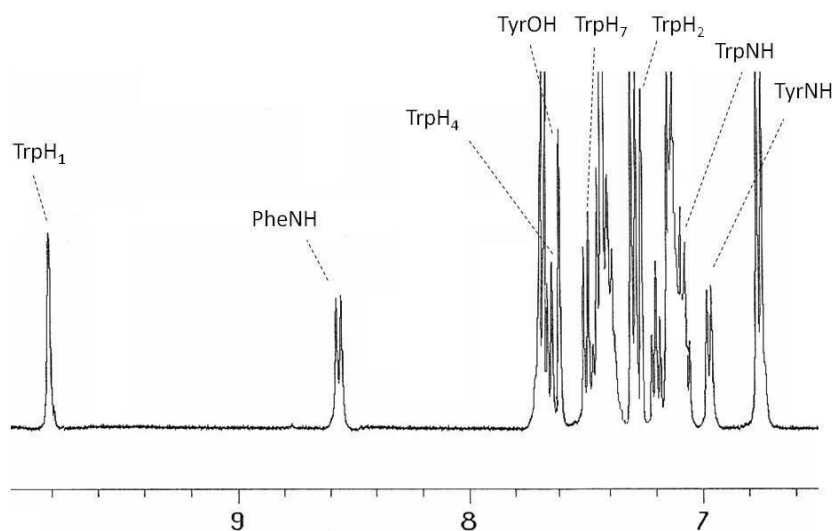


Fig. (1). <sup>1</sup>H NMR spectrum of **2i**, showing the amide and aromatic region

The *trans* conformation of **2i** was confirmed by comparison of the NMR spectroscopic data with that of Oxd-peptides described in the literature<sup>[11,12]</sup>. In Oxd-peptides, the carbonyl group of the cycle introduces a constraint that forces the pseudo-peptide bond to always have the *trans* conformation. This feature should be of help to investigate the bioactive conformation of EM1, which is an aspect that is under investigation.

## 8.2. Conclusions

In this paper we have illustrated the ready synthesis of some representative peptides incorporating a 2-oxo-oxazolidine-4-carboxylate starting from sulfonyl peptides containing Ser or Thr. Interestingly, the outcome of the reaction was practically independent of the distance between the Ser or Thr residues and the sulfonyl group. Tosyl- or Nosyl-protected peptides gave equally excellent results; these sulfonyl groups can be removed under a variety of mild conditions, in particular, the removal of Nosyl gave the deprotected peptide in good yields. The cyclization reaction was performed either in solution or on a solid phase, making the entire process a promising approach to the preparation of this class of constrained peptidomimetics and foldamers. As a representative example, an all-*trans* Oxd analogue of EM1 was prepared.

### 8.3. Experimental Section

**8.3.1. General Methods:** Unless stated otherwise, standard chemicals were obtained from commercial sources and used without further purification. Flash chromatography of **1** was performed on silica gel (230–400 mesh) by using mixtures of distilled solvents. Compounds **1** were analyzed by RP-HPLC and ES-MS. RP-HPLC was performed on an ODS column [4.6  $\mu\text{m}$  particle size, 100  $\text{\AA}$  pore diameter, 250  $\mu\text{m}$ , DAD 210 nm, from  $\text{H}_2\text{O}/\text{CH}_3\text{CN}$  (9:1) to  $\text{H}_2\text{O}/\text{CH}_3\text{CN}$  (2:8) in 20 min] at a flow rate of 1.0 mL/min, followed by 10 min at the same composition. Semipreparative RP-HPLC purification of compounds **2** were performed on a C18 column [7  $\mu\text{m}$  particle size, 21.2 mm x 150 mm, from  $\text{H}_2\text{O}/\text{CH}_3\text{CN}$  (8:2) to 100%  $\text{CH}_3\text{CN}$  in 10 min] at a flow rate of 10 mL/min. The purity of **2** (more than 95%) was assessed by analytical RP-HPLC under the above conditions. Semipreparative and analytical RP-HPLC of compound **4** were performed under the same conditions as reported for **2**, but with the addition of 0.1% TFA in the mobile phase. Compounds **2** and **4** were analyzed by RP-HPLC, ES-MS, and HRMS (FAB).  $^1\text{H}$  NMR spectra were recorded at 400 MHz at room temperature in  $\text{CDCl}_3/[\text{D}_6]\text{DMSO}$  (2:1) by using 5 mm tubes;  $^{13}\text{C}$  NMR spectra were recorded at 75 MHz. Chemical shifts are reported as  $\delta$  values relative to the  $\text{CDCl}_3$  signal.

**Synthesis of 1:** A measure of Fmoc-Rink amide resin (0.5 g, 1.1 mmol/g, resin particle size: 100–200 mesh) was introduced into a reactor of an automated synthesizer apparatus. Fmoc was removed with DMF/piperidine (4:1) (5 mL) under mechanical shaking. After 15 min, the suspension was filtered, the resin was washed with  $\text{CH}_2\text{Cl}_2$  (5 mL) and treated, while shaking, with a second portion of DMF/piperidine (4:1). After 40 min, the suspension was filtered, and the resin was washed three times in sequence with  $\text{CH}_2\text{Cl}_2$  (5 mL) and  $\text{CH}_3\text{OH}$  (5 mL). The resin was swollen in  $\text{CH}_2\text{Cl}_2$  (5 mL), and a solution of the *N*-protected amino acid (1.1 mmol) and HOBt (1.1 mmol) in DMF (4 mL) was added, followed by DCC (1.1 mmol). The mixture was mechanically shaken, and, after 3 h, the resin was filtered and washed three times with the sequence  $\text{CH}_2\text{Cl}_2$  (5 mL) and  $\text{CH}_3\text{OH}$  (5 mL). Coupling efficacy was determined by means of the Kaiser test. The resin-bound peptide was suspended in a solution of TFA (4.8 mL),  $\text{H}_2\text{O}$  (0.20 mL), and PhOH (0.050 g), in  $\text{CH}_2\text{Cl}_2$  (5 mL), and mechanically shaken at room temp. After 2 h, the mixture was filtered, the resin was washed with 10% TFA in  $\text{Et}_2\text{O}$  (2X5 mL) and  $\text{Et}_2\text{O}$  (2X5 mL). Filtrate and washes were collected, and solvent and volatiles were removed under  $\text{N}_2$  flow at room temp. The resulting residue was suspended in  $\text{Et}_2\text{O}$ , and the crude solid that precipitated was triturated and collected by using a centrifuge. The crude solid was purified by flash chromatography on silica gel (eluent:  $\text{EtOAc}$ ; column size: 10 cm x 1.5 cm), giving **1** (70–80 %). The products were analyzed by RP-HPLC and by MS, and the results are summarized in Table 2.

Table 2. RP-HPLC and ES-MS analyses of **1**.

<b>1</b>	ES-MS m/z [M+1] vs calcd	Purity (%) <sup>[a]</sup>	<b>1</b>	ES-MS m/z [M+1] vs calcd	Purity (%) <sup>[a]</sup>
<b>a</b>	371.1/371.1	85	<b>b</b>	406.1/406.2	87
<b>c</b>	503.2/503.1	91	<b>d</b>	477.2/477.1	89
<b>e</b>	491.2/491.1	93	<b>f</b>	508.2/508.2	86
<b>g</b>	548.2/548.1	84	<b>i</b>	755.3/755.2	90

<sup>[a]</sup> Determined by analytical RP-HPLC, see General Methods

**8.3.2. Solution-Phase Synthesis of Oxd-peptides 2b–g and 2i.** DSC (0.45 mmol) was added to a stirred solution of **1** (0.3 mmol) in CH<sub>2</sub>Cl<sub>2</sub>/DMF (4:1) (3 mL) followed by DIPEA (0.45 mmol) at room temp., under an inert gas. After 1 h, the solvent was removed under reduced pressure, the residue was diluted with 0.1 M HCl (5 mL), and the mixture was extracted with CH<sub>2</sub>Cl<sub>2</sub> (3x 5 mL). The combined organic layers were dried with Na<sub>2</sub>SO<sub>4</sub>, filtered, and concentrated under reduced pressure. The residue was purified by flash chromatography on silica gel (hexane/EtOAc, 1:1; column size: 15 cm x 1.0 cm) to give **2** (80–95%; purity higher than 95% as determined by analytical RP-HPLC). Under the same reaction conditions and workup protocol, Ts-Pro-Ser-OMe (**1a**) gave Ts-Pro-DHA-OMe (**3a**) (82%; 95% pure by analytical RP-HPLC).

**8.3.4. Solid-Phase Synthesis of 2h.** Wang resin pre-loaded with Fmoc-Phe (0.5 g, 0.4–0.8 mmol/g, resin particle size: 100–200 mesh) was introduced into a reactor of an automated synthesizer apparatus. Fmoc removal and couplings with the following *N*-protected amino acids were performed as described above; the quantities of the reagents were calculated based on an average resin loading of 0.6 mmol/g. The resin-bound peptide was suspended in CH<sub>2</sub>Cl<sub>2</sub>/DMF (4:1) (5 mL), and DSC (0.75 mmol) and DIPEA (0.75 mmol) were added at room temp. under an inert gas. After 2 h, the mixture was filtered, and the resin-bound peptide was washed three times in sequence with CH<sub>2</sub>Cl<sub>2</sub> (5 mL) and CH<sub>3</sub>OH (5 mL). The resin bound peptide was suspended in a mixture of TFA (1 mL), H<sub>2</sub>O (0.33 mL), ethane-dithiol (0.33 mL), and PhOH (0.33 mL), in CH<sub>2</sub>Cl<sub>2</sub> (8 mL), and mechanically shaken at room temp. After 2 h, the mixture was filtered, the resin was washed with 5% TFA in Et<sub>2</sub>O (2x 5 mL) and Et<sub>2</sub>O (2x 5 mL). The cleavage procedure was repeated, and all of the filtrates and washes were collected; solvent and volatiles were removed under an N<sub>2</sub> flow at room temp. The resulting residue was suspended in Et<sub>2</sub>O, and the crude solid that precipitated was triturated and collected by using a centrifuge. The Oxd-peptide acid **2i** was isolated by semipreparative RP-HPLC (see General Methods) (77% based on the average resin loading of 0.6 mmol/g; 96% pure by analytical RP-HPLC).

**8.3.5. Removal of the Ts Group.** To a suspension of sodium iodide (0.045 g, 0.3 mmol) in CH<sub>3</sub>CN (3 mL), TMSCl (0.038 mL, 0.3 mmol) was added, and the mixture was stirred at 0 °C under an inert gas for 10 min. To this stirred suspension, a solution of **2d** (0.10 g, 0.2 mmol) in CH<sub>3</sub>CN (3 mL) was added, and the reaction mixture was heated to reflux for 3 h. The solvent was removed under reduced pressure, and the residue was diluted with satd. aqueous Na<sub>2</sub>CO<sub>3</sub> (5 mL) and extracted with EtOAc (4x 5 mL). The collected organic layers were dried with anhydrous Na<sub>2</sub>SO<sub>4</sub> and concentrated under reduced pressure. The residue was purified by semipreparative RP-HPLC (see General Methods) to afford **4** (0.045 g, 65 %; 95% pure by analytical RP-HPLC).

**8.3.6. Removal of the Ns Group.** To a stirred solution of **2f** (0.11 g, 0.2 mmol) in DMF (4 mL), PhSH (0.026 mL, 0.24 mmol) and K<sub>2</sub>CO<sub>3</sub> (0.83 g, 0.6 mmol) were added under an inert gas, and the mixture was stirred at room temp. for 1 h. The solvent was removed under reduced pressure, and compound **4** was isolated as described above (0.063 g, 90%; 96% pure by analytical RP-HPLC).

**Ts-Pro-DHA-OMe (3a):** IR (nujol):  $\tilde{\nu}$  = 3050, 1720, 1690  $\text{cm}^{-1}$ .  $^1\text{H}$  NMR:  $\delta$  = 1.58–1.80 (m, 3 H, ProH $\beta$ , ProH $\gamma$ ), 2.15 (m, 1 H, ProH $\beta$ ), 2.42 (s, 3 H, TsCH $_3$ ), 3.20 (m, 1 H, ProH $\delta$ ), 3.46 (m, 1 H, ProH $\delta$ ), 3.85 (s, 3 H, COOCH $_3$ ), 4.15 (dd,  $J$  = 3.2, 8.6 Hz, 1 H, ProH $\alpha$ ), 5.91 (s, 1 H, =CH), 6.57 (s, 1 H, =CH), 7.33 (d,  $J$  = 8.0 Hz, 2 H, ArH), 7.74 (d,  $J$  = 8.0 Hz, 2 H, ArH), 9.15 (br. s, 1 H, NH) ppm.  $^{13}\text{C}$  NMR:  $\delta$  = 19.1, 22.0, 22.4, 40.2, 50.5, 56.8, 105, 125.3, 129.5, 136.3, 138.4, 141.5, 165.3, 171.5 ppm. ES-MS: calcd. for  $\text{C}_{16}\text{H}_{20}\text{N}_2\text{O}_5\text{S}$  [ $\text{M} + 1$ ] $^+$  371.1; found 371.2.

**Ts-Oxd-PheNH $_2$  (2b):** IR (nujol):  $\tilde{\nu}$  = 1777, 1710, 1651  $\text{cm}^{-1}$ .  $^1\text{H}$  NMR:  $\delta$  = 2.43 (s, 3 H, TsCH $_3$ ), 3.15–3.28 (m, 2 H, PheH $\beta$ ), 4.16 (dd,  $J$  = 4.2, 8.6 Hz, 1 H, 4-H), 4.53 (t,  $J$  = 8.8 Hz, 1 H, 5-H), 4.65 (q,  $J$  = 6.8 Hz, 1 H, PheH $\alpha$ ), 5.12 (dd,  $J$  = 4.2, 8.4 Hz, 1 H, 5-H), 6.82 (br. s, 1 H, CONH $_2$ ), 7.23 (br. s, 1 H, CONH $_2$ ), 7.23–7.42 (m, 7 H, ArH), 7.76 (d,  $J$  = 8.0 Hz, 2 H, ArH), 8.60 (d,  $J$  = 8.0 Hz, 1 H, PheNH) ppm.  $^{13}\text{C}$  NMR:  $\delta$  = 19.9, 36.0, 52.7, 55.9, 65.2, 124.1, 125.7, 127.2, 127.9, 128.2, 128.3, 132.5, 133.0, 135.9, 150.2, 166.4, 171.8 ppm. HRMS (FAB): calcd. for  $\text{C}_{20}\text{H}_{22}\text{N}_3\text{O}_6\text{S}$  [ $\text{M} + \text{H}$ ] $^+$  432.1229; found 432.1232.

**Ts-Pro-Oxd-PheNH $_2$  (2c):** IR (nujol):  $\tilde{\nu}$  = 1773, 1715, 1660  $\text{cm}^{-1}$ .  $^1\text{H}$  NMR:  $\delta$  = 1.52 (m, 1 H, ProH $\gamma$ ), 1.72 (m, 1 H, ProH $\gamma$ ), 1.82 (m, 1 H, ProH $\beta$ ), 1.97 (m, 1 H, ProH $\beta$ ), 2.35 (s, 3 H, TsCH $_3$ ), 3.00–3.09 (m, 3 H, ProH $\delta$ , PheH $\beta$ ), 3.42 (m, 1 H, ProH $\delta$ ), 4.22 (dd,  $J$  = 3.6, 9.4 Hz, 1 H, 4-H), 4.51 (t,  $J$  = 9.2 Hz, 1 H, 5-H), 4.62 (q,  $J$  = 7.2 Hz, 1 H, PheH $\alpha$ ), 5.02 (dd,  $J$  = 3.6, 9.2 Hz, 1 H, 5-H), 5.42 (dd,  $J$  = 3.8, 9.0 Hz, 1 H, ProH $\alpha$ ), 6.50 (br. s, 1 H, CONH $_2$ ), 6.73 (br. s, 1 H, CONH $_2$ ), 7.08–7.22 (m, 5 H, ArH), 7.24 (d,  $J$  = 8.4 Hz, 2 H, ArH), 7.62 (d,  $J$  = 8.4 Hz, 2 H, ArH), 7.78 (d,  $J$  = 8.0 Hz, 1 H, PheNH) ppm.  $^{13}\text{C}$  NMR:  $\delta$  = 17.9, 20.7, 23.1, 38.5, 40.7, 49.0, 51.1, 54.8, 56.4, 126.1, 127.8, 128.5, 129.4, 136.9, 139.1, 143.5, 152.6, 170.2, 173.1, 175.0 ppm. HRMS (FAB): calcd. for  $\text{C}_{25}\text{H}_{29}\text{N}_4\text{O}_7\text{S}$  [ $\text{M} + \text{H}$ ] $^+$  529.1757; found 529.1760.

**Ts-Ala-Oxd-PheNH $_2$  (2d):** IR (nujol):  $\tilde{\nu}$  = 1766, 1722, 1649, 1530  $\text{cm}^{-1}$ .  $^1\text{H}$  NMR:  $\delta$  = 1.32 (d,  $J$  = 7.3 Hz, 3 H, AlaCH $_3$ ), 2.40 (s, 3 H, TsCH $_3$ ), 3.00–3.17 (m, 2 H, PheH $\beta$ ), 4.27 (dd,  $J$  = 4.2, 9.3 Hz, 1 H, 4-H), 4.45 (t,  $J$  = 9.3 Hz, 1 H, 5-H), 4.64 (q,  $J$  = 7.4 Hz, 1 H, PheH $\alpha$ ), 4.91 (dd,  $J$  = 4.2, 8.6 Hz, 1 H, 5-H), 5.15 (dq,  $J$  = 7.4, 9.3 Hz, 1 H, AlaH $\alpha$ ), 6.07 (br. s, 1 H, CONH $_2$ ), 6.39 (br. s, 1 H, CONH $_2$ ), 6.41 (d,  $J$  = 9.3 Hz, 1 H, AlaNH), 7.10–7.27 (m, 7 H, ArH), 7.75 (d,  $J$  = 8.4 Hz, 2 H, ArH), 7.98 (d,  $J$  = 8.0 Hz, 1 H, PheNH) ppm.  $^{13}\text{C}$  NMR:  $\delta$  = 18.5, 20.8, 39.1, 47.8, 50.7, 54.9, 56.0, 127.1, 127.3, 128.7, 129.4, 129.8, 136.4, 139.5, 143.9, 152.4, 167.9, 173.5, 174.5 ppm. HRMS (FAB): calcd. for  $\text{C}_{23}\text{H}_{27}\text{N}_4\text{O}_7\text{S}$  [ $\text{M} + \text{H}$ ] $^+$  503.1600; found 503.1598.

**Ts-Ala-(5-Me-Oxd)-PheNH $_2$  (2e):** IR (nujol):  $\tilde{\nu}$  = 1776, 1716, 1633  $\text{cm}^{-1}$ .  $^1\text{H}$  NMR:  $\delta$  = 1.24 (d,  $J$  = 7.2 Hz, 3 H, AlaCH $_3$ ), 1.33 (d,  $J$  = 6.0 Hz, 3 H, 5-CH $_3$ ), 2.36 (s, 3 H, TsCH $_3$ ), 3.03 (d,  $J$  = 6.4 Hz, 2 H, PheH $\beta$ ), 4.22 (d,  $J$  = 4.8 Hz, 1 H, 4-H), 4.42 (t,  $J$  = 5.2 Hz, 1 H, 5-H), 4.55 (q,  $J$  = 7.3 Hz, 1 H, PheH $\alpha$ ), 4.98 (m, 1 H, AlaH $\alpha$ ), 5.70 (br. s, 1 H, CONH $_2$ ), 5.81 (br. s, 1 H, CONH $_2$ ), 6.17 (d,  $J$  = 7.9 Hz, 1 H, AlaNH), 7.09–7.20 (m, 5 H, ArH), 7.22 (d,  $J$  = 7.2 Hz, 2 H, ArH), 7.38 (d,  $J$  = 8.0 Hz, 1 H, PheNH), 7.65 (d,  $J$  = 7.2 Hz, 2 H, ArH) ppm.  $^{13}\text{C}$  NMR:  $\delta$  = 18.5, 20.3, 21.5, 37.8, 51.0, 54.9, 75.0, 75.9, 127.1, 127.3, 128.7, 129.2, 129.8, 136.3, 136.7, 147.5, 151.8, 167.0, 173.0, 174.7 ppm. HRMS (FAB): calcd. for  $\text{C}_{24}\text{H}_{29}\text{N}_4\text{O}_7\text{S}$  [ $\text{M} + \text{H}$ ] $^+$  517.1757; found 517.1761.

**Ns-Ala-Oxd-PheNH<sub>2</sub> (2f):** IR (nujol):  $\tilde{\nu}$  = 1769, 1724, 1648, 1532 cm<sup>-1</sup>. <sup>1</sup>H NMR:  $\delta$  = 1.32 (d,  $J$  = 7.0 Hz, 3 H, AlaCH<sub>3</sub>), 3.00–3.15 (m, 2 H, PheH $\beta$ ), 4.20 (dd,  $J$  = 4.1, 9.1 Hz, 1 H, 4-H), 4.40 (t,  $J$  = 9.1 Hz, 1 H, 5-H), 4.59 (q,  $J$  = 7.3 Hz, 1 H, PheH $\alpha$ ), 4.81 (dd,  $J$  = 4.1, 8.5 Hz, 1 H, 5-H), 5.15 (dq,  $J$  = 7.0, 8.8 Hz, 1 H, AlaH $\alpha$ ), 6.21 (br. s, 1 H, CONH<sub>2</sub>), 6.80 (br. s, 1 H, CONH<sub>2</sub>), 7.10–7.30 (m, 5 H, ArH), 7.37 (d,  $J$  = 8.8 Hz, 1 H, AlaNH), 7.79 (d,  $J$  = 8.0 Hz, 1 H, PheNH), 7.96 (d,  $J$  = 9.0 Hz, 2 H, ArH), 8.22 (d,  $J$  = 9.0 Hz, 2 H, ArH) ppm. <sup>13</sup>C NMR:  $\delta$  = 19.6, 37.1, 50.2, 53.9, 65.8, 123.7, 126.3, 127.8, 127.9, 128.9, 136.2, 146.4, 149.3, 152.3, 167.1, 172.1, 172.4 ppm. HRMS (FAB): calcd. for C<sub>22</sub>H<sub>24</sub>N<sub>5</sub>O<sub>9</sub>S [M + H]<sup>+</sup> 534.1295; found 534.1300.

**Ts-Ala-Ala-Oxd-PheNH<sub>2</sub> (2g):** IR (nujol):  $\tilde{\nu}$  = 1783, 1710, 1705, 1653, 1525 cm<sup>-1</sup>. <sup>1</sup>H NMR:  $\delta$  = 1.20 (d,  $J$  = 6.8 Hz, 3 H, AlaCH<sub>3</sub>), 1.35 (d,  $J$  = 7.2 Hz, 3 H, AlaCH<sub>3</sub>), 2.40 (s, 3 H, TsCH<sub>3</sub>), 3.03 (dd,  $J$  = 6.4, 13.8 Hz, 1 H, PheH $\beta$ ), 3.08 (dd,  $J$  = 6.9, 13.8 Hz, 1 H, PheH $\beta$ ), 3.78 (quint,  $J$  = 7.3 Hz, 1 H, AlaH $\alpha$ ), 4.22 (dd,  $J$  = 4.3, 9.0 Hz, 1 H, 4-H), 4.43 (t,  $J$  = 9.2 Hz, 1 H, 5-H), 4.63 (q,  $J$  = 7.1 Hz, 1 H, PheH $\alpha$ ), 4.91 (dd,  $J$  = 4.3, 8.8 Hz, 1 H, 5-H), 5.28 (quint,  $J$  = 6.8 Hz, 1 H, AlaH $\alpha$ ), 5.80 (br. s, 1 H, CONH<sub>2</sub>), 6.50 (br. s, 1 H, CONH<sub>2</sub>), 6.60 (d,  $J$  = 8.4 Hz, 1 H, AlaNH), 7.10–7.27 (m, 8 H, ArH, AlaNH), 7.72 (d,  $J$  = 8.0 Hz, 2 H, ArH), 7.81 (d,  $J$  = 7.2 Hz, 1 H, PheNH) ppm. <sup>13</sup>C NMR:  $\delta$  = 16.3, 18.0, 20.5, 36.7, 47.1, 51.3, 53.6, 55.2, 64.8, 125.9, 126.1, 127.4, 128.4, 128.7, 135.6, 136.0, 142.6, 151.4, 166.8, 170.6, 171.7, 171.9 ppm. HRMS (FAB): calcd. for C<sub>26</sub>H<sub>32</sub>N<sub>5</sub>O<sub>8</sub>S [M + H]<sup>+</sup> 574.1972; found 574.1977.

**Ts-Ala-Oxd-Phe-OH (2h):** IR (nujol):  $\tilde{\nu}$  = 2800–3450, 1766, 1722, 1716, 1649 cm<sup>-1</sup>. <sup>1</sup>H NMR:  $\delta$  = 1.20 (d,  $J$  = 7.2 Hz, 3 H, AlaCH<sub>3</sub>), 2.41 (s, 3 H, TsCH<sub>3</sub>), 3.05–3.17 (m, 2 H, PheH $\beta$ ), 4.27 (dd,  $J$  = 4.1, 8.5 Hz, 1 H, 4 H), 4.36 (t,  $J$  = 9.2 Hz, 1 H, 5-H), 4.63 (q,  $J$  = 7.6 Hz, 1 H, PheH $\alpha$ ), 4.92 (dd,  $J$  = 4.0, 9.2 Hz, 1 H, 5-H), 5.20 (m, 1 H, AlaH $\alpha$ ), 6.30 (d,  $J$  = 9.0 Hz, 1 H, AlaNH), 7.10–7.25 (m, 5 H, ArH), 7.30 (d,  $J$  = 8.0 Hz, 2 H, ArH), 7.52 (d,  $J$  = 7.6 Hz, 1 H, PheNH), 7.73 (d,  $J$  = 8.0 Hz, 2 H, ArH), 9.32 (br. s, 1 H, COOH) ppm. <sup>13</sup>C NMR:  $\delta$  = 17.9, 20.5, 38.4, 47.9, 50.1, 54.2, 56.4, 126.8, 127.7, 128.2, 129.1, 130.2, 136.3, 139.2, 144.1, 152.4, 168.0, 173.2, 176.0 ppm. HRMS (FAB): calcd. for C<sub>23</sub>H<sub>26</sub>N<sub>3</sub>O<sub>8</sub>S [M + H]<sup>+</sup> 504.1441; found 504.1436.

**Ts-Tyr-Oxd-Trp-PheNH<sub>2</sub> (2i):** IR (nujol):  $\tilde{\nu}$  = 1776, 1718, 1675, 1526 cm<sup>-1</sup>. <sup>1</sup>H NMR:  $\delta$  = 2.38 (s, 3 H, TsCH<sub>3</sub>), 2.42 (dd,  $J$  = 8.0, 14.0 Hz, 1 H, TyrH $\beta$ ), 2.82 (dd,  $J$  = 7.6, 14.2 Hz, 1 H, TrpH $\beta$ ), 2.99 (dd,  $J$  = 6.4, 14.2 Hz, 1 H, TrpH $\beta$ ), 3.15 (dd,  $J$  = 3.0, 14.0 Hz, 1 H, TyrH $\beta$ ), 3.22 (d,  $J$  = 7.6 Hz, 2 H, PheH $\beta$ ), 4.22 (dd,  $J$  = 4.1, 9.2 Hz, 1 H, 4-H), 4.50 (t,  $J$  = 9.2 Hz, 1 H, 5-H), 4.57 (q,  $J$  = 6.8 Hz, 1 H, TrpH $\alpha$ ), 4.92 (q,  $J$  = 7.0 Hz, 1 H, PheH $\alpha$ ), 5.02 (dd,  $J$  = 4.1, 8.8 Hz, 1 H, 5-H), 5.30 (quint,  $J$  = 6.8 Hz, 1 H, TyrH $\alpha$ ), 5.72 (br. s, 1 H, CONH<sub>2</sub>), 6.05 (br. s, 1 H, CONH<sub>2</sub>), 6.75 (d,  $J$  = 8.4 Hz, 2 H, TyrArH), 6.95 (d,  $J$  = 7.8 Hz, 1 H, TyrNH), 7.02–7.15 (m, 4 H, TrpNH, TrpH-5, TyrArH), 7.19 (t,  $J$  = 7.6 Hz, 1 H, TrpH-6), 7.25 (s, 1 H, TrpH-2), 7.30 (d,  $J$  = 8.0 Hz, 2 H, ArH), 7.32–7.45 (m, 5 H, PheArH), 7.50 (d,  $J$  = 8.0 Hz, 1 H, TrpH-7), 7.61 (s, 1 H, TyrOH), 7.66 (d,  $J$  = 7.9 Hz, 1 H, TrpH-4), 7.68 (d,  $J$  = 8.0 Hz, 2 H, ArH), 8.55 (d,  $J$  = 8.8 Hz, 1 H, PheNH), 9.81 (br. s, 1 H, TrpH1) ppm. <sup>13</sup>C NMR:  $\delta$  = 21.4, 31.9, 36.6, 37.3, 49.3, 52.7, 59.2, 60.1, 71.3, 111.8, 112.3, 116.6, 120.2, 121.0, 123.5, 125.0, 126.2, 127.3, 129.5, 132.1, 132.3, 136.2, 137.6, 140.1, 141.3, 155.7, 156.2, 173.2, 174.0, 174.2, 176.0 ppm. HRMS (FAB): calcd. for C<sub>40</sub>H<sub>41</sub>N<sub>6</sub>O<sub>9</sub>S [M + H]<sup>+</sup> 781.2656; found 781.2662.

**H-Ala-Oxd-PheNH<sub>2</sub> (4):** IR (nujol):  $\tilde{\nu}$  = 3352, 3445, 1764, 1722, 1645 cm<sup>-1</sup>. <sup>1</sup>H NMR:  $\delta$  = 1.22 (d,  $J$  = 6.8 Hz, 3 H, AlaCH<sub>3</sub>), 2.96 (dd,  $J$  = 9.8, 13.8 Hz, 1 H, PheH $\beta$ ), 3.12 (dd,  $J$  = 4.6, 13.8 Hz, 1 H, PheH $\beta$ ), 3.30 (q,  $J$  = 6.8 Hz, 1 H, AlaH $\alpha$ ), 4.08 (dd,  $J$  = 4.6, 8.4 Hz, 1 H, 4-H), 4.36 (dd,  $J$  = 4.6, 9.2 Hz, 1 H, 5-H), 4.43 (t,  $J$  = 8.4 Hz, 1 H, 5-H), 4.50 (m, 1 H, PheH $\alpha$ ), 7.10 (br. s, 1 H, CONH<sub>2</sub>), 7.15 (br. s, 1 H, CONH<sub>2</sub>), 7.16–7.30 (m, 5 H, ArH), 8.05–8.25 (m, 3 H, PheNH, AlaNH) ppm. <sup>13</sup>C NMR:  $\delta$  = 17.3, 37.9, 47.7, 49.0, 56.1, 63.2, 126.0, 128.7, 129.2, 137.1, 153.4, 172.4, 173.8, 174.0 ppm. HRMS (FAB): calcd. for C<sub>16</sub>H<sub>21</sub>N<sub>4</sub>O<sub>5</sub> [M + H]<sup>+</sup> 349.1512; found 349.1509.

## REFERENCES

- [1] a) M. Cai, V. V. Kulkarni, V. J. Hruby in *Textbook of Drug Design and Discovery*, 4th ed. (Eds.: U. Madsen, P. Krosggaard-Larsen, K. Stromgaard), Taylor & Francis, London, **2010**, pp.123–134; b) A. Grauer, B. König, *Eur. J. Org. Chem.* **2009**, 5099–5111; c) L. Gentilucci, R. De Marco, L. Cerisoli, *Curr. Pharm. Des.* **2010**, *16*, 3185–3203.
- [2] For a representative example, see: L. Gentilucci, F. Squassabia, R. De Marco, R. Artali, G. Cardillo, A. Tolomelli, S. Spampinato, A. Bedini, *FEBS J.* **2008**, *275*, 2315–2337, and references herein.
- [3] C. Bonauer, T. Walenzyk, B. König, *Synthesis* **2006**, 1–20.
- [4] L. Gentilucci, L. Cerisoli, R. De Marco, A. Tolomelli, *Tetrahedron Lett.* **2010**, *51*, 2576–2579.
- [5] a) A. Polinsky, M. G. Cooney, A. Toy-Palmer, G. Osapay, M. Goodman, *J. Med. Chem.* **1992**, *35*, 4185–4194; for related procedures, see: b) H. Ogura, O. Sato, K. Takeda, *Tetrahedron Lett.* **1981**, *22*, 4817–4818; c) P. M. T. Ferreira, H. L. S. Maia, L. S. Monteiro, J. Sacramento, *J. Chem. Soc. Perkin Trans. 1* **1999**, 3697–3703; d) Y. Zhu, W. A. van der Donk, *Org. Lett.* **2001**, *3*, 1189–1192; e) R. Rojo, J. C. Jimenèz, A. Lòpez-Macià, E. Giral, F. Albericio, *Eur. J. Org. Chem.* **2001**, 45–48; f) B. K. Ayida, K. B. Simonsen, D. Vourloumis, T. Hermann, *Bioorg. Med. Chem. Lett.* **2005**, *15*, 2457–2460; g) T. Mori, H. Tohmiya, Y. Satouchi, S. Higashibayashi, K. Hashimoto, M. Nakata, *Tetrahedron Lett.* **2005**, *46*, 6423–6427; h) R. Ramesh, K. De, S. Chandrasekaran, *Tetrahedron* **2007**, *63*, 10534–10542; i) C. R. Avena, L. Hongquiang, R. P. Vijaya, J. C. Vederas, *J. Am. Chem. Soc.* **2010**, *132*, 462–463.
- [6] D. Seebach, T. L. Sommerfeld, Q. Jiang, L. M. Venanzi, *Helv. Chim. Acta* **1994**, *77*, 1313–1330.
- [7] a) H. Fang, G. Kaur, B. Wang in *Prodrugs: Challenges and Rewards, Part 2* (Eds.: V. Stella, R. T. Borchardt, M. Hageman, R. Oliyai, H. Maag, J. Tilley), Springer, New York, **2007**, pp. 265–288; b) A. Buur, H. Bundgaard, *Int. J. Pharm.* **1988**, *46*, 159–167; c) W. Kamm, P. Raddatz, J. Gante, T. Kissel, *Pharm. Res.* **1999**, *16*, 1527–1533.
- [8] T. Mittag, K. L. Christensen, K. B. Lindsay, N. C. Nielsen, T. Skrydstrup, *J. Org. Chem.* **2008**, *73*, 1088–1092.
- [9] J. Gante, H. Juraszyk, P. Raddatz, H. Wurziger, S. Bernotat- Danielowski, G. Melzer, F. Rippmann, *Bioorg. Med. Chem. Lett.* **1996**, *6*, 2425–2430.
- [10] A. Ali, G. S. Reddy, M. N. Nalam, S. G. Anjum, H. Cao, C. A. Schiffer, T. M. Rana, *J. Med. Chem.* **2010**, *53*, 7699–7708.
- [11] a) G. Angelici, G. Falini, H.-J. Hofmann, D. Huster, M. Monari, C. Tomasini, *Chem. Eur. J.* **2009**, *15*, 8037–8048; b) C. Tomasini, Luppi, M. Monari, *J. Am. Chem. Soc.* **2006**, *128*, 2410–2420.
- [12] G. Angelici, G. Falini, H.-J. Hofmann, D. Huster, M. Monari, C. Tomasini, *Angew. Chem. Int. Ed.* **2008**, *47*, 8075–8078.
- [13] G. Zappia, E. Gacs-Baitz, G. Delle Monache, D. Misiti, L. Nevola, B. Botta, *Curr. Org. Synth.* **2007**, *4*, 81–135.
- [14] a) J. E. Zadina, L. Hackler, L.-J. Ge, A. J. Kastin, *Nature* **1997**, *83*, 499–502; b) L. Gentilucci, *Curr. Top. Med. Chem.* **2004**, *4*, 19–38.
- [15] S. Cutugno, G. Martelli, L. Negro, D. Savoia, *Eur. J. Org. Chem.* **2001**, 517–522.

- [16] M. Ousmer, N. A. Braun, C. Bavoux, M. Perrin, M. A. Ciufolini, *J. Am. Chem. Soc.* **2001**, *123*, 7534–7538.
- [17] X. Deng, N. S. Mani, *Green Chem.* **2006**, *8*, 835–838.
- [18] G. Panda, N. V. Rao, *Synlett* **2004**, 714–716.
- [19] G. Sabitha, B. V. S. Reddy, S. Abraham, J. S. Yadav, *Tetrahedron Lett.* **1999**, *40*, 1569–1570.
- [20] T. Ankner, G. Hilmersson, *Org. Lett.* **2009**, *11*, 503–506.
- [21] T. Fukuyama, C.-K. Jow, M. Cheung, *Tetrahedron Lett.* **1995**, *36*, 6373–6374.
- [22] A. Isidro-Llobet, M. Alvarez, F. Albericio, *Chem. Rev.* **2009**, *109*, 2455–2504.
- [23] L. Gentilucci, A. Tolomelli, F. Squassabia, *Curr. Med. Chem.* **2006**, *13*, 2449–2466.
- [24] a) A. Keresztes, A. Borics, G. Toth, *ChemMedChem* **2010**, *5*, 1176–1196; b) L. Gentilucci, A. Tolomelli, *Curr. Top. Med. Chem.* **2004**, *4*, 105–121; c) B. L. Podlogar, M. G. Paterlini, D. M. Ferguson, G. C. Leo, D. A. Demeter, F. K. Brown, A. B. Reitz, *FEBS Lett.* **1998**, *439*, 13–20; d) S. Fiori, C. Renner, J. Cramer, S. Pegoraro, L. Moroder, *J. Mol. Biol.* **1999**, *291*, 163–175.

---

## Chapter 9

---

# Expedient Synthesis of Pseudo-Pro-Containing Peptides: Towards Constrained Peptidomimetics and Foldamers

---

### 9. Introduction

Determining the receptor-bound structure of biologically active peptides is fundamental in drug design. However, the direct investigation of ligand-receptor complexes has met with considerable practical obstacles; in addition, many native peptides are highly flexible molecules, therefore their conformational analysis is a difficult task. As a consequence, many efforts have been dedicated to the design of conformationally defined peptidomimetics as tools for investigating the key structural and conformational features on which receptor recognition and binding are based<sup>[1]</sup>.

Generally, peptide backbones serve as 3D scaffolds for positioning the side chains involved in ligand-receptor interactions. The presence of Pro residues strongly impacts the structural and conformational properties of the backbones. The cyclic structure of Pro forces the  $\phi$  angle to  $-65^\circ \pm 15^\circ$ , thus preventing the formation of a  $\alpha$ -helix, and promoting the formation of  $\beta$ -turns<sup>[2]</sup>. Turns and inverse turns play important roles in the architecture and bioactivity of native folded proteins<sup>[3]</sup>. Besides, while the barrier to secondary amide *cis/trans* isomerization is circa 10 kcal mol<sup>-1</sup> (Fig. 1), the presence of Pro reduces the barrier to just 2 kcal mol<sup>-1</sup>, increasing the *cis* conformer<sup>[4]</sup>.

Besides to Pro itself, numerous derivatives were found in proteins of microbial or marine origins, in antibiotics or cytotoxic peptides,<sup>[1]</sup> and many other (e.g. 2,4-MePro,  $\Delta^3$ Pro, Azi, Aze, Pip, Nip, etc., Fig. 1)<sup>[6]</sup> were synthesized and utilized to design conformationally constrained peptidomimetics<sup>[7]</sup>. For instance, pseudo-Pro such as thiazolidine- and oxazolidine-4-carboxylic acid (Tc, Oxi) dimethylated at the position 2, are known to be quantitative, or nearly quantitative, inducers of the *cis* conformation around the preceding peptide bond<sup>[8]</sup>, while 1-aminocyclohexane-1-carboxylic acid (Chx) induces the *trans* conformation<sup>[9]</sup>. On the other hand, 5,5-dimethylthiazolidine-4-carboxylic acid (Dtc)<sup>[10]</sup> and azetine-2-carboxylic acid (Aze)<sup>[11]</sup> (Fig. 1) favor angles in the  $\gamma$ -turn region, while 5-*tert*-butylproline (5-*tBu*Pro) stabilizes type VI  $\beta$ -turn conformation<sup>[12]</sup>.

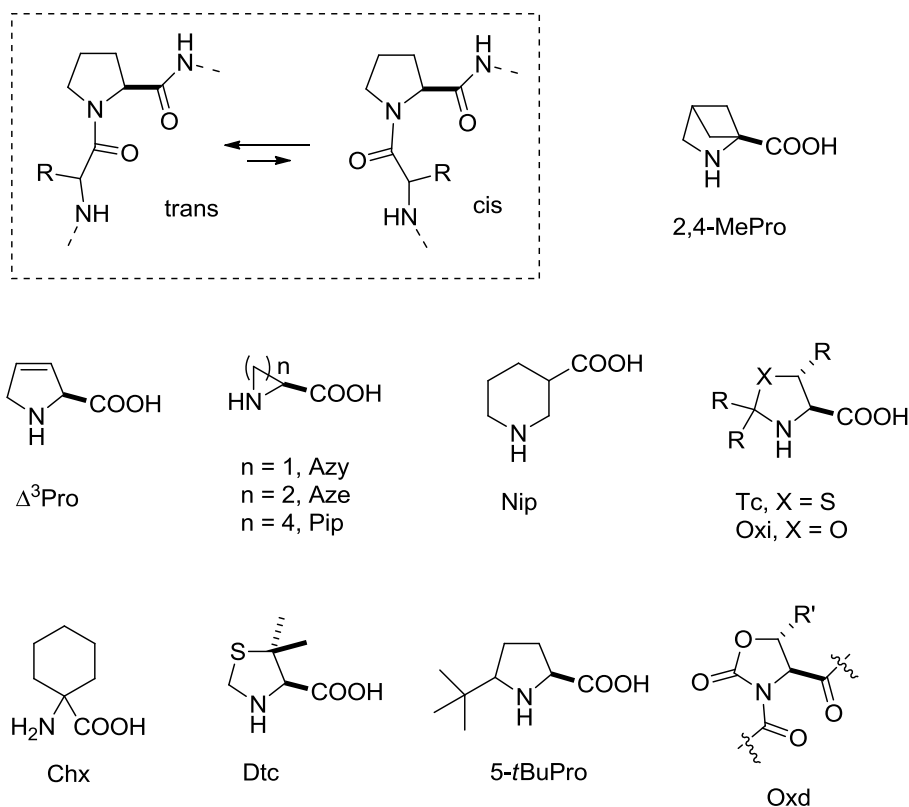


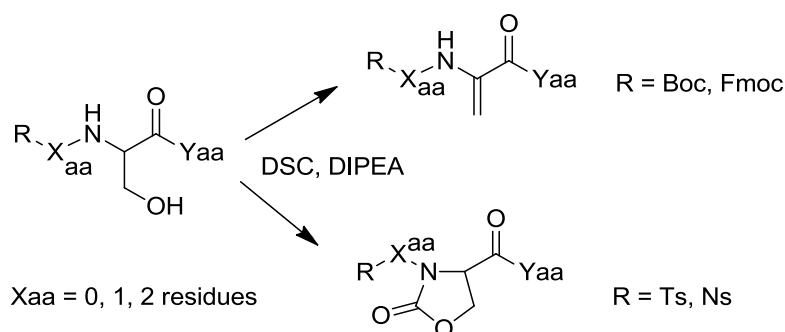
Fig. (1). Selected examples of pseudo-Pro structures.

Finally, pseudo-Pro have found use in the preparation of foldamers<sup>[13]</sup>, short synthetic oligomers which have a tendency to form well-defined secondary structures, stabilized by noncovalent interactions<sup>[14]</sup>.

In the last years, we have been interested in the use of D-Pro,  $\beta$ -Pro, pseudo-Pro and pseudo- $\beta$ -Pro for the preparation of constrained bioactive peptidomimetics<sup>[15]</sup>. In this contest, we recently proposed the 2-oxo-1,3-oxazolidine-4-carboxylate (or oxazolidin-2-one, in short: Oxd) as a constrained pseudo-Pro residue. Indeed, the carbonyl group of the cycle introduces a constraint that enforces the pseudo-peptide bond to always have the *trans* conformation (Fig. 1).

Apart from the different applications in medicinal chemistry<sup>[16]</sup>, Oxd-peptides have been the subject of much interest as foldamers or as self-assembling scaffolds forming nanostructures. The oligomers of the Boc-(L-Ala-D-Oxd)<sub>n</sub>-OBn series exhibit a strong tendency to form helices with 10-membered H-bonded rings in solution<sup>[17]</sup>. The  $\alpha,\beta$ -hybrid oligomers of the Boc-(L- $\beta^3$ -hPhg-D-Oxd)<sub>n</sub>-OBn series, formed helices with 11-membered H-bonded turns for  $n \geq 5$ . The Boc-(L- $\beta^3$ -hPhe-D-Oxd)<sub>n</sub>-OBn series displays chain length-dependent behaviour. In the higher oligomers ( $n > 2$ ), there is a stronger tendency to form intramolecular H-bonds, while the Boc-(L- $\beta^3$ -hPhe-D-Oxd)<sub>2</sub>-OBn motif forms an anti-parallel  $\beta$ -sheet-like structure, where only one intermolecular H-bond stabilizes the fibre-like material besides the hydrophobic forces between the aromatic side-chains<sup>[18]</sup>.

In this work we considerably expand the scope of our preliminarily described preparation of peptides containing the Oxd ring<sup>[19]</sup>. The reaction proceeds by the direct cyclization of *N*-sulfonyl peptides containing a Ser residue (Scheme 1), by treatment with *bis(succinimidyl) carbonate* (DSC) and *diisopropylethylamine* (DIPEA).



**Scheme 1.** Different reactivity of *N*-carbamate and *N*-tosyl (Ts) or nosyl (Ns) oligopeptides.

The distance between the sulfonyl and the Ser in the sequence is relatively unimportant. Indeed, the reaction of peptides having the sulfonyl group directly connected to the Ser, or separated by one or two amino acids (Scheme 1, Xaa = 0, 1, or 2 residues) proceeded with similar results. The reaction of the corresponding Fmoc- or Boc-peptides under the same conditions gave elimination to dehydroalanine (Dha), in agreement to the literature (Scheme 1)<sup>[20]</sup>.

## 9.1. Results and discussion

### 9.1.2.. Optimization of the reaction conditions

The reaction depicted in Scheme 1 represents the first synthesis of a oxazolidin-2-one-4-carboxylate directly within a peptide sequence. Apparently, the reaction outcome depends on the presence of the sulfonyl group (see Introduction). Subsequently, in order to optimize the cyclization of these sulfonyl peptides, we investigated the role of the carbonate, solvent, base, and sulfonyl group, by reacting the model peptides **1a-d** under different conditions (Scheme 2, Table 1).

The preparation of **1a-d** and of the other sulfonyl-protected peptides **4**, **6**, **8**, **11**, and **13**, was conducted by coupling the amino acids under normal conditions, using *1-ethyl-3-[3-dimethylaminopropyl]carbodiimide hydrochloride* (EDC-HCl) and *1-hydroxybenzotriazole hydrate* (HOBt) as activating agents. *N*-Mesyl (Ms), tosyl (Ts), or nosyl (Ns) amino acids were prepared according to the literature<sup>[21]</sup>.

The treatment of **1a** (Table 1) with 1.5 equiv. of DSC and 1.5 equiv. of DIPEA in DCM/CH<sub>3</sub>CN<sup>[Errore. Il segnalibro non è definito.]</sup> gave the oxazolidinone-peptide **2a**, Ts-Ala-Oxd-PheNH<sub>2</sub> (Entry 1) in good yield, together with traces of the corresponding elimination product Ts-Ala-Dha-PheNH<sub>2</sub> (**3**). The substitution of CH<sub>3</sub>CN with DMF allowed increasing the yield, while reducing the reaction time (Entry 2); the use of solely DMF or DMSO (Entry 3, and 4) was not beneficial. Different bases such as DBU (Entry 5) or DMAP (Entry 6) in DCM/DMF gave **2** with comparable yields.

A second set of reactions was designed to test the role of the carbonate. The synthesis of a oxazolidin-2-one ring from an aminoalcohol and different kinds of carbonates or dicarbonates is well documented in the literature<sup>[22]</sup>. Nevertheless, none of the procedures attempted by us gave the oxazolidinone-peptide **2** in a significant yield. The reaction of **1a** with *1,1'-carbonyldiimidazole* (CDI) and DIPEA<sup>[23]</sup> gave Ts-Ala-Dha-PheNH<sub>2</sub> (**3**) as the major product, and only traces of **2a** (Entry 7), the rest being the reagent. The treatment

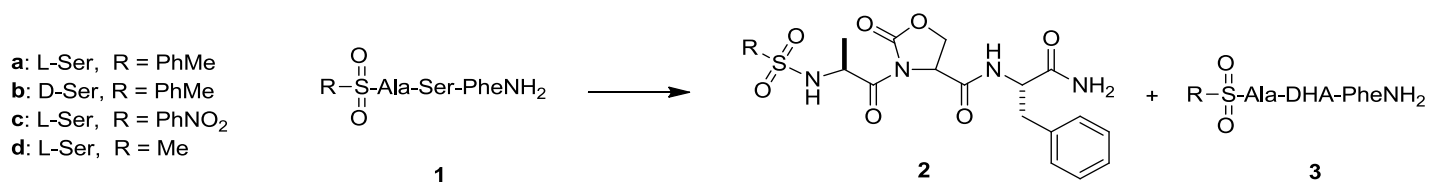
of **1a** with Boc<sub>2</sub>O and DIPEA (Entry 8) or DMAP<sup>[24]</sup> (Entry 9) gave a Boc-derivative of **1** (not isolated) and traces of **2**, as determined by the HPLC-MS analysis of the reaction mixture. Triphosgene gave **2** and **3** only in traces (Entry 10), while *ethylchloroformate* was completely ineffective (entry 11)<sup>[Errore. Il segnalibro non è definito. Errore. Il segnalibro non è definito.,25]</sup>.

Furthermore, we observed that the reaction of **1a** and DSC in the absence of a base did not furnish **2a** (Entry 12). However, the reaction was possible with a catalytic amount of DIPEA (Entry 13) or DMAP (Entry 14), giving **2a** in excellent yield and in reasonable time in a DCM/DMF mixture, but not in DCM alone (Entry 15). By using DSC and a catalytic amount of DIPEA, Ts-Ala-D-Ser-PheNH<sub>2</sub> (**1b**) was converted into Ts-Ala-D-Oxd-PheNH<sub>2</sub> (**2b**) with the same yield of **2a** (Entry 16 compared to Entry 13).

In order to gain more information about the role of the sulfonyl group in the cyclization, we compared the reaction of the Ts-peptide **1a** to that of the peptides **1c** and **1d** carrying the nosyl and mesyl groups, respectively.

Under the same conditions of Entry 13, Ns-Ala-Ser-PheNH<sub>2</sub> (**1c**) gave the corresponding Oxd-peptide Ns-AlaOxd-Phe-NH<sub>2</sub> (**2c**) in very good yield (Entry 17).

On the contrary, the mesyl group failed to promote the cyclization. The treatment of Ms-Ala-Ser-PheNH<sub>2</sub> (**1d**) with DSC in the presence of a catalytic amount of DIPEA did not give rise to the formation of the Oxd-peptide (Entry 18); the use of 1.2 equiv. of DIPEA (Entry 19) or DMAP (Entry 20) afforded the product only in traces.



**Scheme 2.** Reactions of the sulfonyl-peptides **2a**, **c**, **d**, containing L-Ser, and of **2b**, containing D-Ser, under the conditions reported in Table 1.

Taken together, the results reported in Table 1 give several clues on the mechanism of the cyclization process. Albeit an accurate investigation of the reaction mechanism is beyond the scope of this work, we compared the elimination of Boc- or Fmoc-peptides containing a Ser vs a plausible mechanisms of cyclization of the corresponding tosyl peptides (Scheme 3). The two reactions proceed via a common Ser-O-carbonate intermediate **A**. The elimination of the Boc- or Fmoc-intermediate **A** induced by the base (:B) gives Dha, as sketched in pathway **a**.

**Table 1.** Reagents and conditions tested for the synthesis of R-SO<sub>2</sub>-Ala-Oxd-PheNH<sub>2</sub> (**2**) from R-SO<sub>2</sub>-Ala-Ser-PheNH<sub>2</sub> (**1**)

entry	Compd	carbonate (equiv.)	base (equiv.)	solvent	Time (h) <sup>a</sup>	<b>2</b> (%) <sup>b</sup>	<b>3</b> (%)
1	<b>a</b>	DSC (1.5)	DIPEA (1.2)	DCM/CH <sub>3</sub> CN 3:1	2	74	traces <sup>c,d</sup>
2	<b>a</b>	DSC (1.5)	DIPEA (1.2)	DCM/DMF 3:1	1	88	-
3	<b>a</b>	DSC (1.5)	DIPEA (1.2)	DMF	1	80	-
4	<b>a</b>	DSC (1.5)	DIPEA (1.2)	DMSO	1	79	-
5	<b>a</b>	DSC (1.5)	DBU (1.2)	DCM/DMF 3:1	2	85	-
6	<b>a</b>	DSC (1.5)	DMAP (1.2)	DCM/DMF 3:1	3	87	-
7	<b>a</b>	CDI (1.2)	DIPEA (1.2)	DCM	24	traces <sup>c,d</sup>	30 <sup>d,e</sup>
8	<b>a</b>	BOC <sub>2</sub> O (2.1)	DIPEA (1.2)	CH <sub>3</sub> CN	24	- <sup>f,d,e</sup>	-
9	<b>a</b>	BOC <sub>2</sub> O (2.1)	DMAP (1.2)	DCM/DMF 3:1	2	- <sup>f,d,e</sup>	-
10	<b>a</b>	Cl <sub>3</sub> COCOOCCl <sub>3</sub> (0.5)	DIPEA (3.0)	DCM/DMF	24	-	traces <sup>c,d</sup>
11	<b>a</b>	ClCOOMe	DIPEA (1.2)	DCM/DMF 3:1	24	- <sup>g,d,e</sup>	-
12	<b>a</b>	DSC (1.2)	-	DCM/DMF 3:1	24	-	-
13	<b>a</b>	DSC (1.2)	DIPEA (0.1) <sup>h</sup>	DCM/DMF 3:1	3	92	-
14	<b>a</b>	DSC (1.2)	DMAP (0.3) <sup>h</sup>	DCM/DMF 3:1	6	90	-
15	<b>a</b>	DSC (1.2)	DIPEA (0.1) <sup>h</sup>	DCM	24	traces <sup>c,d,e</sup>	-
16	<b>b</b>	DSC (1.2)	DIPEA (0.1) <sup>h</sup>	DCM/DMF 3:1	3	92	-
17	<b>c</b>	DSC (1.2)	DIPEA (0.1) <sup>h</sup>	DCM/DMF 3:1	3	90	-
18	<b>d</b>	DSC (1.2)	DIPEA (0.1) <sup>h</sup>	DCM/DMF 3:1	24	-	-
19	<b>d</b>	DSC (1.5)	DIPEA (1.2)	DCM/DMF 3:1	24	traces <sup>c,d,e</sup>	traces <sup>c,d,e</sup>
20	<b>d</b>	DSC (1.5)	DMAP (1.2)	DCM/DMF 3:1	24	traces <sup>c,d,e</sup>	traces <sup>c,d,e</sup>

<sup>a</sup> The reaction was stopped at the disappearance of the reagent, as determined by the t.l.c. analysis of the reaction, or after 24h. <sup>b</sup> After purification by flash chromatography. <sup>c</sup> <5%. <sup>d</sup> Not isolated, determined by the HPLC-MS analysis. <sup>e</sup> The rest being the reagent **1**. <sup>f</sup> Boc-**1** was the mayor by-product. <sup>g</sup> MeOCO-**1** was the mayor by-product. <sup>h</sup> The lower amount tested.

The alternative cyclization to Oxd was investigated with the aid of theoretical computations performed employing ab initio molecular orbital (MO) theory at the HF/6-31G\*\* level. These led to the proposal of the plausible reaction pathway **b**, which accounts for the experimental observations reported in Table 1. Upon treatment with :B, the Ts- or Ns-intermediate **A** would form the anionic intermediate **B**, which in turn gives rise to the five membered anionic intermediate **C**. The loss of 2,5- dioxopyrrolidin-1-olate from **C** leads to the Oxd-peptide **D**; the protonation of the anionic leaving group by HB<sup>+</sup> would regenerate the free base, which can be utilized in catalytic amount.

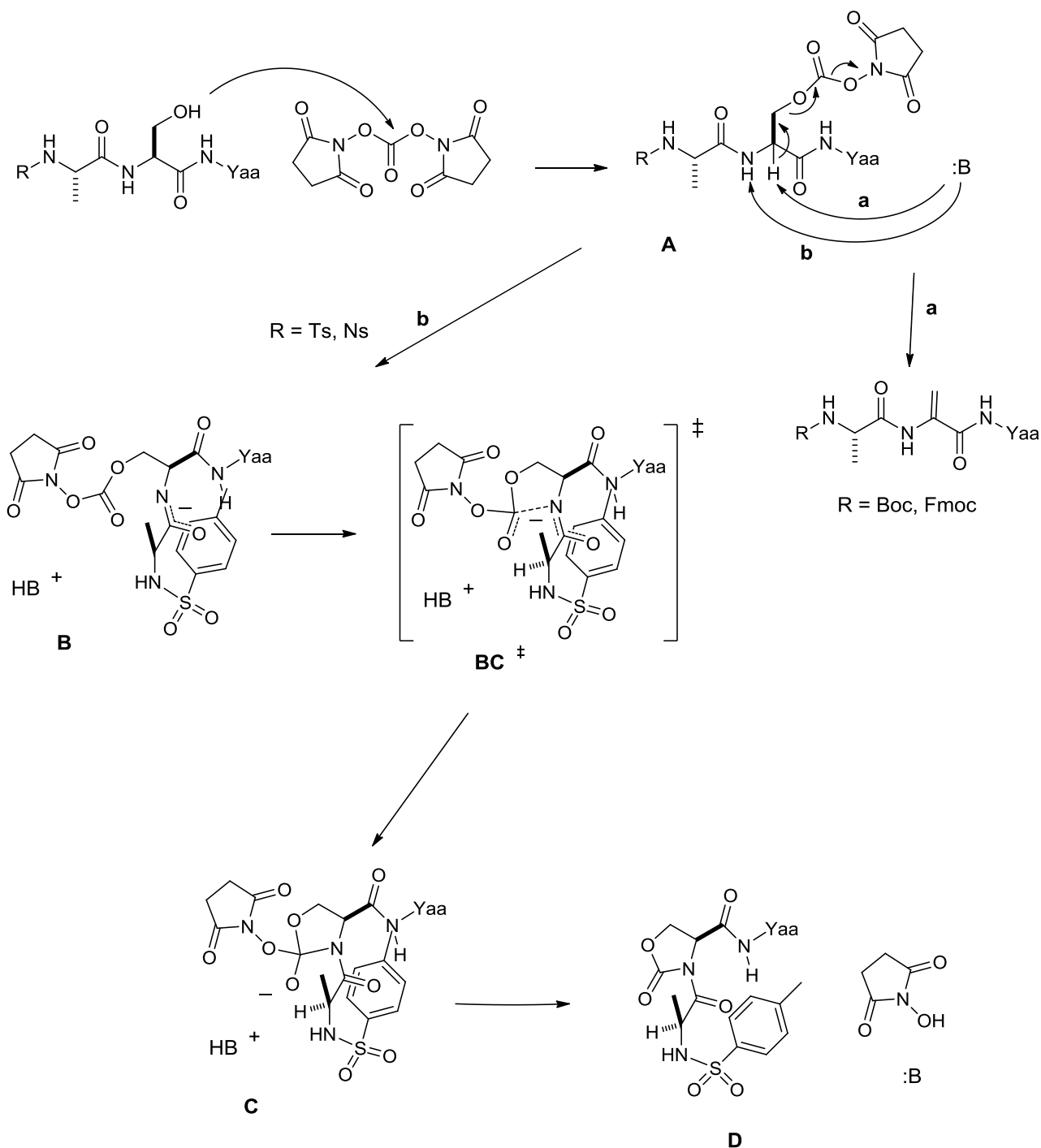
The optimized conformations of **A-D** and the estimated  $\Delta E$  are shown in the Supporting Information section, Scheme S1. The most stable conformation of the anionic intermediate **B** shows the aromatic ring of the sulfonyl group stacked below the delocalized anion at a distance of 3.5 Å; this distance is perfectly compatible with the values reported in the literature for  $\pi$ -stacking interactions<sup>[26]</sup>. The ability of arylsulfonamido groups to form sandwich structures by  $\pi$ -stacking interactions is well described in the literature<sup>[27]</sup>. Besides, electron-poor aromatic rings effectively promote the reactivity of delocalized anions such as enolates, by means of a donor-acceptor  $\pi$ -stacking stabilization of the transition states<sup>[28]</sup>. In a

similar way, it is plausible that sulfonamido groups such as *N*-tosyl and *N*-nosyl, but not mesyl, might stabilize the intermediate anion **B** as well as the plausible transition state **BC** (Scheme 3). This effect would be impossible for Boc- or Fmoc-peptides; consequently, under the same conditions, these peptides undergo elimination to Dha.

Interestingly, the calculated structures of **C** and **D** clearly revealed a AlaCH $\alpha$ ...<sup>1</sup>O-C interaction, and a non-conventional AlaCH $\alpha$ ...O=C(Oxd) hydrogen bond, respectively. The latter interaction was also confirmed by NMR analysis and modeling of the Oxd-peptides. (see next paragraph).

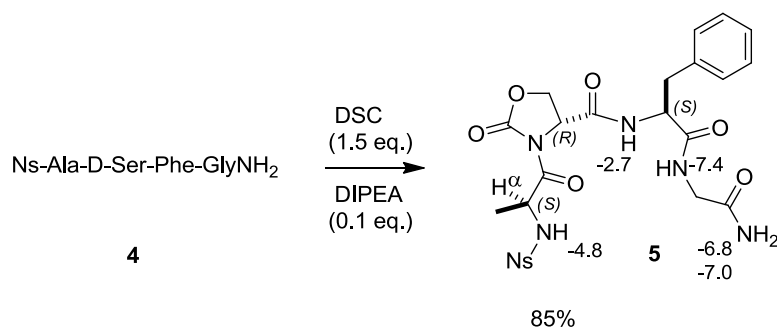
Starting from the calculated structures **A-D**, the dioxopyrrolidin-1-yl group was replaced by other leaving groups resulting from CDI, Boc<sub>2</sub>O, chloroformate, or triphosgene (see Table 1), and these new structures were optimized (not shown). The comparison revealed that the anionic intermediate **C** carrying the dioxopyrrolidin-1-yl is significantly lower in energy with respect to these analogues. This comparatively higher stability might also reflect to the transition state **BC**, accounting for the efficacy of DSC in the cyclization, compared to the other carbonates or dicarbonates, etc., discussed in Table 1, Entries 8-11.

Finally, it is plausible that the  $\pi$ -stacking is functional also at stabilizing the anionic intermediate of type **B** for peptides having the arylsulfonamido group and Ser separated by two amino acids[*Errore. Il segnalibro non è definito.*]. (not calculated).



**Scheme 3.** Plausible reaction pathways for the elimination of carbamate-peptides (pathway **a**) and alternatives for the cyclization of arylsulfonyl peptides (pathway **b**).

Epimerization during the cyclization process was excluded on the basis of the comparison of the NMR and HPLC analyses of **2a** vs **2b**, including the HPLC analysis on a chiral stationary phase (see General Methods). The mild cleavage of the arylsulfonyl groups<sup>[29]</sup> was discussed previously<sup>[Errore. Il segnalibro non è definito.]</sup>. The tosyl group was removed in sufficient yield with iodotrimethylsilane<sup>[30]</sup>, while the treatment with  $\text{Sml}_2/\text{pyrrolidine}/\text{water}$ <sup>[31]</sup> was much less efficient. The cleavage of the Ns group was easily performed with  $\text{K}_2\text{CO}_3/\text{PhSH}$ <sup>[32]</sup>, giving the deprotected peptide in good yield.



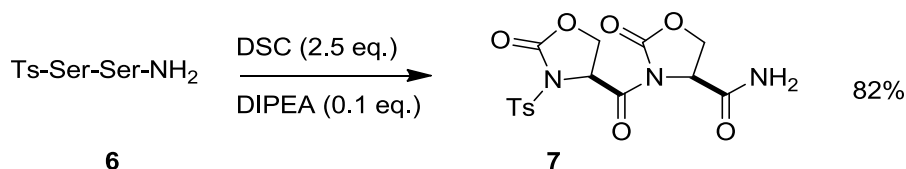
**Scheme 4.** Synthesis of **5** and  $\Delta\delta/\Delta t$  VT-NMR values of the amide protons in 8:2 DMSO- $d_6$ /H $_2$ O.

In summary, the comparison of the results enlisted in Table 1 led us to reckon the conditions of Entry 13 the best for the cyclization reaction. Consequently, the Oxd-tetrapeptide Ns-Ala-D-Oxd-Phe-GlyNH $_2$  (**5**), useful for the investigation of the conformational features of the constrained peptides, was smoothly prepared from Ns-Ala-D-Ser-Phe-GlyNH $_2$  (**4**) by treatment with DSC and 0.1 equiv. of DIPEA in 3:1 DCM/DMF (Scheme 4).

## 2.2 Synthesis of di-Oxd-peptides

Previous results<sup>[19]</sup> demonstrated that the position of a Ser or Thr residue in the sequence of the sulfonyl-peptide is practically unimportant for the cyclization to Oxd-peptide (see above). As a consequence, we envisaged the opportunity to perform a single-step cyclization of sequences containing two Ser, or a Ser and a Thr, consecutive or alternating with other amino acids.

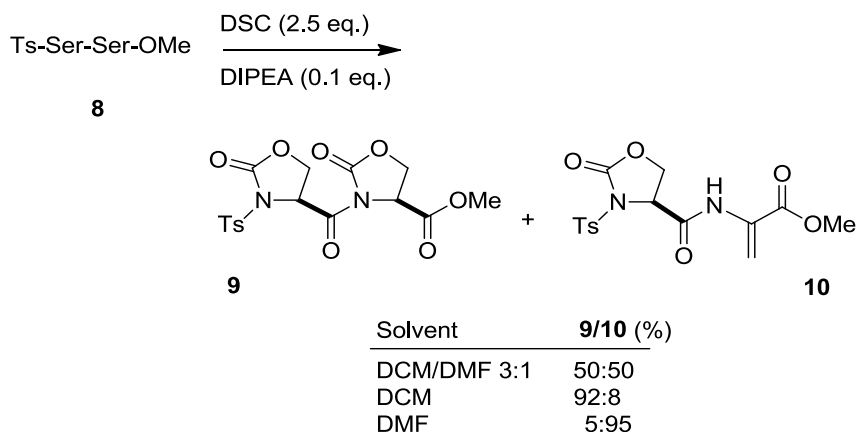
The reaction of Ts-Ser-SerNH $_2$  (**6**) with 2.5 equiv. of DSC in 3:1 DCM/DMF and in the presence of a catalytic amount of DIPEA (0.1 equiv.) gave the corresponding *di*-Oxd-amide **7** in excellent yield (Scheme 5) after isolation by flash chromatography.



**Scheme 5.** Synthesis of the di-Oxd peptide amide **7**.

On the other hand, the reaction of the dipeptide ester Ts-Ser-SerOMe (**8**) under the same reaction conditions gave a circa 1:1 mixture of the expected *di*-Oxd peptide **9** and the dipeptide containing the Dha methyl ester **10** (Scheme 6).

Possibly, this result reflects the comparatively higher acidity of the H $\alpha$  of serine methyl ester with respect to that of the serine amides<sup>[33]</sup>, which promotes the elimination of the intermediate Ser-O-succinimidyl carbonate.

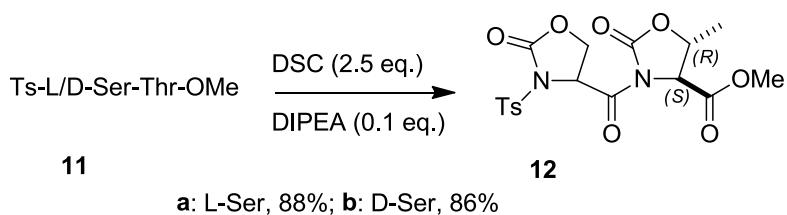


**Scheme 6.** Solvent effect in the alternative formation of the di-Oxd peptide **9** and Oxd-Dha peptide **10**.

Interestingly, the reaction outcome was dependent on the solvent utilized (Scheme 6). Indeed, on performing the reaction in DCM gave Ts-Oxd-OxdOMe (**9**) and Ts-Oxd-Dha-OMe (**10**, Dha = dehydroalanine) in 92:8 ratio (88% overall yield), while in DMF the situation was completely reversed, giving a 95:5 ratio in favor of **10** (86% overall yield).

This dipeptide Ts-Oxd-Dha-OMe is of some interest, since it contains two distinct secondary structure-inducer residues, the Oxd and a dehydroamino acid. Indeed, dehydroamino acids are well known inducer of  $\beta$ -turn structures; for instance, sequential placement of dehydroPhe ( $\Delta$ Phe) in oligomers gives repeated  $\beta$ -turns forming  $3_{10}$  helices [Errore. Il segnalibro non è definito.<sup>34</sup>].

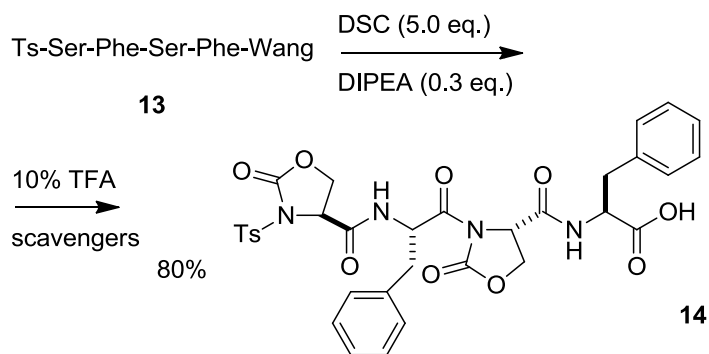
In a similar way as for the preparation of **9**, the cyclization of the peptide esters **11a** and **b** containing L-Ser, Thr, and D-Ser, Thr, respectively, gave in DCM the di-Oxd **12a, b** in high yield (Scheme 7), with only traces of the elimination products.



**Scheme 7.** Synthesis of the di-Oxd peptide esters **12a, b**.

The trans configuration of the 5-methyl-oxazolidin-2-one-4-carboxylate was deduced by the  $^1\text{H-NMR}$  coupling constant of the H4-H5 ( $J$  circa 5.0 Hz), thus retaining the (2*S*,3*R*) stereochemistry of Thr. The comparison of the NMR and HPLC analyses of **12a** vs **12b**, including the HPLC analysis on a chiral stationary phase (see General Methods) allowed considering epimerization negligible.

Finally, the *d*-Oxd-tetrapeptide acid Ts-Oxd-Phe-Oxd-Phe-OH (**14**) was entirely synthesized on solid-phase (Scheme 8). The resin-bound precursor Ts-Ser-Phe-Ser-Phe-Wang (**13**) was prepared under standard conditions, and it was subjected to cyclization by treatment with a 5 equiv. excess of DSC and catalytic DIPEA (0.3 equiv) prior to the cleavage from the resin.



**Scheme 8.** Solid-phase synthesis of **14**.

The cleavage of the di-Oxd-peptide was performed by two consecutive treatments with 10% TFA in DCM in the presence of scavengers. The peptide **14** was isolated by semi-preparative RP-HPLC with a very satisfactory yield.

### 2.3. Conformational aspects of the Oxd peptides

In order to analyze the conformational bias exerted by the Oxd on the overall structure of the peptides, we performed the conformational analyses of the representative examples **2a**, **2b**, **5**, **10**, containing one Oxd, and of **12a**, **12b**, **14**, which contain two consecutive or alternate Oxd rings.

Electronic Circular Dichroism (ECD) is a widely used technique for studying protein and peptide conformations. This technique is intrinsically a low-resolution method; however it can furnish qualitative information on the presence of ordered secondary structures<sup>[35]</sup>, although not too many examples on short peptides are reported<sup>[36]</sup>. ECD measurements of compounds **2a**, **2b**, **5**, **10**, **12a**, **12b**, **14**, were performed at room temperature in TFE<sup>[37]</sup> and methanol; **10** and **12a** also in chloroform (Supporting Information, Figure S2). These analyses gave a few information on the eventual occurrence of secondary structures. Spectra of **2b**, **5**, **10**, and **12b** show a negative  $n\pi^*$  band at *ca.* 235 nm, compatible with  $\beta$ -turn structures<sup>[38]</sup>. Spectra of structurally correlated **2a** **2b**, and of **12a** **12b** show marked differences. CD intensity changes by moving from methanol (and chloroform for **10**) to TFE, indicating that the nature of the solvent may influence the turn population. Different chiroptical properties are associated to the other compounds **2a**, **12a**, **14** in the same spectral region. For instance, by comparing ECD spectra of **12a** with those of **12b**, a specular relationship emerges in the  $n\pi^*$  region, possibly reflecting the inversion of configuration of Oxd<sup>1</sup>. CD spectra of **12a** present a positive band centered at *ca.* 230 nm accompanied by a weak positive shoulder at lower energy, while a negative  $\pi\pi^*$  band is observed at around 200 nm. In both cases magnitude of CD grows up by moving from TFE to methanol and chloroform. These spectral features suggest that for **12a**, a different secondary structure becomes predominant with respect to the one characterizing **12b**, and its stability is increased in chloroform.

The Oxd-peptides were analyzed by NMR experiments using standard techniques at 400 MHz in  $\text{CDCl}_3$ ,  $\text{CH}_3\text{OH}$ , and in the biomimetic medium 8:2  $\text{DMSO-d}_6/\text{H}_2\text{O}$ <sup>[39]</sup>. For most compounds, the <sup>1</sup>H-NMR resonances

of the compounds showed modest variations of the chemical shifts in the different solvents, suggesting conformational stability (exceptions are discussed throughout).

It has been demonstrated that the Oxd confers the preceding amide bond a well defined trans conformation<sup>[Errore. Il segnalibro non è definito. Errore. Il segnalibro non è definito.]</sup>. Accordingly, the <sup>1</sup>H-NMR analyses of all of the Oxd-peptides showed a single set of sharp resonances in each solvent, indicating conformational homogeneity or a fast equilibrium between conformers; generally, linear peptides containing a Pro show two sets of resonances, for the cis and trans conformers (see Introduction).

The <sup>1</sup>H-NMR analyses of all of the compounds showed a significantly downfield position of the H<sub>α</sub> proton of the residue preceding the Oxd. For instance, the AlaH<sub>α</sub> in Ts-Ala-Oxd-PheNH<sub>2</sub> (**2a**) it is at circa 5.1 p.p.m., while in Ts-Ala-Ser-PheNH<sub>2</sub> (**1a**) it is at circa 3.5 p.p.m.; in Ts-Oxd<sup>1</sup>-Oxd<sup>2</sup>-OMe (**9**), the Oxd<sup>1</sup>H<sub>4</sub> is at circa 6.0 p.p.m., while Oxd<sup>2</sup>H<sub>4</sub> is at circa 5.0 p.p.m. This accounts for a strong deshielding effect exerted by Oxd(C=O)<sup>[Errore. Il segnalibro non è definito. Errore. Il segnalibro non è definito.]</sup>, compatible with a non-conventional, CH...O=C intramolecular hydrogen bond<sup>[40]</sup>, and confirms the trans conformation of the amide bond between the Oxd and the preceding, deshielded residue.

Variable temperature (VT)-<sup>1</sup>H-NMR experiments were utilized to deduce the presence of H-bonds (Tables S1-3, Supporting Information). The homochiral Oxd-peptide Ts-Ala-Oxd-PheNH<sub>2</sub> (**2a**) did not manifest the presence of any H-bond: the  $\Delta\delta/\Delta t$  values of AlaNH, PheNH in 8:2 DMSO/H<sub>2</sub>O were -6.8, and -4.3 p.p.b./K, respectively.

On the other hand, for Ts-Ala-D-Oxd-PheNH<sub>2</sub> (**2b**) the  $\Delta\delta/\Delta t$  (p.p.b./K, 8:2 DMSO/H<sub>2</sub>O) values of AlaNH, PheNH were -4.2, and -2.6, and for Ts-Ala-D-Oxd-Phe-GlyNH<sub>2</sub> (**5**) the  $\Delta\delta/\Delta t$  (p.p.b./K, 8:2 DMSO/H<sub>2</sub>O) values of AlaNH, PheNH, and GlyNH were -4.8, -2.7, and -7.4. The comparatively lower VT-<sup>1</sup>H-NMR  $\Delta\delta/\Delta t$  parameters of PheNH for **2b** and **5** are suggestive of the occurrence of a significant amount of folded conformations having PheNH involved in a H-bond ( $|\Delta\delta/\Delta t| < \text{or close to } 2.5 \text{ p.p.b./K}^{-1}$ )<sup>[Errore. Il segnalibro non è definito.]</sup><sup>[41]</sup>. The same trends can be observed also in the other solvents (Table S1, Supporting Information).

Molecular backbone conformations were investigated by 2D ROESY analysis in 8:2 DMSO/H<sub>2</sub>O at 400Mhz, and the intensities of the resulting cross-peak were ranked to infer plausible interproton distances (Tables S4-10 Supporting Information). 2D gCOSY experiments were utilized for the unambiguous assignment of all of the resonances.

Structures consistent with the spectroscopic analyses were obtained by restrained MD simulations, using the distances derived from ROESY as constraints, and minimized with the AMBER force field. The  $\omega$ bonds were set at 180°, as the absence of H<sub>α</sub><sup>*i*</sup>-H<sub>α</sub><sup>*i+1*</sup> cross-peaks excluded cis peptide bonds. Simulations were conducted in a box of explicit, equilibrated TIP3P water molecules. Random structures were generated by unrestrained high-temperature MD; the structures were subjected to high-temperature restrained MD with a scaled force field, followed by a simulation with full restraints. Finally, the system was gradually cooled, and the structures were minimized. The results were clustered by the RMSD analysis of the backbone atoms.

For Ts-Ala-Oxd-PheNH<sub>2</sub> (**2a**) and Ts-Ala-D-Oxd-PheNH<sub>2</sub> (**2b**), the procedure gave one mayor clusters each, comprising circa 80% of the structures. For each compound cluster, the representative geometries with the lowest internal energy were selected and analyzed (Figure 2). The comparison of the two structures show a

clear difference; while **2a** adopts an extended conformation, the peptide containing the D-Oxd shows a preference for a folded conformation, compatible with a  $\beta$ -turn centered on D-Oxd.

To investigate the dynamic behavior of **2a** and **2b**, the structures were analyzed by unrestrained MD for 10 ns in a box of explicit water molecules. Besides the different random conformations, the analysis of the trajectories of **2b**, but not of **2a**, revealed a well-defined  $\beta$ -turn secondary structure stabilized by an explicit H-bond between PheNH and the Ala(C=O), in agreement with the VT-NMR parameters.

For Ns-Ala-D-Oxd-PheGly-NH<sub>2</sub> (**5**), the conformational analysis gave two clusters comprising altogether more than 85% of the structures. For each cluster, the representative geometries **5A** and **5B** with the lowest internal energy were selected and analyzed (Figure 2). They differ almost exclusively by the opposite orientation of the D-Oxd-Phe peptide bond. Possibly, the two structures represent conformers in fast equilibrium. The structure **5A** shows a clear inverse  $\beta$ -turn centered on D-Oxd, and is circa 1.4 Kcal mol<sup>-1</sup> lower in energy than **5B**; the latter shows some violations of the distance constraint involving PheNH.

To investigate the dynamic behavior of **5**, the two conformers **A** and **B** were analyzed by unrestrained MD for 10 ns in a box of standard TIP3P water molecules. The simulation showed the conversion of one conformation into the other. The analysis of the trajectories of **5A** revealed the occurrence of well-defined secondary structures stabilized by an explicit H-bond between Ala(C=O) and PheNH, in agreement with the VT-NMR parameters. On the other hand, the analysis of the trajectories of **5b** revealed that occasionally the structure adopts an inverse  $\beta$ -turn type I conformation, stabilized by an H-bond between GlyNH and the Ala(C=O), but this observation is not supported by the VT-NMR analysis.

The preference for the folded structures shown by **2b** and **5** makes sense. It is well known that linear oligopeptides including a heterochiral Pro show higher propensity to adopt stable inverse  $\beta$ - or  $\gamma$ -turns, the Pro occupying the position  $i+1$ , compared to the peptides composed of all L-amino acids<sup>[42]</sup>. Besides, 10- and 7-membered H-bonded rings form competitively to each other, depending on the solvent<sup>[43]</sup>, on the prevalence of a trans over cis conformation of the amide bond preceding Pro<sup>[44]</sup>, and/or on the nature and steric hindrance of the amino acids preceding and following Pro<sup>[45]</sup>.



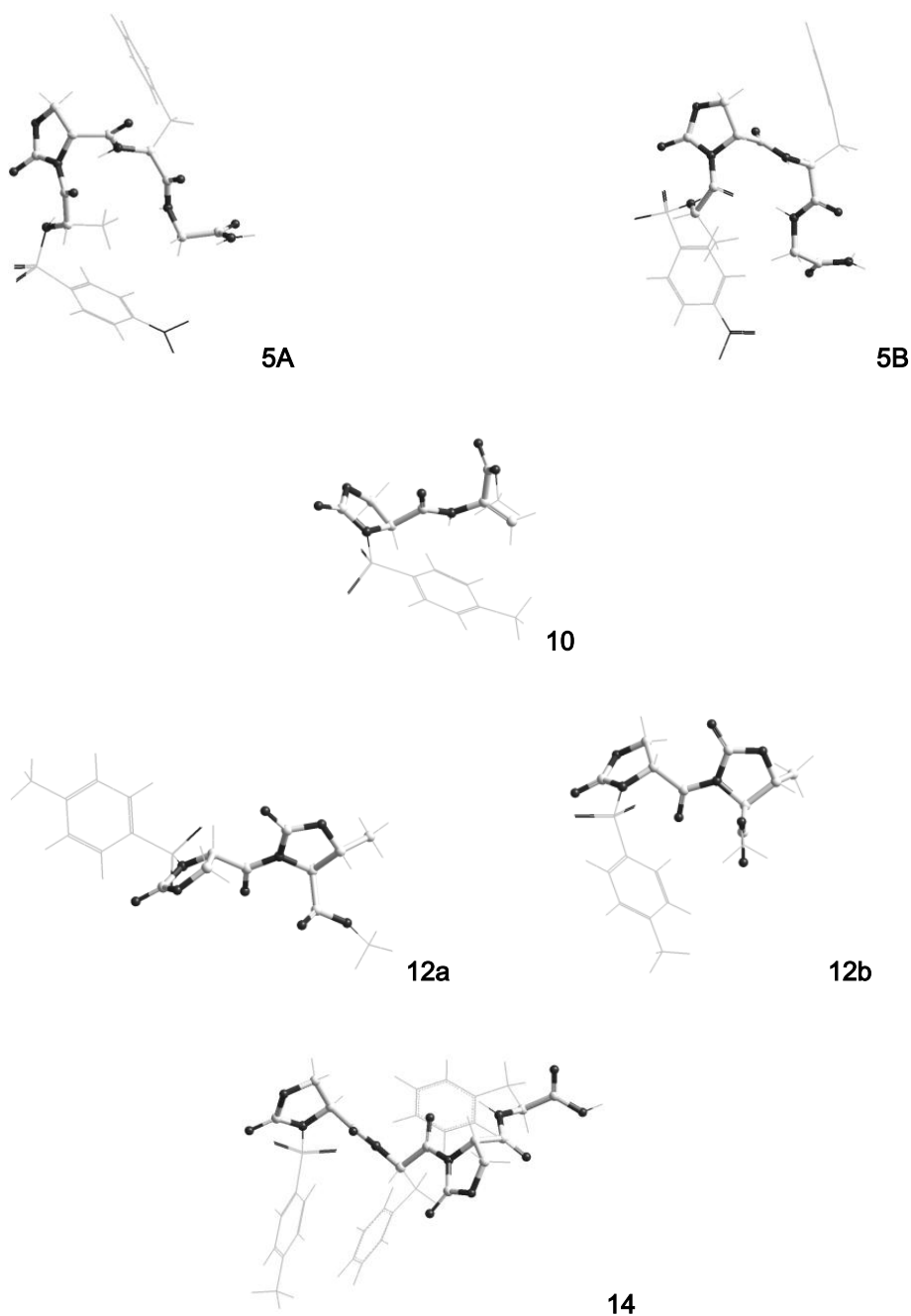


**Fig. (2).** Representative low-energy structures of **2a**, **2d**, **5a**, **5b**, **10**, **12a**, **12b**, **14** consistent with ROESY analysis, calculated by restrained MD in a 30x 30x30 box of standard TIP3P water molecules. Backbones and Oxid are rendered in balls-and cylinders, the rest in sticks.

The conformational analysis of (**10**) gave one clusters comprising the large majority of the structures. The representative geometry with the lowest internal energy is shown in Figure 2. The calculated geometry of the Dha residue perfectly matches the structures reported in the literature<sup>[46]</sup>.

The conformational preference of **10** showed some dependence on the solvent. The <sup>1</sup>H-NMR resonances of the H4 and H5 protons of Oxid in CDCl<sub>3</sub> showed significant differences with respect to 8:2 DMSO/H<sub>2</sub>O and CH<sub>3</sub>OH.

The VT-NMR analysis in CDCl<sub>3</sub> gave DhaNH  $\Delta\delta/\Delta t = -1.8$  p.p.b./K, and in 8:2 DMSO/H<sub>2</sub>O  $\Delta\delta/\Delta t = -4.6$  p.p.b. Apparently, in the less competitive CDCl<sub>3</sub> the DhaNH is involved in a H-bond with one of the S=O, conferring **10** a pseudo  $\beta$ -turn structure, which is not observed in 8:2 DMSO/H<sub>2</sub>O. Accordingly, the unrestrained molecular dynamics simulations for 10ns in explicit water did not show this pseudo  $\beta$ -turn conformation.

The ROESY-restrained MD simulations of Ts-Oxd<sup>1</sup>-(5-Me-Oxd<sup>2</sup>)-OMe (**12a**) and Ts-D-Oxd<sup>1</sup>-(5-Me-Oxd<sup>2</sup>)-OMe (**12b**) gave, after clustering, one clusters each, comprising almost the totality of the structures; the representative ones are shown in Figure 2. The two oxazolidin-2-ones are nearly orthogonal to each other. The unrestrained MD confirmed the rigidity of the conformations, since the rotation of the two Oxd rings one with respect to the other was not observed during the simulations.

The calculated conformation of the Ts-Oxd<sup>1</sup>-Phe<sup>2</sup>-Oxd<sup>3</sup>-Phe<sup>4</sup>-OH (**14**), determined as above described, presents a extended conformation (Figure 2), confirming that homochiral peptides do not tend to fold.

The <sup>1</sup>H-NMR signals of the compound significantly vary in the different environments; for instance, the  $\delta$  of Phe<sup>4</sup>H $\alpha$  in CDCl<sub>3</sub>, 8:2 DMSO/H<sub>2</sub>O, and CH<sub>3</sub>OH is 4.83, 4.53, 4.22, respectively, and the  $\delta$  of Phe<sup>2</sup>H $\alpha$  is 5.78, 5.57, 5.68.

The VT-NMR analysis in 9:1 CDCl<sub>3</sub>/DMSO-d<sub>6</sub> (this compound is not soluble in pure chloroform) indicated some preference for a pseudo  $\beta$ -turn on Oxd<sup>1</sup> stabilized by a H-bond between Oxd<sup>1</sup>(S=O) and Phe<sup>2</sup>NH (Phe<sup>2</sup>NH  $\Delta\delta/\Delta t = -2.9$  p.p.b.). However, as observed for **10**, this conformation is not stable in more polar environments (for instance, in 8:2 DMSO/H<sub>2</sub>O Phe<sup>2</sup>NH  $\Delta\delta/\Delta t = -5.2$  p.p.b.), and it is not observed during the unrestrained MD simulations in explicit water.

### 3. Conclusions

In this work we discuss our methodology for the straightforward preparation of Oxd-peptides starting from arylsulfonyl peptides containing L or D-configured Ser or Thr by treatment with DSC and a base.

The mechanism was investigated by varying the reaction conditions, and the results were rationalized with the aid of theoretical computations. The experiments highlighted the role of the arylsulfonylamido group and DSC. Indeed, while tosyl and nosyl gave the ring closure, the mesyl group was ineffective; further, CDI, Boc<sub>2</sub>O, triphosgene, and ClCOOMe, failed to afford the Oxd-peptides in significant yield. The reaction was performed by using catalytic amounts of DIPEA, DBU, or DMAP.

Essentially, computations suggested that the electron-poor arylsulfonylamido group might effectively stabilize the anionic intermediate which leads to the Oxd ring by a  $\pi$ -stacking interaction. Computations also allowed to rationalize the effectiveness of DSC compared to other carbonates or dicarbonates.

We expanded the scope of the methodology by preparing in a single step *d**i*-Oxd-peptides from peptides containing two consecutive Ser, or Ser and Thr, or two Ser separated by other amino acids. The peptides amide gave the corresponding *d**i*-Oxd-amides, as expected, while peptide methyl ester gave the *d**i*-Oxd-ester or the peptide containing Oxd and Dha-ester, depending on the solvent selected for the reaction. The synthesis of the linear precursors and the cyclization reaction was performed either in solution or in the solid phase, making the entire process a convenient method for the preparation of constrained peptides or foldamers.

These Oxd residues can be regarded to as suitable constrained pseudo-Pro. The peptides containing the Oxd in place of Pro show an all-trans conformation instead of mixtures of cis and trans conformers. Homochiral sequences tend to adopt extended conformations, while the presence of a D-Oxd ring induces folded conformations, with a inverse  $\gamma$ -turn centered on D-Oxd, stabilized by a explicit H-bond.

## 4. Experimental

### 4.1 General Methods

Unless stated otherwise, standard chemicals were obtained from commercial sources and used without further purification. Flash chromatography was performed on silica gel (230-400 mesh), using mixtures of distilled solvents. Analytical RP-HPLC was performed on an ODS column (4.6  $\mu\text{m}$  particle size, 100 Å pore diameter, 250  $\mu\text{m}$ , DAD 210 nm, from a 9:1 H<sub>2</sub>O/CH<sub>3</sub>CN to a 2:8 H<sub>2</sub>O/CH<sub>3</sub>CN in 20 min) at a flow rate of 1.0 mL/min, followed by 10 min at the same composition. Semi-preparative RP-HPLC was performed on a C18 column (7  $\mu\text{m}$  particle size, 21.2mm x 150 mm, from 8:2 H<sub>2</sub>O/CH<sub>3</sub>CN to 100% CH<sub>3</sub>CN in 10 min) at a flow rate of 12 mL/min. Purities were assessed by analytical RP-HPLC under the above reported conditions and elemental analysis. Chiral HPLC analysis was performed on a CHIRALPAK IC column (0.46 cm x 25 cm), n-hexane/2-propanol 1:1, at 0.8 mL min<sup>-1</sup>. Semi-preparative and analytical RP-HPLC of the peptide acid **14** were performed as reported above, with the addition of 0.1% TFA in the mobile phase. Elemental analyses have been performed using a Thermo Flash 2000 CHNS/O analyzer. NMR spectra were recorded on a Varian instrument. Circular Dichroism (CD) spectra were recorded on a Jasco J-710 spectropolarimeter.

#### 4.1.1. Peptide synthesis

A stirred solution of the *N*-protected amino acid in 4:1 DCM/DMF (5 mL) was treated with HOBt (1.2 equiv.), at r.t and under inert atmosphere. After 10 min, the *C*-protected amino acid (1.1 equiv.), EDCI-HCl (1.2 equiv.) and TEA (3 equiv.) were added while stirring at r.t. under inert atmosphere. After 3h, the mixture was concentrated at reduced pressure, and the residue was diluted with EtOAc (25 mL). The solution was washed with 0.1 M HCl (5 mL), and a saturated solution of NaHCO<sub>3</sub> (5 mL). The organic layer was dried over Na<sub>2</sub>SO<sub>4</sub> and the solvent was evaporated at reduced pressure. The crude peptides were analyzed by HPLC-MS analysis, and were used without further purifications.

The intermediate *N*-Boc peptides were deprotected by treatment with 1:2 TFA/DCM (5 mL), while stirring, at r.t. After 15 min, the solution was evaporated at reduced pressure, and the treatment was repeated. The residue was suspended in Et<sub>2</sub>O (20 mL). The peptide-TFA salts which precipitated were used for the next couplings without further purifications.

**Table 1.** RP-HPLC and ES-MS analyses of the linear peptides.

compd	ES-MS m/z [M+1] vs calcd	Purity (%) <sup>[a]</sup>	compd	ES-MS m/z [M+1] vs calcd	Purity (%) <sup>[a]</sup>
<b>1a</b>	477.2/477.1	89	<b>1b</b>	477.1/477.1	86
<b>1c</b>	508.2/508.2	86	<b>1d</b>	401.1/401.1	87
<b>4</b>	565.1/565.2	85	<b>6</b>	346.0/346.1	88
<b>8</b>	361.1/361.1	87	<b>11a</b>	374.1/374.1	90
<b>11b</b>	374.1/374.1	88	<b>13<sup>b</sup></b>	- <sup>c</sup>	- <sup>c</sup>

<sup>a</sup> Determined by analytical RP-HPLC, see General Methods; <sup>b</sup> Ts-Ser-Phe-Ser-Phe-Wang; the following cyclization was performed in solid phase. <sup>c</sup> Not determined.

#### 4.1.2. Mono-Oxd-peptide synthesis

*Ts-Ala-Oxd-Phe-NH<sub>2</sub>* (**2a**). DSC (0.13 g, 0.50 mmol) was added to a stirred solution of the linear peptide Ts-Ala-Ser-Phe-NH<sub>2</sub> (**1a**, 0.20 g, 0.42 mmol), in 3:1 DCM/DMF (4 mL) followed by DIPEA (7.4  $\mu$ L, 0.04 mmol) at r.t. and under inert atmosphere. After 3h, the solvent was removed at reduced pressure, the residue was diluted with 0.1M HCl (5 mL), and the mixture was extracted three times with DCM (5 mL). The combined organic layers were dried over sodium sulphate, filtered, and concentrated at reduced pressure. The residue was purified by flash chromatography over silica-gel (eluant 1:1 hexane/EtOAc, column size: 15 $\times$ 1.0 cm<sup>2</sup>) to give **2a** (0.194 g, 92%, 95% pure by analytical RP-HPLC). IR (nujol)  $\nu$ : 1766, 1722, 1649, 1530 cm<sup>-1</sup>; <sup>1</sup>H-NMR (CDCl<sub>3</sub>)  $\delta$  1.31 (d, J=7.3 Hz, 3H, AlaMe), 2.39 (s, 3H, TsMe), 3.01-3.16 (m, 2H, PheH $\beta$ ), 4.26 (dd, J=4.2, 9.3 Hz, 1H, OxdH5), 4.44 (t, J=9.3 Hz, 1H, OxdH5), 4.63 (q, J=7.4 Hz, 1H, PheH $\alpha$ ), 4.90 (dd, J=4.2, 8.6 Hz, 1H, OxdH4), 5.12 (dq, J=7.4, 9.3 Hz, 1H, AlaH $\alpha$ ), 6.03 (br.s, 1H, CONH<sub>2</sub>), 6.35 (br.s, 1H, CONH<sub>2</sub>), 6.40 (d, J=9.3 Hz, 1H, AlaNH), 7.09-7.26 (m, 7H, ArH), 7.75 (d, J=8.4 Hz, 2H, ArH), 7.96 (d, J=8.0 Hz, 1H, PheNH); <sup>13</sup>C-NMR (2:1 CDCl<sub>3</sub>/DMSO-d<sub>6</sub>)  $\delta$ : 18.5, 20.8, 39.1, 47.8, 50.7, 54.9, 56.0, 127.1, 127.3, 128.7, 129.4, 129.8, 136.4, 139.5, 143.9, 152.4, 167.9, 173.5, 174.5; RP-HPLC (see general methods) 7.01 min; ES-MS  $m/z$  503.2 [M+1], calcd 503.2; Elem. Anal. for C<sub>23</sub>H<sub>26</sub>N<sub>4</sub>O<sub>7</sub>S, calcd: C 54.97, H 5.21, N 11.15, S 6.38; found: C 54.92, H 5.19, N 11.10, S 6.36.

*Ts-Ala-D-Oxd-Phe-NH<sub>2</sub>* (**2b**). The reaction of Ts-Ala-D-Ser-Phe-NH<sub>2</sub> (**1b**, 0.20 g, 0.42 mmol) under the same conditions described for **1a** gave **2b** (0.190 g, 90%, 96% pure by analytical RP-HPLC). IR (nujol)  $\nu$ : 1770, 1717, 1651, 1528 cm<sup>-1</sup>; <sup>1</sup>H-NMR (CDCl<sub>3</sub>)  $\delta$ : 1.25 (d, J=7.2 Hz, 3H, AlaMe), 2.38 (s, 3H, TsMe), 2.85 (dd, J=9.2, 14.0 Hz, 1H, PheH $\beta$ ), 3.25 (dd, J=4.8, 14.0 Hz, 1H, PheH $\beta$ ), 3.75 (dd, J=3.0, 8.4 Hz, 1H, OxdH5), 4.28 (t, J=9.2 Hz, 1H, OxdH5), 4.66 (q, J=7.4 Hz, 1H, PheH $\alpha$ ), 4.72 (dd, J=3.6, 9.2 Hz, 1H, OxdH4), 5.09 (quint, J=7.8 Hz, 1H, AlaH $\alpha$ ), 6.00 (br.s, 1H, CONH<sub>2</sub>), 6.62 (d, J=9.2 Hz, 1H, AlaNH), 6.70 (br.s, 1H, CONH<sub>2</sub>), 7.02-7.29 (m, 7H, ArH), 7.65 (d, J=8.4 Hz, 2H, ArH), 8.23 (d, J=8.4 Hz, 1H, PheNH); <sup>13</sup>C-NMR (2:1 CDCl<sub>3</sub>/DMSO-d<sub>6</sub>)  $\delta$  19.0, 21.1, 40.1, 47.0, 50.2, 55.6, 55.8, 127.3, 127.5, 129.1, 129.5, 130.1, 136.7, 139.9, 143.1, 153.4, 168.1, 173.2, 173.5; RP-HPLC (see general methods) 7.01 min; ES-MS  $m/z$  503.2 [M+1], calcd 503.2; Elem. Anal. for C<sub>23</sub>H<sub>26</sub>N<sub>4</sub>O<sub>7</sub>S, calcd: C 54.97, H 5.21, N 11.15, S 6.38; found: C 54.94, H 5.24, N 11.09, S 6.34.

**Ns-Ala-Oxd-Phe-NH<sub>2</sub> (2c).** The reaction of Ns-Ala-Ser-Phe-NH<sub>2</sub> (**1c**, 0.20 g, 0.39 mmol) under the same conditions described for **1a** gave **2c** (0.189 g, 90%, 96% pure by analytical RP-HPLC). IR (nujol)  $\nu$ : 1783, 1710, 1705, 1653, 1525 cm<sup>-1</sup>; <sup>1</sup>H-NMR (CDCl<sub>3</sub>)  $\delta$ : 1.21 (d, J=6.8 Hz, 3H, AlaMe), 1.33 (d, J=7.2 Hz, 3H, AlaMe), 2.43 (s, 3H, TsMe), 3.02 (dd, J=6.4, 13.8 Hz, 1H, PheH $\beta$ ), 3.06 (dd, J=6.9, 13.8 Hz, 1H, PheH $\beta$ ), 4.22 (dd, J=4.3, 9.0 Hz, 1H, OxdH5), 4.44 (t, J=9.2 Hz, 1H, OxdH5), 4.62 (q, J=7.1 Hz, 1H, PheH $\alpha$ ), 4.92 (dd, J=4.3, 8.8 Hz, 1H, OxdH4), 5.27 (quint, J=6.8 Hz, 1H, AlaH $\alpha$ ), 5.79 (br.s, 1H, CONH<sub>2</sub>), 6.51 (br.s, 1H, CONH<sub>2</sub>), 6.61 (d, J=8.4 Hz, 1H, AlaNH), 7.10-7.28 (m, 8H, ArH+AlaNH), 7.72 (d, J=8.0 Hz, 2H, ArH), 7.80 (d, J=7.2 Hz, 1H, PheNH); <sup>13</sup>C-NMR (2:1 CDCl<sub>3</sub>/DMSO-d<sub>6</sub>)  $\delta$  16.3, 18.0, 20.5, 36.7, 47.1, 51.3, 53.6, 55.2, 64.8, 125.9, 126.1, 127.4, 128.4, 128.7, 135.6, 136.0, 142.6, 151.4, 166.8, 170.6, 171.7, 171.9; Elem. Anal. for C<sub>22</sub>H<sub>23</sub>N<sub>5</sub>O<sub>9</sub>S, calcd: C 49.53, H 4.35, N 13.13, S 6.01; found: C 49.49, H 4.33, N 13.13, S 5.98.

**Ns-Ala-D-Oxd-Phe-Gly-NH<sub>2</sub> (5).** The reaction of Ns-Ala-D-Oxd-Phe-Gly-NH<sub>2</sub> (**4**, 0.20 g, 0.35 mmol) under the same conditions described for **1a** gave **5** (0.178 g, 85%, 96% pure by analytical RP-HPLC). IR (nujol)  $\nu$ : 1768, 1719, 1655, 1534 cm<sup>-1</sup>; <sup>1</sup>H-NMR (9:1 CDCl<sub>3</sub>/DMSO-d<sub>6</sub>)  $\delta$  1.13 (d, J=7.0 Hz, 3H, Me), 3.01 (dd, J=6.2, 13.8 Hz, 1H, PheH $\beta$ ), 3.23 (dd, J=6.8, 13.8 Hz, 1H, PheH $\beta$ ), 3.64 (dd, J=3.1, 8.9 Hz, 1H, D-OxdH5), 3.70-3.79 (m, 2H, GlyH $\alpha$ ), 4.30 (t, J=8.6 Hz, 1H, D-OxdH5), 4.64 (q, J=7.1 Hz, 1H, PheH $\alpha$ ), 4.72 (dd, J=2.9, 9.0 Hz, 1H, D-OxdH4), 5.13 (quint, 7.1 Hz, 1H, AlaH $\alpha$ ), 6.62 (br.s, 1H, CONH<sub>2</sub>), 7.05 (br.s, 1H, CONH<sub>2</sub>), 7.11-7.25 (m, 5H, ArH), 7.90 (d, J=8.4 Hz, 2H, ArH), 8.02 (t, J=7.9 Hz, 1H, GlyNH), 8.29 (d, J=8.0 Hz, 1H, PheNH), 8.35 (d, J=8.4 Hz, 2H, ArH), 8.40 (d, J=9.3 Hz, 1H, AlaNH); <sup>13</sup>C-NMR (DMSO-d<sub>6</sub>)  $\delta$ : 18.0, 37.6, 42.2, 51.6, 56.0, 58.2, 62.4, 125.2, 125.9, 127.8, 128.8, 128.6, 136.7, 150.4, 151.3, 153.9, 169.9, 171.7, 172.3, 173.2; RP-HPLC (see general methods) 7.85 min; ES-MS  $m/z$  591.2 [M+1], calcd 591.1; Elem. Anal. for C<sub>24</sub>H<sub>26</sub>N<sub>6</sub>O<sub>10</sub>S, calcd: C 48.81, H 4.44, N 14.23, S, 5.43; found: C 48.77, H 4.47, N 14.19, S, 5.47.

#### 4.1.3. Di-Oxd-peptide synthesis

**Ts-Oxd<sup>1</sup>-Oxd<sup>2</sup>-NH<sub>2</sub> (7).** To a stirred solution of Ts-Ser-Ser-NH<sub>2</sub> (**6**, 0.2 g, 0.58 mmol) in 3:1 DCM/DMF (4 mL), DSC (0.37 g, 1.45 mmol) and DIPEA (10  $\mu$ L, 0.06 mmol.) were added at r.t. under inert atmosphere. After 4h, work up was performed as described above for **2a**, giving **7** (0.189 g, 82%, 95% pure by analytical RP-HPLC). IR (nujol)  $\nu$ : 1776, 1770, 1725, 1711; <sup>1</sup>H-NMR (CDCl<sub>3</sub>)  $\delta$ : 2.43 (s, 3H, Me), 4.37 (dd, J=2.8, 9.2 Hz, 1H, Oxd<sup>1</sup>H5), 4.48 (dd, J=3.6, 9.6 Hz, 1H, Oxd<sup>2</sup>H5), 4.62-4.71 (m, 2H, Oxd<sup>1</sup>H5+Oxd<sup>2</sup>H5), 5.00 (dd, J=2.8, 8.8 Hz, 1H, Oxd<sup>2</sup>H4), 5.99 (dd, J=3.6, 9.6 Hz, 1H, Oxd<sup>1</sup>H4), 7.07 (s, 1H, CONH<sub>2</sub>), 7.35 (d, J=8.1 Hz, 2H, ArH), 7.76 (s, 1H, CONH<sub>2</sub>), 7.93 (d, J=8.1 Hz, 2H, ArH); <sup>13</sup>C-NMR (9:1 CDCl<sub>3</sub>/DMSO-d<sub>6</sub>)  $\delta$ : 21.1, 50.6, 57.4, 62.9, 63.2, 128.2, 129.7, 132.7, 137.9, 151.4, 154.1, 167.9, 170.6; RP-HPLC (see general methods) 5.7 min; ES-MS  $m/z$  398.0 [M+1], calcd 398.1; Elem. Anal. for C<sub>15</sub>H<sub>15</sub>N<sub>3</sub>O<sub>8</sub>S, calcd: C 45.34, H 3.80, N 10.57, S 8.07; found: C 45.28, H 3.82, N 10.60, S 8.10.

**Ts-Oxd<sup>1</sup>-Oxd<sup>2</sup>-OMe (9).** A stirred solution of Ts-Ser-Ser-OMe (**8**, 0.2 g, 0.56 mmol) in DCM (4 mL), was treated as described above for the synthesis of **7**. The same work up gave **9** (0.187 g, 81%, 94% pure by analytical RP-HPLC) and **10** (0.016 g, 8%), separated by flash chromatography.

**(9)**. IR (nujol)  $\nu$ : 1779, 1769, 1721;  $^1\text{H-NMR}$  ( $\text{CDCl}_3$ )  $\delta$  2.45 (s, 3H, Me), 3.82 (s, 3H, COOMe), 4.39 (dd,  $J=3.6, 9.6$  Hz, 1H, Oxd<sup>1</sup>H5), 4.50 (dd,  $J=2.2, 9.1$  Hz, 1H, Oxd<sup>2</sup>H5), 4.74 (t,  $J=9.4$  Hz, 1H, Oxd<sup>1</sup>H5), 4.76 (t,  $J=9.3$  Hz, 1H, Oxd<sup>2</sup>H5), 5.08 (dd,  $J=1.8, 9.1$  Hz, 1H, Oxd<sup>2</sup>H4), 6.00 (dd,  $J=3.4, 9.6$  Hz, 1H, Oxd<sup>1</sup>H4), 7.36 (d,  $J=8.0$  Hz, 2H, ArH), 7.98 (d,  $J=8.0$  Hz, 2H, ArH);  $^{13}\text{C-NMR}$  (2:1  $\text{CDCl}_3/\text{DMSO-d}_6$ )  $\delta$ : 21.0, 51.5, 52.1, 55.7, 62.1, 62.5, 128.9, 129.3, 133.0, 137.4, 151.3, 153.3, 165.1, 166.6; RP-HPLC (see general methods) 7.81 min; ES-MS  $m/z$  413.0 [M+1], calcd 413.1; Elem. Anal. for  $\text{C}_{16}\text{H}_{16}\text{N}_2\text{O}_9\text{S}$ , calcd: C 46.60, H 3.91, N 6.79, S 7.78; found: C 46.55, H 3.88, N 6.76, S 7.75.

**Ts-Oxd-Dha-OMe (10)**. A stirred solution of **8** (0.20 g, 0.56 mmol) in DMF (3.0 mL) was treated as described above for the synthesis of **7**. The work up gave **10** (0.169 g, 82%, 94% pure by analytical RP-HPLC) and **9** (9.2 mg, 4%), isolated by flash chromatography.

**(10)**. IR (nujol)  $\nu$ : 1768, 1721, 1715;  $^1\text{H-NMR}$  ( $\text{CDCl}_3$ )  $\delta$ : 2.42 (s, 3H, Me), 3.88 (s, 3H, COOMe), 4.45 (dd,  $J=4.6, 9.0$  Hz, 1H, OxdH5), 4.52 (t,  $J=9.2$  Hz, 1H, OxdH5), 4.99 (dd,  $J=4.4, 9.2$  Hz, 1H, OxdH4), 6.05 (s, 1H, =CH), 6.65 (s, 1H, =CH), 7.34 (d,  $J=8.4$  Hz, 2H, ArH), 7.93 (d,  $J=8.4$  Hz, 2H, ArH), 8.54 (s, 1H, DhaNH);  $^{13}\text{C-NMR}$  (2:1  $\text{CDCl}_3/\text{DMSO-d}_6$ )  $\delta$ : 21.4, 52.6, 57.9, 66.0, 111.0, 128.7, 128.9, 129.1, 129.1, 131.0, 133.8, 145.4, 151.5, 163.6, 166.8; RP-HPLC (see general methods) 7.47 min; ES-MS  $m/z$  369.1 [M+1], calcd 369.1; Elem. Anal. for  $\text{C}_{15}\text{H}_{16}\text{N}_2\text{O}_7\text{S}$ , calcd: C 48.91, H 4.38, N 7.60, S 8.70; found: C 48.88, H 4.35, N 7.57, S 8.68.

**Ts-Oxd<sup>1</sup>-(5-Me-Oxd<sup>2</sup>)-OMe (12a)**. A stirred solution of Ts-Ser-ThrOMe (**11a**, 0.20 g, 0.53 mmol) in DCM (4 mL), was treated as described above for the synthesis of **9**, giving **12a** (0.20 g 88%, 94% pure by analytical RP-HPLC). IR (nujol)  $\nu$ : 1788, 1768, 1719;  $^1\text{H-NMR}$  ( $\text{CDCl}_3$ )  $\delta$ : 1.63 (d,  $J=6.0$  Hz, 3H, 5-Me), 2.46 (s, 3H, TsMe), 3.82 (s, 3H, COOMe), 4.39 (dd,  $J=3.2, 9.2$  Hz, 1H, Oxd<sup>1</sup>H5), 4.64 (d,  $J=5.0$  Hz, 1H, Oxd<sup>2</sup>H4), 4.73 (br.t, 2H, Oxd<sup>1</sup>H5+Oxd<sup>2</sup>H5), 6.04 (dd,  $J=4.0, 10.0$  Hz, 1H, Oxd<sup>1</sup>H4), 7.36 (d,  $J=8.0$  Hz, 2H, ArH), 7.99 (d,  $J=8.0$  Hz, 2H, ArH);  $^{13}\text{C-NMR}$  (9:1  $\text{CDCl}_3/\text{DMSO-d}_6$ )  $\delta$ : 20.6, 21.3, 53.5, 57.6, 60.6, 65.0, 75.1, 128.9, 129.0, 133.7, 145.6, 151.2, 152.0, 167.1, 167.7; RP-HPLC (see general methods) 8.33 min; ES-MS  $m/z$  427.3 [M+1], calcd 427.1; Elem. Anal. for  $\text{C}_{17}\text{H}_{18}\text{N}_2\text{O}_9\text{S}$ , calcd: C 47.89, H 4.25, N 6.57, S 7.52; found: C 47.93, H 4.2 N 6.60, S 7.49.

**Ts-D-Oxd<sup>1</sup>-(5-Me-Oxd<sup>2</sup>)-OMe (12b)**. The reaction of Ts-D-Ser-ThrOMe (**11b**, 0.20 g, 0.53 mmol) under the same conditions described for **9** gave **12b** (0.196 g, 86%, 94% pure by analytical RP-HPLC). IR (nujol)  $\nu$ : 1786, 1760, 1724;  $^1\text{H-NMR}$  ( $\text{CDCl}_3$ )  $\delta$ : 1.53 (d,  $J=6.0$  Hz, 3H, 5-Me), 2.45 (s, 3H, TsMe), 3.90 (s, 3H, COOMe), 4.27 (dd,  $J=3.2, 10.0$  Hz, 1H, Oxd<sup>1</sup>H5), 4.53 (d,  $J=5.3$  Hz, 1H, Oxd<sup>2</sup>H4), 4.72 (t,  $J=9.2$  Hz, 1H, Oxd<sup>1</sup>H4), 4.74 (t,  $J=6.0$  Hz, 1H, Oxd<sup>2</sup>H5), 5.98 (dd,  $J=3.2, 9.6$  Hz, 1H, Oxd<sup>1</sup>H4), 7.33 (d,  $J=8.0$  Hz, 2H, ArH), 7.96 (d,  $J=8.0$  Hz, 2H, ArH);  $^{13}\text{C-NMR}$  (2:1  $\text{CDCl}_3/\text{DMSO-d}_6$ )  $\delta$ : 20.9, 21.7, 53.5, 58.2, 61.7, 65.2, 75.3, 129.3, 129.4, 134.2, 145.7, 151.3, 152.2, 167.0, 167.6; RP-HPLC (see general methods) 8.33 min; ES-MS  $m/z$  427.3 [M+1], calcd 427.1; Elem. Anal. for  $\text{C}_{17}\text{H}_{18}\text{N}_2\text{O}_9\text{S}$ , calcd: C 47.89, H 4.25, N 6.57, S 7.52; found: C 47.93, H 4.2 N 6.60, S 7.49.

#### 4.1.4. Di-Oxd-peptide solid-phase synthesis

***Ts-Oxd<sup>1</sup>-Phe<sup>2</sup>-Oxd<sup>3</sup>-Phe<sup>4</sup>-OH (14)***. Wang resin pre-loaded with Fmoc-Phe (0.5 g, 0.4-0.8 mmol/g, resin particle size: 100-200 mesh) was introduced in one reactor of an automated synthesizer apparatus.

Fmoc was removed with 4:1 DMF/piperidine (5 mL) under mechanical shaking. After 15 min, the suspension was filtered, the resin was washed with DCM (5 mL) and treated while shaking with a second portion of 4:1 DMF/piperidine. After 40 min, the suspension was filtered, and the resin was washed three times in sequence with DCM (5 mL) and CH<sub>3</sub>OH (5 mL).

The resin was swollen in DCM (5 mL), and a solution of the *N*-protected amino acid (1.2 equiv.) and HOBt (1.2 equiv.) in DMF (4 mL) was added, followed by DCC (1.2 equiv.). The mixture was mechanically shaken, and after 3h the resin was filtered and washed three times with the sequence DCM (5 mL), CH<sub>3</sub>OH (5 mL). Coupling efficacy was determined by means of the Kaiser test.

The resin-bound peptide was suspended in 5:1 DCM/DMF (5 mL), and DSC (5 equiv.) and DIPEA (0.3 equiv.) were added at r.t. under inert atmosphere. After 3h the mixture was filtered, and the resin-bound peptide was washed three times in sequence with DCM (5 mL) and CH<sub>3</sub>OH (5 mL).

The resin-bound peptide was suspended in a mixture of TFA (1 mL), H<sub>2</sub>O (0.33 mL), ethanedithiol (0.33 mL), and PhOH (0.33 mL), in DCM (8 mL), and mechanically shaken at r.t. After 2 h the mixture was filtered, the resin was washed twice with 5% TFA in Et<sub>2</sub>O (5 mL), twice with Et<sub>2</sub>O (5 mL). The cleavage procedure was repeated, and all of the filtrates and washes were collected; solvent and volatiles were removed under N<sub>2</sub> flow at r.t. The resulting residue was suspended in Et<sub>2</sub>O, and the crude solid which precipitated was triturated and collected by centrifuge. The Oxd-peptide acid **14** was isolated by semipreparative RP-HPLC (General Methods) (80%, 96% pure by analytical RP-HPLC). IR (nujol)  $\nu$ : 3300-2900, 1784, 1776, 1727, 1719; <sup>1</sup>H-NMR (9:1 CDCl<sub>3</sub>/DMSO-d<sub>6</sub>)  $\delta$ : 2.37 (s, 3H, Me), 2.70 (dd, J=3.0, 14.0 Hz, 1H, Phe<sup>2</sup>H $\beta$ ), 3.17 (dd, J=6.0, 13.7 Hz, 1H, Phe<sup>4</sup>H $\beta$ ), 3.27 (dd, J=3.8, 14.0 Hz, 1H, Phe<sup>2</sup>H $\beta$ ), 3.41 (dd, J=5.8, 13.7 Hz, 1H, Phe<sup>4</sup>H $\beta$ ), 3.98 (dd, J=4.0, 8.4 Hz, 1H, Oxd<sup>3</sup>H5), 4.25 (t, J=9.0 Hz, 1H, Oxd<sup>3</sup>H5), 4.45 (t, J=8.9 Hz, 1H, Oxd<sup>1</sup>H5), 4.52 (dd, J=4.1, 8.3 Hz, 1H, Oxd<sup>1</sup>H5), 4.64 (dd, J=4.1, 7.9 Hz, 1H, Oxd<sup>3</sup>H4), 4.79 (dd, J=3.8, 8.4 Hz, 1H, Oxd<sup>1</sup>H4), 4.83 (q, J= 6.6 Hz, 1H, Phe<sup>4</sup>H $\alpha$ ), 5.78 (q, J= 6.8 Hz, 1H, Phe<sup>2</sup>H $\alpha$ ), 6.54 (d, J=7.6 Hz, 1H, Phe<sup>4</sup>NH), 6.67 (d, J=7.2 Hz, 1H, Phe<sup>2</sup>NH), 7.15-7.30 (m, 12H, Phe<sup>2</sup>ArH+Phe<sup>4</sup>ArH+TsArH), 7.76 (d, J=8.4 Hz, 2H, ArH); <sup>13</sup>C-NMR (2:1 CDCl<sub>3</sub>/DMSO-d<sub>6</sub>)  $\delta$  23.9, 36.1, 37.8, 53.4, 54.1, 56.2, 59.2, 61.9, 62.8, 125.9, 127.7, 127.7, 128.3, 128.6, 128.8, 128.9, 129.3, 129.5, 133.7, 136.6, 136.6, 137.6, 151.9, 153.1, 171.7, 171.7, 174.7, 175.2; RP-HPLC (see general methods) 10.39 min; ES-MS *m/z* 693.2 [M+1], calcd 693.2; Elem. Anal. for C<sub>33</sub>H<sub>32</sub>N<sub>4</sub>O<sub>11</sub>S, calcd: C 57.22, H 4.66, N 8.09, S, 4.63; found: C 57.18, H 4.69, N 8.12, S, 4.64.

## 5. Theoretical computations.

All theoretical calculations were performed employing the HyperChem package<sup>[47]</sup>. The structures of the product **D**, and of the plausible reaction intermediates **A**, **C**, and **D**, were calculated employing ab initio molecular orbital (MO) theory. A systematic conformational analysis for the structures was done at the HF/6-31G\* level. The conformers were re-optimized at the HF/6-31G\*\* level. Optimization was performed by conjugate gradient algorithm, convergence at 0.001; energies are expressed in Kcal mol<sup>-1</sup>. The following structures were included in the computations of **A-D**: **A**, DIPEA; **B**, DIPEAH<sup>+</sup>; **C**, DIPEAH<sup>+</sup>; **D**, 1-hydroxypyrrolidine-2,5-dione, and DIPEA.

## 6. Conformational analysis

### 6.1. Circular Dichroism.

ECD spectra were recorded from 200 to 300 nm at 25 °C. Solutions were made up in spectral grade solvents and run in a 0.01 cm quartz cell. For each sample the absorbance value was set to 1.0 at  $\lambda_{\max}$  (225÷260 nm); concentrations used were in the range 5÷11 mM. Data are reported in ellipticity (millidegree).

### 6.2. NMR analyses.

<sup>1</sup>H-NMR spectra were recorded at 400 MHz in 5 mm tubes, using 0.01 M peptide at room temperature. Solvent suppression was performed by the solvent presaturation procedure implemented in Varian (PRESAT). <sup>13</sup>C-NMR spectra were recorded at 75 MHz.

Chemical shifts are reported as  $\delta$  values. The unambiguous assignment of <sup>1</sup>H-NMR resonances was performed by 2D gCOSY, HMBC, and HSQC. gCOSY experiments were conducted with a proton spectral width of 3103 Hz. VT-<sup>1</sup>H-NMR experiments were performed over the range of 298-348 °K. 2D spectra were recorded in the phase sensitive mode and processed using a 90°-shifted, squared sine-bell apodization. 2D ROESY experiments were recorded in the biomimetic medium 8:2 DMSO-*d*<sub>6</sub>/H<sub>2</sub>O, with a 250 ms mixing time with a proton spectral width of 3088 Hz. Peaks were calibrated on DMSO.

### 6.3. ROESY and molecular dynamics.

Only ROESY-derived constraints were included in the restrained molecular dynamics. Cross-peak intensities were classified very strong, strong, medium, and weak, and were associated with distances of 2.2, 2.6, 3.0, and 4.5 Å, respectively. Geminal couplings and other obvious correlations were discarded. For the absence of  $H\alpha(i, i+1)$  ROESY cross peaks, all of the  $\omega$  bonds were set at 180° (force constant: 16 kcal mol<sup>-1</sup>Å<sup>-2</sup>). The restrained MD simulations were conducted using the AMBER force field<sup>[48]</sup> in a 30×30×30 Å box of standard TIP3P models of equilibrated water<sup>[49]</sup>. All water molecules with atoms that come closer than 2.3 Å to a solute atom were eliminated. A 100 ps simulation at 1200 °K was used for generating 50 random structures that were subsequently subjected to a 50 ps restrained MD with a 50 % scaled force field at the same temperature, followed by 50 ps with full restraints (distance force constant of 7 kcal mol<sup>-1</sup> Å<sup>-2</sup>), after which the system was cooled in 20 ps to 50 °K. H-bond interactions were not included, nor were torsion angle restraints. The resulting structures were minimized with 3000 cycles of steepest descent and 3000 cycles of conjugated gradient (convergence of 0.01 kcal Å<sup>-1</sup> mol<sup>-1</sup>). The backbones of the structures were clustered by the rmsd analysis module of HyperChem<sup>[Errore. Il segnalibro non è definito.]</sup>.

Unrestrained MD simulation was performed in a 30×30×30 Å box of standard TIP3P water for 10 ns at 298 °K, at constant temperature and pressure (Berendsen scheme<sup>[50]</sup>, bath relaxation constant of 0.2). For 1-4 scale factors, van der Waals and electrostatic interactions are scaled in AMBER to half their nominal value. The integration time step was set to 0.1 fs.

## 7. Supporting Information

*<sup>1</sup>H-NMR analyses of 2a, 2b, 5, 10, 12a, 12b, 14, in different solvents.*

### ***Ts-Ala-Oxd-Phe-NH<sub>2</sub> (2a).***

<sup>1</sup>H-NMR (8:2 DMSO/H<sub>2</sub>O) δ 1.11 (d, J=7.4 Hz, 3H, AlaMe), 2.39 (s, 3H, TsMe), 2.79 (dd, J=8.4, 13.6 Hz, 1H, PheHβ), 2.97 (dd, J=4.8, 13.6 Hz, 1H, PheHβ), 4.20 (dd, J=2.6, 9.2 Hz, 1H, OxdH5), 4.38 (q, J=8.0 Hz, 1H, PheHα), 4.52 (t, J=8.8 Hz, 1H, OxdH5), 4.69 (dd, J=2.6, 8.8 Hz, 1H, OxdH4), 5.06 (dq, J=6.8, 8.8 Hz, 1H, AlaHα), 7.09 (br.s, 1H, CONH<sub>2</sub>), 7.15-7.30 (m, 5H, ArH), 7.36 (d, J=8.4 Hz, 2H, ArH), 7.51 (br.s, 1H, CONH<sub>2</sub>), 7.65 (d, J=8.4 Hz, 2H, ArH), 8.25 (d, J=9.2 Hz, 1H, AlaNH), 8.42 (d, J=8.0 Hz, 1H, PheNH).

<sup>1</sup>H-NMR (CH<sub>3</sub>OH) δ 1.22 (d, J=7.1 Hz, 3H, AlaMe), 2.41 (s, 3H, TsMe), 2.80 (dd, J=8.0, 13.8 Hz, 1H, PheHβ), 3.03 (dd, J=4.6, 13.8 Hz, 1H, PheHβ), 4.22 (dd, J=3.0, 9.0 Hz, 1H, OxdH5), 4.43 (q, J=7.8 Hz, 1H, PheHα), 4.49-4.70 (m, 2H, OxdH5+OxdH4), 5.19 (quint, J=8.2 Hz, 1H, AlaHα), 7.15-7.30 (m, 6H, ArH+CONH<sub>2</sub>), 7.36 (m, 3H, ArH+CONH<sub>2</sub>), 7.67 (d, J=8.2 Hz, 2H, ArH), 8.36 (d, J=9.0 Hz, 1H, AlaNH), 8.67 (d, J=8.2 Hz, 1H, PheNH).

### ***Ts-Ala-D-Oxd-Phe-NH<sub>2</sub> (2b).***

<sup>1</sup>H-NMR (8:2 DMSO/H<sub>2</sub>O) δ <sup>1</sup>H-NMR (8:2 DMSO/H<sub>2</sub>O) δ 1.06 (d, J=7.2 Hz, 3H, AlaMe), 2.36 (s, 3H, TsMe), 2.73 (dd, J=10.2, 13.0 Hz, 1H, PheHβ), 3.08 (dd, J=4.6, 13.0 Hz, 1H, PheHβ), 3.42 (d, J=8.6 Hz, 1H, D-OxdH5), 4.34 (t, J=8.8 Hz, 1H, D-OxdH5), 4.64 (m, 1H, PheHα), 4.72 (d, J=8.6 Hz, 1H, D-OxdH4), 5.12 (quint, J=7.6 Hz, 1H, AlaHα), 7.15 (br.s, 1H, CONH<sub>2</sub>), 7.16-7.25 (m, 5H, ArH), 7.32 (d, J=7.8 Hz, 2H, ArH), 7.54 (br.s, 1H, CONH<sub>2</sub>), 7.60 (d, J=7.8 Hz, 2H, ArH), 8.07 (d, J=9.2 Hz, 1H, AlaNH), 8.49 (d, J=8.8 Hz, 1H, PheNH).

<sup>1</sup>H-NMR (CH<sub>3</sub>OH) δ <sup>1</sup>H-NMR (8:2 DMSO-d<sub>6</sub>/H<sub>2</sub>O) δ <sup>1</sup>H-NMR (8:2 DMSO/H<sub>2</sub>O) δ 1.30 (d, J=6.8 Hz, 3H, AlaMe), 2.19 (s, 3H, TsMe), 2.84 (dd, J=10.4, 14.0 Hz, 1H, PheHβ), 3.05 (dd, J=4.6, 14.0 Hz, 1H, PheHβ), 3.63 (dd, J=3.5, 8.8 Hz, 1H, D-OxdH5), 4.36 (t, J=9.2 Hz, 1H, D-OxdH5), 4.60 (m, 1H, PheHα), 4.64 (dd, J=4.4, 8.6 Hz, 1H, D-OxdH4), 5.26 (quint, J=6.8 Hz, 1H, AlaHα), 7.15-7.30 (m, 8H, ArH+CONH<sub>2</sub>), 7.44 (br.s, 1H, CONH<sub>2</sub>), 7.67 (d, J=7.8 Hz, 2H, ArH), 8.11 (d, J=9.0 Hz, 1H, AlaNH), 8.54 (d, J=8.2 Hz, 1H, PheNH).

***Ns-Ala-D-Oxd-Phe-Gly-NH<sub>2</sub>* (5).**

<sup>1</sup>H-NMR (8:2 DMSO-d<sub>6</sub>/H<sub>2</sub>O) δ 1.35 (d, J=7.3 Hz, 3H, Me), 2.70 (dd, J=6.4, 13.9 Hz, 1H, PheHβ), 3.12 (dd, J=6.8, 13.9 Hz, 1H, PheHβ), 3.40 (dd, J=4.0, 8.4 Hz, 1H, D-OxdH5), 3.69-3.76 (m, 2H, GlyHα), 4.34 (t, J=9.2 Hz, 1H, D-OxdH5), 4.65-4.74 (m, 2H, D-OxdH4+PheHα), 5.22 (quint, 7.1 Hz, 1H, AlaHα), 7.06 (br.s, 1H, CONH<sub>2</sub>), 7.11-7.25 (m, 6H, ArH+CONH<sub>2</sub>), 7.94 (d, J=8.5 Hz, 2H, ArH), 8.23 (t, J=7.9 Hz, 1H, GlyNH), 8.33 (d, J=8.5 Hz, 2H, ArH), 8.55 (d, J=8.0 Hz, 1H, PheNH), 8.66 (d, J=9.3 Hz, 1H, AlaNH).

<sup>1</sup>H-NMR (CH<sub>3</sub>OH) δ <sup>1</sup>H-NMR (8:2 DMSO-d<sub>6</sub>/H<sub>2</sub>O) δ 1.25 (d, J=7.1 Hz, 3H, Me), 2.86 (dd, J=9.0, 13.9 Hz, 1H, PheHβ), 3.20 (dd, J=6.4, 13.9 Hz, 1H, PheHβ), 3.55 (dd, J=3.9, 8.5 Hz, 1H, D-OxdH5), 3.80-3.90 (m, 2H, GlyHα), 4.33 (dd, J=5.0, 9.0 Hz, 1H, D-OxdH5), 4.64 (ddd, J=6.4, 8.0, 9.0 Hz, 1H, PheHα), 4.72 ((dd, J=2.6, 8.8 Hz, 1H, D-OxdH4), 5.19 (quint, 7.0 Hz, 1H, AlaHα), 7.11 (br.s, 1H, CONH<sub>2</sub>), 7.15-7.25 (m, 6H, ArH+CONH<sub>2</sub>), 7.98 (d, J=8.5 Hz, 2H, ArH), 8.28 (t, J=8.0 Hz, 1H, GlyNH), 8.39 (d, J=8.5 Hz, 2H, ArH), 8.64 (d, J=8.0 Hz, 1H, PheNH), 8.69 (d, J=8.2 Hz, 1H, AlaNH).

***Ts-Oxd-Dha-OMe* (10).**

<sup>1</sup>H-NMR (8:2 DMSO-d<sub>6</sub>/H<sub>2</sub>O) δ 2.41 (s, 3H, Me), 3.89 (s, 3H, COOMe), 4.34 (dd, J=4.0, 9.2 Hz, 1H, OxdH5), 4.62 (t, J=8.8 Hz, 1H, OxdH5), 5.25 (dd, J=3.8, 9.0 Hz, 1H, OxdH4), 6.03 (s, 1H, =CH), 6.47 (s, 1H, =CH), 7.44 (d, J=8.4 Hz, 2H, ArH), 7.94 (d, J=8.4 Hz, 2H, ArH), 10.01 (s, 1H, DhaNH).

<sup>1</sup>H-NMR (CH<sub>3</sub>OH) δ 2.49 (s, 3H, Me), 3.79 (s, 3H, COOMe), 4.28 (dd, J=4.4, 8.6 Hz, 1H, OxdH5), 4.64 (t, J=9.0 Hz, 1H, OxdH5), 5.34 (dd, J=3.4, 9.0 Hz, 1H, OxdH4), 5.86 (s, 1H, =CH), 6.32 (s, 1H, =CH), 7.45 (d, J=8.4 Hz, 2H, ArH), 7.84 (d, J=8.4 Hz, 2H, ArH), 10.12 (s, 1H, DhaNH).

***Ts-Oxd<sup>1</sup>-(5-Me-Oxd<sup>2</sup>)-OMe* (12a).**

<sup>1</sup>H-NMR (8:2 DMSO-d<sub>6</sub>/H<sub>2</sub>O) δ 1.53 (d, J=5.6 Hz, 3H, 5-Me), 2.42 (s, 3H, TsMe), 3.73 (s, 3H, COOMe), 4.32 (dd, J=2.6, 9.0 Hz, 1H, Oxd<sup>1</sup>H5), 4.82-4.93 (m, 2H, Oxd<sup>2</sup>H4+Oxd<sup>1</sup>H5), 4.94 (quint, J=5.8 Hz, 1H, Oxd<sup>2</sup>H5), 6.05 (dd, J=2.4, 9.6 Hz, 1H, Oxd<sup>1</sup>H4), 7.47 (d, J=8.4 Hz, 2H, ArH), 7.93 (d, J=8.4 Hz, 2H, ArH).

<sup>1</sup>H-NMR (CH<sub>3</sub>OH) δ 1.61 (d, J=6.4 Hz, 3H, 5-Me), 2.49 (s, 3H, TsMe), 3.82 (s, 3H, COOMe), 4.42 (dd, J=3.6, 9.2 Hz, 1H, Oxd<sup>1</sup>H5), 4.79-4.83 (m, 2H, Oxd<sup>1</sup>H5+Oxd<sup>2</sup>H4), 4.90 (dq, J=4.0, 6.4 Hz, 1H, Oxd<sup>2</sup>H5), 6.13 (dd, J=3.4, 9.8 Hz, 1H, Oxd<sup>1</sup>H4), 7.43 (d, J=8.2 Hz, 2H, ArH), 8.00 (d, J=8.2 Hz, 2H, ArH).

***Ts-D-Oxd<sup>1</sup>-(5-Me-Oxd<sup>2</sup>)-OMe* (12b).**

<sup>1</sup>H-NMR (8:2 DMSO-d<sub>6</sub>/H<sub>2</sub>O) δ 1.52 (d, J=6.4 Hz, 3H, 5-Me), 2.43 (s, 3H, TsMe), 3.81 (s, 3H, COOMe), 4.57 (d, J=6.0 Hz, 1H, Oxd<sup>2</sup>H4), 4.71 (dd, J=2.8, 8.8 Hz, 1H, D-Oxd<sup>1</sup>H5), 4.74 (t, J=9.2 Hz, 1H, D-Oxd<sup>1</sup>H5), 4.94 (quint, J=6.0 Hz, 1H, Oxd<sup>2</sup>H5), 5.97 (dd, J=3.2, 8.8 Hz, 1H, D-Oxd<sup>1</sup>H4), 7.46 (d, J=8.0 Hz, 2H, ArH), 7.86 (d, J=8.0 Hz, 2H, ArH).

<sup>1</sup>H-NMR (CH<sub>3</sub>OH) δ 1.61 (d, J=6.4 Hz, 3H, 5-Me), 2.49 (s, 3H, TsMe), 3.91 (s, 3H, COOMe), 4.58 (dd, J=3.2, 9.2 Hz, 1H, Oxd<sup>1</sup>H5), 4.63 (d, J=5.6 Hz, 1H, Oxd<sup>2</sup>H4), 4.75 (t, J=9.6 Hz, 1H, Oxd<sup>1</sup>H5), 4.86 (quint, J=6.4 Hz, 1H, Oxd<sup>2</sup>H5), 6.06 (dd, J=3.2, 9.2 Hz, 1H, Oxd<sup>1</sup>H4), 7.43 (d, J=8.0 Hz, 2H, ArH), 7.95 (d, J=8.0 Hz, 2H, ArH).

***Ts-Oxd<sup>1</sup>-Phe<sup>2</sup>-Oxd<sup>3</sup>-Phe<sup>4</sup>-OH* (14).**

<sup>1</sup>H-NMR (8:2 DMSO-d<sub>6</sub>/H<sub>2</sub>O) δ 2.38 (s, 3H, Me), 2.68 (dd, J=3.3, 13.8 Hz, 1H, Phe<sup>2</sup>Hβ), 2.95-3.05 (m, 1H, Phe<sup>4</sup>Hβ), 3.22 (m, 2H, Phe<sup>2</sup>HβPhe<sup>4</sup>Hβ), 4.06 (dd, J=3.8, 8.4 Hz, 1H, Oxd<sup>1</sup>H5), 4.20 (dd, J=4.0, 8.4 Hz, 1H, Oxd<sup>3</sup>H5), 4.53 (q, J= 6.6 Hz, 1H, Phe<sup>4</sup>Ha), 4.67 (t, J=9.0 Hz, 2H, Oxd<sup>1</sup>H5+Oxd<sup>3</sup>H5), 4.98 (dd, J=3.6, 8.8 Hz, 1H, Oxd<sup>3</sup>H4), 5.02 (dd, J=3.8, 9.2 Hz, 1H, Oxd<sup>1</sup>H4), 5.57 (q, J= 6.8 Hz, 1H, Phe<sup>2</sup>Ha), 7.12-7.28 (m, 12H, Phe<sup>2</sup>ArH+Phe<sup>4</sup>ArH+TsArH), 7.64 (d, J=8.4 Hz, 2H, ArH), 8.85 (d, J=6.8 Hz, 1H, Phe<sup>4</sup>NH), 8.93 (d, J=7.6 Hz, 1H, Phe<sup>2</sup>NH).

<sup>1</sup>H-NMR (CH<sub>3</sub>OH) δ 2.45 (s, 3H, Me), 2.70 (dd, J=3.8, 13.6 Hz, 1H, Phe<sup>2</sup>Hβ), 3.00-3.12 (m, 2H, Phe<sup>4</sup>Hβ), 3.18 (dd, J=5.6, 13.6 Hz, 1H, Phe<sup>2</sup>Hβ), 4.14 (dd, J=3.6, 8.6 Hz, 1H, Oxd<sup>1</sup>H5), 4.22 (q, J= 6.6 Hz, 1H, Phe<sup>4</sup>Hα), 4.35 (dd, J=4.1, 8.5 Hz, 1H, Oxd<sup>3</sup>H5), 4.59 (t, J=8.9 Hz, 2H, Oxd<sup>1</sup>H5), 4.64 (t, J=8.8 Hz, 2H, Oxd<sup>1</sup>H5), 4.76 (dd, J=3.8, 8.6 Hz, 1H, Oxd<sup>3</sup>H4), 4.99 (dd, J=3.6, 9.0 Hz, 1H, Oxd<sup>1</sup>H4), 5.68 (q, J= 6.8 Hz, 1H, Phe<sup>2</sup>Ha), 7.18-7.30 (m, 10H, Phe<sup>2</sup>ArH+Phe<sup>4</sup>ArH), 7.38(d, J=8.4 Hz, 2H, ArH), 7.59 (d, J=8.4 Hz, 2H, ArH), 8.90 (d, J=6.8 Hz, 1H, Phe<sup>4</sup>NH), 9.00 (d, J=7.4 Hz, 1H, Phe<sup>2</sup>NH).

**Table S1.** VT-<sup>1</sup>H-NMR Δδ/Δt values (p.p.b./K) of Ts-Ala-L/D-Oxd-Phe-NH<sub>2</sub> (**2a**, **2b**), and Ts-Ala-D-Oxd-Phe-GlyNH<sub>2</sub> (**5**) in different solvents.

compd	solvent	AlaNH	PheNH	GlyNH	CONH <sub>2</sub>
<b>2a</b>	CDCl <sub>3</sub>	-12.9	-9.6	-	-11.2/-9.2
	8:2 DMSO-d <sub>6</sub> /H <sub>2</sub> O	-6.8	-4.3	-	-5.9/-5.4
	CH <sub>3</sub> OH	-7.0	-4.6	-	-6.1/-5.8
<b>2b</b>	CDCl <sub>3</sub>	-6.7	-5.7	-	-5.9/-5.4
	8:2 DMSO-d <sub>6</sub> /H <sub>2</sub> O	-4.2	-2.6	-	-5.6/-6.8
	CH <sub>3</sub> OH	-4.4	-3.0	-	-6.0/-6.9
<b>5</b>	9:1 CDCl <sub>3</sub> /DMSO-d <sub>6</sub>	-5.9	-4.2	-6.5	-6.1/-6.4
	8:2 DMSO-d <sub>6</sub> /H <sub>2</sub> O	-4.8	-2.7	-7.4	-6.0/-6.4
	CH <sub>3</sub> OH	-5.1	-3.1	-6.2	-6.0/-6.4

**Table S2.** VT-<sup>1</sup>H-NMR Δδ/Δt values (p.p.b./K) of Ts-Oxd-DHA-OMe (**10**), in different solvents.

compd	solvent	DHANH
<b>10</b>	CDCl <sub>3</sub>	-1.8
	8:2 DMSO-d <sub>6</sub> /H <sub>2</sub> O	-4.6
	CH <sub>3</sub> OH	-4.9

**Table S3.** VT-<sup>1</sup>H-NMR Δδ/Δt values (p.p.b./K) of Ts-Oxd<sup>1</sup>-Phe<sup>2</sup>-Oxd<sup>3</sup>-Phe<sup>4</sup>-OH (**14**), in different solvents.

compd	solvent	Phe <sup>2</sup> NH	Phe <sup>4</sup> NH
<b>14</b>	9:1 CDCl <sub>3</sub> /DMSO-d <sub>6</sub>	-2.9	-4.2
	8:2 DMSO-d <sub>6</sub> /H <sub>2</sub> O	-5.2	-3.8
	CH <sub>3</sub> OH	-5.6	-4.2



**Table S4.** Non-obvious ROESY cross-peaks observed for Ts-Ala-L-Oxd-Phe-NH<sub>2</sub> (**2a**) in 8:2 DMSO-d<sub>6</sub>/H<sub>2</sub>O.

Cross peak <sup>a</sup>	Intensity <sup>b</sup>	Cross peak <sup>a</sup>	Intensity <sup>b</sup>
PheNH-PheHβ <sub>2,8</sub>	vs	PheNH-PheHβ <sub>3,0</sub>	s
PheNH-OxdH <sub>5,4,2</sub>	s	PheNH-PheHα	m
PheNH-OxdH <sub>4</sub>	vs	PheNH-OxdH <sub>5,4,5</sub>	m
PheNH-PheArH	m	PheNH-CONH <sub>7,3</sub>	m
AlaNH-AlaMe	vs	AlaNH-AlaHα	m
AlaNH-TsArH <sub>7,8</sub>	m	TsArH <sub>7,8</sub> -AlaHα	s
TsArH <sub>7,8</sub> -AlaMe	m	CONH <sub>7,3</sub> -PheHα	vs
CONH <sub>7,3</sub> -PheHβ <sub>3,0</sub>	s	CONH <sub>7,3</sub> -PheHβ <sub>2,8</sub>	s
PheArH-PheHβ <sub>3,0</sub>	s	PheArH-PheHβ <sub>2,8</sub>	s
PheArH-PheHα	s	CONH <sub>7,0</sub> -PheHα	m
PheHα-PheHβ <sub>3,0</sub>	s	PheHα-PheHβ <sub>2,8</sub>	s

<sup>a</sup> Stereochemistry has been omitted. <sup>b</sup> vs = very strong, s = strong, m = medium, w = weak.

**Table S5.** Non-obvious ROESY cross-peaks observed for Ts-Ala-D-Oxd-Phe-NH<sub>2</sub> (**2b**) in 8:2 DMSO-d<sub>6</sub>/H<sub>2</sub>O.

Cross peak <sup>a</sup>	Intensity <sup>b</sup>	Cross peak <sup>a</sup>	Intensity <sup>b</sup>
PheNH-PheHβ <sub>2,7</sub>	s	PheNH-PheHβ <sub>3,1</sub>	w
PheNH-OxdH <sub>5,3,4</sub>	m	PheNH-PheHα	m
PheNH-OxdH <sub>4</sub>	vs	PheNH-PheArH	m
PheNH-CONH <sub>7,6</sub>	m	AlaNH-AlaMe	s
AlaNH-AlaHα	m	TsArH <sub>7,6</sub> -AlaMe	m
TsArH <sub>7,6</sub> -AlaHα	m	TsArH <sub>7,6</sub> -AlaNH	w
CONH <sub>7,6</sub> -PheHβ <sub>3,1</sub>	m	CONH <sub>7,6</sub> -PheHβ <sub>2,7</sub>	w
CONH <sub>7,6</sub> -PheHα	s	CONH <sub>7,3</sub> -PheH <sub>5,3,4</sub>	w
CONH <sub>7,3</sub> -PheHβ <sub>3,1</sub>	w	CONH <sub>7,3</sub> -OxdH <sub>5,3,4</sub>	w
CONH <sub>7,3</sub> -PheHα	w	PheArH-PheHβ <sub>2,7</sub>	s
PheArH-PheHβ <sub>3,1</sub>	s	PheArH-OxdH <sub>5,3,4</sub>	m
PheArH-PheHα	s	OxdH <sub>4</sub> -AlaMe	w
PheHα-PheHβ <sub>2,7</sub>	s	PheHα-PheHβ <sub>3,1</sub>	vs
TsMe-AlaMe	w		

<sup>a</sup> Stereochemistry has been omitted. <sup>b</sup> vs = very strong, s = strong, m = medium, w = weak.

**Table S6.** Non-obvious ROESY cross-peaks observed for Ns-Ala-D-Oxd-Phe-GlyNH<sub>2</sub> (**5**) in 8:2 DMSO-d<sub>6</sub>/H<sub>2</sub>O.

Cross peak <sup>a</sup>	Intensity <sup>b</sup>	Cross peak <sup>a</sup>	Intensity <sup>b</sup>
AlaMe-AlaNH	s	AlaMe-NsArH <sub>7,9</sub>	m
AlaMe-OxdH4	w	AlaNH-PheHa	w
AlaNH-AlaHa	m	PheNH-OxdH <sub>5,4,3</sub>	w
PheNH-GlyNH	w	PheNH-PheArH	w
PheNH-OxdH4	vs	PheNH-PheHa	m
PheNH-OxdH <sub>5,3,4</sub>	m	PheNH-PheHa	vs
PheNH-PheH $\beta$ <sub>3,2</sub>	w	PheNH-GlyHa	w
GlyNH-CONH <sub>7,1</sub>	w	GlyNH-CONH <sub>7,3</sub>	m
GlyNH-PheHa	vs	GlyNH-GlyHa	vs
GlyNH-PheH $\beta$ <sub>3,2</sub>	m	GlyNH-PheH $\beta$ <sub>2,7</sub>	w
GlyNH-AlaHa	w	NsArH <sub>7,9</sub> -AlaHa	w
NsArH <sub>8,2</sub> -AlaMe	w	NsArH <sub>8,2</sub> -AlaHa	w
NsArH <sub>8,2</sub> -GlyHa	w	PheArH-PheH $\beta$ <sub>2,7</sub>	s
PheArH-PheH $\beta$ <sub>3,2</sub>	s	PheArH-OxdH <sub>5,3,4</sub>	m
PheArH-PheHa	s	GlyHa-CONH <sub>7,1</sub>	m
GlyHa-CONH <sub>7,3</sub>	s	PheHa-PheH $\beta$ <sub>2,7</sub>	m
PheHa-PheH $\beta$ <sub>3,2</sub>	s	NsArH <sub>7,9</sub> -PheH $\beta$ <sub>2,7</sub>	w
NsArH <sub>7,9</sub> -PheH $\beta$ <sub>3,2</sub>	m	NsArH <sub>7,9</sub> -GlyHa	w

<sup>a</sup> Stereochemistry has been omitted. <sup>b</sup> vs = very strong, s = strong, m = medium, w = weak.

**Table S7.** Non-obvious ROESY cross-peaks observed for Ts-Oxd-Dha-OMe (**10**) in 8:2 DMSO-d<sub>6</sub>/H<sub>2</sub>O.

Cross peak <sup>a</sup>	Intensity <sup>b</sup>	Cross peak <sup>a</sup>	Intensity <sup>b</sup>
DhaNH-OxdH <sub>5,4,3</sub>	s	DhaNH-OxdH <sub>5,4,7</sub>	w
DhaNH-OxdH4	vs	DhaNH-C=CH <sub>5,9</sub>	w
DhaNH-C=CH <sub>6,3</sub>	m	DhaNH-COOMe	w
TsArH <sub>7,8</sub> -C=CH <sub>5,9</sub>	w	TsArH <sub>7,8</sub> -C=CH <sub>6,3</sub>	w
TsArH <sub>7,8</sub> -OxdH4	s	TsArH <sub>7,8</sub> -COOMe	w
TsArH <sub>7,4</sub> -C=CH <sub>5,9</sub>	w	TsArH <sub>7,4</sub> -C=CH <sub>6,3</sub>	w
TsArH <sub>7,4</sub> -COOMe	w	COOMe-TsMe	w
C=CH <sub>5,9</sub> -COOMe	m	OxdH <sub>5,4,3</sub> -TsMe	w
OxdH <sub>5,4,7</sub> -TsMe	w		

<sup>a</sup> Stereochemistry has been omitted. <sup>b</sup> vs = very strong, s = strong, m = medium, w = weak.

**Table S8.** Non-obvious ROESY cross-peaks observed for Ts-Oxd<sup>1</sup>-(5-Me-Oxd<sup>2</sup>)-OMe (**12a**) in 8:2 DMSO-d<sub>6</sub>/H<sub>2</sub>O.

Cross peak <sup>a</sup>	Intensity <sup>b</sup>	Cross peak <sup>a</sup>	Intensity <sup>b</sup>
TsArH <sub>7,9</sub> -Oxd <sup>2</sup> H4	w	TsArH <sub>7,9</sub> -Oxd <sup>1</sup> H4	m
Oxd <sup>1</sup> H4-Oxd <sup>2</sup> H4	w	Oxd <sup>2</sup> H5-COOMe	m
Oxd <sup>2</sup> H4-COOMe	w	COOMe-Oxd <sup>1</sup> H <sub>5,4,3</sub>	w
COOMe-5'Me	w		

<sup>a</sup> Stereochemistry has been omitted. <sup>b</sup> vs = very strong, s = strong, m = medium, w = weak.

**Table S9.** Non-obvious ROESY cross-peaks observed for Ts-D-Oxd<sup>1</sup>-(5-Me-Oxd<sup>2</sup>)-OMe (**12b**) in 8:2 DMSO-d<sub>6</sub>/H<sub>2</sub>O.

Cross peak <sup>a</sup>	Intensity <sup>b</sup>	Cross peak <sup>a</sup>	Intensity <sup>b</sup>
TsArH <sub>7,9</sub> -Oxd <sup>1</sup> H4	w	TsArH <sub>7,9</sub> -COOMe	w
TsArH <sub>7,5</sub> -COOMe	w	Oxd <sup>1</sup> H4-Oxd <sup>2</sup> H4	w
Oxd <sup>1</sup> H <sub>5,4,3</sub> -5'Me	w	Oxd <sup>2</sup> H5-COOMe	m
Oxd <sup>2</sup> H4-COOMe	w		

<sup>a</sup> Stereochemistry has been omitted. <sup>b</sup> vs = very strong, s = strong, m = medium, w = weak.

**Table S10.** Non-obvious ROESY cross-peaks observed for Ts-Oxd<sup>1</sup>-Phe<sup>2</sup>-Oxd<sup>3</sup>-Phe<sup>4</sup>-OH (**14**), in 8:2 DMSO-d<sub>6</sub>/H<sub>2</sub>O.

Cross peak <sup>a</sup>	Intensity <sup>b</sup>	Cross peak <sup>a</sup>	Intensity <sup>b</sup>
Phe <sup>2</sup> NH-Phe <sup>2</sup> Hβ <sub>2,6</sub>	vs	Phe <sup>2</sup> NH-Phe <sup>2</sup> Hβ <sub>3,2</sub>	w
Phe <sup>2</sup> NH-Oxd <sup>1</sup> H4	vs	Phe <sup>2</sup> NH-Phe <sup>2</sup> Ha	m
Phe <sup>2</sup> NH-TsArH <sub>7,5</sub>	w	Phe <sup>2</sup> NH-Phe <sup>2</sup> ArH	m
Phe <sup>4</sup> NH-Phe <sup>4</sup> Hβ <sub>3,0</sub>	s	Phe <sup>4</sup> NH-Phe <sup>4</sup> Ha	m
Phe <sup>4</sup> NH-Oxd <sup>3</sup> H4	vs	TsArH <sub>7,3</sub> -Oxd <sup>1</sup> H <sub>5,4,7</sub>	w
Phe <sup>4</sup> ArH-Phe <sup>4</sup> Hβ <sub>3,0</sub>	vs	Phe <sup>4</sup> ArH-Phe <sup>4</sup> Ha	m
Phe <sup>2</sup> ArH-Phe <sup>2</sup> Hβ <sub>2,6</sub>	s	Phe <sup>2</sup> ArH-Phe <sup>2</sup> Hβ <sub>3,2</sub>	m
Phe <sup>2</sup> ArH-Phe <sup>2</sup> Ha	m	Phe <sup>4</sup> Ha-Phe <sup>4</sup> Hβ <sub>3,0</sub>	vs
Phe <sup>4</sup> Ha-Phe <sup>4</sup> Hβ <sub>3,2</sub>	w	Phe <sup>2</sup> Ha-Phe <sup>2</sup> Hβ <sub>3,2</sub>	s
Phe <sup>2</sup> Ha-Phe <sup>2</sup> Hβ <sub>2,6</sub>	w		

<sup>a</sup> Stereochemistry has been omitted. <sup>b</sup> vs = very strong, s = strong, m = medium, w = weak.

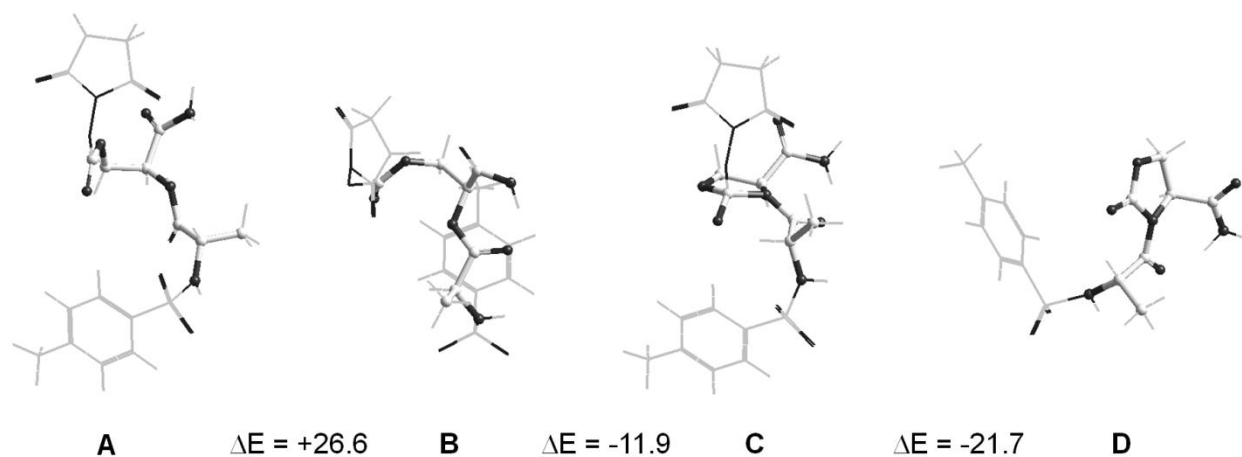


**Figure S1.** Structures and  $\Delta E$  of the intermediates calculated for the cyclization of the model peptide Ts-Ala-Ser-NH<sub>2</sub> with DSC and DIPEA, employing ab initio molecular orbital (MO) theory. A systematic conformational analysis for the structures was done at the HF/6-31G\* level. The conformers were re-optimized at the HF/6-31G\*\* level. Backbones are rendered in balls-and-cylinders, the rest in sticks. Optimization was performed by conjugate gradient algorithm, convergence at 0.001; energies are expressed in Kcal mol<sup>-1</sup>. The following structures were included in the computations of **A-D**, but are not visualized for clarity: **A**, DIPEA; **B**, DIPEAH<sup>+</sup>; **C**, DIPEAH<sup>+</sup>; **D**, 1-hydroxypyrrolidine-2,5-dione and DIPEA.

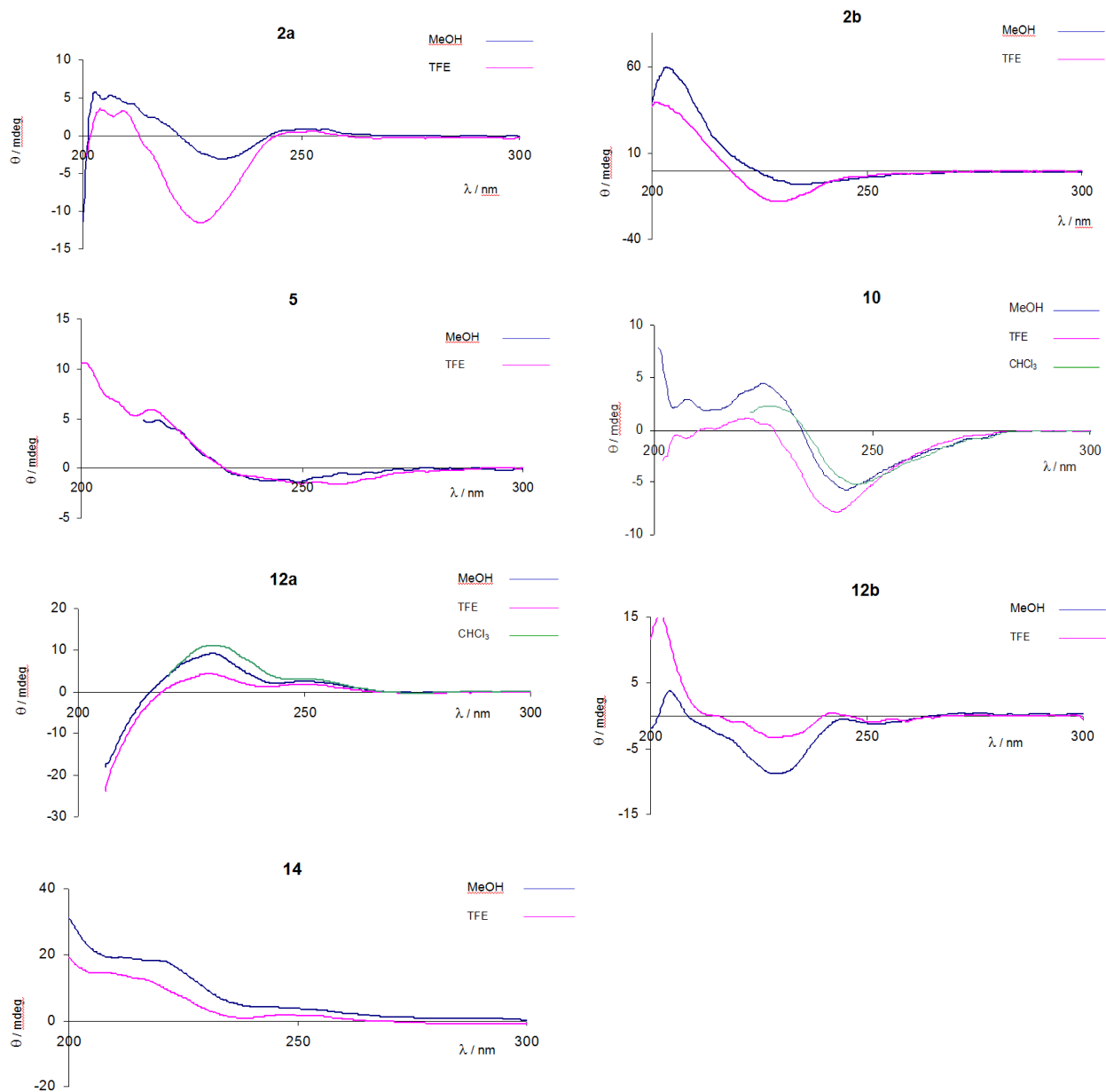


**Figure S2.** ECD spectra were recorded from 200 to 300 nm at 25 °C. Solutions were made up in spectral grade solvents and run in a 0.01 cm quartz cell. For each sample the absorbance value was set to 1.0 at  $\lambda_{\text{max}}$  (225–260 nm); concentrations used were in the range 5–11 mM. Data are reported in ellipticity (millidegree).

## Notes and references

- [1]. V. J. Hruby and P. M. Balse, *Curr. Med. Chem.*, **2000**, 7, 945; A. Grauer and B. König, *Eur. J. Org. Chem.*, **2009**, 5099; L. Gentilucci, R. De Marco and L. Cerisoli, *Curr. Pharm. Des.*, **2010**, 16, 3185.
- [2]. J. S. Richardson and D. C. Richardson, in *Prediction of Protein Structure and the Principle of Protein Conformation*, ed. G. D. Fasman, Plenum Press, New York, **1989**.
- [3]. J. D. A. Tyndall, B. Pfeiffer, G. Abbenante and D. P. Fairlie, *Chem. Rev.*, **2005**, 105, 793.
- [4]. D. E. Stewart, A. Sarkar and J. E. Wampler, *J. Mol. Biol.*, **1990**, 214, 253; M. W. MacArthur and J. M. Thornton, *J. Mol. Biol.*, **1991**, 218, 397; D. K. Chalmers and G. R. Marshall, *J. Am. Chem. Soc.*, **1995**, 117, 5927; T. Hoffmann, H. Lanig, R. Waibel and P. Gmeiner, *Angew. Chem., Int. Ed.*, **2001**, 40, 3361; K. Wookhyun, R. A. McMillan, J. P. Snyder and V. P. Conticello, *J. Am. Chem. Soc.*, **2005**, 127, 18121; H. Bittermann and P. Gmeiner, *J. Org. Chem.*, **2006**, 71, 97; A. P. Vartak and L. L. Johnson, *Org. Lett.*, **2006**, 8, 983.
- [5]. A. B. Mauger, *J. Nat. Prod.*, **1996**, 59, 1205.
- [6]. D. Seebach, T. L. Sommerfeld, Q. Jiang and L. M. Venanzi, *Helv. Chim. Acta*, **1994**, 77, 1313; E. Beausoleil and W. Lubell, *J. Am. Chem. Soc.*, **1996**, 118, 12902; P. Dumy, M. Keller, D. E. Ryan, B. Rohwedder, T. Wöhr and M. Mutter, *J. Am. Chem. Soc.*, **1997**, 119, 918; M. Keller, C. Sager, P. Dumy, M. Schutkowski, G. S. Fischer and M. Mutter, *J. Am. Chem. Soc.*, **1998**, 120, 2714; Y. J. Chung, B. R. Huck, L. A. Christianson, H. E. Stanger, S. Krauthauser, D. R. Powell and S. H. Gellman, *J. Am. Chem. Soc.*, **2000**, 122, 3995; F. Cavelier, B. Vivet, J. Martinez, A. Aubry, C. Didierjean, A. Vicherat and M. Marraud, *J. Am. Chem. Soc.*, **2002**, 124, 2917; J. Quancard, A. Labonne, Y. Jacquot, G. Chassaing, S. Lavielle and P. Karoyan, *J. Org. Chem.*, **2004**, 69, 7940; P. Grieco, L. Giusti, A. Carotenuto, P. Campiglia, V. Calderone, T. Lama, I. Gomez-Monterrey, G. Tartaro, M. R. Mazzoni and E. Novellino, *J. Med. Chem.*, **2005**, 48, 3153; D. Torino, A. Mollica, F. Pinnen, G. Lucente, F. Feliciani, P. Davis, J. Lai, S.-W. Mad, F. Porreca and V. J. Hruby, *Bioorg. Med. Chem. Lett.*, **2009**, 19, 4115.
- [7]. P. Thamm, H. J. Musiol and L. Moroder, Synthesis of peptides containing proline analogues, in *Methods of Organic Chemistry: Synthesis of Peptides and Peptidomimetics*, ed. M. Goodman, Georg Thieme Verlag, Stuttgart, New York, **2003**, vol. 22, pp. 52–86; P. Karoyan, S. Sagan, O. Lequin, J. Quancard, S. Lavielle and G. Chassaing, Substituted prolines: syntheses and applications in structure-activity relationship studies of biologically active peptides, in *Targets in Heterocyclic Systems—Chemistry and Properties*, ed. O. A. Attanasi and D. Spinelli, Royal Society of Chemistry, Cambridge, **2005**, vol. 8, pp. 216–273.
- [8]. M. Keller, C. Boissard, L. Patiny, N. N. Chung, C. Lemieux, M. Mutter and P. W. Schiller, *J. Med. Chem.*, **2001**, 44, 3896.
- [9]. M. Doi, A. Asano, E. Komura and Y. Ueda, *Biochem. Biophys. Res. Commun.*, **2002**, 297, 138.
- [10]. J. Samanen, T. Cash, D. Narindray, E. Brandeis Jr., W. Adams, H. Weideman, T. Yellin and D. Regoli, *J. Med. Chem.*, **1991**, 34, 3036.
- [11]. J. L. Baeza, G. Gerona-Navarro, M. J. Pérez de Vega, M. T. García- López, R. González-Muñiz and M. Martín-Martínez, *J. Org. Chem.*, **2008**, 73, 1704.
- [12]. L. Halab and D.W. Lubell, *J. Am. Chem. Soc.*, **2002**, 124, 2474.

- [13]. S. J. Buhrlage, B. Chen and A. K. Mapp, *Tetrahedron*, **2009**, 65, 3305; J. Farrera-Sinfreu, L. Zaccaro, D. Vidal, X. Salvatella, E. Giralt, M. Pons, F. Albericio and M. Royo, *J. Am. Chem. Soc.*, **2004**, 126, 6048.
- [14]. S. H. Gellman, *Acc. Chem. Res.*, **1998**, 31, 173; J. A. Miller, *Chem. Rev.*, **2001**, 101, 2181; S. Izquierdo, M. J. Kogan, T. Parella, A. G. Moglioni, V. Branchadell, E. Giralt and R. M. Ortuño, *J. Org. Chem.*, **2004**, 69, 5093; D. Seebach and J. Gardiner, *Acc. Chem. Res.*, **2008**, 41, 1366; W. S. Horne and S. H. Gellman, *Acc. Chem. Res.*, **2008**, 41, 1399; T. A. Martinek and F. Fülöp, *Chem. Soc. Rev.*, **2012**, DOI: 10.1039/c1cs15097a.
- [15]. Selected examples: G. Cardillo, L. Gentilucci, A. R. Qasem, F. Sgarzi and S. Spampinato, *J. Med. Chem.*, **2002**, 45, 2571; G. Cardillo, L. Gentilucci, A. Tolomelli, M. Calienni, A. R. Qasem and S. Spampinato, *Org. Biomol. Chem.*, **2003**, 1, 1498; L. Gentilucci, G. Cardillo, F. Squassabia, A. Tolomelli, S. Spampinato, A. Sparta and M. Baiula, *Bioorg. Med. Chem. Lett.*, **2007**, 17, 2329; F. Benfatti, G. Cardillo, E. Mosconi and A. Tolomelli, *Synlett*, **2008**, 17, 2605; F. Benfatti, G. Cardillo, S. Contaldi, L. Gentilucci, E. Mosconi, A. Tolomelli, E. Juaristi and G. Reyes-Rangel, *Tetrahedron*, **2009**, 65, 2478; A. Tolomelli, L. Gentilucci, E. Mosconi, A. Viola and E. Paradisi, *Amino Acids*, **2011**, 4, 575.
- [16]. Selected examples: J. Gante, H. Juraszyk, P. Raddatz, H. Wurziger, S. Bernotat-Danielowski, G. Melzer and F. Rippmann, *Bioorg. Med. Chem. Lett.*, **1996**, 6, 2425; W. Kamm, P. Raddatz, J. Gante and T. Kissel, *Pharm. Res.*, **1999**, 16, 1527; T. Mittag, K. L. Christensen, K. B. Lindsay, N. C. Nielsen and T. Skrydstrup, *J. Org. Chem.*, **2008**, 73, 1088; A. Ali, G. S. Reddy, M. N. Nalam, S. G. Anjum, H. Cao, C. A. Schiffer and T. M. Rana, *J. Med. Chem.*, **2010**, 53, 7699.
- [17]. C. Tomasini, G. Luppi and M. Monari, *J. Am. Chem. Soc.*, **2006**, 128, 2410–2420; G. Angelici, G. Luppi, B. Kaptein, Q. B. Broxterman, H. J. Hofmann and C. Tomasini, *Eur. J. Org. Chem.*, **2007**, 2713.
- [18]. G. Angelici, G. Falini, H.-J. Hofmann, D. Huster, M. Monari and C. Tomasini, *Angew. Chem., Int. Ed.*, **2008**, 47, 8075; G. Angelici, G. Falini, H.-J. Hofmann, D. Huster, M. Monari and C. Tomasini, *Chem.–Eur. J.*, **2009**, 15, 8037.
- [19]. L. Gentilucci, A. Tolomelli, R. De Marco, C. Tomasini and S. Feddersen, *Eur. J. Org. Chem.*, **2011**, 4925.
- [20]. A. Polinsky, M. G. Cooney, A. Toy-Palmer, G. Osapay and M. Goodman, *J. Med. Chem.*, **1992**, 35, 4185; U. Schmidt, A. Lieberknecht and J. Wild, *Synthesis*, **1988**, 159; J. M. Humphrey and A. R. Chamberlin, *Chem. Rev.*, **1997**, 97, 2243; C. Bonauer, T. Walenzyk and B. König, *Synthesis*, **2006**, 1.
- [21]. T. Poloński, *Tetrahedron*, **1985**, 41, 603; M. Ousmer, N. A. Braun, C. Bavoux, M. Perrin and M. A. Ciufolini, *J. Am. Chem. Soc.*, **2001**, 123, 7534; X. Deng and N. S. Mani, *Green Chem.*, **2006**, 8, 835.
- [22]. G. Zappia, E. Gacs-Baitz, G. Delle Monache, D. Misiti, L. Nevola and B. Botta, *Curr. Org. Synth.*, **2007**, 4, 81.
- [23]. S. Cutugno, G. Martelli, L. Negro and D. Savoia, *Eur. J. Org. Chem.*, **2001**, 517.
- [24] P. M. T. Ferreira, H. L. S. Maia, L. S. Monteiro and J. Sacramento, *J. Chem. Soc., Perkin Trans. 1*, **1999**, 3697.
- [25]. E. Falb, A. Nudelman and A. Hassner, *Synth. Commun.*, **1993**, 23, 2839; D. Melon, C. Gravier-Pellettier, Y. Le Merrer and J. C. Depezay, *Bull. Soc. Chim. Fr.*, **1992**, 129, 585.
- [26] G. B. Jones and B. J. Chapman, *Synthesis*, **1995**, 475.

- [27] *Modern Aldol Reactions Vol. 1: Enolates, Organocatalysis, Biocatalysis and Natural Product Synthesis 8 2004*, ed. R. Mahrwald, WILEY-VCH Verlag GmbH & Co. KGaA, Weinheim, pp. 1–328.
- [28]. I. Ojima and H. B. Kwon, *J. Am. Chem. Soc.*, **1988**, 110, 5617; M. Stefano, G. N. Ana and F. M. Carlos, *J. Org. Chem.*, **2009**, 74, 6888.
- [29]. A. Isidro-Llobet, M. Alvarez and F. Albericio, *Chem. Rev.*, **2009**, 109, 2455–2504.
- [30]. G. Sabitha, B. V. S. Reddy, S. Abraham and J. S. Yadav, *Tetrahedron Lett.*, **1999**, 40, 1569.
- [31]. T. Ankner and G. Hilmersson, *Org. Lett.*, **2009**, 11, 503.
- [32]. T. Fukuyama, C.-K. Jow and M. Cheung, *Tetrahedron Lett.*, **1995**, 36, 6373.
- [33]. G. Panda and N. V. Rao, *Synlett*, **2004**, 714.
- [34]. K. R. Rajashankar, S. Ramakumar and V. S. Chauhan, *J. Am. Chem. Soc.*, **1992**, 114, 9225.
- [35]. A. Glaetli, X. Daura, D. Seebach and W. F. van Gunsteren, *J. Am. Chem. Soc.*, **2002**, 124, 12972.
- [36]. N. Sreerama and R. W. Woody, Circular dichroism of peptides and proteins, in *Circular Dichroism – Principles and Applications*, N. Berova, K. Nakanishi and R. W. Woody, ed., Wiley-VCH, New York, **2000**.
- [37]. F. D. Sonnichsen, J. E. Van Eyk, R. S. Hodges and B. D. Sykes, *Biochemistry*, **1992**, 31, 8790.
- [38]. E. Vass, Z. Maier, K. Kohalmy and M. Hollosi, *Chirality*, **2010**, 22, 762; A. Motta, M. Reches, L. Pappalardo, G. Andreotti and E. Gazit, *Biochemistry*, **2005**, 44, 14170; D. Yang, W. Li, S.-W. Luo and Y.-D. Wu, *J. Am. Chem. Soc.*, **2003**, 125, 13018; V. Madison and K. D. Kopple, *J. Am. Chem. Soc.*, **1980**, 102, 4855.
- [39]. P. A. Temussi, D. Picone, G. Saviano, P. Amodeo, A. Motta, T. Tancredi, S. Salvadori and R. Tomatis, *Biopolymers*, **1992**, 32, 367 and references herein.
- [40]. F. Bernardi, M. Garavelli, M. Scatizzi, C. Tomasini, V. Trigari, M. Crisma, F. Formaggio, C. Peggion and C. Toniolo, *Chem.–Eur. J.*, **2002**, 8, 2516.
- [41]. C. Toniolo, *Crit. Rev. Biochem. Mol. Biol.*, **1980**, 9, 1.
- [42]. J. A. Smith and L. G. Pease, *J. Mol. Biol.*, **1980**, 203, 221; B. Imperiali, S. L. Fisher, R. A. Moats and T. J. Prim, *J. Am. Chem. Soc.*, **1992**, 114, 3182; J. Venkatraman, S. C. Shankaramma and P. Balaram, *Chem. Rev.*, **2001**, 101, 3131; R. Rai, S. Raghobama and P. Balaram, *J. Am. Chem. Soc.*, **2006**, 128, 2675.
- [43]. M. Sugawara, K. Tonan and S. Ikawa, *Spectrochim. Acta, Part A*, **2001**, 57, 1305.
- [44]. B. Ishimoto, K. Tonan and S. Ikawa, *Spectrochim. Acta, Part A*, **2000**, 56, 201.
- [45]. Y. Jin, V. Tonan and S. Ikawa, *Spectrochim. Acta, Part A*, **2002**, 58, 2795; W. Chin, M. Mons, J. P. Dognon, F. Piuze, B. Tardivel and I. Dimicoli, *Phys. Chem. Chem. Phys.*, **2004**, 6, 2700.
- [46]. C. A. Jordi Casanovas, *Biopolymers*, **1995**, 36, 71; B. Rzeszotarska, D. Siodlak, M. A. Broda, I. Dybala and A. E. Koziol, *J. Pept. Res.*, **2002**, 59, 79; B. Padmanabhan, S. Dey, B. Khandelwal, G. S. Rao and T. P. Singh, *Biopolymers*, **1992**, 32, 1271.
- [47]. HyperChem Release 8.0.3, Hypercube Inc. 1115 NW 4th St. Gainesville, FL 32608, (USA), 2007.
- [48]. W. D. Cornell, P. Cieplak, C. I. Bayly, I. R. Gould, K. M. Merz, D. M. Ferguson, D. C. Spellmeyer, T. Fox, J. W. Caldwell and P. A. Kollman, *J. Am. Chem. Soc.*, **1995**, 117, 5179.
- [49]. W. L. Jorgensen, J. Chandrasekhar, J. Madura, R. W. Impey and M. L. Klein, *J. Chem. Phys.*, **1983**, 79, 926.

[50]. H. J. C. Berendsen, J. P. M. Postma, W. F. van Gunsteren, A. Di Nola and J. R. Haak, *J. Chem. Phys.*, **1984**, 81, 3684.

## CONCLUSIONS

This manuscript describes the results obtained during my PhD work in the period 2009-2011. The main topic of my experiments has been the synthesis of modified amino acids, and their insertion in peptides and peptidomimetics. Further, I studied the effects exerted by the modifications on structures and biological activities of the compounds so obtained. The last section of the paper deals with the use of the peptidomimetic strategy for designing structurally defined compounds as integrin inhibitors and opioid receptor agonists.

In this regard, I prepared peptide analogues containing unusual amino acids such as halogenated, alkylated (S)- or (R)-tryptophans, useful for the synthesis of mimetics of the endogenous opioid peptide endomorphin-1, or 2-oxo-1,3-oxazolidine-4-carboxylic acids, utilized as pseudo-prolines having a clear all-trans configuration of the preceding peptide bond. The latter gave access to a series of constrained peptidomimetics with potential interest in medicinal chemistry and in the field of the foldamers.

In particular, I have dedicated much efforts to the preparation of cyclopentapeptides containing D-configured, alfa-, or beta-aminoacids, and also of cyclotetrapeptides including the retro-inverso modification. The conformational analyses confirmed that these cyclic compounds can be utilized as rigid scaffolds mimicking gamma- or beta-turns, allowing to generate new molecular and 3D diversity.

Much work has been dedicated to the structural analysis in solution and in the receptor-bound state, fundamental for giving a rationale to the experimentally determined bioactivity, as well as for predicting the activity of virtual compounds (in silico pre-screen). The conformational analyses in solution has been done mostly by NMR (2D gC<sub>osy</sub>, Roesy, VT, molecular dynamics, etc.). A special section is dedicated to the prediction of plausible poses of the ligands when bound to the receptors by Molecular Docking. This computational method proved to be a powerful tool for the investigation of ligand-receptor interactions, and for the design of selective agonists and antagonists.

As a practical application, I synthesized scaffolds based on a partially modified retro-inverso cyclotetrapeptide structure carrying side chains designed to mimic the pharmacophores on the RGD integrin-recognition motive. Indeed, I could demonstrate a antiangiogenic effect of dual and selective  $\alpha_5\beta_1/\alpha_v\beta_3$  integrin antagonists.

Another practical use of cyclic peptidomimetics was the synthesis and biological evaluation of cyclic analogues of endomorphin-1 lacking in a protonable amino group. The studies revealed that a inverse type II beta-turn on D-Trp-Phe constituted the bioactive conformation. To my knowledge, this can be regarded to as a unprecedented pharmacophoric motif for MOR agonists.

In conclusion, the researched described herein demonstrate that the peptidomimetic approach to 3D definite structures allows unambiguous investigation of the structure-activity correlation, giving an access to a wide range bioactive compounds of pharmaceutical interest, as demonstrated by the examples in the integrin and opioid fields.

## CURRICULUM VITAE

### Personal Information

First name: Rossella

Last name: De Marco

Email : rossella.demarco2@unibo.it

Nationality: Italiana

### Academic Information

#### Education

**1993-1998** Diploma in Chemistry (45/60): State Industrial Technical Institute I.T.I.S. "E.Fermi", Castrovillari (CS).

**1998-2007** Laurea (Master) in CTF (97/110): Faculty of Pharmacy, Bologna University (07/03/2007), under the supervision of Prof.ssa A. Bisi, "Bioisosters and models of xantonic derivatives as aromatase inhibitors".

**2009-today** Ph.D. Course in Organic Chemistry, under the supervision of Prof. L. Gentilucci, Dept. of Chemistry "G. Ciamician", Università di Bologna.

**2010** PhD student at the laboratories of Prof. Floris P.J.T.Rutjes of the University of Nijmegen, "Synthesis of peptidomimetic inhibitors of MCH1 receptor".

#### Research and Professional experience

**1996** participation to "chemistry games organized by the Italian Chemical Society (SCI)", ranked 4th at the regional level.

**2007-2008** fellowship dedicated to "Antagonists of opioid receptors for the treatment of addictions", by Fondazione CARISBO, Bologna, under the supervision of Prof. L. Gentilucci

**2008** collaboration with Stepbio Srl for "Development of automated procedures for the synthesis of peptides"

**2008- 2009** fellowship Spinner/ASTER "Novel SPPS methodologies with green chemistry approach and innovative polymers".

**2009- 2011** project on the "Synthesis of modified amino acids for the preparation of peptidomimetics: structural aspects and impact on biological activity".

**2012** project on the "Study of peptidomimetics based on 2D-NMR analysis"

#### Teaching

**2009- today** Member of the group "Knowing Chemistry", that holds demonstrative lessons of Chemistry to both high school students and adults, in the aim of orienting young audience toward scientific studies and improving the knowledge about scientific topics in adult audience.

**2009** Tutorship for the "Laboratory of Organic Chemistry" practises of the Biotechnology students.

**2011** Tutorship for the "Laboratory of Organic Chemistry" practises of the Chemistry students.

### **Scholarships and Awards**

**2009-present** PhD fellowship in the Dept. of Chemistry "G. Ciamician", University of Bologna, by the Italian Ministry of University and Research.

**2010** Research fellowship in the Dept. of Chemistry "G. Ciamician", University of Bologna, by the Italian Ministry of Education through the project PRIN 2008.

### **Technical expertise**

Extremely skilled in a wide range of organic reactions and procedures. Competent with instruments for the identification and analysis of organic compounds: mono and bidimensional NMR, HPLC-MS, chiral HPLC, preparative HPLC, FT-IR, GC-MS. Competent with all word-processing softwares (Word, Openword), presentation tools (Powerpoint), bibliographic databases (Scifinder, Beilstein, Endnote, Reaxys).

**Congress participation: Poster (P) presentation**

**2009** New Perspectives in Medicinal Chemistry, III meeting-workshop, poster communication "DEVELOPMENT AND CHARACTERIZATION OF ENDOMORPHIN-1 ANALOGUES AS NOVEL POTENTIAL ANALGESIC DRUGS", Castelvechio Pascoli (LU), Italy.

**2009** "Tenth Tetrahedron Symposium", poster communication "Tryptophan- and halotryptophan-based opioid peptidomimetics: a new paradigm in the design of atypical analgesics", Paris, France.

**2009** SIGMA ALDRICH YOUNG CHEMISTS SYMPOSIUM - SAYCS, poster communication "Synthesis of Dipeptides Containing modified Trp by 1,4-Addition of Indoles Promoted by Lewis Acids", Pesaro, Italy.

**2009** Meeting of the Società Chimica Italiana (SCI) poster communication "Peptidomimetici oppioidi basati sul Triptofano e alogeno-triptofano: un nuovo modello di analgesici atipici", Bologna, Italy.

**2010** "International Narcotics Research Conference"(INRC) poster communication "Ac-D-Trp-PheNH<sub>2</sub> and Ac-D-Trp-Phe-GlyNH<sub>2</sub>- a new class of unusual opioid peptides", Malmo, Sweden.

**2011** Italian show 5 per thousand, poster communication "NUOVI OPPIOIDI PER IL TRATTAMENTO DEL DOLORE ACUTO E CRONICO", Bologna, Italy.

**2011.** "European Opioid Conference" (EOC) poster communication "DESIGN AND SYNTHESIS OF OPIOID PEPTIDE ANALOGUES AND MIMETICS", Krakow, Polonia.

**2011.** Società Farmacologia Italiana (SFI) poster communication " NOVEL ANTAGONIST OF  $\alpha_v\beta_3$  AND  $\alpha_5\beta_1$  INTEGRINS: ATTRACTIVE TARGETS FOR CANCER AND ANTI-INFLAMMATORY THERAPEUTICS", Bologna, Italy.

**2012.** poster communication

**2012.** oral communication

## List of Publications

1. Gentilucci, L.; Squassabia, F.; De Marco, R.; Artali, R.; Cardillo, G.; Tolomelli, A.; Spampinato, S.; Bedini, A. Investigation of the interaction between the atypical agonist c[YpwFG] and MOR. *FEBS Journal*, 2008, 275, 2315.
2. Gentilucci, L.; Cardillo, G.; Tolomelli, A.; De Marco, R.; Garelli, A.; Spampinato, S.; Spartà, A.; Juaristi, E. Synthesis and Conformational Analysis of Cyclotrapeptide Mimetic beta-Turn Templates and Validation as 3D Scaffolds. *Chem Med Chem*, 2009, 4, 517-23.
3. Gentilucci, L.; Cardillo, G.; Tolomelli, A.; Squassabia, F.; De Marco, R.; Chiriano, G. Cyclopeptide analogs for generating new molecular and 3D diversity. *Comb Chem High Throughput Screen* 2009, 12, 929-39.
4. Gentilucci, L.; Cardillo, G.; Spampinato, S.; Tolomelli, A.; Squassabia, F.; De Marco, R.; Bedini, A.; Baiula, M.; Belvisi, L.; Civera, M. Antiangiogenic effect of dual/selective alpha(5)beta(1)/alpha(v)beta(3) integrin antagonists designed on partially modified retro-inverso cyclotrapeptide mimetics. *J Med Chem* 2010, 1, 106-18.
5. Gentilucci, L.; Cerisoli, L.; De Marco, R.; Tolomelli, A. A simple route towards peptide analogues containing substituted (S)- or (R)-tryptophans. *Tetrahedron Letters* 2010, 51, 2576-79.
6. Bedini, A.; Baiula, M.; Gentilucci, L.; Tolomelli, A.; De Marco, R.; Spampinato, S. Peripheral antinociceptive effects of the cyclic endomorphin-1 analogue c[YpwFG] in a mouse visceral pain model. *Peptides* 2010, 31, 2135-2140.
7. Gentilucci, L.; De Marco, R.; Cerisoli, L. Chemical Modifications Designed to Improve Peptide Stability: incorporation of Non-Natural Amino Acids, Pseudo-Peptide Bonds, and Cyclization. *Curr Pharm Des*, 2010, 16, 3185-3203.
8. The Inverse Type II b-Turn on d-Trp-Phe, a Pharmacophoric Motif for MOR Agonists. L. Gentilucci, A. Tolomelli, R. De Marco, S. Spampinato, A. Bedini, and R. Artali. *Chem. Med. Chem.*, 2011, 9, 1640-53.
9. A Practical Synthesis of Peptides Containing Oxazolidin-2-one 4-Carboxylic Acid. L. Gentilucci, A. Tolomelli, R. De Marco, C. Tomasini, and S. Feddersen, *European Journal of Organic Chemistry* 2011, 18,

3545-51.

**10.** A novel family of minimalist opioid peptides deprived of the classic pharmacophores. L.Gentilucci, R. De Marco, A. Tolomelli, S. Feddersen, S. Spampinato, A. Bedini, R. Artali. *Pharmacological Reports*, 2011, 63, 212.

**11.** Design and synthesis of opioid peptide analogues and mimetics. R.De Marco, L. Gentilucci, A. Tolomelli, S. Feddersen, S. Spampinato, A. Bedini, R. Artali. *Pharmacological Reports*, 2011, 63, 223.

**12.** Expedient Synthesis of Pseudo-Pro-Containing Peptides: Towards Constrained Peptidomimetics and Foldamers. R. De Marco, A. Tolomelli, M. Campitiello, P. Rubini, L. Gentilucci. *Org. Biorg. Chem.*, 2012, 10, 2307-2317.

**13.** Molecular docking of opioid peptides and analogues, a powerful tool for the design of selective agonists and antagonists, and for the investigation of atypical ligand-receptor interactions. L. Gentilucci, A. Tolomelli, R. Artali, R. De Marco. *Curr. Med. Chem.*, 2012, in press.

**14.** Analytical pyrolysis of dipeptides containing proline and amino acids with polar side chains. Novel 2,5-diketopiperazine markers in the pyrolysates of proteins. D. Fabbri, A. Adamiano, G. Falini, R. De Marco, I. Mancini. *J. Anal.Appl.Pyrolysis.*, 2012, submitted.